THE JOURNAL
OF
CHEMICAL PHYSICS

VOLUME 32, NUMBER 5 MAY, 1960

Interactions between Molecules Adsorbed on a Surface

OKTAY SINANOĞLU* AND KENNETH S. PITZER

Lawrence Radiation Laboratory and College of Chemistry, University of California, Berkeley 4, California

(Received August 26, 1959)

The intermolecular potential energy between two inert gas molecules is considerably altered when these molecules are next to a solid surface as in physical adsorption. The change in the interaction is evidenced by the additional long-range repulsion that is often observed between the molecules of a monolayer and also by the additional attractions that must play a role in multilayer formation.

In this article, the two-molecule-surface potential is derived from quantum mechanical third-order perturbation theory. It is shown that this potential consists of two parts just as the energy giving the van der Waals attraction of a single molecule to a surface does. The first part exists only when the surface has a net electrostatic field and this is equivalent to the classical polarization effect. The second part arises from the fluctuations of the surface fields and is of the same origin as the dispersion forces. The third-order energy, i.e., the new intermolecular interaction caused by the surface, is directly related to the zero-coverage heat of adsorption and except for this experimental quantity, the results do not require specific assumptions about the surface. Thus, the theory is applicable to either metal or insulator surfaces. When both the two-molecule-surface and the one-molecule-surface interactions are available experimentally (for example, from the application of virial coefficients treatment in physical adsorption) the electrostatic field of the surface can be estimated.

The fluctuation or dispersion part of the third-order energy is shown to yield a repulsion between two molecules in a monolayer that amounts to 20–40% of the gas phase Lennard-Jones potential minimum ϵ_0. The same energy yields an additional attraction of about 10–20% of ϵ_0 when the two molecules are on top of one another as in multilayer formation. The theory is applicable also when more than two molecules at a time need be considered on the surface.

A. INTRODUCTION

PHYSICAL adsorption is characterized by relatively weak forces as compared to chemisorption and it might be considered a process in which both the adsorbed molecules and the adsorbent surface remain quite unchanged. Thus the van der Waals forces that cause physical adsorption can be understood for the most part through the use of quantum mechanical perturbation theory. The theory of these forces between molecules has been reviwed by Margenau[1] and some recent considerations by Pitzer.[2] Extensive reviews on the forces that cause physical adsorption also exist.[3,4]

Some interesting phenomena such as the formation of monolayers and multilayers on an adsorbent involve the forces between adsorbed molecules themselves as well as with the surface. Such forces can be investigated through the application of statistical mechanics to experimental measurements especially in physical adsorption, and although this is difficult when the adsorbate is dense, it becomes particularly suitable in the dilute case, i.e., relatively high temperature adsorption making use of a theory similar to the virial coefficients treatment of imperfect gases.[5] By such a method it is possible to investigate the adsorption of essentially one molecule, two molecules, etc., at a time on a surface and the potential energies of interaction involved in each case.[5]

Such experimental evidence has long shown[3,5b] that two inert gas atoms adsorbed into a monolayer display a rather different potential energy between themselves as compared to their energy when they are in the gas phase, i.e., the presence of the surface apparently causes a new long-range repulsion to appear between the two molecules of the monolayer and this repulsion tends to counterbalance their usual London attraction. On the other hand, in multilayer formation additional

[1] H. Margenau, Revs. Modern Phys. **11**, 1 (1939).
[2] K. S. Pitzer, *Advances in Chemical Physics* (Interscience Publishers, Inc., New York, 1959), Vol. II; or see K. S. Pitzer, UCRL-8395 (September, 1958).
[3] J. H. de Boer, Advances in Catalysis **8**, 29 (1956).
[4] S. Brunauer, *The Adsorption of Gases and Vapors* (Princeton University Press, Princeton, New Jersey, 1945), p. 180.
[5] (a) W. A. Steele and G. D. Halsey, Jr., J. Chem. Phys. **22**, 979 (1954); see also (b) M. P. Freeman, J. Phys. Chem. **62**, 729 (1958).

Copyright © 1960 by the American Institute of Physics

attractions must exist. These observations are not explainable in terms of second-order perturbation theory of long-range forces. This theory predicts that the total interaction between a system of adsorbed molecules and the surface must be pairwise additive; hence the interaction between molecules would be unaltered.[1] The repulsion in the monolayer has usually been ascribed[3] to the dipoles permanently induced in the nonpolar molecules by an electrostatic field that is known to be present on metal[6] and charcoal[3] surfaces. The magnitude of these induced dipoles can be inferred[3] from the nonideal behavior of the adsorbed two-dimensional gas if the entire additional repulsion in the presence of the surface is attributed to this classical electrostatic effect. However the values so obtained usually seem to be too high in comparison to the estimates from measured contact potentials[6] and work function lowering.[7] It is apparent that part of the many-body repulsion must be caused by a mechanism other than ordinary electrostatic polarization.

Many-body forces between spherical, inert molecules have been investigated quite extensively. When overlap effects are negligible these forces arise for the most part from the triple-dipole interaction in third-order perturbation theory. These three-body forces have been reviewed extensively, along with their application to the third virial coefficient of an imperfect gas, by Kihara.[8] A recent discussion with reference to colloidal particles has been given by Sparnaay.[9] Although the three-body force between three molecules is quite small, it is to be expected that forces of similar origin should become appreciable, as compared to the interaction between two molecules, when the third body is a large surface.

If the two molecules overlap, then even in second-order perturbation appreciable many-body forces should arise as shown by Jansen and McGinnies[10] for three atoms. However, we shall assume that this effect is part of the change that must take place in the short-range repulsive region of the intermolecular potential and concern ourselves with nonoverlap, long-range interactions.

Higher-order perturbations have been studied by Bade[11] using the simple Drude or harmonic oscillator model. It is found that for a system of a few molecules the perturbation series converges quite rapidly and more will be said about convergence in Sec. C.

In the following we shall give a general derivation of some forces that arise between spherical (hence nonpolar) molecules in the presence of a semi-infinite solid surface (metal or insulator) based on a third-order perturbation treatment. Since in this order the energy is triplewise additive[11] (see end of Sec. C) it will be necessary to consider only the system of two molecules and the surface. We shall show that, just as in the case of van der Waals energy between one molecule and the surface,[3] the energy of two molecules and the surface is composed of an "electrostatic" part and a quantum mechanical fluctuation or dispersion part. Moreover, it will be found that each part of the three-body energy can be related directly to the corresponding part of the one molecule adsorption energy. Thus it is often possible to obtain the potential energy of interaction between two molecules, physically adsorbed on a surface, in terms of the experimental zero-coverage heat of adadsorption U_0. On the other hand, the present treatment enables one to estimate the "electrostatic" fraction of U_0, when both U_0 and the surface intermolecular potential are available experimentally. The intimate connection between these two energies makes it necessary to discuss first the van der Waals energy of a single molecule on a surface with comments on the application of some of the existing theories before going into the derivation of the "two-molecule-surface" potential.

B. SECOND-ORDER ENERGY

Let us consider the most general derivation of the van der Waals attraction energy between a spherical, nonpolar molecule such as a rare gas atom and any solid which extends from minus to plus infinity in the x and y directions, defining the surface plane, and is semi-infinite in the perpendicular z direction. We shall use straightforward perturbation theory. If the adsorbed molecule is not too large, the perturbation can be written as

$$J=-\boldsymbol{\mu}_1\cdot\mathbf{F}_1, \tag{1}$$

where $\boldsymbol{\mu}_1$ is the instantaneous dipole moment of the molecule and $\mathbf{F}_1$ is the instantaneous electric field produced by all the electrons and nuclei of the solid at the center of molecule 1. The unperturbed Hamiltonian is simply

$$H^0=H_1+H_s, \tag{2}$$

i.e., the sum of the parts describing the molecule and the surface separately. Where overlap is negligible, the system will be represented by

$$\psi_0=\psi_1^0\psi_s^0, \tag{3}$$

i.e., the product of unperturbed wave functions for the molecule and the surface. When (1) is applied as the perturbing potential on (2) and (3), the first-order energy vanishes. But the second-order energy becomes

$$E_{1s}^{(2)}=\sum_{(\rho,\tau)\neq 0}\frac{|\langle 00\,|\,\boldsymbol{\mu}_1\cdot\mathbf{F}_1\,|\,\rho\tau\rangle|^2}{\delta_{0\rho}+\delta_{0\tau}}, \tag{4}$$

[6] J. C. P. Mignolet, Rec. trav. chim. **74**, 701 (1955).
[7] G. Ehrlich and F. G. Hudda, J. Chem. Phys. **30**, 493 (1959).
[8] T. Kihara, *Advances in Chemical Physics* (Interscience Publishers, Inc., New York, 1958), Vol. I, p. 267; Triple-dipole energy was first discussed by B. M. Axilrod and E. Teller, J. Chem. Phys. **11**, 299 (1943); Axilrod, *ibid.* **19**, 719 (1951).
[9] M. J. Sparnaay, Physica **25**, 217 (1959).
[10] L. Jansen and R. T. McGinnies, Phys. Rev. **104**, 961 (1956).
[11] W. L. Bade, J. Chem. Phys. **27**, 1280, 1284 (1957); **28**, 282 (1958).

where ρ, τ refer to the various unperturbed energy states of the molecule and the "surface" (meaning the semi-infinite solid), respectively, and δ's denote the excitation energies to these various states. Now, if we assume that the δ's can be replaced by some "mean excitation energies" and use the relations

$$\sum_{\rho=0}^{\infty} |\langle 0|\mu_1|\rho\rangle|^2 = \langle 0||\mu_1|^2|0\rangle \equiv \langle|\mu_1|^2\rangle_{00}, \quad (5)$$

and

$$\alpha_1 = \alpha_1^{zz} \cong 2(\langle \mu_{1z}^2\rangle_{00}/\delta_1),$$

for a spherical molecule, Eq. (4) becomes

$$E_{1s}^{(2)} \cong -\tfrac{1}{2}\alpha_1 |\langle 0|\mathbf{F}_1|0\rangle|^2 - \tfrac{1}{2}\alpha_1[\delta_1/(\delta_1+\delta_s)]\sum_{\tau\neq 0}^{\infty} |\langle 0|\mathbf{F}_1|\tau\rangle|^2. \quad (7)$$

The first term is simply the electrostatic polarization of the molecule due to a net field $\langle \mathbf{F}_1\rangle_{00}$ over the surface. This field would be zero if the solid were uniform up to its surface, as is roughly the case for an insulator. But on a metal it arises from an effective dipole layer[12] on the surface which may be caused by electron leakage through the surface barrier.[13(a)] (See, however, Mignolet.[13(b)]) The second term corresponds to the usual "dispersion" type of force. The physical meaning of this force becomes clearer if we write

$$\langle|\mathbf{F}_1|^2\rangle \equiv \sum_{\tau\neq 0}^{\infty} |\langle 0|\mathbf{F}_1|\tau\rangle|^2 = \langle|\mathbf{F}_1|^2\rangle_{00} - |\langle \mathbf{F}_1\rangle_{00}|^2 = \langle|\mathbf{F}_1 - \langle \mathbf{F}_1\rangle_{00}|^2\rangle_{00}. \quad (8)$$

Thus the second term of Eq. (7) may be looked upon as arising from the additional polarization of the molecule due to the nonvanishing of the mean square of the fluctuations of the "surface" electric field about its average value. And of course, when the thermal motion of the nuclei in the solid is negligible, these fluctuations are due primarily to the quantum motion of the electrons. In fact, Eq. (8) can be written[14] in terms of first- and second-order density matrices for the electrons after making the Born-Oppenheimer approximation, in a form most useful when the solid is a metal. However we must be cautious with this interpretation of the second term of Eq. (7) due to the presence of the factor $[\delta_1/(\delta_1+\delta_s)]$. If for a metal the free-electron model is adopted and δ_s assumed negligible compared to δ_1, as was done by Prosen and Sachs,[15] this factor is unity making the above interpretation correct, i.e., only the molecule is polarized. However, the presence of a quite large δ_s, as in insulators and real metals, in effect accounts for the polarization of the surface in turn by the molecule.

Now, all the formulas[3,4] that are used for either insulators or metals can be shown to follow directly or indirectly from the general expression Eq. (7). When the surface is an insulator, Eq. (8) can be evaluated by summing (or integrating) the contributions from each molecule or section that makes up the solid considering these as fluctuating dipoles. Then the over-all van der Waals attraction can be obtained directly from one of the formulas[1–4] which give the intermolecular dispersion energy (such as London's and Kirkwood-Müller's) using empirical quantities such as polarizabilities and diamagnetic susceptibilities. Although a metal should be treated in terms of metallic electrons and it seems at first thought that it could not be divided into sections, the consideration of electron correlation[14] has been shown to lead to essentially the same result as though the metal behaved as an insulator made up of sections of oscillating dipoles.[16] With these considerations in mind, an estimate of the total potential between one molecule and the surface (and the heat of adsorption) can be obtained by assuming the usual Lennard-Jones [12–6] potential, frequently used in imperfect gas theory,[17] to hold between a portion of the solid and the molecule, and integrating.[18] The result which we shall need later is

$$U(R) = [3/2(5)^{\frac{1}{2}}]U_0[(r_0/R)^3 - \tfrac{1}{15}(r_0/R)^9],$$
$$U_0 = -[2(5)^{\frac{1}{2}}/9]\pi n\epsilon_0 r_0^3, \quad (9)$$

with R the distance from the molecule to the surface and ϵ_0, r_0 the parameters of the Lennard-Jones [12–6] potential.[17] Notice that at the minimum, R_0, the attractive portion of energy is simply 1.5 times U_0, the heat of adsorption at zero coverage.

The magnitude of the van der Waals attraction between a molecule and a surface can be estimated by the use of the "nonmetallic" or metallic type formulas some of which we have cited above. (These formulas will be mentioned here only by name; the reader is referred to the general references given for details.) Such estimates are usually found to yield values for the heats of adsorption,[4,19] however, which are too low. A similar situation has existed in the comparison of observed and calculated van der Waals attractions between two molecules.[20] Recently, however, in connection with London forces it has been shown[2,21] that the trouble often lies in the δ's, the "mean excitation

[12] W. G. Pollard, Phys. Rev. **61**, 740(A) (1942).
[13] (a) K. Huang and G. Wyllie, Proc. Phys. Soc. (London) **62**, 180 (1949); (b) J. C. P. Mignolet, in *Chemisorption* (Butterworths Scientific Publications, Ltd., London, 1957), p. 181.
[14] J. Bardeen, Phys. Rev. **58**, 727 (1940).
[15] E. J. R. Prosen and R. G. Sachs, Phys. Rev. **61**, 70 (1942).
[16] H. Margenau and W. G. Pollard, Phys. Rev. **60**, 128 (1941).
[17] See for example, Hirschfelder, Curtiss, and Bird, *Molecular Theory of Gases and Liquids* (John Wiley & Sons, Inc., New York, 1954).
[18] T. L. Hill, J. Phys. Chem. **63**, 456 (1959).
[19] R. A. Pierotti and G. D. Halsey, Jr., J. Phys. Chem. **63**, 680 (1959).
[20] K. S. Pitzer, *Quantum Chemistry* (Prentice-Hall, Inc., New York, 1954), p. 339.
[21] W. E. Donath, University of California, Ph.D. thesis (1958) and UCRL-8385 (July 21, 1958).

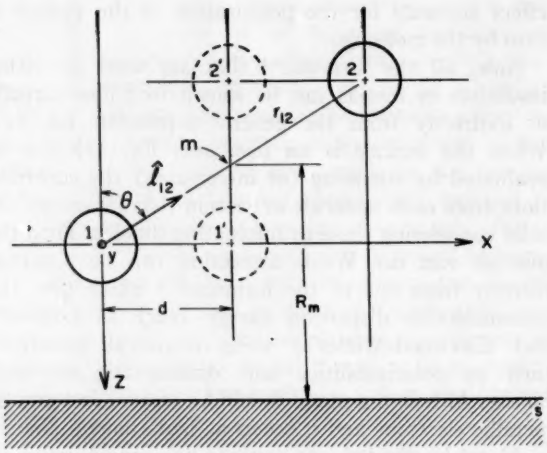

FIG. 1. Coordinates used in the general derivation of $E^{(3)}$.

energies." These also occur in Eq. (7) and in most of the specific formulas mentioned in the foregoing. In adsorption as well as in intermolecular dispersion energies the δ's are usually assumed to be approximately equal to the ionization potentials I. Recent considerations show[2,20,21] that in more than two-electron atoms electron correlation raises the δ by a factor of about 2.1 higher than I. It must be pointed out here that the use of this proper δ (for the molecules and possibly for the solid) will bring the insulator-type adsorption energy formulas such as London's into quite good agreement with experiment. Slater-Kirkwood formula[2,19] involves N, the number of electrons in the outer shell of molecules, instead of δ; here N should be regarded as an empirical parameter and "effective" values used.[2] Kirkwood-Müller formula[2,4,19] does not contain any of these "parameters" and although it is strictly valid for spherical systems,[2] it is still quite successful in adsorption.[19] In the rest of this article, we shall use the appropriate molecular δ's ($2.1I$) instead of I wherever they occur.

The formulas derived from Eq. (7) and Eq. (8) strictly for metals[14,16] also predict heats which are too small.[19] Here the increase in δ_1 has a smaller effect on $E_{1s}^{(2)}$. However, it should be recalled that the δ's appearing as the main feature in both Bardeen's[14] and Margenau's and Pollard's[16] formulas were derived[14] for monovalent metals neglecting the effect of the periodic potential of the lattice and the effect of the polarizability of the ion cores. Thus, such formulas should not be applied to, for instance, transition metals that have incomplete d shells and might show very large "inner core" effects.

The low values predicted for the heats of adsorption by the theories above, in the way that they are often applied, have induced discussion[6] of another type of force, i.e., the charge-transfer[22] force as contributing to van der Waals adsorption on metals. However, in view of the lack of a sufficiently quantitative treatment of these forces in adsorption and considering the preceding discussion, we shall assume that van der Waals attraction of nonpolar molecules to metals as well as to insulators is given primarily by $E_{1s}^{(2)}$ of Eq. (7).

[22] R. S. Mulliken, J. Am. Chem. Soc. **74**, 811 (1952).

C. THIRD-ORDER ENERGY

Now, if instead of a single molecule on the surface several molecules are considered, no new effects arise in the nonoverlap second-order perturbation. The potential energy of the system is simply the sum of London attractions[1] between molecules and their individual van der Waals attractions to the surface as given by Eq. (7). To see the effect of the surface on the long-range interaction between molecules we must turn to the third-order term of the perturbation series. If, as we had done for the second-order term in Eq. (1), we consider the adsorbed molecules to be quite small, and after expanding the instantaneous potential of the molecules in multipole series in the usual fashion,[1] take only the leading dipole terms, the interaction operator between two molecules and the surface becomes

$$J=-\boldsymbol{\mu}_1\cdot\mathbf{F}_1-\boldsymbol{\mu}_2\cdot\mathbf{F}_2+\boldsymbol{\mu}_1\cdot\mathbf{T}_{12}\cdot\boldsymbol{\mu}_2, \tag{10}$$

where again $\mathbf{F}_1$ and $\mathbf{F}_2$ are the instantaneous electric fields produced at the centers of the molecules 1 and 2, respectively, by a given distribution of all the electrons and nuclei that make up the solid. The $\boldsymbol{\mu}$'s are the instantaneous dipole moments of the molecules (here we always mean inert gas atoms or other small quasi-spherical molecules) given by $e\sum_i \bar{r}_i$, i.e., summing the radius vectors of all the electrons of a given atom. The last term of Eq. (10) is the dipole-dipole operator for the interaction between two molecules with the tensor $\mathbf{T}_{12}$ given by

$$\mathbf{T}_{12}=(\mathbf{I}-\mathbf{l}_{12}\mathbf{l}_{12})/r_{12}^3. \tag{11}$$

Here $\mathbf{l}_{12}$ is the unit vector along r_{12}, the distance between the two molecules as shown in Fig. 1.

With the J of Eqs. (10) or (1) the third-order energy becomes[23]

$$E^{(3)}=\sum_{n=0}\sum_{m\neq n,0}\frac{\langle 0\mid J\mid n\rangle\langle n\mid J\mid m\rangle\langle m\mid J\mid 0\rangle}{(E_0-E_n)(E_0-E_m)}. \tag{12}$$

This energy vanishes for one molecule and the surface, i.e., for J given by Eq. (1). If on the other hand, Eq. (10) is substituted into Eq. (12), each matrix element there can be written as a sum of three terms and since the eigenstates of the system are taken in the product form as in Eq. (3) (with each factor forming an ortho-

[23] In general $E^{(3)}$ will have an additional term which is different in different perturbation theories (see: Morse and Feshbach, *Methods of Theoretical Physics* (McGraw-Hill Book Company, Inc., New York, 1953), Vol. II; however, this term vanishes in our case because of the dipole selection rules.

normal set) a typical matrix element is of the form

$$\langle 0 \mid J \mid n\rangle = -\langle 00 \mid \boldsymbol{\mu}_1\cdot\mathbf{F}_1 \mid \rho\tau\rangle\delta_{0\sigma} - \langle 00 \mid \boldsymbol{\mu}_2\cdot\mathbf{F}_2 \mid \sigma\tau\rangle\delta_{0\rho} + (\langle 0 \mid \boldsymbol{\mu}_1 \mid \rho\rangle\cdot\mathbf{T}_{12}\cdot\langle 0 \mid \boldsymbol{\mu}_2 \mid \sigma\rangle)\delta_{0\tau}, \quad (13)$$

where again σ, ρ, τ label the various eigenstates of molecules 1 and 2 and the entire solid (including all the nuclei and electrons that make it up), respectively. [The $\delta_{0\sigma}$, etc. are Kronecker deltas only here and should not be confused with the excitation energies in Eq. (4), Eq. (5), and in the forthcoming equations.] Then, multiplying out such matrix elements in Eq. (12) and using the dipole selection rules for spherical molecules,[24] it can be seen that only certain combinations of transitions giving rise to such terms as

$$\sum_{\tau\neq 0}\sum_{\sigma'\neq 0}\frac{\langle\boldsymbol{\mu}_1\rangle_{0\rho}\cdot\langle\mathbf{F}_1\rangle_{0\tau}\langle\boldsymbol{\mu}_2\rangle_{0\sigma'}\cdot\langle\mathbf{F}_2\rangle_{\tau 0}\langle\boldsymbol{\mu}_1\rangle_{\rho 0}\cdot\mathbf{T}_{12}\cdot\langle\boldsymbol{\mu}_2\rangle_{\sigma' 0}}{[\delta_1(0\rho)+\delta_s(0\tau)][\delta_1(0\rho)+\delta_2(0\sigma')]}, \quad (14)$$

with $\delta_1(0\rho)=E_1{}^{\rho}-E_1{}^{0}$ and similarly δ_s for the surface, contribute to the sum [Eq. (12)]. The derivation follows along quite similar lines to that given by Kihara[8] for three molecules. There are two types of terms designated by transitions such as

$$000\rightarrow\rho 00\rightarrow\rho\sigma' 0\rightarrow 000$$

and

$$\underbrace{000}_{0}\rightarrow\underbrace{0\sigma 0}_{n}\rightarrow\underbrace{\rho'\sigma 0}_{m}\rightarrow\underbrace{000}_{0},$$

in which only the ground state of the solid is involved, and six types of terms corresponding to different double transitions in each matrix element, such as

$$000\rightarrow\rho\sigma 0\rightarrow\rho 0\tau'\rightarrow 000.$$

The numerators of these six are all equivalent [Eq. (14)] but four of the denominators [of the form $(\delta_1+\delta_2)(\delta_1+\delta_s)$] are different from the other two [of the form $(\delta_1+\delta_s)(\delta_2+\delta_s)$]. After using mean excitation energies and polarizabilities for the molecules [Eqs. (5) and (6)] as had been done for $E_{1s}{}^{(2)}$ previously, the result is

$$E_{12s}{}^{(3)}=(\alpha_1{}^2/r_{12}{}^3)[\langle\mathbf{F}_1\rangle_{00}\cdot\langle\mathbf{F}_2\rangle_{00}-3\langle\mathbf{F}_1\rangle_{00}\cdot\mathbf{l}_{12}\mathbf{l}_{12}\cdot\langle\mathbf{F}_2\rangle_{00}] + (\alpha_1{}^2/2r_{12}{}^3)[(2\delta_1+\delta_s)\delta_1/(\delta_1+\delta_s)^2]\sum_{\tau\neq 0}(\langle\mathbf{F}_1\rangle_{0\tau}\cdot\langle\mathbf{F}_2\rangle_{\tau 0} - 3\langle\mathbf{F}_1\cdot\mathbf{l}_{12}\rangle_{0\tau}\langle\mathbf{l}_{12}\cdot\mathbf{F}_2\rangle_{\tau 0}) \quad (15a)$$

or

$$E_{12s}{}^{(3)}\equiv E_{es}{}^{(3)}+E_{fl}{}^{(3)} \quad (15b)$$

where es means electrostatic and fl fluctuation and where for convenience we have assumed molecules 1 and 2 to be identical. In arriving at this result use has been made of relations of the type:

$$\sum_{\rho\neq 0}\langle\boldsymbol{\mu}_1\rangle_{0\rho}\cdot\mathbf{T}'\cdot\langle\boldsymbol{\mu}_1\rangle_{\rho 0}=\sum_{\rho\neq 0}\langle\boldsymbol{\mu}_1\rangle_{0\rho}\langle\boldsymbol{\mu}_1\rangle_{\rho 0}:\mathbf{T}' = \langle\mu_{1z}\rangle_{00}{}^2\mathbf{I}:\mathbf{T}',$$

$$\mathbf{T}'=\langle\mathbf{F}_1\rangle\langle\mathbf{F}_2\rangle\cdot\mathbf{T}_{12}, \quad (17)$$

$$\mathbf{I}:\mathbf{T}'=\mathrm{Trace}\mathbf{T}'=(\langle\mathbf{F}_1\rangle\cdot\langle\mathbf{F}_2\rangle-3\langle\mathbf{F}_2\cdot\mathbf{l}_{12}\rangle\langle\mathbf{F}_1\cdot\mathbf{l}_{12}\rangle)/r_{12}{}^3,$$

and τ in Eq. (15) still refers to an eigenstate of the semi-infinite solid as a whole.

The meaning of Eq. (15) is similar to that of Eq. (7) discussed previously. Again the first part, $E_{es}{}^{(3)}$, exists only when the surface possesses a net average electrostatic field $\langle\mathbf{F}\rangle_{00}$ and within the approximation of Eq. (6), i.e., the substitution of atomic polarizability into Eq. (16), it is the same as the classical interaction between two permanently induced dipoles and already has been considered by de Boer.[3] The second part $E_{fl}{}^{(3)}$, involving the sum

$$\langle\mathbf{F}_1\cdot\mathbf{F}_2-3\mathbf{F}_1\cdot\mathbf{l}_{12}\mathbf{l}_{12}\cdot\mathbf{F}_2\rangle_{\tau}\equiv\sum_{\tau\neq 0}(\langle\mathbf{F}_1\rangle_{0\tau}\cdot\langle\mathbf{F}_2\rangle_{\tau 0} - 3\langle\mathbf{F}_1\cdot\mathbf{l}_{12}\rangle_{0\tau}\langle\mathbf{l}_{12}\cdot\mathbf{F}_2\rangle_{\tau 0}$$

$$=(\langle\mathbf{F}_1\cdot\mathbf{F}_2\rangle_{00}-3\langle\mathbf{F}_1\cdot\mathbf{l}_{12}\mathbf{l}_{12}\cdot\mathbf{F}_2\rangle_{00}) - (\langle\mathbf{F}_1\rangle_{00}\cdot\langle\mathbf{F}_2\rangle_{00}-3\langle\mathbf{F}_1\rangle_{00}\cdot\mathbf{l}_{12}\mathbf{l}_{12}\cdot\langle\mathbf{F}_2\rangle_{00}) \quad (18)$$

is again of the dispersion or fluctuation type. When δ_s is small, it represents the interaction resulting from the additional simultaneous polarization of the molecules by the in phase fluctuations of the surface fields at the points 1 and 2. In fact, Eq. (18) can be simply regarded as the "correlation coefficient" of $\mathbf{F}_1$ and $\mathbf{F}_2$ in the sense of elementary statistics.

The electrostatic or average fields in Eq. (15) must be in the z direction (see Fig. 1) whenever they exist, on account of the symmetry in the xy plane, so that the electrostatic energy in Eq. (15a) is given by

$$E_{es}{}^{(3)}=(\alpha_1{}^2/r_{12}{}^3)\langle F_1{}^z\rangle_{00}\langle F_2{}^z\rangle_{00}(1-3\cos^2\theta), \quad (19)$$

and similarly we have from Eq. (7)

$$E_{es}{}^{(2)}=-\tfrac{1}{2}\alpha_1\langle F_1{}^z\rangle_{00}{}^2. \quad (20)$$

When one of these energies is known the other is obtainable by the appropriate elimination of $\langle F^z\rangle$'s.[3]

On insulators Eq. (19) and (20) are usually unimportant[3] and fluctuation energies constitute the primary effects. On metal and charcoal surfaces both es and fl energies must be taken into account. The discussion of $E^{(3)}$ and $E^{(2)}$ in relation to one another when es terms are not negligible will be deferred until the end of this section, i.e., until after a detailed derivation of what we have called the fluctuation energy between adsorbed molecules, to which we now turn.

[24] Landau and Liftschitz, *Non-Relativistic Quantum Mechanics* (Addison-Wesley Publishing Company, Inc., Reading, Massachusetts, 1958).

The fluctuation parts of Eqs. (7) and (15a) are given by

$$E_{fl}^{(2)}=-\tfrac{1}{2}\alpha_1[\delta_1/(\delta_1+\delta_s)]\langle\,|\,\mathbf{F}_1\,|^2\rangle_\tau, \quad (21a)$$

$$\langle\,|\,\mathbf{F}_1\,|^2\rangle_\tau=\langle(F_1^z)^2\rangle_\tau+2\langle(F_1^x)^2\rangle_\tau, \quad (21b)$$

and

$$E_{fl}^{(3)}=(\alpha_1^2/r_{12}^3)[\delta_1(2\delta_1+\delta_s)/2(\delta_1+\delta_s)^2][\langle\mathbf{F}_1\cdot\mathbf{F}_2\rangle_\tau - 3\langle\mathbf{F}_1\cdot\mathbf{l}_{12}\mathbf{l}_{12}\cdot\mathbf{F}_2\rangle_\tau], \quad (22)$$

where the summations over the eigenstates of the solid not including the $\tau=0$ ground state have been indicated by $\langle\ \ \rangle_\tau$. Eq. (21b) follows from the equivalence of the x and y coordinates over the surface.

In terms of the coordinates shown in Fig. 1, Eq. (22) becomes

$$E_{fl}^{(3)}=(\alpha_1^2/r_{12}^3)[\delta_1(2\delta_1+\delta_s)/2(\delta_1+\delta_s)^2][\langle F_1^xF_2^x\rangle_\tau \cdot(1-3\sin^2\theta)+\langle F_1^yF_2^y\rangle_\tau+\langle F_1^zF_2^z\rangle_\tau(1-3\cos^2\theta) - 3\sin\theta\cos\theta\langle F_1^xF_2^z+F_1^zF_2^x\rangle_\tau], \quad (23)$$

θ denoting the angle between $\mathbf{l}_{12}$ and the normal to the surface. The coordinate axes have been so chosen that z is along the normal and the xz plane contains $\mathbf{l}_{12}$ (Fig. 1). Notice also that, e.g., $\langle F_1^zF_2^z\rangle_\tau$ is identical with $\langle F_1^zF_2^z\rangle_{00}$ i.e., the expectation value over the ground state of the solid, because $\langle F_1^x\rangle_{00}$ is zero [see Eqs. (8) and (18)]. Equation (23) can be simplified considerably by noting that $\langle F_1^zF_2^z\rangle_{00}$ and $\langle F_1^zF_2^x\rangle_{00}$ vanish because F^z is an odd function in all the x coordinates involved (i.e., all electrons and nuclei of the solid). In addition the matrix elements, $\langle F_1^xF_2^x\rangle_\tau$, $\cdots$, can be replaced to a good approximation by the corresponding quantities $\langle F_{1'}^xF_{2'}^x\rangle_\tau$, $\cdots$ (Fig. 1); i.e., the points 1 and 2 can be brought on top of one another along the normal to the surface passing through the midpoint m of r_{12}. This approximation can be partly justified in the following manner.

Since the states of the solid, $\psi_0, \psi_\tau\cdots$, form an orthonormal set, we have, as in Eq. (18),

$$\langle F_1^zF_2^z\rangle_\tau=\sum_{\tau\neq0}^{\infty}\langle F_1^z\rangle_{0\tau}\langle F_2^z\rangle_{\tau0}, \quad (24)$$

and similarly for x and y. Now because of translational symmetry the over-all eigenstates describing the solid must be of generalized Bloch function form; i.e.,

$$\psi_\tau=[\exp(i\mathbf{k}_\tau\cdot\mathbf{R})]u_\tau(\mathbf{R}), \quad (25)$$

where $\mathbf{R}$ denotes the coordinates of *all* the electrons and nuclei, $\mathbf{k}_\tau$ is a generalized wave vector and u_τ a periodic function of $\mathbf{R}$ depending on the symmetry of the solid (In the xy plane) Thus the matrix elements such as $\langle F_1^z\rangle_{0\tau}$ will be of the form

$$\langle F_1^z\rangle_{0\tau}=\int\exp(i\mathbf{k}_\tau'\cdot\mathbf{R})F_1^zu_0^*u_\tau d\mathbf{R}. \quad (26)$$

Here F_1^z is the sum of the instantaneous electric fields of all the electrons and nuclei in the solid, and these electrons and nuclei may be assumed to be quite uniformly distributed at *all* instances. This assumption allows us to consider $\mathbf{F}_1$ as a nearly periodic operator in the sense that if all the electrons and nuclei were to be translated by a lattice constant in the x or y directions, it would remain quite unchanged. In this case, according to group theory, only those matrix elements [Eq. (26)] for which the $\mathbf{k}_\tau'(x, y)$ equals zero would be nonvanishing.[25,26] Even though this selection rule is not rigorously applicable here because $\mathbf{F}_1$ is not really a "periodic" operator, nevertheless it suggests that the greatest contribution to Eq. (24) will come from excitations for which the generalized wave vector $\mathbf{k}(x, y)$ in the xy plane is approximately unchanged. It is interesting to note that even when the crude free-electron approximation is made when the solid is a metal, a similar conclusion can be shown[15] to follow; in this case where the assumption of the periodicity of $\mathbf{F}_1$ cannot be made at all, Eq. (26) reduces to a single electron matrix element involving ordinary one-electron Bloch functions. Nevertheless it is found[15] that even these matrix elements have appreciable values only when the changes in the wavelength (in the xy plane) of an electron are small compared with the reciprocal of a distance of the order of a lattice constant. [See Eq. (14) of reference 15].

If then, it is further assumed that d (Fig. 1) is either much smaller than or approximately equal to a lattice constant of the "surface," the origin of the coordinates for the wave functions in Eq. (26) can be shifted from 1 and 2 to 1′ or 2′, respectively, and in view of the translational properties just discussed, one gets

$$\langle F_1^xF_2^x\rangle_\tau=\sum_{\tau\neq0}^{\infty}\langle F_1^x\rangle_{0\tau}\langle F_2^x\rangle_{\tau0}\cong\sum_{\tau\neq0}^{\infty}\langle F_{1'}^x\rangle_{0\tau}\langle F_{2'}^x\rangle_{\tau0} = \langle F_{1'}^xF_{2'}^x\rangle_\tau \quad (27)$$

and similarly for y and z. Eq. (27) makes the x and y matrix elements in Eq. (23) equivalent and hence

$$E_{fl}^{(3)}\approx(\alpha_1^2/r_{12}^3)[\delta_1(2\delta_1+\delta_s)/2(\delta_1+\delta_s)^2][\langle F_{1'}^zF_{2'}^z\rangle_\tau - \langle F_{1'}^xF_{2'}^x\rangle_\tau](1-3\cos^2\theta). \quad (28)$$

When the two molecules are the same distances from the surface ($\theta=90°$), the points 1′ and 2′ coincide with m the midpoint of r_{12} and we already have $\langle F_{1'}^zF_{2'}^z\rangle_\tau$ and $\langle F_{1'}^xF_{2'}^x\rangle_\tau$ going over into $\langle(F_m^z)^2\rangle_\tau$ and $\langle(F_m^x)^2\rangle_\tau$, which are the same matrix elements appearing in $E_{fl}^{(2)}$. [Eq. (21)]. On the other hand when θ differs from 90° so that 1′ and 2′ are above and below m, by writing

$$\langle\mathbf{F}_{1'}\cdot\mathbf{F}_{2'}\rangle_\tau\sim\langle\,|\,\mathbf{F}_m\,|^2\rangle_\tau \quad (29)$$

---

[25] N. F. Mott and H. Jones, *The Theory of the Properties of Metals and Alloys* (reprinted by Dover Publishers, Inc., New York, 1936), p. 59.

[26] M. Tinkham, *Advanced Quantum Mechanics of Atoms, Molecules, and Solids* (A. S. U. C. Store, University of California, Berkeley, 1958), p. 94.

we might be expected to provide a reasonable approximation. Actually somewhat later we shall give another quite different derivation of $E_{fl}^{(3)}$ which will show among other assumptions made in the foregoing, the validity of Eq. (29).

It is, by this time, apparent that Eqs. (28) and (29) would permit the replacement of the matrix elements in $E_{fl}^{(3)}$ in terms of $E_{fl}^{(2)}$ (which might eventually be viewed as an empirical quantity) provided a simple relation can be found among the various components of $\langle|\mathbf{F}|^2\rangle_\tau$. Fortunately such a relation does indeed exist. The same proportionality constant between $\langle(F^x)^2\rangle_\tau$ and $\langle(F^z)^2\rangle_\tau$ is obtained upon an examination of two very different models of a solid and the result is perhaps perfectly general. First, it has been shown[15] that in the nondegenerate or degenerate free-electron gas model of a metal,

$$\langle(F^x)^2\rangle_\tau=\langle(F^y)^2\rangle_\tau=\tfrac{1}{2}\langle(F^z)^2\rangle_\tau. \tag{30}$$

Secondly, if we consider an insulator or a metal (Margenau-Pollard[16] model) as made up of fluctuating-dipole sections (in the sense of dispersion forces) then $\langle(\mathbf{F}^x)^2\rangle_{00}$ etc. can be calculated from

$$\langle|\mathbf{F}_m|^2\rangle_{00}\cong\int\langle|\mathbf{F}_{m\omega}|^2\rangle_{00}d\omega, \tag{31}$$

where $d\omega$ refers to an infinitesimal volume element in the solid and $\langle|\mathbf{F}_{m\omega}|^2\rangle_{00}$ is the expectation value of the square of the field produced at m by the section $d\omega$. By using

$$\mathbf{F}_{m\omega}=-\mathbf{T}_{m\omega}\cdot\boldsymbol{\mu}_\omega, \tag{32}$$

where $\mathbf{T}_{m\omega}$ and $r_{m\omega}$ are analogous to $\mathbf{T}_{12}$ and r_{12} of Eq. (11) we find for the components

$$\langle(F_{m\omega}^x)^2\rangle_{00}=[\langle(\mu_\omega^x)^2\rangle_{00}/r_{m\omega}^6][1+3(l_{\omega m}^x)^2], \tag{33}$$

and similarly for y and z, $l_{\omega m}^x$ being the x component of the unit vector in the direction from ω to m. Equation (31) can be integrated separately for each component; e.g.,

$$\langle(F_m^x)^2\rangle_{00}\cong\langle(\mu_x)^2\rangle_{00}\int_{R_m}^{\infty}\int_{-\infty}^{\infty}\int_{-\infty}^{\infty}[(1+3x^2/r^2)/r^6]dxdydz; \tag{34}$$

and $\langle(\mu_x)^2\rangle_{00}$ is related to the polarizability of the solid per unit volume [Eqs. (5), (6)]. Equations (33) and (34) again lead to exactly the same result as Eq. (30) after performing the elementary integrations. Thus we take Eq. (30) as a sufficiently general result.

Finally, combining Eqs. (21), (22), and (28)–(30), we have an approximate relation between $E_{fl}^{(3)}$ and $E_{fl}^{(2)}$ analogous to the relation between the es energies in Eqs. (19) and (20):

$$E_{fl}^{(3)}\cong(\alpha_1/r_{12}^3)\Delta_0\,|\,E_{fl}^{(2)}(R_m)\,|\,\tfrac{1}{4}(1-3\cos^2\theta), \tag{35}$$

where

$$\Delta_0=(2\delta_1+\delta_s)/(\delta_1+\delta_s),$$

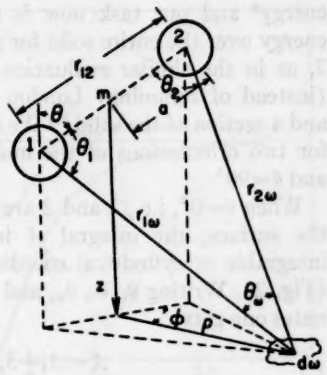

FIG. 2. Derivation of $E^{(3)}$ by integration.

and $E_{fl}^{(2)}(R_m)$ usually[3,4,14,16] is of the form

$$E_{fl}^{(2)}=-K_f/R_m^3, \tag{36}$$

with K_f a constant (to be determined empirically when $E_{es}^{(2)}\sim0$, or from the theories discussed in Sec. B) and R_m the distance from m to the surface.

The derivation presented has the advantage of being general and independent of the nature of the solid. Everything that would specifically involve the solid has been taken care of by $E_{fl}^{(2)}$ which of course may be viewed if necessary as an experimental quantity. However a crucial assumption has been made in Eq. (27) depending on the uniformity of electron and nuclear distribution at *all* times, an assumption which seems reasonable intuitively but cannot be fully justified. We shall give another derivation of $E_{fl}^{(3)}$, however, which is quite independent of the first one, yet leads essentially to the same results as Eq. (35).

The matrix elements of the electric fields appearing in Eq. (22) can be evaluated directly if a specific model is adopted for the solid. This evaluation would be possible, for instance, for the free-electron model of a metal[15]; however this model is not suitable because van der Waals interactions are very strongly influenced by electron correlation.[2,14,21] The oscillating-dipoles model which we have already discussed is a valid one for insulators and even for metals.[16] To evaluate $E_{fl}^{(3)}$ for this model we again consider the solid to consist of small elementary portions $d\omega$ and write as in Eq. (31)

$$\langle\mathbf{F}_1\cdot\mathbf{F}_2\rangle_\tau-3\langle\mathbf{F}_1\cdot\mathbf{l}_{12}\mathbf{l}_{12}\cdot\mathbf{F}_2\rangle_\tau$$
$$\cong\int[\langle\mathbf{F}_{1\omega}\cdot\mathbf{F}_{2\omega}\rangle_{00}-3\langle\mathbf{F}_{1\omega}\cdot\mathbf{l}_{12}\mathbf{l}_{12}\cdot\mathbf{F}_{2\omega}\rangle_{00}]d\omega, \tag{37}$$

where $\mathbf{F}_{1\omega}$ and $\mathbf{F}_{2\omega}$ are the fields due to the section $d\omega$ at the points 1 and 2. After substituting Eq. (32) and some manipulation the integral in Eq. (37) becomes

$$3\langle(\mu_\omega^x)^2\rangle_{00}\int\frac{(3\cos\theta_1\cos\theta_2\cos\theta_\omega+1)d\omega}{r_{1\omega}^3r_{2\omega}^3} \tag{38}$$

in terms of the angles and distances defining the triangle 12ω as shown in Fig. 2. Of course the integrand is just the expression that appears in the triple-dipole

energy[8] and our task now is the integration of this energy over the entire solid for given positions of 1 and 2, as in the similar evaluation of $E^{(2)}$ by integrating (instead of summing) London forces between 1, say, and a section of the solid.[3,4] We shall integrate Eq. (38) for two orientations of the molecules only, i.e., $\theta=0°$ and $\theta=90°$.

When $\theta=0°$, i.e., 1 and 2 are on the same normal to the surface, the integral A in Eq. (38) is exactly integrable in cylindrical coordinates with origin at m (Fig. 2). Writing θ_1, θ_2, θ_ω, and $r_{1\omega}$, $r_{2\omega}$ in these coordinates one gets

$$A=A_1+3A_c \tag{39}$$

where

$$A_1=\int\frac{dV}{r_{1\omega}{}^3r_{2\omega}{}^3}=2\pi\int_{R_m}^{\infty}\int_0^{\infty}\frac{\rho d\rho dz}{[b^4-4a^2z^2]^{\frac{3}{2}}},$$

$$A_c=\int\frac{\cos\theta_1\cos\theta_2\cos\theta_\omega dV}{r_{1\omega}{}^3r_{2\omega}{}^3}$$

$$=-2\pi\int_{R_m}^{\infty}\int_0^{\infty}\frac{(z^2-a^2)(z^2-a^2+\rho^2)\rho d\rho dz}{[b^4-4a^2z^2]^{5/2}},$$

and $b^2\equiv z^2+\rho^2+a^2$.

The result is

$$A(\theta=0°)=-\pi/6R_m{}^3. \tag{40}$$

On the other hand, when $\theta=90°$, i.e., when 1 and 2 are in the same monolayer, the integration is somewhat more involved owing to the appearance of $\cos\phi$ in the denominators of

$$A_1=\int\frac{dV}{b^6(1-k^2\cos^2\phi)^{\frac{3}{2}}},$$

and

$$A_c=\int\frac{a^2(1-2a^2/b^2)(1-\rho^2\cos^2\phi/a^2)dV}{b^8(1-k^2\cos^2\phi)^{5/2}},$$

$$(k^2\equiv 4a^2\rho^2/b^4). \tag{41}$$

Nevertheless, by expanding these denominators in binomial series and keeping 3–4 terms, A is obtained to about one percent accuracy:

$$A(\theta=90°)\cong(0.34\pi/R_m{}^3)f(a, R_m),$$

$$f(a, R_m)=\{[(2R_m{}^2-a^2)/3(R_m{}^2+a^2)]$$

$$+0.320[a^2R_m{}^4/(R_m{}^2+a^2)^3]-0.422[R_m{}^4/(R_m{}^2+a^2)^2]$$

$$+(a^2/5R_m{}^2)-(a^4/7R_m{}^4)+(a^6/9R_m{}^6)-\cdots\}, \tag{42}$$

where the arctan resulting from the final z integration has also been expanded in a power series of (a/R_m).

The connection between these and the result of the former derivation, Eq. (35), becomes apparent when we substitute the troublesome quantity $\langle(\mu_\omega{}^x)^2\rangle_{00}$, related to the polarizability of the metal, in Eq. (38) from $E^{(2)}$ based on the same model[16] [see Eq. (34)]. One obtains

$$E_{\mathrm{fl}}{}^{(3)}(\theta=0°)=-(\alpha_1/2r_{12}{}^3)\Delta_0(K_t/R_m{}^3) \tag{43a}$$

and

$$E_{\mathrm{fl}}{}^{(3)}(\theta=90°)\cong(\alpha_1/r_{12}{}^3)\Delta_0(K_t/R_m{}^3)f(a, R_m). \tag{43b}$$

Equation (43a) is exactly the same as Eq. (35) provided a $R_m{}^{-3}$ law is assumed for $E_{\mathrm{fl}}{}^{(2)}(R_m)$, and this result lends additional support to the assumption of Eq. (29) that had been made in the previous derivation. On the other hand, Eq. (43b) would also be the same as Eq. (35) if $f(a, R_m)$ of the former were to equal the factor of $\frac{1}{4}$ in the latter. An examination of the Eq. (42) reveals that $f(a, R_m)$ is a very slowly varying function of both a and R_m, and its value remains within about $\pm 15\%$ of 0.25 over the relevant ranges of these variables.

The previous derivation of Eq. (35) had been quite independent of the nature of the solid, and, for instance, the **F**'s are not restricted to dipole fields as in the second derivation. Yet, when the proper (e.g., empirical when $\langle\mathbf{F}\rangle_{00}\sim 0$) $E^{(2)}$'s are used in both, the two derivations lead essentially to the same result (at least for the interesting cases, $\theta=0°$ and $\theta=90°$, examined). This is not surprising, however, since any differences that would have arisen between the results of the two derivations as a consequence of the specific model used in the second, are largely cancelled in the elimination of $\langle(\mu_\omega{}^x)^2\rangle_{00}$ which is common to both $E_{\mathrm{fl}}{}^{(2)}$ and $E_{\mathrm{fl}}{}^{(3)}$.

$E_{\mathrm{es}}{}^{(3)}$ and $E_{\mathrm{fl}}{}^{(3)}$ in Eqs. (19) and (35) have the same dependence on θ and r_{12} and can be combined together giving the total surface intermolecular potential $E_{12s}{}^{(3)}$,

$$E_{12s}{}^{(3)}\cong(\alpha_1/r_{12}{}^3)(1-3\cos^2\theta)\{\alpha_1\langle F_m{}^z\rangle_{00}{}^2$$

$$+\tfrac{1}{4}\Delta_0\,|\,E_{\mathrm{fl}}{}^{(2)}(R_m)\,|\,\}. \tag{44}$$

The electrostatic or average field $\langle F^z\rangle_{00}$ is independent of the x, y coordinates on the surface and we have also made the approximation

$$\langle F_1{}^z\rangle_{00}\langle F_2{}^z\rangle_{00}\approx\langle F_m{}^z\rangle_{00}{}^2 \tag{45}$$

and used the average field at m. The total $E_{12s}{}^{(3)}$ cannot be related to the total $E_{1s}{}^{(2)}$, because the relative importance of the es terms are quite different in each case. Nevertheless Eq. (44) can be put into a very useful form after substituting for $\langle F_m{}^z\rangle_{00}$ from Eq. (20),

$$E_{12s}{}^{(3)}\cong(\alpha_1/r_{12}{}^3)(1-3\cos^2\theta)\,|\,E_{1s}{}^{(2)}(R_m)\,|$$

$$\times[(\Delta_0+\gamma_m\Delta_1)/4], \tag{46}$$

where

$$\Delta_1\equiv[(6\delta_1+7\delta_s)/(\delta_1+\delta_s)],$$

and we have defined the parameter

$$\gamma_m\equiv E_{\mathrm{es}}{}^{(2)}(R_m)/E_{1s}{}^{(2)}(R_m)$$

$$=E_{\mathrm{es}}{}^{(2)}/(E_{\mathrm{es}}{}^{(2)}+E_{\mathrm{fl}}{}^{(2)}), \tag{47}$$

i.e., the electrostatic fraction of the *total* van der Waals attraction of a molecule at m to the surface. Here γ_m is not a constant but depends on R_m, because $E_{fl}^{(2)}$ varies in general[3,4] as R_m^{-3}, whereas $E_{es}^{(2)}$ falls off exponentially.[13] However if we are interested in the behavior of molecules strictly in a monolayer, then we find a simple proportionality between $E^{(3)}$ and $E^{(2)}$. In general the range of R_m that is important for $E^{(3)}$ is not very large so that we might replace γ_m by an average $\bar{\gamma}$ either over the whole range or at least up to a certain R_m^0 and then assume $\gamma_m=0$ for $R_m>R_m^0$.

If a Lennard-Jones (12–6) potential had been assumed between two molecules (e.g., in inert gases), when the molecules are adsorbed on a surface the new intermolecular potential is modified and now becomes

$$\epsilon'(r_{12})=\epsilon_0[(r_0/r_{12})^{12}-2(r_0/r_{12})^6]+[S(R_m)/r_{12}^3](1-3\cos^2\theta), \quad (48)$$

provided the original r_{12}^{-12} repulsion has not been altered appreciably by the surface. Here ϵ_0 and r_0 are unchanged and are the gas phase parameters[17]; $S(R_m)$ includes both the es and fl contributions [Eq. (46)]. When more than two molecules are considered on the surface, the total potential energy of interaction *between* the molecules themselves will be obtained by summing ϵ_{12}' over all pairs. In other words, the *intermolecular* energy is still "pairwise additive" to the same extent as the gas phase Lennard-Jones potential. Bade[11] has found that for a system of molecules the third-order energy is triplewise additive. With a system of molecules and the surface the only additional triplets that we haven't included in $E^{(3)}$ is the triple-dipole energy[8] of three adsorbed molecules and this of course is the same as in the gas phase. Then, pairwise additivity of $\epsilon'(r_{12})$, Eq. (48), to the same extent as the Lennard-Jones (12–6)$\epsilon(r_{12})$ follows. An estimate of the contribution of higher order perturbations to $\epsilon'(r_{12})$ can also be obtained from the work of Bade[11] with reference to the model we have used in the second derivation of $E^{(3)}$. Replacing summation over the solid by integration as in Eq. (37) the effect of higher order perturbations on ϵ_{12}' can be shown to be negligible. This is to be expected since the higher terms involve higher inverse powers of the distances.

The full use of Eqs. (46)–(48) in conjunction with experimental data and relative magnitudes of $E_{fl}^{(3)}$ and $E_{es}^{(3)}$ will be discussed in the next section.

D. APPLICATIONS AND MAGNITUDES

$E^{(3)}$ as given by Eq. (46) can be obtained most directly when the electrostatic effects are quite unimportant as on most insulators.[3] One only has to substitute for $E_{1s}^{(2)}$. Especially in a monolayer the repulsion between two atoms can be estimated simply by using $1.5U_0$ for $E_{1s}^{(2)}$, [Eq. (9)], if we assume the atoms to be restricted to their minimum energy distances (R_0) from the surface and behave like a two-dimensional gas; then one does not need an estimate of this distance $R_m=R_0$ but only U_0, the energy of adsorption at zero coverage.

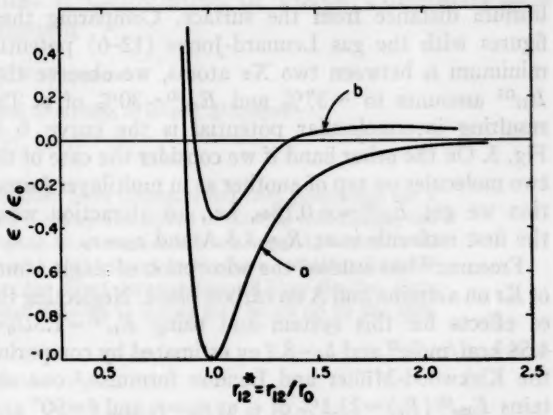

FIG. 3. Potential energy of interaction between two Xe atoms; curve a, Lennard-Jones (12–6) potential in the gas phase; curve b, Lennard-Jones (12–6) plus the third-order repulsion between two Xe atoms in a monolayer on tungsten. Both atoms are the same distance R_0, from the surface.

The most straightforward application of Eq. (46) is in connection with the virial coefficients treatment of physical adsorption.[5] There, $E_{1s}^{(2)}$ can be obtained without the complications of nonzero coverage from B_{1s}, the "second-surface virial coefficient" involving a single molecule and the surface.[5] When $\bar{\gamma}$ is not negligible, the total $E^{(2)}$ might be approximated by a general R_m^{-n} law and its parameters obtained from a best fit to B_{1s} data. Similarly $E_{12s}^{(3)}$ is related to C_{12s}, the two-molecule-surface virial coefficient.[5b] A combination of B_{1s} and C_{12s} would enable one to get an estimate of an average $\bar{\gamma}$. Notice that although in general it is difficult to estimate a reliable value for δ_s, the surface mean excitation energy, its appearance in Δ_0 and Δ_1 of Eq. (46) is not critical. Because Δ_0 varies only from unity to two, and Δ_1 from six to seven as (δ_s/δ_1) ranges from infinity to zero. In general Δ_0 will lie close to 1.5 and Δ_1 to 6.5.

A few applications with actual data will serve to demonstrate the use of some of these ideas and at the same time show the relative magnitudes of $E_{fl}^{(3)}$ and $E_{es}^{(3)}$.

Ehrlich and Hudda[7] have estimated the heat of desorption of Xe on tungsten to be about 8 kcal/mole and $E_{es}^{(2)}\sim 1.6$ kcal/mole. If we neglect any effects of nonzero coverage and assume that (8–1.6) = 6.4 kcal/mole represents the energy minimum U_0 of a Lennard-Jones (9–3) potential, then $E_{fl}^{(2)}(R_0)\sim 9.6$ kcal/mole.

The same value is obtained from Kirkwood-Müller formula[2,4] at $R_m=3.1$ A, so that this estimate is reasonable. Taking δ_s very roughly as twice the ionization potential I of tungsten atom (see Sec. B about δ_1's), $\Delta_0\sim 1.59$. With these values one gets $E_{fl}^{(3)}\sim 0.163$ kcal/mole and $E_{es}^{(3)}\sim 0.133$ kcal/mole, at $r_{12}=r_0$ and when $\theta=90°$ and the two molecules are at their equi-

librium distance from the surface. Comparing these figures with the gas Lennard-Jones (12–6) potential minimum ϵ_0 between two Xe atoms, we observe that $E_{fl}^{(3)}$ amounts to $\sim 37\%$ and $E_{es}^{(3)} \sim 30\%$ of ϵ_0. The resulting intermolecular potential is the curve b in Fig. 3. On the other hand if we consider the case of the two molecules on top of another as in multilayer formation we get $E_{fl}^{(3)} \sim -0.18\epsilon_0$, i.e., an attraction when the first molecule is at $R_1 \sim 3.5$ A and $r_{12}=r_0$.

Freeman[27] has studied the adsorption of single atoms of Kr on alumina and A on carbon black. Neglecting the es effects for this system and using $E_{1s}^{(2)}=1.5U_0=4.58$ kcal/mole[27] and $\delta_s \sim 8.2$ ev estimated by comparing the Kirkwood-Müller and London formulas,[2] one obtains $E_{12s}^{(3)}(R_0) \sim 23.1\%$ of ϵ_0 at $r_{12}=r_0$ and $\theta=90°$ and about -10% ϵ_0 attraction when $\theta=0°$.

Of course very often it is also possible to estimate $E^{(3)}$ using a calculated value of $E_{fl}^{(2)}$, e.g., from Kirkwood-Müller's formula. For instance, the attraction of Kr to tungsten, $E_{fl}^{(2)}$, is found to be ~ 6.9 kcal/mole at a distance of $R_0 \sim 3$ A by this formula. This leads to 0.32 ϵ_0 repulsion in the monolayer at $r_{12}=r_0$. (The Lennard-Jones parameters ϵ_0, r_0 in the above calculations as well as I's have been taken from reference 20, p. 339).

Finally the estimation of $\bar{\gamma}$ from data can be demonstrated on the system: A and carbon black. At the distance of minimum energy R_0 one has

$$E_{fl}^{(2)} \sim 1.5U_0(1-\gamma)/[1+(\gamma/2)] \qquad (49)$$

if it is assumed that a Lennard-Jones (9–3) potential has been fitted only to $E_{fl}^{(2)}$ excluding $E_{es}^{(2)}$. We take $\delta_s \sim 2I=22.4$ ev and from Freeman[27] $1.5U_0=5.8$ kcal/mole. Then for a *total* repulsion, $E_{12s}^{(3)}$ between two A atoms in a monolayer that would amount to about 70% of ϵ_0 at $r_{12}=r_0$, as in the Xe–W case, one would get $\bar{\gamma} \sim 38\%$. This number compares favorably with $\bar{\gamma} \sim 30\%$ that one gets from Eq. (49) after calculating $E_{fl}^{(2)}$ from Kirkwood-Müller's formula at $R_0=2.94$ A.[27]

The results presented above might be summarized by stating that the third-order perturbation introduces, aside from the "electrostatic" effect, a repulsion between the molecules in a monolayer which amounts to about 20–40% of their gas phase potential minimum, ϵ_0(at $r_{12}=r_0$). The same third-order fluctuation energy gives rise to an attraction, if two molecules lie on top of one another, which might be about 10–20% of ϵ_0. This attraction is among the factors contributing to the formation of multilayers (multimolecular adsorption).

It is well known that with a relatively dense adsorbate resembling a liquid only a small amount of additional attraction above and beyond the heat of liquefaction of the adsorbate is needed to provide for the formation of multilayers.[3] Although the greater portion of this energy is provided by the ordinary van der Waals field of the surface,[28] i.e., by $E_{fl}^{(2)}$, (es effects decreasing exponentially from the surface, might be negligible in the additional layers) $E_{fl}^{(3)}$ as discussed above is also a contributing factor; in the Xe–W example with only two molecules on the surface $E_{12s}^{(3)}$ amounts to roughly ten percent of the $E_{fl}^{(2)}$ acting on the top molecule at $R_2 \sim 8$ A.

ACKNOWLEDGMENT

We are indebted to Dr. Mark P. Freeman who attracted our attention to this problem.

This research was performed under the auspices of the U. S. Atomic Energy Commission.

[27] M. P. Freeman, J. Phys. Chem. **62**, 723 (1958).

[28] T. L. Hill, Advances in Catalysis **4**, 236 (1952); G. D. Halsey, *op. cit.*, p. 265.

Transferability of Urey-Bradley Force Constants. I. Calculation of Force Constants on a Digital Computer

JOHN OVEREND AND J. R. SCHERER

Spectroscopy Laboratory, The Dow Chemical Company, Midland, Michigan

(Received July 22, 1959)

An algorithm for the systematic calculation of Urey-Bradley force constants has been programed for a digital computer (the Datatron 204). The secular equation is set up and solved in internal coordinates, the potential energy being transformed from Urey-Bradley space to internal-coordinate space by a matrix **Z**. This same matrix is also used to transform the Jacobian of λ with respect to the force constants from internal-coordinate to Urey-Bradley space, thereby allowing the direct determination of Urey-Bradley force constants. A method is described whereby the **Z** matrix and Wilson's **G** matrix may be set up by the computer from the geometrical parameters of the molecule.

INTRODUCTION

FOR many years the interpretation of vibrational spectra has followed two distinct paths. On the one hand spectra of thousands of compounds have been measured and cataloged and empirical correlations have been drawn between the observed frequencies and the molecular structures.[1] but relatively few of these spectra have, on the other hand, been subject to the detailed vibrational analysis which yields potential constants and normal coordinates. There appear to be two reasons for this state of affairs.

First, the amount of computation involved in a force-constant calculation is well known to anyone with experience in the field, and this has in the past been a major factor determining the type of molecule studied—those with few atoms and a high degree of symmetry have enjoyed considerable popularity. Now that high-speed digital computers are becoming increasingly available the computational burden becomes less onerous and the way is opened to vibrational analyses of many larger molecules of greater chemical interest. Thus, with suitably programed computer, it should be possible to extract more information from the present compilation of spectroscopic data and to make further systematic correlations between the force constants and the molecular parameters.

However before proceeding, we must consider the second limitation which militates against force-constant calculations for large molecules, viz., the number of force constants in a realistic potential function usually exceeds the number of vibrational frequencies from which the former must be determined. In certain cases frequency data have been supplemented by rotational constants (e.g., ζ and D_J), which are also functions of the potential constants, and by data from isotopically substituted molecules where these are available. Alternatively, the embarrassment of too many parameters in the potential function may be overcome by taking only selected cross terms, by taking a different physical model with fewer parameters, (e.g., the Urey-Bradley force field[2] or the orbital following force field[3]) or by transferring force constants from related molecules. While it appears that the general quadratic force field is superior when the available data are in excess of the minimum necessary to fix the force constants and the potential function is carefully fitted by least squares, it is rare indeed that all this information is available, even for a small molecule with four or five atoms. Thus, it would appear that if we are to embark upon an extensive program of force-constant calculations with an extension to large and complex molecules in mind, one of the simpler force fields is preferable to the general quadratic one. Our preference for the Urey-Bradley field was determined by the following considerations.

(i) Relatively few parameters are necessary for a complete description of the potential energy.

(ii) The Urey-Bradley field contains no quadratic cross terms as such but rather they are implicit in the interactions between nonbonded atoms. These interactions are often more easily visualized than quadratic cross terms and should be easier to correlate, particularly in the case of fairly large molecules with many vibrational degrees of freedom.

(iii) The calculations of Shimanouchi[4,5] and coworkers have demonstrated the general validity of this type of potential function and have already established typical values for a number of Urey-Bradley force constants.

This paper describes the basic computational techniques we have developed for the calculation of Urey-Bradley force constants from the observed vibrational frequencies. The perturbation treatment on which our program is based originated in Dr. Bryce Crawford's laboratory at the University of Minnesota and we

[1] The current literature has been summarized by Bellamy [*The Infrared Spectra of Complex Molecules* (Methuen and Company, Ltd., London, 1958)]. However, many more spectra and correlations exist in the working files of practicing spectroscopists; for example, our file at The Dow Chemical Company contains more than 12 000 spectra of pure compounds.

[2] H. C. Urey and C. A. Bradley, Phys. Rev. **38**, 1969 (1931).

[3] D. F. Heath and J. W. Linnett, Trans. Faraday Soc. **44**, 873 (1948).

[4] T. Shimanouchi, J. Chem. Phys. **17**, 245, 848 (1949).

[5] T. Shimanouchi, J. Chem. Soc. Japan **74**, 266 (1953).

should like to take this opportunity to acknowledge our indebtedness to Dr. Shimanouchi, Dr. King, Dr. Curtis, and to Dr. Crawford for many of the underlying ideas.

APOLOGIA

To discuss the procedure for calculating force constants at such length, particularly when some of the details are already in the scientific literature, requires justification. However, as we have abandoned the customary approach in which large transformation matrices are expressed as explicit functions of the geometrical parameters, and have programed a computer to construct these matrices from a minimal input, it is imperative that we give full details of our method, for our results are always open to the criticism that they are "machine calculations which can be assumed to be numerically correct although they cannot be checked···."[6]

The only real evidence we can offer for the correctness of our results is the detailed description of the method on which our program is based and our assurance that we have tested it fully, and, to the best of our knowledge, the logic of the program is correct. We have also taken several test cases ($COCl_2$, COH_2, C_2Cl_4, and C_2H_4) which have previously been calculated by other methods and have been able to reproduce the results with our program.

Therefore we feel justified in devoting the first paper of this series to a detailed description of the basic techniques, not only to give perspective to our developments of the method, but also because we hope that this description will provide the key to the interpretation of subsequent papers in this series.

CALCULATION OF FORCE CONSTANTS

While in principle the intramolecular force constants may be expressed as explicit functions of the vibrational frequencies by expansion of the secular determinant in minors, in practice this method is cumbersome and eventually becomes impracticable as one proceeds to higher order problems. Those iterative methods which gradually refine a trial set of force constants to fit certain criteria (e.g., the vibrational frequencies) are much more powerful and our method is based on such a procedure described by King.[7]

Consider the potential energy in the Urey-Bradley form,[5]

$$2V=\sum_i[2K_i'r_i\Delta r_i+K_i(\Delta r_i)^2]+\sum_{i<j}[2H_{ij}'r_0^2\Delta\alpha_{ij}+H_{ij}(r_0\Delta\alpha_{ij})^2]+\sum_{i<j}[2F_{ij}'q_{ij}\Delta q_{ij}+F_{ij}(\Delta q_{ij})^2], \quad (1)$$

noting that it is a function of the coordinates Δr_i (valence-bond stretches), $\Delta\alpha_{ij}$ (valence-angle bends), and Δq_{ij} (displacements between nonbonded atoms). After removal of the redundant coordinates Δq_{ij} and substitution of the minimum condition, V is left as a function of n' variables which may be independent or, if we chose to include more than the minimum number of internal coordinates necessary for a complete description of the molecular configuration, may still contain local or cyclic redundancies.[8] The potential energy now appears as a quadratic form in the internal coordinates $\mathbf{R}$, viz.,

$$2\mathbf{V}=\mathbf{R}'\mathbf{F}\mathbf{R}, \quad (2)$$

where the individual elements of the $\mathbf{F}$ matrix are linear functions of the Urey-Bradley force constants,

$$F_j{}^i=\sum_k a_{jk}{}^i\phi_k, \quad (3)$$

the coefficients $a_{jk}{}^i$ being determined by the molecular geometry.

The $(n')^2$ row-and-column indices[9] of the entries in $\mathbf{F}$ are then arranged in arbitrary order as a vector $\mathbf{f}$ (the F-index vector) and the individual elements of $\mathbf{F}$ are similarly arranged as a second vector $\mathbf{F}$ so that there is a one-to-one correspondence between the elements of $\mathbf{f}$ and $\mathbf{F}$.

This procedure allows us to define a transformation matrix $\mathbf{Z}$ such that

$$\mathbf{F}=\mathbf{Z}\Phi, \quad (4)$$

where Φ is a vector of Urey-Bradley force constants; the order of the elements of $\mathbf{F}$ and the rows of $\mathbf{Z}$ is determined by the $\mathbf{f}$ vector. We shall defer examination of the $\mathbf{Z}$ matrix and for the moment be satisfied by the fact that such a transformation exists. The information contained in the F-index vector can be used to rearrange the $\mathbf{F}$ vector into the $\mathbf{F}$ matrix.

It is often advantageous to take the internal coordinates $\mathbf{R}$ in linear combination, i.e.,

$$\mathbf{S}=\mathbf{U}\mathbf{R} \quad (5)$$

and to set up the secular equation in these coordinates. The utility of this approach is twofold: in the transformation $\mathbf{U}$ lies the opportunity to remove local and cyclic redundancies and also to introduce any symmetry which the molecule might have.[10] When this coordinate transformation is applied to the $\mathbf{F}$ matrix, there results a new force-constant matrix $\mathfrak{F}$ which is taken with an appropriate $\mathfrak{G}$ matrix[11] to form the

[6] H. C. Urey, Nature **181**, 1458 (1958).
[7] W. T. King, dissertation, University of Minnesota (1956).
[8] J. C. Decius, J. Chem. Phys. **17**, 1315 (1949).
[9] Actually, because of the symmetrical nature of F it is necessary to take only $\frac{1}{2}n'(n'+1)$ indices.
[10] In machine computation the advantage of molecular symmetry is not so much in the reduction of the order of the problem but rather in the fact that, once the observed frequencies have been separated into different species by inferrences from band shapes, depolarization ratios, etc., this separation may be retained throughout the calculation.
[11] E. B. Wilson, Jr., J. Chem. Phys. **7**, 1047 (1939).

secular equation. If the symmetry coordinates contain one or more redundant coordinates, $\mathcal{F}$ will be of order n' and $\mathcal{G}$ of order n. In forming the product $\mathcal{GF}$, the $n\times n$ submatrix of $\mathcal{F}$ is used and the indeterminate force constants corresponding to the redundant (i.e., null) coordinates are thrown away. The secular equation in the form

$$[\mathcal{GF}]\mathcal{L}_i=\mathcal{L}_i\lambda_i^{(c)} \tag{6}$$

is then solved for eigenvectors $\mathcal{L}_i$ and eigenvalues $\lambda_i^{(c)}$.

In as much as the exact Urey-Bradley force constants in the vector $\mathbf{\Phi}$ are seldom known in advance but are usually approximated, the roots of the secular equation will not be exactly equal to the observed-frequency parameters ($\lambda_i^{(o)}=4\pi^2\nu_i^2$). We therefore use first-order perturbation theory to refine the approximate force constants so that the fit between observed and calculated λ's is improved; i.e., we seek a correction to $\mathcal{F}$ such that $[\lambda_i^{(c)}-\lambda_i^{(o)}]$ will be zero. Assuming the zeroth-order normal coordinates to be fairly close to the true ones, this criterion implies that

$$[\mathcal{G}(\mathcal{F}^0+\Delta\mathcal{F})]\mathcal{L}^0\cong\mathcal{L}^0\mathbf{\Lambda}^0$$

or

$$\mathcal{GF}^0\mathcal{L}^0+\mathcal{G}(\Delta\mathcal{F})\mathcal{L}^0\cong\mathcal{L}^0\mathbf{\Lambda}, \tag{7}$$

where $\mathbf{\Lambda}^0$ is a diagonal matrix of the $\lambda_i^{(0)}$. Combining (6) and (7) gives

$$\mathcal{G}(\Delta\mathcal{F})\mathcal{L}^0\cong\mathcal{L}^0(\mathbf{\Lambda}^c-\mathbf{\Lambda}^0)=\mathcal{L}^0(\Delta\mathbf{\Lambda}). \tag{8}$$

The eigenvectors of the secular equation are normalized so that

$$\mathcal{L}'\mathcal{F}\mathcal{L}=\mathbf{\Lambda} \tag{9}$$

and

$$\mathcal{L}\mathcal{L}'=\mathcal{G} \tag{10}$$

whence (8) reduces to

$$(\mathcal{L}^0)'(\Delta\mathcal{F})\mathcal{L}^0=(\Delta\mathbf{\Lambda}). \tag{11}$$

Rewriting the diagonal terms of (9) as a series of n equations, one for each root we immediately recognize the Jacobian of $\mathbf{\Lambda}$ with respect to $\mathcal{F}$:

$$(\mathcal{L}^0)_i^1(\mathcal{L}_i^0)_i^1\Delta\mathcal{F}_{11}+(\mathcal{L}^0)_i^2(\mathcal{L}^0)_i^2\Delta\mathcal{F}_{22}+\cdots$$
$$+2(\mathcal{L}^0)_i^1(\mathcal{L}_0)_i^2\Delta\mathcal{F}_{12}+2(\mathcal{L}^0)_i^1(\mathcal{L}^0)_i^1\Delta\mathcal{F}_{13}+\cdots=\Delta\lambda_i, \tag{12}$$

or in matrix notation

$$\mathcal{J}(\Delta\mathcal{F})=(\Delta\mathbf{\Lambda}). \tag{13}$$

By solving these n equations it is possible, in principle, to determine n corrections to $\mathcal{F}$.

However, in the present analysis we are not particularly interested in the elements of $\mathcal{F}$, these being merely force constants in the working coordinates, but rather we wish to determine the corrections to the Urey-Bradley force constants, and thus we wish to transform the Jacobian (13) to Urey-Bradley space. The symmetry we introduced in (5) now becomes an inconvenience and so, before setting up the matrix $\mathcal{J}$, the normal coordinates are desymmetrized by the transformation

$$\mathbf{L}=\mathbf{U}^{-1}\mathcal{L} \tag{14}$$

and the $\mathbf{J}$ matrix is set up from these normal coordinates. Then, as the F's are linear functions of the Urey-Bradley force constants, (4) also holds for the difference form

$$\Delta\mathbf{F}=\mathbf{Z}\Delta\mathbf{\Phi}. \tag{15}$$

By combining (14) and (15), we see

$$\mathbf{JZ}\Delta\mathbf{\Phi}=\Delta\mathbf{\Lambda}. \tag{16}$$

The matrix $(\mathbf{JZ})$ is $n\times m$ where n is the order of the secular equation and m is the number of Urey-Bradley force constants; it may be simply interpreted as the Jacobian of $\mathbf{\Lambda}$ with respect to $\mathbf{\Phi}$.[12]

Clearly it is impossible to solve (16) if $m>n$ and if more than n Urey-Bradley force constants are required for a realistic potential function, either some of these must be constrained and the columns omitted from the $(\mathbf{JZ})$ matrix or data from isotopic molecules may be included to give extra rows in $(\mathbf{JZ})$. If there are fewer than n Urey-Bradley force constants, it is more satisfying to solve (16) by least squares; we accomplish this in the usual way[13] by introducing a diagonal weight matrix $\mathbf{P}$ and forming the matrix equation

$$(\mathbf{JZ})'\mathbf{P}(\mathbf{JZ})(\Delta\mathbf{\Phi})=(\mathbf{JZ})'\mathbf{P}(\Delta\mathbf{\Lambda}). \tag{17}$$

The solutions of this equation $\Delta\mathbf{\Phi}$ are the least-square corrections we seek to the Urey-Bradley force constants. However, as the normal coordinates in (12) were only approximate, the corrected force constants will still deviate from the true values and the perturbation must be repeated using the revised normal coordinates to set up a new $\mathbf{J}$ matrix. The cycle is repeated until the calculated λ's converge to the observed-frequency parameters, or in the case where the potential function is over determined, until further refinement produces no change in the resulting force constants.

[12] Previous workers have used a Jacobian method to determine Urey-Bradley force constants, but have used different approaches to obtain the $\mathbf{J}$ matrix. Miyazawa [J. Chem. Soc. Japan, Pure Chem. Sec. **76**, 1132 (1955)] considers a variation δK_λ in one of the UB force constants K_λ and through a matrix $\mathbf{A}_\lambda(F=\Sigma\mathbf{A}_\lambda K_\lambda)$, obtains $J_{a\lambda}$ (i.e., $\partial\lambda a/\partial K_\lambda$) which is equivalent to a single element of $(\mathbf{JZ})$ Mann, Shimanouchi, Meal, and Fano,[13] obtained the Jacobian by a method similar to Miyazawa's, but contrary to our practice, they did not redetermine the Jacobian for each refinement but merely at the beginning and before the final refinement. Curtis [dissertation, University of Minnesota (1959)] has independently developed a method of handling $\mathbf{J}$ exactly like ours with the exception that he prefers to express $\mathbf{Z}$ in symmetry coordinates, thereby sacrificing the convenience of assembling $\mathbf{Z}$ from standard submatrices with a computer.

[13] D. E. Mann, T. Shimanouchi, J. H. Meal, and L. Fano, J. Chem. Phys. **27**, 43 (1957).

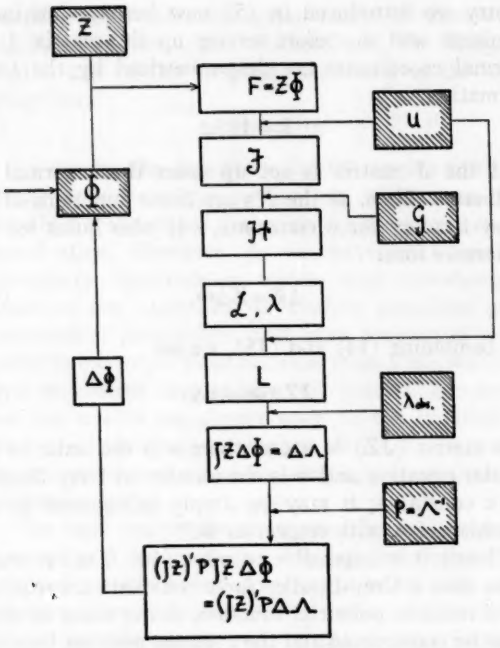

FIG. 1. Block diagram of the main perturbation cycle. Shaded blocks represent the necessary input data.

COMPUTER PROGRAM

It is not our intention to present a detailed description of our computer program as many of its features are determined by the peculiar characteristics of the Datatron 204 computer. However, our experience has brought to light certain points of general interest in the calculation of normal coordinates on a digital computer and we shall briefly review our technique.

A block diagram of the main perturbation cycle is shown in Fig. 1. The required input is as follows:

(i) A vector of approximate Urey-Bradley force constants Φ_0, which are usually estimated by comparison with similar molecules or groups.

(ii) A **Z** matrix.

(iii) A **G** matrix.

(iv) The symmetry-coordinate transformation **U**.

(v) Λ_{obs}, a vector of the observed frequency parameters arranged in descending order of magnitude within each symmetry block, the blocks being arranged in the same order as in the **U** matrix.

(vi) A weight matrix **P**, usually taken as $\mathbf{A}^{-1}$.

In our program the secular equation is unsymmetrical and we have used a particularly apt method of solution described by Wilkinson.[14] This method, although using an iterative procedure to determine the dominant root and its modal column, uses a similarity deflation which circumvents the calculation of left eigenvectors.

In our preliminary studies we used the eigenvectors of **GF** to set up the matrix **J** and then found **JZ** by simple matrix multiplication. However, for a secular determinant of order n, the width of **J** is $\frac{1}{2}n(n+1)$ and the length of **Z** is similar and even for problems of moderate size these matrices make excessive demands on storage. With our relatively small computer these demands proved to be a severe limitation on the size of problem we could tackle. Now as soon as we construct **JZ**, the $\frac{1}{2}n(n+1)$ dimension disappears and the problem returns to moderate bounds. Thus we have abandoned the direct matrix-multiplication approach to **JZ** in favor of an indirect method which allows us to assemble it without forming **J** explicitly. Expanding **JZ** in terms of the elements of the eigenvectors, the typical element of **JZ** has the form

$$(JZ)_{pr}=\sum_{i=1}^{n}\sum_{j=1}^{n}L_i^pL_j^pZ_{ij}^r. \qquad (18)$$

Thus, having ready access to the eigenvectors, we may take the elements of **Z**, one by one, and determine their contribution to the sum in (18), and by accumulating these contributions in storage cells assigned to the elements of **JZ**, we have been able to assemble this matrix within limited storage.

We have not fully tested the convergence of the perturbation but our preliminary results on the carbonyl halides and ethylene were very encouraging, indicating that even when the starting vector Φ_0 is a poor approximation convergence is relatively good. In the particular case of COF_2 we have been able to go from a set of force constants which gave frequencies differing by several hundred wave numbers from the observed values to a converged set of force constants in four cycles by applying the calculated values of $\Delta\Phi$ directly. However, we have found that oscillations sometimes occur when the problem has almost converged and in these cases the final solution is difficult to find. We are presently investigating the effect of scaling the corrections to $\Delta\Phi$ before adding them in and our preliminary results indicate that this effectively overcomes the oscillation problem.

THE G MATRIX

The **G** matrix, first proposed by Wilson,[11] is a convenient way of introducing the kinetic energy into the molecular-vibrational problem. This well-known matrix is quite tedious to set up algebraically and in the past several short cuts have been proposed.[15] However, the construction of this matrix still remains a major problem and provides innumerable opportunities for slips which can invalidate all subsequent work.

Faced with the task of setting up a large number of these **G** matrices, we decided to use a computer for as much as possible of this work, for the fatigue factor, which is responsible for most of the errors incurred

[14] J. H. Wilkinson, Proc. Cambridge Phil. Soc. **50**, 536 (1954).

[15] See, for example, the Decius tables of G-matrix elements. E. B. Wilson, J. C. Decius, and P. C. Cross, *Molecular Vibrations* (McGraw-Hill Book Company, Inc., New York, 1955), p. 55 ff.

when setting up a transformation algebraically, is entirely eliminated in a digital computer.

The numerical **G** matrix may be computed by the simple matrix operation

$$\mathbf{G}=\mathbf{B}\mathbf{M}^{-1}\mathbf{B}', \tag{19}$$

where $\mathbf{M}^{-1}$ is a diagonal matrix of the reciprocal atomic masses and **B** is the transformation from Cartesian to internal coordinates,

$$\mathbf{R}=\mathbf{B}\mathbf{x}. \tag{20}$$

Thus, with standard subroutines for matrix operation, the calculation of the **G** matrix reduces to the determination of the transformation **B** from the molecular geometry.

In our program we have introduced the geometrical parameters in the most general way as the Cartesian coordinates of the atoms in an arbitrary reference frame, the atoms being identified by a code number which is recorded on a master plan of the molecule. The internal coordinates used to describe the molecular vibrations fall into a limited number of types (i.e., valence-bond stretches, valence-angle bends, out-of-plane deformations, and torsions) differing only in the atoms involved. Wilson[15] has given explicit expressions for the **s** vectors for these types of coordinate and the entries of the **B** matrix are just the components of these vectors in the x, y, and z directions. If the Cartesian coordinates of the ith atom are subtracted from those of the jth atom, we obtain a vector $\mathbf{r}_{ij}$ of length r_{ij} and pointing from i to j, i.e.,

$$\mathbf{r}_{ij}=(x_j-x_i)\mathbf{i}-(y_j-y_i)\mathbf{j}-(z_j-z_i)\mathbf{k}. \tag{21}$$

On normalization of $\mathbf{r}_{ij}$ to unit length,

$$\mathbf{e}_{ij}=\mathbf{r}_{ij}(\mathbf{r}_{ij}\cdot\mathbf{r}_{ij})^{-\frac{1}{2}}, \tag{22}$$

we then obtain the vector $\mathbf{e}_{ij}$ which may be substituted in Wilson's formulas. The trigonometric ratios which are also required are determined from the **e** vectors by forming scalar and vector products.

The several coordinate types mentioned in the preceeding are reduced to a simple numerical code and the coordinate exactly defined for the computer input by the code designation and the numbers of the atoms involved (e.g., [01 i,j] represents Δr_{ij}, [02 i,j,k] represents $r_{ij}\Delta\alpha_{ijk}$, etc.) This coded input is broken down in the computer and the coordinate code used to transfer control to a subroutine which will construct the **s** vectors for the particular coordinate type. The indices i, j, and k are used to pick up the Cartesian coordinates of the appropriate atoms and it is then merely a matter of straightforward computation to determine the rows of the **B** matrix, one at a time.

We have programed the calculation of **B** matrices of order 60×20 and **G** matrices of order 20×20 and are able to dump these from the computer in a form suitable for input to the perturbation calculation. To date we have not tackled a problem requiring larger matrices but they could easily be set up as mosaics with our present program.

We have found it convenient to introduce symmetry in two different ways—either by operating on the **B** matrix or by transforming the final **G** matrix; i.e.,

$$\mathfrak{B}=\mathbf{U}\mathbf{B}, \qquad \mathfrak{G}=\mathfrak{B}\mathbf{M}^{-1}\mathfrak{B}' \tag{23}$$

or

$$\mathfrak{G}=\mathbf{U}\mathbf{G}\mathbf{U}'. \tag{23}$$

Although we have succeeded in removing the fatigue factor from the preliminaries to the vibrational problem, our technique is not without its attendant perils. We are reasonably confident that the program logic is correct as we have been able to reproduce many **G** matrices which had previously been set up by more conventional methods: in particular CH_3F, CD_3F, CH_3Cl, CD_3Cl, CH_3Br, CD_3Br, CH_3I, CD_3I, CH_3CCH, C_2H_3Br (8 isotopic species), C_2H_3F, (8 isotopic species), B_2H_6, B_2D_6, and $COCl_2$. In those cases where we were able to reproduce the geometrical parameters exactly, the differences were in the seventh or eighth significant figure; in a few cases where we approximated the angles the agreement was good to only five figures. However, errors may still occur in preparing the input to the program, and although we have programed logical checks on the input data, there still remains a slight possibility of introducing an undetected error.

THE Z MATRIX

In order to make clear the construction of the **Z** matrix it is necessary to review briefly the problem of the Urey-Bradley force field. As the potential energy is expressed in terms of the Δr_i, $\Delta\alpha_{ij}$, and Δq_{ij} which are not independent coordinates, the equilibrium condition that $\delta v=0$ does not necessarily imply that $\partial v/\partial r_i=0$, etc. If the redundant coordinates Δq_{ij} are removed by a substitution such as[4]

$$\begin{aligned}\Delta q_{ij}=s_{ij}(\Delta r_i)+s_{ji}(\Delta r_j)+(t_{ij}t_{ji})^{\frac{1}{2}}(r_j/r_i)^{\frac{1}{2}}(r_i\Delta\alpha_{ij})\\ +1/2q_{ij}\{t_{ij}^2(\Delta r_i)^2+t_{ji}^2(\Delta r_j)^2-s_{ij}s_{ji}(r_j/r_i)(r_i\Delta\alpha_{ij})^2\\ -2t_{ij}t_{ji}(\Delta r_i\Delta r_j)+2t_{ij}s_{ji}(r_j/r_i)(\Delta r_i r_i\Delta\alpha_{ij})\\ +2t_{ji}s_{ij}(\Delta r_i r_i\Delta\alpha_{ij})\}\end{aligned} \tag{24}$$

where

$$s_{ij}=(r_i-r_j\cos\alpha_{ij})/q_{ij}, \quad \text{and} \quad t_{ij}=(r_j\sin\alpha_{ij})/q_{ij},$$

the potential energy is then expressed in an independent set of coordinates, and the partials $\partial v/\partial r_i$ and $\partial v/\partial\alpha_{ij}$ may be equated to zero and the linear terms removed from V. However, this substitution (24) has the effect of introducing the F_{ij}' into the coefficients of the quadratic terms and we must determine these linear force constants along with the quadratic ones. There is an equation similar to (24) for each Δq_{ij} and the **Z** matrix is formed from the coefficients of these substitution relationships.

TABLE I. Contributions to **Z** matrix from gem q_{ij}, the notation is defined in Eq. (24).

f vector	F_{ij}	F'_{ij}
$(\Delta r_i)^2$	s_{ij}^2	t_{ij}^2
$(\Delta r_j)^2$	s_{ji}^2	t_{ji}^2
$(r_i\Delta\alpha_{ij})^2$	$t_{ij}t_{ji}(r_j/r_i)$	$-s_{ij}s_{ji}(r_j/r_i)$
$(\Delta r_i\Delta r_j)$	$s_{ij}s_{ji}$	$-t_{ij}t_{ji}$
$(\Delta r_i r_i\Delta\alpha_{ij})$	$s_{ij}(t_{ij}t_{ji})^{\frac{1}{2}}(r_j/r_i)^{\frac{1}{2}}$	$t_{ij}s_{ji}(r_j/r_i)$
$(\Delta r_j r_i\Delta\alpha_{ij})$	$s_{ji}(t_{ij}t_{ji})^{\frac{1}{2}}(r_j/r_i)^{\frac{1}{2}}$	$t_{ji}s_{ij}$

At present we recognize two important types of q_{ij}; that where atoms i and j are bonded to a common atom k (gem q_{ij}), and that where atoms i and j are bonded respectively to two other atoms k and l which are in turn connected by a bond kl, atoms i and j lying on the same side of the bond kl (cis q_{ij}).

To illustrate the construction of the **Z** matrix consider the relatively simple gem q_{ij}. Inspection of (24) reveals that removal of this Δq_{ij} introduces F_{ij} and F_{ij}' into the coefficients of the diagonal terms $(\Delta r_i)^2$, $(\Delta r_j)^2$, and $(\Delta\alpha_{ij})^2$ of the **F** matrix and into the off-diagonal terms $(\Delta r_i\cdot\Delta r_j)$, $(\Delta r_i\cdot\Delta\alpha_{ij})$, and $(\Delta r_j\cdot\Delta\alpha_{ij})$. The coefficients of these terms are shown in Table I and this submatrix is the contribution of Δq_{ij}(gem) to the **Z** matrix. The Δq_{ij}(cis) submatrix may be obtained in a similar way and is shown in Table II. The diagonal force constants K_i and H_{ij} are unaffected by the removal of the redundant Δq_{ij}'s and therefore each is represented by a single unit energy in **Z**, under the appropriate column and in the row corresponding to the diagonal element of **F** for that particular coordinate.

As with the **B** matrix it is necessary to introduce the Cartesian coordinates of the atoms and the internal coordinates in a coded representation. These latter must be extended to include the Δq_{ij}: at present our arsenal is limited to the gem q_{ij} (07 i, j, k) and a cis q_{ij} for the most general planar case (10 i, j, k, l) although other types can readily be added as need arises. The program for construction of the **Z** matrix picks up each coordinate in turn and tests for the coordinate type. If it is a Δr_i or $\Delta\alpha_{ij}$ type, a one is entered in the appropriate cell of **Z**; if it is a Δq_{ij}, the type index is used to transfer control to a subroutine which constructs the necessary geometrical parameters by vector analysis (cf. the **B** matrix) and enters the appropriate submatrix in **Z**. Provision is made for closing up the columns of the **Z** matrix and substituting F_{ij}' as a predetermined function of F_{ij} before the matrix is dumped on IBM cards.

LOCAL AND CYCLIC REDUNDANCIES

As we previously remarked, it is often desirable to include more than the minimum number of valence coordinates necessary for a complete description of the molecular configuration[16] and therefore when the Δq_{ij}'s have been removed the coordinates are still not independent but are related by one or more redundancy relations, $R_a(\Delta r_i, \Delta\alpha_{ij})$. Thus in order to introduce the equilibrium condition we must use Lagrange's method of undetermined multipliers and seek the unrestricted minimum of

$$V' = V(\Delta r_i, \Delta\alpha_{ij}) + \sum_a \kappa_a R_a(\Delta r_i, \Delta\alpha_{ij}). \qquad (25)$$

The redundancy relationship is generally expressed in a Taylor series, taking terms through the quadratic. Thus, when V' is minimized, the potential energy will contain the quadratic terms in R_a as coefficient of a force constant κ_a, the intramolecular tension: this force constant will contribute a column to the **Z** matrix.

In the particular case of a planar group, e.g., $=CH_2$, the *exact* redundancy relationship contains only first-

TABLE II. Contributions to **Z** matrix from planar cis q_{ij}.[a]

f vector	F_{ij}	F'_{ij}
$(\Delta r_i)^2$	v_{ij}^2	$(1-v_{ij}^2)$
$(\Delta r_j)^2$	v_{ji}^2	$(1-v_{ji}^2)$
$(\Delta R_{kl})^2$	a_{ij}^2	b_{ij}^2
$(\Delta r_i\Delta r_j)$	$v_{ij}v_{ji}$	$[\cos(\alpha_{il}+\alpha_{jk})-v_{ij}v_{ji}]$
$(\Delta r_i\Delta R_{kl})$	$-a_{ij}v_{ij}$	$(a_{ij}v_{ij}-\cos\alpha_{il})$
$(\Delta r_j\Delta R_{kl})$	$-a_{ij}v_{ji}$	$(a_{ij}v_{ji}-\cos\alpha_{jk})$
$(r_i\Delta\alpha_{il})^2$	u_{ij}^2	$[(v_{ij}q_{ij}/r_i)+(1-u_{ij}^2)]$
$(r_j\Delta\alpha_{jk})^2$	u_{ji}^2	$[(v_{ji}q_{ij}/r_j)+(1-u_{ji}^2)]$
$(r_i\Delta\alpha_{il}r_j\Delta\alpha_{jk})$	$u_{ij}u_{ji}$	$-[\cos(\alpha_{jk}+\alpha_{il})+u_{ij}u_{ji}]$
$(r_i\Delta\alpha_{il}\Delta r_i)$	$-u_{ij}v_{ij}$	$u_{ij}(q_{ij}+r_iv_{ij})/r_i$
$(r_i\Delta\alpha_{il}\Delta r_j)$	$-u_{ij}v_{ji}$	$[v_{ji}u_{ij}-\sin(\alpha_{jk}+\alpha_{il})]$
$(r_i\Delta\alpha_{il}\Delta R_{kl})$	$u_{ij}a_{ij}$	$(\sin\alpha_{il}-a_{ij}u_{ij})$
$(r_j\Delta\alpha_{jk}\Delta r_i)$	$-u_{ji}v_{ij}$	$[v_{ij}u_{ji}-\sin(\alpha_{jk}+\alpha_{il})]$
$(r_j\Delta\alpha_{jk}\Delta r_j)$	$-u_{ji}v_{ji}$	$u_{ji}(q_{ij}+r_jv_{ji})/r_j$
$(r_j\Delta\alpha_{jk}\Delta R_{kl})$	$u_{ji}a_{ij}$	$(\sin\alpha_{jk}-a_{ij}u_{ji})$

[a] Notation. The cis q_{ij} represents the interaction between atoms i and j which are bonded, respectively, to atoms l and k which are in turn joined by a bond kl. Angles α_{il}, α_{jk} lie between 0 and π. We have patterned our notation on that adopted Mann *et al.*,[10] i.e.,

$a_{ij}=(R_{kl}-r_i\cos\alpha_{il}-r_j\cos\alpha_{jk})/q_{ij}$, $b_{ij}=(r_i\sin\alpha_{il}-r_j\sin\alpha_{jk})/q_{ij}$

$u_{ij}=(a_{ij}\sin\alpha_{il}+b_{ij}\cos\alpha_{il})$, $u_{ji}=(a_{ij}\sin\alpha_{jk}-b_{ij}\cos\alpha_{jk})$,

$v_{ij}=(a_{ij}\cos\alpha_{il}-b_{ij}\sin\alpha_{il})$ and $v_{ji}=(a_{ij}\cos\alpha_{jk}+b_{ij}\sin\alpha_{jk})$.

[16] In a symmetrical molecule this complication arises when we wish to include complete sets of equivalent coordinates to carry the molecular symmetry through into the secular equation. However, even with molecules of lower symmetry we have found that inclusion of redundant coordinates improves the Urey-Bradley force field: for example, in a study of the planar vibrations of the carbonyl halides we found it impossible to transfer force constants calculated from a force field which included only two of the angles around the carbon atom.

order terms if the *motion is restricted to a plane* and therefore no intramolecular tension enters the quadratic part of V. The same is true for planar cyclic molecules or groups.[17] Although in principle one should always consider the molecule in its most general displaced configuration, in which case the intramolecular tension should be included even when the equilibrium configuration is planar, we have adopted the simplified model for a number of planar molecules and to date have found no reason to include the intramolecular tension.

CARTESIAN DISPLACEMENTS AND POTENTIAL ENERGY IN UREY-BRADLEY SPACE

While the eigenvalues of the secular equation contain a complete description of the normal modes of vibration, these are not particularly easy to interpret. They are much more readily visualized when transformed to a Cartesian reference frame and in this representation the normal coordinates can be plotted to give a two-dimensional projection of the normal modes of vibration.

The transformation from Cartesian to internal coordinates (20) has no inverse, the reverse transformation being defined by a new matrix $\mathbf{A}$,

$$\mathbf{x}=\mathbf{AR}. \tag{26}$$

To relate $\mathbf{A}$ and $\mathbf{B}$ it is necessary to augment the internal coordinates with translations and rotations, where it may easily be shown that[18]

$$\mathbf{BA}=\mathbf{I}_{3n-6}; \tag{27}$$

However, we know

$$\mathbf{BM}^{-1}\mathbf{B}'=\mathbf{G},$$

whence

$$\mathbf{BM}^{-1}\mathbf{B}'\mathbf{G}^{-1}=\mathbf{I}_{3n-6}, \tag{28}$$

and after combining (27) and (28), we find

$$\mathbf{A}=\mathbf{M}^{-1}\mathbf{B}'\mathbf{G}^{-1}. \tag{29}$$

[17] S. Califano (private communication).

[18] B. L. Crawford and W. H. Fletcher, J. Chem. Phys. **19**, 141 (1951); Bryce L. Crawford, Jr., *ibid.* **20**, 977 (1952).

Then, as $\mathbf{R}=\mathbf{LQ}$, we see

$$\mathbf{x}=\mathbf{ALQ}=(\mathbf{M}^{-1}\mathbf{B}'\mathbf{G}^{-1}\mathbf{L})\mathbf{Q}. \tag{30}$$

We may avoid the inversion of the G matrix by substitution from (6), whence

$$\mathbf{x}=(\mathbf{M}^{-1}\mathbf{BFL}\Lambda^{-1})\mathbf{Q}. \tag{31}$$

Equations (30) and (31) are equivalent; however we chose to use (31) which circumvents the matrix inversion. This transformation of the normal coordinates to a Cartesian reference frame is incorporated into the dump routine and at any time we may take out the Cartesian displacements for inspection.

We have also found it worthwhile to display the contributions of the various Urey-Bradley force constants to the different normal modes; that is, to construct the potential-energy distributions in Urey-Bradley space. This we accomplish by forming the matrix product

$$\Lambda^{-1}\mathbf{J}\,\mathbf{Z}\Phi^*,$$

where Φ^* is a diagonal matrix of the Urey-Bradley force constants, and the other matrices have the definition given previously. The elements of this matrix are the fractional contributions to the λ_i from the work terms associated with each Urey-Bradley coordinate. Again, we have programed the construction of this matrix into our dump routine and routinely print it out with our final output.

As we do not have an algebraic check on our starting matrices, and it always remains a possibility to misread the input data, at the end of each problem we print out the Urey-Bradley force constants Φ, the calculated λ's and ν's, and the matrices $\mathbf{G}$, $\mathbf{F}$, $\mathbf{L}$, $\mathbf{Z}$, and $\mathbf{U}$. Clearly we cannot reproduce the whole of this output, and we have selected Φ, $\mathbf{u}$, $\mathbf{L}$, and ν as the most important results for inclusion in subsequent papers in this series.

ACKNOWLEDGMENT

We are indebted to Dr. C. D. Alstad for his help and advice in the planning of the computer program, and to Dr. B. L. Crawford, Dr. E. C. Curtis, and Dr. W. T. King for helpful discussions. We should also like to express our gratitude to Dr. N. Wright and Dr. W. J. Potts for their continued encouragement in this work.

Transferability of Urey-Bradley Force Constants. II. Carbonyl Halides and Related Molecules

JOHN OVEREND AND J. R. SCHERER

Spectroscopy Laboratory, The Dow Chemical Company, Midland, Michigan

(Received July 22, 1959)

Urey-Bradley force constants have been fitted to the observed vibrational frequencies of COF_2, $COCl_2$, and $COBr_2$ by the method described in the previous paper. These force constants have been used to calculate the frequencies of COClF, COBrF, and COBrCl. Normal coordinates and the potential energy distribution among the various Urey-Bradley coordinates have also been calculated. It is found that, despite the fact that the carbonyl stretching frequencies fall over a range of 100 cm^{-1}, the carbonyl stretching force constant is essentially the same for all molecules in the carbonyl halide series.

INTRODUCTION

ALTHOUGH the carbonyl halides are of limited chemical interest, they nevertheless constitute a simple series of molecules belonging to that important class of compounds containing carbonyl groups. Their simplicity makes them particularly attractive for a trial of the method of calculating force constants described in the previous paper, and one may reasonably hope that some of the results may be transferred to other more complex molecules containing the carbonyl group. In addition, a treatment of these molecules by the Urey-Bradley force field should be particularly rewarding as the interactions between nonbonded atoms have been found to be sizable in halogen compounds.[1,2] Also, vibrational frequencies and reliable assignments are now available for many molecules in this series; these are summarized in Table I. With the exception of COF_2, which is discussed in the following, we have found the presently accepted vibrational assignments in perfect harmony with the results of our calculations.

Recently Mann *et al.*[2] have calculated force constants for a series of perhaloethylenes by using an eight-parameter Urey-Bradley potential function for the C_2X_4 molecules. They fitted these force constants by a method of least squares to nine observed fundamentals and obtained good agreement between observed and calculated frequencies. The structural similarities[3] of these molecules to the carbonyl halides suggested a comparison of the force constants and in our work we have used the values obtained by Mann *et al.* as starting approximations and in some instances have boldly transferred their force constants to the corresponding carbonyl halide molecules.

SYMMETRICAL MOLECULES, COX_2[4]

The potential function was taken in the form

$$2V=\sum_{i=1}^{3}[2K_i'r_i\Delta r_i+K_i(\Delta r_i)^2]+\sum_{i<j}[2H_{ij}'r_0^2\Delta\alpha_{ij}+H_{ij}(r_0\Delta\alpha_i)^2]+\sum_{i<j}[2F_{ij}'q_{ij}\Delta q_{ij}+F_{ij}(\Delta q_{ij})^2] \quad (1)$$

where the coordinates Δr_i are the valence-bond stretches, $\Delta\alpha_{ij}$ the valence-angle bends, and the Δq_{ij} the changes in nonbonded interatomic distances. The scaling bond lengths r_0 were taken as r_{CX} for all the angles in the symmetric molecules. The out-of-plane deformations fall in a separate class and have been discussed elsewhere[5]; accordingly, this coordinate is not included in (1). After the Δq_{ij}'s have been removed, the potential function contains eight force constants in the coefficients of the quadratic terms, *viz.*, K_O, K_X, H_{OX}, H_{XX}, F_{OX}, F_{OX}', F_{XX}, and F_{XX}'. These cannot all be determined from only five vibrational frequencies and we must introduce further simplifications. Following the precedent set by Shimanouchi,[2,6] we have taken $F_{ij}'=-0.1F_{ij}$ and thereby reduced the number of parameters to six. Thus, if we assume a value for any one, the remaining five force constants may be evaluated by the method of the previous paper. At this stage, the potential energy is expressed in terms of a set of six valence coordinates which includes a redundancy in the angles around the carbon atom. We have not reproduced the **F** matrices here, but have given in Table II the final **Φ** vectors for all the symmetrical molecules, and in Table III the numerical **Z** matrix[7] for $COCl_2$. The en-

[1] T. Shimanouchi, J. Chem. Phys. **17**, 848 (1949).

[2] D. E. Mann, T. Shimanouchi, J. H. Meal, and L. Fano, J. Chem. Phys. **27**, 43 (1957).

[3] The geometrical parameters Mann *et al.* used for the perhaloethylenes are shown as follows: $r_{CF}=1.31$ A, $r_{CCl}=1.72$ A, and $r_{CBr}=1.90$ A, and $\alpha_{XCX}=114°$.

[4] The frequencies of $COCl_2$ have been calculated previously by Miyazawa [J. Chem. Soc. Japan **74**, 915 (1953)] from a set of Urey-Bradley force constants. His adopted values were $K_{Cl}=1.75$, $K_O=12.5$, $H_{ClCl}=0.1$, $H_{ClO}=0.3$, $F_{ClCl}=0.65$, and $F_{ClO}=1.0$ md/A.

[5] J. Overend and J. C. Evans, Trans. Faraday Soc. **55**, 1817 (1959).

[6] Y. Morino, K. Kuchitso, and T. Shimanouchi, J. Chem. Phys. **20**, 726 (1952).

[7] J. Overend and J. R. Scherer, J. Chem. Phys. **32**, 1289 (1960), this issue.

TABLE I. Carbonyl halides and related molecules; fundamental frequencies in cm^{-1} and assignments.

Molecule	ν_1	ν_2	ν_3	ν_4	ν_5	ν_6	Source
COF_2	965	1928	626	1249	584	774	Nielsen *et al.*
$COCl_2$	567	1827	285	849	440	580	Catalano and Pitzer
$COBr_2$	425	1828	181	757	350	512	Overend and Evans
COClF	776	1868	501	1095	415	667	Nielsen *et al.*
COBrF	721	1874	398	1068	335	620	Patty and Lagemann
COClBr	517	1828	240	806	372	547	Overend and Evans

TABLE II. Urey-Bradley force constants for symmetric molecules, md/A.

Molecule	Comments	K_O	K_X	H_{XX}	H_{OX}	F_{OX}	F_{XX}
COF_2 (i)	Nielsen assignment	13.20	4.162	0	0.674	0.626	2.990
COF_2 (ii)	Alternative assignment	13.23	4.332	0	0.497	1.236	2.137
*COF_2 (iii)	Nielsen assignment	12.79	4.64	0.450	0.250	1.298	1.604
*COF_2 (iv)	Alternative assignment	12.85	4.528	0.450	0.261	1.578	1.120
COF_2 (v)	Nielsen assignment	12.82	4.660	0.425	0.246	1.261	1.659
COF_2 (vi)	Alternative assignment	12.87	4.53	0.425	0.265	1.561	1.166
$COCl_2$ (i)		12.68	2.004	0	0.327	0.861	0.736
*$COCl_2$ (ii)		12.61	1.99	0.11	0.145	0.860	0.523
$COBr_2$ (i)		12.85	1.653	0	0.318	0.631	0.639
*$COBr_2$ (ii)		12.83	1.565	0.060	0.104	0.631	0.528

tires in the **Z** matrices for the other molecules differ slightly from this on account of the geometrical nature of the terms, but all the matrices have similar form.

The internal coordinates were taken in linear combination as symmetry coordinates to factor the secular equation and remove the redundancy in the angles. These symmetry coordinates are

$$S_1=\Delta r_0,$$

$$S_2=1/\sqrt{2}(\Delta r_X^1+\Delta r_X^2),$$

$$S_3=r_{CX}/(6)^{\frac{1}{2}}(2\Delta\alpha_{XX}-\Delta\alpha_{XO}^1-\Delta\alpha_{XO}^2),$$

$$S_4=1/\sqrt{2}(\Delta r_X^1-\Delta r_X^2),$$

$$S_5=r_{CX}/\sqrt{2}(\Delta\alpha_{XO}^1-\Delta\alpha_{XO}^2),$$

redundant coordinate

$$S_6=r_{CX}/\sqrt{3}(\Delta\alpha_{XX}+\Delta\alpha_{XO}^1+\Delta\alpha_{XO}^2), \quad (2)$$

and these coordinates must be taken with the **L** matrices given in Table IV.

The geometrical parameters for COF_2 were obtained from the microwave results of Smith[8] although, as his data were limited to one molecule, the geometry is not uniquely determined. By combining his results with the electron diffraction data,[9] we find $r_{C-O}=1.17$ A, $r_{CF}=1.32$ A, and $\alpha_{FCF}=112°30'$. Robinson[10] has determined the geometry of $COCl_2$ from microwave measurements and gives $r_{CO}=1.166$ A, $r_{CCl}=1.746$ A, and $\alpha_{ClCCl}=111°18'$. The geometry of $COBr_2$ was taken from the electron diffraction results of Dornte[11] who gives $r_{CO}=1.13$ A, $r_{CBr}=2.05$ A, and $\alpha_{BrCBr}=110°$. No experimental data are available for the structures of the mixed halides, and we have transferred the foregoing interatomic distances and angles from the symmetrical molecules, using linear interpolation where necessary.

A complication arises from the fact that the vibrational assignment of COF_2 given by Nielsen *et al.*[12] is not entirely free from ambiguity. The spectrum con-

TABLE III. *Z* matrix $COCl_2$; $R_1=\Delta r_{CO}$, $R_2=\Delta r_{CX}^1$, $R_3=\Delta r_{CX}^2$, $R_4=r_{CX}\Delta\alpha_{OX}^1$, $R_5=r_{CX}\Delta\alpha_{OX}^2$, and $R_6=r_{CX}\Delta\alpha_{XX}$

f	K_O	K_{Cl}	H_{ClCl}	H_{OCl}	F_{OCl}	F_{ClCl}
1.1	1.0				1.3182401	
2.2		1.0			0.84797666	0.64979524
3.3		1.0			0.84797666	0.64979524
4.4			1.0			0.38653112
5.5				1.0	0.18970403	
6.6				1.0	0.18970403	
1.2					0.79188485	
1.3					0.79188485	
1.4						
1.5					0.25715056	
1.6					0.25715056	
2.3						0.71346882
2.4						0.41925876
2.5					0.32448897	
2.6						
3.4						0.41925876
3.5						
3.6					0.32448897	
4.5						
4.6						
5.6						

[8] D. F. Smith (private communication).
[9] T. T. Broun and R. L. Livingston, J. Am. Chem. Soc. **74**, 6084 (1952).
[10] D. W. Robinson, J. Chem. Phys. **21**, 1741 (1953).
[11] R. W. Dornte, J. Am. Chem. Soc. **55**, 4126 (1933).
[12] A. H. Nielsen, T. G. Burke, P. J. H. Woltz, and E. A. Jones, J. Chem. Phys. **20**, 596 (1952).

TABLE IV. L' matrices, symmetric molecules.

	ν, cm^{-1}	S_1 (Δr_{CO})	S_2(Δr_{CX})	S_3 ($r_{CX}\Delta\alpha$)	S_4 (Δr_{CX})	S_5 ($r_{CX}\Delta\alpha$)
	1928.18	0.37950814	−0.19813167	0.48508783		
	964.99	0.04079931	0.25054195	−0.23152197		
COF_2	584.48	0.01075333	−0.04493011	−0.46314641		
	1250.07				0.40597376	0.64441555
	627.75				−0.05469062	0.51847825
	1827.87	0.38162997	−0.18115573	0.45370953		
	564.75	−0.01264356	−0.21746583	0.30442801		
$CoCl_2$	284.80	−0.00231234	−0.03902969	0.35768890		
	847.87				0.36122393	0.91314027
	439.28				−0.10804602	0.42805826
	1828.04	0.38173152	−0.18141821	0.44672887		
	429.04	−0.00931456	−0.18315612	0.33705956		
$COBr_2$	181.00	−0.00096676	0.02941229	0.24443000		
	757.46				0.33191419	1.1132310
	350.00				−0.11891306	0.36678771

tains two overlapping bands at 626 and 584 cm^{-1} which they assigned to ν_3 and ν_5, respectively, basing their arguments on the relative intensities of the bands in the Raman spectrum, the 620-cm^{-1} band being more intense than the 571-cm^{-1} band. In view of the tenuous nature of their assignment, we have calculated two complete sets of force constants for COF_2; the one using Nielsen's assignment and the other taking ν_3 at 584 and ν_5 at 626 cm^{-1}. Both sets of force constants are given in Table II, and the relative merits of the alternative assignments are discussed in the following.

As already remarked, before proceeding with the actual calculation of force constants it was necessary to supply a value for one of the six. We have explored several possibilities and our final preference is for the set obtained by transferring H_{XX} from the perhaloethylenes[2] (see Table V). A second set of force constants was calculated for each molecule of the type COX_2 by constraining H_{XX} to be zero. Our original intention had been to use this simplified potential function, and our preliminary calculations on $COCl_2$ and $COBr_2$ were encouraging, the transferred force constants giving an excellent fit to COClBr. However, when an attempt was made to use this simplified potential with COF_2, its deficiencies immediately became apparent. Indeed, in our experience the fluorine-containing compounds show considerably more sensitivity to the form of the potential function. We also tried transferring the value of F_{FF} from perfluoroethylene to COF_2 as the F—F distance is almost the same in the two molecules, but under this constraint the other force constants converged to most improbable values—K_F becoming as low as 1.5 md/A.

TABLE V. Urey-Bradley force constants in md/A for ethylene-type molecules (in-plane).

Molecule	K_{CC}	K_{CX}	H_{XX}	H_{CX}	F_{XX}	F_{CX}	C
C_2F_4[a]	8.84	5.20	0.45	0.10	0.67	1.37	−0.09
C_2CL_4[a]	6.98	2.66	0.11	0.07	0.60	0.92	0.61
C_2Br_4[a]	7.01	2.11	0.06	0.05	0.50	0.71	0.21
C_2H_4[b]	7.4	4.7	0.31	0.145	0	0.70	

[a] See footnote 2.
[b] T. Shimanouchi, J. Chem. Phys. 26, 594 (1957).

In our final dump from the computer we calculated the transformation **L** from normal coordinates to symmetry coordinates (the eigenvectors of the secular equation), the transformation from normal coordinates to Cartesian displacement coordinates, and the potential energy distribution of each normal mode in Urey-Bradley configurational space. We also dumped, in each case, the **G** matrix, the **F** matrix, the roots of the secular equation, and the calculated frequencies.

UNSYMMETRICAL MOLECULES, COXY

The potential energy function for the unsymmetrical molecules was taken in the same form as Eq. (1), but in this case there are twelve independent force constants: with the approximation that $F'=-0.1F$, this number is reduced to nine. These were determined by transferring the values just obtained (Table II) and using linear interpolation for K_O, H_{XY}, and F_{XY}, and we show these sets of force constants in Table VI. The ambiguity in the assignment of COF_2 leads to two sets of force constants for each molecule containing fluorine. That designated (ii) is in each case obtained by transferring the COF_2 force constants derived from the Nielsen assignment[12] and the other set (i) from the alternative assignment. These Φ vectors were taken in turn with the appropriate **Z** and **G** matrices in the calculation of vibrational frequencies and the results are summarized in Table VII.

The practice of multiplying by a bond length to scale the angle coordinates leads to complications in the unsymmetrical molecules. As before, it is advantageous to remove the redundancy in the angles, but Eq. (2) no longer accomplishes this because the angles are

TABLE VI. Force constants used in calculation of mixed carbonyl halides, md/A.

CoClF	(i)	(ii)	CoBrF	(i)	(ii)	(iii)	COClBr	(i)
K_O	12.73	12.69	K_O	12.84	12.82	12.84	K_O	12.72
K_F	4.528	4.64	K_F	4.528	4.64	4.528	K_{Br}	1.565
K_{Cl}	1.99	1.99	K_{Br}	1.565	1.565	1.565	K_{Cl}	1.99
H_{FCl}	0.321	0.321	H_{FBr}	0.297	0.297	0.297	H_{BrCl}	0.07
H_{OF}	0.261	0.250	H_{OF}	0.261	0.261	0.261	H_{OBr}	0.104
H_{OCl}	0.145	0.145	H_{OBr}	0.104	0.104	0.104	H_{OCl}	0.145
F_{OF}	1.578	1.298	F_{OF}	1.578	1.298	0.578	F_{OBr}	0.631
F_{OCl}	0.860	0.860	F_{OBr}	0.631	0.631	0.631	F_{OCl}	0.860
F_{FCl}	0.821	1.063	F_{FBr}	0.824	1.066	0.779	F_{BrCl}	0.525

TABLE VII. COXY molecules, observed and calculated frequencies in cm^{-1}. ($\Delta\nu=\nu_{obs}-\nu_{calc}$). The sets designated (i) and (ii) correspond to the alternative sets of force constants (see Table VI).

	ν_{obs}	ν_{calc}	$\Delta\nu$	%	ν_{calc}	$\Delta\nu$	%	
COClF		(i)				(ii)		
	776	762	14	1.8	739	37	4.8	*
	1868	1877	−9	0.5	1876	−8	0.4	
	501	485	16	3.2	486	15	3.0	
	1095	1117	−22	2.0	1116	−21	1.9	
	415	425	−10	2.4	448	−33	8.0	*
		(i)				(ii)		
COBrF	721	731	−10	1.4	702	19	2.6	*
	1874	1876	−2	0.1	1877	−3	0.2	
	398	384	14	3.5	404	−6	1.5	
	1068	1099	−31	2.9	1099	−31	2.9	
	335	374	−39	11.6	382	−47	14.0	*
COBrCl	517	519	−2	0.4				
	1828	1828	0	0				
	240	236	4	1.7				
	806	806	0	0				
	372	371	1	0.3				

necessarily scaled differently. We have used the transformation[13] for the unsymmetrical molecules.

$$S_1=\Delta r_0,$$

$$S_2=\Delta r_X,$$

$$S_3=\Delta r_Y,$$

$$S_4=1/\sqrt{2}(R_{XO}-R_{XY}),$$

$$S_5=1/A[-R_{XO}-R_{XY}+2(r_X/r_Y)R_{YO},$$

redundant coordinate

$$S_6=1/B[R_{XO}+R_{XY}+(r_X/r_Y)R_{YO}], \quad (3)$$

where

$$A=[4(r_X/r_Y)^2+2]^{\frac{1}{2}},$$

$$B=[2+(r_X/r_Y)^2]^{\frac{1}{2}}, \quad (4)$$

and $R_{XO}=r_X\Delta\alpha_{XO}$, $R_{XY}=r_X\Delta\alpha_{XY}$, and $R_{YO}=r_Y\Delta\alpha_{YO}$.

[13] This **U** matrix, although normalized, is not orthogonal, and consequently one is no longer able to substitute **U'** for $\mathbf{U}^{-1}$. Accordingly, we have symmetrized **F** by $\mathfrak{F}=(\mathbf{U}^{-1})'\mathbf{F}\mathbf{U}^{-1}$ rather than the more familiar **UFU'**, which requires orthonormal symmetry coordinates.

In each case we operated on **B** and **G** with (3) and were able to demonstrate that this transformation gave essentially null elements in these matrices for the redundant coordinate, thereby giving us a cross check on some of the geometrical transformations. It should be noted that these coordinates (3) are the ones to be used in interpreting the **L** matrices for the unsymmetrical molecules in Table VIII.

VIBRATIONAL ASSIGNMENT OF COF_2

Before discussing these results in detail, we first consider the assignment of COF_2. As was stated in the preceding, Nielsen *et al.* chose their assignment ($\nu_3=626$ cm^{-1}, $\nu_6=584$ cm^{-1}) so that the A_1 mode has the stronger Raman line: they also noted that this puts the rocking mode at higher frequency than the *s* bending mode. When we first calculated Urey-Bradley force constants from Nielsen's assignment, we were much surprized by the high value of F_{FF}(1.604 md/A) compared with previously obtained values (C_2F_4; $F_{FF}=0.67$ md/A[2], CF_4, etc.; $F_{FF}=1.35$ md/A[1]; we had, in fact, expected a value close to that in C_2F_4. Accordingly, we reversed the assignment of ν_3 and ν_6 and

TABLE VIII. L' matrices, unsymmetrical molecules.

	ν, cm^{-1}	S_1	S_2	S_3	S_4	S_5
	1877.33	0.38025657	−0.14963816	−0.11962609	0.35623365	−0.23741102
	1117.15	0.02920943	0.32996055	−0.18787041	0.28396011	0.57929435
COClF	761.61	0.01733796	0.06508049	0.20373284	−0.46859462	−0.31166544
	485.08	0.00437586	−0.00575749	0.14124634	0.14274351	0.29287982
	424.68	0.00621691	−0.01979349	−0.02882866	−0.24587533	0.34276317
	1876.25	0.38029887	−0.15013201	−0.11948637	0.33667796	−0.22216618
	1099.52	0.03071775	0.33245739	−0.17153374	0.28449274	0.59196057
COBrF	730.69	0.01357487	0.05124932	0.17547726	−0.50813017	−0.41161469
	383.90	0.00700221	−0.01139463	0.10155914	−0.07658195	0.39157079
	373.71	0.00158794	−0.01010338	−0.10492222	−0.19806976	0.14675014
	1827.84	0.38168034	−0.12760624	−0.12878001	0.41383131	−0.23407869
	805.73	0.00277236	−0.22547058	0.26663709	−0.51989834	−0.84466540
COBrCl	518.67	0.01017689	0.11355943	0.15166406	−0.12986113	0.37879652
	370.55	0.00364276	0.12115168	−0.02928164	−0.31436288	−0.20875475
	235.58	0.00149865	−0.03349295	−0.01885081	−0.29008034	0.14159634

TABLE IX. Unsymmetrical molecules COXY. Potential energy distributions in Urey-Bradley space.

COClF	ν cm^{-1}	K_O	K_F	K_{Cl}	H_{FCl}	H_{OF}	H_{OCl}	F_{OF}	F_{OCl}	F_{FCl}	
	1877	89	5	1	2	...	...	1	1	1	
	1117	1	67	10	...	6	6	9	2	1	
	762	1	6	24	5	15	3	38	4	4	*
	485	...	...	29	...	8	7	13	35	8	
	425	...	2	2	26	1	13	1	12	44	*
COBrF	ν cm^{-1}	K_O	K_F	K_{Br}	H_{FBr}	H_{OF}	H_{OBr}	F_{OF}	F_{OBr}	F_{FBr}	
	1876	90	5	1	1	0	0	1	1	1	
	1100	2	70	6	...	6	5	9	2	...	
	731	1	4	15	5	20	5	44	2	3	*
	384	1	1	19	11	1	18	3	42	5	
	374	1	...	21	13	3	3	3	3	54	*
COBrCl	ν cm^{-1}	K_O	K_{Br}	K_{Cl}	H_{BrCl}	H_{OBr}	H_{OCl}	F_{OBr}	F_{OCl}	F_{BrCl}	
	1828	94	1	2	1	...	...	1	1	...	
	806	...	21	37	...	15	16	5	6	−1	
	519	1	13	29	3	...	8	3	37	5	
	371	...	28	2	1	13	5	41	9	1	
	236	...	5	2	16	6	5	2	33	59	

calculated a second set of force constants which is somewhat more appealing because the value of F_{FF} drops to 1.120 and that of F_{OF} rises to 1.578 md/A. This order is the same as that previously found in the chloro compounds, e.g., $F_{OCl}=1.0$[14] and $F_{ClCl}=0.65$ md/A.[1] Also, the fact that the values of the carbon-halogen stretching force constants K_X, obtained in the present analysis, fall between those of the CX_4 type molecules and those of the C_2X_4 type seems to favor that value of F_{XX} in COF_2 which lies between those found in CF_4 and C_2F_4, i.e., F_{FF} (COF_2) = 1.120 md/A).

TABLE X. Summary of Urey-Bradley force constants, md/A.

Molecules	K_O	K_X	H_{XX}	H_{OX}	F_{OX}	F_{XX}
COF_2	12.85	4.528	0.450[a]	0.261	1.578	1.120
$COCl_2$	12.61	1.99	0.11[a]	0.145	0.860	0.523
$COBr_2$	12.83	1.565	0.060[a]	0.104	0.631	0.528

[a] These values assumed and constrained.

[14] I. Nakagawa, I. Ichishima, K. Kurtari, T. Miyazawa, T. Schimanouchi, and S. Mizushima, J. Chem. Phys. **20**, 1720 (1952).

Further evidence supporting the alternative assignment of COF_2 is supplied by the calculations on the unsymmetrical species, COClF and COBrF. While the two alternative sets of force constants yield similar values for the calculated frequencies, in each molecule the agreement of calculated and observed frequencies is slightly better with set (i) than with set (ii). Inspection of Table VI reveals that the two sets of force constants for the unsymmetrical molecules differ significantly only in the values of F_{OF} and F_{XF}, and turning to the distributions of the potential energy in the Urey-Bradley coordinates (Table IX), we see that certain frequencies are strong functions[15] of these particular

[15] It must be admitted that the potential energy distributions we reproduce were calculated from the preferred sets of force constants, i.e., those corresponding to the alternative assignment in COF_2. However, the Nielsen assignment gives very similar distributions, and for this argument the choice is immaterial.

TABLE XI. Symmetric molecules COXY, potential energy distribution in Urey-Bradley space.

COF_2[a]		ν cm^{-1}	K_O	K_F	H_{FF}	H_{OF}	F_{OF}	F_{FF}
		965	4	52	3	1	31	9
	A_1	1928	84	8	3	1	2	1
		584	1	5	32	9	11	43
	B_1	1249	...	81	...	12	8	−1
		626	...	6	...	30	64	...
COF_2[b]		ν cm^{-1}	K_O	K_F	H_{FF}	H_{OF}	F_{OF}	F_{FF}
		965	5	53	2	...	25	15
	A_1	1928	84	9	3	1	2	2
		626	1	1	30	8	11	47
	B_1	1249	...	84	...	11	7	−2
		584	...	6	...	34	60	...
$COCl_2$		ν cm^{-1}	K_O	K_{Cl}	H_{ClCl}	H_{OCl}	F_{OCl}	F_{ClCl}
		567	1	50	4	2	36	7
	A_1	1827	93	3	1	...	2	...
		285	...	6	19	13	8	53
	B_1	849	...	61	...	28	11	−1
		440	...	20	...	23	56	...
$COBr_2$		ν cm^{-1}	K_O	K_{Br}	H_{BrBr}	H_{OBr}	F_{OBr}	F_{BrBr}
		425	1	48	4	4	35	7
	A_1	1828	95	3	...	...	1	...
		181	...	7	12	11	4	66
	B_1	757	...	51	...	38	12	−1
		350	...	31	...	19	51	−1

[a] Present assignment.
[b] See reference 10.

force constants, and hence, the calculated values of these particular frequencies should prove a useful criterion in choosing an assignment for COF_2. In COClF, ν_5 is dominated by F_{FCl} and the deviations between observed and calculated values of this frequency are 1.8% for set (i) and 4.8 for set (ii), thereby indicating a preference for set (i). Similar results are found for the other molecules, and in Table V we have indicated those frequencies which are sensitive to F_{OX} and F_{FX}. In each case, set (i) gives calculated frequencies closer to the observed ones.

Thus, while it is not possible to make an unequivocal assignment, the wealth of evidence favors a reversal of Nielsen's assignment, with ν_2 being taken at 584 cm^{-1} and ν_5 at 626 cm^{-1}. For the purposes of this discussion, we assume the revised assignment to be correct.

DISCUSSION

The force constants of the COX_2 molecules summarized in Table X parallel those of the C_2X_4 molecules (Table IV). The values of K_X are significantly lower in the former series, which fits in well with the relative stabilities.

The constancy of the C—O stretching force constant within the series of carbonyl halides is quite remarkable, the total variation being only about 2%, and is in good agreement with the results of the structure determinations which show the CO bond to be roughly the same length in COF_2, $COCl_2$, and $COBr_2$. (The apparently lower value of K_{Cl} is anomalous, but a similar result is found in the perhaloethylenes which is slightly comforting.) Now Table I shows that the frequencies of the CO stretching vibrations vary over a range of 100 cm^{-1} (i.e., 5%) in going from COF_2 to $COCl_2$ and $COBr_2$, and if all this variation were to be explained by differences in the strength of the CO bond, the variation in K_O would have to amount to 10%, which is clearly contrary to our observations. From where, then, does the high frequency of $\nu_2(COF_2)$ derive?

Halford[16] has shown that the CO stretching frequency of the molecule COX_2 is relatively insensitive to the mass of the atom X and if $m_X > 12$ amu, variations in ν_{CO} stemming from the kinetic energy terms are entirely negligible; therefore, the origin of the high frequency of the CO stretching mode in COF_2 must be sought in the potential energy. Turning to Table XI, where we display the potential energy distributions in Urey-Bradley space, we find that in COF_2 only 84% of λ_2 derives from K_O, the remainder coming from K_F (8%), H_{FF} (3%),

[16] J. O. Halford, J. Chem. Phys. 24, 830 (1956).

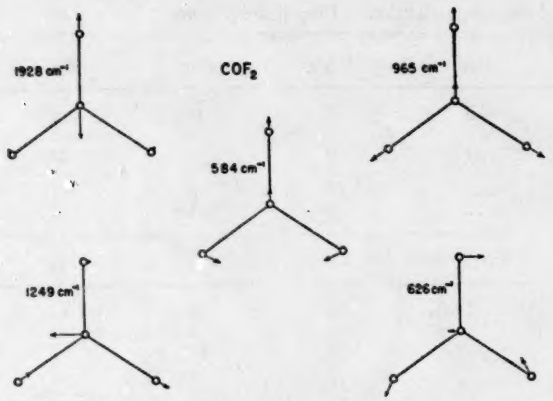

FIG. 1. The normal modes of COF_2 in Cartesian displacements. The displacement vectors, corresponding to unit change in the normal coordinate, are drawn to twice the scale of the interatomic distances.

and F_{OF} (2%). It is the contribution from these work terms over and above the CO stretching constant that causes the frequency of ν_{CO} to be so high. The physical origin of the effect is illustrated most strikingly in Fig. 1 which shows the relative displacements of the atoms in the different normal vibrations of COF_2. In ν_2 we note that as the CO bond stretches, the carbon atom moves back into the two fluorine atoms, thereby compressing the CF bonds and opening up the FCF angle.[17] Now, in COF_2 the force constants associated with these secondary displacements are relatively large, and consequently, these work terms make an extraordinary contribution to ν_2. The 2% contribution from F_{OF} is not unusual, cf. $COCl_2$ and $COBr_2$.

A puzzling feature of these results is the high value of F_{FF} in COF_2 compared with the values of the corresponding force constants in the C_2X_4 series. In view of the assumptions made about the form of the F_{FF} potential (i.e., that $F'=-0.1F$), this could indicate either that the potential energy hypersurface has higher curvature in this coordinate, corresponding to greater overlap between the two fluorine atoms, or that the slope of the potential energy is greater, indicating a much larger repulsive term in COF_2 than in C_2F_4. Neither explanation is particularly compatible with the chemical facts and known structures which suggest that the two values of F_{FF} should have similar magnitudes, and our result may well be due to a deficiency of the simplified potential function.

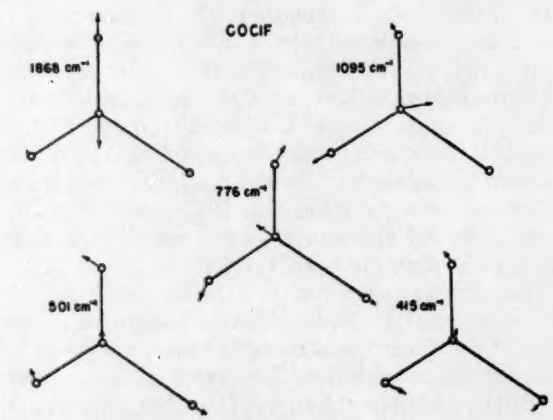

FIG. 2. The normal modes of COClF in Cartesian displacements. Vectors twice the scale of interatomic distances. Note that there is no single vibration corresponding to the symmetric stretch in Fig. 1.

[17] The same argument applies, *mutatis mutandis*, for compression of the CO bond.

For each molecule, we routinely calculated the normal coordinates expressed in terms of the symmetry coordinates and also in terms of Cartesian displacements. The latter are much easier to visualize, particularly in the case of a planar molecule, when they may be plotted out so as to display the normal modes pictorially. From our results, we have selected the pictures of COF_2, COClF, and COBrCl, which we reproduce in Figs. 1–3. Figure 1, which is typical of all the COX_2 molecules, shows that the popular descriptions of the vibrations of the symmetric molecules, *viz.*, CO stretch, symmetric CX stretch, XCX bend, asymmetric CX stretch, and CO rock, correspond reasonably well with the true normal modes. However, the vibrations of the unsymmetrical molecules are more complex as may be seen in Figs. 2 and 3, and although ν_1 may be fairly accurately described as an XCY asymmetric stretch, there is no single vibration which may be assigned as the corresponding symmetric stretch, but this coordinate, mixed up with the bending motions, contributes to both ν_3 and ν_4.

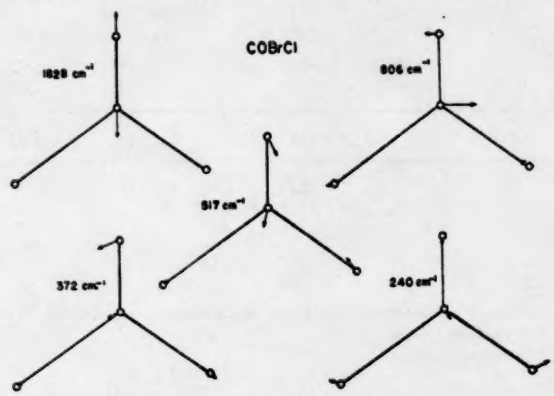

FIG. 3. COBrCl; Normal modes expressed in Cartesian displacements. Displacement vectors twice the scale of interatomic distances.

TRANSFERABILITY OF UREY-BRADLEY FORCE CONSTANTS

In conclusion, it is pertinent to review the results of these calculations in an evaluation of the transferability of Urey-Bradley force constants, both within this series of closely related molecules and in the much more gen-

eral field of carbonyl- and halogen-containing molecules. Referring to Table VII, we find that the vibrational frequencies COBrCl calculated from the transferred force constants are in quite good agreement with the observed frequencies, and our results for COClF are almost as encouraging. Mann, Meal, Fano, and Shimanouchi met with similar success when they transferred Urey-Bradley force constants from the symmetrical perhaloethylenes to the mixed chlorofluoroethylenes.

COBrF does not show particularly good agreement between observed and calculated frequencies, but we note that the differences are systematically negative, i.e., the calculated frequency is invariably too high. The discrepancy is most serious in ν_5 which, by Table IX, contains a major contributions from F_{FBr}. It would be possible to alleviate this discrepancy by lowering this particular force constant, remembering that it was obtained from COF_2 and $COBr_2$ by linear interpolation, but it also appears from the general trend of the calculated frequencies that the molecule is, in general, somewhat "looser" than a linear hybrid of COF_2 and $COBr_2$.

With these reservations, we conclude that Urey-Bradley force constants may be transferred within the carbonyl halide series to give fairly accurate representations of the potential energy. Further studies on the acetyl halides are presently in hand, and we hope to fit these into the same scheme as the carbonyl halides.

On the broader question of the transferability of Urey-Bradley force constants to molecules outside this limited series, it is not yet possible to formulate general principles. Comparison of the present results with the perhaloethylenes reveals marked parallels, but it is obvious that there are significant differences. We hope to use the present technique of machine computation to accumulate many data on different molecules and to correlate empirically some of these differences in the Urey-Bradley force constants with other structural parameters and so facilitate their transfer.

ACKNOWLEDGMENT

We should like to thank Dr. L. K. Frevel and Dr. W. J. Potts for helpful discussions and Dr. M. Nakamura for his invaluable assistance in interpreting the Japanese papers.

Computation of the Equilibrium Composition of Burnt Gases

ROBERT L. POTTER* AND WOUTER VANDERKULK†

Bell Aircraft Corporation, Buffalo, New York

(Received May 15, 1958)

The multicomponent chemical equilibrium composition problem is discussed generally and a formulation of it is presented in a form suitable for digital computer calculations. A geometric interpretation of the equations used to specify the chemical system is also given.

1. INTRODUCTION

WITH the advent of high-speed computing machines it has become feasible to formulate and solve problems involving the equilibrium composition attained in multicomponent homogeneous and heterogeneous systems. The solutions thus obtained are useful in flame temperature, detonation, and shock calculations, and in the analysis of engine cycles. Several such programs have been formulated and published.[1] A computational method is being developed at Bell Aircraft Corporation, which has features that are in some ways similar to methods developed by Brinkley[1] and by Huff *et al.*[1]; however, there are distinct features in it that are unusual. Because this problem is important and evokes continued interest, it seems appropriate to communicate at this time some of the methods which have proven satisfactory to date. After this was written and submitted to this journal the article by White, Johnson, and Dantzig[2] came to the attention of the authors.

The plan will be to discuss the specification of the system first in familiar terms, and then it will be shown how these equations may be transformed into the new forms required in the present scheme. Like Brinkley, it is found convenient to focus attention on certain species and to call these components. It is found that a very simple system for ideal gases results when the sum of the mole fractions in the gas phase is used as the dependent variable, and the chemical potentials are used as independent variables. In particular, the component conservation equations are related to the components of the gradient of the sum of the mole fractions of gas species in chemical potential space. The proof of this is given for the general case, and the results then are specialized to the ideal gas case. The number of equations specifying the system is one greater in general than those required by Brinkley, because he removes algebraically the total number of gas moles by normalizing the components to one. However, the procedure of normalizing the components to one is not always possible over the entire range of mixture strengths for all choices of components. It turns out to be just as convenient to keep the extra equation and the extra unknown. Further, it is not necessary to separate the program into various parts depending on mixture strength, thus resulting in use of different components at various mixture strengths. With the use of one set of components, a simple initial value program is required to give suitable starting values for the iteration procedure. It also turns out to be possible to treat solids within the same framework. The rapidity of the program is remarkable, even with the inclusion of the extra equation specifying the system.

2. SYSTEM SPECIFICATIONS

A chemical system, at a fixed pressure and temperature, is specified by the moles of all the species present, n_i, $i=1, \cdots N$. Of these, any independent set of M may be chosen as components. These are the "ultimate components" of Gibbs.[3] Then, if a denotes gaseous component, λ_{ia} is the coefficient of component a exhibiting the production of species i. The component balance equations are

$$q_a=\sum_{i=1}^{N}\lambda_{ia}n_i, \quad a=1, \cdots M, \tag{2-1}$$

where the q_a is the moles of component a. The sum is to extend over all phases. Brinkley[1] normalizes the q_a. However, this is not always possible for a particular choice of components. If some of the species are ionized gases and free electrons are present, it is convenient to choose electrons as a new component, and if the gas is electrically neutral, setting q (electrons)$=0$ automatically satisfies the requirements of electrical neutrality. In case solids are formed, it is not necessary

* Present address: American Cyanamid Co., Stamford, Conn.

† Present address: IBM Corp., Dept. 513, Owego, New York.

[1] S. R. Brinkley, Jr., J. Chem. Phys. **14** 563, 686 (1946); **15** 113 (1947); S. R. Brinkley, Jr., and B. Lewis, U. S. Bureau of Mines Report Investigation 4806 (1952); S. R. Brinkley, Jr., Ind. Eng. Chem. **43** 2471 (1951). S. R. Brinkley, Jr., *High Speed Aerodynamics and Jet Propulsion* (Princeton University Press, Princeton, N. J., 1956), Part 1, Sec. C; *Combustion Processes*, ibid, Vol. II. F. J. Krieger and W. B. White, J. Chem. Phys. **16**, 358 (1948); V. N. Huff and C. S. Calvert, NACA TN 1653 1948); P. F. Winternitz, *Third Symposium on Combustion and Flame and Explosion Phenomena*, (Williams and Wilkins, Baltimore, Maryland, 1949), p. 623. D. S. Villars, NAVORD Rept. 5326 (October 16, 1956). Huff, Gordon, and Morrell, NACA Rept. 1037 (1951). J. S. Martinez and G. W. Elverum, Jr., Jet Propulsion Laboratory, California Institute of Technology Memo 20-121, (1955). N. M. Williams and W. S. McEwan, NAVORD Rept. 3421 (January 12, 1955).

[2] White, Johnson, and Dantzig, J. Chem. Phys. **28** 751 (1958).

[3] *The Collected Works of J. Willard Gibbs* (Longmans, Green and Company, Inc., New York, 1931), Vol. 1, p. 172.

to choose them as components, however, species that coexist in gas and condensed phases cannot simultaneously be chosen as components.

3. THERMODYNAMIC EQUILIBRIUM EQUATIONS

The Gibbs free energy, G, is minimized subject to the constraints Eq. (2-1). There result linear relations between the chemical potentials μ, thus,

$$\mu_i = \sum_a \lambda_{ia}\mu_a. \tag{3-1}$$

These can be transformed into the familiar equations involving the n_i, the pressure p, and the temperature T. There are a total of N equations between Eqs. (2-1) and (3-1), and hence the N unknowns n_i can be solved, assuming p and T are known.

4. EQUATIONS IN TERMS OF CHEMICAL POTENTIALS

We shall, in the present section, rewrite the equations of Secs. 2 and 3 in terms of the chemical potentials μ_a of the gaseous components. We split G into G_g for the gas phase, and $\mu_{i_c}{}^0 n_{i_c} + \cdots$ for the condensed phases where g denotes gas and c condensed phase. We assume each solid species forms a separate phase. G_g further can be written as $n\phi$ where ϕ is the free energy per mole and n is the sum of the moles of gaseous species. We define a chemical potential by

$$\mu_{i_g}' = (\partial\phi/\partial y_{i_g}) + \frac{\phi - \sum_j y_{j_g}(\partial\phi/\partial y_{j_g})}{\sum y_{j_g}}, \tag{4-1}$$

which reduces to μ_{i_g} at $\sum y_{j_g} = 1$. The y_j are the mole fractions of j in the gas phase. The y_{j_g} can be obtained from the μ_{i_g}'. We further define a function,

$$F = \sum_{i_g=1}^{N_g} y_{i_g}. \tag{4-2}$$

It follows that

$$\sigma dF = -\sum_{i_g} y_{i_g} d\mu_{i_g}' + (\partial\phi/\partial p)_{y_{i_g},T} dp + (\partial\phi/\partial T)_{y_{i_g},p} dT, \tag{4-3}$$

in which

$$\sigma = \frac{\phi - \sum_j y_{j_g}(\partial\phi/\partial y_{j_g})}{\sum_{j_g} y_{j_g}}. \tag{4-4}$$

In case ϕ is given by

$$\phi = \sum_{i_g} y_{i_g}[\mu_{i_g}{}^0(T) + RT \ln p y_{i_g} + \mu_{i_g}{}^E(y_{j_g}, p, T)] \tag{4-5}$$

where $\mu_{i_g}{}^E$, the excess chemical potential, is homogeneous of degree zero in the y_{j_g}, Eq. (4-4) reduces to

$$\sigma = -RT.$$

At equilibrium, in view of Eq. (3-1), it follows that

$$-\sigma(\partial F/\partial \mu_a') = \sum_{i_g}^{N_g} \lambda_{i_g a} y_{i_g}. \tag{4-6}$$

And in view of Eq. (2-1), it is seen that

$$-\sigma(\partial F/\partial \mu_a')_{\mu_a' - \mu_a} = (q_a/n) - \sum_{i_c} \lambda_{i_c a} \cdot (n_{i_c}/n), \qquad a = 1, \cdots M. \tag{4-7}$$

The left-hand side of this is related to the components of the gradient of the sum of the mole fractions of the gas in chemical potential space. Equation (4-6) cannot be obtained using the normal definition of μ_{i_g}. Equation (4-1) has the advantage that the form of μ_{i_g}' is identical with μ_{i_g} even when F does not equal one. It is important to note that during the iteration procedure developed below F only attains one at the conclusion of the iterations. The set of equations to be solved is then Eq. (4-7), Eq. (4-2), specialized so that $F = 1$, and Eq. (2-1) for each solid phase formed from gaseous components. Thus, the equations are

$$\text{(i)} \quad \sum_{a=1}^{M} \lambda_{i_c a}\mu_a = \mu_{i_c}{}^0 \quad (N_c \leq M-1)$$

$$\text{(ii)} \quad F(\mu_a', p, T)_{\mu_a' - \mu_a} = 1 \quad (1)$$

$$\text{(iii)} \quad -\sigma(\partial F/\partial \mu_a')_{\mu_a' - \mu_a} = (q_a/n) - \sum_{i_c} \lambda_{i_c a}(n_{i_c}/n) \quad (M) \tag{4-8}$$

from which n_{i_c}/n, $1/n$, and μ_a can be solved as functions of p and T. Once μ_a is known as a function of p and T, the mole fractions y_j can be obtained.

There is some duality between the system (2-1), and (3-1), on the one hand, and the system described above. The first system is obtained by *minimizing* a nonlinear function, G, on a *linear* $(N-M)$-dimensional space defined by the balance of matter equations, the second system is obtained by *maximizing*

$$G = \sum_{a=1}^{M} q_a \mu_a'$$

on the *nonlinear* $(M-1-N_c)$-dimensional surface Y defined by Eqs. (4-8) (i) and (ii).

The $(M-1)$-dimensional surface Z defined by $F = 1$ is convex; moreover, it is "open," i.e., is unbounded. Since Y is the intersection of Z with the linear space defined by Eq. (4-8) (i), Y is also convex. However, Y can be open or closed depending on the direction of the linear space

$$\sum_{a=1}^{M} \lambda_{i_c a}\mu_a = \mu_{i_c}.$$

In case condensed phases are present, this set of equations will have one solution μ_a when Y is open and will possess two solutions when Y is closed. The following criterion, in the case of ideal gases, will discriminate between these two possibilities in the event only one species is allowed to coexist in both gas and condensed phases. Let S be this species. If S lies outside the convex cone spanned by all the remaining species,

then only one solution is possible. Otherwise, two solutions are possible. The convex cone is defined as the collection of all vectors of the form

$$k_1 S_{i_1} + \cdots k_K S_{i_K}; \qquad k_1 \geq 0, \cdots k_K \geq 0 \quad (4\text{–}9)$$

where S_i denotes a mole of species i.

It can be also shown that the Eq. (4–8) will admit a solution if it is true that the vector

$$\sum_{a=1}^{M} q_a S_a$$

lies in the interior of the convex cone spanned by all the species S_i in the system.

5. ITERATION EQUATIONS FOR IDEAL GASES

In the event the gas phase is ideal then the function G_g in Sec. 4 is defined (with the $\mu_i^E = 0$) by

$$G_g = \sum_{i_g} n_{i_g} [\mu_{i_g}^0(T) + RT \ln p(n_{i_g}/n)] \quad (5\text{–}1)$$

where n is the sum of moles of gas. From this we see that ϕ can be chosen as follows;

$$\phi = \sum_{i_g} y_{i_g} (\mu_{i_g}^0 + RT \ln p y_{i_g}). \quad (5\text{–}2)$$

Solution of y_{i_g} in terms of μ_{i_g}' yields

$$y_{i_g} = p^{-1} \exp[(\mu_{i_g}' - \mu_{i_g}^0)/RT]. \quad (5\text{–}3)$$

Hence, utilizing Eq. (3–1), y_{i_g} is described as a function of the μ_a' by the formula,

$$y_{i_g} = p^{-1} \exp[-(\mu_{i_g}^0/RT) + \sum_a \lambda_{i_g a} \cdot (\mu_a'/RT)] \quad (5\text{–}4)$$

and F by

$$F = \sum_{i_g} p^{-1} \exp[-(\mu_{i_g}^0/RT) + \sum_a \lambda_{i_g a} \cdot (\mu_a'/RT)]. \quad (5\text{–}5)$$

Introducing

$$Z_a = -\ln p + [(\mu_a' - \mu_a^0)/RT] = \ln(n_a/n), \quad (5\text{–}6)$$

we can write Eq. (5–4) as follows,

$$n_{i_g}/n = K_{i_g} \exp(\sum_a \lambda_{i_g a} Z_a) \quad (5\text{–}7)$$

where

$$K_{i_g} = p^{[-1+\sum_a \lambda_{i_g a}]} \cdot \exp(-\mu_{i_g}^0 + \sum_a \lambda_{i_g a} \mu_a^0)/RT, \quad (5\text{–}8)$$

F can be described in terms of Z_a by

$$F = \sum_{i_g} K_{i_g} \exp(\sum_a \lambda_{i_g a} Z_a), \quad (5\text{–}9)$$

and the Eq. (4–8) becomes

$$\text{(i)} \quad -\ln K_{i_c} = (\mu_{i_c}^0 - \sum_a \lambda_{i_c a} \mu_a^0)/RT - \sum_a \lambda_{i_c a} \cdot \ln p = \sum_a \lambda_{i_c a} Z_a,$$

$$\text{(ii)} \quad F(Z_a, p, T) = 1,$$

$$\text{(iii)} \quad \partial F/\partial Z_a = (q_a/n) - \sum_a \lambda_{i_c a} (n_{i_c}/n). \quad (5\text{–}10)$$

The Eqs. (5–10) can be solved numerically by an iteration method obtained by linearization of F. However, more rapid convergence is obtained by first rewriting Eq. (5–10) in terms of the function $f = \ln F$, and then linearizing f. The reason for this is that of the two convex functions F and f, f is 'more' linear than F, i.e., f has smaller second derivatives than F. For the system of equations involved here, savings of 50% in the number of necessary iterations were experienced when using f instead of F.

Let $Z_a^{(k)}$ denote the kth approximation to the solution Z_a of Eq. (5–10). Then the kth approximation, $y_{i_g}^{(k)}$ to the mole fraction n_{i_g}/n of the gaseous species S_{i_g} can be computed from Eq. (5–7).

The kth approximation for $1/n$ and n_{i_c}/n may be found by solving N_c+1 of the Eq. (5–10) (iii). The adequacy of the kth approximation can be tested by substitution of this approximation into Eq. 5–10, and by comparing the left sides of the equations so obtained with the corresponding right sides. If it is necessary to calculate a $(k+1)$st approximation one can proceed as follows,

$$\xi_a = Z_a^{(k+1)} - Z_a^{(k)}. \quad (5\text{–}11)$$

Then, linearization of Eq. (5–10), using f in place of F, i.e.,

$$f^{(k+1)} = f^{(k)} + \sum_a (\partial f/\partial Z_a) \xi_a = 0,$$

yields the following equations

$$\text{(i)} \quad \sum_a \lambda_{i_c a} \xi_a = 0,$$

$$\text{(ii)} \quad F^{(k)} \cdot \ln F^{(k)} + \sum_a F_a^{(k)} \xi_a = 0, \quad (5\text{–}12)$$

$$\text{(iii)} \quad F_a^{(k)} \cdot (1 + \ln F^{(k)}) + \sum_b F_{a,b}^{(k)} \xi_b = \nu q_a - \sum_{i_c} \lambda_{i_c a} \nu_{i_c}$$

where

$$F^{(k)} = \sum_{i_g} y_{i_g}^{(k)}; \qquad F_a^{(k)} = \sum_{i_g} \lambda_{i_g a} y_{i_g}^{(k)},$$

$$F_{a,b}^{(k)} = \sum_{i_g} \lambda_{i_g a} \lambda_{i_g b} y_{i_g}^{(k)}; \quad \nu = 1/n; \quad \nu_{i_c} = n_{i_c}/n. \quad (5\text{–}13)$$

From the N_c+1+M Eq. (5–12), one can solve for ξ_a. From this one can find $Z_a^{(k+1)}$ [cf. Eq. (5–11)] and

repeat the cycle. This iterative technique presupposes a fixed pressure and temperature.

To illustrate how solids are handled, we shall discuss the case of carbon which is allowed to coexist in the gas and condensed phase. Calculations are permitted under either one of the hypotheses: solid carbon present and solid carbon absent. Usually, such information is available. However, near the boundary where solid carbon forms, such information is not readily obtainable. In order to handle these cases near the solid carbon boundary, a feature is added to the program by means of which at the end of each calculation, the hypothesis inserted at the start of the calculation can be checked in order to be sure it is indeed correct. If incorrect, the computer automatically restarts the calculation with the correct hypothesis. The mechanism used for this feature will now be described.

If solid carbon present is assumed, the computer tests whether n_{C_s}/n is positive. If not, the computer is automatically instructed to repeat the calculation with solid carbon absent as hypothesis. If solid carbon absent is assumed, the computer tests whether the partial pressure pn_{C_g}/n, of carbon gas exceeds the vapor pressure of solid carbon at the temperature specified. If so, the computer automatically repeats the calculations with solid carbon present as hypothesis.

6. INTERATION EQUATIONS FOR NONIDEAL GASES

When the gaseous species are nonideal, the function ϕ introduced in Sec. 4 is given by Eq. (4–5) where the quantities $\mu_{i_g}{}^E$, instead of being zero as in the ideal gas case, are known functions of the y_{j_g}, p, and T. As a consequence, explicit analytical determination of y_{j_g} and F as functions of μ_a', p, and T becomes cumbersome, if not impossible. Yet it is still possible to use substantially the same iterative technique used for ideal gases and discussed in Sec. 5.

For nonideal gases parameters K_{i_g}' are necessary, similar to those defined by Eq. (5–8), which not only are functions of p and T, but also depend on the mole fractions n_{j_g}/n. We shall represent K_{i_g}' by

$$K_{i_g}'=\Psi_{i_g}(n_{j_g}/n, p, T)=K_{i_g}\cdot\exp\Big(\sum_a \lambda_{i_g a}\mu_a{}^E-\mu_{i_g}{}^E\Big) \tag{6-1}$$

where the right-hand side must be thought of as a *known* function of the N_g+2 parameters n_{j_g}/n, p, T. The K_{i_g} are defined by Eq. (5–8). The iterative technique proposed for the nonideal case is the same as that for ideal gases with the exception that the K_{i_g}''s after each iteration must be 'updated' with the information gained from the previous iteration. This can be done in various ways. We shall outline here two different methods.

Let us by $K_{i_g}{}'^{(k)}$, $y_{i_g}{}^{(k)}$, and $Z_a{}^{(k)}$ denote the kth estimates for K_{i_g}', n_{i_g}/n, and Z_a. Before executing the next iteration, new estimates $K_{i_g}{}'^{(k+1)}$ can be obtained by using either the formula

$$K_{i_g}{}'^{(k+1)}=\Psi_{i_g}(y_{j_g}{}^{(k)}, p, T) \tag{6-2}$$

where

$$y_{i_g}{}^{(k)}=\Psi_{i_g}(y_{j_g}{}^{(k-1)}, p, T)\exp\Big(\sum \lambda_{i_g a}Z_a{}^{(k)}\Big),$$

or the formulas

$$K_{i_g}{}'^{(k+1)}=\Psi_{i_g}(\bar{y}_{j_g}{}^{(k)}, p, T), \tag{6-3}$$

and

$$\bar{y}_{j_g}{}^{(k)}=\Psi_{i_g}(y_{j_g}{}^{(k)}, p, T)\exp\Big(\sum_a \lambda_{i_g a}Z_a{}^{(k)}\Big). \tag{6-4}$$

Statistical Mechanical Theory of the Diffusion Coefficients in Binary Liquid Solutions

RICHARD J. BEARMAN

Department of Chemistry, University of Kansas, Lawrence, Kansas

(Received November 17, 1959)

The statistical mechanical theory of the diffusion coefficients in binary liquid solutions is developed from the viewpoint of the pair space linear relations. Equations for the composition dependence of the ratios of the friction and diffusion coefficients are developed. For solutions which are regular it is found that the ratio of the two self-diffusion coefficients is in the inverse ratio of the corresponding molar volumes. The assumptions of the theory are discussed critically.

I. INTRODUCTION

THE complexity of the diffusion process in liquids has led to the development of numerous theories, each designed to explain or elucidate some given aspect of the phenomenon.[1] The researches of Fick paved the way to various formal descriptions which have culminated in the development of the so-called phenomenological relations that serve to describe heat conduction and thermal transport of matter as well as ordinary diffusion. The classical investigations of Einstein on the theory of Brownian motion[2] have stimulated the study of diffusion as a manifestation of the irregularity of molecular motion. In the more recent past, Eyring and his school[3] have fruitfully regarded diffusion as an activated rate process analogous to those of chemical kinetics and have achieved rather useful results based upon the cell model of the liquid state.

Recently, we have succeeded in deriving the hydrodynamic equations of transport for multicomponent fluid systems from the Liouville theorem of statistical mechanics and have obtained the phenomenological relations from the exact equations by the postulation of linear expressions for the distribution functions in terms of the velocities of the components and gradient of temperature.[4] Explicit evaluation of transport coefficients is not to be achieved from such general considerations, and, viewed in this perspective, the objective of more detailed theories is to determine the precise forms of the nonequilibrium distribution functions. To accomplish this, it has been assumed variously that only binary collisions are of importance, that it suffices to use the equilibrium distribution functions, or that cell or lattice models accurately describe the molecular configuration of the liquid state. We have been able to avoid these hypotheses by the introduction of a plausible assumption that falls within the spirit of the linear phenomenological theory and which we believe to have considerable merit. To introduce it, we first observe that the average force plays an important role in determining the motion of a fluid. Thus, we have found it possible[4] to define a mean frictional force $\mathbf{F}_\alpha^{(1,1)*}$ on a molecule of species α in a ν component system, such that, isothermally,

$$\mathbf{F}_\alpha^{(1,1)*} = -\sum_{\beta=1}^{\nu} c_\beta \zeta_{\alpha\beta}(\mathbf{u}_\alpha - \mathbf{u}_\beta), \tag{1.1}$$

where $\mathbf{u}_\alpha$ is the mean velocity of species α, c_α is the concentration of the species and $\zeta_{\alpha\beta}$ are well-defined friction coefficients. The principal assumption, mentioned in the foregoing, consists of two parts and is concerned with the mean frictional force $\mathbf{F}_{\alpha\beta,1}^{(2,1)}$ on a molecule of species α under conditions when a second molecule of species β is located in its neighborhood. We assume first that it is a linear function of the average velocity $\mathbf{u}_{\alpha\beta,1}^{(2)}$ of α in the presence of β, with associated friction tensors $\boldsymbol{\zeta}_{\alpha\beta,\gamma\nu}^{(2)}$. Secondly, we replace the friction tensors, which in principle depend upon the distance between the two molecules, by their values at large distances where they are simply related to the ordinary friction coefficients $\zeta_{\alpha\beta}$. In physical terms, we suppose that the mean frictional force on α in the presence of β is related to the velocities in precisely the same way as in its absence, provided that the correct average velocity of α, namely, $\mathbf{u}_{\alpha\beta,1}^{(2)}$, is introduced. Stated thus physically, the assumption has considerable intuitive appeal combined with the virtue of simplicity. Using it, we derive a differential equation which relates the nonequilibrium pair correlation function to the radial distribution function, and this then permits the expression of the transport parameters as averages over equilibrium ensembles.

We have previously applied our technique to the study of the heat of transport,[5] thermal conductivity,[6] and thermal diffusion[7] in binary solutions. In these theories the diffusion coefficients have arisen as parameters which must be evaluated experimentally. We now find again that we cannot predict the magnitude of the diffusion and friction coefficients. We are able to obtain,

[1] For a recent review of some of the current theories as well as a summary of available experimental data, we refer the reader to P. A. Johnson and A. L. Babb, Chem. Revs. **56**, 387 (1956).

[2] A. Einstein, *Investigations on the Theory of the Brownian Movement* (Dover Publications, Inc., New York, 1956).

[3] S. Glasstone, K. J. Laidler, and H. Eyring, *The Theory of Rate Processes* (McGraw-Hill Book Company, Inc., New York, 1941).

[4] R. J. Bearman and J. G. Kirkwood, J. Chem. Phys. **28**, 136 (1958).

[5] R. J. Bearman, J. G. Kirkwood, and M. Fixman, Advances in Chem. Phys. **1**, 1 (1958).

[6] R. J. Bearman, J. Chem. Phys. **29**, 1278 (1958).

[7] R. J. Bearman, J. Chem. Phys. **30**, 835 (1959).

however, equations for their ratios which are of interest in their own right. Furthermore, only the ratios of self-diffusion coefficients appear in the equations for the heat of transport and thermal diffusion factor, so that it becomes possible to express these coefficients entirely in terms of equilibrium parameters. The reader may prove this readily by substituting our present results into the formulas derived in the references.

Because the equilibrium theory of solutions is as yet incomplete, we introduce further simplifying assumptions to obtain numerical results. In the present instance, we find that for solutions which in a certain sense are regular the ratio of the two self-diffusion coefficients are in the inverse ratio of the molar volumes of two components. However, our general results, although unwieldy, do not depend upon the hypotheses of any specialized solution theory.

It is a feature of our approach that the diffusion coefficients can be treated independently of the viscosity coefficient. In our treatment of viscous flow, which we hope to publish later, the familiar products of the viscosity coefficient and diffusion coefficients do appear.

II. PHENOMENOLOGICAL THEORY

Diffusion exists when the components of a system undergo relative motion. Its magnitude at a point of interest is measured in terms of the fluxes of each component across a plane moving with an arbitrary velocity. For theoretical purposes,[8] the most convenient velocity is that of the center of mass which we may denote by $\mathbf{u}$, and the flux of α is then $c_\alpha(\mathbf{u}_\alpha-\mathbf{u})$. However, in experimental arrangements, the volume velocity $\mathbf{u}^0$, defined by the relation

$$\mathbf{u}^0=\sum_{\alpha=1}^{r}c_\alpha\bar{v}_\alpha\mathbf{u}_\alpha \tag{2.1}$$

may often be taken to be zero,[9] so that diffusion coefficients are measured with reference to it. For this reason we shall be concerned in this paper solely with the diffusion fluxes $\mathbf{j}_\alpha\equiv c_\alpha(\mathbf{u}_\alpha-\mathbf{u}^0)$. These are evidently subject to the condition

$$\sum_\alpha\bar{v}_\alpha\mathbf{j}_\alpha=0. \tag{2.2}$$

Mutual Diffusion

Restricting ourselves to the case of two components, we may write the phenomenological equations for isothermal mutual diffusion[8]

$$-\mathbf{j}_\alpha=\sum_{\beta=1}^{2}\Omega_{\alpha\beta}\nabla\mu_\beta,\qquad\alpha=1,2, \tag{2.3}$$

where μ_β are the chemical potentials and $\Omega_{\alpha\beta}$ are the phenomenological coefficients. When in addition the system is at uniform pressure, Fick's law follows from Eq. (2.3) and the Gibbs-Duhem equation,

$$-\mathbf{j}_1=D\nabla c_1 \tag{2.4}$$

$$D=\frac{1}{c_2}\left(\frac{\partial\mu_1}{\partial c_1}\right)_{T,P}(c_2\Omega_{11}-c_1\Omega_{12}),$$

where T is absolute temperature and p is pressure. An alternative diffusion coefficient may be defined by writing Fick's law for the second component, but by Eq. (2.2) and the relationship

$$\bar{v}_1\nabla c_1+\bar{v}_2\nabla c_2=0 \tag{2.5}$$

it also is equal to D. In other frames of reference the two coefficients will not be equal.

Strictly speaking, there exists a slight approximation in the application of Fick's law under the assumption that the volume velocity is zero. For, when it vanishes, the center of mass velocity $\mathbf{u}$ does not, and by the Newtonian equation of motion[8] a gradient of pressure will in general be present. This gradient then contributes to the phenomenological equation, creating an additional term in Fick's law. In practice, the correction is usually completely negligible.

Self-Diffusion

Self-diffusion is the name given to the diffusion through a system, otherwise in equilibrium, of a trace of a substance identical with one of the components, save for some trivial distinguishing characteristic. It is described by a Fick's law equation for the motion of the trace component. For example, denoting the labeled component corresponding to the first component by 1*, we have

$$-\mathbf{j}_{1*}=D_1\nabla c_{1*} \tag{2.6}$$

$$\mathbf{j}_{1*}=c_{1*}\mathbf{u}_{1*}$$

where D_1 is the self-diffusion coefficient of component 1.

III. STATISTICAL MECHANICAL THEORY

The mean nonequilibrium force $\mathbf{F}_\alpha^{(1)}$ on a molecule of species α may be represented as the sum of the average forces exerted by all other molecules in the system,[4,6]

$$c_\alpha\mathbf{F}_\alpha^{(1)}=\sum_{\beta=1}^{r}\int\frac{dV_{\beta\alpha}}{dr}\frac{\mathbf{r}}{r}c_{\alpha\beta}^{(2)}(\mathbf{r}_1,\mathbf{r})\,d^3\mathbf{r}, \tag{3.1}$$

where $V_{\beta\alpha}(r)$ is the potential of intermolecular force, assumed central and pairwise additive, between molecules of species α and β, $\mathbf{r}\equiv\mathbf{r}_2-\mathbf{r}_1$ is the position, with magnitude r, of the center of mass of the β molecule at $\mathbf{r}_2$ relative to that of the α molecule at $\mathbf{r}_1$, and $c_{\alpha\beta}^{(2)}(\mathbf{r}_1,\mathbf{r})$, defined more completely in the references, is the density in pair configuration space of molecules of species α at $\mathbf{r}_1$ and β at $\mathbf{r}_2$. The integral in Eq. (3.1) may be represented with trivial inaccuracy as the sum of two

[8] R. J. Bearman, J. Chem. Phys. **28**, 662 (1958).
[9] L. J. Gosting, Advances in Protein Chem. **11**, 429 (1956).

terms, the first of which leads to the phenomenological equations for the heat and matter fluxes while the second leads to the Newtonian stress tensor,[4,6]

$$c_\alpha \bar{\mathbf{F}}_\alpha^{(1)} = c_\alpha \bar{\mathbf{F}}_\alpha^{(1)*} + \tfrac{1}{2}\nabla_{r_1} \cdot \sum_{\beta=1}^{\nu} c_\alpha(\mathbf{r}_1) c_\beta(\mathbf{r}_1) \int \frac{\mathbf{r}\mathbf{r}}{r} \frac{dV_{\beta\alpha}}{dr} g_{\beta\alpha}^{(2)}(\mathbf{r}_1, \mathbf{r}) d^3\mathbf{r},$$

$$c_\alpha \bar{\mathbf{F}}_\alpha^{(1)*} = \tfrac{1}{2} \sum_{\beta=1}^{\nu} c_\alpha(\mathbf{r}_1) c_\beta(\mathbf{r}_1) \int \frac{\mathbf{r}}{r} \frac{dV_{\beta\alpha}}{dr} [g_{\alpha\beta}^{(2)}(\mathbf{r}_1, \mathbf{r}) - g_{\beta\alpha}^{(2)}(\mathbf{r}_1, \mathbf{r})] d^3\mathbf{r}, \quad (3.2)$$

$$g_{\alpha\beta}^{(2)}(\mathbf{r}_1, \mathbf{r}) \equiv c_{\alpha\beta}^{(2)} / c_\alpha(\mathbf{r}_1) c_\beta(\mathbf{r}_2).$$

In Eq. (3.2), $g_{\alpha\beta}^{(2)}$ is the pair correlation function.

Intuitively, we may regard the total force on a molecule not in equilibrium to be the sum of two contributions. One of these is nonvanishing even at equilibrium and is due to the presence of concentration gradients. The other, a frictional force, is of primary interest and arises from the existence of velocities and temperature gradients. Accordingly, we define the frictional force for the isothermal case as the actual force $\bar{\mathbf{F}}_\alpha^{(1)}$ less the force $\bar{\mathbf{F}}_\alpha^{(1,0)}$ in an equilibrium, enforced by the presence of external fields and assured by the Gibbs' criteria, in which the concentration distribution is the same as in the diffusing system.[4,6] Thus,

$$\bar{\mathbf{F}}_\alpha^{(1,1)} = \bar{\mathbf{F}}_\alpha^{(1)} - \bar{\mathbf{F}}_\alpha^{(1,0)}$$

$$\bar{\mathbf{F}}_\alpha^{(1,1)*} = \bar{\mathbf{F}}_\alpha^{(1)*} - \bar{\mathbf{F}}_\alpha^{(1,0)*}$$

$$c_\alpha \bar{\mathbf{F}}_\alpha^{(1,0)} = c_\alpha \bar{\mathbf{F}}_\alpha^{(1,0)*} + \tfrac{1}{2}\nabla_{r_1} \cdot \sum_{\beta=1}^{\nu} c_\alpha c_\beta \int \frac{\mathbf{r}\mathbf{r}}{r} \frac{dV_{\beta\alpha}}{dr} g_{\beta\alpha}^{(2,0)}(\mathbf{r}_1, \mathbf{r}) d^3\mathbf{r}$$

$$c_\alpha \bar{\mathbf{F}}_\alpha^{(1,0)*} = \tfrac{1}{2} \sum_{\beta=1}^{\nu} c_\alpha c_\beta \int \frac{\mathbf{r}}{r} \frac{dV_{\beta\alpha}}{dr} [g_{\alpha\beta}^{(2,0)} - g_{\beta\alpha}^{(2,0)}] d^3\mathbf{r} \quad (3.3)$$

$$g_{\alpha\beta}^{(2,1)} = g_{\alpha\beta}^{(2)} - g_{\alpha\beta}^{(2,0)}$$

where the equilibrium pair correlation function $g_{\alpha\beta}^{(2,0)}$ is the ordinary radial distribution function of statistical mechanics. To proceed further we now introduce linear expressions for the distribution function perturbations, conditioned by the restrictions that the microscopic equations must lead to the phenomenological relations for the matter flux and to the Newtonian stress tensor,[4]

$$g_{\alpha\beta}^{(2,1)} / g_{\alpha\beta}^{(2,0)} = \psi_{\alpha\beta}^{(1)}(r) \frac{\mathbf{r}}{r} \cdot (\mathbf{u}_\beta - \mathbf{u}_\alpha) + \psi_{\alpha\beta}^{(0)}(r) \nabla \cdot \mathbf{u} + \psi_{\alpha\beta}^{(2)}(r) \frac{\mathbf{r} \cdot \dot{\boldsymbol{\varepsilon}}^* \cdot \mathbf{r}}{r^2} \quad (3.4)$$

$$\dot{\boldsymbol{\varepsilon}}^* = \mathrm{sym}\nabla\mathbf{u} - \tfrac{1}{3}\nabla \cdot \mathbf{u}\mathbf{1}$$

$$\mathrm{sym}\nabla\mathbf{u} = \tfrac{1}{2}(\nabla\mathbf{u} + \nabla\mathbf{u}^{\mathrm{transpose}}).$$

The first term in Eq. (3.4), a first-order spherical harmonic, contributes to $\bar{\mathbf{F}}_\alpha^{(1,1)*}$ whereas the second and third terms, zero and second-order spherical harmonics, lead to the formula for the stress tensor. By the definition of simple Fickian diffusion which we treat here, the viscous terms will be negligible, and thus from Eqs. (3.3) and (3.4) we are led to the result,[4]

$$\bar{\mathbf{F}}_\alpha^{(1,1)*} = \bar{\mathbf{F}}_\alpha^{(1,1)} = -\sum_{\beta=1}^{\nu} c_\beta \zeta_{\alpha\beta} (\mathbf{u}_\alpha - \mathbf{u}_\beta)$$

$$\zeta_{\alpha\beta} = \tfrac{1}{6} \int \frac{dV_{\alpha\beta}}{dr} [\psi_{\alpha\beta}^{(1)} + \psi_{\beta\alpha}^{(1)}] g_{\beta\alpha}^{(2,0)} d^3\mathbf{r} \quad (3.5)$$

where the friction coefficients $\zeta_{\alpha\beta}$ are defined by the second of Eqs. (3.5).

The partial equations of motion of Bearman and Kirkwood[4] reduce to the simple form,

$$\bar{\mathbf{F}}_\alpha^{(1,1)*} = \nabla\mu_\alpha \quad (3.6)$$

for quasistationary isothermal, isobaric diffusion processes. From Eqs. (3.5) and (3.6) we find that the gradients of chemical potential are linearly related through the friction coefficients to the relative velocities of the components,

$$\nabla\mu_\alpha = -\sum_{\beta=1}^{\nu} c_\beta \zeta_{\alpha\beta} (\mathbf{u}_\alpha - \mathbf{u}_\beta). \quad (3.7)$$

From Eq. (3.7) it is possible to derive the following expressions for the mutual and self-diffusion coefficients in a two-component fluid[10]:

$$D = (\bar{v}_1 kT/\zeta_{12}) \left[1 + \left(\frac{\partial \ln f_2}{\partial \ln c_2}\right)_{T,P}\right] = (\bar{v}_2 kT/\zeta_{12}) \left[1 + \left(\frac{\partial \ln f_1}{\partial \ln c_1}\right)_{P,T}\right]$$

$$D_\alpha = kT/\zeta_\alpha, \qquad \zeta_\alpha = \sum_{\beta=1}^{2} c_\beta \zeta_{\alpha\beta} \quad (3.8)$$

where f_1 and f_2 are the activity coefficients of 1 and 2, respectively, $\bar{v}_1$ and $\bar{v}_2$ are their partial molar volumes, and k is the Boltzmann constant.

Up to this point our considerations have been of a fairly general nature, combining statistical mechanics with the ordinary phenomenological theory of irreversible processes. We are now prepared to introduce our final major assumption, which concerns the average frictional force on a molecule when it is in the neighborhood of another molecule. The average force on a molecule of species α at point $\mathbf{r}_1$ in the system when a second

[10] Footnote reference 6, Appendix.

molecule of species β is at $\mathbf{r}_2$ may be denoted by $\mathbf{F}_{\alpha\beta,1}^{(2)}(\mathbf{r}_1, \mathbf{r}_2)$,[11] and the average force on the second molecule by $\mathbf{F}_{\alpha\beta,2}^{(2)}(\mathbf{r}_1, \mathbf{r}_2)$. It is convenient to combine these formally into a vector of six components, $\mathbf{F}_{\alpha\beta}^{(2)}(\mathbf{r}_1, \mathbf{r}_2)$, which may be written as their direct sum,

$$\mathbf{F}_{\alpha\beta}^{(2)}(\mathbf{r}_1, \mathbf{r}_2) = \mathbf{F}_{\alpha\beta,1}^{(2)} \oplus \mathbf{F}_{\alpha\beta,2}^{(2)}. \tag{3.9}$$

Similarly the average velocities of the two molecules $\mathbf{u}_{\alpha\beta,1}^{(2)}(\mathbf{r}_1, \mathbf{r}_2)$ and $\mathbf{u}_{\alpha\beta,2}^{(2)}(\mathbf{r}_1, \mathbf{r}_2)$ may be combined into the six-space vector $\mathbf{u}_{\alpha\beta}^{(2)}(\mathbf{r}_1, \mathbf{r}_2)$,

$$\mathbf{u}_{\alpha\beta}^{(2)}(\mathbf{r}_1, \mathbf{r}_2) = \mathbf{u}_{\alpha\beta,1}^{(2)} \oplus \mathbf{u}_{\alpha\beta,2}^{(2)}. \tag{3.10}$$

The pair space frictional force $\mathbf{F}_{\alpha\beta}^{(2,1)}$ is simply the difference between $\mathbf{F}_{\alpha\beta}^{(2)}$ and the corresponding force $\mathbf{F}_{\alpha\beta}^{(2,0)}$ in the equilibrium state specified above. We suppose (i) that the frictional force obeys the linear relation,

$$\mathbf{F}_{\alpha\beta}^{(2)} - \mathbf{F}_{\alpha\beta}^{(2,0)} \equiv \mathbf{F}_{\alpha\beta}^{(2,1)} = -\sum_{\gamma}\sum_{\sigma} \tfrac{1}{2}\zeta_{\alpha\beta;\gamma\sigma} \cdot \{\mathbf{u}_{\alpha\beta}^{(2)}(\mathbf{r}_1, \mathbf{r}_2) - (\mathbf{u}_{\gamma}(\mathbf{r}_1) \oplus \mathbf{u}_{\sigma}(\mathbf{r}_2))\}, \tag{3.11}$$

and (ii) that the pair friction tensor $\zeta_{\alpha\beta;\gamma\sigma}$ may be replaced by its asymptotic form obtained upon comparison of the relations for the singlet and pair forces with recognition that the pair and singlet forces, and also velocities, must approach each other at large distances between molecular pairs so that,

$$\zeta_{\alpha\beta;\gamma\sigma} = c_{\gamma}\zeta_{\alpha\gamma}\mathbf{1}_1 \oplus c_{\sigma}\zeta_{\beta\sigma}\mathbf{1}_2, \tag{3.12}$$

where $\mathbf{1}_1$ and $\mathbf{1}_2$ are the unit tensors at $\mathbf{r}_1$ and $\mathbf{r}_2$, respectively. Equations (3.11) and (3.12), taken together, are the principal assumptions which permit unification of the theories of the several transport parameters in simple liquid mixtures, and form the basis of our current series of papers. Combined with the partial equations of motion and Eq. (3.4) for the distribution function perturbations, they provide differential equations[5] for the reduced perturbation parameters $\psi_{\alpha\beta} \equiv (D_\alpha + D_\beta)\psi_{\alpha\beta}^{(1)}$ in terms of the equilibrium radial distribution functions $g_{\alpha\beta}^{(2,0)}$,

$$g_{\alpha\beta}^{(2,0)}\frac{d^2\psi_{\alpha\beta}}{dr^2} + \left(\frac{dg_{\alpha\beta}^{(2,0)}}{dr} + \frac{2}{r}g_{\alpha\beta}^{(2,0)}\right)\frac{d\psi_{\alpha\beta}}{dr} - \frac{2g_{\alpha\beta}^{(2,0)}}{r^2}\psi_{\alpha\beta} = \frac{dg_{\alpha\beta}^{(2,0)}}{dr}, \tag{3.13}$$

subject to the boundary conditions that $\psi_{\alpha\beta}$ approach zero as r approaches infinity and, for potentials which are infinite for $r \leq b$,

$$\lim_{r \to b+} \frac{d\psi_{\alpha\beta}}{dr} = 1.$$[12]

From Eq. (3.5) and the definition of $\psi_{\alpha\beta}$, we may write down expressions for the ratios of the friction coefficients,

$$\zeta_{11}vkT/(x_1\zeta_{11} + x_2\zeta_{12}) = \tfrac{1}{6}\int \frac{dV_{11}}{dr}\psi_{11}g_{11}^{(2,0)}d^3\mathbf{r},$$

$$vkT\zeta_{12}\{1/(x_1\zeta_{11} + x_2\zeta_{12}) + 1/(x_2\zeta_{22} + x_1\zeta_{12})\} = \tfrac{1}{3}\int \frac{dV_{12}}{dr}\psi_{12}g_{12}^{(2,0)}d^3\mathbf{r}, \tag{3.14}$$

$$\zeta_{22}vkT/(x_2\zeta_{22} + x_1\zeta_{12}) = \tfrac{1}{6}\int \frac{dV_{22}}{dr}\psi_{22}g_{22}^{(2,0)}d^3\mathbf{r},$$

where v is the molar volume of solution and x_1 and x_2 are the mole fractions. The friction coefficient ζ_{21} need not be considered separately, for, by its definition in Eq. (3.5), it is equal to ζ_{12}. Since there are only two independent ratios of three quantities, the second of Eqs. (3.14) must follow from the other two. We have not shown this generally, but we have discovered in the special case discussed in the following that the three relations appear to be consistent. Although we are unable to calculate the magnitude of each of the friction coefficients, they are well defined experimentally, for they may be evaluated with the use of Eq. (3.8) and data on the two self-diffusion coefficients and one mutual diffusion coefficient at any given composition.

In principle, each of the integrals appearing in Eq. (3.14) may be calculated from the solutions to the differential equations, Eq. (3.13), and a knowledge of the equilibrium radial distribution functions $g_{\alpha\beta}^{(2,0)}$ and the potentials of intermolecular force $V_{\alpha\beta}$. In practice, however, even for the simplest molecules, the labor involved is formidable. Upon reflection, this appears reasonable, for this situation is already encountered in equilibrium statistical mechanical theory, and we would not expect the theory of transport to be any simpler. To achieve comparison with experiment, one must introduce simplified physical models or appropriate mathematical approximations. In the present instance, we find it most convenient to adopt the viewpoint of the theory of regular solutions of Hildebrand[13]

[11] For more precise definitions in terms of ensemble averages the reader is referred to footnote references 5 and 6.

[12] The approach of Bearman, Kirkwood, and Fixman,[5] which preceded the general formulation of Bearman and Kirkwood[4] and the nonisothermal theory of Bearman,[6] is readily altered to conform to the later developments without change of any equations. It should be observed also that Eq. (3.13), derived for two-component systems, holds, subject to our hypotheses, for all multicomponent systems including those undergoing self-diffusion. There, the trace species is treated as an extra component with intermolecular potential parameters identical with those of one of the other species.

[13] J. H. Hildebrand and R. L. Scott, *The Solubility of Nonelectrolytes* (Reinhold Publishing Corporation, New York, 1950), 3rd ed., Chap. VII.

wherein volumes are assumed additive and the radial distribution functions are taken to be independent of composition. It then follows from Eq. (3.13) that the distribution function perturbations $\psi_{\alpha\beta}$ are also composition independent, and therefore the integrals of Eq. (3.14) are similarly constant. Their values may be determined by letting the mole fractions approach unity. We thus find

$$\tfrac{1}{6}\int\frac{dV_{11}}{dr}\psi_{11}g_{11}^{(2,0)}d^3\mathbf{r}=v_1kT,$$

$$\tfrac{1}{6}\int\frac{dV_{22}}{dr}\psi_{22}g_{22}^{(2,0)}d^3\mathbf{r}=v_2kT,$$

$$\zeta_{12}/\zeta_{11}=v_2/v_1, \qquad (3.15)$$

$$\zeta_{12}/\zeta_{22}=v_1/v_2.$$

Substitution of Eq. (3.15) into the left-hand side of the second of Eqs. (3.14) gives

$$\tfrac{1}{3}\int\frac{dV_{12}}{dr}\psi_{12}g_{12}^{(2,0)}d^3\mathbf{r}=(v_1+v_2)kT. \qquad (3.16)$$

All three of Eqs. (3.14) are therefore consistent with the assumption that the radial distribution functions are composition independent. By Eq. (3.15) for the friction coefficient ratios and Eq. (3.8) for the diffusion coefficients, we find the simple relations

$$D_1/D_2=v_2/v_1,$$

$$\zeta_{22}/\zeta_{11}=(D_1/D_2)^2, \qquad (3.17)$$

$$D=D_1\left[1+\left(\frac{\partial\ \ln f_1}{\partial\ \ln c_1}\right)_{T,P}\right].$$

The last equation is identical with one proposed previously[14] from more heuristic considerations. The present derivation provides a formal basis, and, as well, suggests the limitations of the result.

IV. DISCUSSION

Our principal assumptions fall into three categories concerning (i) the dynamical behavior of the molecules, (ii) their nonequilibrium statistical behavior, and (iii) their equilibrium behavior. With respect to the first, we have assumed that the molecules obey the laws of classical mechanics and that they have pairwise additive central forces dependent only upon the magnitude of the distance separating the centers of mass of the molecular pairs and not upon their relative orientations. It is evident that of all species the heavier rare gas molecules most nearly approximate this behavior, and even with these the assumption of additivity is by no means exact.[15] For more complex molecules the assumptions apply with rapidly diminishing accuracy, so that in many cases of interest they have only qualitative application. With respect to the second category, the most important assumption is contained in the equations which linearly relate the pair space forces to the velocities through the use of asymptotic friction coefficients. To justify the equations, we note that they are plausible, that they lead to relatively simple results, and, not the least important, that they permit the unification of the theories of the transport parameters in simple liquid mixtures. Moreover, the consequences of the equations are in agreement with current theories of electrolytes[16] and the Kirkwood theory of Brownian motion.[17] The degree of approximation which is involved can be better understood by comparison of our current theory[5] of the heat of transport with those of earlier workers. Previous results were obtained on the assumption that the pair space velocity $\mathbf{u}_{\alpha\beta,1}^{(2)}$ may be set equal to $\mathbf{u}_\alpha$, or, equivalently, that nonequilibrium perturbations to the distribution functions may be neglected. In our formulation we take into account the differences between the velocities, although we retain the condition that the friction tensor maintains its asymptotic value. Thus, in this sense our theory represents a second approximation to the final answer. With respect to the third category, we have assumed for the purposes of simplifying our results that the radial distribution functions, like those of the regular solution theory, are composition independent. At the present time it is difficult to assess the importance of this approximation and separate it from the others. The work of Alder[18] on mixtures of hard spheres suggests that it is not particularly good, except, perhaps, when the molecules are of the same size. Its effect on our final equations, however, depends upon the sensitivity of the integrals in Eq. (3.14) to the values of the distribution functions, and we have not yet determined this.

From the foregoing analysis, it appears that, because of their simplicity, the best systems for the comparison of the theory with experiment are the liquified rare gas mixtures. However, because experimental data are still scarce, we are forced to turn to more complex systems. The values of both self-diffusion coefficients have been obtained by Carman and Stein[19] for the system ethyl iodide(1)–*n*–butyl bromide(2). The ratios of the diffusion coefficients, D_1/D_2, at 19.35°C, calculated from parabolic least squares fits of the data, are presented in Table I as a function of composition. The ratio is fairly constant over most of the range, but is lower than the ratio v_2/v_1 which is 1.41.[20] To two significant figures the agreement is good—1.1 for D_1/D_2 compared with 1.4 for v_2/v_1. It appears better when it is remembered that

[14] Footnote reference 1, Eq. (114).

[15] T. Kihara, Advances in Chem. Phys. **1**, 267 (1958).

[16] E. Helfand and J. G. Kirkwood, "Theory of the heat of transport of electrolytic solutions" (to be published).

[17] J. G. Kirkwood, J. Chem. Phys. **14**, 180 (1946).

[18] B. J. Alder, J. Chem. Phys. **23**, 263 (1955).

[19] P. C. Carman and L. H. Stein, Trans. Faraday Soc. **52**, 619 (1956).

[20] J. Timmermans, *Physico Chemical Constants of Pure Organic Compounds* (Elsevier Publishing Company, Inc., New York, 1950).

equilibrium solution theories have also not been eminently successful in quantitative prediction.[21] The classical Stokes-Einstein relation,[2] derived for the Brownian motion of particles of macroscopic dimension, predicts that the product of the diffusion coefficient and viscosity is proportional to the reciprocal of the radius of the particle. The extension to the present case would suggest that the ratio of the self-diffusion coefficients should be in the inverse ratio of the cube root of the molar volumes.[22] For the ethyl iodide-*n*-butyl bromide system this is 1.1, and is therefore closer to the experimental value than our prediction. However, this need not be interpreted as a failure of the theory presented here since the system under consideration does not meet all of the requirements for the validity of the simplified formulas. In particular, we should not expect the radial distribution functions to be composition independent since the molar volume of *n*-butyl iodide is one and a half times greater than that of ethyl iodide. In the limit when the volumes become equal, the ratio of volumes approaches one, as does the cube root of the ratio, so that a critical comparison of the two theories may not be feasible.

Finally, we would like to suggest that our formulation may be extended readily in a variety of ways, some of which could prove useful for the empirical representation of data.[23] We shall consider only the simplest case in which we assume arbitrarily that the friction coefficients are independent of comparison. From Eq. (3.8) we find

$$D_1^0=v_1kT/\zeta_{11}, \qquad D_1^\infty=v_2kT/\zeta_{12},$$
$$D_2^0=v_2kT/\zeta_{22}, \qquad D_2^\infty=v_1kT/\zeta_{12}, \tag{4.1}$$

where D_1^0, D_2^0 are the self-diffusion coefficients of (1) and (2) in pure (1) and (2), respectively, and D_1^∞ and D_2^∞ are the coefficients of each at infinite dilution. We

[21] I. Prigogine, *The Molecular Theory of Solutions* (Interscience Publishers, New York, 1957), Chap. XI.

[22] J. C. M. Li and P. Chang, J. Chem. Phys. **23**, 518 (1955).

[23] In this connection, we would like to call attention to the similar approach of R. W. Laity, J. Phys. Chem. **63**, 80 (1956), who attacked the problem with purely phenomenological techniques.

TABLE I. D_1/D_2 for the system ethyl iodide (1)-*n*-butyl iodide (2).

x_1	D_1/D_2
0	1.13
0.1	1.14
0.2	1.14
0.3	1.14
0.4	1.13
0.5	1.12
0.6	1.12
0.7	1.11
0.8	1.11
0.9	1.08
1.0	1.07

then have

$$D_1^\infty/D_2^\infty=v_2/v_1. \tag{4.2}$$

If we combine Eq. (4.1) and Eq. (3.8), assuming additivity of volumes, we may express the composition dependence of D_1 in terms of D_1^0 and D_1^∞ or alternatively in terms of D_1^0 and D_2^∞,

$$1/D_1=(x_1v_1D_1^\infty+x_2v_2D_1^0)/vD_1^0D_1^\infty$$
$$=\frac{v_1}{v}\left(\frac{x_1}{D_1^0}+\frac{x_2}{D_2^\infty}\right). \tag{4.3}$$

If, in addition, we introduce the assumption that the radial distribution functions are independent of composition and therefore that $v_2/v_1=D_1/D_2=D_1^0/D_2^\infty$, we then find from Eq. (4.3) that $D_1=D_1^0$, or that the self-diffusion coefficient is constant over the entire composition range. Thus, sufficient conditions for the constancy of the self-diffusion coefficients are the additivity of volumes and the independence of the radial distribution functions and friction coefficients on composition. By Eq. (3.8), the mutual diffusion coefficient is constant when the volumes are additive, the activity coefficient is unity, and the friction coefficient ζ_{12} is composition independent.

ACKNOWLEDGMENT

I am grateful to Peter F. Jones for carrying out the numerical calculations in connection with this work.

Measurements of Multicomponent Diffusion Coefficients for the CO_2—He—N_2 System Using the Point Source Technique*

R. E. WALKER, N. DEHAAS, AND A. A. WESTENBERG

Applied Physics Laboratory, The Johns Hopkins University, Silver Spring, Maryland

(Received October 21, 1959)

Measurements of the diffusion coefficient for a trace of carbon dioxide in a mixture of helium and nitrogen of varying composition have been made at room temperature and atmospheric pressure using the point source technique. The results are shown to be in agreement with the results of Fairbanks and Wilke in that an equation of the form

$$D_{i-mix}=\left[\sum_{k\neq i}(x_k/\mathfrak{D}_{ik})\right]^{-1}$$

can be used to relate the diffusion coefficient of a trace of species i in a mixture of composition given by the mole fraction x_k to the binary diffusion coefficients $\mathfrak{D}_{ik}$. Some data are presented on the separation of the mixture in the diffusion zone.

IN a recent paper,[1] a detailed study of a new method of measuring molecular diffusion coefficients in gaseous systems was presented. This technique uses the change in concentration downstream of a point source of a trace gas located in a uniform laminar jet of a second gas to determine the binary diffusion coefficient. The technique has good precision (±1–2%) and, because the trace gas concentration is essentially zero, the ambiguity in the conventional diffusion measurements arising because of composition changes can be conveniently avoided. In fact, this feature has been used to measure the small effects of concentration on binary diffusion coefficients.[2,3] The present paper is concerned with another interesting application of the point source method. If a multicomponent mixture is used for the carrier gas, the diffusion of the trace gas through the mixture can be studied. This is actually a multicomponent diffusion process, but the unique feature of the point source technique (a trace amount of one component) simplifies the necessary theoretical considerations and permits a simple relation between the measured diffusion coefficient and the individual binary diffusion coefficients to be established. Measurements of this type provide a check on the complex kinetic theory of multicomponent systems.[4]

THEORY

The theoretical foundation for the problem of diffusion from a point source of a trace gas into a uniform laminar jet of a second (carrier) gas has already been given,[1] although it is necessary to reproduce in part some of the derivation for the case of a multicomponent carrier gas. The theory is developed for a binary carrier gas (species 2 and 3), although extension to more complicated mixtures is easily accomplished. The assumptions employed in reference 1 are used here, namely, (a) steady state, (b) no chemical reaction, (c) constant unidimensional stream velocity U, (d) no external forces, (e) constant temperature and pressure, and (f) species 1 present only as a trace. Assumptions (e) and (f) permit one to assume that the gas density ρ and the various multicomponent diffusion coefficients D_{ij} are constant. By using these many assumptions, the differential equation for the trace component becomes

$$U(\partial n_1/\partial z)+(n^2/\rho)[m_2D_{12}\nabla^2(n_2/n)+m_3D_{13}\nabla^2(n_3/n)]=0 \quad (1)$$

with $n=n_1+n_2+n_3$. In this equation, m_i is the molecular mass of the ith component and n is the (constant) molecular density. The multicomponent diffusion coefficients are related to the several binary diffusion coefficients by a complicated expression involving concentration of species, molecular masses, and binary diffusion coefficients.[4] For this particular problem, where it can be assumed that the mole fraction $x_1\approx 0$ and x_2 and x_3 are constant, Eq. (1) can be simplified to

$$U(\partial n_1/\partial z)+[(x_2/\mathfrak{D}_{12})+(x_3/\mathfrak{D}_{13})]^{-1}\nabla^2 n_1=0. \quad (2)$$

Equations for species 2 and 3 become complicated expressions involving all three pertinent binary diffusion coefficients ($\mathfrak{D}_{12}$, $\mathfrak{D}_{23}$, $\mathfrak{D}_{13}$), and the presence of species 1 indicates that ordinarily the species 2 and 3 will separate in the presence of the trace gas—it has been the assumption in this analysis that the amount of separation is small and could be neglected in evaluating the diffusion coefficients. That this is the case is demonstrated in the following experimental study. A quantitative understanding of this separation phenomenon would require the solution of equivalent equations for species 2 and 3.

Equation (2) has a form identical to the equation for a single-component carrier gas except the binary

* Supported by contract with the Bureau of Ordnance, U. S. Navy.

[1] R. E. Walker and A. A. Westenberg, J. Chem. Phys. **29**, 1139 (1958).

[2] R. E. Walker and A. A. Westenberg, J. Chem. Phys. **29**, 1147 (1958).

[3] R. E. Walker and A. A. Westenberg, J. Chem. Phys. **31**, 519 (1959).

[4] J. O. Hirschfelder, C. F. Curtiss, and R. B. Bird, *The Molecular Theory of Gases and Liquids* (John Wiley & Sons, Inc., New York, 1954), p. 541.

diffusion coefficient has been replaced with an effective diffusion coefficient

$$D_{1-\text{mix}}=[(x_2/\mathfrak{D}_{12})+(x_3/\mathfrak{D}_{13})]^{-1}. \quad (3)$$

For a mixture of more than two components, Eq. (3) is given as

$$D_{i-\text{mix}}=[\sum_{i\neq j}(x_i/\mathfrak{D}_{ij})]^{-1}. \quad (4)$$

Equation (4) has been given by Hirschfelder and Curtiss[5] and Fairbanks and Wilke[6] for multicomponent diffusion with one component present in trace amounts. The application of Eq. (3) to the point source method of measuring diffusion coefficients permits an independent method of checking multicomponent kinetic theory. Fairbanks and Wilke[6] have already reported data in substantial agreement with Eq. (4) for the diffusion of ethyl propionate into hydrogen-air mixtures and toluene into hydrogen-argon mixtures.

APPARATUS

The experimental measurements reported in this paper were obtained in much the same manner as the data reported in reference 1. In view of the separation of the carrier gas species, however, it became necessary to modify the sampling and thermal-conductivity gas analysis apparatus used to detect the small concentration of trace gas. Ordinarily, a gas sample was continuously removed from the flow system with a quartz microprobe and passed to one cell of the thermal-conductivity gas analysis cell, the cell pressure being regulated at about 1 cm Hg. The reference cell was continually purged at 1 atm with pure carrier gas.

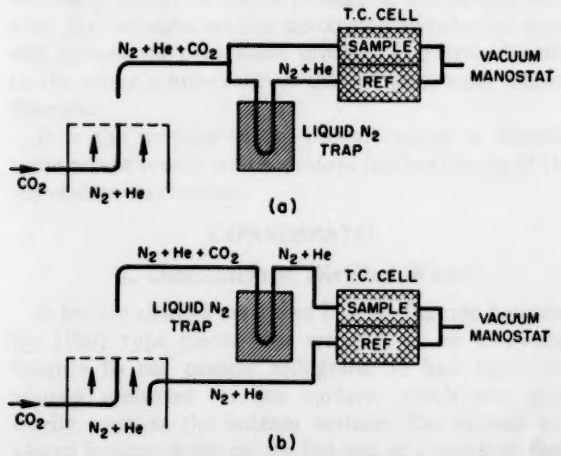

FIG. 1. Schematic of gas sampling and analysis system. (a) Method of measuring CO_2 concentration. (b) Method of measuring separation of the He—N_2 carrier gas.

[5] J. O. Hirschfelder and C. F. Curtiss, *Third Symposium on Combustion, Flame and Explosion Phenomena* (Williams and Wilkins, Baltimore, Maryland, 1949), p. 124.

[6] D. F. Fairbanks and C. R. Wilke, Ind. Eng. Chem. **42**, 471 (1950).

TABLE I. Comparison of measured effective diffusion coefficients for the CO_2(trace)—He—N_2 system and computed values (using experimental end points) ($T=299°K$; $p=1$ atm).

Mole fraction helium x_{He}	Mole fraction nitrogen x_{N_2}	Experimental D_{CO_2-mix} cm²/sec	Calculated $\frac{x_{He}}{\mathfrak{D}_{CO_2-He}}+\frac{x_{N_2}}{\mathfrak{D}_{CO_2-N_2}}$ cm²/sec
0	1.000	0.171	(0.171)
0.207	0.793	0.206	0.201
0.407	0.593	0.242	0.242
0.607	0.393	0.312	0.304
0.798	0.202	0.402	0.402
1.000	0	0.611	(0.611)

By using carbon dioxide as a trace gas, it was possible to obtain quantitative trace gas composition measurements with the usual thermal-conductivity gas analysis by splitting the sample. Part of the sampled gas was passed to the reference cell through a liquid nitrogen trap to remove the carbon dioxide. See Fig. 1(a). In this way, the carbon dioxide concentration could be measured against a slightly varying reference gas composition and the data handled in the usual fashion. Checks were made with binary systems (CO_2–N_2 and CO_2–He) to insure that the split lines were sufficiently long to insure isolation between the reference and sample cells and that the carbon dioxide was quantitatively removed by the liquid nitrogen trap.

Measurement of the amount of separation of the helium and nitrogen carrier was accomplished by purging the reference cell with sampled, carrier-gas mixture, where the sample withdrawn from the mixing zone was passed through a liquid nitrogen trap to remove the carbon dioxide before being analyzed. See Fig. 1(b).

The helium and nitrogen gas flows were regulated through critical orifices and the mixture proportions were continually monitored with a Gow-Mac thermal-conductivity cell. The nitrogen (super dry) and carbon dioxide (extra dry) were supplied by the Southern Oxygen Company and the helium was supplied by the Naval Gun Factory. The purity of the carbon dioxide was checked with a mass spectrometer and found to be sufficiently free from light gases and condensables.

RESULTS

Experimental measurements of the effective diffusion coefficients for the CO_2(trace)–He–N_2 system are given in Table I and Fig. 2. The entries in Table I represent average values of four or more runs (the reproducibility of these runs was about ±1%). Various mixtures of helium and nitrogen carrier gas were investigated. Also included in Table I are values of the effective diffusion coefficients calculated with Eq. (3) using the experimental values of the binary diffusion coefficients ($\mathfrak{D}_{CO_2-N_2}$ and $\mathfrak{D}_{CO_2-He}$) determined at the

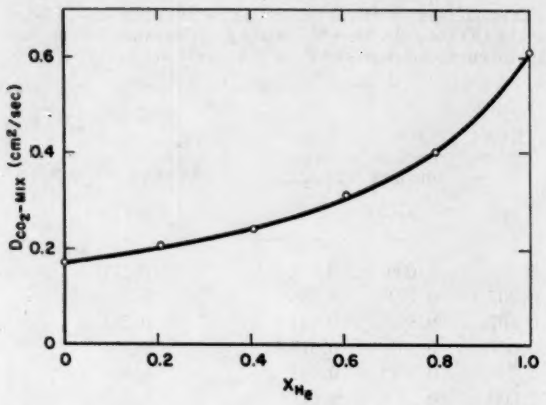

FIG. 2. Measured and calculated values of D_{CO_2-mix} as a function of carrier gas composition.

end points. The end point values of the binary diffusion coefficients are for carbon dioxide as the trace species (this procedure avoids the concentration effect that would be important in the He–CO_2 system). The agreement between the experimental values and the calculated values of the effective diffusion coefficient is good and substantiates that Eq. (3) is quite satisfactory in expressing the effective diffusion coefficient for multicomponent systems where one component is present as a trace.

In addition to the measurements of multicomponent diffusion coefficients, we have made a cursory set of measurements to determine the amount of separation of the carrier gas mixture in the diffusion zone. One such set of profiles for the three components is given in Fig. 3. This figure is to be regarded as a qualitative

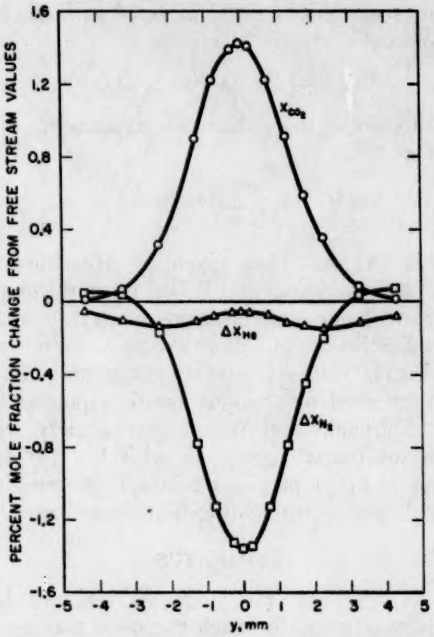

FIG. 3. Profiles of concentration changes downstream of a point source of CO_2 in a He—N_2 jet. ($z=1.00$ cm, $x_{He}=0.498$).

picture of the separation phenomenon and the details of the helium and nitrogen profiles are not to be considered real. In contrast to the profile of the change in the nitrogen concentration, it is of interest to note the nearly uniform and low value of the change in the helium concentration. The transverse profile for the CO_2 concentration agrees well with the point source equation.[1]

Dislocation Etchings

GERALD W. SEARS

General Electric Research Laboratory, Schenectady, New York

(Received October 16, 1959)

The theory of preferential etching at dislocations has been presented by Cabrera. In the present report the theory is reviewed and compared to empirical observations on the dissolution of lithium fluoride. The observed dissolution behavior is consistent with Cabrera's theory as modified by the effect of dissolution poisons.

INTRODUCTION

THE correspondence of etch pits to emergent dislocations was first suggested by Shockley and Read[1] to account for certain etch patterns observed by Lacombe and co-workers[2] on high purity aluminum. Since that time the preferential etching at dislocations has been observed on a wide variety of crystals. The comprehensive work of Gilman and Johnston[3] on dislocation motion in lithium fluoride indicates the mass of information that can be obtained by simple etching techniques.

The theory of preferential etching at dislocations has been presented by Cabrera.[4] He has demonstrated the existence of a region of undersaturation such that dissolution should proceed preferentially at dislocations as opposed to perfect surfaces.

Recently it has been shown[5] that the preferential etching of lithium fluoride by dilute ferric fluoride solutions agrees in all qualitative detail with Cabrera's conclusions subject to one modification. It is insufficient to preferentially create dissolution steps at dislocation sites to obtain a sharply defined etch pit. It is also necessary to have a solute present in the etching solution that adsorbs at the advancing dissolution steps and poisons the dissolution process. The ferric fluoride in the water solution serves that purpose with lithium fluoride.

It is the purpose of the present paper to describe some recent results which confirm further details of the dissolution mechanism.

EXPERIMENTAL

A. Dissolution in Distilled Water

A freshly cleaved crystal of lithium fluoride bounded by {100} type planes was weighed on an analytical balance to the nearest milligram. It had been previously scratched on one surface, which was arbitrarily used as the bottom surface. The crystal was placed bottom down on the bottom of a two-liter flask containing 1000 g of water. A motor driven glass stirrer was introduced through a six-inch length of glass tubing fitted by a ground joint to the neck of the dissolution flask to avoid evaporation of solvent. The stirring rate was slow enough to avoid moving the crystal over the surface of the flask.

After two weeks the crystal was removed, dried, and weighed. Only 0.401 g had dissolved compared to the reported 1.33 g/ liter solubility at 25°C.[6,7] The upper surface did not recede uniformly during the dissolution process as can be seen in the photomicrograph of Fig. 1 at 300 ×. In Fig. 2, an edge of the crystal is shown at 500 × showing the lack of uniformity in solution rate. Thin tapered platelets of lithium fluoride are banded by repeated interference colors. They remain attached to the main crystal.

To view the crystal in cross section, it was cleaved and observed through the cleavage surface. The cleavage plane is a {100} type and is normal to the top and bottom surfaces of the crystal. In Fig. 3 the crystal is viewed at 300 × (parallel) to the top surface. Large tapered pits can be observed which are at most 200 μ in depth and correspond to the large rectangular holes shown in Fig. 1.

An even more striking effect is seen when the crystal is viewed through a cleavage plane at the bottom surface. The large pits characterizing the top surface are absent. Figure 4 is a photomicrograph at 500 × taken below the cleavage plane showing interference colored channels which run predominantly in a {100} direction with some segments in a {110} direction. The channels have uniform interference colors over short segments indicating that they frequently jog from a {100} direction. They are about 2 μ wide as observed at 500 × and less than 1μ thick as judged by their interference colors and 100 μ in length.

B. Dissolution in the Presence of Antedotal Solutes

It was known that ferric fluoride in very low concentrations is a poison for both the dissolution[5] and growth[8] of lithium fluoride in aqueous solutions. It was suspected that the solution process in current experiments was inhibited by ferric fluoride provided by the

[1] W. Shockley and W. T. Read, Phys. Rev. 78, 275 (1950).
[2] P. Lacombe, *Report on Conference on Strengths of Solids* (Physical Society of London, 1948), p. 91.
[3] J. J. Gilman and W. G. Johnston, *Dislocations and Mechanical Properties of Crystals* (John Wiley & Sons, Inc., New York, 1957), p. 116.
[4] N. Cabrera, J. Chem. Phys. 53, 675 (1956).
[5] J. J. Gilman, W. G. Johnston, and G. W. Sears, J. Appl. Phys. 29, 747 (1958).
[6] J. H. Payne, J. Am. Chem. Soc. 56, 947 (1937).
[7] K. H. Meyer and M. Dunkel, Z. Physik. Chem. (Bodenstein Festband) 556 (1931).
[8] G. W. Sears (unpublished results).

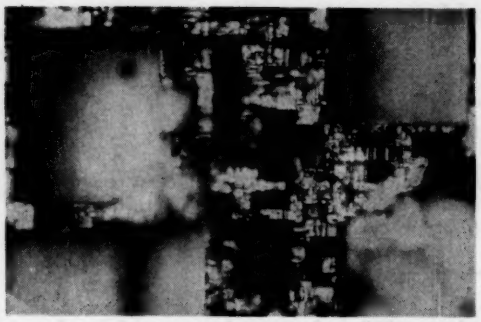

FIG. 1. Upper surface LiF crystal after 14 days dissolution in distilled water. 500× (reduction 60%).

dissolving crystal. This possibility was investigated by studying the dissolution of lithium fluoride in dilute solutions with two solutes that reduce the ferric ion concentration in solution below the value characteristic of a ferric fluoride complex ion, sodium cyanide and ammonium hydroxide.

The dissolution of lithium fluoride in 0.044 molal ammonium hydroxide was carried out as before. After 24 hr the cleaved sample was removed from solution, dried and reweighed. A weight loss of 0.750 g was found. The weight loss increased to 0.936 g after a second 24-hr solution period.

The upper surface was more uniformly dissolved than in the absence of ammonium hydroxide. In Fig. 5, a region of the upper surface is observed at 1057.5× after 24-hr dissolution. The surface is covered with tiny tiny holes and what appear to be foreign particles. In Fig. 6, the surface of a lithium fluoride platelet grown from aqueous solution is photographed at 1000× for comparison.

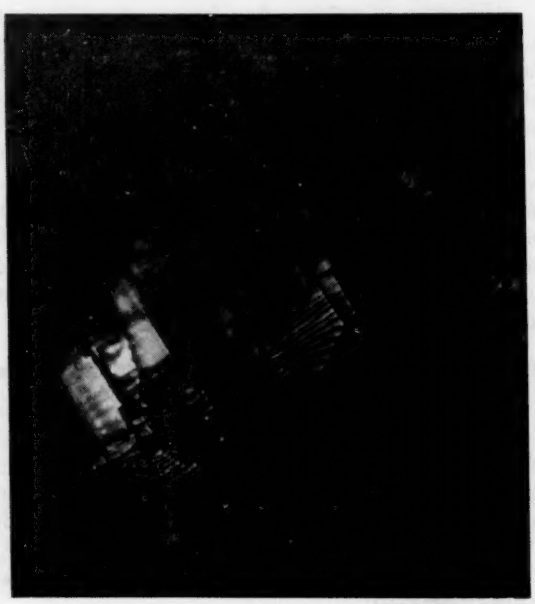

FIG. 2. Upper edge of crystal in Fig. 1. 500×.

FIG. 3. Crystal in Fig. 1 viewed parallel to the top surface through a cleavage surface. 500× (reduction 60%).

The dissolution of lithium fluoride in 0.01 molal NaCN solution was next studied. After 21 hr a weight loss of 0.893 g was measured. In an additional 20 hr, the weight loss had increased to 1.009 g. The surface was even more uniformly dissolved than in the presence of ammonium hydroxide. In Fig. 7, a surface area is photographed at 750× to indicate that the same type of surface roughness shown in Fig. 5 is present on a crystal that has been dissolved in the presence of sodium cyanide.

DISCUSSION

A. Preferential Dissolution at Dislocations

The formation of long narrow channels in [100] directions is attributed to preferential etching along

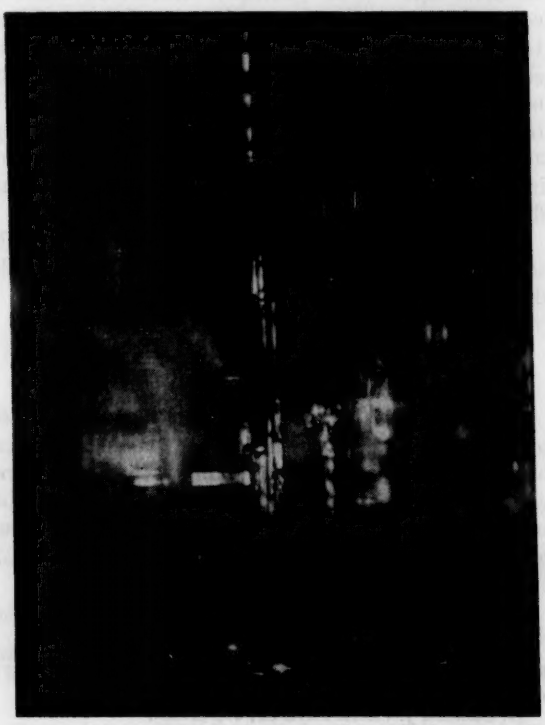

FIG. 4. Crystal in Fig. 1 viewed parallel to the bottom surface through a cleavage surface. 500×.

dislocations in the presence of a poison contributed by the dissolving crystal phase. The channels may be regarded as negative whiskers. Their morphology is determined by undersaturations in an analogous way by which supersaturations determine whisker morphologies. It may be deduced that preferential etching of the channels occurs at quite low undersaturations. Channels were observed after etching in a 0.01 molal NaCN solution containing an initial concentration of 0.936 g/liter of LiF. These channels were as much as 0.1 mm deep, and were formed in a 20-hr etching period.

It will be assumed that the concentration gradient along a channel is constant. An approximate equation for estimating the average concentration difference is

$$\langle \Delta c \rangle_{Av} \cong (10^3 \rho l^2 / 20 \cdot \Delta t) \text{ (g/liter)}. \quad (1)$$

Introducing the numerical values $l = 10^{-2}$ cm, $D = 10^{-5}$ cm^2 sec^{-1}, $\Delta t = 7 \times 10^4$ sec, and $\rho = 2.6$ g/cm^3, a value of

FIG. 5. Upper surface of LiF crystal after 24 hr in 0.044 molal NH_4OH. 1410× (reduction 75%).

concentration difference between the tip of a channel and the solution is calculated as

$$\langle \Delta c \rangle_{Av} \approx 0.2 \text{ g/liter}.$$

This difference in concentration combined with the body concentration gives an approximate concentration of 1.14 g/liter at the dissolving end of a channel. The average concentration difference is not overestimated. It is concluded that the preferential etching of channels in LiF may occur at undersaturation ratios at least as large as 0.85, i.e., at near saturation.

If $\alpha_c = 0.85$ is taken as that saturation ratio at which $\Delta f^* = 0$ for dissolution at a dislocation, Eq. (A 10b) may be solved for the surface energy of lithium fluoride in contact with its water solution. It is written

$$\gamma = (b/\pi) \{ G \rho RT \ln \alpha_c / M(1-\nu) \}^{\frac{1}{3}}. \quad (2)$$

Introducing the values $G = 5.5 \times 10^{11}$ dynes/cm^2,[9] $\nu =$ 0.33, $b = 4.01 \times 10^{-8}$ cm[10] in Eq. (A 10b) yields the result

$$\gamma = 165 \text{ erg/cm}^2.$$

This value is an upper limit since the value of α_c was not underestimated. It is noted that the interfacial energy of potassium chloride in contact with aqueous solution[11] (11) is 46 erg/cm^2 as compared to ~80 erg/cm^2 [12] for fused potassium chloride. The ratio of the interfacial tension to the fused salt value is 0.58. The surface tension of fused lithium fluoride[12] is 250 erg/cm^2 and the corresponding ratio is 0.66.

Consider the saturation ratio α_1 necessary to cause unit nucleation rate on a perfect surface. (Nucleation rate is such a sensitive function of undersaturation that unit rate and measurable rate are synonomous).

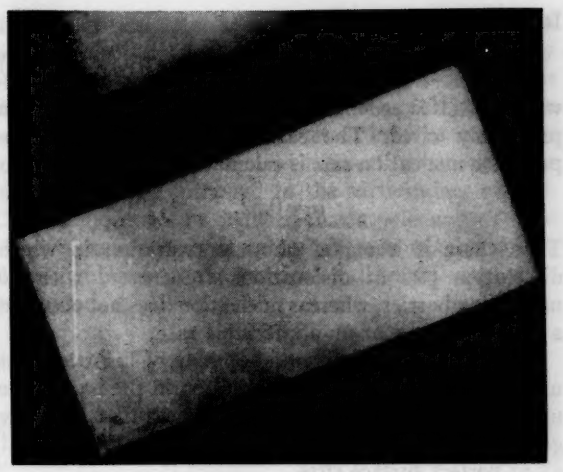

FIG. 6. As-grown surface of LiF crystal from distilled water. 1000×.

FIG. 7. Upper surface of LiF crystal after 21 hr in 0.01 molal NaCN. 1000× (reduction 75%).

[9] J. J. Gilman, Trans. Am. Inst. Mining, Met. Petrol. Engrs. **209**, 449 (1957).

[10] *Handbook of Chemistry and Physics* (Chemical Rubber Publishing Company, Cleveland, Ohio, 1952), 34th ed., p. 2265.

[11] G. W. Sears, J. Chem. Phys. **29**, 979 (1958).

[12] *Handbook of Chemistry and Physics* (Chemical Rubber Publishing Company, Cleveland, Ohio, 1959), 40th ed., p. 2143.

It is written that

$$\alpha_1=\exp\{-\pi a\gamma^2 M/\rho RkT^2 \ln B\}, \quad (3)$$

where $B\cong 10^{20}$ sec^{-1} and the other values have been previously cited. The saturation ratio for an appreciable nucleation rate is calculated as

$$\alpha_1=0.52.$$

Thus there is a region of undersaturation in which dissolution pits at dislocations are created with no nucleation barrier, whereas nucleation does not occur on a perfect surface at an appreciable rate.

It appears that preferential etching of LiF occurs at undersaturation ratios in the solution in the immediate neighborhood of the crystal surface such that steps are generated spontaneously at dislocations and not at all at perfect surface sites.

Equation (A 10b) shows that the pertinent elastic modulus and the surface energy determine the upper bound of undersaturation for which spontaneous dissolution may occur at a dislocation for a given crystal. Since Gb^2 is almost as large for LiF as for a metal crystal, while the pertinent surface energy is larger for a metal crystal, spontaneous dissolution will occur at dislocations in metal crystals only at very small undersaturation ratios. There is a well-defined region of undersaturation in which preferential etching can occur at dislocations in metal crystals, but the upper limit of undersaturation ratio is quite small. Vermilyea[13] recognized this feature and attributed the difficulty in dislocation etching pure metals to the fact that small undersaturation ratios cannot be maintained in the solution phase. Real crystals used in etching experiments have many steps and sources of steps not involving nucleation processes, i.e., crystal edges, screw dislocations, and high index planes. The empirical inability to maintain small undersaturation ratios over a specific metal crystal implies the absence of a sufficiently effective dissolution poison.

B. Dissolution Poisoning

The most important effect of a poison in the formation of etch pits depends upon the inhibition of the dissolution process. It has been shown that severe hindrance[14] of growth and solution at a step is associated with complete coverage of the adsorption sites on the step. It is necessary to postulate that an originally clean step moving across a crystal surface is rapidly poisoned by diffusion of poison from the body of solution. If this did not occur the solution would become saturated in the neighborhood of the crystal surface and preferential dissolution at dislocations could not occur.

It is possible to make an estimate of the poisoning time for an initially clean set of steps by the following procedure. Suppose that the interstep spacing is 10^{-6} cm. The available sites for adsorption of poison would be approximately 10^{13} cm^{-2}. This quantity of poison would be contained in the solution within 10^{-7} cm of the surface if the poison concentration was 10^{-6} mole fraction. If the diffusion constant, D, for poison is established at 10^{-5} cm^2 sec^{-1}, the Einstein equation

$$2D\tau=\lambda_s^2, \quad (4)$$

relating mean free path of diffusion λ_s and diffusion time τ can be solved to give a poisoning time of 10^{-9} sec. Even including a generous allowance for a material accommodation coefficient of less than unity, a poisoning time larger than 1 μsec is hardly conceivable.

The formation of an etch pit at a dislocation occurs by the generation of loops of step concentric to the dislocation. As a given loop expands the number of adsorption sites, s, for poison increases according to the equation

$$\dot{s}=2\pi N_0\dot{r}, \quad (5)$$

where N_0 is the number of sites per unit length of step. The pit size is limited by the largest diameter loop of step. It is expected that the half-life of an adsorbed poison molecule is long so that interchange between adsorption sites can be ignored with respect to diffusion transport from solution. The validity of this assumption can be deduced from earlier results.[5] In a solution having a body undersaturation ratio of 0.15 with respect to LiF, pits at edge dislocations were much deeper than pits at screw dislocations although the diameter of both types of pits was identical. Since the pits at edge dislocations must necessarily involve a larger number of total poison adsorption sites, the rate of pit growth involves primarily the effect of the lengthening step given in Eq. (5) rather than the total number of adsorption sites at a dislocation.

The equiconcentration lines in the diffusion field will be approximately hemispherical about a dislocation. The net effect of expanding step loops and the diffusive transport of poison will be to establish a quasi-steady-state population of filled adsorption sites on the collection of steps comprising the etch pit. The population will depend upon the undersaturation of the solution with respect to the dissolving crystal phase, the concentration of poison in the etchant, the radius of an etch pit and the spatial relation of etch pits one to another. The further complexity of different types of dislocations and dislocation directions with respect to the surface, as well as varying degrees and kinds of adsorption and/or precipitation upon dislocations from solid solution will be ignored in the present discussion. It was found[5] that it was necessary to reduce the poison content in an etching solution having an undersaturation ratio of 0.15 in LiF to maintain the same pit size for a given etching period as in the absence of LiF. For a given poison concentration in solution and a given etch pit radius, the steady-state population of

[13] D. Vermilyea, Acta Met. **6**, 381 (1958).
[14] G. W. Sears, J. Chem. Phys. **29**, 1045 (1958).

filled adsorption sites would be larger for slower rates of step motion. The population of poisoned sites can also be changed by modifying the diffusion field, i.e., reducing the poison content in the etching solution will reduce the rate of transport of poison to a surface site. Qualitatively the observed reduction in poison content in solution was necessary to maintain a poison concentration on the step at a value such that a fixed step motion was maintained in the presence of a partial saturation of LiF.

Since the dissolution rate at a step is a sensitive function of the fractional coverage of adsorbed poison, it is expected that the poisoning action characteristic of a given poison concentration in solution should be sensitive in some cases to the temperature of the system. The etching of sodium chloride crystals by glacial acetic acid containing small amounts of ferric ion shows an effect attributed to change in adsorption isotherm with temperature.[14] The size of etch pits after a 1-min etch is many times larger if the etching is carried out at 50°C than at 25°C.

C. Antedotal Action

The very slow rate of solution of lithium fluoride in distilled water was attributed to the presence of poison contained in the lithium fluoride crystal. The approximately thirty-fold increase in solution rate in the presence of ammonium hydroxide and sodium cyanide gives strong confirmation to the interpretation.

The uneven dissolution rate over the crystal into distilled water is characteristic of the action of poisons during growth. The tapered platelets showing consecutive bands of interference colors is similar to the formation of tapered laths of LiF colored by interference bands when grown from a solution containing small amounts of ferric fluoride.

The identity of the active poison is believed to be ferric ion impurity in the lithium fluoride crystal. The impurity might be either in solid solution or as precipitate particles in the parent crystal.

The etching behavior is complicated by the presence of many precipitate particles which litter the surface of a heavily etched crystal as shown in Figs. 5 and 7. The grown surface of Fig. 6 contrasts in the absence of particles. The growth step undergoes repeating pinning and release from precipitate particles. This action tends to pile up growth steps to form step heights that are multiples of unit steps and whose dissolution behavior differs from that of steps of unit height.

CONCLUSIONS

Empirical observations on dislocation etching of lithium fluoride are consistent in great detail with the predictions of Cabrera's theory of etching as modified by the effect of dissolution poisons. The formation of etch pits occurs when the undersaturation ratio in the immediate neighborhood of the crystal surface is less than the critical value at which spontaneous dissolution occurs at dislocation sites. Etch pitting can only occur in the presence of dissolution poisons since this is the only way in which the local undersaturation can be maintained below the critical level. Poisons also serve to pile up step loops around dislocations so that the pits are visibly contrasted to the surrounding crystal. Conversely, it can be deduced that a polishing solution ideally requires the complete absence of any solute that might poison the particular dissolution reaction being used.

APPENDIX

Résumé of Cabrera's Treatment

It is convenient to briefly review Cabrera's theory of dissolution at a dislocation before discussing the present results. A formulation used by Cahn[15] for the nucleation of an incoherent second phase from solid solution upon a dislocation line is followed.

The dissolution nucleus is taken as a cylindrical hole in the crystal surface, one atom layer deep, a, and of radius r, with the dislocation normal to the surface. The free energy of nucleation, Δf consists of a strain energy term, Δf_e, a surface energy term, Δf_s and a volume energy term Δf_v. It is written that

$$\Delta f=\Delta f_e+\Delta f_s+\Delta f_v. \tag{A1}$$

The strain energy contribution is given by

$$\Delta f_e=-aA\ln(r/r_0)+B \quad (r\geq r_0), \tag{A2}$$

where A and B are dependent upon the nature of the dislocation and the degree of solute adsorption upon the dislocation. For a clean edge dislocation, $A=Gb^2/4\pi(1-\nu)$ and for a clean screw dislocation $A=Gb^2/4\pi$ where G is the elastic shear modulus, ν is the Poisson ratio and b is the Burgers vector of the dislocation. It follows that

$$\Delta f=-aA\ln(r/r_0)+2\pi a\gamma r-\pi r^2 af+B, \tag{A3}$$

where γ is the appropriate interfacial energy and f is the negative of the volume free energy of dissolution, i.e., $f>0$ for dissolution to occur.

The behavior of the free energy curve is determined by considering the first two derivatives of Δf

$$d\Delta f/dr=-aA/r+2\pi a\gamma-2\pi arf, \tag{A4a}$$

$$d^2\Delta f/dr=aA/r^2-2\pi af. \tag{A4b}$$

Equating the first derivative to zero gives a quadratic equation having two roots

$$\left.\begin{matrix} r_+ \\ r_- \end{matrix}\right\}=\frac{\gamma}{2f}\left\{\begin{matrix} 1+(1-\xi)^{\frac{1}{2}} \\ 1-(1-\xi)^{\frac{1}{2}} \end{matrix}\right\}, \tag{A5}$$

where $\xi=2Af/\pi\gamma^2$. When $0<\xi<1$ there are two real roots, r_+ corresponding to a maximum and r_- corresponding to a minimum. When $\xi=1$, there is a double

[15] J. W. Cahn, Acta Met. 5, 169 (1957).

root $r_+=r_-=\gamma/2f$. When $\xi>1$ there are no real roots, i.e., there is no nucleation barrier to the formation of a dissolution nucleus.

When the second derivative is equated to zero, there is a single positive real root

$$r^*=\xi^{\frac{1}{2}}(\gamma/2f). \quad \text{(A6)}$$

Thus every free energy curve has an inflection point. For $\xi=1$ the slope of the free energy curve is zero at the inflection point. The equation for the slope at the inflection point is obtained by combining Eqs. (A4a) and (A6) to give

$$(d\Delta f/dr)^*=(d\Delta f/dr)_{r^*}=2\pi a\gamma(1-\xi)^{\frac{1}{2}}. \quad \text{(A7)}$$

For $\xi<1$ the slope is positive at the inflection point while for $\xi>1$ the slope is negative at the inflection.

The undersaturation in the immediate neighborhood of a surface site is pertinent in determining the nucleation rate of monolayer holes in that area. For a given solute-solvent system ξ can be changed only by altering the undersaturation in the etching solution, i.e., by changing the free energy of dissolution.

For $\xi<1$ the critical free energy for nucleation of a monolayer hole at a dislocation is written

$$\Delta f^*=\Delta f(r^+)-\Delta f(r^-). \quad \text{(A8)}$$

The combination of Eqs. (A3), (A5), and (A8) yields

$$\Delta f^*=(\pi a\gamma^2/f)(1-\xi)^{\frac{1}{2}}+Aa\ln\frac{1-(1-\xi)^{\frac{1}{2}}}{1+(1-\xi)^{\frac{1}{2}}}, \quad \text{(A9)}$$

which is valid for $r\geq r_0$ and $\xi\leq 1$. When

$$\xi\rightarrow 1 \qquad \Delta f^*\rightarrow 0 \quad \text{(A10a)}$$

or when

$$f\rightarrow\pi\gamma^2/2A \qquad \Delta f^*\rightarrow 0. \quad \text{(A10b)}$$

For $\xi\rightarrow 1$, the second term on the right hand side of Eq. (A9) approaches zero more rapidly than the first term and it is written

$$\Delta f^*\cong(\pi a\gamma^2/f)(1-\xi)^{\frac{1}{2}} \quad \text{for} \quad \xi\sim 1. \quad \text{(A11)}$$

The competing process of nucleating a monolayer hole in a perfect crystal surface has a critical free energy, Δf_0^*, given by

$$\Delta f_0^*=\pi a\gamma^2/f. \quad \text{(A12)}$$

It is apparent for $\xi>1$, i.e., $f>\pi\gamma^2/2A$, that there is no barrier to the formation of a dissolution nucleus at a dislocation, while there is a nucleation barrier at a site on a perfect surface. For $\xi\lesssim 1$ the nucleation barrier is smaller by the factor $(1-\xi)^{\frac{1}{2}}$ at a dislocation than at a perfect surface site.

The dissolution rate in layers per second at a dislocation must exceed the net dissolution rate on the surrounding perfect crystal surface. On one hand, the number of perfect surface sites is much greater than the number of dislocation sites. On the other hand, some of the perfect surface nuclei are wasted in that many more holes may be nucleated in a given layer than are sufficient for the dissolution process.

Calculation of the Coupling Terms Neglected in Performing the Born-Oppenheimer Separation for the Hydrogen Molecule Ion*

DONALD W. JEPSEN AND JOSEPH O. HIRSCHFELDER

University of Wisconsin Theoretical Chemistry Laboratory, Madison, Wisconsin

(Received June 17, 1959)

A method is given for calculating the coupling between the nuclear and electronic motion in the hydrogen molecule ion using the exact wave functions. Calculations are carried out for the transition $1s\sigma - 2s\sigma$ and compared with values obtained from simple approximate methods. Estimates are made of the cross sections for excitation and capture into the $2s$ state during a proton-hydrogen atom collision, using approximate H_3^+ wave functions to describe the state during collision. Finally, it is shown that a Born-Oppenheimer separation carried out in relative coordinates should be slightly more accurate than the usual treatment using fixed space coordinates. Two different types of relative coordinates suggest themselves for use at different ranges of internuclear separation.

I. INTRODUCTION

THE quantum mechanics of molecules is greatly simplified by the Born-Oppenheimer separation,[1,1a] which makes it possible to study the motion of the electrons and the motion of the nuclei separately. In this procedure, the electronic motion is calculated with the nuclei held in fixed positions and then the slower motion of the nuclei is calculated using a potential energy produced by the moving cloud of electrons.

This separation explains the Franck-Condon principle, and is consistent with the characteristics of most molecular spectra. The size and character of the interactions between nuclear and electronic motion which are neglected in performing the separation is not clear, though a number of physical effects are known to be due to its failure. Kronig has explained the perturbations sometimes observed in spectra and the process of predissociation as an interaction of otherwise independent states.[2] Similarly, Van Vleck has shown that the coupling terms dropped in performing the separation provide an explanation of the phenomenon of Λ doubling.[3]

The analyses made of these effects reproduce the observed selection rules and the observed dependence on rotational quantum numbers, and also predict the proper order of magnitude for the effects. Only crude estimates of the electronic matrix elements of the coupling are needed to show that the mechanism of the process is properly described. Consequently, more accurate analyses which show how the coupling terms depend upon the properties of the electronic motion have not been made.

The most interesting cases of nonadiabatic transition arise in chemical reaction kinetics. Pelzer and Wigner have shown that, at least in simple substitution reactions, nonadiabatic behavior is likely only at points where the potential surfaces corresponding to different electronic states have nearly the same energy.[4]

It appears that the greatest probability of nonadiabatic transition is found between electronic energy states which approach each other but do not cross because of the Wigner-Witmer noncrossing rule. Such cases can be handled by a simple procedure due to London.[5] Two zero-order wave functions can usually be written down for this pair of states. The energy curves for these zero-order functions actually cross. New approximations of the true wave functions are then formed which are linear combinations of these two functions. The combination constants are obtained by the variational principle. The energy curves of the new functions do not cross. Passing through the crossing region, the mixture of the two zero-order wave functions in each of the new wave functions changes so that each new wave function is nearly one zero-order function in the first region and nearly the other beyond the crossing point. The variation of the coefficients in these linear combinations in the region of transition gives the wave functions a strong dependence on the nuclear coordinates, and hence, as can be seen from our formulas, gives large matrix elements of coupling. The calculation of the corresponding transition probability has been worked out by a number of authors.[6] The probability of transition is large both because these matrix elements are large and because the states are close together.

This type of situation is probably responsible for most of the observed nonadiabatic transitions, but may not be involved in all observed phenomena pro-

* This work was supported by the U. S. Atomic Energy Commission.

[1] M. Born and J. R. Oppenheimer, Ann. Phys. **84**, 457 (1927).

[1a] We will sometimes use the phrase BO separation or BO approximation. This should not be confused with the modification of the Born approximation of scattering theory to include exchange which is also called the Born-Oppenheimer approximation.

[2] R. Kronig, Z. Physik **50**, 347 (1928).

[3] J. Van Vleck, Phys. Rev. **33**, 467 (1929).

[4] H. Pelzer and E. Wigner, Z. Phys. Chem. **B15**, 445 (1932).

[5] F. London, Z. Physik **74**, 143 (1932).

[6] L. Landau, Physik. Z. Sowjetunion **1**, 89 (1932); **2**, 46 (1932); C. M. Zener, Proc. Roy. Soc. (London) **A137**, 696 (1933); **A140**, 660 (1933); E. C. G. Stueckelberg, Helv. Phys. Acta **5**, 370 (1932).

duced by coupling between the electronic and nuclear motions. A much weaker coupling should be capable of producing transitions from stable states where it has plenty of time to act. In particular it would seem likely that weak forms of predissociation with less diffuse lines may not involve the enhanced coupling due to curve crossing. It is thus interesting to study the nature of the coupling terms for the spontaneous transitions between states whose electronic energy curves are far apart. In this case the calculation is more difficult.

In this paper the Born-Oppenheimer (which we shall refer to as the BO) cross terms between two states of the hydrogen molecule ion are obtained. By using the exact wave functions in this problem we feel that we are assured that the curves obtained as a function of internuclear separation describe physical effects and are not merely properties of the wave functions employed. The matrix elements between the states $1s\sigma^a$ and $2s\sigma_g$ are calculated. For this pair of states the cross terms involve partial derivatives of the electronic wave function with respect to the internuclear separation, and hence might be given erroneously by approximate wave functions. Comparison is made with the result from LCAO calculations and from a perturbation calculation using the united atom wave functions. The magnitude of the coupling between this pair of states is then estimated by a calculation of the excited cross section.

Calculations have been carried out by Dalgarno and McCarroll[7] on the coupling terms between the states $1s\sigma_g$ and $3d\pi_g$. This matrix element is a coupling of electronic and nuclear angular momenta rather than between the electronic motion and the vibrationlike transition studied here. This work is part of a large group of calculations of molecular properties, using exact wave functions, carried out by the group at Belfast. It is hoped that our work will fit into their program.

Recently there has been interest in the diagonal terms of the Born-Oppenheimer separation which are due to differentiation of the electronic wave function with respect to nuclear variables. As Born showed, the diagonal terms should be added to the electronic energy to obtain the potential of the nuclear motion.[8] The diagonal terms are the corrections to the solutions of the Schrödinger equation for clamped nuclei, which must be made in order to account for the reactions of the nuclei to the electronic motions. These terms do not vanish for either the united atom or the separated atom configurations. As a matter of fact, in these limits, the diagonal terms correspond to the corrections resulting from using the effective masses of the electrons in place of the actual electron mass. This suggests the desirability of considering, as the first approximation, the separation between the centers of mass of the reacting species to be held clamped rather than the corresponding nuclei. When the centers of mass of each of the reacting species are held clamped, both the diagonal and nondiagonal BO correction terms become zero at infinite separations. Since different methods of clamping establish different relationships between the variables and since the correction terms depend upon the derivatives with respect to these variables, different results can be obtained by considering different methods of clamping. From the standpoint of physical meaningfulness, the best procedure would lead to the smallest correction terms. At the present time we do not know the best way of considering problems involving intermediate separations.

Actually one obtains different correction terms if one separates off the motion of the center of mass of the system before separating the motions of the electrons and nuclei rather than following the usual procedure of calculating the electronic motion with the nuclei held fixed in space. All these various possibilities are discussed presently.

II. BORN-OPPENHEIMER SEPARATION

Instead of basing our discussion of the BO separation on the original treatment of Born and Oppenheimer, we will follow a later method which has been given by a number of authors.[9] The original method is more involved and assumes explicitly that the nuclei remain near a minimum of the electronic energy. The latter method avoids this "near equilibrium" assumption and gives the terms which must be neglected to achieve separation in a more convenient form.

The quantum mechanical motion of the system of L electrons with coordinates r_i, $i=1, \cdots, L$, and N nuclei with coordinates R_α, $\alpha=1, \cdots, N$, is given by the Schrödinger equation

$$[\sum_i(\mathbf{p}_i^2/2m)+\sum_\alpha(\mathbf{p}_\alpha^2/2M_\alpha)+V(r,R)]\Psi = i\hbar(\partial/\partial t)\Psi. \quad (1)$$

The electron mass is denoted by m, and the nuclear masses by M_α. We denote by $\mathbf{p}_u$ the quantum-mechanical operator for the momentum of particle u. The arguments r and R in V signify dependence on all

[7] A. Dalgarno and R. McCarroll, Proc. Phys. Soc. (London) **A70**, 502 (1957).

[8] Wu and Bhatia made calculations of the diagonal terms for interactions of hydrogen and helium atoms and found that they are not negligible at large separations [T. Y. Wu, and A. B. Bhatia, J. Chem. Phys. **24**, 48 (1956); T. Y. Wu, *ibid.* **24**, 444 (1956)]. However, the calculations of Dalgarno and McCarroll [A. Dalgarno and R. McCarroll, Proc. Roy. Soc. (London) **A237**, 383 (1956); **A239**, 413 (1957)], do not agree with those of Wu and Bhatia. They found that the diagonal terms are only appreciable for the interaction of atoms in excited states.

[9] M. Born and K. Huang, *Dynamical Theory of Crystal Lattices* (Oxford University Press, New York, 1954), pp. 406–407; M. Born, Nachr. Akad. Wiss. Gottingen **1** (1951); J. O. Hirschfelder, and C. F. Curtiss, and R. B. Bird, *The Molecular Theory of Gases and Liquids* (John Wiley & Sons, Inc., New York, 1954), pp. 925–929; R. Kronig, Z. Physik **46**, 814 (1927); **50**, 347 (1928); H. S. W. Massey and R. A. Smith, Proc. Roy. Soc. (London) **A142**, 142 (1933).

the electronic and all the nuclear coordinates, respectively.

By dropping the nuclear kinetic energy terms from the Hamiltonian we obtain an "electronic" Hamiltonian $\mathcal{H}_e$ which contains the nuclear coordinates as parameters rather than variables. The eigenfunctions ψ_n of this Hamiltonian, satisfying

$$\mathcal{H}_e\psi_n(r, R)=E_n^{(e)}(R)\psi_n(r, R), \tag{2}$$

describe the motion of the electrons when the nuclei are held fixed.

The ψ_n form a complete set in the space of electronic variables, so it is possible to expand the wave function of the system of electrons and nuclei in the form

$$\Psi=\sum_n\chi_n(R)\psi_n(r, R). \tag{3}$$

Since the ψ_n's are known, we have reduced the problem to finding the χ_n's which are functions of the nuclear coordinates only. Substituting this series into the Schrödinger equation and forming matrix elements in the electronic variables, we obtain the following set of coupled equations for the χ_n's:

$$[\sum_\alpha(\mathbf{p}_\alpha^2/2M_\alpha)+E_{n'}^{(e)}(R)+(\hbar/i)(\partial/\partial t)]\chi_{n'}(R)=-\sum_n C_{n'n}(R, P)\chi_n(R).$$

Here the $C_{n'n}(R, P)$ is a function of both the internuclear separations (indicated by the R) and the nuclear momenta (indicated by the P),

$$C_{n'n}=\sum_\alpha(1/M_\alpha)(\mathbf{A}_{n'n}^{(\alpha)}\cdot\mathbf{p}_\alpha+B_{n'n}^{(\alpha)})$$

$$\mathbf{A}_{n'n}^{(\alpha)}=\int\psi_{n'}^*(r, R)\,\mathbf{p}_\alpha\psi_n(r, R)\,d\tau_e$$

$$B_{n'n}^{(\alpha)}=\tfrac{1}{2}\int\psi_{n'}^*(r, R)\,\mathbf{p}_\alpha^2\psi_n(r, R)\,d\tau_e. \tag{4}$$

If the ψ_n are chosen to be real, the diagonal elements $\mathbf{A}_{nn}^{(\alpha)}$ can be written as a gradient of the normalization integral,

$$\mathbf{A}_{nn}^{(\alpha)}(R)=-\tfrac{1}{2}(i\hbar)(\partial/\partial\mathbf{R}_\alpha)\left\{\int\psi_n\psi_n d\tau_e\right\}=0. \tag{5}$$

This enables us to combine C_{nn} with $E_n^e(R)$ to give the nuclear potential function

$$U_{n'}^{(e)}(R)=E_{n'}^{(e)}(R)+\sum_\alpha(1/M_\alpha)B_{n'n'}^{(\alpha)}(R). \tag{6}$$

The equations can now be written

$$[\sum_\alpha(\mathbf{p}_\alpha^2/2M_\alpha)+U_{n'}^{(e)}(R)+(\hbar/i)(\partial/\partial t)]\chi_{n'}(R)=-\sum_{n\neq n'}C_{n'n}\chi_n(R). \tag{4'}$$

The zeroth-order approximation corresponds to dropping the terms on the right side of this equation to give the usual nuclear Schrödinger equation,

$$[\sum_\alpha(p_\alpha^2/2M_\alpha)+U_{n'}^{(e)}(R)+(\hbar/i)(\partial/\partial t)]\chi_{n'}^0(R)=0. \tag{7}$$

The wave function for the whole system becomes

$$\Psi^0=\psi_{n'}(r, R)\chi_{n'}^0(R), \tag{8}$$

where $\chi_{n'}^0$ is some solution of the nuclear equation, Eq. (7).

The original perturbation method of Born and Oppenheimer led to a power series expansion in $(m/M)^{\frac{1}{4}}$ and showed that under the conditions imposed, the zeroth-order approximation is valid up to the fourth power of $(m/M)^{\frac{1}{4}}$. The experimental evidence also shows that the influence of the terms neglected in performing the separation is very small. Thus we may use the ψ and χ^0 obtained by performing the separation to determine the size and character of the quantities $\mathbf{A}_{n'n}^{(\alpha)}$ and $B_{n'n}^{(\alpha)}$ which make up the error terms.

For a homonuclear diatomic molecule it is simplest to use the relative coordinates

$$\mathbf{R}=\mathbf{R}_{12}=\mathbf{R}_2-\mathbf{R}_1 \qquad \mathbf{A}=\tfrac{1}{2}(\mathbf{R}_1+\mathbf{R}_2) \tag{9}$$

to describe the positions of the two nuclei. In these coordinates the expressions for the cross terms become

$$\mathbf{A}_{n'n}=\int\psi_{n'}^*(\partial/\partial\mathbf{R}_{12})\psi_n d\tau_e,$$

$$B_{n'n}=\int\psi_{n'}^*\nabla_{R_{12}}^2\psi_n d\tau_e,$$

$$\mathbf{D}_{n'n}=\int\psi_{n'}^*(\partial/\partial\mathbf{A})\psi_n d\tau_e,$$

$$F_{n'n}=\tfrac{1}{4}\int\psi_{n'}^*\nabla_A^2\psi_n d\tau_e,$$

$$\mathbf{A}_{n'n}^{(1)}=(\hbar/i)(-\mathbf{A}_{n'n}+\tfrac{1}{2}\mathbf{D}_{n'n}),$$

$$\mathbf{A}_{n'n}^{(2)}=(\hbar/i)(+\mathbf{A}_{n'n}+\tfrac{1}{2}\mathbf{D}_{n'n}), \tag{10}$$

$$B_{n'n}^{(1)}+B_{n'n}^{(2)}=-\hbar^2(B_{n'n}+F_{n'n}).$$

Some of these expressions can be put in a more easily calculated form by the use of a relation satisfied by the electronic wave function. The momentum operator for the system as a whole is the sum of the momentum operators for all of the particles. That is,

$$\mathbf{p}_{\text{total}}=\sum_i \mathbf{p}_i+\sum_\alpha \mathbf{p}_\alpha \tag{11}$$

Since $\mathbf{p}_{\text{total}}$ is the total momentum of the system, changing to relative coordinates would give

$$\mathbf{p}_{\text{total}}=(\hbar/i)\,(\partial/\partial\mathbf{R}_c). \tag{12}$$

Here $\mathbf{R}_c$ is the position of the center of gravity of the molecule. Since the usual electronic wave functions are written in coordinates measured relative to the nuclei, they do not depend on the position of the center of mass. Hence we have

$$(\partial/\partial\mathbf{R}_c)\psi=(i/\hbar)\,\mathbf{p}_{\text{total}}\psi=0. \tag{13}$$

This relation enables us to write the gradient of the electronic wave function with respect to the center of mass of the nuclei $(\partial/\partial\mathbf{\Lambda})\psi$ in terms of electronic derivatives. Since the sum of the momentum operators of the nuclei is the momentum of their center of mass

$$\frac{\hbar}{i}\frac{\partial}{\partial\mathbf{\Lambda}}\psi=\frac{\hbar}{i}\sum_\alpha\frac{\partial}{\partial\mathbf{R}_\alpha}\psi$$

$$=-\frac{\hbar}{i}\sum_\alpha\frac{\partial}{\partial\mathbf{r}_i}\psi. \tag{14}$$

In particular, this gives for the hydrogen molecule ion

$$(\partial/\partial\mathbf{\Lambda})\psi=-(\partial/\partial\mathbf{r}_e)\psi \qquad \nabla_\Lambda^2\psi=\nabla_{r_e}^2\psi. \tag{15}$$

Hence,

$$\mathbf{D}_{n'n}=-\int\psi_{n'}^*(\partial/\partial\mathbf{r}_e)\psi_n d\tau_e,$$

$$F_{n'n}=\tfrac{1}{4}\int\psi_{n'}^*\nabla_{r_e}^2\psi_n d\tau_e. \tag{16}$$

These formulas relate $\mathbf{D}_{n'n}$ and $F_{n'n}$ to the momentum dipole and kinetic energy of the electron, respectively. The quantity $\mathbf{D}_{n'n}$ is related to the dipole matrix element by the formula

$$\mathbf{D}_{n'n}=(m/\hbar^2)\,(E_{n'}^{(e)}-E_n^{(e)})\int\psi_{n'}^*\mathbf{r}_e\psi_n d\tau_e. \tag{17}$$

This formula is a trivial consequence of the commutation rule

$$[\mathcal{H}_e,\,\mathbf{r}_e]=-(\hbar^2/m)\,(\partial/\partial\mathbf{r}_e). \tag{18}$$

We shall not discuss $\mathbf{D}_{n'n}$ further, since it vanishes by the optical selection rules for the transition studied here. Calculations have been made for a number of pairs of states.[10]

If we use the Schrödinger equation, we find that

$$F_{n'n}=(m/2\hbar^2)\int\psi_{n'}V\psi_n d\tau_e-(m/2\hbar^2)\,E^{(e)}\delta_{n'n}, \tag{19}$$

where V is the electronic potential.

In order to carry out the differentiation with respect to the nuclear variables in $\mathbf{A}_{n'n}$ and $B_{n'n}$, either the coordinate system or the form of the derivatives must be changed. The coordinate system usually used for the electrons in these integrals is fixed to the nuclear skeleton, hence some of the nuclear coordinates do not appear as parameters in the wave function. It is usually easier to transform the derivatives to a coordinate system moving with the nuclei than to carry out the differentiation on the complicated function obtained when the wave function is expressed in fixed coordinates.

The Z axis of the coordinates system used in the electronic Schrödinger equation for a diatomic molecule is usually along the axis of the molecule. The azimuthal angle of the electronic motion can be measured from any line perpendicular to this axis. As the molecule rotates about its center of mass, the direction of the molecular axis can be given by the spherical coordinates α and β measured in a fixed reference frame. The azimuth of the axis of the molecule is α and its zenith is β. We measure the azimuthal angles for electronic motion from the line perpendicular to the molecular axis which lies in the fixed XY plane. The positive direction on this new X axis is chosen so that the angle β, which can be considered to be a rotation about this axis, is a positive rotation. The relation of the coordinate systems is shown in Fig. 1.

The transformation of the derivatives to this moving system is[11]

$$\partial/\partial\mathbf{R}_{12}=\bar{R}(\partial/\partial R)+R^{-1}\bar{\beta}[(\partial/\partial\beta)-(i/\hbar)\,J_z]$$

$$+(\bar{\alpha}/R\sin\beta)[(\partial/\partial\alpha)-(i/\hbar)\,(\cos\beta)\,J_z-(i/\hbar)\,(\sin\beta)\,J_y]$$

$$\nabla_{R_{12}}^2=(1/R^2)\,(\partial/\partial R)[R^2(\partial/\partial R)]+(R^2\sin\beta)^{-1}$$

$$\times[(\partial/\partial\beta)-(i/\hbar)\,J_x]\sin\beta[(\partial/\partial\beta)-(i/\hbar)\,J_x]$$

$$+(R^2\sin^2\beta)^{-1}[(\partial/\partial\alpha)-(i/\hbar)\,(\cos\beta)\,J_z$$

$$-(i/\hbar)\,(\sin\beta)\,J_y]^2. \tag{20}$$

The symbols $\bar{R}$, $\bar{\beta}$, and $\bar{\alpha}$ are unit vectors forming the

[10] D. R. Bates, J. Chem. Phys. **19**, 1122–1124 (1951); A. Dalgarno and J. T. Lewis, Proc. Phys. Soc. (London) **A69**, 285–292 (1956), and references cited.

[11] R. Kronig, Z. Physik **46**, 814 (1928); **50**, 347 (1928), J. Van Vleck, Phys. Rev. **33**, 467 (1929). This form of the relations can be found in D. R. Bates, H. S. Massey, and A. L. Stewart, Proc. Roy. Soc. (London) **A216**, 457 (1953).

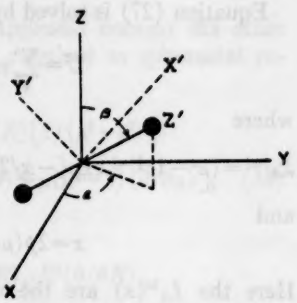

FIG. 1. Relationship between the space fixed coordinates axes XYZ and the molecular coordinate axes X'Y'Z'.

basis in the spherical coordinate system. The derivatives in these expressions are to be taken with the coordinates of the electrons in the moving system held constant. Actually the derivatives with respect to α and β are not needed because the wave function does not contain these variables. In these formulas $\mathbf{J}$ is the electronic angular momentum, which may or may not contain the spin, depending on the type of coupling chosen. In Hund's case A the spin is included and in B it is omitted.[12]

We can simplify the selection rules for the matrix elements by rearranging terms and making a slight change in the choice of the basis vectors. We form a row vector $\mathbf{e}$ whose components are made up of combinations of the symbols $\bar{R}$, $\bar{\beta}$, and $\bar{\alpha}$, and write the expression for $\mathbf{A}_{n'n}$ as the matrix product of $\mathbf{e}$ with a column vector of scalar components. Thus

$$\mathbf{e}=[\bar{R},\ (\bar{\beta}-i\bar{\alpha})/2R,\ (\bar{\beta}+i\bar{\alpha})/2R]$$

$$\partial/\partial\mathbf{R}_{12}=[R,\ (\bar{\beta}-i\bar{\alpha})/2R,\ (\bar{\beta}+i\bar{\alpha}/2R)]\begin{pmatrix}\partial/\partial R\\ -iJ_+/\hbar\\ -iJ_-/\hbar\end{pmatrix}$$

$$-(i/\hbar)\bar{\alpha}(\cot\beta/R)\,J_z$$

$$\nabla_{R_{12}}{}^2=(1/R^2)(\partial/\partial R)[R^2(\partial/\partial R)]-(\hbar^2R^2)^{-1}\mathbf{J}^2$$

$$-(\hbar^2R^2)^{-1}(\cot^2\beta-1)\,J_z^2$$

$$+(i/\hbar^2R^2)\cot\beta(J_+-J_-)\,J_z. \quad (21)$$

Here J_+ and J_- are the familiar raising and lowering operators.

If the spin of the system is quantised along the axis of the molecule, $\mathbf{J}$ equals $\mathbf{L}+\mathbf{S}$ in these formulas. Denoting the spin quantum numbers of the initial and final wave functions by S and S' and the corresponding Z component quantum numbers by Σ and Σ' we may determine the spin dependence of these expressions.

[12] G. Herzberg, *Spectra of Diatomic Molecules* (D. Van Nostrand Company, Inc., Princeton, New Jersey, 1950), second edition, p. 218.

In this way we obtain

$$\partial/\partial\mathbf{R}_{12}=\delta_{S',S}\{[\mathbf{e}\begin{pmatrix}\partial/\partial R\\ -(i/\hbar)L_+\\ -(i/\hbar)L_-\end{pmatrix}-(i/\hbar)\bar{\alpha}(\cot\beta/R)L_z]\delta_{\Sigma'\Sigma}$$

$$-\frac{i\Sigma\bar{\alpha}}{R}\cot\beta\delta_{\Sigma',\Sigma}-\frac{\bar{\alpha}+i\bar{\beta}}{2R}[(S+\Sigma+1)(S-\Sigma)]^{\frac{1}{2}}\delta_{\Sigma',\Sigma+1}$$

$$+\frac{\bar{\alpha}-i\bar{\beta}}{2R}[(S-\Sigma+1)(S+\Sigma)]^{\frac{1}{2}}\delta_{\Sigma',\Sigma-1}\Big\},$$

$$\nabla_{R_{12}}{}^2=\delta_{S',S}\Big\{\Big[(1/R^2)(\partial/\partial R)\Big(R^2\frac{\partial}{\partial R}\Big)-(\hbar^2R^2)^{-1}\mathbf{L}^2$$

$$+(\hbar^2R^2)^{-1}(1-\cot^2\beta)\,L_z^2+(i/\hbar^2R^2)\cot\beta(L_+-L_-)\,L_z$$

$$-(2\Sigma/\hbar R^2)\,L_z-\frac{S(S+1)}{R^2}+\frac{(1-\cot^2\beta)\Sigma}{R^2}\Big(\frac{2}{\hbar}L_z+\Sigma\Big)$$

$$+(i\Sigma/\hbar R^2)\cot\beta(L_+-L_-)\Big]\delta_{\Sigma',\Sigma}$$

$$-[(S-\Sigma+1)(S+\Sigma)]^{\frac{1}{2}}\Big[\frac{1}{\hbar R^2}L_+$$

$$+\frac{i}{R^2}\cot\beta\Big(\frac{1}{\hbar}L_z+\Sigma\Big)\Big]\delta_{\Sigma',\Sigma-1}$$

$$+[(S+\Sigma+1)(S-\Sigma)]^{\frac{1}{2}}[-(\hbar R^2)^{-1}L_-$$

$$+(i/R^2)\cot\beta(\hbar^{-1}L_z+\Sigma)]\delta_{\Sigma',\Sigma+1}\Big\}.$$

The explicit expressions for L_+ and L_- are given in Eq. (37). For the transition considered in our calculation, the spins are coupled to fixed axes so that we set $\mathbf{J}=\mathbf{L}$ in Eq. (21) and omit all further consideration of spin.

III. CALCULATION OF COUPLING TERMS USING THE EXACT WAVE FUNCTIONS OF THE HYDROGEN MOLECULE ION

The electronic Schrödinger equation for the hydrogen molecule ion has the form

$$-\tfrac{1}{2}\nabla^2\psi+[-(1/r_1)-(1/r_2)+(1/R)]\psi=E\psi. \quad (23)$$

Here r_1 and r_2 are the distances of the electron from the nuclei and R is the internuclear separation. All quantities are expressed in atomic units. This equation can be separated in the prolate spheroidal coordinates.

$$\mu=(r_1+r_2)/R,\quad \nu=(r_1-r_2)/R,\quad \phi, \quad (24)$$

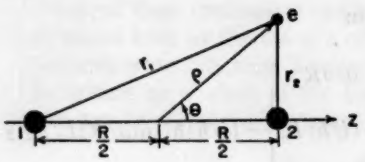

FIG. 2. Geometrical relations used in connection with the spheroidal coordinates.

to yield the equations

$$(d^2/d\phi^2)\Phi=-m^2\Phi, \tag{25}$$

$$(d/d\nu)[(1-\nu^2)(d/d\nu)S]+\{p^2\nu^2-A-[m^2/(1-\nu^2)]\}S=0, \tag{26}$$

$$(d/d\mu)[(\mu^2-1)(d/d\mu)U]+\{-p^2\mu^2+2R\mu+A-[m^2/(\mu^2-1)]\}U=0, \tag{27}$$

where

$$\psi=N^{-1}\Phi SU,$$

$$p^2=-(E-R^{-1})\tfrac{1}{2}R^2. \tag{28}$$

This p^2 is the symbol for the energy parameter usually used in the equations for H_2^+. It is not related to the momentum. The factor N^{-1} is the normalization; A and m are separation constants. We solve these equations by the methods instituted by Hylleraas.[13]

Equation (25) gives immediately

$$\Phi=\exp(im\phi) \qquad m=0,\pm1,\pm2,\pm3,\cdots. \tag{29}$$

Equation (26) is solved by expanding S in the form

$$S^{(m)}(A,p;\nu)=\sum_i d_i(A,p)\,P_{|m|+i}^{|m|}(\nu), \tag{30}$$

where P_n^m is the associated Legendre function. Substitution in (26) yields a three-term recursion relation for the coefficients

$$\frac{i(i-1)}{(2i+2\,|\,m\,|-1)(2i+2\,|\,m\,|-3)}d_{i-2}+\frac{(i+2\,|\,m\,|+1)(i+2\,|\,m\,|+2)}{(2i+2\,|\,m\,|+3)(2i+2\,|\,m\,|+5)}d_{i+2}+\left[\frac{2(i+|\,m\,|)(i+|\,m\,|+1)-2\,|\,m\,|^2-1}{(2i+2\,|\,m\,|+3)(2i+2\,|\,m\,|-1)}-\frac{(i+|\,m\,|)(i+|\,m\,|+1)+A}{p^2}\right]d_i=0. \tag{31}$$

For any given p, the separation constant A is determined by requiring the convergence of a certain continued fraction obtained from this recursion relation.

[13] E. A. Hylleraas, Z. Physik **71**, 739 (1931); see also W. T. Baber and H. R. Hasse, Proc. Cambridge Phil. Soc. **31**, 564 (1935).

Equation (27) is solved by expanding U in the form

$$U=\sum_k \gamma_k \mathfrak{L}_k^{|m|}, \tag{32}$$

where

$$\mathfrak{L}_k^{|m|}=(\mu^2-1)^{\frac{1}{2}|m|}\exp(-x/2)\,L_{k+|m|}^{|m|}(x)/(|\,m\,|+k)!$$

and

$$x=2p(\mu-1). \tag{33}$$

Here the $L_k^m(x)$ are the usual associated Laguerre polynomials.[14] Substitution of the expansion (32) into Eq. (27) gives the three-term recursion relation for the coefficients:

$$(|\,m\,|+k+1)[k+1-(R/p)]\gamma_{k+1}+k[k+|\,m\,|-(R/p)]\gamma_{k-1}+\{(k+|\,m\,|)(|\,m\,|+1)-p^2+2R+A-(2k+|\,m\,|+1)[2p+|\,m\,|+k+1-(R/p)]\}\gamma_k=0. \tag{34}$$

For a given p and a value of A obtained in the solution of Eq. (26), this recursion relation, converted to a continued fraction, implicitly determines R. Values of p and A as functions of R are tabulated in the literature.[15]

In order to perform calculations with these wave functions, the expressions (21) must be written in spheroidal coordinates. The necessary relations can be obtained from the geometry of Fig. 2 and Eq. (24):

$$\rho^2=\tfrac{1}{4}R^2(\mu^2+\nu^2-1), \qquad \cos\theta=\mu\nu/(\mu^2+\nu^2-1)^{\frac{1}{2}}. \tag{35}$$

The first derivatives we need are given by

$$\rho(\partial/\partial\rho)=(\mu^2-\nu^2)^{-1}[\nu(1-\nu^2)(\partial/\partial\nu)+\mu(\mu^2-1)(\partial/\partial\mu)],$$

$$\partial/\partial\theta=\frac{[(\mu^2-1)(1-\nu^2)]^{\frac{1}{2}}}{\mu^2-\nu^2}[\nu(\partial/\partial\mu)-\mu(\partial/\partial\nu)]. \tag{36}$$

From these expressions we obtain formulas for the angular momentum operators,

$$L_\pm=\hbar\delta_{m\pm1,m}\mathfrak{L}_\pm$$

$$\mathfrak{L}_\pm=(\partial/\partial\theta)\mp m\cot\theta$$

$$=\frac{\nu(1-\nu^2)^{\frac{1}{2}}}{\mu^2-\nu^2}\left[(\mu^2-1)^{\frac{1}{2}}\left(\frac{\partial}{\partial\mu}\mp m\frac{\mu}{\mu^2-1}\right)\right]-\frac{\mu(\mu^2-1)^{\frac{1}{2}}}{\mu^2-\nu^2}\left[(1-\nu^2)^{\frac{1}{2}}\left(\frac{\partial}{\partial\nu}\pm m\frac{\nu}{1-\nu^2}\right)\right]. \tag{37}$$

[14] L. Pauling and E. B. Wilson, Jr., *Introduction to Quantum Mechanics* (McGraw-Hill Book Company, Inc., New York, 1935), p. 131.

[15] D. R. Bates, K. Ledsham, and A. L. Stewart, Phil. Trans. Roy. Soc. (London) **A246**, 215 (1953); R. F. Wallis and H. Hulburt, J. Chem. Phys. **22**, 774 (1954).

Relations derived in the Appendix convert the other two expressions which are required to spheroidal coordinates:

$$(\partial/\partial R)_{\theta,\rho}=(\partial/\partial R)_{\mu,\nu}-(1/R)[1/(\mu^2-\nu^2)]\times[\nu(1-\nu^2)(\partial/\partial\nu)+\mu(\mu^2-1)(\partial/\partial\mu)], \quad (38)$$

$$\nabla_{R\theta\phi}^2=\tfrac{1}{4}(\mu^2+\nu^2-1)\nabla_{\mu,\nu,\phi}^2+(1/R^2)(\partial/\partial R)_{\mu\nu}R^2(\partial/\partial R)_{\mu,\nu}-[2/R(\mu^2-\nu^2)][\nu(1-\nu^2)(\partial/\partial\nu)+\mu(\mu^2-1)(\partial/\partial\mu)](\partial/\partial R)_{\mu,\nu}-[2/R^2(\mu_2-\nu^2)][\nu(1-\nu^2)(\partial/\partial\nu)+\mu(\mu^2-1)(\partial/\partial\mu)]. \quad (39)$$

After making these substitutions, it is possible to write the expressions in a form so that all integrations can be carried out analytically. Complicated expressions are obtained involving the expansion coefficients, parameters, and the first derivatives of these quantities with respect to R. These expressions can be evaluated by using the tables in the literature.[16]

IV. RESULTS OF THE CALCULATIONS

Calculations of the matrix elements A, B, and F of Eq. (10) were made for the transition $1s\sigma_g-2s\sigma_g$ for internuclear separations between 1 and 5 Bohr radii. The various series involved for these states all converge rapidly and only two to three terms were required in each of them to obtain accurate wave functions. However, the matrix elements depend in a sensitive fashion on the exact shape of the wave functions, so that their accuracy is not as great. The dependence of the wave functions on the internuclear separation R is complicated by the fact that the spheroidal coordinates themselves contain R as a scale factor. This dependence is larger than the actual physical effect and leads to internal cancelation in the calculations. This greatly reduces tne accuracy of the results, particularly at small values of R. Thus, the inaccuracy in the final results for $B_{1s\sigma,2s\sigma}$, which involves the most complicated calculation, is probably about 10%. The matrix element A should be more accurate. The results for A and B are shown in Figs. 3 and 4, respectively, along with results obtained from LCAO wave functions and from perturbation theory.

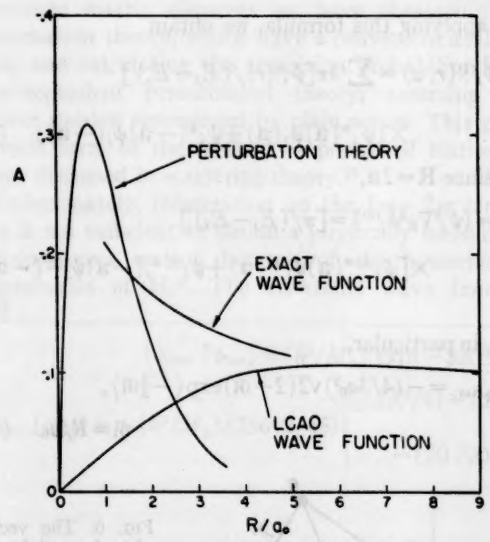

FIG. 3. A as a function of internuclear separation for $1s\sigma_g-2s\sigma_g$.

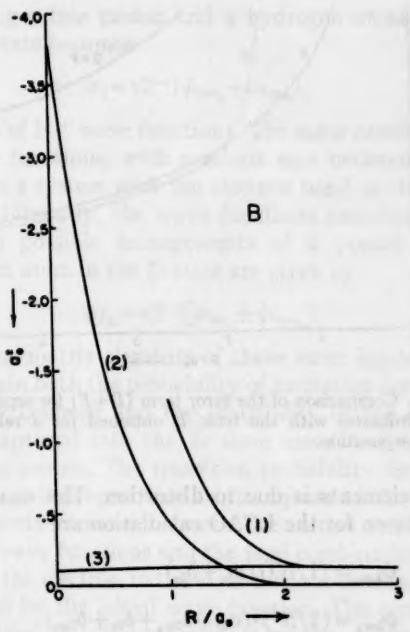

FIG. 4. B as a function of internuclear separation calculated (1) from exact wave functions, (2) from perturbation theory, and (3) from LCAO wave functions.

According to Eq. (10), the quantity F should be added to B to give the complete contribution to the coupling. However, F no longer appears as one of the cross terms if the center of mass motion is removed from the equations before the Born-Oppenheimer separation is carried out. This will be shown in Sec. VI. Consequently we have graphed B rather than $B+F$ in Fig. 4. For the united atom, F is 11% of B. The comparison at larger internuclear separations is given in Fig. 5.

Comparison of the curves for A and B calculated from the exact functions with the results of the LCAO method show clearly that most of the size of the

[16] The details of this work are given in University of Wisconsin Naval Research Laboratory Report WIS-AEC-19, September, 1958, which is available on request.

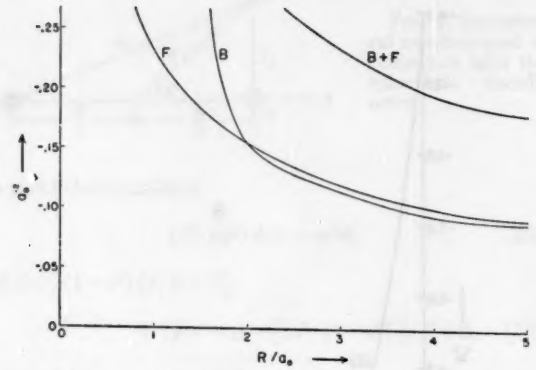

FIG. 5. Comparison of the error term $(B+F)$ for separation in fixed coordinates with the term B obtained for a relative coordinate separation.

matrix elements is due to distortion. The wave functions chosen for the LCAO calculation are

$$\psi_{1s\sigma_g}=(1/N^{\frac{1}{2}})(a_{1s}+b_{1s})$$
$$\psi_{2s\sigma_g}=(1/N')^{\frac{1}{2}}(a_{2s}+a_{2p_s}+b_{2s}+b_{2p_s}). \quad (40)$$

The atomic orbitals used here are hydrogenic wave functions. These functions are exact at infinite separation.[17] The wave functions are not orthogonal, but it was found that, including the differentiation of the normalization factor, the results of the calculation are negligibly different from those obtained when a small amount of the $1s\sigma$ function is mixed into the $2s\sigma$ function to obtain orthogonality.

Unfortunately, the method used for calculating the exact results has not proved practical for small values of the internuclear distance. Consequently, it is desirable to obtain some information at small internuclear separations by a perturbation method using the wave functions of the united atom He^+. These results are exact at zero internuclear separation, but do not fit together with the exact results obtained at $R=1$. The method should also be useful for other molecules.

The Schrödinger equation for the motion of the electron in H_2^+ an be written as

$$[\mathfrak{H}^{(0)}+\mathfrak{H}^{(1)}]\psi=E\psi$$

where

$$E=E^{(e)}-R^{-1},$$
$$\mathfrak{H}^{(0)}=-\tfrac{1}{2}\nabla^2-2\,|\,\mathbf{r}\,|^{-1},$$
$$\mathfrak{H}^{(1)}=-\,|\,\mathbf{r}-\mathbf{a}\,|^{-1}-|\,\mathbf{r}+\mathbf{a}\,|^{-1}+2\,|\,\mathbf{r}\,|^{-1}. \quad (41)$$

$\mathfrak{H}^{(0)}$ is the Hamiltonian for the united atom, and $\mathfrak{H}^{(1)}$ is to be treated as the perturbation. The nuclei have positions $\mathbf{a}$ and $-\mathbf{a}$; $\mathbf{r}$ is the electronic coordinate.

[17] A level diagram is given by H. Bethe, *Handbuch der Physik* (Springer-Verlag, Berlin, 1933), p. 528.

This is shown in Fig. 6. The usual formula of first-order perturbation theory is

$$\psi_j^{(1)}(\mathbf{r},\mathbf{a})=\psi_j^{(0)}(\mathbf{r})+\sum_{i;\,i\neq j}[(\psi_i^{0}\mathfrak{H}^{(1)}\psi_j^{(0)})/(E_j-E_i)]\psi_i^{(0)}(\mathbf{r}). \quad (42)$$

After taking the gradient of this expression with respect to $\mathbf{a}$ we obtain

$$(\partial/\partial\mathbf{a})\psi_j^{(1)}(\mathbf{r},\mathbf{a})=\sum_i{}'[\psi_i^{0}(r)/(E_j-E_i)](\partial/\partial\mathbf{a})(\psi_i^{(0)}\mathfrak{H}^{(1)}\psi_j^{(0)}). \quad (43)$$

By another differentiation the Laplacian can be obtained:

$$(\partial/\partial\mathbf{a})\cdot(\partial/\partial\mathbf{a})\psi_j^{(1)}(\mathbf{r},\mathbf{a})=\sum_i{}'[\psi_i^{(0)}(r)/(E_j-E_i)]\nabla_a^2\int\psi_i^{*}\times[-\,|\,\mathbf{r}-\mathbf{a}\,|^{-1}-|\,\mathbf{r}+\mathbf{a}\,|^{-1}+(2/r)]\psi_j d\tau. \quad (44)$$

It is well known in electrostatics that if

$$V(\mathbf{a})=\int[\rho(\mathbf{r})/|\,\mathbf{r}-\mathbf{a}\,|]d\tau_r, \quad (45)$$

then

$$\nabla^2V(\mathbf{a})=-4\pi\rho(\mathbf{a}), \quad (46)$$

which means

$$\nabla_a^2\left\{\int[\rho(r)/|\,\mathbf{r}-\mathbf{a}\,|]d\tau_r\right\}=-4\pi\rho(a). \quad (47)$$

On applying this formula, we obtain

$$\nabla_a^2\psi_j^{(1)}(r,a)=\sum_i{}'4\pi[\psi_i^{0}(r)/(E_j-E_i)]\times(\psi_i^{*}(\mathbf{a})\psi_j(\mathbf{a})+\psi_i^{*}(-\mathbf{a})\psi_j(-\mathbf{a})) \quad (48)$$

or, since $\mathbf{R}=2\mathbf{a}$,

$$B_{ij}=(\psi_i^{0}\nabla_R^2\psi_j^{(0)})=[\pi/(E_j-E_i)]\times[\psi_i^{(0)*}(\mathbf{a})\psi_j^{(0)}(\mathbf{a})+\psi_i^{(0)*},(-\mathbf{a})\psi_j^{(0)}(-\mathbf{a})), \quad (49)$$

and, in particular,

$$B_{2s\sigma_g,1s\sigma_g}=-(4/3a_0^2)\sqrt{2}(2-\mathfrak{R})\exp(-\tfrac{3}{2}\mathfrak{R}),\qquad \mathfrak{R}=R/a_0. \quad (50)$$

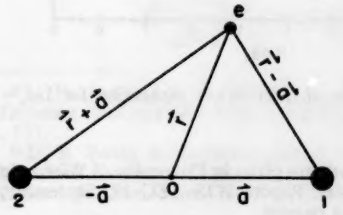

FIG. 6. The vectors used in determining the matrix elements approximately by perturbation theory.

Examination of the higher orders of the perturbation shows that these results are exact at $R=0$. To obtain a similar expression for A we use the Neumann expansions of the potentials appearing in Eq. (43).[18]

$$1/r_{12}=\sum_n[(r_<)^n/(r_>)^{n+1}]P_n(\cos\theta_{12})$$

$$3\mathcal{C}^{(1)}=-2\sum_{n=1}^{\infty}r^{-1}(a/r)^{2n}P_{2n}(\cos\theta) \quad a<r$$

$$3\mathcal{C}^{(1)}=(2/r)-2\sum_{n=0}^{\infty}a^{-1}(r/a)^{2n}P_{2n}(\cos\theta) \quad a>r. \tag{51}$$

For the transition $1s\sigma-2s\sigma$ all of the terms except for $n=0$ integrate to zero by symmetry. This leaves

$$A_{2s\sigma,1s\sigma}=[\psi_{2s}^{(0)}(\partial/\partial R)\psi_{1s}^{(0)}]$$

$$=[2\pi/(E_{1s}-E_{2s})(\partial/\partial a)\int_0^a\psi_{2s}[(2/r)-(2/a)]\psi_{1s}r^2dr \tag{52}$$

or

$$A_{2s\sigma,1s\sigma}=-(8\sqrt{2}/9a_0)\,\mathfrak{R}\exp(-3\mathfrak{R}/2) \tag{53}$$

where $\mathfrak{R}=R/a_0$.

V. CALCULATION OF THE CROSS SECTION

It is interesting to check whether the A's and the B's are of the proper size to give inelastic collision probabilities in agreement with those obtained using other methods of scattering theory. A simple answer to this question can be obtained by using the approximate matrix elements we have obtained from perturbation theory, which have a convenient analytic form, and calculating the transition probability from time-dependent perturbation theory, assuming the nuclear motion represented by plain waves. This gives a crude form of the method of perturbed stationary states discussed in scattering theory.[19]

Unfortunately, information on the $1s\sigma-2s\sigma$ transition is not sufficient to obtain a physically meaningful collision cross section because of the homonuclear degeneracies of H_2^+. The electronic wave function describing a free proton and a hydrogen atom in the ground state becomes

$$\phi_i=\sqrt{2}^{-1}(\psi_{1s\sigma_g}+\psi_{2p\sigma_u}),$$

in terms of H_2^+ wave functions. The same combination of wave functions, with a minus sign between them, describes a system with the electron bond to the other proton. Similarly, the wave functions associated with the two possible arrangements of a proton and a hydrogen atom in the $2s$ state are given by

$$\phi_{f\pm}=\sqrt{2}^{-1}[\psi_{2s\sigma_g}\pm\psi_{ep\sigma_u}].$$

From the matrix elements of these wave functions we can obtain both the probability of excitation into the $2s$ state by collision and the probability of the electron being captured into the $2s$ state associated with the colliding proton. The transition probability for excitation P_{excit} is proportional to the square of the interaction matrix element between the initial combination of H_2^+ wave functions and the final combination which assigns the electron to the same nucleus to which it was assigned by the initial wave function. The probability of capture P_{cap} is proportional to the square of the matrix element involving the transition between the initial wave function and the $2s$ combination which assigns the electron to the opposite nucleus. Thus, we have

$$\begin{aligned}P_{\text{excit, cap}}&\propto|(\phi_{f\pm},I\phi_I)|^2\\&\propto\tfrac{1}{4}|(2s\sigma_g,I1s\sigma_g)|^2\\&\quad\pm\tfrac{1}{2}(3p\sigma_u,I2p\sigma_u)(2s\sigma_g,I1s\sigma_g)\\&\quad+\tfrac{1}{4}|(3p\sigma_u,I2p\sigma_u)|^2.\end{aligned} \tag{54}$$

The $g-g$, $u-u$ selection rule eliminates the other terms which might be expected in this formula. Each matrix element, of course, also includes integration over the nuclear variables.

Knowledge of the matrix elements for the $2p\sigma-3p\sigma$ transition is necessary to calculate either of these cross sections. It is hoped that the same perturbation method used for $1s\sigma-2p\sigma$ gives a reasonable approximation to the corresponding exact results in this case. Thus, expressing R in Bohr units, we have

$$(\phi_{2s\sigma},I\phi_{1s\sigma})=(\hbar^2/M_p)\exp(-3R/2)[(4\sqrt{2}/3)(2-R)+(16\sqrt{2}/9)R(\partial/\partial R)], \tag{55}$$

$$\begin{aligned}(\phi_{3p\sigma},I\phi_{2p\sigma})&=+(\hbar^2/M_p)(256\sqrt{2}/45)\begin{Bmatrix}[(3R^2/4)-(R^3/8)]\exp(-5R/6)\\-(30\,720/R^4)(\tfrac{3}{5})^9(\partial/\partial R)\end{Bmatrix}\\&\quad+\tfrac{1}{3}(\hbar^2/M_p)(32\,768\sqrt{2})\begin{Bmatrix}(16/R^4)(\tfrac{3}{5})^9+(8/R^3)(\tfrac{3}{5})^8\\+(2/R^2)(\tfrac{3}{5})^7+(1/3R)(\tfrac{3}{5})^6\\+\tfrac{1}{4}(\tfrac{3}{5})^5+(R/480)(\tfrac{3}{5})^3+(R^3/12\,800)\end{Bmatrix}\exp(-5R/6)(\partial/\partial R).\end{aligned} \tag{56}$$

[18] H. Eyring, J. Walter, and G. E. Kimball, *Quantum Chemistry* (John Wiley & Sons, Inc., New York, 1944), p. 370, v. 6.
[19] N. F. Mott and H. S. Massey, *The Theory of Atomic Collisions* (Clarendon Press, Oxford, 1949), second edition, p. 153 ff; D. R. Bates, H. S. Massey, and A. L. Stewart, Proc. Roy. Soc. (London) **A216**, 457 (1953).

These expressions are substituted into the usual formula of time-dependent perturbation theory which gives the differential cross section for excitation, $\sigma_{\text{excit}}(\theta)$, and the differential cross section for capture,[20] $\theta_{\text{cap}}(\theta)$:

$$\sigma_{\text{excit,cap}}(\theta)=(k/k_0)\,(\mu_{\text{nuc}}/2\pi\hbar^2)^2\left|\int \exp[(-i\mathbf{k}\cdot\mathbf{R})](\phi_{f\pm},I\phi_i)\,\exp(i\mathbf{k}_0\cdot\mathbf{R})\,d\tau\right|^2. \quad (57)$$

Unlike the exact results, the approximate expressions for the matrix elements go to zero for large separations of the nuclei. This error is actually fortunate since scattering theory is not possible without this property. The exact results would also go to zero in this way if the BO separation were carried out in a suitable set of relative coordinates, but the Schrödinger equation could not be solved by separation. A simple change to relative coordinates also justifies dropping the terms in the interaction arising from the motion of the nuclear center of mass, as we have done to obtain Eq. (57). Both these points will be discussed in the last section of this paper.

TABLE I. Total cross sections for the proton hydrogen atom collision. Here Q_{excit} is the total cross section for excitation from the $1s$ to the $2s$ atomic state. The Q_{cap} corresponds to the capture of the $1s$ electron into the $2s$ state of the collising proton.

Energy (ev)	$Q_{\text{excit}}/\pi a_0^2$	$Q_{\text{cap}}/\pi a_0^2$
20.39	0.000	0.000
25.15	1.789×10^{-8}	1.543×10^{-8}
30.87	1.094×10^{-7}	8.806×10^{-8}
33.46	1.979×10^{-7}	1.545×10^{-7}
36.47	3.562×10^{-7}	2.687×10^{-7}
39.95	6.384×10^{-7}	4.630×10^{-7}
43.95	1.140×10^{-6}	7.901×10^{-7}
48.57	2.030×10^{-6}	1.335×10^{-6}
53.86	3.604×10^{-6}	2.232×10^{-6}
59.94	6.387×10^{-6}	3.689×10^{-6}
66.90	1.130×10^{-5}	6.023×10^{-6}
74.88	1.996×10^{-5}	9.698×10^{-6}
84.01	3.523×10^{-5}	1.537×10^{-5}
94.46	6.217×10^{-5}	2.392×10^{-5}
106.4	1.097×10^{-4}	3.645×10^{-5}
120.1	1.935×10^{-4}	5.413×10^{-5}
135.7	3.417×10^{-4}	7.789×10^{-5}
153.6	6.035×10^{-4}	1.078×10^{-4}
174.0	1.067×10^{-3}	1.417×10^{-4}
197.4	1.887×10^{-3}	1.742×10^{-4}
224.1	3.340×10^{-3}	1.954×10^{-4}
254.6	5.912×10^{-3}	1.945×10^{-4}
289.5	1.047×10^{-2}	1.740×10^{-4}
329.4	1.851×10^{-2}	1.960×10^{-4}
375.0	3.269×10^{-2}	4.982×10^{-4}
427.1	5.756×10^{-2}	1.758×10^{-3}
486.6	1.010×10^{-1}	5.643×10^{-3}
554.7	1.760×10^{-1}	1.589×10^{-2}
632.5	3.044×10^{-1}	4.022×10^{-2}
721.3	5.211×10^{-1}	9.362×10^{-2}
822.9	8.803×10^{-1}	2.032×10^{-1}
939.0	1.463	4.152×10^{-1}
1072	2.385	8.020×10^{-1}
1223	3.795	1.468
1397	5.871	2.548
1595	8.788	4.186

[20] See L. I. Schiff, *Quantum Mechanics* (McGraw-Hill Book Company, New York, 1949), second edition, Chap. 8, especially pp. 199–201 and 205–208.

The differential cross section becomes

$$\sigma_{\text{excit,cap}}(\theta)=2^{23}(k/k_0)\left\{\mp[\rho/3(4K^2+9)^3]+2^6\left[\frac{(\frac{25}{27}-(4K^2/5)\rho}{[4K^2+(25/9)]^5}\right.\right.$$
$$\left.\left.+(\rho+K^2)\left(\frac{(11/125)-(108K^2/625)+(7776K^4/78\,125)}{[4K^2+(25/9)]^3}-\frac{4374}{1\,953\,125}\ln\left(1+\frac{25}{36K^2}\right)\right)\right]\right\}^2, \quad (58)$$

where

$$K^2=k_0^2+k^2-2kk_0\cos\theta,$$

and

$$k_0^2-k^2=\rho=3M_p/8\mu_e.$$

The minus sign gives the differential cross section for excitation, and the plus sign gives the cross section for capture. It is difficult to determine which $2s$ wave function assigns the electron to which nucleus, so this assignment has been made on the physical assumption that the excitation cross section is larger than the capture cross section.

The Ferranti Mercury computing machine at Oxford was used to integrate numerically the differential cross section $\sigma(\theta)$ over all angles θ to obtain the total cross sections Q. The resulting total cross sections Q_{excit} and Q_{cap} are given in Table I. The cross section for transition of particles in the $1s\sigma$ state to the $2s\sigma$ state which is obtained by using the expression of Eq. (55) as the interaction is

$$\sigma(\theta)=k/k_0(M_p/\mu_e)^2[2^{17}/(4K^2+9)^6],$$
$$Q_{s-s}/\pi a_0^2=(2^{15}/5k_0^2)\,(M_p/\mu_e)^2[(4[k_0-k]^2+9)^{-5}-(4[k_0+k]^2+9)^{-5}]. \quad (59)$$

For some reason this is exactly the Born approximation for the excitation of the atom to the $2s$ state by collision with the proton as given by a simple adaptation of the treatment given by Schiff.[18] Figure 7 shows the behavior of these cross sections. At low energies the $1s\sigma-2s\sigma$ transition gives the predominant contribution to both the excitation and capture cross sections. The contribution from the $2p\sigma-3p\sigma$ transition is small at low energies, but becomes larger than the $1s\sigma-2s\sigma$ part around 300 ev. The two contributions add to give the excitation cross section and subtract to give the cross section for capture. At higher energies our calculated values of the $2p\sigma-3p\sigma$ contribution continue to increase

until the results become too large to be physically sensible. The Born approximation curve (3) in Fig. 7 should indicate the proper behavior at high energies. This type of failure of the theory has been discussed in detail by Bates[21] for a very similar method for treating scattering. It appears that the electron cannot follow the rapid rotation of the nuclei in the "molecular complex" formed during the collision.

It is tempting to believe that the proper exact matrix elements would give similar but slightly smaller cross section curves. The approximate A curve obtained by the perturbation calculation would match up with the exact curve at $R=1$ if it were reduced by a factor of the square root of two. This would reduce the cross sections obtained by about one-half. However, definite conclusions await calculation of the exact curves for smaller internuclear separation. This work is being considered.

VI. BORN-OPPENHEIMER SEPARATION IN RELATIVE COORDINATES

Instead of directly performing the BO separation as already outlined, it is possible to separate off the motion of the center of mass from the Schrödinger equation before performing the separation. The two approaches give essentially different Born-Oppenheimer separations, with different accuracy and somewhat different cross terms between the electronic and nuclear motions. If the center of mass motion is removed from the Schrödinger equation, the center of mass of the system

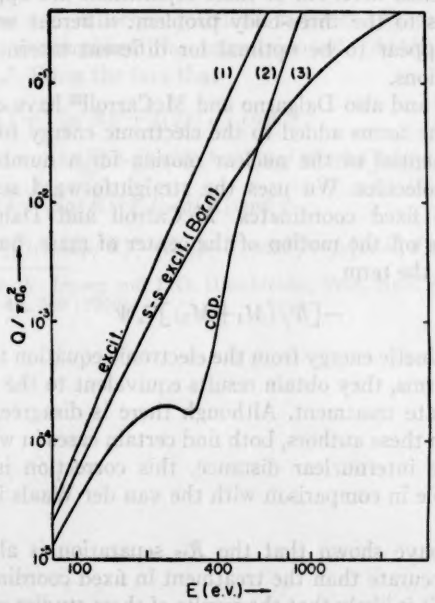

FIG. 7. Total cross sections for proton-H atom collision. Here the three curves are (1) Excitation to $2s$ state; (2) capture into $2s$ state on the colliding proton; (3) excitation cross section obtained using the Born approximation, $Q_{e\to}$.

[21] D. R. Bates, Proc. Roy. Soc. (London) **A243**, 15 (1957); **A245**, 299 (1958).

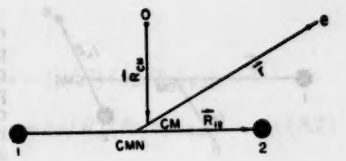

FIG. 8. The "R_{12}" relative coordinate system. The point marked CM is the center of mass of the system. The point marked CMN is the center of mass of the nuclei.

remains fixed in space because it has been separated from the equations exactly. As the electrons carry out the motion described by the electronic Schrödinger equation, the nuclei must move slightly to balance the motion of the electrons and keep the center of mass of the system fixed.

The most convenient set of relative coordinates for the hydrogen molecule ion gives the Schrödinger equation

$$\{-\tfrac{1}{2}\hbar^2[(M_1+M_2)^{-1}+m_e^{-1}]\nabla_e^2-\tfrac{1}{2}\hbar^2(M_1^{-1}+M_2^{-1})\nabla_{R_{12}}^2+V\}\Psi=i\hbar(\partial/\partial t)\Psi. \quad (60)$$

The electron coordinates are referred to the center of mass of the nuclei, r_1 and r_2 are the distances of the electron from nuclei 1 and 2, respectively, and the R_{12} coordinate is the distance between the two nuclei. This coordinate system is shown in Fig. 8. We choose the electronic Schrödinger equation to be

$$\{-\tfrac{1}{2}\hbar^2[(M_1+M_2)^{-1}+m_e^{-1}]\nabla_e^2-r_1^{-1}-r_2^{-1}+R^{-1}\}\Psi=E_e\psi. \quad (61)$$

Note that the kinetic energy term contains a relative mass. Putting

$$\Psi=\sum_n\chi_n(R_{12})\psi_n(r,R_{12}), \quad (62)$$

and carrying through the separation procedure in the obvious way, we obtain only the two correction terms

$$\mathbf{A}_{n'n}=\int\psi_{n'}^*(\partial/\partial\mathbf{R}_{12})\psi_n d\tau_e,$$
$$B_{n'n}=\int\psi_{n'}^*\nabla_{R_{12}}^2\psi_n d\tau_e, \quad (63)$$

instead of the four quantities given in Eq. (10). These quantities appear with the same coefficients as in the previous treatment. Calculation of the coupling terms gives us the opportunity to determine which of these two ways of performing the separation more effectively isolates the electronic motion from the nuclear motion. Although the difference is small, Fig. 5 shows that the terms B and F add rather than subtract, so that removing the center of mass motion before performing the separation, at least between this pair of states, decreases the amount of coupling The coupling is probably decreased for most of the other transitions as well, as we shall see.

The Born-Oppenheimer separation performed after the center of mass motion has been removed from the

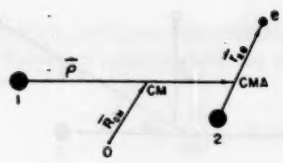

FIG. 9. The "ρ" relative coordinate system. The point marked CM is the center of the system. The point marked CMA is the center of mass of the atom made up of the electron and nucleus 2.

equations is not unique. By using different sets of relative coordinates it is possible to obtain different BO separations. For example, another separation in relative coordinates is possible which is particularly appropriate to the atom plus particle problem. The coordinates are the position of the center of mass of the system, $\mathbf{R}_{CM}$, the relative position of the particle from the center of mass of the atom $\boldsymbol{\rho}$ and the position of the electron relative to the nucleus of the atom $\mathbf{r}_{2e}$. These coordinates are shown in Fig. 9.

To illustrate the different separations, it is convenient to write down the cross terms in the special case when the nuclei are far apart and the electron is bound to one of them only. For this case we can obtain three different sets of cross terms depending upon whether we use fixed coordinates or either of the two sets of relative coordinates. We assume that the electron is on nucleus 2, and that the mass of each nucleus is M_p. The Schrödinger equation for the last set of coordinates is

$$[-\tfrac{1}{2}\hbar^2(M_p^{-1}+m_e^{-1})\nabla_e^2-\tfrac{1}{2}\hbar^2[M_p^{-1}+(M_p+m_e)^{-1}]\nabla_\rho^2 +V]\Psi=i\hbar(\partial/\partial t)\Psi. \quad (64)$$

The Schrödinger equations for the other two separations are given in Eqs. (1) and (60). The three separations beginning with the three equations (1), (60), and (64) will be referred to as the fixed coordinate separation, the R_{12} separation, and the ρ separation, respectively.

The electronic Schrödinger equations, obtained by dropping the nuclear kinetic energy terms in these equations, are all nearly the same. In calculating the cross terms we will use the same electronic wave functions for all three cases. Using the proper wave functions for each case would not change the results appreciably.

The true wave functions for this case can be obtained without any BO separation since nucleus 1 is assumed to be far away. They are the wave functions of the hydrogen atom. These wave functions depend only on the vector between nucleus 2 and the electron $\mathbf{r}_e-\mathbf{R}_2$.

We convert all of the nuclear derivatives to the fixed set of coordinates so that they can be compared with each other as follows:

$$\partial/\partial\mathbf{R}_{12}=\tfrac{1}{2}[(\partial/\partial\mathbf{R}_2)-(\partial/\partial\mathbf{R}_1)],$$

$$\partial/\partial\boldsymbol{\rho}=-\frac{M_p+m_e}{2M_p+m_e}\frac{\partial}{\partial\mathbf{R}_1}+\frac{M_p}{2M_p+m_e}\left(\frac{\partial}{\partial\mathbf{R}_2}+\frac{\partial}{\partial\mathbf{r}_e}\right). \quad (65)$$

Since the wave functions depend only on $\mathbf{r}_e-\mathbf{R}_2$,

$$(\partial/\partial\mathbf{R}_2)\psi_e=-(\partial/\partial\mathbf{r}_e)\psi_e, \qquad \nabla_{R_2}^2\psi_e=\nabla_e^2\psi_e,$$
$$(\partial/\partial\mathbf{R}_1)\psi_e=0. \quad (66)$$

This enables us to write the cross terms for the three separations as:

I. Separation in fixed coordinates

$$C_{n'n}=-(\hbar^2/M_p)\int\psi_{n'}^*(\partial/\partial\mathbf{r}_e)\psi_n d\tau_e\cdot(\partial/\partial\mathbf{R}_2) -(\hbar^2/2M_p)\int\psi_{n'}^*\nabla_e^2\psi_n d\tau_e.$$

II. The R_{12} separation

$$C_{n'n}=-(\hbar^2/2M_p)\int\psi_{n'}^*(\partial/\partial\mathbf{r}_e)\psi_n d\tau_e \cdot[(\partial/\partial\mathbf{R}_2)-(\partial/\partial\mathbf{R}_1)]-(\hbar^2/4M_p)\int\psi_{n'}^*\nabla_e^2\psi_n d\tau_e.$$

III. The ρ separation

$$C_{n'n}=0. \quad (67)$$

These values for I and II agree with the limits at infinite separation of the graphs of Fig. 9. We see that the ρ separation is exact in this limit. The R_{12} separation is probably more accurate when the nuclei are close together. Unfortunately our evaluation of the cross terms cannot be adapted to the ρ separation, so this will not be checked here. All of these separations are approximations to the three-body problem: different separations appear to be optimal for different internuclear separations.

Wu[22] and also Dalgarno and McCarroll[23] have calculated the terms added to the electronic energy to give the potential of the nuclear motion for a number of light molecules. Wu uses the straightforward separation in fixed coordinates. McCarroll and Dalgarno separate off the motion of the center of mass, but, by moving the term

$$-[\hbar^2/(M_1+M_2)]\nabla_e^2\Psi$$

in the kinetic energy from the electronic equation to the cross terms, they obtain results equivalent to the fixed coordinate treatment. Although there is disagreement between these authors, both find certain cases in which, at large internuclear distance, this correction is not negligible in comparison with the van der Waals interaction.

We have shown that the R_{12} separation is always more accurate than the treatment in fixed coordinates, so that it is likely that the results of these studies would be more meaningful if based upon a relative coordinate

[22] T. Y. Wu and A. B. Bhatia, J. Chem. Phys. **24**, 48 (1956); T. Y. Wu, *ibid.* **24**, 444 (1956).

[23] A. Dalgarno and R. McCarroll, Proc. Roy. Soc. (London) **A237**, 383 (1956); **A239**, 413 (1957).

separation. We believe that the ρ separation would be the logical choice of relative coordinates for such studies on H_2^+, and would probably yield the smallest correction. For more than three particles the number of possible sets of relative coordinates increases.[24] This makes possible a greater variety of different Born-Oppenheimer separations than in the case of three particles. Again an appropriate separation can be picked out which is exact at infinite separation of the colliding systems by choosing the vector between the centers of mass of the two systems as a coordinate. This system probably gives the smallest correction terms. It should be pointed out that a fundamental difficulty arises for a general chemical reaction of the form A+B→C+D because the coordinates which are appropriate initially, when the reactants are far apart, will not be appropriate after reaction, when the products are at large distances from each other.

ACKNOWLEDGMENT

The authors would like to thank the computing staff of the University of Wisconsin Naval Research Laboratory for extensive calculations to obtain the matrix elements, and the Oxford University Computing Laboratory for use of their Ferranti Mercury for the cross section calculations. The authors are most grateful to Elizabeth Hirschfelder for her help in revising this manuscript.

APPENDIX

The use of other relations between R, θ, ϕ and μ, ν, ϕ simplifies the conversion of $(\partial/\partial R)_{\theta,\rho}$ and $\nabla_{R,\theta,\phi}^2$. From the fact that

$$\mu=\tfrac{1}{2}[1+(2\rho/R)^2+2(2\rho/R)\cos\theta]^{\frac{1}{2}}+\tfrac{1}{2}[1+(2\rho/R)^2-2(2\rho/R)\cos\theta]^{\frac{1}{2}}=f_1(\rho/R,\theta),$$

$$\nu=\tfrac{1}{2}[1+(2\rho/R)^2+2(2\rho/R)\cos\theta]^{\frac{1}{2}}-\tfrac{1}{2}[1+(2\rho/R)^2-2(2\rho/R)\cos\theta]^{\frac{1}{2}}=f_2(\rho/R,\theta), \quad \text{(A1)}$$

it follows that

$$(\partial\mu/\partial R)_{\theta,\rho}=-(\rho/R)(\partial\mu/\partial\rho)_{\theta,R},$$

$$(\partial\nu/\partial R)_{\theta,\rho}=-(\rho/R)(\partial\nu/\partial\rho)_{\theta,R}, \quad \text{(A2)}$$

and thus we obtain

$$(\partial/\partial R)_{\theta,\rho}=(\partial/\partial R)_{\mu,\nu}-(\rho/R)(\partial/\partial\rho)_{\theta,R}. \quad \text{(A3)}$$

If we combine Eq. (A3) with one of the formulas of (36), we get the conversion of $(\partial/\partial R)_{\theta,\rho}$ as

$$(\partial/\partial R)_{\theta,\rho}=(\partial/\partial R)_{\mu,\nu}-R^{-1}\cdot(\mu^2-\nu^2)^{-1}\times[\nu(1-\nu^2)(\partial/\partial\nu)+\mu(\mu^2-1)(\partial/\partial\mu)]. \quad (38')$$

Rearranging (A3) and squaring gives

$$(\partial^2/\partial R^2)_{\mu,\nu}=(\partial^2/\partial R^2)_{\theta,\rho}+2(\rho/R)(\partial/\partial\rho)_{\theta,R}(\partial/\partial R)_{\theta,\rho}+(\rho^2/R^2)(\partial^2/\partial\rho^2)_{\theta,R}. \quad \text{(A4)}$$

We use this expression along with (A3) to convert $\nabla_{(R,\theta,\phi)}^2$ to $(\rho^2/R^2)\nabla_{(\rho,\theta,\phi)}^2$ plus first derivatives in ρ and derivatives with respect to R with μ and ν held constant, obtaining finally

$$\nabla_{(R,\theta,\phi)}^2=(\rho^2/R^2)\nabla_{(\rho,\theta,\phi)}^2+(1/R^2)(\partial/\partial R)_{\mu,\nu}R^2(\partial/\partial R)_{\mu,\nu}-(2\rho/R)(\partial/\partial\rho)_{\theta,R}(\partial/\partial R)_{\mu,\nu}-(2\rho/R^2)(\partial/\partial\rho)_{\theta,R}, \quad \text{(A5)}$$

or, using (36) again,

$$\nabla_{(R,\theta,\phi)}^2=\tfrac{1}{4}(\mu^2+\nu^2-1)\nabla_{(\mu,\nu,\phi)}^2+(1/R^2)(\partial/\partial R)_{\mu,\nu}R^2(\partial/\partial R)_{\mu,\nu}-[2/R(\mu^2-\nu^2)][\nu(1-\nu^2)(\partial/\partial\nu)+\mu(\mu^2-1)(\partial/\partial\mu)](\partial/\partial R)_{\mu,\nu}-[2/R^2(\mu^2-\nu^2)][\nu(1-\nu^2)(\partial/\partial\nu)+\mu(\mu^2-1)(\partial/\partial\mu)]. \quad (39')$$

[24] D. W. Jepsen and J. O. Hirschfelder, Proc. Natl. Acad. Sci. U. S. 45, 249 (1959).

Extended Theory of Sputtering

DON E. HARRISON, JR.

University of Toledo, Toledo, Ohio

(Received October 13, 1959)

The author's earlier theory of sputtering has been simplified to a form from which direct computations are possible without extended numerical analysis. A considerable analytic simplification is obtained by a new choice of boundary conditions, and certain mathematical expressions have been modified by physical considerations where a detailed analysis is not justified by the present state of experimental information. The special cases of very high and very low energy sputtering are examined in some detail. The $(\ln E_0)/E_0$ high-energy results of Goldman and Simon are shown to be fortuitous but still significant. Low energy results are of the form reported by Wehner.

I. INTRODUCTION

IN two earlier papers[1] the author has presented a theoretical treatment of the cathode sputtering problem. This paper discusses a simplification and extension of the theory detailed in (A), with particular attention devoted to the regions of very high and very low sputtering energies where significant simplification of the model is possible.

The mathematical structure of the theory will be much easier to follow if we examine the physical model in some detail. Consider a monoenergetic beam of particles normally incident upon the surface of a metal. Except in two-body interactions we ignore all charge effects. The metal is assumed to be polycrystalline so that any crystal structure can be neglected. We consider a process in which these ions penetrate into the surface where they "cool" into thermal equilibrium with the lattice by making collisions with the lattice atoms. Because of these collisions a number of lattice atoms acquire enough energy to escape their lattice sites; but they too must "cool," contributing to the breeding process. The final steady state is determined by two distributions of moving atoms, one describing "incident" atoms and one describing "struck" atoms, interacting with the stationary lattice which provides a sink for both energy and momentum which are transported from the surface into the metal by Debye waves. A more detailed discussion of the distribution functions was presented in (A).

For very low energies both distribution functions will be nearly symmetric, and a P_1 Legendre polynomial approximation appears to be satisfactory into the 10–20 kev energy range. At very high energies the incident particle mean free path becomes very large, implying deep penetration before the first collision; which in turn suggests that only the first collision will contribute viable particles to the lattice particle distribution because subsequent collisions are so deeply buried that there is no chance for the struck particles to escape.

Each individual collision is strongly influenced by a trapping parameter, $h_m=\sigma_D/(\sigma_D+\sigma_t)$, where σ_D is the displacement cross section, and σ_t is the cross section for trapping by the lattice. At low energies both h_m (see Table I) should be small, dominated by the σ_t. At high energies for the first collision h_i (incident particle) should approach unity, as σ_t approaches zero much more rapidly than σ_D. Any attempt to account for this energy dependence of the h_m leads to an impossibly difficult mathematical theory; so to make a beginning we assume that the h_m are constants, with the understanding that the values assigned to this constant may differ in different energy ranges.

All interactions are assumed to be "smooth hard-sphere," but "radii" and cross sections are calculated from a Coulomb interaction.

In this work the lethargy variable $u=\ln E_0/E$ is more convenient than the energy. Note that as the energy decreases from E_0, the lethargy increases from zero. All final results are expressed in terms of energies.

Both distribution functions are assumed to be solutions of the transport form of the Boltzmann equation. These equations, called the first and second fundamental equations in the remaining work, take the form

$$[p/\eta_m(u)]d/dz[L_m(u,z,p)]=L_m(u,z,p)+W_m(u,z,p)$$
$$+\int dp'\int du' L_m(u',z,p')f_m(u',u,p_0)h_m(u'). \quad \text{(I)}$$

Here u is the logarithmic energy, or *lethargy*, p the velocity direction cosine with respect to the z axis, $L=N\nu\eta$, the collision frequency, η the bulk displacement cross section, f the lethargy transition function, h the trapping parameter, and W describes the source of particles for the distribution. The definitions and functional meanings of these parameters are discussed in (A). For the first fundamental equation, W_i is defined by an exponentially decaying beam; while for the second fundamental equation, W_j consists of contributions from three sources: the beam, the "incident particle" distribution, and the "lattice particle" distribution; the actual forms are discussed in (A).

[1] D. E. Harrison, Phys. Rev. **102**, 1473 (1956) [hereafter (A)]; *ibid.* **105**, 1202 (1957).

As before, two lethargy transition functions are required. One, the *direct* function f_m correlates lethargy change and scattering angle for the initially moving particle, while the other, the *indirect* function F_m describes the lethargy and recoil direction of the struck particle. These functions were discussed in (A), where they are called energy transition functions. The p_N approximation enters the theory because of our interest in the Legendre polynomial expansion coefficients of the functions

$$f_{mn}\equiv 2\pi\int_{-1}^{1} dp[P_n(p)f_m(p)].$$

In particular,

$$f_{m1}=2\pi\int_{-1}^{1} dp[pf_m(p)],$$

which is discontinuous, and has the complicated Laplace transform (L.T.) exhibited in (A). To simplify the analysis we assume that

$$f_{m1}=p_N\int_{-1}^{1} dpf_m(p),$$

or

$$f_{m1}=p_N f_{m0},$$

where, when $x=u-u'$,

$$p_N=\bar{p}\equiv\int_0^{\epsilon_m} dx[\theta_m(x)f_m(x)].$$

For $\mu\leq 1$, $\bar{p}=\frac{2}{3}\mu$.

II. ANALYTIC PROCEDURE

We begin the solution of Eq. (I) for either case by assuming that L_m can be expanded in a series of Legendre polynomials, assuming that the η_m are constants. At this stage Eq. (I) has become an infinite set of integro-differential equations in the expansion coefficients L_{mn}. Next we calculate the L.T. of each term in each equation, assuming that s is the transform variable corresponding to u, and the equations mentioned in the foregoing become a set of simultaneous differential equations for the $\bar{L}_{mn}$, where

$$\bar{L}_{mn}(s,z)\equiv\int_0^{\infty}\exp(-su)\,L_{mn}(u,z)du.$$

Assuming that L_m is nearly symmetric we retain only the $\bar{L}_{m0}$ and $\bar{L}_{m1}$ terms. For the incident particle distribution function we retain the equations

$$\begin{aligned}\eta_i^{-1}d\bar{L}_{i1}/dz&=-\gamma_{i0}\bar{L}_{i0}+\bar{W}_{i0},\\ \tfrac{1}{3}\eta_i^{-1}d\bar{L}_{i0}/dz&=-\gamma_{i1}\bar{L}_{i1}+\bar{W}_{i1}\end{aligned}\qquad(1)$$

(see Table II for the meaning of undefined functions). Upon eliminating $\bar{L}_{i1}$, we obtain, finally,

$$d^2\bar{L}_{i0}/dz^2=\omega_i^2(s)\bar{L}_{i0}(s,z)+\bar{K}_0(s)\exp(-\eta_i z).\qquad(2)$$

TABLE I. Physically significant quantities which appear in the theory. The functional definition is omitted if it appears in the text.

E_0	Energy of an incident ion
E	Energy of a moving particle
E_a	Threshold energy for the process
u	Logarithmic energy
p_m	Direction cosine of the velocity
p_0	Scattering angle in a single collision
q	Direction cosine of recoil angle
v	Velocity of a moving particle
N_m	Distribution function for type m particles
$L_m=N_m v\eta_m$	Collision frequency per unit volume
f_m	Direct lethargy transition function
F_m	Indirect lethargy transition function
i	Subscript referring to incident particles
j	Subscript referring to lattice particles
m	Subscript referring to any moving particle
n	Order of Legendre expansion coefficient
N_e	Incident beam particle density
$N=N_e v\eta_i$	Amplitude of source strength
W_m	Source strength
ϵ_m	Maximum logarithmic energy transferable
ν_m	Minimum logarithmic energy receivable
σ_D	Cross section for displacement of a lattice particle
σ_t	Cross section for trapping by the lattice
h_m	Trapping parameter
η_m	Bulk cross section
$\eta=\eta_i/\eta_j$	Cross-section ratio
$\mu=M_i/M_j$	Mass ratio

which must now be solved subject to appropriate boundary conditions. The general solution which vanishes as $z\to\infty$ is

$$\bar{L}_{i0}(s,z)=\bar{A}(s)\exp[-\omega_i(s)z]+\bar{B}(s)\exp(-\eta_i z).\qquad(3)$$

The second boundary condition is very difficult to establish. For example, the choice made in (*A*) is physically appealing, but the resulting analysis is much too complicated for simple interpretation. In neutron diffusion work it is customary to use the measurable neutron flux as a boundary condition, but here we wish to determine the flux so this choice is not practical. Similarly, we do not know anything about the particle distribution function at the surface, so boundary conditions on $\bar{L}_{i0}$ itself are not practical. Thus we are forced to consider conditions on d^2L_{i0}/dz^2 at $z=0$.

Now specification of $d^2\bar{L}_{i0}/dz^2$ at the boundary fixes only the profile of the "energy front" of the distribution

TABLE II. Mathematical functions defined in the course of the analysis are collected here for easy reference. In some cases considerable tedious algebra is required to pass from one equation to the next. Except for $\bar{A}(s)$ all forms are identical to the corresponding functions in (A), which should be consulted for additional detail of their derivation.

$$\gamma_{in}=1-h_i\bar{f}_{in}(s)$$
$$\Gamma_{jm}=1-h_j\bar{f}_{jm}(s)-\bar{F}_{jm}(s)$$

$$\omega_i^2=3\eta_i^2\gamma_{i0}\gamma_{i1}$$
$$\omega_j^2=3\eta_j^2\Gamma_{j0}\Gamma_{j1}$$

$$\bar{W}_{i0}=N\bar{f}_{i1}$$
$$\bar{W}_{i1}=N\bar{f}_{i0}p_i$$

$$K_0(s)=3N\eta_i^2[\bar{f}_{i0}(s)\gamma_{i1}(s)+\bar{f}_{i1}(s)]$$
$$K_1(s)=3\omega_j^2h_i[N+\bar{B}(s)][\bar{F}_{i0}\Gamma_{j1}+F_{i1}/\gamma_{i1}]$$
$$K_2(s)=3\omega_j^2h_i[\bar{F}_{i0}\Gamma_{j1}+\omega_i\bar{F}_{i1}/\eta_i\gamma_{i1}]\bar{A}(s)$$

$$\bar{A}(s)=-\bar{B}(s)[\eta_i^2/\omega_i^2]$$
$$\bar{B}(s)=\bar{K}_0(s)/[\omega_i^2-\eta_i^2]$$
$$\bar{J}_1(s)=\bar{K}_1(s)/[\omega_j^2-\eta_i^2]$$
$$\bar{J}_2(s)=\bar{K}_2(s)/[\omega_j^2-\omega_i^2]$$
$$\bar{J}_3(s)=[1/\omega_j^2(s)][\eta_i^2J_1(s)+\omega_i^2\bar{J}_2(s)]$$

function at the surface, while the particles actually involved in the flux may come from points located well behind this front. Thus we might expect the flux to be relatively insensitive to the "curvature" at the surface.

This hypothesis is certainly not intuitively obvious, but it can be verified by making different assumptions on d^2L_{i0}/dz^2 and then examining the resulting distribution functions. Such an analysis of the actual curves, rather than just the functional dependence, indicates the hypothesis is at least good as the others upon which the theory is based. Present measurements just are not sufficiently sensitive to distinguish between different assumptions.

As the physical information is not conclusive, we allow ourselves to be guided by conditions of mathematical simplicity and require that the curvature vanish at the boundary,

$$\lim_{z\to 0} d^2\bar{L}_{m0}/dz^2=0,$$

which greatly simplifies the analysis. This assumption leads to the forms of $\bar{A}(s)$ and $\bar{B}(s)$ which appear in Table II. Now $\bar{L}_{i1}$ is readily determined, and upon completing the analysis, we obtain

$$\bar{L}_i(s,z,p)=\tfrac{1}{2}\bar{B}(s)\{[1+(p/\gamma_{i1})]\exp(-\eta_i z)-(\eta_i^2/\omega_i^2)[1+(p\omega_i/\eta_i\gamma_{i1})]\exp(-\omega_i z)\} \quad (4)$$

for the L.T. of the "incident particle" distribution function to the $P_1(p)$ approximation.

The analysis of the second fundamental equation is identical, and requires no further comment. In its final form, to the $P_0(p)$ approximation, we find

$$\bar{L}_{j0}(s,z)=\bar{J}_1(s)\exp(-\eta_i z)+\bar{J}_2(s)\exp(-\omega_i z)+\bar{J}_3(s)\exp(-\omega_j z), \quad (5)$$

where the functions are defined in Table II.

III. SPUTTERING RATIO

To determine the sputtering ratio, we must invert Eq. (3) back to lethargy space, multiply by a suitable emission probability and integrate over z and p, obtaining the number of particles sputtered with a given lethargy. When integrated over u, this function will give the total sputtering ratio for a given incident ion energy. This procedure can be considerably simplified if the steps are performed in a different order.

Consider the physical meaning of a transformation to "s space." Such a transformation is known to convert a "variable energy" diffusion process into a mathematically equivalent steady-state diffusion process in transform space. Suppose that the distribution of particles in (s, z) space is described by a function $Q(s)\,e^{-q(s)z}$. Then so long as we remain in this space it seems reasonable to treat $q(s)$ as a constant bulk cross section which describes the diffusion of these particles in (s, z). We make use of this simplification by determining the number of particles emitted from the surface $z=0$ *with a given* s, then perform the process equivalent to integration in u space, and finally make the inversion to lethargy space.

Unfortunately, our problem is further complicated by the angular variable p; however, if we assume a simple collision kinetic picture in "s space," $q(s)\exp[-q(s)z/p]$ appears to be a reasonable emission probability as it corresponds to a normalized e^{-kr} probability of diffusion without collision.

Upon multiplying the terms of Eq. (3) by this probability function, noting that each term has its own appropriate bulk cross section, and integrating over the range $0\leq z\leq\infty$, and then over the range, $-1\leq p\leq 0$, we obtain

$$\bar{L}_{j0}(s)=0.699(\bar{J}_1(s)+\bar{J}_2(s)+\bar{J}_3(s)). \quad (6)$$

This procedure may be compared with the approximation described in (A) which leads to Eq. (19) of that paper. The final expressions are essentially equivalent. When the definitions are substituted into Eq. (6) the result is

$$\bar{L}_{j0}(s)=(2.1\eta_j^2h_i/\omega_j^2)\left\{[N+(\bar{K}_0/\omega_i^2)]\bar{F}_{i0}\Gamma_{j1}+\left[N+\frac{\bar{B}}{\gamma_{i1}}\left(1-\frac{\eta_i}{\omega_i}\right)\right]\bar{F}_{i1}\right\}. \quad (7)$$

In this expression the factor $[\bar{B}/\gamma_{i1}][1-(\eta_i/\omega_i)]$ of the second term will be neglected when compared to N, because it contributes only small terms. Thus we obtain

to a "zeroth" approximation

$$\bar{L}_{j0}^{(0)}(s)=[2.1\eta_j^2 h_i/\omega_j^2][(N+\bar{K}_0/\omega_i^2)\bar{F}_{i0}\Gamma_{ji}+N\bar{F}_{i1}].$$

Finally, in terms of the collision frequency $L_j(u)$, the sputtering ratio is

$$R^{(0)}=\tfrac{1}{2}(\eta_i/\eta_j)N^{-1}\int_0^{u_a}L_j^{(0)}(u)\,du,$$

where N is the incident beam current density, and u_a will be defined later. The Laplace transform of this expression is

$$\bar{R}^{(0)}(s)=\tfrac{1}{2}(\eta N^{-1})\bar{L}_j^{(0)}(s)/s. \tag{8}$$

Here $\eta=\eta_i/\eta_j$, and s is now the transform variable corresponding to u_a. Equation (8) indicates that our problem is solved if it is possible to obtain the Laplace inverse of $\bar{L}_j^{(0)}(s)/s$. As in (A), we set $v=s+1$, and use the p_N approximation in $\bar{f}_1$ and an equivalent q_N approximation in $\bar{F}_1$. Upon carrying out the algebra, we find

$$\bar{R}^{(0)}(v)=R_0\left\{\frac{E_2(v)}{v-1}\left[\frac{1}{v-r_3}+\frac{v\bar{q}_i}{(v-r_3)(v-r_4)}+\frac{(vr_1\hat{p}_i+r_2^2/\hat{p}_i)E_1(v)}{(v-r_3)[v-r_1E_1(v)][v-r_2E_1(v)]}\right]\right\} \tag{9}$$

where $E_1(v)=1-\exp(-\epsilon_i v)$, $E_2(v)=\exp(-\nu_i v)$, $\hat{p}_i=1-\bar{p}_i$, $R_0=0.35\eta b_i h_i$, $r_1=a_i h_i$, $r_2=a_i h_i\bar{p}_i$, $r_3=h_j(a_j+b_j)=2h_j$, $r_4=h_j(a_j\bar{p}_j+b_j\bar{q}_j)=4h_j/3$.

A physical interpretation of $E_2(v)$ is presented in (A), and need not be repeated here. The only effect of this factor will be to change the lethargy reference energy from the incident beam energy, E_0; $u=\ln E_0/E$; to a new reference energy E_a which may be interpreted as the threshold energy for sputtering from an ideal plane surface at normal incidence. In terms of E_a, $u=\ln(E/E_a)$ and we now see that $u_a=\ln(E_0/E_a)$.

The factor $E_1(v)$ which appears at several points in Eq. (9) can be interpreted as an extremely complicated type of "jump function," which when convoluted with the other factors appears as a fine structure in the distribution function. Calculations based upon the earlier work indicate that this fine structure is always small compared to the actual function; so the factor $E_1(v)$ will be set equal to unity, (see Appendix I). From Eq. (9), after collecting terms, we can write

$$R^{(0)}(s)=R_0\sum_{n=1}^{4}m_n/[s(s-t_m)] \tag{11}$$

where $t_n=r_n-1$, and upon performing the Laplace inversion, obtain the final result

$$R^{(0)}(u_a)=R^{(0)}\sum_{n=1}^{4}R_n[\exp(t_n u_a)-1]. \tag{12}$$

For reference, the coefficients t_n are

$$\begin{aligned}t_1&=a_i h_i-1,\\ t_2&=a_i h_i\bar{p}_i-1,\\ t_3&=2h_j-1,\\ t_4&=(4h_j/3)-1,\end{aligned} \tag{13}$$

and the coefficients R_n are

$$\begin{aligned}R_1&=[a_i h_i/t_1\hat{p}_i][1/(a_i h_i-2h_j)]\\ R_2&=[1/t_2\hat{p}_i][a_i h_i\bar{p}_i(1+\hat{p}_i)/(2h_j-a_i h_i\bar{p}_i)]\\ R_3&=t_3^{-1}[1+3h_j\bar{q}_i\\ &\quad+(a_i h_i\{2h_j\hat{p}_i+a_i h_i\bar{p}_i\}/\{2h_j-a_i h_i\}\{2h_j-a_i h_i\bar{p}_i\})]\\ R_4&=-2\bar{q}_i.\end{aligned} \tag{14}$$

In all cases examined to date R_4 has been negligible compared to the remaining terms.

IV. CROSS-SECTION RATIO

Goldman and Simon[2] have shown that the method of Seitz and Koehler[3] may be used to determine displacement cross sections. Accepting this work, the cross section ratio $\eta=\eta_i/\eta_j=\sigma_i/\sigma_j$ (where the σ's are displacement cross sections) is readily evaluated. Converting to the notation of the present paper, their cross-section expressions become

$$\sigma_i=\pi\mu Z_i^2 Z_j^2 e^4/E_0E_d$$

and

$$\sigma_j=\pi Z_j^4 e^4/E_jE_d$$

where Z's are atomic numbers, e the electronic charge, E_d the displacement energy (20 ev?), and E_j the energy of a moving lattice particle. Goldman and Simon have shown that E_j is not a sensitive function of E_0, so we replace it by its average value $\bar{E}_j$.

Combining all results,

$$R_0=0.35(1+\mu)^2(Z_i/Z_j)^2\bar{E}_j/E_0,$$

and expressing u_a in terms of E_0, we find

$$R(E_0)=R_0\sum_{n=1}^{4}R_n[(E_0/E_a)^{t_n}-1] \tag{15}$$

when all t_n are positive. If any t_n is negative the factor becomes $1-(E_0/E_a)^{t_n}$ and the absolute value of this t_n should be used in the corresponding R_n. If one of the t_n is zero, $R(E_0)$ must be recalculated.

V. HIGH-ENERGY APPROXIMATION

For very high-energy incident particles, η_i is sufficiently larger than η_j that we consider only the "beam" term in the source of the second fundamental equation. In this case we may also set $h_i=1$, for the incident particle trapping cross section is negligible at these

[2] D. T. Goldman and A. Simon, Phys. Rev. 111, 383 (1958).
[3] F. Seitz and J. S. Koehler, Solid State Phys. 2, 321 (1956).

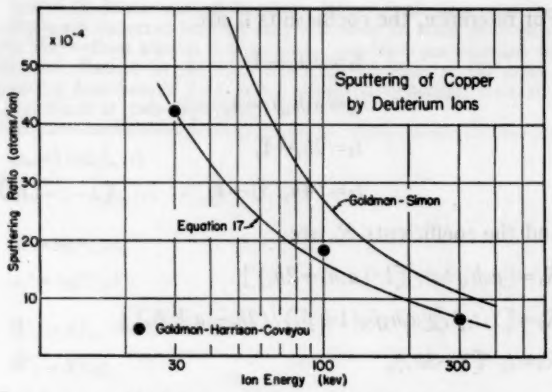

FIG. 1. Comparison of data obtained from the Monte Carlo sputtering program of Goldman *et al.*[4] (the points ●) with the Goldman-Simon analytic function $(\ln E_0)/E_0$, and the sputtering ratio of Eq. (17) (using $E_a=25$ ev, $h_j=0.66$). It is interesting that the function $E_0^{-0.80}$ is indistinguishable on the graph from Eq. (17). The fit of Eq. (17), which is the best fit possible for all three points, could be improved by reducing E_a. As the simplifying approximations may not be valid at the 30-kev point; it might be better to fit only the two high-energy points.

energies. In this approximation the terms in $\bar{A}(s)$ and $\bar{B}(s)$ do not contribute, and $R(s)$ reduces to

$$R_H(s)=R_0\{[1/s(s-t_3)]+[\bar{q}_i(s+1)/s(s-t_3)(s-t_4)]\}. \tag{16}$$

Note that in this approximation Eq. (16) is exact; i.e., no terms have been neglected during the analysis. Inversion of this equation is very simple, giving, for the high-energy approximation

$$R_H(E_0)=0.35\bar{E}_j(1+\mu)^2(Z_i/Z_j)^2 \times\{(H_1/E_0)[H_2(E_0/E_a)^{t_3}+H_3(E_0/E_a)^{t_4}+1]\} \tag{17}$$

$$H_1=(3t_4-2)/3t_3t_4$$
$$H_2=t_4(5t_3-3t_4)/(t_3-t_4)(3t_4-2)$$
$$H_3=-3t_3/(t_3-t_4)(3t_4-2). \tag{18}$$

Note that t_3 and t_4 must appear in the H_i with appropriate signs, so it is not feasible to rewrite the H_i in terms of h_j.

Although direct comparison between theoretical results has no physical significance, it is interesting to see how this analytic theory compares with the results of Goldman and Simon,[2] and also Goldman, Harrison, and Coveyou,[4] which describes a Monte Carlo calculation on deuterium-copper sputtering at high energies. The results are displayed in Fig. 1. Clearly, the results are somewhat better than the Goldman-Simon $(\ln E_0)/E_0$, but not much better than a simple reciprocal fractional power fit.

An exact fit of the Monte Carlo data requires that $\bar{E}_j$ be 3.90 kev, which may be compared with 3.96 kev and 11.9 kev which are the maximum energies transferable to a metal atom for the 30 kev and 100 kev cases, respectively. This value of $\bar{E}_j$ is possible but not realistic; however, when we recall that $(Z_i/Z_j)^2$ appears because the cross section was calculated from pure Coulomb scattering, it is evident that a small screening reduction of Z_j will significantly reduce $\bar{E}_j$.

It is also instructive to consider two special cases, and in particular derive the Goldman-Simon relation.

Case A

Goldman and Simon have considered the special case where $\sigma_D=\sigma_t$, giving $h_j=0.5$. This value of h_j makes $t_3=0.0$ and $t_4=-\frac{1}{3}$. The result of the inversion, including the second-order pole, is

$$R_A(u_a)=4R_0\{u_a-(\tfrac{1}{3}\mu)[1-\exp(-u_a/3)]\}$$

which, in the limit of large u_a, becomes

$$R_A(E_0)=0.35\bar{E}_j(1+\mu)^2(Z_i/Z_j)^2[(1/E_0)\ln(E_0/E_a)] \tag{19}$$

when written in terms of E_0. Goldman and Simon report the same energy dependence but a different mass ratio dependence.

Case B

To indicate how the energy dependence is sensitive to the choice of h_j, set $h_j=0.75$ so that $t_3=0.5$, $t_4=0.0$. The analysis is simple, giving

$$R_B(E_0)=0.17_5\bar{E}_j(1+\mu)^2(1+2\mu)(Z_i/Z_j)^2(E_0E_a)^{-\frac{1}{2}} \tag{20}$$

which is a similar, but analytically different, energy dependence. Apparently, the energy dependence reported by Goldman and Simon is fortuitous, depending on the choice of h_j, and other dependences are just as plausible.

We conclude that, depending upon the choice of trapping parameter, the asymptotic energy dependence lies in the range of reciprocal fractional powers of E_0, and includes $E_0^{-1}\ln E_0$ as a special case.

VI. LOW-ENERGY APPROXIMATION

If the incident particle energy E_0 is very near the threshold energy E_a, the lethargy u_a is small, and Eq. (15) becomes

$$R(u_a)=R_0\sum_{n=1}^{4}R_nt_nu_a. \tag{21}$$

Further, we can approximate the lethargy from the identity

$$\ln x=(x-1)-\tfrac{1}{2}(x-1)^2+\tfrac{1}{3}(x-1)^3-\cdots 0\leq x\leq 2,$$

[4] D. T. Goldman, D. E. Harrison, and R. R. Coveyou, Oak Ridge National Laboratory Report 2729 (1959).

which converges most rapidly when x is near unity. Combining these approximations, we obtain

$$R(E_0)=(R_0/E_a)(E_0-E_a)\sum_{n=1}^{4}R_n l_n, \qquad (22)$$

if we assume that the cross-section ratio is constant in this narrow energy range.

Equation (22) exhibits the linear energy dependence reported by Wehner[5] for the majority of his cases, and the slightly better logarithmic approximation should account for the cases in which he reports some curvature in the sputtering ratio vs ion energy curve. No attempt will be made to fit Eq. (22) to Wehner's data because it contains E_j, h_i, h_j, and η as undetermined parameters.

Actually, the success of Eq. (20) is rather surprising, for it is built upon at least one highly improbable assumption, i.e., that the transport equation is valid when only one or two collisions are required for cooling. This is clearly nonsense, but the theory obtained from it is consistent with present experimental data.

APPENDIX I

Factors of the form $[(v-a)+ae^{-bv}]^{-1}$ appear in the functions which must be inverted to lethargy space. Here, as before, we have set $v=s+1$. Upon expanding in series, this function may be rewritten as

$$[(v-a)+ae^{-bv}]^{-1}=(v-a)^{-1}\sum_{r=0}^{\infty}[-a/(v-a)]^r e^{-brv},$$

which appears as the convolution of a simple pole at $v=a$ and the inversion of the series expression. Let us examine the inversion of a general term in the expansion

$$S_r=[-a/(v-a)]^r e^{-brv}.$$

Inverting just the first factor,

$$T^{-1}[-a/(v-a)]^r=[(-a)^r/(r-1)!]q^{r-1}e^{-aq}$$

and applying a general theorem, we find

$$T^{-1}\{[-a/(v-a)]^r e^{-brv}\}$$
$$=\exp[-a(q-br)][(-a)^r/(r-1)!]U(q-br)$$

where

$$U=0, \quad q\leq br$$
$$=1, \quad q>br.$$

Finally, writing in terms of s rather than v, we obtain

$$T^{-r}\{S_r\}=(u-br)^{r-1}[(-a)^r/(r-1)!]$$
$$\times\exp-[(a+1)u+abr]U(u-br).$$

Now consider the physical implications of this term. Clearly, it does not contribute until $u>br$. Further, if we set $u=br$, the exponential function becomes e^{-bu}, which will be small for physically interesting values of b.

Detailed analysis of the term for $r=1$ indicates that normally it contributes a magnitude less than 10% of the total convolution, and much lower values are common. Under the circumstances, the entire effect of the series has been neglected. It can be included at any time when an increase in experimental precision justifies the extra labor.

[5] G. K. Wehner, Phys. Rev. 112, 1120 (1958).

Intermolecular Coupling of Vibrations in Molecular Crystals*

DAVID A. DOWS

Department of Chemistry, University of Southern California, Los Angeles 7, California

(Received August 24, 1959)

The connection between intermolecular potential energies and the unit cell vibrational frequencies in molecular crystals is summarized in Sec. I. Details of the treatment of potentials which can be written as functions of intermolecular atom-atom distances are developed. The frequencies of vibration of methyl chloride in the crystal are treated by the methods discussed in Sec. II. Dipole-dipole interactions are insufficient to explain the observed splittings. For vibrations which are primarily hydrogen motions, an intermolecular hydrogen-hydrogen repulsion potential accounts satisfactorily for the observed effects.

THE effects of intermolecular forces on the vibrational spectra of crystals have been known for some time. A decade ago, Hornig[1] and Winston and Halford[2] discussed the spectra in terms primarily of the symmetry of the crystal. In particular, the selection rules and number of frequencies resulting from a given molecular vibration in a dynamically pure crystal (consisting of one isotopic variety of a single pure compound) are now regarded as well known. Methods involving isotopically substituted crystals have been developed[3] to differentiate between "factor group" and "site group" splitting,[2] and to determine the values of force constants coupling vibrational modes in adjacent molecules.[4]

In addition to predicting the number and type of frequencies to be expected in the vibrational spectrum of a crystal, it has been shown (in reference 1 and elsewhere) in general terms how to calculate the frequencies and splittings from intermolecular force constants, and vice versa. Unfortunately, there has been a lack of success in computing the force constants from independent data, and thus there is a gap in understanding their origin. Recently, there have been efforts to bridge this gap. Decius,[5] and Hornig and Hiebert[4] have assumed a dipole-dipole interaction between neighboring molecules or ions and have had at least semiquantitative success in some cases. Stein[6] has taken another approach, using a potential derived from compressibility measurements on hydrocarbon crystals, again with some success on one frequency.

In Sec. I of this article, the method of calculating crystal frequencies from intermolecular potential functions is summarized. One objective is to make clear the assumptions and approximations to be used later. The other is to detail the treatment of certain types of potentials which have proved of value. Section II gives the result of applying these methods to the case of methyl chloride.

I. THEORY

We begin with Hornig's[1] potential function for the crystal but with the assumption that only the terms shown need be considered,

$$V=V_{\text{int}}+V_{\text{int-int}} \tag{I-1}$$

where V_{int} is the internal energy of all the molecules in the crystal, and the second term represents the coupling between internal motions of different molecules. This potential assumes no coupling between internal and lattice motions. We also assume

$$V=\sum V_k \tag{I-2}$$

where the sum is over the various normal coordinates of an isolated molecule. This assumption of no coupling between unlike normal coordinates should, of course, be closely scrutinized when two nearby frequencies have the same symmetry in the crystal. Hereafter, we drop the summation over k, intending that each normal vibration be separately treated.

The potential may now be written more specifically as

$$V=\sum_n (V_n^0+\sum_{m>n} V_{nm}) \tag{I-3}$$

where V_n^0 is the potential of an isolated molecule n, and V_{nm} is the intermolecular potential between molecules n and m. This specifically assumes pairwise interactions between molecules.

In calculating crystal frequencies, we may restrict our attention to one unit cell.[1] Equation (I-3) then is interpreted as involving sums over the Z unit cell occupants. It is understood, however, that V_{nm} is the potential connecting molecule n with *m and all molecules identical to m under translation*.

We may now write the F and G matrices[7] for the coupled unit cell, using as basis coordinates the normal coordinates of the Z cell unit occupants. Thus, $G_{nm}=$

* This work was supported by the Office of Ordnance Research, U.S. Army.

[1] D. F. Hornig, J. Chem. Phys. **16**, 1063 (1948).

[2] H. Winston and R. S. Halford, J. Chem. Phys. **17**, 607 (1949).

[3] (a) H. J. Hrostowski and G. C. Pimentel, J. Chem. Phys. **19**, 661 (1951); (b) G. L. Hiebert and D. F. Hornig, *ibid.* **20**, 918 (1952).

[4] D. F. Hornig and G. L. Hiebert, J. Chem. Phys. **27**, 752 (1957).

[5] J. C. Decius, J. Chem. Phys. **22**, 1941, 1946 (1954); **23**, 1290 (1955).

[6] R. S. Stein, J. Chem. Phys. **23**, 734 (1955).

[7] E. B. Wilson, J. C. Decius, and P. C. Cross, *Molecular Vibrations* (McGraw-Hill Book Company, Inc., New York, 1955).

δ_{nm}, and the F-matrix elements are given by

$$F_{nn}=\lambda^0+\sum_m \partial^2 V_{nm}/\partial Q_n^2=\lambda^0+f_n \qquad \text{(I-4a)}$$

$$F_{nm}=\sum_m \partial^2 V_{nm}{}^m/\partial Q_n \partial Q_m=f_{nm} \qquad \text{(I-4b)}$$

where λ^0 is the value of $4\pi^2c^2\nu^2$ for the isolated molecule for the normal coordinate in question (for the isolated molecule $F=\lambda^0$ and $G=1$). The symmetry is then used to construct symmetry coordinates[7] for the unit cell based on the molecular normal coordinates. The symmetry coordinate transformation then factors the GF matrix in the usual way, and the resulting blocks form secular equations soluble for the unit cell frequencies.

Intermolecular Potentials

At this point, it is convenient to make an arbitrary and not too clean-cut distinction between two types of potentials: (a) those which can be written as

$$V_{nm}=\sum_i \sum_j V_{in,jm}(r_{ij}) \qquad \text{(I-5)}$$

and (b) those which are better left simply in the form V_{nm}. We refer to those of type (a) as interatomic potentials, i being an atom of molecule n, etc., and r_{ij} the interatomic distance. The object of this separation is the further treatment possible for interatomic potentials. It should be noted that the work of Decius[5] and Hiebert and Hornig[4] concerns the treatment of certain potentials of type (b). In these cases, V_{nm} is the dipole interaction potential and the intermolecular force constant f_{nm} involves geometrical terms and dipole derivatives, the latter in principle available from absolute intensity measurements on the absorption bands.

Potentials of type (a) can be expected to include repulsive potentials between molecules, and perhaps to a cruder approximation one might assume the London forces to be sums over atom pair terms. It is the feeling of this author that the usefulness of such a breakdown will be decided by experiment, though definitive theoretical discussion by those more knowledgable in the field of intermolecular forces would be of great assistance in the attempts. For potentials which cannot be written as in (I-5), efforts must be made to calculate values of f_n and f_{nm} in other ways; for interatomic potentials we present the following further details.

Atom-Atom Potentials

On the assumption of (I-5), the derivatives used in (I-4) become

$$\partial^2 V_{nm}/\partial Q_n^2=\sum_i \sum_j [(\partial^2 V_{nm}/\partial r_{ij}^2)(\partial r_{ij}/\partial Q_n)^2 + (\partial V_{nm}/\partial r_{ij})(\partial^2 r_{ij}/\partial Q_n^2)] \qquad \text{(I-6a)}$$

$$\partial^2 V_{nm}/\partial Q_n \partial Q_m = \sum_i \sum_j [(\partial^2 V_{nm}/\partial r_{ij}^2)(\partial r_{ij}/\partial Q_n)(\partial r_{ij}/\partial Q_m) + (\partial V_{nm}/\partial r_{ij})(\partial^2 r_{ij}/\partial Q_n \partial Q_m)]. \qquad \text{(I-6b)}$$

It will be indicated (Appendix I) that the terms in (I-6) in $\partial V/\partial r$ are usually small compared to those in $\partial^2 V/\partial r^2$, so we neglect them in the remainder of this work. Equations (I-6) may be rewritten in terms of the vector positions of the ith and jth atoms (of molecules n and m, respectively) as

$$f_n=\partial^2 V/\partial Q_n^2=\sum_i \sum_j (\partial^2 V/\partial r_{ij}^2)[(\partial r_{ij}/\partial r_i)(\partial r_i/\partial Q_n)]^2 \qquad \text{(I-7a)}$$

$$f_{nm}=\partial^2 V/\partial Q_n \partial Q_m = \sum_i \sum_j (\partial^2 V/\partial r_{ij}^2)[(\partial r_{ij}/\partial r_i)(\partial r_i/\partial Q_n)] \times [(\partial r_{ij}/\partial r_j)(\partial r_j/\partial Q_m)], \qquad \text{(I-7b)}$$

where the quantities $\partial r_{ij}/\partial r_i$ and $\partial r_{ij}/\partial r_j$ are just the cosines of the angles between the normal displacements of the atoms and the interatomic distances.

The calculation of the F-matrix elements now reduces to postulating a potential function $V_{nm}(r_{ij})$ and finding the terms $\partial r_i/\partial Q_n$. The latter are the elements of a matrix $\mathbf{C}$ such that

$$\mathbf{r}=\mathbf{CQ}. \qquad \text{(I-8)}$$

If we take the r's as referred to a coordinate system fixed in the crystal and defined for each molecule by the molecule's principle axes, we may leave until later the simple rotations of axes necessary to find the terms $\partial r_{ij}/\partial r_i$, etc., and the matrix $\mathbf{C}$ will be the same for all molecules. The $\mathbf{C}$ matrix is simply the product of other matrices long in favor:

$$\mathbf{C}=\mathbf{D}^{-1}\mathbf{U}'\mathbf{L}, \qquad \text{(I-9)}$$

where $\mathbf{D}^{-1}$ is the matrix of the transformation from internal coordinates into cartesian coordinates, $\mathbf{U}'$ is the matrix taking symmetry coordinates into internal coordinates, and $\mathbf{L}$ is the matrix of the transformation from normal to symmetry coordinates. The last two are obtained in the usual normal coordinate analysis of the molecule, while $\mathbf{D}^{-1}$ may be obtained in a variety of ways.[8] The definition of $\mathbf{D}^{-1}$ includes the conditions that the center of gravity and angular momenta are unchanged, as must be the case if we consider molecules rigidly fixed in the crystal.

Discussion

The procedure for calculating unit cell frequencies in molecular crystals (where the assumptions made above are most likely to be appropriate) yields the limiting modes of vibration, which include those active in the infrared or Raman effect.[1] The procedure must be followed for each normal vibration of the isolated molecule. If the potential function seemingly most appropriate for intermolecular coupling includes terms of types (a) and (b), one may treat each term separately, since the f_n and f_{nm} terms are simply additive.

[8] S. R. Polo, J. Chem. Phys. **24**, 1133 (1956) gives a direct method. Another is to write $\mathbf{D}$ by inspection and invert on a computer or by the method given in Appendix II.

TABLE I. Correlation diagram for methyl chloride.

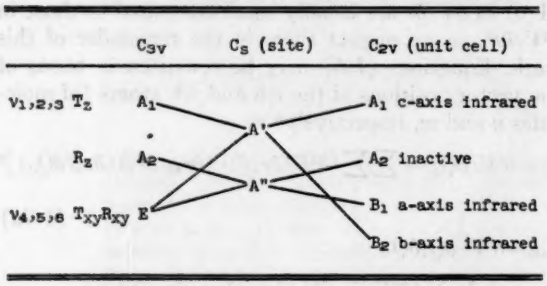

The method given for interatomic potentials includes Stein's treatment[6] of the rocking modes of normal paraffins, with the added attraction that his approximations involving the form of such motions are obviated. Application of the foregoing treatment to Stein's case, retaining his approximations, is in agreement with his results; substitution of the more accurate forms of the molecular motion would not be expected to change his results greatly, since the vibrations are in actuality almost entirely motions of the hydrogen atoms, as he assumed.

Section II applies the preceding methods to the case of methyl chloride.

II. INTERMOLECULAR FORCES IN CRYSTALLINE METHYL CHLORIDE

The infrared spectrum of crystalline methyl chloride has been reported previously.[9] All fundamental bands but one are observed to be split by crystal coupling. In this section, we apply the theory of Sec. I in an attempt to explain the coupling observed.

The crystal structure of CH_3Cl is orthorhombic,[10] with $Z=4$ and space group $Cmc2_1\cdots C_2^{12}$. We accept Burbank's[10] "orientation 1" for the hydrogen atoms. As has been pointed out by Hexter,[11] the primitive cell may be considered to be smaller ($Z=2$), but it will be seen that proceeding with the larger cell reflecting the entire symmetry of the crystal gives results in agreement with Hexter's discussion. He gives an analysis of the symmetry requirements on the number and activity of the unit cell frequencies which we only summarize here.

The correlation diagram connecting free molecules with unit cell and site symmetries is given in Table I. For each of the A' (of C_s) frequencies (one from each of ν_1 through ν_{6a}) we construct from the molecular normal coordinates Q_1, Q_2, Q_3, Q_4 a symmetry coordinate of type A_1 and one of type B_2. For each A'' frequency (from ν_{4b} through ν_{6b} only) we construct coordinates of type A_2 and B_1. The subscripts on the Q's refer to four molecules of the unit cell, and the numbering follows Burbank.[10] The symmetry coordinates are

$$S_{A_1}=\tfrac{1}{2}(Q_1+Q_2+Q_3+Q_4),$$
$$S_{B_2}=\tfrac{1}{2}(Q_1-Q_2+Q_3-Q_4),$$
$$S_{A_2}=\tfrac{1}{2}(Q_1+Q_2-Q_3-Q_4),$$
$$S_{B_1}=\tfrac{1}{2}(Q_1-Q_2+Q_3+Q_4). \qquad \text{(II-1)}$$

We write the F matrix for the unit cell by assuming interactions between all molecules

$$F=\begin{vmatrix} \lambda^0+f & f_{12} & f_{13} & f_{14} \\ f_{12} & \lambda^0+f & f_{23} & f_{24} \\ f_{13} & f_{23} & \lambda^0+f & f_{34} \\ f_{14} & f_{24} & f_{34} & \lambda^0+f \end{vmatrix} \qquad \text{(II-2)}$$

where the notation follows Sec. I. The G matrix is the unit matrix. Application of the symmetry coordinate transformation factors the F matrix. Noting that f is the same for all four molecules, but different for A' and A'' frequencies of the same fundamental due to different directions of vibration, letting $f_{||}=f$ for A' and $f_\perp=f$ for A'', and noting that by symmetry $f_{12}=f_{34}$, $f_{13}=f_{24}$, and $f_{14}=f_{23}$, we finally write the unit cell λ's as

$$\lambda_{A_1}=\lambda^0+f_{||}+f_{12}+f_{13}+f_{14},$$
$$\lambda_{B_2}=\lambda^0+f_{||}+f_{13}-f_{14}-f_{12},$$
$$\lambda_{A_2}=\lambda^0+f_\perp+f_{14}-f_{12}-f_{13},$$
$$\lambda_{B_1}=\lambda^0+f_\perp+f_{12}-f_{13}-f_{14}. \qquad \text{(II-3)}$$

The site splitting appears here as $\Delta\lambda(\text{site})=(f_{||}+f_{13})-(f_\perp-f_{13})$. The appearance of f_{13} only as a site splitting term is in agreement with the smaller unit cell of Hexter.[11] The factor group splitting of the A' frequencies is given by $\Delta\lambda(\text{factor})=2(f_{12}+f_{14})$, and of the A'' frequencies by $\Delta\lambda(\text{factor})=2(f_{12}-f_{14})$.

The observed splittings[9] for the A_1 frequencies of CH_3Cl must be of the factor group variety. Only the case of ν_3 is complicated by isotope effects, as discussed before.[9] In the case of E frequencies, the assignment is not clear, except perhaps for ν_5 where we now assume the central component is B_1. Table II lists the

TABLE II. Observed band splittings for methyl chloride.

ν	$\Delta\nu$ cm^{-1}	$\Delta\lambda$ (10^{28} sec^{-2})
1	4.3	±0.090
2	10.4	±0.098
3	~5	±0.025
4	5	±0.106
5	7.6	±0.078
6	<3[a]	±<0.02

[a] The line width is roughly 4.5 cm^{-1}, larger than that of other bands.

[9] D. A. Dows, J. Chem. Phys. **29**, 484 (1958).
[10] R. D. Burbank, J. Am. Chem. Soc. **75**, 1211 (1953).
[11] R. M. Hexter, J. Chem. Phys. **25**, 1286 (1956).

observed splittings and the computed values of $\Delta\lambda(=8\pi^2c^2\nu\Delta\nu)$.

Dipole Coupling

We first apply the treatment of Decius[5] to calculate splittings due to dipole-dipole coupling. For coupling between a pair of molecules n and m,

$$f_{nm}=-[2(r_1\cdot r)(r_2\cdot r)-(r_1 x r)\cdot(r_2 x r)/|r|^5](\partial\mu/\partial Q)^2 \qquad \text{(II-4)}$$

which is an alternate way of expressing Decius' formula. Here, r is the $n-m$ vector, r_1 and r_2 are unit vectors in the directions of $\partial\mu_n/\partial Q_n$ and $\partial\mu_m/\partial Q_m$. As pointed out previously,[9] there is question as to the positions defining r and the directions of r_1 and r_2. We assume the latter are fixed along (or perpendicular to) C—Cl axes (as indicated by the gas-phase molecular symmetry) and in (or perpendicular to) the crystal bc plane.

We have calculated f_{nm} based on vectors r defined both by the Cl atoms and by the C atoms. For illustration, we take those defined by the C_n and C_m positions, since the calculated value of f_{nm} is larger in this case than on most other reasonable definitions of r. The values thus are maxima, and since we feel that dipole coupling is not important except perhaps in one band, this assumption will give the strongest test of our feeling. Values of $(\partial\mu/\partial Q)^2$ are from Dickson et al.[12] It may be that these values are changed in the crystal, but very rough relative band intensity measurements indicate that such changes are not great, and we use Dickson's data unchanged. Table III presents the calculated f_{nm} values, considering only nearest-neighbor molecules II and IV as coupling with I.

In Table III and elsewhere in this paper, account has been taken of the number of equivalent molecules coupling to a given one. Thus, f_{12} and f_{14} include factors of 2 and 4 because of the neighboring unit cell occupants identical to molecules II and IV with respect to molecule I. The results of the dipole calculation indicate (in comparison with Table II) that except for ν_1 (25%) and ν_3 (100%), the predicted splittings are less than 10% of those observed. It does not seem likely, in contradiction to our previous statement,[9] that changes in the treatment such as including further neighbors can make these coupling constants sufficiently important to consider as other than corrections, so we ignore all but those two mentioned in the remainder of this article.

Atom-Atom Potentials

A study of the crystal structure indicates that certain atom-atom interactions might prove a profitable field of study. The contracts in the crystal are of the type H···Cl between molecules I and IV and between I and III. The distance is 3.00 A, just the sum of the van der Waals radii. The distance between hydrogen atoms of I and II is 2.87 A. Repulsive forces of these types seem of likely importance. We treat only the H···H repulsion in some detail, assuming a potential connecting H atoms of I with H atoms of II and II$(00\bar{1})$. There are four such interatomic pairs connected with molecule I, all to be added to contribute to f_{12}. f_{13} and f_{14} are zero.

TABLE III. Dipole coupling force constants in methyl chloride.

ν	f_{12}[a]	f_{14}[a]	$\Delta\lambda$[a,b] (factor splitting)
1	−0.0074	−0.0040	−0.023
2	−0.0023	−0.0013	−0.0072
3	−0.0078	−0.0042	−0.024
$4A'$	−0.0017	−0.0009	+0.0052
$4A''$	−0.0014	+0.0003	+0.0034
$5A'$	−0.0022	−0.0012	+0.0068
$5A''$	−0.0018	+0.0003	+0.0042
$6A'$	−0.0007	−0.0004	+0.0022
$6A''$	−0.0006	+0.0001	+0.0014

[a] All in units of 10^{38} erg/g cm^2=10^{38} sec^{-2}.
[b] A negative sign indicates $\lambda A_1<\lambda B_2$, etc.

In applying Eqs. (I-7) to find f_{12}, we take $\partial^2V/\partial r^2=\beta$ (where r is the H···H distance) out as a factor. The terms $\partial r_{ij}/\partial r_i$ are calculated from the crystal structure[10] when the directions of the r_i's are known. The latter, included in $\partial r_i/\partial Q$ are the elements of the matrix $\mathbf{C}$(I-9). A normal coordinate analysis of the methyl halides has been carried out by King et al.,[13] who give the matrices $\mathbf{L}^{-1}$ and $\mathbf{U}$. The $\mathbf{L}$ matrix was obtained by direct inversion after correction of the typographical error in sign of L_{33}^{-1} for methyl chloride from King's paper. The $\mathbf{U}$ matrix was taken to include a row for the redundancy condition, and was therefore a 10×10 matrix (including separate rows for the degenerate pairs). The D matrix was written by inspection and included a column for the redundancy and rows for the center of gravity and angular momenta conditions. It was inverted directly through the courtesy of the Western Data Processing Center (UCLA). Multiplication of the matrices to obtain C was performed on a computer on this campus, and was spot-checked manually along with general checks on symmetry and reasonableness of the results. The C matrices for CH_3Cl and CD_3Cl, and the $\mathbf{D}^{-1}$ matrices for the other halides are available.

By using the results obtained and Eqs. (I-7), we calculate the constants f_{12} for interatomic potentials apart from the factor β. Conversely, we may calculate the values of β from the observed $\Delta\lambda$'s. Since approximate values are our goal at this time, we have not

[12] A. D. Dickson, I. M. Mills, and B. Crawford, Jr., J. Chem. Phys. 27, 445 (1957).

[13] W. T. King, I. M. Mills, and B. Crawford, Jr., J. Chem. Phys. 27, 455 (1957).

TABLE IV. Calculated values[a] of $\lambda-\lambda^0$ for a H···H repulsion potential in CH_3Cl.

ν	$f_{\parallel}$	$f_{\perp}$	f_{12}	$\lambda_{A_1}-\lambda^0$	$\lambda_{B_2}-\lambda^0$
1	0.0464	...	0.0292	0.0756	0.0172
2	0.0468	...	0.0248	0.0716	0.0220
3	0.0036	...	0.0070	0.0114	−0.0034
$4A'$	0.0668	...	0.0162	0.0830	0.0504
$5A'$	0.0222	...	0.0222	0.0444	0.0000
$6A'$	0.0348	...	−0.0308	0.0040	0.0656
				(A_2 and B_1)	
$4A''$	...	0.0020	0	0.0020	
$5A''$	...	0.0054	0	0.0054	
$6A''$	...	0.0206	0	0.0206	

[a] All values in 10^{28} sec^{-2}. Values include all equivalent nearest neighbor interactions.

made any check of the approximation discussed in Appendix I.

To evaluate β, we take a theoretical equation for the hydrogen repulsion energy. Because of its mathematical simplicity, and because it is not clear to us which of several such theoretical papers is most appropriate, we adopt the results of deBoer.[14] His repulsive potential (for two H_2 molecules) is a sum of terms in the interatomic distances, of which we extract just one, since we consider only one H···H distance at a time. The potential assumed is then

$$V=(2.78e^2/a_0)\exp(-1.87r/a_0), \qquad \text{(II-5)}$$

or $V=1.20\times10^{-10}\exp(-3.52\times10^8 r)$ erg. Thus, at the H···H distance in the crystal, $\beta=6.1\times10^2$ erg/cm^2. By applying this factor to the rest of the terms of (I-7), we get Table IV of calculated $\lambda-\lambda^0$ values.

A cursory examination of the differences between the A_1 and B_2 frequencies in Table IV shows that the predicted splittings agree within a factor of 2 for ν_1 and ν_2. For ν_4 the site splitting predicted more nearly matches the observed value. For ν_5 the factor group splitting predicted is again twofold low. In ν too much splitting is predicted. We take the rather arbitrary position that the factor β given by the deBoer formula (as used in the foregoing) is actually low by a factor of two. Then we may summarize the results of our calculations of the splittings (factor group variety except for ν_4). This is done in Table V, which includes the H···H repulsion results (with the factor of two applied) and the dipole results.

The calculated values for ν_1, ν_2, ν_4, ν_5 are in agreement with observations to well within the expected reliability of the approximations used. This result was obtained with one parameter (β) adjusted only by a factor of two from its theoretical value (which is of questionable validity under these conditions anyway).

[14] J. deBoer, Physica **9**, 363 (1942); J. O. Hirschfelder, C. F. Curtiss, and R. B. Bird, *Molecular Theory of Gases and Liquids* (John Wiley & Sons, Inc., New York, 1954), p. 1085.

TABLE V. Final calculated and observed splittings in CH_3Cl.

ν	$\Delta\lambda$obs[a]	$\Delta\lambda$calc[a]
1	0.090	0.098
2	0.098	0.0966
3	0.024	0.004
4	0.106	{0.064 (site) {0.032 (factor)
5	0.078	0.088
6	<0.040	0.128

[a] In units of 10^{28} sec^{-2}.

There are weaknesses in the results in the prediction of site splittings (e.g., ν_5) and in general band shifts from the gas phase because we have left out such obvious points as dielectric effects and molecule I-molecule III dipole interactions, which might well cause such splittings and shifts. The unfortunate results for ν_3 and ν_6 are not surprising, as these frequencies most seriously involve motions of the Cl atoms, whose interactions have been entirely ignored.

The point of interest is the reasonable prediction, based on H-atom interaction, of the splitting of all vibrations largely consisting of H-atom motion. The value used in Table V for the parameter β may be considered the first intermolecular potential constant to emerge from the use of the theory of Sec. I.

SUMMARY

Two types of intermolecular potentials, dipole-dipole and hydrogen repulsion, have been assumed in order to calculate the intermolecular coupling constants and frequency splittings in crystalline CH_3Cl. It is found that the latter suffices to account for the greater part of the observed effects in four bands, while the former is of major importance for only one. At this time, it does not seem profitable to attempt a better fit by the addition, say, of a H···Cl repulsion or a dispersion force term. Work is in progress on the deuterated analogue of methyl chloride, whose splittings should provide a check on the present results and perhaps shed more light on other interactions.

ACKNOWLEDGMENTS

The author is grateful to several persons, particularly Professor W. B. Person and Dr. R. M. Hexter for valuable discussions and encouragement. Dr. Hexter has made analyses similar to those parts of this work on dipole coupling in CH_3Cl. The facilities of the Western Data Processing Laboratory, University of California at Los Angeles, made possible the convenient calculation of some of the matrices employed, and the author was assisted in the use of these facilities by Dr. G. Palenik.

APPENDIX I

To indicate that the terms of (I-6) involving $\partial V/\partial r_{ij}$ are negligible we consider f_{nm}, rewriting as in

(I-7) (only one atom pair considered):

$$f_{nm}=(\partial^2V/\partial r_{ij})[(\partial r_{ij}/\partial r_i)(\partial r_i/\partial Q_n)]$$
$$\times[(\partial r_{ij}/\partial r_j)(\partial r_j/\partial Q_m)]$$
$$+(\partial V/\partial r_{ij})(\partial^2 r_{ij}/\partial r_j\partial r_j)(\partial r_i/\partial Q_n)(\partial r_j/\partial Q_m). \quad (A\text{-}1)$$

The terms $\partial r_{ij}/\partial r_i$, etc., can be written as $\cos\phi_i$, where ϕ_i is the angle between the normal displacement vector of the atoms and the vector r_{ij}. It is easily shown that $\partial^2 r_{ij}/\partial r_i\partial r_j=\sin\phi_i\sin\phi_j\cos\theta/r_{ij}$, where θ is the dihedral angle formed by the three vectors involved. Thus,

$$f_{nm}=\left[(\partial^2V/\partial r_{ij}^2)(\cos\phi_i\cos\phi_j)\right.$$
$$\left.+(\partial V/\partial r_{ij})\frac{\sin\phi_i\sin\phi_j\cos\theta}{r_{ij}}\right](\partial r_i/\partial Q_n)(\partial r_j/\partial Q_m). \quad (A\text{-}2)$$

If we now assume that the interatomic potential is of the inverse-p type ($V=d/r_{ij}^p$) we may take derivatives as indicated and write

$$f_{nm}=[p(p+1)/r_{ij}^2]\cdot(d/r_{ij}^p)[\cos\phi_i\cos\phi_j$$
$$+(p+1)^{-1}\sin\phi_i\sin\phi_j\cos\theta](\partial r_i/\partial Q_n)(\partial r_j/\partial Q_m). \quad (A\text{-}3)$$

Since the term p will ordinarily be large for those potentials which can reasonably be written on an atom-atom basis (e.g., repulsive potentials where $p\cong 12$ and possibly dispersion potentials, where $p\cong 6$) the maximum value of the second term in parentheses will be small [one $(p+1)$th of the maximum of the first]. Especially for repulsive potentials it will be most profitable to ignore the second term unless an examination shows that *both* the angles ϕ and θ are such as to necessitate its consideration.

APPENDIX II

It is desired to obtain the $\mathbf{D}^{-1}$ matrix. We define the following transformation matrices

$$\mathbf{q}=\mathbf{D}v,$$
$$\mathbf{S}=\mathbf{U}q,$$
$$\mathfrak{s}=\mathfrak{U}v,$$
$$\mathbf{S}=\mathfrak{D}\mathfrak{s}, \quad (A\text{-}4)$$

where q and v are column vectors in internal and external (cartesian) coordinates, respectively, and $\mathbf{S}$ and $\mathfrak{s}$ are internal and external symmetry coordinates, respectively.[7] The transformations $\mathbf{U}$ and $\mathfrak{U}$ being orthogonal, their reverse transformations are given by the transpose matrices $\mathbf{U}'$ and $\mathfrak{U}'$. Then,

$$\mathfrak{D}=\mathbf{U}\mathbf{D}\mathfrak{U}' \quad (A\text{-}5)$$

and due to the choice of symmetry coordinates, $\mathfrak{D}$ will be factored into blocks which will be of a much more convenient magnitude. $\mathfrak{D}$ may then be inverted directly to give $\mathbf{D}^{-1}$, the inversion process being greatly simpler than direct inversion of $\mathbf{D}$ itself. To accomplish the inversion, $\mathfrak{D}$ must be a square matrix. The rows of $\mathfrak{D}$ which must be added are simply the conditions of conservation of center of gravity and angular momentum, expressed in external symmetry coordinates. Of course, the conditions may be put in $\mathbf{D}$ at the beginning and carried through.

Having obtained $\mathbf{D}^{-1}$, it is also directly a consequence of the definitions that

$$\mathbf{D}^{-1}=\mathfrak{U}'\mathfrak{D}^{-1}\mathbf{U}. \quad (A\text{-}6)$$

Of course, it may be of value to obtain instead of $\mathbf{D}^{-1}$ the transformation directly from internal symmetry coordinates to cartesian coordinates. This transformation is given simply by $\mathfrak{U}'\mathfrak{D}^{-1}$.

It should be noted that the cartesian coordinates considered throughout this paper are *not* the mass-weighted ones discussed by Polo,[8] though the difference is merely one of convenience.

Electron Capture by Neutral Molecules

R. E. STANTON

Department of Chemistry, Canisius College, Buffalo, New York

(Received October 14, 1959)

The problem of calculating the probability of electron capture by neutral molecules is analyzed. It is shown that capture is possible only through the breakdown of the separation of nuclear and electronic motion in the Schrödinger equation, and that this is equivalent to the use of the nuclear kinetic energy as a perturbation operator. For diatomic molecules, it is found that capture is improbable except for those states of the negative ion whose major configuration contains at least as many MSO's of a given spin-symmetry type as the neutral molecule. Experimental verification of this result is found in the case of hydrogen.

I. INTRODUCTION

WITHIN the last year or so, a number of experimenters have shown increased interest in electron capture by neutral molecules. We shall be particularly concerned with the work of Khvostenko and Dukel'skii[1] and Schulz[2] on electron capture by H_2. A sampling of other workers in the field is given in reference 3. Further references may be obtained by consulting their papers.

On the other hand, there seems to have been no attempt to attack the problem of capture cross sections from a theoretical standpoint since the early work of Bloch and Bradbury[4] and Massey.[5] The present paper is an attempt to explore the possibilities of a theoretical analysis, particularly with regard to finding selection rules. It is hoped that this will facilitate the interpretation of experiment in cases where several electronic states of the negative ion are possible.

II. PERTURBATION SCHEME

It seems advisable to begin with a defense of the use of the nuclear kinetic energy operator as the perturbation bringing about capture. While Massey has laid down the physical grounds for this approach, he has not demonstrated its uniqueness; in particular, he has not shown the impossibility of accounting for capture in terms of the electrostatic interaction between the electron and the neutral molecule. These points may be brought out quite clearly if we examine the usual procedure for separating nuclear and electronic motion in a molecule.[6]

We may write the Schrödinger equation for the combined system of neutral molecule and free (or bound) electron as

$$\mathbf{H}\Psi = i\hbar(\partial\Psi/\partial t) \tag{1}$$

$$\mathbf{H} = \mathbf{H}^{(e)} + \mathbf{H}^{(n)} \tag{2}$$

$$\mathbf{H}^{(e)} = -\Sigma(\hbar^2/2n)\nabla_i^2 + V_{ne} + V_{ee} \tag{3}$$

$$\mathbf{H}^{(n)} = -\Sigma(\hbar_2/2m_\alpha)\nabla_\alpha^2, \tag{4}$$

where all symbols have their customary meaning in molecular theory.

On writing Ψ as

$$\Psi = \Sigma x_i \xi_i \Sigma y_{ij} \mathbf{n}_{ij} \exp(-i\omega_{ij} t) \tag{5}$$

$$= \Sigma f_{ij} \phi_{ij} \exp(-i\omega_{ij} t), \tag{6}$$

where

$$\mathbf{H}^{(e)} \xi_i = E^{(e)} \xi_i \tag{7}$$

and

$$(\mathbf{H}^{(n)} + E_i^{(e)}) \mathbf{n}_{ij} = E_{ij} \mathbf{n}_{ij} \tag{8}$$

we find

$$\dot{x}_i = \dot{y}_{ij} = \dot{f}_{ij} = 0, \tag{9}$$

provided only that we may ignore all derivatives of ξ_i with respect to the nuclear coordinates. Let us refer to this as the adiabatic approximation.[7]

Equation (9) states that within the adiabatic approximation, no transitions occur between the eigenfunctions of $\mathbf{H}^{(e)}$. We shall demonstrate that to the same approximation this means capture is impossible. To do this, we need simply show that in an actual physical situation the initial wave function of a system composed of a neutral molecule and an impinging electron contains no contribution from any negative ion eigenstate.

For purposes of clarity we shall first restrict our attention to a system composed of a single hydrogen atom and an extra electron. There can be no question of the fact that there exists a true eigenstate ξ_B of this system in which both electrons are bound to the atom. Obviously, there also exist other eigenstates in which one or both of the electrons are free. The general state of this two-electron system may be represented as a

[1] V. I. Khvostenko and V. M. Dukel'skii, J. Exptl. Theoret. Phys. (U.S.S.R.) **33**, 851 (1958); [Translation: Soviet Phys.—JETP **6**, 657 (1958)].

[2] G. J. Schulz, Phys. Rev. **113**, 816 (1959).

[3] D. C. Frost and C. A. McDowell, J. Chem. Phys. **29**, 503 (1958); V. M. Hickam and D. Berg, *ibid.* **29**, 517 (1958); B. E. Knox and B. P. Burtt, *ibid.* **28**, 1256 (1958); M. A. Biondi and R. E. Fox, Phys. Rev. **109**, 2012 (1958).

[4] F. Bloch and N. E. Bradbury, Phys. Rev. **48**, 689 (1935).

[5] H. S. W. Massey, *Negative Ions* (Cambridge University Press, Cambridge, England, 1950), 2nd ed., p. 50.

[6] H. Eyring, J. Walter, and G. E. Kimball, *Quantum Chemistry* (John Wiley & Sons, Inc., New York, 1944), pp. 190–191.

[7] We prefer to restrict the expression "Born-Oppenheimer approximation" to the somewhat different separation scheme which they employed in their famous paper.

superposition of all possible bound states and all possible free states:

$$\psi=\Sigma x_i\xi_i\exp(-i\omega_i t) \tag{10}$$

with

$$\dot{x}_i=0. \tag{11}$$

Now let us consider the sort of experiment we perform in measuring capture cross sections. We begin with one electron roughly localized at some macroscopically significant distance from the atom. This means that the wave function ψ, which represents the system at $t=0$, must be vanishingly small if the coordinates of both electrons are given values in the vicinity of the nucleus. Therefore, at $t=0$ there will be no overlap between ψ and ξ_B, and

$$x_B=\int\xi_B^*\psi(t=0)d\tau,$$

$$=0. \tag{12}$$

This geometric argument breaks down at later times, but Eq. (11) ensures that x_B will remain zero at all times. Thus, we see that capture is impossible (except by radiative means with which we are not concerned).

Now let us consider what happens with a hydrogen molecule. For very large values of the internuclear distance R it is clear that there will be two bound states of $H_2^{(+)}$, appropriate *gerade* and *ungerade* combinations of states in which the extra electron is bound to one or the other of the atoms. As the internuclear distance is decreased the two states ξ_{Bg}, and ξ_{Bu} will change their characteristics continuously. In particular, since helium probably has no electron affinity, there will be a tendency for the electron distribution of each state to become more and more diffuse until at a short enough distance R_e the two states lose their bound character and the electron distribution spreads out to infinity. The discussion of the possibility of capture varies according to whether this critical distance is less or greater than the normal internuclear distance R_e.

If $R_c<R_e$ the overlap argument previously carried out for the atomic case carries through unchanged. Once again,

$$\psi(t=0)=\Sigma x_i\xi_i\Sigma y_{ij}\mathfrak{n}_{ij} \tag{13}$$

$$\left.\begin{aligned} x_{Bg}&\propto\int\xi_{Bg}^*\psi(t=0)d\tau\\ &=0\end{aligned}\right\} \tag{14}$$

$$\left.\begin{aligned} x_{Bu}&\propto\int\xi_{Bu}^*\psi(t=0)d\tau\\ &=0\end{aligned}\right\} \tag{15}$$

because of nonoverlap, and since $\dot{x}_i=0$ we see that the bound states never make a contribution to ψ.

If $R_c>R_e$ an apparent difficulty arises since ξ_{Bg} and ξ_{Bu} extend to infinity. We note, however, that ξ_{Bg} and ξ_{Bu} can extend to infinity only at the expense of becoming infinitesimal everywhere. Since $\psi(t=0)$ is localized we have once more

$$x_{Bg}=0 \tag{14'}$$

$$x_{Bu}=0. \tag{15'}$$

A word about Eqs. (14'), (15'): in most cases where a state extends to infinity the infinitesimal overlap with a localized wave function retains significance because there are an infinity of other states with only infinitesimally different physical characteristics which overlap with the localized wave function in the same way, and it is the sum of all of these infinitesimal overlaps that is of interest. In the present problem, however, there are only two states involved and the sum of x_{Bg} and x_{Bu} remains infinitesimal. Capture remains impossible within the adiabatic approximation. It is, moreover, clear that the argument is completely general in its applicability and is not restricted to hydrogen.

On the other hand, when we drop the adiabatic approximation we find

$$i\hbar\dot{f}_{kl}=\sum_{\alpha,i,j}f_{ij}\hbar^2/2m_\alpha \times\int\xi_k^*\mathfrak{n}_{kl}^*\{(\nabla_\alpha^2\xi_i)\eta_{ij}+\nabla_\alpha\xi_0\cdot\nabla_\alpha\mathfrak{n}_{ij}\}d\tau \times\exp[i(\omega_{kl}-\omega_{ij})t]. \tag{16}$$

If ϕ_{kl} represents a bound eigenstate, and if we take into account the orthogonality of ξ_k and ξ_i, and the absence of bound states from the initial wave function, then within the limits of first-order perturbation theory (16) becomes

$$i\hbar\dot{f}_{kl}=\exp(i\omega_{kl}t)\int\phi_{kl}^*T\psi d\tau, \tag{17}$$

where T is the nuclear kinetic energy operator. This is essentially Massey's expression.

III. SELECTION RULES

We assume that, to a good approximation, both the initial and the bound states may be represented by a single determinant for the electronic part together with an associated nuclear wave function:

$$\psi(t\to0)=\xi_F(t)\mathfrak{n}_F\exp(-i\omega t) \tag{18}$$

$$\phi_B=\xi_B\mathfrak{n}_B \tag{19}$$

$$\xi_F=(n!)^{-\frac{1}{2}}\,|\,\xi_1(1)\xi_2(2)\cdots\xi_{n-1}(n-1)\xi_F(n,t)\,| \tag{20}$$

$$\xi_B=(n!)^{-\frac{1}{2}}\,|\,\xi_1'(1)\xi_2'(2)\cdots\xi_{n-1}'(n-1)\xi_n'(n)\,| \tag{21}$$

In order to assure the accuracy of this approximation, we allow the ξ_i' and the ξ_i to be drawn from different sets. $\xi_F(t)$ represents the free electron. Without loss of generality it may be assumed to have been orthogonalized to the other ξ_i.

Let us now examine the conditions under which the nuclear kinetic energy matrix element vanishes. No completely rigorous conditions may be derived. The reason is simply that the uncertain nature of $\xi_F(t)$ makes it impossible to assign any definite symmetry species or total spin to ξ_F. Insofar, however, as the single determinant approximations of Eqs. (18)–(21) are valid, one may hope to derive selection rules for electron capture based upon the symmetry species and spin character of the individual MSO's, which enter into ξ_F and ξ_B.

From (16), we see that f_{BI} depends upon the vector quantity $\langle \xi_B \mid \Sigma \nabla_\alpha/m_\alpha \mid \xi_F \rangle$ and the scalar quantity $\langle \xi_B \mid \nabla_\alpha^2/m_\alpha \mid \xi_F \rangle$. Since ∇_α acts only on the nuclear coordinates, both of these may be expressed as sums of products of one-electron integrals; e.g.,

$$\langle \xi_B \mid \nabla_\alpha \mid \xi_F \rangle = (n!)^{-1}\{\cdots + \langle \xi_i' \mid \xi_j \rangle \langle \xi_k' \mid \xi_l \rangle \cdots \langle \xi_m' \mid \nabla_\alpha \mid \xi_P \rangle \cdots + \cdots\}. \quad (22)$$

One of the factors in the typical term indicated will contain $\xi_F(t)$. Since, as previously noted, this function has no precise spin or symmetry character, there is no reason why the integral involving it should vanish. The vanishing or nonvanishing of the entire term depends then on the other factors. Now, it is clear that ∇_α has no effect on the spin part of ξ_P. It can also be shown that *for diatomic molecules*, ∇_α does not change the symmetry species.[8]

It follows that the entire kinetic energy matrix element will vanish if ξ_B does not contain at least as many MSO's of a given spin-symmetry type as does ξ_F, since at least one of the factors in each term of the expansions of $\langle \xi_B \mid \nabla_\alpha \mid \xi_F \rangle$ and $\langle \xi_B \mid \nabla_\alpha^2 \mid \xi_F \rangle$ will vanish if this condition is not met.

[8] We may expand each MSO in a Taylor series about the equilibrium value of (R) in the *neutral* molecule. The coefficients of all powers of $(x_\alpha - x_{\alpha 0})$, etc., must have the same symmetry characteristics. Since ∇_α does not affect these coefficients, it follows that ξ_i and $\nabla_\alpha \xi_i$ belong to the same symmetry species.

Experimental verification of these ideas is available in the case of hydrogen. As previously noted there are two states of H_2^- which may be formed from $H+H^-$, both in their ground states. The major configurations of each may be designated by

$$\xi_{Bu} = (3!)^{-1} \mid 1s\sigma_g'\alpha(1) \quad 1s\sigma_g'\beta(2) \quad 2p\sigma_u'\alpha(3) \mid$$

and

$$\xi_{Bg} = (3!)^{-1} \mid 1s\sigma_g''\alpha(1) \quad 2p\sigma_u''\alpha(2) \quad 2p\sigma_u''\beta(3) \mid.$$

If we compare these with

$$\xi_F = (3!)^{-1} \mid 1s\sigma_g\alpha(1) \quad 1s\sigma_g(2) \quad \xi_F(3,t) \mid,$$

we see that capture should be possible only into ξ_{Bu}.

This prediction seems to be fulfilled by experiment. Both Schulz and the Russian group of Khvostenko and Dukel'skii found that the process

$$H_2 + e \rightarrow H + H^-$$

occurs in two energy intervals, from about 8 to 10 ev, and from about 14 to 16 ev. If the H atom produced were in its ground state in both cases, then our theoretical predictions would seem to be in error. Actually, however, Schulz concluded from measurements of the kinetic energy of the H^- ions that the H atom must be excited when produced by electrons of energy between 14 and 16 ev.

In the low-energy region, Schulz's plot of cross section vs electron energy shows a very slight dip in the maximum. This does not appear in Khvostenko and Dukel'skii's data. However, they express less confidence in their low-energy data than in their high-energy data, and the possibility must be considered that this dip results from an overlap of two capture processes, one leading to the *gerade* state of the negative ion and one leading to the *ungerade* state. Once again, the measurements of the kinetic energy of the H^- ion are informative. From these measurements, Schulz was able to show that if capture into both states were possible then the potential energy diagrams of the two states *must coincide* for values of R near the equilibrium separation of H_2. This conclusion does violence to all predictions of molecular orbital theory. It seems much more reasonable to accept our conclusion that capture into the *gerade* state is forbidden.

Thermodynamic Excess Functions for Electrolyte Solutions

HAROLD L. FRIEDMAN,*

Department of Chemistry, University of Southern California, Los Angeles, California

(Received February 6, 1959)

A system of excess functions is developed for electrolyte solutions and other solutions with an essentially unsymmetrical solvent-solute relation. These new functions vanish for a solution whose practical (molal scale) osmotic coefficient is unity at all compositions, temperatures and pressures. The use of these excess functions offers some advantages over other methods of comparing Mayer's ionic solution theory with experiment, of representing the properties of solutions of single or mixed electrolytes, and of making qualitative interpretations of the molecular basis of thermodynamic properties.

Graphs showing the ionic-strength dependence of the excess free energy, excess enthalpy, excess entropy, and excess volume are given for several aqueous solutions of single electrolytes up to 6 molal. Experimental values of the cluster integral sum, the characteristic function of the Mayer theory, have also been calculated. The concentration dependence of this function is very similar to that of the excess free energy.

1. INTRODUCTION

THE use of excess functions to represent the thermodynamic properties of solutions of nonelectrolytes, which was introduced by Scatchard[1] and Scatchard and Raymond,[2] offers the most convenient way to describe the deviation from ideality of the solution as a whole.[3–5] Activity coefficients, which have been in much more general use than the excess free energy, are suited for applications in which the behavior of a particular component of the solution is of special interest, as in the distribution of this component between two phases or in the chemical reaction of this component in the solution. These applications provide the only way to investigate the free energy of mixing in condensed phases, but for other directly measurable thermodynamic properties, such as enthalpy, volume, and heat capacity, there is no corresponding unique significance of the partial molal quantities. On the other hand, the excess free energy is the term in the total configurational free energy of the solution that is characteristic of the mixture, and the configurational energy is closely related to the configuration integral whose evaluation is the direct objective of most statistical calculations from a model for the solution. Also, graphs which show the dependence of the various excess functions upon the composition of the solution are simpler and more susceptible to qualitative interpretation in terms of molecular interaction in the solution than the corresponding graphs of the various partial molar excess functions.

One may expect the same advantages to be found in a suitably defined system of excess functions for electrolyte solutions and other solutions with an essentially unsymmetrical solvent-solute relationship. Indeed such functions have occasionally been employed before now,[6–11] but there is a need for a systematic exposition of their properties such as the one offered in Sec. 2 of this paper. The excess functions for electrolyte solutions in the Debye-Hückel limiting law (DHLL) range are given in Sec. 3. In Sec. 4 there is a development of the relation of the excess Gibbs free energy to the cluster integral sum of the McMillan-Mayer solution theory and Mayer's ionic solution theory. When excess functions rather than activity or osmotic coefficients are used to represent the data it becomes unnecessary to differentiate the irreducible cluster integrals of the Mayer theory with respect to concentration in order to make a comparison with experiment, and this advantage has been the stimulus to the present development.

It seems appropriate to include some examples of the description of the thermodynamic properties of aqueous electrolyte solutions by excess functions. This is done for solutions of single electrolytes in Sec. 5 along with several comments on the relevance of these descriptions to some earlier qualitative discussions of the molecular basis of the thermodynamic behavior of electrolyte solutions. Some special advantages in the use of total excess functions to represent the properties of electrolyte mixtures are demonstrated in Sec. 6.

2. FORMULATION OF EXCESS FUNCTIONS FOR UNSYMMETRICAL SOLUTIONS

We designate one component of the solution as the solvent and choose as composition variables the

* Present address: IBM Research Center, P. O. Box 218, Yorktown Heights, New York.

[1] G. Scatchard, Chem. Revs. **8**, 321 (1931); **44**, 7 (1949).

[2] G. Scatchard and C. Raymond, J. Am. Chem. Soc. **60**, 1278 (1938).

[3] I. Prigogine and R. Defay, *Chemical Thermodynamics* (Longmans, Green and Company, Inc., New York, 1952).

[4] I. Prigogine, *The Molecular Theory of Solutions* (Interscience Publishers, Inc., New York, 1957).

[5] E. Guggenheim, *Thermodynamics* (Interscience Publishers, New York, 1957), 3rd ed.

[6] G. Scatchard and S. Prentiss, J. Am. Chem. Soc. **56**, 1486 (1934).

[7] G. Scatchard, Chem. Revs. **19**, 309 (1936).

[8] R. Fowler, *Statistical Mechanics* (Cambridge University Press, New York, 1936), 2nd ed.

[9] R. Fowler and E. Guggenheim, *Statistical Thermodynamics* (Cambridge University Press, New York, 1952).

[10] H. L. Friedman and R. Schug, J. Am. Chem. Soc. **78**, 3881 (1956).

[11] H. L. Friedman, Discussions Faraday Soc. **24**, 74 (1957).

molalities, m_s, of each of the solute species ($s=1, 2, \cdots$). The chemical potential of any solute may be expressed as

$$\mu_s=\mu_s^0+RT\ln m_s\gamma_s \tag{2.1}$$

We specify that the activity coefficient, γ_s, is unity when all of the m_s are zero. Then μ_s^0 is the chemical potential of solute species s in the usual hypothetical one molal reference state at the same T and P as the solution. By applying the Gibbs-Duhem equation we find that Eq. (2.1) implies that the chemical potential of the solvent, μ_w, is related to the total molality of solute species,[11a]

$$m=\sum m_s, \quad s=1, 2, \cdots$$

by the equation

$$\mu_w=\mu_w^0-RTM_w m\phi/1000 \tag{2.2}$$

where μ_w^0 is the chemical potential of the pure solvent at the same T and P as the solution, M_w is the molecular weight of the solvent, and ϕ is the osmotic coefficient, given by

$$\phi=1+(1/)m\int_{m=0}^{m}\sum m_s d\ln\gamma_s. \tag{2.3}$$

At this point, we introduce an innovation which simplifies many of the equations in this paper. This is to use as the basic quantity of solvent not the mole, but the kilogram, and to express all specific total solution functions as the extensive function for the quantity of solution containing a kilogram of solvent. We retain the mole as the basic quantity of each solute, and continue to employ partial molal quantities for the solutes. This asymmetry of the notation is merely a logical consequence of the use of the molal rather than mole ratio or mole fraction concentration scale. Also, we use not the partial molal, but the partial specific (per kg) free energy of the solvent, G_w:

$$G_w=[\partial\mathcal{G}/\partial\mathcal{W}]_{T,P,n_s},$$

where $\mathcal{W}$ is the mass of solvent.[11b]

Equation (2.2) then becomes

$$G_w=G_w^0-RTm\phi. \tag{2.2'}$$

We also introduce a hypothetical reference solution in which all of the activity coefficients are unity at any temperature, pressure, and composition. For such a solution, the osmotic coefficient is also unity [Eq. (2.3)], and the partial free energies are given by

$$\mu_s^*=\mu_s^0+RT\ln m_s \tag{2.4}$$

$$G_w^*=G_w^0-RTm \tag{2.5}$$

It is apparent that γ_s and ϕ are simply related to partial excess functions, which express the difference in properties of a real solution and of a hypothetical reference solution of the same composition, temperature, and pressure:

$$\mu_s^{ex}=\mu_s-\mu_s^*=RT\ln\gamma_s \tag{2.6}$$

$$G_w^{ex}=G_w-G_w^*=RTm(1-\phi). \tag{2.7}$$

The *total* excess Gibbs free energy of a quantity of a real solution containing a kilogram of solvent is

$$G^{ex}=G-G^*=G_w^{ex}+\sum m_s\mu_s^{ex} \tag{2.8}$$

$$=RTm[1-\phi+\sum x_s\ln\gamma_s] \tag{2.9}$$

where

$$x_s=m_s/m \tag{2.10}$$

is the solute fraction of species s. It is convenient to define a mean solute quantity,

$$Y_\pm=\sum x_s Y_s \tag{2.11}$$

corresponding to any partial molar solute quantity, Y_s. This reduces to the usual mean ionic quantity[12] when the solute is obtained by the dissociation of a single strong electrolyte. Equation (2.11) may be applied to $Y_s=\ln\gamma_s$ and then we obtain

$$G^{ex}=RTm[1-\phi+\ln\gamma_\pm], \tag{2.12}$$

which is valid in general and which, for an electrolyte solution with a single solute, provides a way to calculate G^{ex} from the usual[12,13] tabulated values of ϕ and $\gamma_\pm$.

We now consider several derivatives of G^{ex}. The partial molal derivatives are

$$(\partial G^{ex}/\partial m_s)_{T,P,m_{i\neq s}=m_s}=\mu_s^{ex} \tag{2.13}$$

and

$$\left[\frac{\partial(G^{ex}/m)}{\partial(1/m)}\right]_{T,P,\text{ all }x_s}=G_w^{ex}. \tag{2.14}$$

The excess enthalpy is

$$H^{ex}=\left[\frac{\partial(G^{ex}/T)}{\partial(1/T)}\right]_{P,\text{m, all }x_s}=H_w^{ex}+m_s H_s^{ex}, \tag{2.15}$$

and equations for the excess entropy, excess volume, etc., are obtained in analogous fashion.

In the case of solutions of a single electrolyte, there are functions discussed in Harned and Owen,[12] which correspond to some of the excess functions which we define in this way. Some relations between the two sets

[11a] A dictionary of the present nomenclature in relation to the more familiar Harned and Owen[12] nomenclature is given in Appendix A. Note especially the distinction between the two m's.

[11b] Script capitals are employed in this paper to represent extensive quantities.

[12] H. Harned and B. Owen, *The Physical Chemistry of Electrolyte Solutions* (Reinhold Publishing Corporation, New York, 1958), 3rd ed.

[13] R. Robinson and R. Stokes, *Electrolyte Solutions* (Butterworths Scientific Publications, Ltd., London, 1955).

of enthalpy and volume functions are given in Appendix A.

It is apparent that the excess functions, G^{ex}, H^{ex}, S^{ex}, and V^{ex} for unsymmetrical solutions are interrelated in the same way as the fundamental thermodynamic variables $\mathcal{G}$, $\mathcal{H}$, $\mathcal{S}$, and $\mathcal{V}$. For instance, we have

$$TS^{ex}=H^{ex}-G^{ex}.$$

The same interrelation exists for the excess functions which are convenient for the description of symmetrical solutions, but not for the functions $\gamma_{\pm}$, ϕ, ϕ_L, ϕ_V, etc. which have most often been used to describe the properties of electrolyte solutions. On the other hand, the excess functions for symmetrical solutions include the effects of solvation as well as solute-solute interaction and give a complete description of the formation of a solution from its components, while the excess functions proposed here include only that part of the solute-solvent interaction which changes with the concentration of the solution. The new excess functions must, therefore, be supplemented by the thermodynamics of formation of the solutes in their reference states in solution from pure forms, in order to give a complete description of the formation of the solution from its components. It may also be pointed out that making the assumption of ideal mixing would lead to definite contributions to S^{ex} and G^{ex} as defined for unsymmetrical solutions.

3. EXCESS FUNCTIONS IN ELECTROLYTE SOLUTIONS AND THE DEBYE-HÜCKEL THEORY

The Debye-Hückel theory may be formulated to lead directly to $\mathcal{G}^{el}$, the extra Gibbs free energy due to the interionic forces in electrolyte solutions [cf. Fowler and Guggenheim,[9] Eq. (9.17.3)]. This in turn leads to

$$G^{ex}=-kTV\kappa^3/12\pi \qquad (3.1)$$

in the DHLL range. Here, κ is the usual Debye parameter. It is useful to record the following relations between the relative functions and the molal ionic strength I in the DHLL range:

$$G^{ex}=-\tfrac{4}{3}RTI^{\frac{3}{2}}[\ln 10]\mathcal{S}_f/w'(V_w^0)^{\frac{1}{2}} \qquad (3.2)$$

$$H^{ex}=-\tfrac{4}{3}I^{\frac{3}{2}}\mathcal{S}_H/vw'(V_w^0)^{\frac{1}{2}} \qquad (3.3)$$

$$V^{ex}=\tfrac{4}{3}I^{\frac{3}{2}}\mathcal{S}_V/vw'(V_w^0)^{\frac{1}{2}}. \qquad (3.4)$$

The functions $\mathcal{S}_F/w'$, $\mathcal{S}_H/vw'$, and $\mathcal{S}_V/vw'$ are tabulated by Harned and Owen[12] for aqueous solutions at several temperatures. The volume of pure solvent per kg, V_w(pure), is abbreviated V_w^0 in these equations.

It is interesting to compare the values for these relative functions for water at 25° and for a hypothetical solvent with the same dielectric constant, but with vanishing temperature and pressure derivatives ofthe dielectric constant:

	Water	Hypothetical solvent
G^{ex}	$-926I^{\frac{3}{2}}$ cal	$-926I^{\frac{3}{2}}$ cal
H^{ex}	$+472I^{\frac{3}{2}}$ cal	$-1389I^{\frac{3}{2}}$ cal
S^{ex}	$+4.7I^{\frac{3}{2}}$ cal/deg	$-1.55I^{\frac{3}{2}}$ cal/deg
V^{ex}	$+2.5I^{\frac{3}{2}}$ cm^3	0.

In the hypothetical solvent, the structural interpretation of S^{ex} is that it is a measure of the loss of freedom of motion of the ions, and that this loss corresponds to the order implied by the existence of the ion atmosphere.[14] The difference between this and S^{ex} for the real solution must be associated with the change of entropy of water in the electric field of the ions since[15]

$$[\partial S/\partial(E^2)]_{\mu,T}=V(8\pi)^{-1}[\partial D/\partial T]_{P,E} \qquad (3.5)$$

where D is the dielectric constant and E the electric field strength.[15a] The contribution to S^{ex} from this effect is positive because the electric fields of the ions overlap and partially cancel in the real solution, but not in the hypothetical reference solution. Therefore, the effective E^2 acting upon the solvent increases more rapidly in the reference solution. Another way of stating this is that the electric field from an ion is more effective in decreasing the entropy of the solvent when the ion is added to pure solvent than when it is added to a real solution of finite concentration.

The preceding discussion of the entropy effects in the DHLL range may be taken as superseding and correcting that given by Frank and Robinson.[14] The author is indebted to Professor H. S. Frank for a discussion leading to the clarification of this matter.

4. EXCESS FUNCTIONS AND CLUSTER SOLUTION THEORIES

The McMillan-Mayer statistical thermodynamic theory of multicomponent mixtures[16] is the starting point of the Mayer ionic solution theory.[17] The essential point for the present purpose is that the McMillan-Mayer theory leads to a series expansion (in powers of concentration) of a thermodynamic function which we shall designate $\mathcal{G}$, the cluster integral sum, and that the Mayer ionic solution theory leads to a different expansion[18] for this function which is useful for ionic solutions. The function $\mathcal{G}$ is the same in either case, but

[14a] N. Bjerrum, Z. physik. Chem. (Leipzig) **119**, 145 (1926).
[14b] H. Frank and R. Robinson, J. Chem. Phys. **8**, 933 (1940).
[15] H. Frank, J. Chem. Phys. **23**, 2023 (1955).
[15a] There is a smaller term arising from the contribution of $(\partial V/\partial T)_p$, which is omitted in this discussion.
[16] W. G. McMillan and J. E. Mayer, J. Chem. Phys. **13**, 276 (1945).
[17] J. E. Mayer, J. Chem. Phys. **18**, 1426 (1950).
[18] H. L. Friedman, Mol. Phys. **2**, 23 (1959).

for the present purpose of relating it to G^{ex}, it is much easier to work with the McMillan-Mayer expansion,[18a]

$$\mathcal{S}=\sum B_{\mathbf{n}}c^{n}\prod x_s^{n_s}. \tag{4.1}$$

In this equation, $\mathbf{n}$ is a set,

$$\mathbf{n}=n_1, n_2, n_3, \cdots, \tag{4.2}$$

of molecules, n_1 molecules of species 1, n_2 molecules of species 2, etc., and

$$n=n_1+n_2+n_3+\cdots \tag{4.3}$$

is the total number of molecules in the set. The summation in (4.1) is over every set $\mathbf{n}$, such that $n\geq 2$ and $\mathbf{n}$ is a subset of the set comprising all the solute particles in the solution. The function $B_{\mathbf{n}}$ cannot be described in a simple way, but it is sufficient to note for the present purpose that it is independent of the concentration of solutes, but does depend upon the properties of the set of ions $\mathbf{n}$, in the pure solvent at a particular temperature T, and pressure P_0. This function is represented as B_{0n}* by McMillan and Mayer,[16] as B_n by Mayer,[17] and as $B_{\mathbf{n}}$ by Friedman.[18] In Eq. (4.1), c is the total solute particle number density (molecules per unit volume) and x_s is the solute fraction as defined in Eq. (2.10). The product is over all exponentials, $x_s^{n_s}$, corresponding to the set $\mathbf{n}$. For a given solvent the composition of the solution is specified by fixing c and the set $\mathbf{x}$

$$\mathbf{x}=x_1, x_2, x_3, \cdots. \tag{4.4}$$

In relating $\mathcal{S}$ to G^{ex}, our starting point is Eq. (85c) of McMillan and Mayer[16] which is, in the present notation

$$\pi/kT=c-\sum(n-1)c^{n}B_{\mathbf{n}}\prod x_s^{n_s}, \tag{4.5}$$

where the sum is over the same sets as in Eq. (4.1). This equation may be interpreted in terms of the usual osmotic pressure experiment employing a membrane permeable only to solvent species. Each $B_{\mathbf{n}}$ in the equation is a function of P_0, the pressure on the pure solvent, and T, both assumed constant throughout this section. We may independently adjust $\mathbf{x}$ and c by appropriate addition of solutes and adjustment of the volume accessible to the solute molecules. After the attainment of osmotic equilibrium, with the pressure on the solvent maintained at P_0, the pressure on the solution is $\pi+P_0$. The osmotic pressure π is given by (4.5). It is clear that π is a function of $\mathbf{x}$, c, and T as shown explicitly in (3.4) and that it also depends upon T, P_0, and the nature of the solvent through the $B_{\mathbf{n}}$. In all the differentiations, integrations, and other processes which we consider in the remainder of this section and in Appendix B we assume that c is the only one of these independent variables that is changing. There is no loss of generality in this procedure and it greatly simplifies the calculations.

With this assumption in mind, and comparing (4.1) and (4.5), it is apparent that the latter may be written as

$$\pi/kT=c+\partial(\mathcal{S}/c)/\partial(1/c), \tag{4.6}$$

which we take as the fundamental thermodynamic relation for $\mathcal{S}$ [compare with Eq. (19′) of Mayer].[17]

The development from this point on is a purely formal thermodynamic one and before undertaking it, it seems wise to obtain a more intuitive interpretation of the meaning of $\mathcal{S}$ by comparing (4.6) with a similar expression for an imperfect gas:

$$P/kT=c-\partial(\mathfrak{F}^{int}/c\mathcal{V}kT)/\partial(1/c). \tag{4.7}$$

This equation may also be related to the osmotic pressure experiment by omitting the solvent. Then $P_0\rightarrow 0$, $\pi\rightarrow P$, the pressure of the gas, and the semipermeable membrane is an ordinary wall. $\mathfrak{F}^{int}$ is the part of the Helmholtz free energy which arises from the intermolecular forces, i.e., the nonideal part. This equation may be deduced from Eqs. (701.9), (701.11), and (701.19) of Fowler and Guggenheim,[9] the last equation being the familiar relation,

$$P/kT=\partial \ln\Omega/\partial\mathcal{V},$$

of the pressure to the configuration integral, Ω. Equation (4.7) follows upon separating the ideal and nonideal parts of the configuration integral and changing variables from $\mathcal{V}$ to c.

Evidently $\mathcal{S}$ in the osmotic pressure equation corresponds to $-\mathfrak{F}^{int}/kT\mathcal{V}$ in the equation for an imperfect gas, and $-kT\mathcal{S}\mathcal{V}$ may be interpreted as that part of the Helmholtz free energy which corresponds to solute-solute interaction (including concentration-dependent solute-solvent interaction) in the solution. We will return to this analogy in the discussion at the end of this section. This correspondence between the osmotic pressure and imperfect gas equations has already been emphasized by McMillan and Mayer,[16] but the important point to be made here is that it shows that $\mathcal{S}$ has the character of an excess free energy. It remains to relate $\mathcal{S}$ exactly to G^{ex}.

The first step is the formal integration of Eq. (4.6) to obtain

$$\mathcal{S}/c=\int_{c=0}^{c}[\pi/kT-c]d(1/c) \tag{4.8}$$

where the upper limit of integration and $\mathcal{S}/c$ correspond to the same state. The integration is over a continuous series of osmotic equilibrium states. Now we change variables as follows:

$$c=Nm/V(m, \pi+P_0) \tag{4.9}$$

[18a] The function, $\mathcal{S}$, does not appear in reference 16 explicitly, but it corresponds to S of reference 17, Eq. (18) and $\mathbf{S}$ of reference 18, Eq. (7). The designation $\mathcal{S}$ is preferred to either of the others in thermodynamic treatments because S may be confused with the entropy and $\mathbf{S}$ implies[16] a set.

where N is Avogadro's number and $V(m, P)$ is the volume of solution per kg of solvent at molality m and pressure P. It is not necessary to specify $\mathbf{x}$, T, etc., because these independent variables are fixed in this discussion, but it *is* necessary to specify the m and P to which V, V_w, and $V_\pm$ apply in order to avoid confusion in the remainder of this section and in Appendix B. Neglecting P_0,[18b] we obtain from Eq. (4.8),

$$\mathcal{O}/c=\int_0^m[\pi V(m,\pi)/RT-m]d(1/m)+\int_0^m[\pi/mRT]dV(m,\pi)+\ln[V(0,0)/V(m,\pi)], \quad (4.10)$$

with the same path of integration as before

A similar relation may be obtained for G^{ex}. We begin with the general relation between the partial specific free energy of the solvent in the solution and in the pure state, both at pressure P_0:

$$G_w(m)=G_w^0-\int_{P_0}^{P_0+\pi}V_w(m,P)dP \quad (4.11)$$

where π is the osmotic pressure of the solution and V_w is the partial specific volume of the solvent in the solution.

We subtract (2.5) from (4.11) to obtain the excess partial specific free energy of the solvent

$$G_w^{ex}=RTm-\int_{P_0}^{P_0+\pi}V_w(m,P)dP=RTm-\pi V_w(m,\pi)+\int_0^\pi PdV_w(m,P) \quad (4.12)$$

where the second step is obtained by letting $P_0=0$ and integrating by parts. Equation (4.12) is then substituted into (2.14) and the result integrated to obtain

$$G^{ex}/mRT=-\int_0^m\{[\pi V_w(m,\pi)/RT]-m\}d(1/m)+(1/RT)\int_0^m d(1/m)\int_0^\pi PdV_w(m,P). \quad (4.13)$$

Now we combine Eqs. (4.10) and (4.13)

$$(\mathcal{O}/c)+(G^{ex}/mRT)=\int_0^m(\pi/RT)mV_\pm(m,\pi)d(1/m)+\ln[V(0,0)/V(m,\pi)]+\int_0^m\{\pi dV(m,\pi)/RTm]+d(1/m)\int_0^\pi[PdV_w(m,P)/RT]\}. \quad (4.14)$$

[18b] P_0 is generally neglected in the following derivation in order to simplify the equations. Usually, both G^{ex} and the B_n correspond to $P_0=1$ atm rather than $P_0=0$, but the difference, as estimated directly by carrying P_0 in the equations, is far smaller than the uncertainty in G^{ex} from the best data available.

We note the identity,

$$mV_\pm d(1/m)+(dV/m)=-V_\pm[dm/m]+V_\pm[dm/m]+(1/m)[\partial V/\partial P]_m dP, \quad (4.15)$$

which enables us to convert (4.14) into the following simpler form,

$$(\mathcal{O}/c)+(G^{ex}/mRT)=\ln[(V(0,0)/V(m,\pi)]+(1/RT)\int_0^m(\pi/m)[\partial V(m,\pi)/\partial P][\partial\pi/\partial m]dm+(1/RT)\int_0^m d(1/m)\int_{P=0}^\pi P[\partial V_w(m,P)/\partial P]dP. \quad (4.16)$$

This equation is useful for the exact comparison of values of $\mathcal{O}$ obtained from theory with values of G^{ex} obtained from experiment provided that the function $V(m, P)$ is known over a sufficient range of the variables. In principle this may be obtained from the theory but it will probably be more practical in most cases to employ experimental data for $V(m, P)$. A procedure for evaluating the right-hand side of (4.16) on the basis of experimental data for $V(m, P)$ for aqueous electrolyte solutions is developed in detail in Appendix B.

Some of the results which are presented in the following section show that in several systems,

$$\mathcal{O}/c\simeq -G^{ex}/mRT \quad (4.17)$$

is a useful approximation and it seems probable that this is true in general. It is proposed that this approximation may serve as a basis for qualitative discussions of the molecular-scale effects which are responsible for the thermodynamic properties of solutions. We proceed by noting that (4.17) is equivalent to

$$-kT\mathcal{U}\mathcal{O}\simeq\mathcal{W}G^{ex}=\mathcal{G}^{ex} \quad (4.18)$$

where, from the definition of G^{ex}, $\mathcal{G}^{ex}$ is the part of the Gibbs free energy of the solution at P_0 which is due to solute-solute interaction. Now, as pointed out earlier in this section, $-kT\mathcal{U}\mathcal{O}$ corresponds to $\mathcal{F}^{int}$ for an imperfect gas. So far the approximate relation (4.18) is at least consistent with our previous notions about the meaning of both $\mathcal{G}^{ex}$ and $\mathcal{F}^{int}$. But in addition, the analogy established by McMillan and Mayer[16] between the osmotic pressure equation and the imperfect gas equation provides the basis for writing a configuration integral for the former, which is analogous to the well known configuration integral for the latter. In this way we find

$$\mathcal{G}^{ex}=-kT\mathcal{U}\mathcal{O}=-kT\ln[\mathcal{U}^{-N}\int\exp[-W(\{N\})/kT]d\{N\}] \quad (4.19)$$

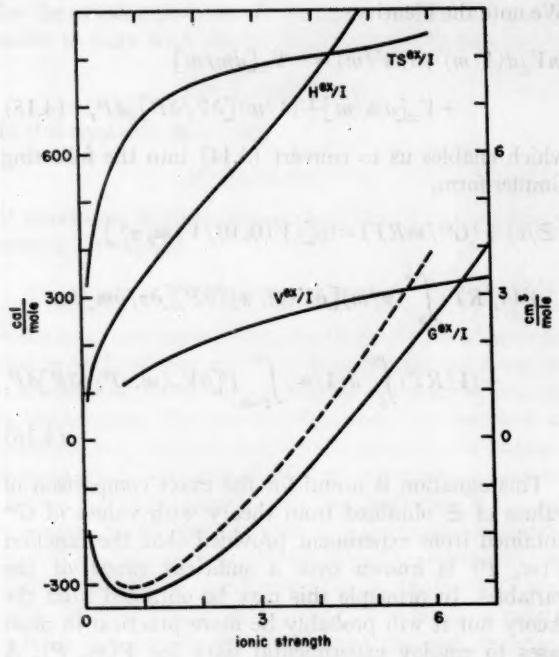

FIG. 1. Excess functions for aqueous LiCl solutions at 25°. The ordinate scale for V^{ex}/I is on the right, the others are on the left. The broken curve is $-2RT\lambda\mathfrak{S}/\kappa^3$, calculated by (B.19).

where N is the total number of solute particles, $\{N\}$ is a set of coordinates of all the solute particles, and the integration is over all coordinates consistent with the volume $\mathcal{V}$. The potential energy of the system when the solute particles are at the coordinates $\{N\}$ in the solvent, relative to the widely separated solute particles in the solvent as zero, is $W(\{N\})$. This potential energy involves an average over the coordinates of the solvent molecules and the internal coordinates of the solute molecules so it is a temperature dependent potential of average force. The application of this equation is illustrated in Sec. 5.

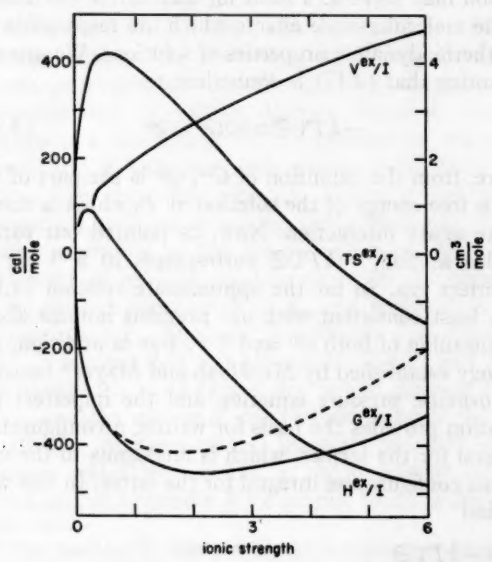

FIG. 2. Excess functions for aqueous NaCl solutions at 25°. The ordinate scale for V^{ex} is on the right, the others are on the left. The broken curve is $-2RT\lambda\mathfrak{S}/\kappa^3$, calculated by (B.19).

5. EXPERIMENTAL EXCESS FUNCTIONS FOR SOLUTIONS OF A SINGLE ELECTROLYTE

This section is intended only to illustrate the appearance of the excess function data and to suggest the relevancy of these data to any qualitative discussion of the structure of electrolyte solutions. It is felt that this is important because, owing to the complexity of rigorous approaches to the calculation of the equilibrium properties of electrolyte solutions, we shall have to rely heavily on more qualitative methods for some time to come.

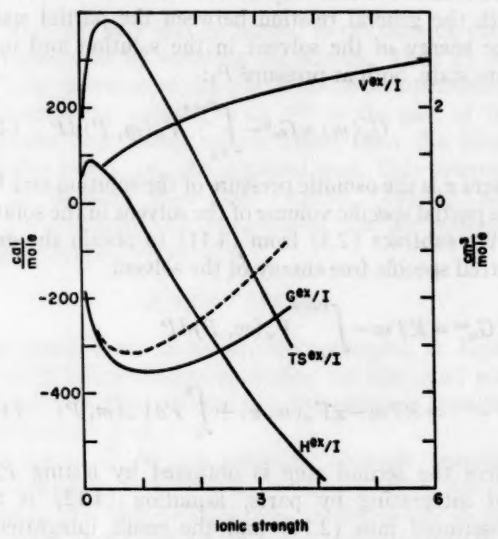

FIG. 3. Excess functions for aqueous NaI solutions at 25°. The ordinate scale for V^{ex}/I is on the right, the others are on the left. The broken curve is $-2RT\lambda\mathfrak{S}/\kappa^3$, calculated by (B.19).

Complete sets of excess functions for several typical systems are given in Figs. 1–4 to illustrate the characteristic features, and the excess entropy curves are assembled in Fig. 5 for all the systems for which they have been calculated. The excess functions divided by I, rather than the excess functions themselves, are plotted as a convenience in scaling the figures. These graphs differ significantly from the more familiar graphs of excess functions for symmetrical solutions vs mole fraction in that Bakhuis-Roozeboom constructions[3] are not possible on the present graphs. This is the price we pay for using the molal concentration scale. However, with Eqs. (2.13) and (2.14) in mind, it it possible to visualize the course of the partial function curves as we examine these graphs.

It is clear that the G^{ex}/I curves are similar in shape to the more familiar graphs of $\gamma_\pm$ or log $\gamma_\pm$ vs I, and in fact this similarity even extends to the order of displacement of the curves as in the series LiCl, NaCl, KCl, RbCl, CsCl; or NaCl, NaBr, NaI. Therefore, the rather reasonable discussions, of which the one by Diamond[19] is a recent example, which have been devoted to the interpretation of these shifts are directly applicable to the G^{ex}/I curves. It must be emphasized that this is fortuitous, as may be illustrated by the following example.

Diamond[19] has suggested that "localized hydrolysis" is responsible for the order of the $\gamma_\pm$ curves of the alkali halides. It is proposed that a water molecule immediately between two ions of opposite charge becomes strongly polarized, the more so the smaller the ions and the higher their charges, and this may lead to incipient dissociation of the water molecule:

$$M^+HO^-\cdots H^+X^-.$$

Thus, two such ions that are near to each other become hydrolyzed by a cooperative effect, even when each has a negligible tendency to hydrolysis when isolated from other ions in the solvent. It is argued that this effect tends to reduce the partial free energy of the solute. However, it has not been explicitly recognized that a process such as this, which nearly dissociates a water molecule, also tends to lower the partial free

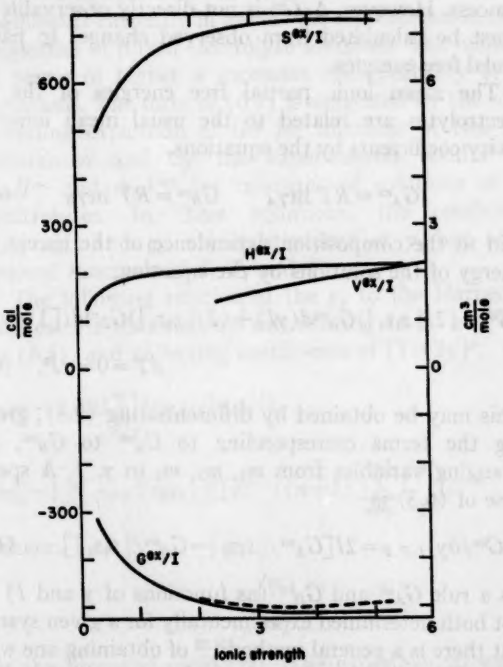

FIG. 4. Excess functions for aqueous $BaCl_2$ solutions at 25°. The ordinate scale for V^{ex}/I is on the right, the others are on the left. The broken curve is $-2RT\lambda\mathfrak{S}/\kappa^3$, calculated by (B.19).

[19] R. M. Diamond, J. Am. Chem. Soc. **80**, 4808 (1958).

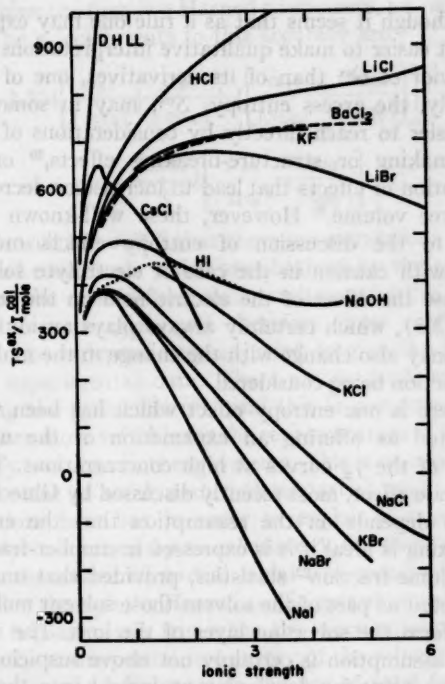

FIG. 5. Excess entropies of several aqueous electrolyte solutions at 25°. These are based upon activity and osmotic coefficients tabulated by Robinson and Stokes[13] and enthalpy data tabulated by Harned and Owen[18] or National Bureau of Standards Circ. 500 ("Selected values of chemical thermodynamic properties", by F. R. Rossini, D. D. Wagman, W. H. Evans, S. Levine, and I. Jaffe.)

energy of the solvent. On the other hand, we cannot have separate explanations for the concentration dependence of both G_w^{ex} and $G_\pm^{ex}$ because they are not independent:

$$dG_w^{ex}/dm + m dG_\pm^{ex}/dm = 0, \quad dT = dP = d\mathbf{x} = 0$$

and in fact, an effect which tends to increase G_w^{ex} tends to decrease $G_\pm^{ex}$.

We suggest that a better way to proceed toward the objective of a qualitative interpretation of the observations in terms of molecular structure is to look at the effect of the interaction in question on the integral of Eq. (4.19). In the case of an example cited, "localized hydrolysis" reduces (more negative) the potential of the interaction of a positive and a negative ion when they are one water molecule apart and does not otherwise affect the potential, $W(\{N\})$. Therefore, for any configuration, $\{N\}$, that corresponds to having some cations one water molecule distant from anions, this effect makes a negative contribution to $W(\{N\})$, a positive contribution to the configuration integral, and finally a negative contribution to G^{ex}. So, we conclude that localized hydrolysis tends to lower G^{ex}. Now, in order to determine the sign of its effect on $\gamma_\pm$ we must determine the concentration dependence of its effect on the configuration integral. There is no argument corresponding to this step in the paper cited.[19]

Although it seems that as a rule one may expect to find it easier to make qualitative interpretations of the behavior of G^{ex} than of its derivatives, one of these, namely, the excess entropy, S^{ex}, may in some cases be easier to reach directly by considerations of structure-making or structure-breaking effects,[20] or consideration of effects that lead to increase or decrease of the free volume.[21] However, these well-known shortcuts to the discussion of entropy effects must be used with caution in the case of electrolyte solutions because the effect of the electric field on the solvent, Eq. (3.5), which certainly always plays an important role, may also change with the change in the molecular interaction being considered.

There is one entropy effect which has been widely accepted as offering an explanation of the upward trend of the $\gamma_\pm$ curves at high concentrations. This is the scale effect, most recently discussed by Glueckauf,[22] which depends on the assumption that the entropy of mixing is ideal if it is expressed in number-fraction[23] or volume-fraction[22] statistics, provided that one does not count as part of the solvent those solvent molecules that form the solvation layer of the ions. The underlying assumption is certainly not above suspicion as a starting point for developing an insight into the equilibrium behavior of electrolyte solutions, but the present criticism of this approach is leveled in the same empirical spirit as that in which the scale correction itself has been offered. That is, that a minimum expectation on the basis of this theory would be that the order of increasing upward curvature of the $\gamma_\pm$ curves is the same as the order of increasing downward curvature of the S^{ex} curves. However, a typical sequence of $\gamma_\pm$ curves (increasing upward curvature) is KCl, KBr, KI, NaCl, NaOH, NaBr, NaI, LiCl, LiBr, HCl; while the corresponding series of S^{ex} curves (increasing downward curvature) is HCl, LiCl, LiBr, NaOH, KCl, NaCl, KBr, NaBr, NaI. Only the anion dependence seems to conform to the requirement of the scale factor effect. In fact, the cation dependence is more important because the cations are supposed to be more highly hydrated, so these observations seem to challenge the revelance of the scale factor effect.

An equivalent way of stating this criticism is to point out that the Stokes and Robinson[23] and Glueckauf[22] theories assume that H^{ex} conforms to the Debye-Hückel limiting law, but in fact the deviations of H^{ex} are as large and characteristic as those of G^{ex} or TS^{ex}.

6. EXCESS FUNCTIONS FOR MIXED ELECTROLYTE SOLUTIONS

The use of total excess functions for the representation of the properties of mixed electrolyte solutions offers two advantages over the use of partial molal quantities for this purpose which find no parallel in the preceding discussions of simpler systems. These advantages will be pointed out in the course of the following development.

We consider here only the simple case of a solution containing electrolyte A (ions 1 and 3) and electrolyte B (ions 2 and 3). For composition variables, we choose the total ionic strength of the solution, I, and the mixing fraction y, defined as the fraction of the ionic strength contributed by ions from electrolyte A. The excess free energy of the solution may be expressed as

$$G^{ex}(y, I) = \Delta_m G^{ex}(y, I) + yG^{ex}(1, I) + [1-y]G^{ex}(0, I) \tag{6.1}$$

where $G^{ex}(1, I)$ applies to a solution of pure A and $G^{ex}(0, I)$ applies to a solution of pure B. Each term of the equation pertains to a solution of the same ionic strength, temperature, and pressure, although the last two variables are not exhibited. The quantity, $\Delta_m G^{ex}$, is clearly the increase in excess free energy on forming the mixture from the component solutions at the same I, T, and P and is a measure of the change in molecular interactions in this process. By appropriate differentiation of (6.1) we may obtain expressions for the corresponding enthalpy and volume changes, $\Delta_m H^{ex}$ and $\Delta_m V^{ex}$, which are the directly observable increases in enthalpy and volume, respectively, in this same process. However, $\Delta_m G^{ex}$ is not directly observable but must be calculated from observed changes in partial molal free energies.

The mean ionic partial free energies of the two electrolytes are related to the usual mean ionic activity coefficients by the equations,

$$G_A^{ex} = RT \ln \gamma_A \qquad G_B^{ex} = RT \ln \gamma_B \tag{6.2}$$

and to the composition dependence of the excess free energy of the solutions by the equation,

$$dG^{ex} = (2/|z_1 z_3|) G_A^{ex} d(yI) + (2/|z_2 z_3|) G_B^{ex} d([1-y]I), \qquad dT = 0 = dP. \tag{6.3}$$

This may be obtained by differentiating (2.8), grouping the terms corresponding to G_A^{ex} to G_B^{ex}, and changing variables from m_1, m_2, m_3 to y, I. A special case of (6.3) is

$$(\partial G^{ex}/\partial y)_{I,T,P} = 2I[G_A^{ex}/|z_1 z_3| - G_B^{ex}/|z_2 z_3|]. \tag{6.4}$$

As a rule G_A^{ex} and G_B^{ex} (as functions of y and I) are not both determined experimentally for a given system, but there is a general method[24,25] of obtaining one when the other is known. If both are known we may calculate $\Delta_m G^{ex}$ by the following equation, obtained by

[20] H. Frank and M. Evans, J. Chem. Phys. **13**, 504 (1945).
[21] H. Frank, J. Chem. Phys. **13**, 478, 493 (1945).
[22] E. Glueckauf, Trans. Faraday Soc. **51**, 1235 (1955); **53**, 305 (1957).
[23] R. H. Stokes and R. Robinson, J. Am. Chem. Soc. **70**, 1870 (1948); Trans. Faraday Soc. **53**, 301 (1957).
[24] E. Glueckauf, H. McKay, and A. R. Matheson, Trans. Faraday Soc. **47**, 428 (1951).
[25] H. A. C. McKay, Nature **169**, 464 (1952).

integrating (6.4) between the limits 0, y and 0, 1 and applying Eq. (6.1),

$$\Delta_m G^{ex}(y,I)/2I=\int_0^y [G_A{}^{ex}/|z_1z_3|-G_B{}^{ex}/|z_2z_3|]dy$$

$$-y\int_0^1 [G_A{}^{ex}/|z_1z_3|-G_B{}^{ex}/|z_2z_3|]dy \quad (6.5)$$

where I, T, and P are constant in both integrations. This equation is perfectly general for the system being discussed, but for comparison with other methods of treating this system it is convenient to make some assumptions about the *form* of the y dependence of $G_A{}^{ex}$, $G_B{}^{ex}$, and $\Delta_m G^{ex}$.

We assume

$$G_A{}^{ex}(y,I)-G_A{}^{ex}(1,I)=-2.30RT\sum\alpha_{An}I^n[1-y]^n,$$

$$G_B{}^{ex}(y,I)-G_B{}^{ex}(0,I)=-2.303RT\sum\alpha_{Bn}I^n y^n,$$

$$n=1,2,\cdots \quad (6.6)$$

$$\Delta_m G^{ex}(y,I)=I^2RTy[1-y]\sum g_p[1-2y]^p,$$

$$p=0,1,2,\cdots. \quad (6.7)$$

If the terms for $n>1$ are omitted, (6.6) reduces to the original form of Harned's rule (Harned and Owen,[12] Eqs. (14-4-3) and (14-4-4)). The inclusion of terms for $n=2$ is equivalent to the definition of the Harned coefficients currently in use for the representation of the properties of mixed electrolyte solutions. The inclusion of terms of higher n increases the generality of the equations. The form of (6.7) is suggested by the corresponding expansion of G^{ex} for mixtures of two pure substances and by the experimental results[26] for $\Delta_m H^{ex}$ and $\Delta_m V^{ex}$ for mixtures of solutions of 1-1 electrolytes. In these equations, the coefficients, α_{An}, α_{Bn}, and g_p, are independent of y, but are in general functions of I, T, and P.

The following relation of the g_p to the Harned coefficients is obtained by substituting (6.6) and (6.7) in (6.5), and collecting coefficients of $[1-2y]^p$.

$$g_p=-2.303\sum_{n>p}\{(\alpha_{An}/|z_1z_3|)$$

$$+[-1]^p[\alpha_{Bn}/|z_2z_3|]\}[I^{n-1}/(n+1)]\sum_{m=p}^{n-1}\binom{m}{p}2^{1-m} \quad (6.8)$$

where

$$\binom{m}{p}$$

is the binomial coefficient. The experimental work in the current literature is only accurate enough to determine the first two Harned coefficients, i.e., α_{A1} and α_{A2}. The g_p coefficients to this accuracy are

$$g_0=-2.303\left[\frac{\alpha_{A1}}{|z_1z_3|}+\frac{\alpha_{B1}}{|z_2z_3|}+I\left[\frac{\alpha_{A2}}{|z_1z_3|}+\frac{\alpha_{B2}}{|z_2z_3|}\right]\right] \quad (6.9)$$

$$g_1=-\frac{2.303}{3}I\left[\frac{\alpha_{A2}}{|z_1z_3|}-\frac{\alpha_{B2}}{|z_2z_3|}\right]. \quad (6.10)$$

It is well known[24,25] that there are restrictions on the Harned coefficients which are obtained by the application of the cross-differentiation relations to the partial molal free energies, and therefore these coefficients cannot be independently adjusted to give the best fit with experimental data. There are no such relations among the g_p coefficients, and this is one reason why they are more suitable for the representation of the free energy relations in these systems. This is an advantage in the use of total, rather than partial molal, excess functions here but in order to exploit it most completely it is necessary to calculate $\Delta_m G^{ex}$ more directly from the measured partial molal free energy than the relation through the Harned coefficients obtained above. This is particularly true when the measurements relate directly to the partial free energy of the solvent.

The second advantage in the use of total functions here is most simply illustrated by considering a mixture of two 1-1 electrolytes with a common ion in a concentration range where Harned's rule is a good approximation. Then we have, to this approximation,

$$g_0=-2.303[\alpha_{A1}+\alpha_{B1}], \qquad g_p=0 \quad \text{for} \quad p>0.$$

It is also true in this case that the difference in partial excess free energy of solvent in the end solutions is given by

$$G_w{}^{ex}(1,I)-G_w{}^{ex}(0,I)=2.303RTI^2[\alpha_{A1}-\alpha_{B1}].$$

Then the sum of Harned coefficients is a measure of interactions characterizing the mixture but the difference in Harned coefficients merely reflects a difference in properties of the end solutions.

In general, the individual Harned coefficients include a measure of the difference in properties of the end solutions and must be combined according to (6.8) to obtain quantities that characterize the changes in molecular interaction that occur when the mixture is formed from the end solutions. Therefore, it is advantageous to formulate the thermodynamic properties of these systems in terms of total excess functions if the objective is to represent and correlate these properties of mixed electrolyte solutions which cannot be deduced by thermodynamic methods from measurements on the end solutions alone.

Some of the experimental results for mixed electrolyte solutions have been expressed in terms of total excess functions in contributions by Young[26] and McKay[27] and in a recent paper by the present author.

[26] T. F. Young and M. B. Smith, J. Phys. Chem. **58**, 716 (1954); T. F. Young, Y. C. Wu, and A. A. Krawetz, Discussions Faraday Soc. **24**, 37 (1957).

[27] H. A. C. McKay, Discussions Faraday Soc. **24**, 76 (1957).

APPENDIX A
DICTIONARY OF NOMENCLATURE

This paper	Description	Harned and Owen
m_s	molality (moles per kg of solvent) of sth solute species (ion or molecule)	m_s
m	$\sum m_s$	νm [a,b]
I	molal ionic strength, $\frac{1}{2}\sum m_s z_s^2$	μ
x_s	m_s/m, solute fraction	ν_+/ν or ν_-/ν [a]
γ_s	practical activity coefficient of species s	γ_+ or γ_-
ϕ	practical osmotic coefficient	ϕ
$\gamma_\pm$	$\prod \gamma_s^{x_s}$, mean solute activity coefficient	$\gamma_\pm$ [a]
G_w	partial specific (per kg) Gibbs free energy of solvent	$1000\bar{F}_1 M_1$
μ_s	partial molal Gibbs free energy of solute species s	$\bar{F}_s$
$G_\pm$	$\sum x_s \mu_s$, mean partial molal Gibbs free energy of solutes	$\bar{F}_2/\nu$ [a]
H^{ex}	excess enthalpy	$m\phi_L = -m\Delta H_D$ [a,b]
H_s^{ex}	excess partial molal enthalpy of solute species s	$\bar{L}_s$
$H_\pm$	$\sum H_s x_s$	$\bar{L}_2/\nu$ [a]
V^{ex}	excess volume	$m(\phi_v - \bar{V}_2^0)$ [a,b]
V_s^{ex}	excess partial molal volume of solute species s	$\bar{V}_s - \bar{V}_s^0$
$V_\pm^{ex}$	$\sum x_s V_s^{ex}$	$(\bar{V}_2 - \bar{V}_2^0)/\nu$ [a]

[a] This correspondence exists only if the solution has exactly one electrolytic solute.
[b] This m in the Harned and Owen nomenclature is the molality of *electrolyte*. If we represent it by M, then for a solution of a single electrolyte, $M = m/\nu$, where m is the total molality of solute ions as used in this paper.

APPENDIX B

We consider here the evaluation of the right-hand side of Eq. (4.16) for the case of aqueous electrolyte solutions. We abbreviate the three terms on the right-hand side of this equation as R_1, R_2 and R_3, reading from left to right. A logical procedure would be to expand $V(m, P)$ in a Taylor series in m and P (or $m^{\frac{1}{2}}$ and P) around $m=0$, $P=0$. This may be convenient at low m,[28] but it is clear from the work of R. E. Gibson[29–31] (reviewed in Harned and Owen,[12] Sec. 8.7) that it requires many terms of such a series to represent the pressure dependence of $V(m, P)$ in an adequate way.

A more satisfactory procedure for $m>1$ molal is to use the modification of the Tait equation that has been proposed by Gibson. In our nomenclature this is

$$V(m, P) = V(m, 0) + \tilde{C} \ln[(B+P_e)/(B+P_e+P)] - (m/\nu) P v_c \beta_c, \quad \text{(B.1)}$$

where $2.303\tilde{C}/V(0, 0) = C/V(0, 0)$, a parameter which is independent of temperature and nearly independent of the composition of the liquid (Harned and Owen,[12] Table 8-7-2) (for water it is 0.3150); B is a characteristic pressure which is a function of temperature alone for a given solvent (for water at 25° it is 2996 bars); v_c is the molar volume of the pure crystalline solute at $P=0$; β_c is the compressibility of the pure crystalline solute; P_e is a characteristic pressure which depends on the composition of the solution and on T;

Gibson found[31] that for aqueous solutions of 1-1 electrolytes,

$$B + P_e = mL/\nu V^2(m, 0) + BV^2(0, 0)/V^2(m, 0), \quad \text{(B.2)}$$

where L is a parameter which is characteristic of the solute. For the chloride, bromide, and iodide of lithium, $L = 318\, l^2$ bar/kg mole, while for these same salts of Na and K, and also for the bromide of Cs, $L = 468\, l^2$ bar/kg mole. These coefficients have been obtained from Fig. 9 of footnote reference 31, except for the value for LiI which has been calculated from a similar figure in footnote reference 30.

For some other salts, including some of the higher charge type, and for calculations of higher accuracy, P_e may be obtained from graphs given by Gibson in the articles cited. These are mostly based on measurements of $V(m, 1000 \text{ bars}) - V(m, 1 \text{ bar})$, but in those cases

[28] J. Poirier, J. Chem. Phys. **21**, 965, 972 (1953).
[29] R. E. Gibson, J. Am. Chem. Soc. **56**, 4 (1934).
[30] R. E. Gibson, J. Am. Chem. Soc. **57**, 284 (1935).
[31] R. E. Gibson, Sci. Monthly **46**, 103 (1938).

in which verification has been attempted, Eq. (B.1) is found to give the pressure dependence of $V(m, P)$ within the experimental error (see Harned and Owen,[12] Table 8.7–4).

We regard Eq. (B.1) as a useful empirical representation of the pressure dependence of $V(m, P)$, which may be used together with experimental data for $V(m, 0)$ in evaluating the right-hand side of Eq. (4.16). It has been found to be convenient to use an empirical representation of the concentration dependence of $V(m, 0)$ based on Masson's law for the apparent molal volume e.g., Harned and Owen,[12] Eq. (9–8–1) and Table 8–9–2.

We also need the following functions which may be calculated from (B.1) by standard thermodynamic methods:

$$\partial V(m, P)/\partial P = -\bar{C}/(B+P_e+P) - mv_c\beta_c/\nu \quad \text{(B.3)}$$

$$V_w(m, P) = V_w(m, 0) + \bar{C}\ln[(B+P_e)/(B+P_e+P)] - \bar{C}m[\partial P_e/\partial m][(B+P_e)^{-1} - (B+P_e+P)^{-1}] \quad \text{(B.4)}$$

$$\partial V_w(m, P)/\partial P = \bar{C}/(B+P_e+P) - \bar{C}m[\partial P_e/\partial m]/[B+P_e+P]^2. \quad \text{(B.5)}$$

Finally, we need $\pi(m)$, the osmotic pressure as a function of m. By combining (2.2′) and (4.11) we obtain,

$$mRT\phi = \int_{P_0}^{P_0+\pi} V_w(m, P)dP. \quad \text{(B.6)}$$

Now we let $P_0 \to 0$, combine (B.6) with (B.4), and perform the integration to obtain

$$mRT\phi = \pi V_w(m, 0) + \bar{C}(B+P_E+\pi)\ln[(B+P_e)/(B+P_e+\pi)] + \bar{C}\pi + \bar{C}m[\partial P_e/\partial m]\{\ln[(B+P_e+\pi)/(B+P_e)] - [\pi/(B+P_e)]\} \quad \text{(B.7)}$$

We note that for $\pi < B+P_e$ there is a term in Eq. (B.7) which cancels the first-order term in the series expansion of each of the logarithmic functions. A similar situation arises again later in this development, and therefore it is convenient to define an incomplete logarithmic function as follows:

$$L_p(x) = \ln(1+x) + \sum_{1\le n<p}(-x)^n/n = -\sum_{n\ge p}(-x)^n/n \quad \text{(B.8)}$$

Then we may rearrange (B.7) to read

$$\pi = mRT\phi/[V_w(m, 0) + \delta(m, \pi)]; \quad \text{(B.9)}$$

where

$$\delta(m, \pi)/\bar{C} = \sum_{n\ge 1}\frac{\{-\pi/[B+P_e]\}^n}{n[n+1]} + (m/\pi)(\partial P_e/\partial m)L_2[\pi/(B+P_e)]. \quad \text{(B.10)}$$

The osmotic pressure may readily be calculated from (B.9) and (B.10) by successive approximations. If experimental values of ϕ, $V(m, 0)$ and P_e are used, then the only source of error in the calculated π is the assumption that Eq. (B.1) correctly represents the pressure dependence of $V(m, P)$.

Equations (B.1) and (B.9) enable us to evaluate R_1. Now we turn to the evaluation of R_3. We substitute (B.5) in the expression for R_3 and obtain

$$R_3 = (\bar{C}/RT)\int_0^m \left\{[B+P_e]L_2[\pi/(B+P_e)] - m\frac{\partial P_e}{\partial m}\left[\frac{\pi}{B+P_e} - \frac{\pi}{B+P_e+\pi} + L_2\left(\frac{\pi}{B+P_e}\right)\right]\right\} d(1/m). \quad \text{(B.11)}$$

Now we evaluate R_2 with the aid of (B.1) and combine the resulting expression with (B.11) to obtain

$$RT(R_2+R_3) = -\bar{C}\int_0^m \left\{(\pi/m)\frac{\partial(\pi+P_e)/\partial m}{B+P_e+\pi} + \tfrac{1}{2}[\pi/m]^2(B+P_e)^{-1} + \frac{B+P_e}{m^2}L_3\left(\frac{\pi}{B+P_e}\right) + m^{-1}\frac{\partial P_e}{\partial m}\left[-\frac{\pi}{B+P_e} + \frac{\pi^2}{[B+P_e]^2} - L_3\left(\frac{\pi}{B+P_e}\right)\right] + (\pi/\bar{C}v)(\partial\pi/\partial m)v_c\beta_c\right\} dm. \quad \text{(B.12)}$$

This result may be simplified by noting the following identities:

$$(\pi/m)\left[\frac{\partial(\pi+P_e)/\partial m}{B+P_e+\pi} - \frac{\partial P_e/\partial m}{B+P_e}\right] = \frac{\partial}{\partial m}\left[\frac{\pi}{m}\ln\frac{B+P_e+\pi}{B+P_e}\right] - \frac{\partial(\pi/m)}{\partial m}\left[\frac{\pi}{B+P_e} - \frac{\pi^2}{2(B+P_e)^2} + L_3\left(\frac{\pi}{B+P_e}\right)\right] \quad \text{(B.13)}$$

$$(1/m)\frac{\partial P}{\partial m}\frac{\pi^2}{(B+P_e)^2} + \frac{\partial}{\partial m}\left[\frac{\pi^2}{m[B+P_e]}\right] = \frac{1}{(B+P_e)}\frac{\partial(\pi^2/m)}{\partial m} \quad \text{(B.14)}$$

$$[\pi/m]^2 + 2\pi\frac{\partial(\pi/m)}{\partial m} = \frac{\partial(\pi^2/m)}{\partial m} \quad \text{(B.15)}$$

TABLE B.I Terms on the right of Eq. (4.16) for $6M$ aqueous solutions of several electrolytes at 25°.

Solute	LiCl	NaCl	CsCl	NaI
$-R_1$	0.097	0.110	0.224	0.193
$-R_2-R_3$	0.016	0.008	0.005	0.012
$-R_1-R_2-R_3$	0.114	0.118	0.230	0.205
$\ln[V(m,0)/V(0,0)]$	0.113	0.120	0.234	0.205

Then we obtain

$$RT(R_2+R_3)=-\bar{C}[\pi/m]\ln\left(\frac{B+P_e+\pi}{B+P_e}\right)+\frac{\bar{C}\pi^2}{2m}(B+P_e)^{-1}-(2\nu)^{-1}\pi^2 v_e\beta_e-\bar{C}\int_0^m\left\{\frac{\pi^2}{2(B+P_e)^2}\frac{\partial(\pi/m)}{\partial m}+\left[\frac{B+P_e}{m^2}-m^{-1}\frac{\partial P_e}{\partial m}-\frac{\partial(\pi/m)}{\partial m}\right]L_3\left(\frac{\pi}{B+P_e}\right)\right\}dm \quad \text{(B.16)}$$

A rough numerical analysis indicates that for $m\leq 12$ molal the value of R_2+R_3 is affected by less than 1% if the unevaluated integral in (B.16) is omitted. This is an absolute error of less than 10^{-4} and will usually be small compared to the experimental error in G^{ex}/mRT. Therefore, we neglect the unevaluated integral and obtain

$$\frac{\mathfrak{S}}{c}=-(G^{ex}/mRT)+\ln[V(0,0)/V(m,\pi)]+\frac{\bar{C}}{RT}\left[\frac{\pi}{m}\ln\left(\frac{B+P_e}{B+P_e+\pi}\right)+\frac{\pi^2}{2m}\frac{1}{B+P_e}\right]-\frac{\pi^2}{2\nu RT}v_e\beta_e+\cdots. \quad \text{(B.17)}$$

At the expense of making a somewhat larger error of the order of

$$\bar{C}\pi^3/4mRT(B+P_e)^2<10^{-3} \quad \text{for} \quad m\leq 12 \quad \text{molal},$$

(B.17) may be replaced by the following much simpler form:

$$\frac{\mathfrak{S}}{c}=-(G^{ex}/mRT)+\ln[V(0,0)/V(m,\pi)]+(\pi/2mRT)[V(m,\pi)-V(m,0)]+\cdots. \quad \text{(B.18)}$$

It is often convenient to replace c and m by κ and I, respectively, as independent variables. We have

$$I/m=\tfrac{1}{2}\sum x_s z_s^2=\tfrac{1}{2}\kappa^2/\lambda c,$$

where κ is the usual Debye reciprocal ion-atmosphere radius and

$$\lambda=4\pi\epsilon^2/DkT$$

is the usual Coulomb length in the medium of dielectric constant, D. (This is the dielectric constant of the pure solvent at P_0 in the Mayer theory.) Then (B.18) becomes

$$2\mathfrak{S}\lambda/\kappa^3=-(G^{ex}/IRT)+(2/\sum x_s z_s^2)\times\{\ln[V(0,0)/V(m,\pi)]+(\pi/2mRT)[V(m,\pi)-V(m,0)]+\cdots\}. \quad \text{(B.19)}$$

This equation, together with (B.1) and (B.9), has been used to calculate the curves of $2RT\lambda\mathfrak{S}/\kappa^3$ from those of G^{ex}/I in the graphs of Sec. 5. It is found that $R_1+R_2+R_3$ for a given solute is nearly proportional to m. The contributions to this term for several solutions are listed in Table B.I. The entries in the last row of this table show that the pressure dependence of $V(m, P)$ makes a much smaller contribution to the right-hand side of Eq. 4.16 than the concentration dependence of $V(m, P)$.

ACKNOWLEDGMENT

Part of the work reported here was done while the author was at the Free University of Brussels in the Department of Professor I. Prigogine. The author is also grateful to the John Simon Guggenheim Memorial Foundation for financial assistance during this period.

Mass Spectrometric Investigation of the Sublimation of Molybdenum Dioxide*

R. P. BURNS, G. DEMARIA,† J. DROWART,‡ AND R. T. GRIMLEY

Department of Physics, University of Chicago, Chicago, Illinois

(Received November 30, 1959)

A mass spectrometric investigation of the vapor in thermodynamic equilibrium with powdered molybdenum dioxide has shown the vapor phase to consist, in decreasing order of importance, of the species MoO_3, $(MoO_3)_2$, MoO_2, and $(MoO_3)_3$. The heats, entropies, and free energies of reaction have been determined for the reactions ($T=1600°K$):

$\frac{1}{2}x\ MoO_2(s)\rightarrow(MoO_3)_x(g)+\frac{1}{2}x\ Mo(s)$	where $x=1, 2, 3$
$MoO_2(s)\rightarrow MoO_2(g)$	$\Delta H_T=134.4\pm7$ kcal/mole
$2MoO_3(g)\rightarrow(MoO_3)_2(g)$	$\Delta H_T=-110.2\pm8$ kcal/mole
$3MoO_3(g)\rightarrow(MoO_3)_3(g)$	$\Delta H_T=-222.8\pm13$ kcal/mole

For the case $x=1, 2, 3$ the ΔH_T's are 121.8 ± 3, 133.4 ± 7, and 142.6 ± 13 kcal/mole, respectively. Entropies of the gaseous molecules MoO_3, $(MoO_3)_2$, $(MoO_3)_3$, and MoO_2 at $T=1600°K$ are 96.6, 151.0, 201.2, and 85.5 eu, respectively. In addition, the atomization energies ($\Delta H_0°$) for the reaction

$$MoO_x(g)\rightarrow Mo(g)+xO(g)$$

were calculated to be 277.4 ± 7 and 419.7 ± 10 kcal/mole for $x=2$ and 3, respectively.

INTRODUCTION

THE only previously reported study of the vaporization of $MoO_2(s)$ is that of Blackburn, Hoch, and Johnston,[1] who have examined the system employing the Knudsen effusion technique. The conclusion of the previous work is that the vaporization takes place mainly by disproportionation of $MoO_2(s)$ to $MoO_3(g)$ and $Mo(s)$ with the side reaction $MoO_2(s)\rightarrow MoO_2(g)$ accounting for the remainder of the gaseous species.

The present mass spectrometric investigation was undertaken in order to determine the importance of polymers in the vapor over $MoO_2(s)$.

EXPERIMENTAL TECHNIQUE

The general characteristics of the experimental technique have been described previously.[2] In the present work a molybdenum outer cell was used in conjunction with a Morganite recrystallized alumina liner.[3] An alumina lid was used which had an effusion hole 1 mm in diameter. In order to maintain a more uniform thermal distribution in the cell, a molybdenum cover having a 3-mm hole was used over the alumina lid. Temperatures were read from a blackbody hole in the base of the molybdenum cell, using a Leeds and Northrup optical pyrometer which was calibrated against a National Bureau of Standards calibrated lamp.[4]

Two samples of MoO_2 powder were used in this work. The first experiments were conducted with a sample[5] whose x-ray pattern indicated mainly MoO_2 with a possible trace of MoO_3 impurity, while later experiments were conducted with a high-purity sample (98.56% MoO_2).[6]

EXPERIMENTAL RESULTS

As the temperature of the Knudsen cell assembly was increased to about 850°K, the ion $(MoO_3)_3^+$ corresponding to the molecule $(MoO_3)_3$ was observed. Since $MoO_3(s)$ vaporizes as $(MoO_3)_3(g)$ in this temperature range,[7] the peak was attributed to small quantities of MoO_3 impurity.

Sample A was found to contain less MoO_3 impurity than sample B used in earlier work. However, in both cases, the sample was heated in the 800–900°K range until no further trimer could be detected.

The temperature was then increased and the instrument sensitivity obtained by means of a quantitative vaporization of a weighed amount of silver.[2] After the calibration, the temperature was again increased until the vapor species from $MoO_2(s)$ were observed.

The temperature range 1500–1780°K was examined and the most important species found to be MoO_3^+, $(MoO_3)_2^+$, MoO_2^+, and $(MoO_3)_3^+$. In addition, small peaks of $Mo_2O_5^+$, $Mo_2O_4^+$, and $Mo_3O_8^+$ were found.

* Supported in part by the Office of Ordnance Research, U. S. Army, and in part by the National Science Foundation.

† On leave of absence from Instituto di Chimica Fisica, Universitá degli Studi, Rome, Italy.

‡ On leave of absence from Laboratoire de Chemie Physique Moléculaire, Université Libre de Bruxelles, Brussels, Belgium.

[1] P. E. Blackburn, M. Hoch, and H. L. Johnston, J. Phys. Chem. **62**, 769 (1958).

[2] M. G. Inghram and J. Drowart, "Mass spectroscopy applied to high temperature chemistry," appearing in *International Symposium on High Temperature Chemistry at Asilomar, California* (Stanford Research Institute, Palo Alto, California, 1959).

[3] Morganite Incorporated, Long Island City, New York.

[4] National Bureau of Standards Ribbon Filament Lamp Test No. G-18631a (1956).

[5] Sample B, prepared by Dr. Joan Berkowitz, Arthur D. Little Company, Cambridge, Massachusetts.

[6] Sample A, Shattuck Chemical Company, Denver, Colorado.

[7] J. Berkowitz, M. G. Inghram, and W. Chupka, J. Chem. Phys. **26**, 842 (1957).

TABLE I. Partial pressures of $MoO_3(g)$ in equilibrium with $MoO_2(s)$.

Expt.	T°K	P(atm)	Expt.	T°K	P(atm)	Expt.	T°K	P(atm)
A18	1481	1.4×10^{-8}	B12	1640	7.7×10^{-7}	B15	1716	4.1×10^{-6}
A17	1512	3.1×10^{-8}	A4	1647	9.5×10^{-7}	A9	1720	4.4×10^{-6}
A16	1540	6.2×10^{-8}	A3	1652	1.0×10^{-6}	B7	1721	5.1×10^{-6}
B14	1566	1.4×10^{-7}	A12	1657	1.1×10^{-6}	B9	1728	5.8×10^{-6}
A15	1575	1.6×10^{-7}	A11	1675	2.0×10^{-6}	A7	1732	5.4×10^{-6}
B6	1596	3.3×10^{-7}	B2	1679	2.3×10^{-6}	A8	1735	5.9×10^{-6}
B5	1598	2.8×10^{-7}	B1	1681	2.8×10^{-6}	A20	1747	7.9×10^{-6}
A14	1605	3.6×10^{-7}	B3	1683	2.6×10^{-6}	B11	1765	1.0×10^{-5}
A2	1608	4.0×10^{-7}	B4	1687	2.9×10^{-6}	B16	1773	1.1×10^{-5}
A1	1610	3.5×10^{-7}	A10	1696	2.9×10^{-6}	B10	1777	1.4×10^{-5}
B13	1632	6.5×10^{-7}	A5	1702	3.0×10^{-6}			
A13	1636	7.5×10^{-7}	A6	1709	3.0×10^{-6}			

No Al_xO_y species were observed, nor was any reaction between $MoO_2(s)$ or $Mo(s)$ and Al_2O_3 apparent.

Approximate appearance potentials were determined using the linear extrapolation method, using mercury as the standard for the energy scale. The corrected appearance potentials were MoO_3^+, 12.0±0.6 ev; $(MoO_3)_2^+$, 12.1±0.6 ev; $(MoO_3)_3^+$, 12.0±1.0 ev, and MoO_2^+, 9.4±0.6 ev. Ionization efficiency curves indicated that MoO_3^+, $(MoO_3)_2^+$, and $(MoO_3)_3^+$ were all produced by direct ionization of the corresponding neutral molecule. In the case of MoO_2^+, however, a break in the ionization curve (13.5−14 ev) was noted which indicated that at 17 ev slightly less than half the MoO_2^+ peak was the result of ionization of the MoO_2 molecule. Of the possible parent molecules, energetic considerations indicate that MoO_3 is the most likely source of that part of the MoO_2^+ peak which is a fragment, since the electron energy required for fragmentation in the case of the dimer and trimer is well in excess of bombardment energies employed (17 ev). Thus, the intensity of the MoO_3^+ ion was increased by approximately 6% to correct for fragmentation loss. Examination of the ionization efficiency curve of $Mo_2O_6^+$ revealed thresholds at approximately 10 and 14.5 ev, whereas for $Mo_3O_8^+$ a similar double threshold was found with values of 12.2 and 14.5 ev. In both cases the higher valued threshold resulted from the onset of a fragmentation process whereas the lower threshold appeared to result from a simple ionization process of the parent Mo_2O_6 and Mo_3O_8 molecules. Approximate pressures were calculated to be Mo_2O_6, 1.0×10^{-7} atm and Mo_3O_8, 1.2×10^{-8} atm at 1774°K. The presence of a parent Mo_2O_4 molecule must be considered doubtful, but the upper limit of possible Mo_2O_4 at 1774°K was found to be 2.4×10^{-7} atm.

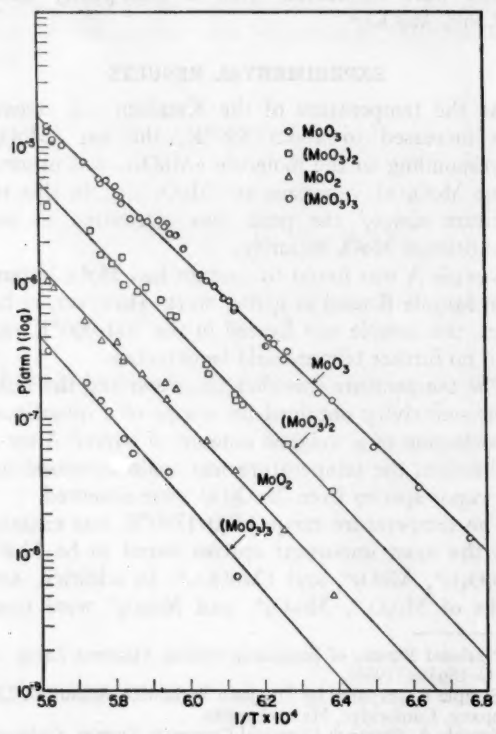

FIG. 1. Partial pressures (atm) of the vapor species over MoO_2 solid as a function of $1/T\times10^4$ deg K^{-1}.

After repeated cyclings of the sample to higher temperatures (ca. 1775°K), it was noted that the partial pressures of the vapor species began to decrease with time. This effect was attributed to a molybdenum metal coating on the sample surface which caused a diffusion-limited vaporization process. In this study all data were taken before the onset of the reduced activity. It is interesting to note that data obtained from the 98.56% pure sample (A) and the slightly less pure sample (B) agree well within the error of the pressure calibrations. (See Table I and Fig. 1).

The relative ionization cross sections used were Ag=34.8, MoO_2=59.1, MoO_3=62.4, $(MoO_3)_2$=124.8, and $(MoO_3)_3$=187.2.[8] Pressures were calculated by using the above cross sections together with corrections for multiplier efficiency and molecular effects.[2] Partial pressure (atm) data for the vapor species over solid MoO_2 are presented in Tables I and II and in Fig. 1. The capital letters in the first column of Tables I and II

[8] J. W. Otvos and D. P. Stevenson, J. Am. Chem. Soc. 78, 546 (1956).

TABLE II. Partial pressure of species in equilibrium with $MoO_2(s)$.

Expt.	T°K	MoO_3 (atm)	$(MoO_3)_2$ (atm)	MoO_2 (atm)	$(MoO_3)_3$ (atm)
B14	1566	1.4×10^{-7}	2.9×10^{-8}	4.9×10^{-9}	...
B6	1596	3.3×10^{-7}	6.5×10^{-8}	...	...
B5	1598	2.8×10^{-7}	...	1.5×10^{-8}	...
A19	1627	...	1.3×10^{-7}	...	...
B13	1632	6.5×10^{-7}	1.4×10^{-7}	4.1×10^{-8}	6.9×10^{-9}
A3	1652	1.0×10^{-6}	2.3×10^{-7}	6.9×10^{-8}	...
A11	1675	2.0×10^{-6}	5.7×10^{-7}	1.6×10^{-7}	...
B2	1679	2.3×10^{-6}	5.8×10^{-7}	...	...
B3	1683	2.6×10^{-6}	...	1.6×10^{-7}	3.8×10^{-8}
B4	1687	2.9×10^{-6}	7.5×10^{-7}	...	...
A10	1696	2.9×10^{-6}	9.4×10^{-7}	...	...
A5	1702	3.0×10^{-6}	8.7×10^{-7}	2.1×10^{-7}	...
A6	1709	3.0×10^{-6}	...	...	5.6×10^{-8}
B15	1716	4.1×10^{-6}	1.3×10^{-6}	2.7×10^{-7}	7.1×10^{-8}
B7	1721	5.1×10^{-6}	...	3.6×10^{-7}	...
B8	1725	...	1.4×10^{-6}	...	...
B9	1728	5.8×10^{-6}	...	...	1.1×10^{-7}
A7	1732	5.4×10^{-6}	1.6×10^{-6}	3.7×10^{-7}	1.4×10^{-7}
A20	1747	7.9×10^{-6}	...	5.2×10^{-7}	1.9×10^{-7}
B16	1773	1.1×10^{-5}	...	9.2×10^{-7}	...
B10	1777	1.4×10^{-5}	3.7×10^{-6}	1.0×10^{-6}	3.1×10^{-7}

refer to the sample of MoO_2 used, while the numbers refer to the order in which the data points were taken.

DISCUSSION

The present work confirms the estimate of Kelley[9] and the findings of Blackburn *et al.*[1] regarding the importance of the disproportionation reaction in the vaporization of $MoO_2(s)$. On the other hand, it is found that $MoO_2(g)$ is of considerably less importance than concluded by Blackburn *et al.* and also that the $(MoO_3)_2(g)$ molecule is of more importance than their estimate.

Equations for $\log P$ vs $1/T$ are given in Table III and are the result of least squares fits of the data in Tables I and II. The reaction energies ΔH_T, ΔS_T, and $\Delta F_T(T=1600°K)$ calculated from the experimental data are given in Table IV. $\Delta H_0°=123.9$ kcal/mole for reaction I, Table IV, is to be compared with $\Delta H_0°=133.6$ kcal/mole given by Blackburn, *et al.*[1] Also $\Delta H_0°=137.4$ kcal/mole for reaction 3 is to be compared with $\Delta H_0°=129.8$ kcal/mole, and $\Delta H_T=228.8$ kcal/mole for reaction 6 to $\Delta H_0°=220.9$ kcal/mole obtained by the same authors.

The slight discrepancies in some of the reaction enthalpies can be attributed to a combination of one or

TABLE III. Log P vs $1/T$ for the vapor species in equilibrium with $MoO_2(s)$.

$\log P_{MoO_3(g)}$	$=-2.661\times10^4/T+10.130$
$\log P_{(MoO_3)_2(g)}$	$=-2.915\times10^4/T+11.067$
$\log P_{(MoO_3)_3(g)}$	$=-3.117\times10^4/T+11.067$
$\log P_{MoO_2(g)}$	$=-2.936\times10^4/T+10.574$

[9] K. K. Kelley, Climax Molybdenum Bulletin Cdb-2 (1954).

TABLE IV. Summary of experimentally determined reaction enthalpies, entropies, and free energies.

No.	Reaction	$T=1600°K$ ΔH_T kcal/mole	ΔS_T eu	$\Delta F_T°$ kcal/mole
1.	$3/2MoO_2(s)\rightarrow MoO_3(g)+\frac{1}{2}Mo(s)$	121.8±3	46.4	47.6
2.	$3MoO_2(s)\rightarrow(MoO_3)_2(g)+Mo(s)$	133.4±7	50.6	52.4
3.	$MoO_3(s)\rightarrow MoO_2(g)$	134.4±7	48.4	56.9
4.	$9/2MoO_2(s)\rightarrow(MoO_3)_3(g)+3/2Mo(s)$	142.6±13	50.6	61.6
5.	$2MoO_3(g)\rightarrow(MoO_3)_2(g)$	−110.2±8	−42.1	−42.8
6.	$3MoO_3(g)\rightarrow(MoO_3)_3(g)$	−222.8±13	−88.6	−81.1

more of the following causes. Blackburn *et al.* underestimated the contribution of $(MoO_3)_2(g)$ and overestimated the contribution of $MoO_2(g)$ to the total pressure. These authors determined the relative amounts of the gaseous species indirectly by two quantitative vaporizations assuming that $MoO_3(g)$ and $MoO_2(g)$ were the main vapor species and reported the vapor to consist of 22 wt % $MoO_2(g)$ in one experiment and 36 wt % $MoO_2(g)$ in the other. Since the results of quantitative vaporizations are extremely sensitive to the amount of impurity, we prefer to determine the composition of the gas phase mass spectrometrically. Furthermore, S_{298} for $MoO_2(s)$ used by Blackburn *et al.* has been determined by King[10] to be substantially lower than the previously reported value. As was mentioned before, the present work indicated that when measurements were attempted above ~1800°K, a gradual reduction in activity occurred. Since Blackburn *et al.* investigated the temperature range 1800–2000°K, an additional possibility exists that these authors encountered some reduction in activity at the temperatures of their measurements.

The entropies of the gaseous oxides at 1600°K are given in Table V. The values in the first row are calculated from the experimental data, $S_{298}MoO_2(s)=11.06$ eu[10] and $S_T-S_{298}MoO_2(s)=37.1$ eu which was estimated by an extension to high temperatures of the method of Latimer[11] in which the entropy of Mo(s) was combined with an average contribution of O^{--}

TABLE V. Entropies of gaseous molybdenum oxides $T=1600°K$.

	S_T (MoO_3) eu	S_T $(MoO_3)_2$ eu	S_T $(MoO_3)_3$ eu	S_T (MoO_2) eu
This work	96.6	151.0	201.2	85.5
Chandrasekharaiah and Brewer[a]	...	...	...	85.5
DeMaria *et al.*[b]	96.3	...	...	87.4

[a] Footnote 13.
[b] Footnote 14.

[10] E. G. King, J. Am. Chem. Soc. **80**, 1799 (1958).
[11] W. M. Latimer, J. Am. Chem. Soc. **73**, 1480 (1951).

obtained from other XO_2 type compounds[12] (X=Ti, Zr, Mn, Si, Th, or U). The data in the second and third rows are calculated from free energy and enthalpy functions with the data of Chandrasekharaiah and Brewer[13] and DeMaria *et al.*[14] The agreement is seen to be quite good for $MoO_3(g)$ and $MoO_2(g)$. The value $S_{1600}(MoO_3)_3(g)=201.2$ eu is to be compared to $S_{900}(MoO_3)_3(g)=193.1$ eu given by Berkowitz *et al.*[7]

By combining the heat of formation of MoO_2[15,16] with the experimental data and calculated data mentioned in the foregoing the atomization energies $\Delta H_0°$ for the reactions $MoO_2(g)\rightarrow Mo(g)+2O(g)$ and $MoO_3(g)\rightarrow Mo(g)+3O(g)$ are calculated to be 277.4± 7 kcal 419.7±10 kcal/mole, respectively. These values are to be compared to the values 262 and 411 kcal/mole given by DeMaria *et al.*[14] to the values 285 and 410 kcal/mole of Blackburn *et al.*,[1] and to the values 295 and 426 kcal/mole derived from the data of Blackburn *et al.* using the free energy functions mentioned previously.[13,14] Dissociation energies for the molecules Mo_2O_5 and Mo_3O_8 are not given since accurate free energy functions for these molecules are lacking.

[12] K. K. Kelley, U. S. Bureau of Mines Bulletin 476 (1949).
[13] M. S. Chandrasekharaiah and L. Brewer, UCRL-8736 (University of California, Berkeley, California).
[14] G. DeMaria, R. Burns, J. Drowart, and M. G. Inghram, J. Chem. Phys. **32**, 1373 (1960), this issue.
[15] B. A. Staskiewicz, J. R. Tucker, and P. E. Snyder, J. Am. Chem. Soc. **77**, 2987 (1955).
[16] A. D. Mah, J. Phys. Chem. **61**, 1572 (1957).

ACKNOWLEDGMENTS

The authors wish to acknowledge the kindness of the S. W. Shattuck Company, of the Climax Molybdenum Company, and of Dr. Joan Berkowitz, Arthur D. Little Company, for providing the samples used in this work. The help of Miss Anne Plettinger in providing x-ray data is appreciated.

Particular thanks are given to Dr. Mark G. Inghram for his suggestions and interest in this work.

THE JOURNAL OF CHEMICAL PHYSICS VOLUME 32, NUMBER 5 MAY, 1960

Thermodynamic Study of Al_2O_3 Using a Mass Spectrometer*

J. DROWART,† G. DEMARIA,‡ R. P. BURNS, AND M. G. INGHRAM

Department of Physics, The University of Chicago, Chicago, Illinois

(Received November 5, 1959)

The evaporation of alumina under nearly neutral conditions in tungsten and molybdenum Knudsen cells has been investigated by mass spectrometric methods. The atomization energies of the gaseous molecules are $D_0°(AlO)=115\pm5$ kcal/mole; $D_0°(Al_2O)=245\pm7$ kcal/mole; $D_0°(Al_2O_2)=365\pm7$ kcal/mole.

INTRODUCTION

IN a study of the vaporization of alumina under reducing conditions (Al_2O_3-Si) Grube, Schneider, Esch, and Fled[1] concluded that Al_2O is the major aluminum-containing species in the vapor. From a comparative vapor pressure study (in tungsten Knudsen cells) of the aluminum-oxygen system under reducing (Al_2O_3-Al) and under nearly neutral conditions (Al_2O_3) Brewer and Searcy[2] concluded that under reducing conditions Al and Al_2O are the principal vapor species while under neutral conditions AlO and atomic oxygen are the principal vapor components. Cochran[3] confirmed the predominance of Al_2O under reducing conditions. Ackermann and Thorn,[4,5] however, compared the weight loss of alumina-loaded tungsten effusion cells with the amount of alumina evaporated near 2600°K. They concluded that the ratio of tungsten to alumina weight losses might be accounted for by reduction of alumina by tungsten and the vaporization of one or more gaseous aluminum oxides and one or more gaseous tungsten oxides. A similar view has been held by von Wartenberg.[6] On the other hand, Medvedev[7] has calculated that the molecule Al_2O_3 is of major importance in the vapor of aluminum oxide under neutral conditions.

A mass spectrometric analysis[8] of the vapor in thermodynamic equilibrium with Al-Al_2O_3 showed the predominant gaseous species to be Al and Al_2O and gave

* Supported in part by the Office of Ordnance Research, U.S. Army, and in part by the National Science Foundation.
† On leave of absence from Laboratoire de Chimie Physique Moleculaire, Université Libre de Bruxelles, Brussels, Belgium.
‡ On leave of absence from Istituto di Chimica Fisica, Universitá degli Studi, Rome, Italy.
[1] G. Grube, A. Schneider, U. Esch, and M. Fled, Z. anorg. Chem. **260**, 120 (1949).
[2] L. Brewer and A. W. Searcy, J. Am. Chem. Soc. **73**, 5308 (1951).
[3] C. N. Cochran, J. Am. Chem. Soc. **77**, 2190 (1955).
[4] R. J. Ackermann and R. J. Thorn, J. Am. Chem. Soc. **78**, 4169 (1956).
[5] R. J. Ackermann and R. J. Thorn, Proceedings of the 16th International Congress of Pure and Applied Chemistry (Paris, 1957), p. 667.
[6] H. vonWartenberg, Z. anorg. u. allgem. Chem. **269**, 76 (1952)
[7] V. A. Medvedev, Zhur. fiz. Khim. **32**, 1690 (1958).
[8] R. F. Porter, P. Schissel, and M. G. Inghram, J. Chem. Phys. **23**, 399 (1955).

thermodynamic properties for Al_2O in agreement with those obtained by Brewer and Searcy.[2] In a similar mass spectrometric investigation[9] of the vapor effusing from a tungsten cell containing Al_2O_3, i.e., closer to neutral conditions, gaseous Al and Al_2O were again identified. The ratio Al_2O^+/Al^+ changed from about 1 in the Al-Al_2O_3 system to 0.1 in the W-Al_2O_3 system. A search for the AlO molecule was difficult, owing to the background at mass 43. It was established, however, that the ratio of the AlO^+ to Al^+ intensities was smaller than 0.1, indicating that AlO is not the major species under such conditions. On the basis of these results, Brewer[10] has compared the experimentally measured pressure[2] of alumina contained in tungsten cells with the pressure for the elements Al and O calculated from the thermodynamic data for condensed alumina. This discussion showed that the measured pressure[2] is a factor of about 4 higher than that calculated, assuming the vapor to contain only Al and O.

In the present work, the systems W-Al_2O_3 and Mo-Al_2O_3 have been investigated in a mass spectrometer to determine the composition of the vapor under conditions of thermodynamic equilibrium. The results obtained in the W-Al_2O_3 system have been briefly reported earlier.[11]

EXPERIMENTAL ARRANGEMENT

The general characteristics of the experimental technique have already been described.[8] In the present work, molybdenum and tungsten Knudsen cells were used. The effusion hole was usually 1 mm in diameter. The thickness of the walls was usually 3 mm. Four blackbody holes were drilled into the sides of each tungsten and molybdenum cell at 6-mm intervals; and one blackbody hole was drilled in the bottom of each cell. Temperatures were determined using two Leeds and Northrup optical pyrometers, calibrated against a National Bureau of Standards ribbon filament lamp.[12] The temperatures read from the bottom and from the two lower side holes were the same within experimental error. The temperature read from the upper side hole was about 30° lower. The maximum temperature difference within the Knudsen cell was therefore estimated to be less than 50°, the coldest part being the cover. An alumina liner, 2.5 cm high, 1.2 cm in diameter, with a wall thickness of about 1.5 mm, was inserted into the tungsten or into the molybdenum cell. No alumina cover was placed on the top of this liner since the liner was melted purposely during the course of the experiment. The liners of recrystallized alumina, grade Triangle RR, were obtained from Morganite Incorporated.[13] The ratio of σ effusing to vaporizing surfaces was smaller than 0.001 for solid and, at the most, 0.01 for molten Al_2O_3.

EXPERIMENTAL RESULTS

(a) Composition of the Vapor

The observed atomic and molecular ions characteristic of the Al-O system were O^+, O_2^+, Al^+, AlO^+, Al_2O^+, and $Al_2O_2^+$. In addition, using tungsten and molybdenum cells, the ions WO^+, WO_2^+, and WO_3^+, and MoO^+, MoO_2^+, and MoO_3^+ were observed. No other $Al_xO_y^+$ ions were found, the search being made up to mass 600. No $(XO)_n^+$, $(XO_2)_n^+$, or $(XO_3)_n^+$ ions were observed (X=W or Mo, and $n=2, 3$); nor were any molecular ions found that contained simultaneously one or more Al and W or Mo atoms. Upper limits on such species are 1×10^{-5} of the Al^+ intensity at 2500°K.

In order to establish that the observed ions were produced from the corresponding molecules, approximate ionization efficiency curves were measured. The linear extrapolation method was used to obtain these appearance potentials, and the energy scale was calibrated with mercury as a standard. The corrected appearance potentials were 13.6, 6.0, 9.5, 7.7, and 9.9 ev, respectively, for O^+, Al^+, AlO^+, Al_2O^+, and $Al_2O_2^+$. The uncertainty was about ±0.5 ev. The first two appearance potentials agree with the spectroscopic ionization potentials[14] of oxygen and of aluminum. The appearance potential for Al_2O measured here is the same as that obtained by Porter, Schissel, and Inghram.[8] The appearance potential for AlO^+, as well as measured ion intensity ratios for the peaks 40 and 43, shows that the ion $^{43}Ca^+$ (a possible impurity) does not interfere with the measurements. The appearance potentials for O^+, Al^+, AlO^+, Al_2O^+, and $Al_2O_2^+$ indicate that, at low ionizing electron energies, these ions are parent ions produced by simple ionization of the molecules O, Al, AlO, Al_2O, and Al_2O_2, respectively. The ion Al_2^+, which was also observed, was identified by its appearance potential to be mainly a fragment from Al_2O.

(b) Pressure Data

Relative partial pressures were derived from the ion intensities by the relation

$$\frac{P_1}{P_2}=\frac{I_1\times\sigma_2\times(E-A_2)\times S_2\times T_1}{1_2\times\sigma_1\times(E-A_1)\times S_1\times T_2} \quad (1)$$

where P=partial pressure, I=ion intensity; σ=relative cross section[15] at the maximum of the ionization efficiency curve; A=appearance potential in ev; E=energy of ionizing electrons, in ev (in the present experiments this quantity was always less than 15

[9] R. F. Porter and M. G. Inghram, results mentioned by M. G. Inghram, W. A. Chupka, and J. Berkowitz, Mem. soc. roy. sci. Liege, 4e ser. 18, 513 (1957).
[10] L. Brewer (private communication).
[11] G. DeMaria, J. Drowart, and M. G. Inghram, J. Chem. Phys. 30, 318 (1959).
[12] National Bureau of Standards, Ribbon filament lamp test No. G-18631a (1956).
[13] Morganite Incorporated, Long Island City, New York.
[14] C. E. Moore, Natl. Bur. Standards (U.S.) Circ. 467, Vol. III (1958).
[15] J. W. Otvos and D. P. Stevenson, J. Am. Chem. Soc. 78, 546 (1956).

TABLE I. Partial pressures in the system $W+Al_2O_3$.

Expt.	T°K	P_O (atm)	P_{Al} (atm)	P_{AlO} (atm)	P_{Al_2O} (atm)	$P_{Al_2O_2}$ (atm)
1a	2188	1.5×10^{-7}	2.0×10^{-7}	9.6×10^{-9}	7.5×10^{-9}	...
11a	2191	1.6×10^{-7}	2.1×10^{-7}	1.0×10^{-8}	9.4×10^{-9}	...
1c	2213	2.3×10^{-7}	2.9×10^{-7}	1.6×10^{-8}	1.2×10^{-8}	...
12a	2226	2.7×10^{-7}	3.4×10^{-7}	1.5×10^{-8}	1.5×10^{-8}	...
1b	2233	3.0×10^{-7}	4.0×10^{-7}	2.3×10^{-8}	1.6×10^{-8}	...
3a	2240	3.4×10^{-7}	4.3×10^{-7}	1.8×10^{-8}	1.0×10^{-8}	...
2a	2264	4.8×10^{-7}	4.8×10^{-7}	3.5×10^{-8}	2.2×10^{-8}	...
4a	2275	5.6×10^{-7}	7.2×10^{-7}	3.9×10^{-8}	2.4×10^{-8}	...
9a	2325	1.1×10^{-6}	1.4×10^{-6}	9.7×10^{-8}	7.2×10^{-8}	....
9b	2335	1.2×10^{-6}	1.8×10^{-6}	7.6×10^{-8}	5.6×10^{-8}	...
6a	2350	1.5×10^{-6}	2.0×10^{-6}	1.5×10^{-7}	8.3×10^{-8}	...
9c	2390	2.5×10^{-6}	3.3×10^{-6}	1.3×10^{-7}	1.1×10^{-7}	...
10a	2464	6.0×10^{-6}	9.0×10^{-6}	5.6×10^{-7}	5.0×10^{-7}	1.4×10^{-9}
5a	2475	6.8×10^{-6}	1.0×10^{-5}	7.1×10^{-7}	3.4×10^{-7}	3.2×10^{-9}
7a	2470	6.6×10^{-6}	1.0×10^{-5}	1.1×10^{-6}	4.9×10^{-7}	2.3×10^{-9}
8a	2514	1.1×10^{-5}	1.4×10^{-5}	1.2×10^{-6}	5.4×10^{-7}	3.5×10^{-9}
8b	2594	2.5×10^{-5}	3.5×10^{-5}	1.8×10^{-6}	8.9×10^{-7}	6.0×10^{-9}

ev); S=multiplier efficiency,[16] corrected for molecular effects if necessary[17]; and T=absolute temperature.

In order to derive the absolute value of the pressure, calibrations were made using the following independent methods:

(*1*) *Silver calibration.* In each experiment, a known amount of silver (3–5 mg) was vaporized at constant temperature, usually in the range 1300–1350°K. Immediately afterwards the cell temperatures were increased and the intensities of the peaks characteristic of the investigated system were measured. The pressures were then obtained from Eq. (1) and from the relationship

$$p=Z(2\pi mkT)^{\frac{1}{2}} \qquad (2)$$

where Z=number of calibrating atoms effusing per cm^2 per sec, m=molecular weight of vaporizing species, and k=Boltzmann's constant.

(*2*) *O/O_2 calibration.* When possible, the ratio between the O^+ and O_2^+ ion intensities was measured. Since the equilibrium constant for the dissociation of O_2 is known,[18,19] this ratio can be used for determining the absolute pressure of these species. In making the O/O_2 calibration the O^+/O_2^+ ratio must be corrected (using appropriate cross sections,[15] appearance potentials,[20] and secondary electron yields[16,17]) in order to obtain the O/O_2 ratio. From this calibration and from Eq. (1), the pressures of the other vapor species can be calculated.

(*3*) *Quantitative vaporization self-calibration.* Weighed alumina samples (about 10 mg) were completely vaporized from either molybdenum or tungsten cells, and each of the peaks Al^+, AlO^+, Al_2O^+ was measured as a function of time. By using the number of Al atoms in the original sample and the integrated peak intensities the pressure responsible for one unit of aluminum intensity was calculated from Eqs. (1) and (2).

(*4*) *Molybdenum calibration.* In the experiments carried out in molybdenum cells, the intensity profile of the molecular beam[21] allowed one to distinguish between the molybdenum effusing from the inside of the Knudsen cell and the molybdenum vaporizing from the outer surface of the cell. The pressure of Mo was derived from this intensity using one of the foregoing calibrations (e.g., a silver calibration). This derived pressure was then compared with the vapor pressure of Mo calculated from the thermodynamic data,[19] and the agreement served as a further check on the pressure calibration.

In the silver, O/O_2 and Mo calibrations, the relative ionization cross sections enter directly into the calculations and must be estimated for all species. The quantitative vaporization self-calibration has one advantage over these calibrations. Namely, that any uncertainties in the Al pressure resulting from an estimate of relative ionization cross section will be only of second order importance. This is due to the fact that the intensity of all gaseous species of the type Al_xO_y is small. Relative values used for the ionization cross section were O=3.3, O_2=6.6, AlO=18.7, Al_2O=34.1, Al_2O_2=37.4, Ag=34.8, and Mo=52.5.[15] By comparison with U (for which the cross section was measured directly[22]) and with Mo, the relative ionization cross section of W was taken as 50.

Pressure data for the tungsten-Al_2O_3 system are presented in Table I and Fig. 1. In column 1 (also in column 1 of Table II) the number refers to the number of the experiment, while the lower case letter refers to

[16] M. G. Inghram, R. J. Hayden and D. C. Hess, Natl. Bur. Standards (U.S.) Circ. 522, 257 (1953).
[17] H. E. Stanton, W. A. Chupka, and M. G. Inghram, Rev. Sci. Instr. **27**, 109 (1956).
[18] P. Brix and G. Herzberg, Can. J. Phys. **32**, 110 (1954).
[19] D. R. Stull and G. C. Sinke, *Thermodynamic Properties of the Elements* (Am. Chem. Soc., Washington, D.C., 1956).
[20] F. H. Field and J. L. Franklin, *Electron Impact Phenomena* (Academic Press, Inc., New York, 1957).
[21] M. G. Inghram, W. A. Chupka and R. F. Porter, J. Chem. Phys. **23**, 2159 (1955).
[22] G. DeMaria, R. P. Burns, J. Drowart, and M. G. Inghram, J. Chem. Phys. **32**, 1373 (1960), this issue.

the order of each data point within one experiment. Data obtained with effusion holes 1.0 mm and 1.9 mm in diameter are in agreement. After a long series of experiments it was observed that the effusion hole became clogged with liquid alumina. Surface vaporization then occurred from molten alumina for which the vaporizing area was essentially that of the effusion hole, as verified from the intensity profile. The relative and absolute intensities of O^+, Al^+, AlO^+, and Al_2O^+ under these conditions were observed to be about the same as from a Knudsen cell. Both of these experiments indicate that the vaporization coefficients for these species are close to one and, hence, that within a Knudsen cell with a σ of 0.001, equilibrium is certainly established. A further indirect proof is that the values for the dissociation energies of WO_2 and WO_3 obtained in the present work (see next paper[22]) are in agreement with the values obtained for these molecules by Chupka *et al.* from the study of the BeO-W system.[23]

Pressure data for the molybdenum-Al_2O_3 system are presented in Table II and Fig. 2. During the initial part of this measurement the Al pressure was close to that calculated for neutral conditions. After some time and at higher temperatures, some reduction was evident

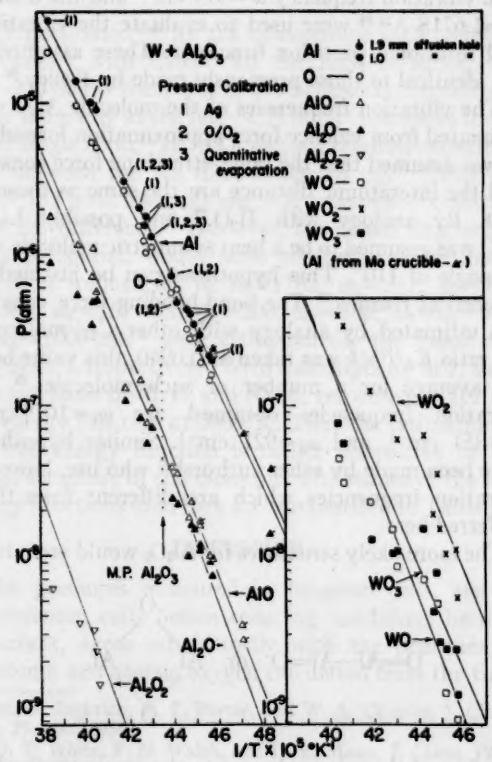

FIG. 1. Pressure data in the W—Al_2O_3 system as a function of $1/T\times10^5°K^{-1}$. The data above and below the melting point of Al_2O_3 are separated by the dotted line labeled M.P. Al_2O_3.

[22] W. A. Chupka, J. Berkowitz, and C. S. Giese, J. Chem. Phys. 30, 827 (1959).

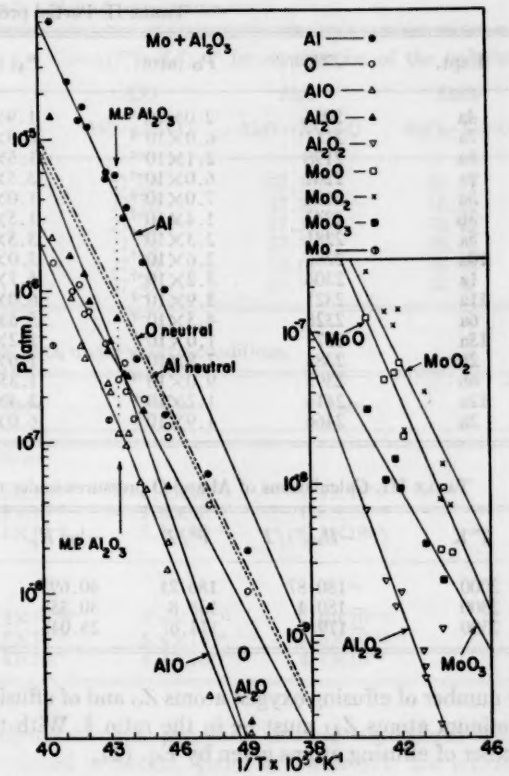

FIG. 2. Pressure data in the Mo—Al_2O_3 system as a function of $1/T\times10^5°K^{-1}$. The data above and below the melting point of Al_2O_3 are separated by the dotted line labeled M.P. Al_2O_3.

as is seen from a comparison of the Al and Al_2O intensities. It was also observed that pressures over solid alumina taken before and after melting the sample did not agree. This was attributed to liquid Al_2O_3 spreading over the internal surface. When solidified, the resulting Al_2O_3 layer tended to reduce the activity of molybdenum and hence the degree of reduction.

Since the experimental data show that the amount of reduction caused by tungsten is small for the vaporization reaction

$$Al_2O_3(s,l)=2Al(g)+3O(g),$$

pressures of Al and O can be calculated from the available thermodynamic data. On combining the heat of formation of Al_2O_3,[24] the heat of sublimation of Al,[2,19] and the dissociation energy of O_2[18], $\Delta H_{298}°=734.15\pm4$ kcal/mole is obtained for this reaction. The entropy data[10] for this reaction, measured for solid and estimated for liquid Al_2O_3, are summarized in Table III, column 2. Since under strictly neutral conditions, no condensed phase other than Al_2O_3 is formed, the composition of the constant boiling vapor will maintain the stoichiometric composition of the condensed phase Al_2O_3. Thus, in vaporization under Knudsen conditions,

[24] J. P. Coughlin, Bur. of Mines Bull. 542 (1954).

TABLE II. Partial pressures in the system $Mo+Al_2O_3$.

Expt.	$T°K$	P_O (atm)	P_{Al} (atm)	P_{AlO} (atm)	P_{Al_2O} (atm)	$P_{Al_2O_2}$ (atm)
4a	2036	2.0×10^{-8}	1.9×10^{-8}	1.2×10^{-9}	1.4×10^{-9}	..
7a	2111	6.0×10^{-8}	6.0×10^{-8}	2.1×10^{-9}	8.1×10^{-9}	...
8a	2198	2.1×10^{-7}	1.5×10^{-7}	1.4×10^{-8}	...	...
9a	2262	6.0×10^{-7}	3.5×10^{-7}	5.3×10^{-8}	...	...
3a	2194	7.0×10^{-8}	1.0×10^{-6}	2.1×10^{-8}	5.0×10^{-8}	...
3b	2243	1.4×10^{-7}	1.5×10^{-6}	4.8×10^{-8}	1.6×10^{-7}	...
5a	2281	2.3×10^{-7}	3.5×10^{-6}	1.1×10^{-7}	2.7×10^{-7}	1.1×10^{-9}
10a	2287	2.6×10^{-7}	3.0×10^{-6}	9.4×10^{-8}	2.8×10^{-7}	2.6×10^{-10}
1a	2304	3.2×10^{-7}	5.7×10^{-6}	1.1×10^{-7}	6.6×10^{-7}	...
11a	2321	3.9×10^{-7}	6.0×10^{-6}	2.1×10^{-7}	4.7×10^{-7}	6.2×10^{-10}
6a	2328	4.3×10^{-7}	5.5×10^{-6}	2.4×10^{-7}	4.0×10^{-7}	8.0×10^{-10}
13a	2371	1.0×10^{-7}	1.2×10^{-5}	...	8.4×10^{-7}	...
2b	2384	7.8×10^{-7}	1.6×10^{-5}	3.5×10^{-7}	1.3×10^{-6}	1.9×10^{-9}
6b	2395	9.0×10^{-7}	1.35×10^{-5}	4.3×10^{-7}	...	1.5×10^{-9}
12a	2416	1.2×10^{-6}	2.4×10^{-5}	8.9×10^{-7}	1.7×10^{-6}	2.3×10^{-9}
2a	2466	1.9×10^{-6}	6.0×10^{-5}	2.2×10^{-6}	1.4×10^{-5}	6.7×10^{-9}

TABLE III. Calculations of Al and O pressures under neutral conditions. (Values in second column are from Brewer[10].)

$T°K$	$(F°-H_{298}°)/T$	$F°/T$	$-\log K_p$	$-5\log P_{Al}$	$-\log P_{Al}$	$-\log P_O$	P_{Al}	P_O
2000	−180.87	186.21	40.695	40.882	8.176	8.113	6.7×10^{-9}	7.7×10^{-9}
2300	−180.4	138.8	30.334	30.521	6.104	6.041	7.86×10^{-7}	9.1×10^{-7}
2500	−179.1	114.6	25.045	25.232	5.046	4.983	9.0×10^{-6}	1.0×10^{-5}

the number of effusing oxygen atoms Z_O and of effusing aluminum atoms Z_{Al} must be in the ratio $\frac{3}{2}$. With the number of effusing atoms given by Eq. (2),

$$P_{Al}=0.867P_O$$

and

$$K_p\equiv(P_{Al}^2)(P_O^3)=1.54P_{Al}^5$$

are obtained. The oxygen and aluminum pressures calculated in this way are summarized in Table III and included graphically in Fig. 2. The slopes shown in Figs. 1 and 2 for the AlO, Al_2O, and Al_2O_2 pressures (below the melting point of Al_2O_3) were calculated from the dissociation energies of the molecules, the change in free energy function for the dissociation, and the measured pressures of Al and O. The slopes above the melting point of Al_2O_3 are estimated from the change in the heat of vaporization at the melting point. It is apparent in Fig. 1 that, at the highest temperature, the data on the molecules are systematically low. The solid lines are those which we believe to be the best fit of all the experimental data.

EVALUATION OF FREE ENERGY FUNCTIONS

To calculate dissociation energies from the measured pressures, free energy functions were estimated for the different molecules encountered in this work.[25-27]

For AlO spectroscopic information is available. It was assumed that the $X^2\Sigma^+$ state[25,28] is the ground state. The vibration frequency $\omega=979$ cm^{-1} and the distance $r_e=1.6718$ A[25,28] were used to evaluate the vibrational and rotational partition functions. These assumptions are identical to those previously made by Kelley.[26]

The vibration frequencies of the molecule Al_2O were estimated from valence force approximation formulas.[27] It was assumed that the bond-stretching force constant and the interatomic distance are the same as those for AlO. By analogy with H_2O,[27] and possibly Li_2O,[29] Al_2O was assumed to be a bent symmetric molecule with an angle of 110°. This hypothesis can be justified for theoretical reasons.[30] The bond-bending force constant was estimated by analogy with other C_{2V} molecules; the ratio $K_\delta/l^2\times k$ was taken as 0.0940, this value being the average for a number of such molecules.[28] The vibration frequencies obtained are $\omega_1=1079$ cm^{-1}, $\omega_2=351$ cm^{-1}, and $\omega_3=921$ cm^{-1}. Similar hypotheses have been made by other authors[5,31] who use, however, vibration frequencies which are different from those preferred here.

The more likely structures for Al_2O_2 would seem to be

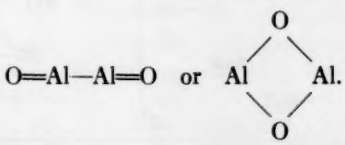

The first of these is analogous to the structure O=B—

[25] G. Herzberg, *Diatomic Molecules* (D. Van Nostrand Company, Inc., Princeton, New Jersey, 1950).
[26] K. K. Kelley, Bur. of Mines Bull. 477 (1950).
[27] G. Herzberg, *Infrared and Raman Spectra* (D. Van Nostrand Company, Inc., Princeton, New Jersey, 1945).
[28] A. Lagerqvist, N. E. L. Nilson, and R. F. Barrow, Arkiv. Fys. **12**, 543 (1957).
[29] P. A. Akishin and N. G. Rambidi, Doklady Akad Nauk SSSR **118**, 973 (1958).
[30] J. A. Pople, Quart Rev. **11**, 273 (1957).
[31] M. A. Cook, A. S. Filler, R. T. Keyes, W. S. Partridge, and W. O. Ursenbach, J. Phys. Chem. **61**, 189 (1957).

TABLE IV. Free energy functions as a function of temperature.

	$-(F°-H_0°)/T$ cal mole^{-1} deg^{-1}			$-\Delta(F°-H_0°)/T$ for atomization of the molecules		
				AlO	Al_2O	Al_2O_2
T°K	AlO	Al_2O	Al_2O_2	$AlO \rightarrow Al+O$	$Al_2O \rightarrow 2Al+O$	$Al_2O_2 \rightarrow 2AlO$
2000	59.69	73.33	80.86	27.08	57.11	38.52
2100	60.09	73.94	81.69	27.18	57.26	38.50
2200	60.48	74.50	82.48	27.25	57.39	38.48
2300	60.86	75.06	83.25	27.31	57.50	38.46
2400	61.21	75.60	83.98	27.40	57.61	38.44
2500	61.56	76.12	84.70	27.47	57.71	38.42

TABLE V. Pressures of the vapor species over Al_2O_3 under various conditions.

T°K	P_{Al}	P_O	P_{AlO}	P_{Al_2O}	$P_{Al_2O_2}$
			Under neutral conditions		
2000	6.7×10^{-9}	7.7×10^{-9}	2.5×10^{-10}	6.4×10^{-11}	1.3×10^{-13}
2300	7.9×10^{-7}	9.1×10^{-7}	7.1×10^{-8}	2.8×10^{-8}	1.3×10^{-10}
2500	9.0×10^{-6}	1.0×10^{-5}	1.1×10^{-6}	5.0×10^{-7}	3.1×10^{-9}
			In a W cell		
2000	7.1×10^{-9}	6.3×10^{-9}	2.2×10^{-10}	9.4×10^{-11}	1.0×10^{-13}
2300	1.0×10^{-6}	7.8×10^{-7}	6.8×10^{-8}	5.4×10^{-8}	1.5×10^{-10}
2500	1.2×10^{-5}	8.7×10^{-6}	1.4×10^{-6}	8.7×10^{-7}	4.1×10^{-9}

B═O, postulated[32,33] for the isoelectronic B_2O_2 molecule by analogy with C_2N_2.[34] In the B_2O_2 molecule, the OB—BO bond[32] compares to the B_2 dissociation energy[25] in the same way as the NC—CN bond[34] compares to the C—C single bond.[34] In Al_2O_2 no such relation appears to hold between the Al_2 dissociation energy[35,36] and the OAl—AlO bond although electron promotion[25] could explain the difference.[37] However, the closed ring, either plane or spatial, would seem somewhat more likely. Vibration frequencies of $\omega_1=1782$, $\omega_2=531$, $\omega_3=979$, $\omega_4=366$, $\omega_5=151$ and $\omega_1=200$, $\omega_2=600$, $\omega_3=\omega_4=930$, $\omega_5=\omega_6=1000$ cm^{-1} were estimated for the linear and ring models, respectively. With a multiplicity of 2, these lead to values of 81.47 and 80.86, respectively, for the free energy function at 2000°K. Thus the estimation of the free energy function is rather insensitive to the actual structure of the molecule. The values of the free energy functions used here are summarized in Table IV.

DISCUSSION

The pressures measured in tungsten cells, and in molybdenum cells before reducing conditions become important, agree satisfactorily with the pressures of aluminum and atomic oxygen calculated from the thermodynamic data, assuming neutral conditions. These calculated pressures, given in Table III, are included in Table V together with the pressures of the AlO, Al_2O, and Al_2O_2 molecules derived from the dissociation energies obtained here.

Sears and Navais[38] have studied the evaporation of alumina under Langmuir conditions and have reported on evaporation coefficient of about 1/200. Observations in the present work, showed that the relative intensities of the species vaporizing from a Knudsen cell and from a clogged effusion orifice are about the same. It is therefore concluded that liquid alumina has an accommodation coefficient greater than 0.1. This conclusion is supported by the agreement between the pressures measured over large samples (Fig. 1) and over small samples in the quantitative evaporation (points numbered 3, Fig. 1). The quantitative evaporation also showed the pressure to be constant with time, thus yielding information indicating the absence of formation of Al-O phases different from Al_2O_3.

There is a discrepancy between the amount of reduction of alumina by tungsten as determined here, and the weight loss ratio of alumina and tungsten (about 1.1 at 2600°K) as measured by Ackermann and Thorn.[4,5] Similarly there is a discrepancy between the amount of reduction in the alumina-molybdenum system and the pressure of the gaseous MoO_n ($n=1, 2, 3$) oxides. This discrepancy cannot be attributed to the ionization cross section of the gaseous oxides since in order to explain the difference, these cross sections would have

[32] M. G. Inghram, R. F. Porter, and W. A. Chupka, J. Chem. Phys. **25**, 498 (1956).
[33] D. T. White, P. N. Walsh, and D. E. Mann, J. Chem. Phys. **28**, 508 (1958).
[34] T. L. Cottrell, *The Strength of Chemical Bonds* (Butterworths Scientific Publications, London, 1958).
[35] J. Drowart and R. E. Honig, J. Phys. Chem. **61**, 890 (1957).
[36] W. A. Chupka, J. Berkowitz, C. S. Giese, and M. G. Inghram, J. Phys. Chem. **62**, 611 (1958).
[37] R. S. Mulliken (private communication).
[38] G. W. Sears and L. Navias, J. Chem. Phys. **30**, 1111 (1959).

TABLE VI. Experimentally measured heats of reaction $\Delta H_0°$(kcal/mole).

Reaction	Al_2O_3+Mo	Al_2O_3+U+MO	Al_2O_3+W	Average
$Al_2O_2(g) \rightarrow 2AlO(g)$	134.3	...	135.8	135.0±5
$Al_2O(g) \rightarrow AlO(g)+Al(g)$	131.0	130.2	131.7	131.0±5
$AlO(g) \rightarrow Al(g)+O(g)$	115.5	115.7	113.9	115.0±5
$Al_2O(g) \rightarrow 2Al(g)+O(g)$	245.3	245.9	243.4	244.8±7

to be about ten times less than the values used in this work. One possible explanation of these discrepancies might be the formation of condensed oxides, soluble in alumina and/or in the metals W or Mo. Another possible explanation of the difference in weight losses in the W-Al_2O_3 system as measured by Ackermann and Thorn and as calculated here is that a binary gaseous oxide of the type Al_2WO_4 becomes important at temperatures higher than those used in the present experiments. The isoelectronic molecule In_2MoO_4 is observed in the system Mo—In_2O_3,[39] as are $BaWO_4$+ and $BaMoO_4$+ [40] in the systems BaO-W and BaO-Mo. A final possible explanation of the discrepancy is that the residual pressure of O_2 in the Ackermann and Thorn experiments was sufficient to give appreciable tungsten oxide transport from the outer surface of the Knudsen cell.

The values for the atomization energy of the molecules AlO, Al_2O and for the dimerization energy of Al_2O_2 are summarized in Table VI. The dissociation energy of the molecule AlO, 115 kcal/mole or 4.95 ev, is substantially higher than the value 4.25 ev, obtained by a linear Birge-Sponer extrapolation of the vibration frequencies of the $^2\Sigma^+$ state of this molecule, as already pointed out by Brewer. The dissociation energy found here confirms the lower limit derived from the earlier mass spectrometric measurements.[9]

The atomization energy of Al_2O, $D_0°=245\pm7$ or $D_{298}°=247\pm7$ kcal/mole agrees within the experimental uncertainty with the values $\Delta H_{298}°=247\pm7$[2] obtained from thermochemical measurements and $\Delta H_{298}°=256\pm7$ kcal/mole based on second law measurements of the heat of formation of Al_2O from Al-Al_2O_3.[8] Comparison of the AlO and Al_2O dissociation energies indicates that a link between the two Al atoms might contribute to the enhanced stability of Al_2O. The dimerization energy of the molecule Al_2O_2, 135 kcal/mole, is higher than that of the isoelectronic molecule B_2O_2, 115 kcal/mole, and may indicate a difference in structure.

The heats of formation from the elements in their standard states at 298°K, derived from these measurements are $\Delta H_{298}°(AlO)_f=+20.8$ kcal/mole, $\Delta H_{298}°(Al_2O)_f=-33.0$ kcal/mole, and $\Delta H_{298}°(Al_2O_2)_f=-93.1$ kcal/mole.

The calculation of Medvedev[7] that Al_2O_3 is an important vapor species over Al_2O_3 under neutral conditions is not borne out by the present experiments. It is to be expected that the Al_2O_3 molecule may be detected in the vapor under oxidizing conditions.

Dissociation energies of the molecules MoO, MoO_2, and MoO_3, WO, WO_2, and WO_3 which can also be derived from the present measurements are treated in the following paper.

ACKNOWLEDGMENTS

We wish to thank Professor L. Brewer for permission to use the thermodynamic data from an unpublished paper on the Al-O system. Numerous crystal structures determined by Miss A. Plettinger are gratefully acknowledged. Valuable technical assistance from Mr. E. Kuziel and Mr. T. Earp is greatly appreciated.

[39] J. Drowart, G. DeMaria, and R. P. Burns (to be published).
[40] L. T. Aldrich, J. Appl. Phys. **22**, 1168 (1951).

Mass Spectrometric Study of Gaseous Molybdenum, Tungsten, and Uranium Oxides*

G. DEMARIA,† R. P. BURNS, J. DROWART,‡ AND M. G. INGHRAM

Department of Physics, University of Chicago, Chicago, Illinois

(Received November 5, 1959)

Partial pressures of the gaseous oxides MoO, MoO_2, MoO_3, WO, WO_2, WO_3, UO, UO_2, and UO_3 in the systems Mo—Al_2O_3 and U—Al_2O_3 have been measured by mass spectrometric methods. The vapor pressure of uranium has also been determined. The reaction enthalpies derived from these measurements are:

Reaction	$\Delta H_0°$ kcal/mole
$MoO(g) \rightarrow Mo(g)+O(g)$	116±15
$MoO_2(g) \rightarrow Mo(g)+2O(g)$	262±10
$MoO_3(g) \rightarrow Mo(g)+3O(g)$	411±7
$WO(g) \rightarrow W(g)+O(g)$	154±10
$WO_2(g) \rightarrow W(g)+2O(g)$	296±7
$WO_3(g) \rightarrow W(g)+3O(g)$	443±7
$UO(g) \rightarrow U(g)+O(g)$	179±7
$UO_2(g) \rightarrow U(g)+2O(g)$	340±7
$UO_3(g) \rightarrow U(g)+3O(g)$	493±7
$U(s) \rightarrow U(g)$	126±5.

INTRODUCTION

IN the preceeding paper[1] describing the evaporation of alumina from both molybdenum and tungsten Knudsen cells, partial pressures were obtained for the gaseous oxides MoO, MoO_2, MoO_3, WO, WO_2, and WO_3. These pressures are here used to calculate thermodynamic quantities for these molecules. To make possible similar calculations for the analogous gaseous oxides UO, UO_2, and UO_3, the measurements have been extended to include the system U—Al_2O_3.

Published work in the Mo—O and W—O systems includes mass spectrometric studies of the sublimation of MoO_3[2] and WO_3[3], both of which vaporize predominantly as polymers $(XO_3)_n$ ($n=3$, 4 and 5; X=Mo or W); the vaporization of the BeO—W system which includes the molecules WO_2 and WO_3 in the vapor phase[4]; and pressure determinations in the systems MoO_2, Mo—MoO_2, Mo_4O_{11}, WO_3 and W—WO_2.[5] Studies of the U—O system include the measurement of the vapor pressure of UO_2 from which the dissociation energy of UO_2 was deduced,[6] and a mass spectrometric study of the U—O system in which dissociation energies for UO and UO_3 were derived.[7]

EXPERIMENTAL TECHNIQUE AND RESULTS

The essentials of the mass spectrometric procedure have been described in the preceding paper. That paper also gives vapor pressure data (Figs. 1 and 2) for the gaseous molybdenum and tungsten oxides. To obtain analogous data for uranium oxides, two types of experiments were performed in molybdenum crucibles. In one, excess metallic uranium was added to a small amount of Al_2O_3. In the other, metallic uranium was added to an excess of Al_2O_3. In the latter experiment the uranium reacted rapidly with alumina to form solutions of UO_2 in Al_2O_3.[8] This method for studying the U—O system presents the advantage that the vaporization is congruent, and that the composition of the vapor is constant with time.

The metal oxide ions observed in the three systems, together with the measured first appearance potentials in ev, are:

$MoO=8.0\pm0.6$	$WO=9.1\pm1$	$UO=4.7\pm0.6$
$MoO_2=9.4\pm0.6$	$WO_2=9.9\pm0.6$	$UO_2=4.3\pm0.6$
$MoO_3=12.0\pm0.6$	$WO_3=11.7\pm0.6$	$UO_3=10.4\pm0.6$.

At low ionizing electron energies ($E \leqslant 15$ ev), the ionization efficiency curves showed all 9 ions to be produced predominantly by direct ionization of the corresponding

* Supported in part by the Office of Ordnance Research, U.S. Army, and in part by the National Science Foundation.

† On leave of absence from Istituto di Chimica Fisica, Universitá degli Studi, Rome, Italy.

‡ On leave of absence from Laboratoire de Chimie Physique Moleculaire, Université Libre de Bruxelles, Brussels, Belgium.

[1] J. Drowart, G. DeMaria, R. P. Burns and M. G. Inghram, J. Chem. Phys. **32**, (1960), this issue.

[2] J. Berkowitz, W. A. Chupka, and M. G. Inghram, J. Chem. Phys. **26**, 842 (1957).

[3] J. Berkowitz, W. A. Chupka, and M. G. Inghram, J. Chem. Phys. **27**, 85 (1957).

[4] W. A. Chupka, J. Berkowitz, and C. F. Giese, J. Chem. Phys. **30**, 827 (1959).

[5] P. E. Blackburn, M. Hoch, and H. L. Johnston, J. Phys. Chem. **62**, 769 (1958).

[6] R. J. Ackermann, P. W. Gilles, and R. J. Thorn, J. Chem. Phys. **25**, 1089 (1956).

[7] W. A. Chupka, Argonne National Laboratory Rept. 5753 (1957), p. 65; and Rept. 5786 (1957), p. 73.

[8] E. M. Levin, H. F. McMurdie, and F. P. Hall, *Phase Diagrams for Ceramists* (American Ceramic Society, 1956), p. 64.

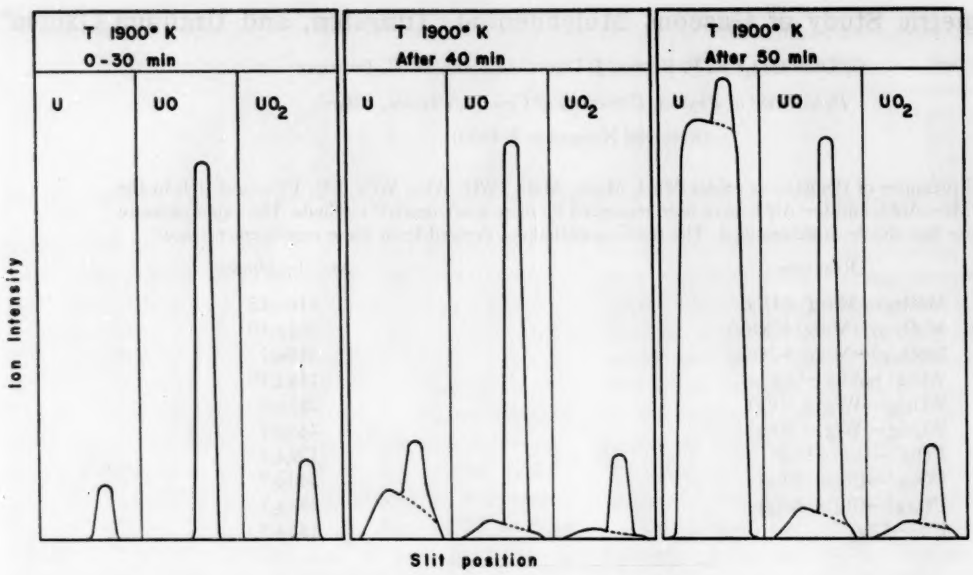

FIG. 1. Intensity profile in the molecular beam as a function of time, as determined using the movable beam defining slit.

neutral molecule. In addition, the ion Mo^+, produced from atomic Mo, was observed in the system Mo—Al_2O_3. The Mo pressure (derived from the Mo^+ intensity) was, under most conditions, in agreement with the Mo pressure given by Stull and Sinke[9] indicating Mo to have unit activity within the cell. In a few measurements after the Al_2O_3 had melted and solidified, Mo was observed not to have unit activity within the Knudsen cell. This was evidently because the Mo surface was covered with solid Al_2O_3. In these cases, as discussed in the preceeding paper, the pressures of the alumina species were also different. Such data have not been included in the calculations of dissociation energies of gaseous MoO_n molecules.

In the initial part of the experiment U(excess)+Al_2O_3 the ions U^+, UO^+, and UO_2^+ were observed. The appearance potential of U^+(5.4±0.3 ev) identified this ion as resulting from the ionization of atomic uranium. Movement of uranium from the inside to the outer surface of the cell necessitated special care in the determination of pressure ratios of uranium to UO and UO_2 within the cell. Use of the movable beam slit showed that, during the initial part of an experiment, uranium in the molecular beam came only from the inside of the cell. (See Fig. 1). After 30 min of operation at 1900°K the molecular beam intensity distribution showed that uranium was beginning to come from the outer surface of the cell. After 50 min of operation the ratio of atomic uranium coming from the effusion hole to the total uranium beam visible through the movable beam defining slit was about 0.1. This ratio remained constant for long periods of time.

The movement of metallic uranium to the outer surface of a Knudsen cell has been observed earlier by mass

TABLE I. Partial pressures in the system W+Al_2O_3.

Expt.	T°K	P_O (atm)	P_{WO} (atm)	P_{WO_2} (atm)	P_{WO_3} (atm)
1a	2188	1.5×10^{-7}	8.4×10^{-10}	5.3×10^{-9}	1.2×10^{-9}
5a	2191	1.6×10^{-7}	...	1.1×10^{-8}	2.4×10^{-9}
1b	2213	2.2×10^{-7}	1.2×10^{-9}	1.0×10^{-8}	2.4×10^{-9}
5b	2226	2.7×10^{-7}	...	1.5×10^{-8}	2.7×10^{-9}
1c	2233	3.0×10^{-7}	4.9×10^{-9}	3.6×10^{-8}	7.7×10^{-9}
2a	2240	3.5×10^{-7}	...	1.9×10^{-8}	4.3×10^{-9}
1d	2264	4.7×10^{-7}	7.1×10^{-9}	6.3×10^{-8}	1.5×10^{-8}
3a	2325	1.1×10^{-6}	8.6×10^{-7}	6.0×10^{-8}	1.1×10^{-8}
3b	2335	1.2×10^{-6}	1.5×10^{-6}	8.3×10^{-8}	1.1×10^{-8}
3c	2390	2.5×10^{-6}	2.3×10^{-8}	1.2×10^{-7}	1.3×10^{-8}
4	2462	5.7×10^{-6}	3.0×10^{-8}	3.3×10^{-7}	5.6×10^{-8}
2b	2475	6.6×10^{-6}	4.5×10^{-8}	4.0×10^{-7}	7.5×10^{-8}

[9] D. R. Stull and G. C. Sinke, Am. Chem. Soc. Rept. No. 18 (1956).

TABLE II. Partial pressures in the system Mo+Al_2O_3.

Expt.	T°K	P_O (atm)	P_{MoO} (atm)	P_{MoO_2} (atm)	P_{MoO_3} (atm)
2c	2262	1.4×10^{-7}	3.5×10^{-9}	7.2×10^{-9}	...
2a	2281	2.3×10^{-7}	9.5×10^{-9}	1.3×10^{-8}	2.3×10^{-9}
2d	2287	2.6×10^{-7}	3.7×10^{-9}	7.9×10^{-9}	...
2e	2321	3.9×10^{-7}	...	4.1×10^{-8}	2.4×10^{-9}
2g	2371	7.0×10^{-7}	2.0×10^{-9}	2.2×10^{-8}	...
1b	2384	7.8×10^{-7}	6.2×10^{-8}	1.4×10^{-7}	9.4×10^{-9}
2b	2395	9.0×10^{-7}	5.4×10^{-8}	1.1×10^{-7}	1.4×10^{-8}
2f	2416	1.2×10^{-6}	4.8×10^{-8}	1.4×10^{-7}	1.1×10^{-8}
1a	2466	1.9×10^{-6}	1.2×10^{-7}	2.5×10^{-7}	3.1×10^{-8}

TABLE III. Partial pressures in the system U (excess)+Al_2O_3.

Expt.	T	P_O (atm)	P_U (atm)	P_{UO} (atm)	P_{UO_2} (atm)	P_{UO_3} (atm)
1a	1876	...	5.2×10^{-9}	9.6×10^{-8}	1.4×10^{-8}	...
1c	1902	...	1.4×10^{-8}	2.0×10^{-7}	2.4×10^{-6}	...
1b	1909	...	1.5×10^{-8}	2.0×10^{-7}	2.6×10^{-6}	...

TABLE IV. Partial pressures in the system $U+Al_2O_3$ (excess) $UO_2+Al_2O_3$.

Expt.	T	P_O (atm)	P_U (atm)	P_{UO} (atm)	P_{UO_2} (atm)	P_{UO_3} (atm)
2b, g	2200	2.9×10^{-8}	...	1.5×10^{-9}	5.6×10^{-7}	4.6×10^{-8}
2f	2219	3.2×10^{-8}	...	1.8×10^{-9}	6.6×10^{-7}	4.6×10^{-8}
2e	2244	9.1×10^{-8}	...	2.5×10^{-9}	1.3×10^{-6}	1.1×10^{-7}
2a	2246	1.0×10^{-7}	...	2.6×10^{-9}	1.4×10^{-6}	1.5×10^{-7}
2d	2286	1.7×10^{-7}	...	3.9×10^{-9}	1.4×10^{-6}	1.1×10^{-7}
2c	2322	2.3×10^{-7}	...	4.0×10^{-9}	1.1×10^{-6}	1.2×10^{-7}

TABLE V. Summary of hypotheses used for free energy functions.

Molecule	Vibration frequency (cm^{-1}) 1	2	3	4	Interatomic distance (A)	Analogous electronic state	Electronic partition function cal deg^{-1} $mole^{-1}$ 2000°K	2200°K	2500°K
MoO	950[a]	...	...	...	1.66[e]	Zr	5.33	5.48	5.66
WO	1060[b]	...	...	...	1.70[e]	Hf^{I}	3.80	3.92	4.08
UO	920[c]	...	...	...	1.96[e]	Th^{I}	3.56	3.64	3.75
MoO_2	920	420	980	...	1.66	Mo^{V}	4.14	4.25	4.39
WO_2	1040	470	1080	...	1.70	La^{II}, Cr^{V}	5.35	5.51	5.71
UO_2	900	400	925	...	1.96	Th^{III}	5.93	6.08	6.30
MoO_3	800	390	830[d]	340[d]	...	...		1	
WO_3	780	340	810[d]	320[d]	...	...		1	
UO_3	750	320	780[d]	280[d]	...	...		1	

[a] T. M. Swaminathan and S. G. Krishnamurthy, Current Sci. 23, 258 (1954).
[b] V. Vittalachar and S. G. Krishnamurthy, Current Sci. 23, 357 (1954).
[c] From the force constant given by K. W. F. Kohlrausch, *Ramanspektren* (Becker and Erler, Leipzig, 1943).
[d] Doubly degenerate.
[e] Guggenheimer relation, K. M. Guggenheimer, Proc. Phys. Soc. (London) 58, 456 (1946).

spectrometric methods.[7] In that case the amount of uranium inserted within the tantalum cell was large and, because the solubility of tantalum in liquid uranium is 15% at 2000°K,[10] a hole was formed through the base of the cell. In the present experiment the base of the Mo cell employed was 1 cm thick, and only 0.6 g of metallic uranium was placed in the cell. Thus solution of Mo in liquid uranium (30% at 1900°K)[11] could not dissolve sufficient material to penetrate the wall. In addition, no visible evidence for liquid flow through the walls could be found. The probable explanations for the movement of uranium here observed are surface mobility and diffusion through the solid cell walls. It is interesting to note that even after a short experiment, although no evidence could be found for change in size of the effusion orifice or in the cell dimensions, the lid broke into pieces when force was applied to remove it. Thus considerable alloying was indicated.

The pressure calibrations were explained in the previous paper for the molybdenum and tungsten oxides. During the uranium studies the sensitivity of the mass spectrometer was calibrated with silver before and after each uranium experiment. The equilibria among O, Al, AlO, and Al_2O molecules were used as secondary standards. The relative ionization cross section of Mo (52.5) was taken from Otvos and Stevenson.[12] An experimental value for the ionization cross section of atomic uranium was obtained by vaporizing known weights of UF_4 and silver in one experiment. The gaseous UF_4 molecule, to which solid UF_4 vaporizes, ionizes predominantly to UF_3^+ under electron impact. In this respect it is similar to many halides, particularly tetra and hexa halides. At 50 ev, the relative intensities of the ions UF_4^+, UF_3^+, UF_2^+, UF^+, and U^+ were 0.054; 1.00; 0.157; 0.132, and 0.049, respectively. From this data[13,14] the total ionization cross section of U was cal-

TABLE VI. Free energy functions $-(F°-H_0°)/T$ in cal deg^{-1} $mole^{-1}$ for gaseous oxides.

T°K	2000	2100	2200	2300	2400	2500
MoO	67.36	67.84	68.29	69.73	69.15	69.56
MoO_2	78.80	79.46	80.09	80.70	81.29	81.56
MoO_3	83.01	83.87	84.70	85.50	86.25	86.98
WO	67.54	68.00	68.44	68.88	69.29	69.69
WO_2	81.31	81.78	82.63	83.25	83.85	84.44
WO_3	84.99	85.85	86.78	87.47	88.22	88.97
UO	68.89	69.31	69.72	70.11	70.49	70.86
UO_2	84.26	84.94	85.60	86.23	86.84	87.44
UO_3	87.25	88.12	88.94	89.75	90.51	91.25

[10] C. H. Schramm, A. R. Gordon, and A. R. Kaufman (AECD-2686), J. Metals 2, (1949).
[11] D. Ahmann, A. I. Snow, and A. S. Wilson, CT-2946 (July, 1945), referred to in *Phase Diagrams of the U System* (Battelle Memorial Institute, Columbus, Ohio) (1955).
[12] J. W. Otvos and D. P. Stevenson, J. Am. Chem. Soc. 73, 546 (1956).
[13] M. G. Inghram, R. J. Hayden, and D. C. Hess, Natl. Bur. Standards Circ. No. 522, 257 (1953).
[14] H. E. Stanton, W. K. Chupka, and M. G. Inghram, Rev. Sci. Instr. 27, 109 (1956).

TABLE VII. Summary of reaction enthalpy changes.

Reaction	$H_0°$ (measured) (kcal mole^{-1})	Pressure data from Table	Deduced atomization energy $D_0°$ (kcal mole^{-1}) $XO_n(g)\rightarrow X(g)+nO(g)$	Atomization energy from literature: Original value (kcal mole^{-1})	Atomization energy from literature: Recalculated value (kcal mole^{-1})	Reference
$MoO(g)\rightarrow Mo(s)+O(g)$	-40.7 ± 15	II	116.4 ± 15	...	...	
$MoO_2(g)\rightarrow Mo(s)+2O(g)$	104.4 ± 10	II	261.5 ± 10	285 ± 2	295 ± 2	5
$MoO_3(g)\rightarrow Mo(s)+3O(g)$	254.0 ± 7	II	411.1 ± 7	410 ± 2	426 ± 2	5
$WO(g)\rightarrow W(s)+O(g)$	-45.7 ± 10	I	154.0 ± 10	...	...	
$WO_2(g)\rightarrow W(s)+2O(g)$	96.0 ± 7	I	295.7 ± 7	313 ± 10	301 ± 10	4
$WO_3(g)\rightarrow W(s)+3O(g)$	243.3 ± 7	I	443.0 ± 7	444 ± 10	449 ± 10	4
$U(s)\rightarrow U(g)$	126.0 ± 5	III		116.6 ± 0.1 125[a]		19
$2UO(g)\rightarrow UO_2(g)+U(g)$	16.6 ± 5	III				
$2UO_2(g)\rightarrow UO_3(g)+UO(g)$	9.6 ± 5	IV				
$UO_2(g)\rightarrow UO(g)+O(g)$	161.9 ± 5	IV				
$UO_3(g)\rightarrow UO_2(g)+O(g)$	152.7 ± 5	IV				
$UO(g)\rightarrow U(g)+O(g)$	178.5 ± 7	III, IV		174	(172)	7
$UO_2(g)\rightarrow U(g)+2O(g)$	340.4 ± 7	III, IV		343 ± 5	(334)	6
$UO_3(g)\rightarrow U(g)+3O(g)$	493.1 ± 7	III, IV		483	(480)	7

[a] Leo Brewer, *National Nuclear Energy Series IV-19B* (McGraw-Hill Book Company, Inc., New York, 1950).

culated to be $\sigma_U=50\pm5$. By analogy with $\sigma_U=50$, so obtained, and $\sigma_{Mo}=52.5$, the relative cross section of tungsten was taken to be $\sigma_W=50$. Pressures for the various oxides are summarized in Tables I through IV (for Mo and W oxides, see also Figs. 1 and 2, preceding paper[1]). The experiment numbers in column 1 of Tables I–IV refer to different Knudsen cell assemblies, while the lower case letters refer to the order in which the data were taken within a given experiment.

EVALUATION OF THE FREE ENERGY FUNCTIONS

The evaluation of the free energy functions of the XO_n oxides was based on experimentally measured vibration frequencies and interatomic distances evaluated from the Guggenheimer relation.[15] The electronic partition functions of the XO and XO_2 molecules were derived[16] from the multiplicities and energy levels of isoelectronic atoms or ions.[17]

All the XO_2 molecules were assumed to have C_{2v} symmetry by an extension of Walsh's[18] conclusions concerning the relationship of shape to the number of valence electrons. The average angle of 107° for such molecules was used. Vibration frequencies were evaluated from the force constant of the corresponding XO molecule, assuming the ratio between bond bending and bond stretching constants k_σ/l^2k_1 to be 0.0940. The XO_3 molecules were assumed to be planar, with all O—X—O angles 120°. The free energy functions derived from these hypotheses, given in Table V, are summarized in Table VI.

[15] K. M. Guggenheimer, Proc. Phys. Soc. (London) **58**, 456 (1946).
[16] L. Brewer (private communication).
[17] C. E. Moore, Natl. Bur. Standards Circ. No. 467 (1949).
[18] A. D. Walsh, J. Chem. Soc. (1953), 2266.

DISCUSSION

Assuming the solubility of molybdenum in liquid uranium to be 30 atom %,[11] i.e., that the activity of uranium is 0.7, the heat of sublimation of uranium derived from the pressures given in Table III is $\Delta H_0°=126\pm5$ kcal/mole. This is to be compared with $\Delta H_0°=116.6\pm0.1$ kcal/mole obtained by Rauh and Thorn.[19] In discussing their result Rauh and Thorn have suggested that uranium inside an effusion cell is coated by a containuous layer of oxide through which the passage of uranium is diffusion limited and that the thickness of the oxide layer depends on the oxygen pressure. In the experiments described here, the oxygen pressure inside the Knudsen cell was 10^2 times below that quoted by Rauh and Thorn as sufficient to effect the results. This pressure was calculated from a knowledge of the equilibrium constant under slightly oxidizing conditions and from the pressures of UO and UO_2 measured under reducing conditions. In addition, the ratio of effusing to geometric vaporizing area σ was less than 10^{-3}. Hence the effect of the diffusion limited process in our experiments is reduced by more than a factor of 10 below that in the Rauh and Thorn experiment. Therefore, under the conditions of our experiment the vaporization of uranium will not be diffusion limited but will be an equilibrium process. The discrepancy between the vapor pressure quoted by Rauh and Thorn and that observed in this experiment is reasonably explained by vaporization of uranium from the surface of the crucible (which must have occurred in the Rauh and Thorn experiments[19]) and by the difference in ratio of effusion hole area to vaporizing area. It is of interest

[19] E. G. Rauh and R. J. Thorn, J. Chem. Phys. **22**, 1414 (1954).

to note that the value for the heat of vaporization of uranium of 125 kcal/mole given by Brewer[20] is in good agreement with the value determined here.

Dissociation energies of the gaseous oxides XO_n derived from the pressures given in Tables I through IV are summarized in Table VII. In addition to the reactions given in Table VII, all gas phase equilibria of the type $UO_2+Al \rightarrow AlO+UO$, etc., were measured for which the equilibrium constant is dimensionless and hence less sensitive to uncertainties in pressure calibrations. These reactions give dissociation energies in good agreement with the above calculations. Atomization energies given by other authors, column 5, Table VII, have been recalculated in column 6 using the free energy functions given here.

The atomization energies of MoO_2 and MoO_3 cannot be compared directly to the values 285 and 410 kcal/mole obtained by Blackburn, Hoch, and Johnston,[5] since the mass spectrometric analysis of the vapor in the Mo—MoO_2 system has shown[20] the vapor in this system to be more complex than assumed by the former authors.

After taking into account a systematic difference (resulting from the use of different assumptions to estimate free energy functions) the atomization energies of WO_2 and WO_3 obtained here are in good agreement with the values calculated from partial pressures in the BeO—W system.[4]

The atomization energy of UO_2, $\Delta H_0^\circ = 340$ kcal/mole, is in good agreement with the atomization energy derived by Ackermann, Gilles, and Thorn[6] from the Clausius-Clapeyron relation applied to the vapor pressure of UO_2. The value 343 kcal/mole obtained by the latter authors using $\Delta H_0^\circ(U) = 117$ kcal/mole is reduced to $334 \pm$ kcal/mole when using $\Delta H_0^\circ(U) = 126 \pm 5$ kcal/mole. The dissociation energies of UO and UO_3 are in agreement with the values 174 kcal/mole obtained by Chupka[5] from second and third law measurements. There are no data available with which to compare the dissociation energies obtained for MoO and WO.

[20] R. P. Burns, G. DeMaria, J. Drowart, and R. T. Grimley, J. Chem. Phys. 32, 1363 (1960), this issue.

Nuclear Magnetic Resonance Spectra of Some Simple Epoxides

C. A. REILLY AND J. D. SWALEN

Shell Development Company, Emeryville, California

(Received August 28, 1959)

High resolution NMR spectra of four epoxides have been observed at 40 Mcps and analyzed. These epoxides are of the type

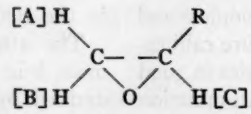

where R is a phenyl group (styrene oxide), a cyanide group (glycidonitrile), an acetyl group (1,2-epoxy-3-butanone), and a carboxyl group (glycidic acid). For each molecule the spin-spin coupling constants and nuclear magnetic screening parameters for the *A*, *B*, and *C* protons were derived from the experimentally determined energy levels. The method for obtaining numerical values for the energy levels from the spectra is described fully. *ABK* and *AA'K* approximations as well as an iterative *ABC* method of solution are described and illustrated.

Corresponding coupling constants are found to be about the same in all four molecules with $J_{AB}=5.8\pm0.5$ cps, $J_{AC}=2.2\pm0.5$ cps and $J_{BC}=4.6\pm0.5$ cps. However, the variations from molecule to molecule are considerably greater than the estimated precision of ±0.05 cps. The *ABX* approximation is shown to be inadequate either for the precise determination of the constants or for the calculation of relative intensities. As compared with the iterated *ABC* solution, the *ABK* or *AA'K* approximation leads to good values for the constants and adequately describes the relative intensities.

INTRODUCTION

THE analysis of nuclear magnetic resonance spectra leads to a determination of the nuclear screening parameters and the indirect spin-spin coupling constants. These are presumably related to the molecular structures and to the electronic and magnetic properties of the molecules. Although most of the results to date have been analyzed in terms of a phenomenological theory, the true relationships between the spin-spin coupling constants and the molecular structures and also between the screening parameters and the molecular structures are still rather obscure. In order to aid in the development of an understanding of these magnetic properties we have studied the NMR spectra of four structurally related epoxides of the type

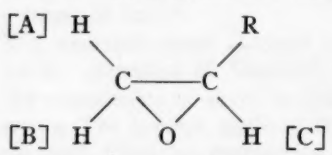

where R is a phenyl group (styrene oxide), a cyanide group (glycidonitrile), an acetyl group (1,2-epoxy-3-butanone), and a carboxyl group (glycidic acid).

The resonance from the R group, except in the case of the cyanide where there are no protons, is well removed and the protons in this group were not measurably spin-spin coupled to any of the other protons (a slight broadening was noticed in the *C* lines of styrene oxide due to the phenyl protons). Therefore, resonances from the three ring protons in each of these compounds were treated as an *ABX* system, as an *ABK* (perturbed *ABX*) system, and as an *ABC* system of three spins. Although the line positions and spin energy levels could be calculated satisfactorily by an *ABX* approximation[1] the intensities could be accounted for only by including perturbation or by a complete solution. In addition it was found that a substantial error can result in some of the spin-spin coupling constants as an *ABX* system approaches an *ABC* system, i.e., as it becomes an *ABK* system. As will be seen later this error can be much larger than one might expect by comparing observed and calculated line positions only.

According to Bernstein, Pople, and Schneider,[1] the *ABX* approximation utilizes two 2×2 rotations. One such rotation is applied to the *ABC* submatrix for the $F_z=\frac{1}{2}$ energy levels and the other to the submatrix for the $F_z=-\frac{1}{2}$ energy levels, the off-diagonal elements $\frac{1}{2}J_{AC}$ and $\frac{1}{2}J_{BC}$ being neglected in each case. In the *ABK* approximation the same rotations are applied but all the off-diagonal elements are included. For example, for the $F_z=+\frac{1}{2}$ matrix the transformation is

$$\begin{pmatrix} \cos\phi_+ & \sin\phi_+ & 0 \\ -\sin\phi_+ & \cos\phi_+ & 0 \\ 0 & 0 & 1 \end{pmatrix} \begin{pmatrix} H_{22} & \frac{1}{2}J_{AB} & \frac{1}{2}J_{AK} \\ \frac{1}{2}J_{AB} & H_{33} & \frac{1}{2}J_{BK} \\ \frac{1}{2}J_{AK} & \frac{1}{2}J_{BK} & H_{44} \end{pmatrix} \cdot \begin{pmatrix} \cos\phi_+ & -\sin\phi_+ & 0 \\ \sin\phi_+ & \cos\phi_+ & 0 \\ 0 & 0 & 1 \end{pmatrix},$$

[1] H. J. Bernstein, J. A. Pople, and W. G. Schneider, Can. J. Chem. **35**, 65 (1957).

TABLE I. Energy levels and wave functions in the ABK and $AA'K$ approximations.

State	Energy	Wave function
1	H_{11}	ψ_1
2	$H'_{22}+\delta_{24}^2\Delta_{24}^{-1}$	$\psi_2\cos\phi_+ + \psi_3\sin\phi_+ + \delta_{24}\Delta_{24}^{-1}\psi_4$
3	$H'_{33}+\delta_{34}^2\Delta_{34}^{-1}$	$-\psi_2\sin\phi_+ + \psi_3\cos\phi_+ + \delta_{34}\Delta_{34}^{-1}\psi_4$
4	$H_{44}-\delta_{24}^2\Delta_{24}^{-1}-\delta_{34}^2\Delta_{34}^{-1}$	$\psi_2[\delta_{34}\Delta_{34}^{-1}\sin\phi_+ - \delta_{24}\Delta_{24}^{-1}\cos\phi_+] - \psi_3[\delta_{34}\Delta_{34}^{-1}\cos\phi_+ + \delta_{24}\Delta_{24}^{-1}\sin\phi_+] + \psi_4$
5	$H_{55}+\delta_{56}^2\Delta_{56}^{-1}+\delta_{57}^2\Delta_{57}^{-1}$	$\psi_5 - \psi_6[\delta_{57}\Delta_{57}^{-1}\sin\phi_- - \delta_{56}\Delta_{56}^{-1}\cos\phi_-] + \psi_7[\delta_{57}\Delta_{57}^{-1}\cos\phi_- + \delta_{56}\Delta_{56}^{-1}\sin\phi_-]$
6	$H'_{66}-\delta_{56}^2\Delta_{56}^{-1}$	$-\delta_{56}\Delta_{56}^{-1}\psi_5 + \psi_6\cos\phi_- + \psi_7\sin\phi_-$
7	$H'_{77}-\delta_{57}^2\Delta_{57}^{-1}$	$-\delta_{57}\Delta_{57}^{-1}\psi_5 - \psi_6\sin\phi_- + \psi_7\cos\phi_-$
8	H_{88}	ψ_8

where:

	ABK	$AA'K$		ABK	$AA'K$
H_{11}	$h_A+h_B+h_K+J+j$	$h_A+h_{A'}+h_K+J+j$	δ_{24}	$\frac{1}{2}J_{AK}\cos\phi_+ + \frac{1}{2}J_{BK}\sin\phi_+$	$\sqrt{2}j\cos\phi_+ + \sqrt{2}j'\sin\phi_+$
H'_{22}	h_K-J+D_+	h_K-J+D_+	δ_{34}	$-\frac{1}{2}J_{AK}\sin\phi_+ + \frac{1}{2}J_{BK}\cos\phi_+$	$-\sqrt{2}j\sin\phi_+ + \sqrt{2}j'\cos\phi_+$
H'_{33}	h_K-J-D_+	h_K-J-D_+	δ_{56}	$\frac{1}{2}J_{AK}\sin\phi_- + \frac{1}{2}J_{BK}\cos\phi_-$	$\sqrt{2}j'\sin\phi_- + \sqrt{2}j\cos\phi_-$
H_{44}	$h_A+h_B-h_K+J-j$	$h_A+h_{A'}-h_K+J-j$	δ_{57}	$\frac{1}{2}J_{AK}\cos\phi_- - \frac{1}{2}J_{BK}\sin\phi_-$	$\sqrt{2}j'\cos\phi_- - \sqrt{2}j\sin\phi_-$
H_{55}	$-h_A-h_B+h_K+J-j$	$-h_A-h_{A'}+h_K+J-j$	Δ_{24}	$H'_{22}-H_{44}$	$H'_{22}-H_{44}$
H'_{66}	$-h_K-J+D_-$	$-h_K-J+D_-$	Δ_{34}	$H'_{33}-H_{44}$	$H'_{33}-H_{44}$
H'_{77}	$-h_K-J-D_-$	$-h_K-J-D_-$	Δ_{56}	$H_{55}-H'_{66}$	$H_{55}-H'_{66}$
H_{88}	$-h_A-h_B-h_K+J+j$	$-h_A-h_{A'}-h_K+J+j$	Δ_{57}	$H_{55}-H'_{77}$	$H_{55}-H'_{77}$
h_i	$\frac{1}{2}\gamma_i H_0\,(1-\sigma_i)$	$\frac{1}{2}\gamma_i H_0\,(1-\sigma_i)$	ψ_1	$\alpha\alpha\alpha$	$\alpha\alpha\alpha$
J	$\frac{1}{4}J_{AB}$	$\frac{1}{4}J_{AA'}$	ψ_2	$\beta\alpha\alpha$	$1/\sqrt{2}\,(\beta\alpha+\alpha\beta)\alpha$
j	$\frac{1}{4}(J_{AK}+J_{BK})$	$\frac{1}{4}(J_{AK}+J_{A'K})$	ψ_3	$\alpha\beta\alpha$	$1/\sqrt{2}\,(\beta\alpha-\alpha\beta)\alpha$
j'	$\frac{1}{4}(J_{AK}-J_{BK})$	$\frac{1}{4}(J_{AK}-J_{A'K})$	ψ_4	$\alpha\alpha\beta$	$\alpha\alpha\beta$
$D_+\cos2\phi_+$	$(h_B-h_A)-j'$	$2J$	ψ_5	$\beta\beta\alpha$	$\beta\beta\alpha$
$D_-\cos2\phi_-$	$(h_B-h_A)+j'$	$2J$	ψ_6	$\beta\alpha\beta$	$1/\sqrt{2}\,(\beta\alpha+\alpha\beta)\beta$
$D_+\sin2\phi_+$	$2J$	$(h_{A'}-h_A)-j'$	ψ_7	$\alpha\beta\beta$	$1/\sqrt{2}\,(-\beta\alpha+\alpha\beta)\beta$
$D_-\sin2\phi_-$	$2J$	$-(h_{A'}-h_A)-j'$	ψ_8	$\beta\beta\beta$	$\beta\beta\beta$

and the transformed matrix becomes

$$\begin{pmatrix} H'_{22} & 0 & \delta_{24} \\ 0 & H'_{33} & \delta_{34} \\ \delta_{24} & \delta_{34} & H_{44} \end{pmatrix},$$

where the elements are defined in Table I. The corresponding matrix for $F_z=-\frac{1}{2}$ is

$$\begin{pmatrix} H_{55} & \delta_{56} & \delta_{57} \\ \delta_{56} & H'_{66} & 0 \\ \delta_{57} & 0 & H'_{77} \end{pmatrix}.$$

Second-order perturbation is now applied in order to obtain ABK energy levels and wave functions given in Table I. Another approximation that may be useful is the $AA'K$. In this approximation symmetric and antisymmetric combinations of spin functions are used for some of the basis functions. The $AA'C$ matrices can either be derived directly from the spin angular momentum properties or they can be obtained from the ABC matrices by the transformation $\mathbf{SHS}^{-1}$, where

$$\mathbf{S}=(1/\sqrt{2})\begin{pmatrix} 1 & 1 & 0 \\ 1 & -1 & 0 \\ 0 & 0 & \sqrt{2} \end{pmatrix} \quad \text{for } F_z=+\tfrac{1}{2}$$

and

$$\mathbf{S}=(1/\sqrt{2})\begin{pmatrix} \sqrt{2} & 0 & 1 \\ 0 & 1 & 1 \\ 0 & -1 & 1 \end{pmatrix} \quad \text{for } F_z=-\tfrac{1}{2}.$$

TABLE II. Labeling scheme for transitions.

Transition No.	Origin	Type
1	7←8	A
2	3←5	A
3	4←6	A
4	1←2	A
5	6←8	A', B
6	2←5	A', B
7	4←7	A', B
8	1←3	A', B
9	5←8	C, X, K
10	2←6	C, X, K
11	3←7	C, X, K
12	1←4	C, X, K
13	4←5	Comb.
14	3←6	Comb.
15	2←7	Comb.

The resulting matrices have the same form as the ABK ones but the definitions of the elements are different (see Table I). The $AA'K$ energy levels and wave functions are also given in Table I. It is evident that one of the foregoing procedures should yield more accurate results than when second order perturbation is applied directly to the original ABC or $AA'C$ matrices.

In the ABC iterative method as in the ABK (or $AA'K$) method the derived energy levels themselves, instead of the transitions, are used in order to solve for the coupling and shielding constants. Not only are the energy levels more accurately determined by the sum rule—viz., the sums of the various transitions connecting two energy levels ($\Delta F_z \geq 2$) by all possible paths must be equal—but also the iterative procedure is easier to apply. When the trial spin Hamiltonian is diagonalized by a transformation, $\mathbf{U}$,

$$\mathbf{U}^{-1}\mathbf{H}\mathbf{U}=\mathbf{\Lambda},$$

the eigenvectors (the columns of U) can be reapplied to the energy levels, Λ_{exp} derived from the spectrum. Schematically our procedure is as follows:

$$h_i\text{'s}, J_{ij}\text{'s} \rightarrow \mathbf{H} \rightarrow \mathbf{\Lambda}, \mathbf{U}$$

$$\mathbf{U}\mathbf{\Lambda}_{exp}\mathbf{U}^{-1}=\mathbf{H}_{exp}.$$

Now $\mathbf{H}_{exp}$ is a set of linear equations relating the various constants. These can be solved to determine new values for the constants. In the present study only the diagonal values $(\mathbf{H}_{exp})_{nn}$ have been used, but in principle all the elements could be used. Since the eigenvectors vary in a higher order than the eigenvalues, these new constants should converge to a consistent solution after several iterations. The iterative ABC method is easy to apply if an electronic computer is available. Otherwise the ABK (or $AA'K$) method may be the more convenient, but it may not always converge.

Finally it should be noted that the labeling of the energy levels and transitions (Tables I and II) differs slightly from that of reference 1. This was done in order to have the lines from an ABC system of nuclei increase in energy in both alphabetical and numerical order when $\sigma_A \gg \sigma_B \gg \sigma_C$ and $J_{AC} > J_{BC} > 0$, $J_{AB} > 0$. We have found such a scheme to be especially useful in computer programming for the analysis of spectra.

METHODS OF ANALYSIS

After an assignment has been made (even a partial assignment may be adequate) the energy levels can be derived by the sum rule and the fact that the sum of all the energy levels must vanish (trace $H=0$). In a complicated spin system when all the transitions can not initially be assigned, the energy level diagram [see, for example, Fig. 1(b)] can often be used to assign other transitions. Either an average solution or a least-squares solution can be used to derive the best values for these energy levels. The effect of an error in a given transition on the derived constants is minimized by this procedure. If the transitions themselves are used, small errors are more likely to be reflected in the derived constants. Also, the sum rule can be applied independently of the degree of perturbation, whereas the line separations can be influenced considerably by large perturbations. Finally, by the deviations of the spectrum calculated from these derived energy levels, a separation can be effected between the experimental errors and the mathematical errors in the approximation used.

In the ABK ($AA'K$) approximation the energy levels are first analyzed by the ABX ($AA'X$) approximation (see Tables I and II) from which initial values of the coupling and screening constants are obtained. These are then used to calculate the δ's and Δ's. The correction terms are applied to the derived experimental energy levels as necessary according to Table I. An ABX analysis is then repeated. This procedure can be iterated several times until a convergent solution is obtained. Finally, the corrected wave functions given in Table I and the relative intensities can be calculated.

In the ABC solution the ABK parameters (without iteration) can be used as initial values and the matrices can then be easily iterated to a consistent solution with the aid of an electronic computer. The relative intensities follow as before from the eigenvectors.

For the particular compounds studied here empirical data on screening constants suggest that the C proton in styrene oxide should have the smallest screening parameter, i.e., it should occur at a higher frequency (lower magnetic field) than either the A or B proton. Further, it has been observed[2] that in epoxides of the structure

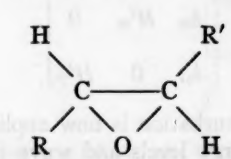

[2] C. A. Reilly and J. D. Swalen (to be published).

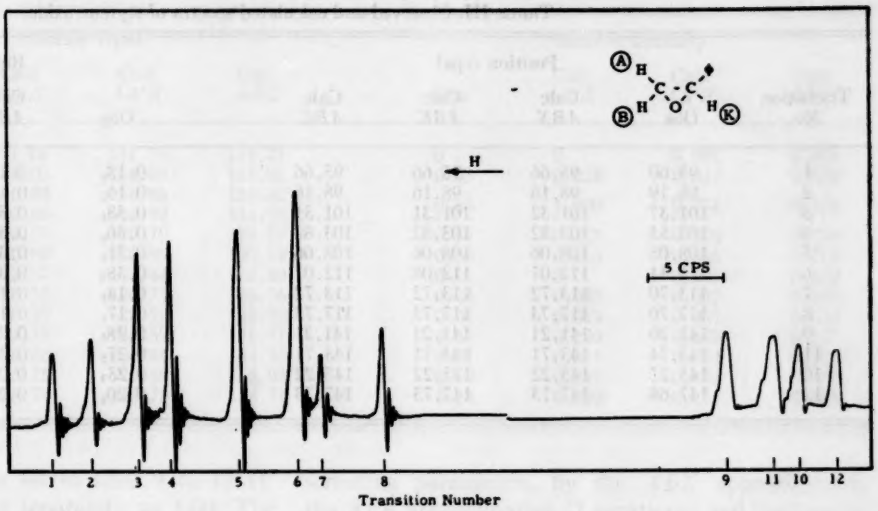

FIG. 1. (a) NMR spectrum of the *ABK* protons in styrene oxide.

the spin-spin coupling constant between the two protons trans to one another is about 2 cps. These two observations formed the bases for our analysis of the various spectra. Resonances from the *C* proton were readily located by the first criterion and resonances from the *A* proton (trans to *C*) were readily determined by the size of the two spin-spin coupling constants, J_{AC} and J_{BC} such that $J_{AC} \approx 2$ cps.

EXPERIMENTAL

A sample of each of the compounds: styrene oxide,[3] glycidonitrile, 1,2-epoxy-3-butanone, and glycidic acid, containing a few percent of tetramethylsilane (TMS) as an internal reference was degassed and sealed under vacuum in a precision bore pyrex tube (i.d. 0.1130 in, o.d. 0.1524 in.). Since glycidic acid is a solid at room temperature a saturated acetone solution containing TMS was used.

The high resolution NMR spectra were observed at about 25°C on a modified Varian Model V-4300 spectrometer equipped with a Field stabilizer and operated at 39.996 Mcps. The position of any resonance line in the spectra with respect to either the internal (TMS) or external (benzene) reference was obtained to approximately ±0.2 cps using a standard side band technique.[4] The separations between the individual lines in a spectrum were obtained from the separation between two side bands of known frequency recorded simultaneously. Such separations reported are average values of several recordings and are estimated to be accurate to ±0.05 cps.

In all the spectra, the *ABC* lines fell within the range 120 to 180 cps from the external reference, benzene. In styrene oxide, a resonance observed at −12.3 cps from benzene arises from the protons in the phenyl group. In glycidic acid a resonance observed at −146.0 cps from benzene is due to the proton in the carboxyl group and that observed at 187.7 cps is due to the solvent, acetone. In 1,2-epoxy-3-butanone a resonance observed at 191.9 cps from benzene is from the protons in the methyl group.

RESULTS

Styrene Oxide

The spectrum of the *ABC* protons of styrene oxide is shown in Fig. 1(a) and the energy levels are shown in Fig. 1(b). The spectrum is presented with increasing frequency (decreasing field) to the right. The position of each line in cps from the internal reference (TMS) was determined by averaging 12 separate recordings. The assignment corresponds to an *ABC* spectrum.

The peak height of each of the lines was measured. The set of lines, 1 to 8 (*A* and *B* resonances) was

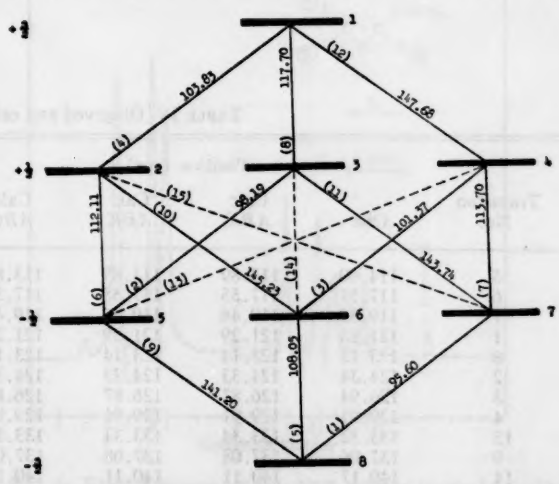

FIG. 1. (b) NMR energy level diagram (schematic) for styrene oxide; dashed lines represent combination transitions (not observed).

[3] Eastman Kodak Catalog No. 4789.
[4] J. T. Arnold and M. E. Packard, J. Chem. Phys. **19**, 1608 (1951).

TABLE III. Observed and calculated spectra of styrene oxide.

Transition No.	Position (cps) Obs	Calc *ABX*	Calc *ABK*	Calc *ABC*	Relative intensity Obs	Calc *ABX*	Calc *ABK*	Calc *ABC*
1	95.60	95.66	95.66	95.66	0.13_4	0.136	0.130	0.133
2	98.19	98.16	98.16	98.16	0.16_2	0.148	0.157	0.153
3	101.37	101.32	101.31	101.31	0.33_1	0.364	0.341	0.339
4	103.83	103.82	103.82	103.82	0.36_4	0.352	0.372	0.376
5	108.05	108.06	108.06	108.06	0.31_2	0.364	0.321	0.320
6	112.11	112.07	112.08	112.07	0.38_0	0.352	0.393	0.395
7	113.70	113.72	113.72	113.72	0.14_1	0.136	0.117	0.118
8	117.70	117.73	117.73	117.73	0.17_4	0.148	0.171	0.168
9	141.20	141.21	141.21	141.21	0.28_6	0.250	0.298	0.298
11	143.74	143.71	143.71	143.71	0.27_2	0.250	0.264	0.264
10	145.23	145.22	145.22	145.22	0.23_9	0.250	0.231	0.231
12	147.68	147.73	147.73	147.73	0.20_3	0.250	0.206	0.207

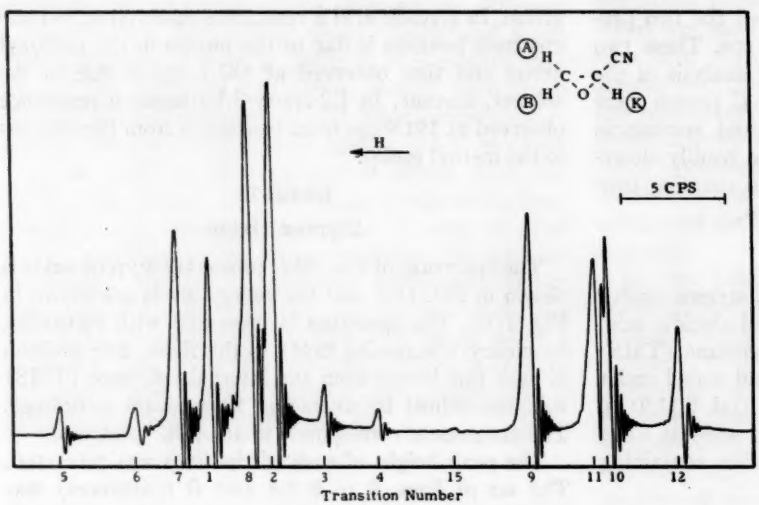

FIG. 2. NMR spectrum of the *ABK* protons in glycidonitrile.

TABLE IV. Observed and calculated spectra of glycidonitrile.

Transiton No.	Position (cps) Obs	Calc *ABX*	Calc *ABK*	Calc *ABC*	Relative intensity Obs	Calc *ABX*	Calc *ABK*	Calc *ABC*
5	114.00	113.89	113.89	113.89	0.05_1	0.065	0.050	0.056
6	117.51	117.55	117.55	117.55	0.04_7	0.030	0.045	0.046
7	119.37	119.48	119.48	119.47	0.35_0	0.434	0.361	0.351
1	121.23	121.29	121.29	121.29	0.34_2	0.434	0.343	0.340
8	123.13	123.14	123.14	123.14	0.54_9	0.461	0.539	0.542
2	124.34	124.33	124.33	124.33	0.55_4	0.461	0.567	0.558
3	126.94	126.87	126.87	126.88	0.07_2	0.065	0.065	0.070
4	129.91	129.91	129.91	129.91	0.03_6	0.039	0.036	0.037
15	133.32	133.34	133.34	133.33	0.00_4	0.002	0.005	0.007
9	137.06	137.08	137.08	137.08	0.32_6	0.250	0.355	0.354
11	140.17	140.11	140.11	140.11	0.26_2	0.248	0.234	0.232
10	140.77	140.74	140.74	140.74	0.26_2	0.248	0.230	0.234
12	143.78	143.77	143.77	143.78	0.16_3	0.250	0.169	0.171

TABLE V. Observed and calculated spectra of 1,2-epoxy-3-butanone.

Transition No.	Position (cps) Obs	Calc *AA'X*	Calc *AA'K*	Calc *ABC*	Relative intensity Obs	Calc *AA'X*	Calc *AA'K*	Calc *ABC*
1	...	111.03	111.16	111.21	0	0	0.001	0.003
2	113.90	114.02	114.03	114.01	0.03	0.038	0.047	0.034
5	116.74	116.80	116.68	116.62	0.85	1.000	0.774	0.766
3	116.74	116.80	116.92	116.98				
4	119.86	119.79	119.79	119.79	0.54	0.463	0.510	0.539
6	120.96	120.99	120.99	120.99	0.58	0.463	0.585	0.593
7	...	122.57	122.44	122.40	0	0	0.005	0.002
8	126.84	126.75	126.75	126.76	0.04	0.038	0.082	0.063
14	128.99	128.79	128.92	128.96	0.01	0.019	0.052	0.034
9	131.58	131.57	131.57	131.57	0.35	0.250	0.370	0.377
11	134.38	134.56	134.44	134.38	0.27	0.231	0.232	0.245
10	135.85	135.75	135.88	135.93	0.19	0.231	0.184	0.190
12	138.67	138.74	138.75	138.74	0.14	0.250	0.148	0.148

normalized to 2.00 and the set of lines 9 to 12 (*C* resonances) was normalized separately to 1.00. The *C* resonances were normalized separately because the broadening due to spin-spin coupling to the protons in the phenyl group would make peak height comparisons to the *A* and *B* resonances incorrect. The observed relative intensities were found by averaging a number of recordings and the estimated error is somewhat less than 0.02. In Table III the observed and calculated spectra are given. Although the positions of the lines could be accounted for by two different nonequivalent assignments, J_{AC} and J_{BC}, with the same signs or different signs, the intensities are much more in agreement when J_{AC} and J_{BC} have the same sign. Equivalent assignments could be obtained by positive or negative J_{AB} with positive or negative J_{AC}, respectively, so we have chosen both to be positive. Therefore all the spin-spin coupling terms are taken to be positive. These are given in Table VII along with the various screening parameters, by the *ABX* approximation, the *ABK* approximation (2 iterations) and the iterated *ABC* solution.

Glycidonitrile

In Fig. 2 the spectrum of glycidonitrile is shown. Whereas the NMR spectrum of styrene oxide was analyzed as an *ABC* one, the spectrum of glycidonitrile must be analyzed as a *BAC* one in order to have $J_{AC} \approx 2$ cps. It should also be noticed that there is an overlapping of the *A* and *B* patterns and that a combination line (15) is observable.

In Table IV the observed and calculated spectra are given. Here, as in the styrene oxide, the energy levels and line positions can be treated adequately by the *ABX* approximation, by the *ABK* approximation, or by the *ABC* solution; but notice the variation in J_{AC} and J_{BC} given in Table VII. These differences for the

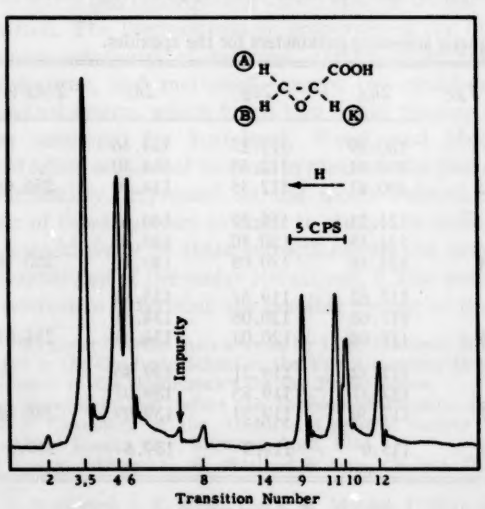

FIG. 3. NMR spectrum of the *ABK* protons in 1,2-epoxy-3-butanone.

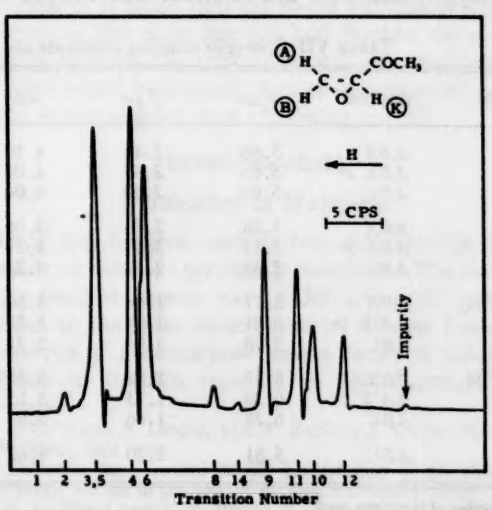

FIG. 4. NMR spectrum of the *ABK* protons in glycidic acid (dissolved in acetone).

TABLE VI. Observed and calculated spectra of glycidic acid.

Transition No.	Position (cps) Obs	Calc $AA'X$	Calc $AA'K$	Calc ABC
1	...	110.28	110.38	110.40
2	113.06	113.19	113.19	113.20
5	116.50	116.55	116.46	116.43
3	116.50	116.55	116.64	116.67
4	119.54	119.46	119.45	119.47
6	120.51	120.51	120.52	120.50
7	...	122.82	122.72	122.70
8	126.90	126.78	126.78	126.77
14	132.80	132.66	132.75	132.79
9	136.10	136.02	136.02	136.02
11	138.76	138.93	138.83	138.82
10	139.96	139.98	140.08	140.09
12	142.87	142.89	142.89	142.89

ABX approximation are about six times the experimental uncertainty. Furthermore, it is evident from the intensities that the ABK approximation is a substantial improvement over the ABX approximation. A second assignment, similar to that in styrene oxide, was made, but it did not agree with the observed intensities satisfactorily and is not included in the table.

1,2-Epoxy-3-butanone

The spectrum of 1,2-epoxy-3-butanone is shown in Fig. 3. At first glance the pattern in Fig. 3 bears little resemblance to the ABC (Fig. 1) pattern or the BAC (Fig. 2) pattern. Evidently there is more overlapping in the A and B portions of the spectrum. A successful analysis of this spectrum, given in Table V, was finally made by assuming that transitions 1 and 7 were too weak to be observed and also that transitions 3 and 5 overlapped and were not resolved. The derived constants are given in Table VII. Notice also the combination line (14) observed in this spectrum.

Glycidic Acid

The spectrum of glycidic acid is shown in Fig. 4. The portion shown in this figure resembles that of 1,2-epoxy-3-butanone and the analysis followed in a similar manner.

The results are given in Tables VI and VII. An impurity line in this spectrum added to the complexity of analysis at first but clearly did not belong to the glycidic acid spectrum. Its origin is unknown. The intensities were calculated for this spectrum but since they give no additional information they are not included.

DISCUSSION

In Table VII are given the best values for the NMR molecular parameters derived from the energy levels by the ABX approximation, by the ABK (or $AA'K$) approximation, and by the iterated ABC solution. The ABC values for the indirect spin-spin coupling constants, J_{ij}, are probably accurate to ± 0.05 cps and the screening constant parameters to ± 0.2 cps. It is evident that coupling constants derived from a spectrum may be in error by a substantial amount unless great care is taken to use an adequate approximation in the analysis.

Corresponding coupling constants are approximately the same from molecule to molecule but the sum $(J_{AC}+J_{BC})$ shows less variation than either J_{AC} or J_{BC}.

It is of considerable interest that the cis coupling constant in epoxides is greater than the trans one. This is opposite to the results found experimentally[5,6] and estimated theoretically[7] for olefins. The present results are undoubtedly a reflection of the different type of bonding in the epoxides and appear to be consistent

TABLE VII. Spin-spin coupling constants and nuclear magnetic screening parameters for the epoxides.

R	Approx	J_{AB}	J_{AC}	J_{BC}	$J_{AC}+J_{BC}$	$2h_A$	$2h_B$	$2h_C$	$2(h_B+h_C)$
ϕ	ABX	5.66	2.42	4.10		100.39	112.25	144.46	
	ABK 2[a]	5.65	2.49	4.04		100.41	112.38	144.30	
	ABC	5.65	2.49	4.04	6.53	100.41	112.38	144.30	256.68
CN	ABX	5.58	2.84	3.86		124.23	119.89	140.43	
	ABK 3[a]	5.53	2.47	4.27		124.35	120.10	140.10	
	ABC	5.53	2.51	4.23	6.74	124.36	120.08	140.10	260.18
$COCH_3$	ABX	5.77	1.64	5.54		117.62	119.57	135.16	
	$AA'K$ 1[a]	5.81	1.91	5.23		117.66	120.08	134.61	
	ABC	5.78	1.95	5.21	7.16	117.68	120.03	134.64	254.67
COOH	ABX	6.27	1.54	5.33		117.32	119.21	139.46	
	$AA'K$ 1[a]	6.29	1.73	5.13		117.37	119.55	139.07	
	ABC	6.28	1.86	5.01	6.87	117.36	119.53	139.09	258.62
Av.	ABC	5.81	2.20	4.62	6.83	115.0	118.0	139.5	257.5

[a] Number of iterations used.

[5] H. M. McConnell, C. A. Reilly, and A. D. McLean, J. Chem. Phys. **24**, 479 (1956).
[6] S. Alexander, J. Chem. Phys. **28**, 358 (1958).

with theoretical estimates[7] on the basis of an eclipsed "ethane-like" model.

It was anticipated that the screening constant parameter for nucleus C would be most affected by changing the R group. However, the parameter for nucleus A is most affected. Furthermore, it appears that the R group has the opposite effect on the screening parameters for nuclei B and C in that the sum of these two parameters, $2(h_B+h_C)$ is somewhat more constant than the individual ones.

[7] M. Karplus, J. Chem. Phys. **30**, 6, 11 (1959).

ACKNOWLEDGMENT

We wish to thank G. B. Payne of this laboratory for preparing the samples of glycidonitrile, 1,2-epoxy-3-butanone, and glycidic acid.

THE JOURNAL OF CHEMICAL PHYSICS VOLUME 32, NUMBER 5 MAY, 1960

Refractive Index and Dispersion of the Benzene-Carbon Tetrachloride System*†

SCOTT E. WOOD, *Department of Chemistry, Illinois Institute of Technology, Chicago 16, Illinois*

AND

CHARLES H. MASLAND, 3RD,‡ *Department of Chemistry, Yale University, New Haven, Connecticut*

(Received December 9, 1959)

The refractive indices of the benzene-carbon tetrachloride system have been measured at seven different wavelengths in the visible region. These indices show only slight departure from linearity in the mole fraction. The molar refractions, calculated according to the Lorentz-Lorenz equation, are not additive in the mole fraction. Moreover, no simple relation between the molar refractions and the frequency of the light source is obtained.

THE properties of liquid nonpolar solutions are determined in a large measure by the London dispersion forces operating between the molecules in the solution. These forces in turn are dependent upon the electronic polarizability of the molecules. In solutions containing polar as well as nonpolar molecules, the attractive forces would be mainly the London dispersion forces and the dipole-dipole forces. From our present knowledge the forces between the induced dipole in a molecule and the dipole in another molecule would be of much less consequence unless specific interactions occurred. The thermodynamic properties of the binary systems composed of benzene, carbon tetrachloride, cyclohexane, and methanol (except the cyclohexane-methanol system which forms two liquid phases) have been measured by Scatchard, Wood, and Mochel.[1] It therefore seemed of interest to measure the electronic polarizability, expressed as the molar refraction, of some of these systems in order to study the additivity or nonadditivity of these refractions. In the event of nonadditivity of the molar refractions, it also would be of interest to determine the possible change of the frequency of the dispersion electrons and of the number of dispersion electrons with composition. Therefore, the refractive indices of the benzene-carbon tetrachloride system and of the benzene-methanol system have been measured at seven wavelengths in the visible range at 25°.

This paper reports the refractive indices of the benzene-carbon tetrachloride system at approximately each eighth mole fraction. The molar refractions have been calculated according to the Lorentz-Lorenz equation. It is found that the molar refractions are not additive in the mole fraction and further, no simple relation between the refractions and the frequency of the light source is obtained. A more extensive discussion of the results is given in the following paper.[2]

EXPERIMENTAL[3]

Purification of Materials

Both the benzene and carbon tetrachloride were purified by methods previously described.[4] The density of the purified benzene was 0.87366 g/cc at 25° in comparison to the same value given in *Selected Values of Properties of Hydrocarbons*[5] and a range of values of 0.87360 to 0.87376 reported in the literature. Its

* This paper is taken from a thesis by C. H. Masland, 3rd, submitted to the Graduate School of the Yale University in partial fulfillment of the requirements for the Ph.D. degree.

† Presented in part before the Division of Physical and Inorganic Chemistry of the American Chemical Society at its meeting at Kansas City, Missouri, April, 1954.

‡ Present address: C. H. Masland & Sons, Carlisle, Pennsylvania.

[1] G. Scatchard, S. E. Wood, and J. M. Mochel, J. Phys. Chem. **43**, 119 (1939); J. Am. Chem. Soc. **61**, 3206 (1939); **62**, 712 (1940); **68**, 1957, 1961 (1946).

[2] S. E. Wood, S. Langer, and R. Battino, J. Chem. Phys. **32**, 1389 (1960), this issue.

[3] Extensive experimental details are given in C. H. Masland, 3rd, thesis, on file in the library of Yale University (1950).

[4] S. E. Wood and J. P. Brusie, J. Am. Chem. Soc. **65**, 1891 (1943).

[5] Natl. Bur. Standards Circ. No. **C461**, (1947).

TABLE I.

	Wavelength mμ	Frequency ($\times 10^{-14}$ sec^{-1})
H α	656.28	4.5678
Na D'	589.59	5.0845
Hg α′	579.07	5.1769
Hg β	546.07	5.4897
H β	486.13	6.1666
Hg γ	435.83	6.8783
Hg δ	404.67	7.4079

refractive index for the Na D line at 25° was 1.49792 in comparison to 1.49790 reported in footnote 5 and 1.49794 given by Hubbard.[6] The density of the purified carbon tetrachloride was 1.58427 g/cc at 25° in comparison to a range of values of 1.5841 to 1.5848 reported in the literature. Its refractive index at 25° for the Na D line was 1.45729 in comparison to 1.45732 reported by Hubbard.[6]

Preparation of Solutions

Solutions were prepared by weight at approximately each eighth mole fraction in special bottles described by Wood and Brusie.[4] All buoyancy corrections were made for each weighing, and corrections also were made for the weight of each component in the vapor phase after the two liquids were mixed. Two series of determinations were made, one in which benzene was always weighed first, and the other in which carbon tetrachloride was weighed first. In this manner a check was made on the accuracy of the corrections. Satisfactory duplication of the results were obtained.

Apparatus

A Pulfrich refractometer (Carl Zeiss, Model No. 299669) was used to measure the refractive indices. In order to obtain the highest precision extreme care had to be taken in adjusting the optical system and in illuminating the scales. This included careful placing of the light sources and focusing of the light onto the prism, adjustment of the aperture of the telescope to reduce the amount of light scattered from the mat surface of the prism to a minimum, and the construction of a device which would necessitate the placing of the eye always in the same position relative to the eyepiece of the telescope in order to reduce the effect of chromatic parallax.[7] In addition, a special device was constructed which allowed careful adjustment of the slit width of the light prior to entering the cell and which could be rapidly opened to obtain full illumination of the cross hairs when necessary. The illumination of the room was always maintained at the same level for all measurements. The graduations on the circle and the reference mark adjacent to the circle and the scale of the micrometer screw were illuminated by small 6-v bulbs. The setting of the circle graduations to the reference mark was also aided by a three power lens.

The refractometer was calibrated in two steps. First, each half degree interval from 30 to 68°, the range used in the measurements, was compared with the same interval of the micrometer screw. The values scattered about the mean and showed no trend. The value of each half-degree interval was then adjusted so that the mean of all the values was 30 min. The units at this point are arbitrary. The zero reading of the normal to the prism, the deviations of the graduations from 0° to 30°, and the factor for conversion from the arbitrary units to true degrees or radians were determined collectively by measuring the refractive index of samples of toluene, methylcyclohexane, and 2,2,4-trimethylpentane. These substances were obtained from the National Bureau of Standards and their refractive indices were certified by the Bureau. Four different wavelengths were used in this calibration. The certified values were relative to air and as a consequence the refractive indices reported in this paper are also relative to air.

The index of the prism at 25° and the seven wavelengths used in the experiment were determined from the indices at 20° furnished with the instrument. The temperature dependence of the refractive indices for a medium flint glass[8] were used to change the indices of the prism from 20° to 25°.

A sodium arc and a mercury arc, both obtained from George W. Gates & Company, and a hydrogen discharge tube were used to obtain the seven different lines used in the experiments. The hydrogen arc was constructed of Pyrex glass No. 7740 and consisted essentially of a 2-liter flask and a side arm in which the discharge was formed. The 2-liter flask was used to furnish a ballast and help maintain the pressure of hydrogen in the flask constant during the discharge.[9] Two aluminum electrodes were sealed to the side arm and perpendicular to its axis. The discharge in the side arm between the two electrodes was confined to a 3-mm tube about 3 cm long. A relatively intense source of light was thus formed in the small tube. This light source was viewed from the end through a glass window. The hydrogen was purified by passing it through activated charcoal contained in a trap which was held at liquid nitrogen temperatures.

The designation of the seven lines used in this research together with their wavelengths[10] and frequencies are given in Table I. The Na D, Hg α, Hg γ, and Hg δ lines are actually composed of two or three lines. The choice between the particular lines was determined by the appearance of the critical edge of the line observed in the telescope of the refractometer and also by the relative intensity of the lines. The critical edge of the

[6] J. C. Hubbard, Phys. Rev. I, **30**, 761 (1910).
[7] J. Guild, Proc. Phys. Soc. (London) **29**, 311 (1917).
[8] L. W. Tilton, J. Research Natl. Bur. Standards **17**, 389 (1936).
[9] J. Guild, Proc. Phys. Soc. (London) **28**, 60 (1915).
[10] H. Kayser and R. Ritschl, *Tabelle der Hauptlinien der Linienspectren aller Elemente nach Wellenlange geordnet* (Springer-Verlag, Berlin, Vienna, 1939), 2nd ed.

Na *D* line was extremely sharp and did not appear to be a superposition of two lines. Consequently the wave length of the Na *D'* line was used. The Hg α line consists of three lines, Hg α, Hg α', and Hg α''. Two lines were apparent in the field of the telescope and the upper one was used. It was assumed to be the Hg α' line because the Hg α line has a very low intensity. The lower of the two Hg γ lines has a lower intensity than the other and was assumed to be hidden in the trailing edge of the upper line. The critical edge for the Hg δ line was rather indistinct and it was assumed that the two lines were essentially superimposed. Here the average of the wavelengths of the two lines was used.

The temperature of the cell, and the prism, was controlled by pumping water through them from a thermostated water bath. The thermoregulator was placed in the stream of water going to the refractometer so that the temperature of the cell rather than that of the bath would be controlled. The temperature was $24.99\pm0.02°$.

Operation

Preliminary experiments with solutions showed that the refractive index of the solution in the cell changed with time. The change was rapid at first and then became essentially linear. The first change was probably due to the change of the temperature of the solution as it approached thermal equilibrium. The second change was probably caused by evaporation of the solution even though the cell was closed by a flat plate or by solution of the cement[11] used to seal the cylinder to the prism from the cell. A standard procedure was adopted to correct for these changes. After the solution was placed in the cell, the micrometer screw was adjusted and the telescope and circle were clamped in position so that the position of the critical edges of all seven lines could be determined on the scale of the screw. One set of readings consisted of determining the position of the seven critical edges in the order of the hydrogen, sodium, and mercury lines. The time was recorded to the nearest minute at the beginning and at the end of a set. First, four sets were determined with a rest of a minute between each set. Then twelve more sets were determined in groups of three with ten minutes rest between each group. The rest periods were necessary to reduce eye fatigue. These sixteen readings for each critical edge were then extrapolated to zero time. The first few points which did not seem to lie on the line were eliminated in the extrapolation. The extrapolated value of the position of the critical edge was then taken to be the position of the critical edge for the original solution placed in the cell at the temperature of the cell.

After a considerable rest period (usually overnight), the angle between the position of the critical edge and the normal to the prism was determined. The approximate angle was read from the circle (to the nearest half degree). Then the micrometer screw reading corresponding to each half degree mark of the circle on each side of the position of a critical edge was determined. Ten observation were made on each mark and the average used in the calculations. The fractional part of the half degree corresponding to each critical edge was then determined by interpolation. In this way the sensitivity of the screw was determined at each half degree used in the calculations.[12]

Accuracy

A very careful and detailed study of the accuracy of the experimental measurements led to an estimate of the precision of the mole fraction of ±3.7–8.4×10^{-5} except for the first three solutions. There, the estimate is ±10–18×10^{-5}. For the refractive index, the estimated precision is ±6–15×10^{-5}. The root-mean-square deviation of the experimental values of the refractive index from smoothed values, which will be discussed in the next section, is $\pm9\times10^{-5}$. The accuracy of the measurements on the H β, Hg γ, and Hg δ lines is somewhat less than on the other lines because of the low intensity of these lines when observed against a dark background.

RESULTS AND DISCUSSION

The experimental values of the refractive indices of the pure components and the solutions are given in Table II. The first column gives the mole fraction of carbon tetrachloride. The second column gives the molar volumes used in calculating the molar refractions.[4] The other columns give the refractive indices at the seven frequencies. At each wavelength the refractive indices are almost linear in the mole fraction but each curve has a slight curvature, concave downward. These values are in excellent agreement with those of Hubbard[6] at four common wavelengths and of Scatchard and Ticknor[13] at the Na *D* line.

The molar refraction was calculated from these values and the data of Wood and Brusie[4] on the volume of mixing by the Lorentz-Lorenz equation. These values were then fitted to equations in terms of the mole fraction and frequency. The smoothed values of the refractive indices mentioned in the previous section were calculated back from these equations. According to the simple theory, the molar refraction should be additive in the mole fraction, but the deviation from linearity was even more marked for these values than for the refractive indices themselves and were definitely functions of both the mole fraction and frequency.

[11] The cement was made by slowly dissolving 3 g of gelatin in a solution of $K_2Cr_2O_7$ in 15 cc of water at 60°. The seal formed between the cylinder and the prism with this cement was irradiated for over 15 hr with the mercury arc placed about 1 in. away.

[12] The micrometer screw moves tangentially to the circle. Consequently, the sensitivity of the screw is not uniform over its entire length for any single clamped position of the circle. See J. Guild, Proc. Phys. Soc. (Lundon) **30**, 166 (1918); and L. W. Tilton, J. Research Natl. Bur. Standards **30**, 322 (1943).

[13] G. Scatchard and L. B. Ticknor, J. Am. Chem. Soc. **74**, 3724 (1952).

TABLE II. Refractive indices of benzene-carbon tetrachloride solutions at 25°.

Mole fraction, x_1, CCl_4	Molar volume, $\tilde{V}$, cc	Frequencies ($\times 10^{-4}$ sec^{-1}) 4.5678	5.0845	5.1769	5.4897	6.1666	6.8783	7.4079
		Refractive indices						
0.00000	89.403	1.49330	1.49792	1.49880	1.50200	1.50986	1.51975	1.52813
0.13823[a]	90.480	1.48807	1.49241	1.49324	1.49626	1.50367	1.51295	1.52079
0.14036[b]	90.496	1.48797	1.49231	1.49315	1.49616	1.50356	1.51282	1.52062
0.25793[b]	91.402	1.48349	1.48766	1.48845	1.49128	1.49824	1.50698	1.51436
0.26069[a]	91.423	1.48335	1.48755	1.48835	1.49112	1.49807	1.50683	1.51420
0.37053[b]	92.267	1.47911	1.48304	1.48378	1.48644	1.49305	1.50131	1.50816
0.37326[a]	92.288	1.47899	1.48289	1.48364	1.48637	1.49297	1.50119	1.50805
0.49852[b]	93.252	1.47421	1.47786	1.47858	1.48106	1.48721	1.49487	1.50123
0.50362[a]	93.291	1.47386	1.47755	1.47822	1.48075	1.48687	1.49448	1.50080
0.61484[b]	94.150	1.46969	1.47308	1.47376	1.47609	1.48188	1.48901	1.49488
0.61580[a]	94.157	1.46967	1.47293	1.47355	1.47593	1.48165	1.48871	1.49461
0.74509[b]	95.155	1.46456	1.46777	1.46839	1.47054	1.47579	1.48232	1.48769
0.74686[a]	95.169	1.46437	1.46756	1.46818	1.47031	1.47559	1.48210	1.48741
0.85739[b]	96.019	1.46022	1.46313	1.46367	1.46571	1.47061	1.47661	1.48150
0.86429[a]	96.072	1.45989	1.46281	1.46334	1.46536	1.47023	1.47619	1.48104
1.00000	97.103	1.45460	1.45729	1.45959	1.45959	1.46400	1.46932	1.47357

[a] Carbon tetrachloride weighed first in making solutions.
[b] Benzene weighed first in making solutions.

The theory of dispersion of the refractive index[14] yields an equation of the form

$$\tilde{R}=\sum_i A_i/(\nu_i^2-\nu_0^2), \qquad (1)$$

where each A_i is proportional to the oscillator strength associated with the characteristic frequency ν_i. The symbol ν_0 represents the frequency of the light used. If only one term of the sum is predominate, a linear equation of the form

$$1/\tilde{R}=(\nu_i^2/A_i)-(\nu_0^2/A_i)$$

can be derived. When the reciprocal of the molar refraction, R, is plotted against ν_0^2, a straight line is obtained for carbon tetrachloride. However, for benzene and for the solutions a curve is obtained. Attempts were made to fit the curve with a two term equation of the form of Eq. (1), but the results were physically meaningless. The second term appeared as a small correction term to the first term and furthermore, the characteristic frequency of the second term was imaginary!

Certainly the Lorentz-Lorenz equation is not strictly applicable to the liquid phase. In view of this and the nonlinearity of the molar refraction with mole fraction, additional calculations using the Böttcher equation have been done but further discussion is postponed to the following paper.

[14] H. Eyring, J. Walter, and G. E. Kimball, *Quantum Chemistry* (John Wiley & Sons, Inc., New York, 1944).

Refractive Index and Dispersion of the Benzene-Methanol System*†

SCOTT E. WOOD, SIDNEY LANGER, AND RUBIN BATTINO
Department of Chemistry, Illinois Institute of Technology, Chicago 16, Illinois

(Received December 9, 1959)

The refractive indices of the benzene–methanol system have been measured at 25° at seven wavelengths in the visible region. The electronic polarizability of benzene, methanol, and carbon tetrachloride have been calculated from the refractive indices of this system and those of the benzene-carbon tetrachloride system by use of the Böttcher equation. The data are then used to calculate the molar electronic polarizations of the carbon tetrachloride-methanol system which are found to be in good agreement with experimentally determined values. These results show that, within the experimental error, the electronic polarizabilities of the three components are independent of the composition and hence of the environment. The electronic polarizabilities of the three substances are found to follow a dispersion equation with only one term.

THIS paper is a continuation of the preceding paper.[1] The refractive indices of solutions of benzene and methanol have been measured at 25° at approximately each eighth mole fraction and the same seven wavelengths in the visible region. The electronic polarizability of the solutions, calculated according to the Lorentz-Lorenz equation, showed marked deviations from additivity in terms of the mole fraction. Moreover, the dispersion of the polarizability of benzene and methanol as well as the solutions were not simple functions of the frequency. Because of these difficulties and the fact that the Lorentz-Lorenz equation is not strictly applicable to the liquid phase, an equation developed by Böttcher[2] has been used to analyze the data for this system and for the benzene-carbon tetrachloride system. It is found that the electronic polarizability of the three components remain the same in the solutions and are independent of the composition. Also the dispersion of the polarizability is a simple function of the frequency.

EXPERIMENTAL[3]

Purification of Materials

The benzene was purified by fractional crystallization and distillation as described in the previous paper.[1] In addition, the purified product was allowed to stand over calcium hydride under a vacuum for several hours. The benzene was then distilled into small ampoules which were sealed from the vacuum line when full. The amount of benzene contained in each ampoule was just sufficient to make a solution for a single determination of the refractive indices. Two samples were taken, one at the beginning of the distillation of the dried benzene and the second at the end of the distillation, for the determination of the density of the benzene. The average value of the density of the two samples was 0.87364 g/cc at 25°; the individual densities of the two samples agreed within 0.00002 g/cc. The refractive index of the purified material was 1.49793 at 25° for the Na *D* line. These values are in good agreement with those obtained by Masland.[1]

The methanol was purified by fractional distillation in an atmosphere of dry nitrogen in order to prevent the absorption of water from the air. It was further dried by allowing it to stand over calcium hydride under a vacuum for several hours. The methanol was then distilled into small ampoules which were sealed under vacuum. Two samples for density measurements were also obtained. The difference between the two densities was 0.00008 g/cc. The average density was 0.78660 g/cc at 25°. This compares to a range of values from 0.78651 to 0.78668, found in the literature. The refractive index for the Na *D* line at 25° of the purified product was 1.32652 compared with 1.32657, a value determined[4] at 15° and then corrected to 25°.

The solutions were prepared in the manner described in the preceding paper.[1]

Apparatus

A Bellingham and Stanley critical angle refractometer (1948 model, No. 37221) was used for the refractometric measurements. This refractometer is similar in principle to the Pulfrich refractometer. It has a 60° prism rather than a 90° one and is constructed so that the observing telescope can be rotated through an angle of about 180°. By this means the angle of the prism and the refractive index of the glass can be measured directly. The observing telescope is attached to a circular glass plate on which the circular scale is engraved. The

* This paper is taken from a thesis by Sidney Langer submitted to the Graduate School of the Illinois Institute of Technology in partial fulfillment of the requirements for the Ph.D. degree.

† The partial support of the National Science Foundation and U.S. Atomic Energy Commission is gratefully acknowledged. The data and initial calculations were presented before the Division of Physical Chemistry of the American Chemical Society at its meeting at Kansas City, Missouri, April, 1954, and the final calculations were presented at the meeting in Boston, Massachusetts, April, 1959.

[1] S. E. Wood and C. H. Masland, 3rd, J. Chem. Phys. 32, 1385 (1960) this issue.

[2] C. J. F. Böttcher, *The Theory of Electric Polarization* (Elsevier Publishing Company, Amsterdam, 1952), p. 177.

[3] Extensive experimental details are given in Sidney Langer, thesis, on file in the library of Illinois Institute of Technology.

[4] A. G. Dorochewski, Zhur. Russ. Fiz. Chim. Obshchestra 43, 66 (1911).

readings of the scale are made by means of a reading telescope in which two images of the scale, 180° apart, are seen adjacent to each other. The readings on each image are made separately. Two values of any measured angle are thus obtained from these readings and the average of these two values is used as the actual value. Any eccentricity of the scale tends to be cancelled by this method. The cell was constructed by placing a glass cylinder, ground to fit the curved portion of the prism, upon the prism. A heavy stopcock grease was used to hold the cylinder in place. (The cement used for the benzene-carbon tetrachloride system was attacked by the liquids of this system.) The housing of the prism was constructed as a water jacket. Another water jacket was furnished which fit around and over the cylinder. This jacket carried a water-cooled finger which dipped inside the cell. A rather large space existed between the jacket and cylinder, which allowed excessive evaporation to take place. Consequently, a stainless steel collar was fashioned which fit snugly within the water jacket and over the cylinder so that evaporation losses were reduced to a minimum. The instrument is a precision instrument but unfortunately the equation used to calculate the refractive index from the observed angles is more sensitive to errors than the corresponding equation for the Pulfrich refractometer.

The refractometer was calibrated in a manner similar to that described previously.[1] Each half-degree interval of the circular scale was compared to the same section of the micrometer screw. This comparison showed that each interval was identical in size within the experimental accuracy. The sensitivity of the micrometer screw in terms of the change of the reading of the scale per unit of angle of rotation of the circle was found to be uniform over the length of the scale used in the measurements. The units of the micrometer scale and of the circular scale were also proved to be identical within the experimental reproducibility of the measurements. Finally, the angle of the prism and the refractive indices of the prism at the seven wavelengths were measured directly.[5]

The sodium and mercury light sources and all the wavelengths were the same as those used for the study of the previous system. A new hydrogen arc, similar to the previous one, was constructed of Vycor glass (No. 7900). Cylindrical electrodes were placed within the side tube, in which the arc was formed, so that the axes of the cylinders coincided with the axis of the tube and of the arc.

[5] The refractive indices of the three standard liquids used in the preceding paper were also determined with this instrument. However, the equations used to determine the angle of the prism and the conversion factor from arbitrary units to degrees from these measurements were not sensitive to the unknown quantities. Consequently, the angle of the prism was measured directly. Also, since the entire circle was graduated and each half-degree interval of the circle was the same for that part of the circle which was calibrated, it was assumed that the uniformity of the divisions was the same in the entire circle and consequently each half-degree interval was a true half-degree.

The temperature of the prism and cell was controlled by pumping water from a thermostat through the water jackets surrounding the cell and prism and back to the thermostat. A specially constructed thermometer well was placed in the return line just after the refractometer. The temperature of the water was regulated at this point at 25.00±0.025°.

As in the previous study precautions were taken against parallax in the observing and reading telescopes of the refractometer. It was also found necessary to design a special shutter to regulate the width of the line observed in the telescope and to reduce scattered and reflected light to a minimum.

The refractometer was housed in a walk-in booth. All settings of the refractometer were made in total darkness and the circular scale and the scale of the micrometer screw were illuminated by small pilot lights only at the time of taking readings.

Operation

The procedure for measuring the refractive indices was somewhat similar to that previously used. After the solutions had been prepared and a sample placed in the cell, ten successive determinations of the position of the normal to the prism face were made. The observing telescope was then clamped in a position so that the critical edges of all seven lines could be measured on the micrometer screw. Four successive sets of readings consisting of five settings of the micrometer screw on each critical edge were made at intervals of about 20 min. Within this time ten settings of the micrometer screw on two half-degree marks on the circle (180° apart) were also made. After the position of the critical edge had been determined, the position of the normal was again determined. The average of the two normal positions was used in the subsequent calculations.

In order to determine the position of a critical edge at the time that the sample was placed in the cell when no evaporation or change of composition could have taken place, the means of the four settings at each 20-min interval were plotted against the time. The four points usually lay close to a straight line. The experiment was repeated with a freshly prepared sample if this was not the case. The value of the position of the critical edge was then obtained by numerical extrapolation.

Accuracy

Again a very careful and detailed study was made of the experimental measurements to obtain an estimate of their precision. For the mole fraction a precision of $\pm 1\times10^{-4}$ is expected. For the refractive index, the estimated precision is $\pm 1.4\times10^{-4}$. The root-mean-square deviations of the refractive indices from smoothed values, which will be discussed in the next section is $\pm 1.6\times10^{-4}$. The values of the mole fractions and the refractive indices reported in Table I (see the

TABLE I. Refractive indices of benzene–methanol solutions at 25°.

Mole fraction, x_2, methanol	Molar volume, $\tilde{V}$, cc	Frequencies ($\times 10^{-14}$ sec^{-1}) 4.5678	5.0845	5.1769	5.4897	6.1666	6.8783	7.4079
		Refractive indices						
0.00000	89.405	1.49331	1.49793	1.49889	1.50208	1.51000	1.51965	1.52858
0.12988[a]	83.112	1.48257	1.48696	1.48788	1.49096	1.49855	1.50782	1.51635
0.13461[b]	82.882	1.48174	1.48606	1.48681	1.48995	1.49761	1.50679	1.51491
0.25397[b]	77.067	1.47033	1.47466	1.47529	1.47829	1.48559	1.49440	1.50236
0.26234[a]	76.659	1.46926	1.47353	1.47444	1.47731	1.48445	1.49315	1.50129
0.36777[b]	71.519	1.45751	1.46148	1.46220	1.46506	1.47179	1.48013	1.48765
0.36893[a]	71.462	1.45725	1.46148	1.46194	1.46474	1.47149	1.47951	1.48720
0.49280[b]	65.419	1.44088	1.44446	1.44523	1.44745	1.45398	1.46149	...
0.49842[a]	65.145	1.43988	1.44350	1.44437	1.44677	1.45266	1.46039	1.46717
0.61696[b]	59.363	1.42106	1.42426	1.42493	1.42722	1.43280	1.43952	1.44586
0.62142[a]	59.146	1.42024	1.42348	1.42410	1.42638	1.43185	1.43876	1.44497
0.74600[b]	53.077	1.39580	1.39862	1.39931	1.40111	1.40587	1.41148	1.41682
0.74890[a]	52.936	1.39518	1.39801	1.39859	1.40054	1.40518	1.41089	1.41616
0.74979[b]	52.893	1.39482	1.39763	1.39819	1.40017	1.40466	1.41037	1.41571
0.87456[b]	46.824	1.36429	1.36651	1.36695	1.36852	1.37228	1.37656	1.38061
0.87755[a]	46.679	1.36345	1.36563	1.36604	1.36766	1.37120	1.37565	1.37993
1.00000	40.735	1.32496	1.32652	1.32685	1.32792	1.33034	1.33320	1.33613

[a] Methanol weighed first in making solutions.
[b] Benzene weighed first in making solutions.

next section) are given to five figures to protect the accuracy in any calculations. As in the previous system, the accuracy of the measurements on the Hβ, Hgγ, and Hgδ lines is somewhat less than on the others because of the low intensity of these lines when observed against a dark background.

RESULTS AND DISCUSSION

The experimental values of the refractive indices of the pure components and the solutions are given in Table I. The entries for the pure substances are averages of three determinations. The first column gives the mole fraction of methanol.[6] The second column gives the molar volumes used in calculating the molar refractions or polarizations. The other columns give the refractive indices at the seven frequencies. The observed values for the Na D line are in good agreement with the values reported by Scatchard and Ticknor[7] and Pesce and Evdokimoff.[8] The refractive indices of the solutions are not additive in the mole fractions but show positive deviations.

The molar refractions were first calculated by the Lorentz-Lorenz equation. This equation predicts additivity of the refractions in terms of the mole fractions. However, the results show a slight positive deviation from additivity. Therefore a deviation function was set up in terms of the mole fraction. The coefficients of this equation were determined by the method of least squares. These coefficients were then in turn determined as functions of the frequency. Smooth values of the refractive indices were calculated from the resulting equations. The root-mean-square deviation of the smooth values from the observed values has been reported in the preceding section.

The dispersion of the molar refraction of the pure substances is given by an equation of the form

$$\tilde{R}=\sum_i[A_i/(\nu_i^2-\nu_0^2)], \qquad (1)$$

where the sum is to be taken over all the characteristic frequencies ν_i. If only one term of the sum predominates, then the reciprocal of the molar refraction becomes a linear function of the square of the frequency of the light. This function shows a slight curvature, concave downward, for the pure substances. The behavior of benzene is exactly the same as that observed in the previous paper.

The Lorentz-Lorenz equation is not strictly applicable to the liquid phase. It is therefore a question whether the nonadditivity of the molar refractions and the nonlinearity of the dispersion is characteristic of the system or a result of the use of the Lorentz-Lorenz equation. Consequently it was decided to use an equation developed by Böttcher[4] to calculate the electronic polarizability of the pure substances and the solutions. The difference between the two equations is that the reaction field of the immediate neighbors of any molecule is taken into account by Böttcher, while this field is assumed to be zero in the Lorentz-Lorenz equation. For light in the visible range, the Böttcher equation is

$$\tilde{P}_B=[(n^2-1)(2n^2+1)/9n^2]\tilde{V}=(4\pi N/3)\sum_i x_i\alpha_i^* \qquad (2)$$

where α_i^* is

$$\alpha_i^*=\frac{\alpha_i}{1-[\alpha_i(2n^2-2)/a_i^3(2n^2+1)]}. \qquad (3)$$

[6] The subscript 1 is used to represent benzene and the subscript 2 to represent methanol.
[7] G. Scatchard and L. B. Ticknor, J. Am. Chem. Soc. **74**, 3725 (1952).
[8] B. Pesce and V. Evdokimoff, Gazz. chim. ital. **70**, 723 (1940).

TABLE II. Calculated values of α and a^3 for benzene, methanol, and carbon tetrachloride.

Frequency ($\times 10^{-14}$ sec^{-1})	Polarizability ($\times 10^{24}$ cm^3) αC_6H_6	αCH_3OH	$\alpha_1 CCl_4$
4.5678	4.7120	1.7506	4.8902
5.0845	4.7135	1.7518	4.8915
5.1769	4.7135	1.7520	4.8917
5.4897	4.7143	1.7528	4.8924
6.1666	4.7156	1.7545	4.8941
6.8783	4.7165	1.7564	4.8957
7.4079	4.7168	1.7584	4.8968
a^3	3.523	1.179	3.563

The quantity $\bar{P}_B$ will be called the Böttcher molar polarization. In this equation $\bar{V}$ is the molar volume of the liquid; a_i is a parameter whose dimensions are in cm; and α_i is the electronic polarizability.

A least-squares method was used to determine α_1 and α_3 for benzene and carbon tetrachloride[9] from the data of the previous paper.[1] In so doing, a_1 and a_3 were eliminated from the Böttcher equation in terms of the Böttcher polarization of the pure substances and α_1 and α_3. This was done on the premise that the data for the pure substances were more accurate than those for the solutions. The values of α_1 and α_3 were then determined at each frequency by a method of least squares and, from these values, those of a_1 and a_3 were finally calculated. These values of a_1 and a_3 showed a dependence on frequency of about 3–4% over the range of frequency. But the a parameter can be conceived as the radius of a spherical cavity and consequently should be independent of frequency. Moreover, the Böttcher equation is of such a form that, for a given set of data, α and a are not independent. It was therefore decided to make a independent of the frequency. The mean value of a for the set obtained from the original least-squares calculation was used in the succeeding calculations. A new set of values for α_1 and α_3 was then determined.

For the benzene-methanol system, α_1^* was first computed by Eq. (3) with the values of α_1 and a_1 determined from the previous system. Values of α_2^* were then obtained by the use of Eq. (2) and the Böttcher molar polarizations obtained from the experimental data. The values of α_2 and a_2 at each frequency were then obtained from graphs of $1/\alpha_2^*$ against $(2n^2-2)/(2n^2+1)$. According to Eq. (3) such plots should be straight lines and straight lines were indeed obtained within the experimental accuracy. Again a_3 showed a slight dependency on the frequency. Consequently, the mean value was used and α_2 redetermined at each frequency.

The values of α, the electronic polarizability and a^3 so determined for the three substances are given in Table II. The first column of the table gives the frequencies and the last three columns give the electronic polarizability of benzene, methanol, and carbon tetrachloride, respectively. The last line of the table gives the values of a^3 for the three substances.

Graphs of $1/\alpha$ against the square of the frequency gave straight lines within experimental accuracy for each of the three substances in conformity with Eq. (1) with the assumption that only one term in the sum is predominant. This behavior is in contrast with that obtained when the Lorentz-Lorenz equation was used to determine the electronic polarizability.

As a final check, the Böttcher molar polarizations for the Na D line were calculated for the three binary systems, benzene-carbon tetrachloride, benzene-methanol, and carbon tetrachloride-methanol, and compared with the observed values determined from the experimental refractive indices. The data of Scatchard and Ticknor[7] were used for carbon tetrachloride-methanol system. This comparison is shown in Table III where the first column gives the mole fraction of benzene for the first two systems and of carbon tetrachloride for the third system. The next two columns give the observed and calculated Böttcher molar polarizations respectively. The last column gives the difference. The uncertainty of the polarizations for the first two systems is estimated to be ± 0.01; the figure in the third decimal place is retained for purposes of comparison. The agreement is quite satisfactory. This is especially true for the carbon tetrachloride-methanol system

TABLE III. Comparison of observed and calculated molar polarizations at the Na D line.

x_1	$\bar{P}_B$ (cm^3) obs	$\bar{P}_B$ (cm^3) calc	$\Delta \times 10^3$
	Benzene–carbon tetrachloride		
1.0000	30.218	30.220	2
0.8618	30.217	30.218	1
0.6295	30.183	30.185	2
0.4964	30.146	30.148	2
0.2549	30.075	30.072	−3
0.1357	30.020	30.017	−3
0.0000	29.956	29.956	0
	Benzene-methanol		
1.0000	30.218	30.220	
0.8701	27.425	27.424	−1
0.7460	24.742	24.741	−1
0.6322	22.280	22.274	−6
0.5072	19.580	19.565	−15
0.3830	16.912	16.886	−26
0.2511	14.100	14.063	−37
0.1225	11.378	11.346	−32
0.0000	8.830	8.831	1
	Carbon tetrachloride-methanol		
x_3			
1.0000	29.956	29.956	0
0.9000	27.826	27.819	−7
0.7000	23.588	23.569	−19
0.5000	19.346	19.320	−26
0.3000	15.114	15.086	−28
0.1000	10.918	10.896	−22
0.0000	8.830	8.831	1

[9] The subscript 3 is used to denote carbon tetrachloride.

because the calculated values have been determined from values of the electronic polarizability and the a parameter of the two components which, in turn, were determined from the data of the other systems and not from the carbon tetrachloride-methanol system itself.

The arbitrariness of using the average value for the a parameter and the effect of a change in the value of a on the Böttcher molar polarization was tested by calculating the molar polarization of the benzene-methanol system using an a parameter 10% and 1% smaller and 1% larger than the average value. The average deviations of the molar polarizations calculated in this way were ± 0.0589 for 10% smaller, ± 0.005 for 1% smaller, and ± 0.012 for 1% greater compared to ± 0.007 when the average value is used. The accuracy of a therefore seems to be about 1%.

From this study it is evident that, within the experimental accuracy, the electronic polarizability of each component in all three solutions is independent of the composition, that is, for any central molecule, its electronic polarizability is independent of the environment of the molecule. This observation is particularly important for the solutions containing methanol. Certainly such behavior would be expected for the benzene-carbon tetrachloride system where only the London dispersion forces are operative in addition to the repulsive forces. In the methanol solutions dipole-dipole forces and also dipole-induced dipole forces will be present. There also may be specific interactions between the dipoles of the C–Cl group of carbon tetrachloride and the O–H group of methanol. Such interactions might be sufficiently great to perturb the electronic polarizability. If this were the case, the electronic polarizability of a component would be a function of the composition. The magnitude of such an effect would be extremely difficult to determine and is probably unknown at the present time. We can only say at this time that, within the accuracy of the experiments and the applicability of the Böttcher equation, the effect has not been observed.

THE JOURNAL OF CHEMICAL PHYSICS VOLUME 32, NUMBER 5 MAY, 1960

Determination of the Dipole Moment Function from Infrared Band Intensities of Diatomic Molecules

ROBERT HERMAN

Research Laboratories, General Motors Corporation, Detroit, Michigan

AND

ROBERT J. RUBIN

National Bureau of Standards, Washington, D. C.

(Received December 14, 1959)

A discussion is given of the relations which exist among vibrational matrix elements for diatomic molecules represented as Morse oscillators. This is done according to the wave function approximation of Trischka and Salwen. It is shown how the matrix element of the dipole moment $\mathfrak{M}_{v'}$ is related to the matrix elements $\mathfrak{M}_0{}^i$ where $v'-v \leqslant i \leqslant v'+v$ with $v'>v$. This relation is examined for the case of the 1—2 band of HCl. It is also shown how the matrix element $\mathfrak{M}_0{}^1$ for DCl can be related to the matrix elements of HCl. Finally, the influence of the vibration-rotation interaction is incorporated in the wave function approximation. In an example, it is shown that the matrix element $\mathfrak{M}_{0,J}{}^{1,J+1}$ can be expressed in terms of the set of matrix elements $\{\mathfrak{M}_{0,0}{}^{i,1}\}$, $i=0, 1, \cdots$.

I. INTRODUCTION

THERE has been a great deal of interest recently in the study of the intensities of individual lines as well as integrated intensities of vibration-rotation bands of diatomic molecules. This information is of importance in the spectroscopic determination of population distributions, or rotational and vibrational temperatures, and in the fundamental study of line shape and width. In these studies a quantity which is basic to the understanding or interpretation of such measurements is the dipole moment function of the molecule, i.e., the dipole moment of the molecule as a function of the internuclear distance, $M(r)$.

In a recent paper Trischka and Salwen[1] have discussed the connection between the dipole moment function and its matrix elements for the diatomic case. They have been concerned particularly with the problem of approximating the dipole moment function from a finite number of known matrix elements. They have employed a new approach in which the product of the dipole moment function and a vibrational wave function

[1] J. Trischka and H. Salwen, J. Chem. Phys. 31, 218 (1959).

TABLE I. Matrix elements and Morse constants.

Matrix element[a]	HCl	DCl
$\lvert\mathfrak{M}_0^1\rvert$	6.70×10^{-2} debyes	5.63×10^{-2} debyes
$\lvert\mathfrak{M}_0^2\rvert$	7.03×10^{-3}	4.99×10^{-3}
$\lvert\mathfrak{M}_0^3\rvert$	5.16×10^{-4}	3.08×10^{-4}
$\lvert\mathfrak{M}_1^2\rvert$	9.71×10^{-2}	...
Constants[b]		
s	49.82	71.17
β	1.868×10^8 cm^{-1}	[c]

[a] The experimental matrix elements for HCl and DCl were obtained from W. S. Benedict, R. Herman, E. E. Moore, and S. Silverman, J. Chem. Phys. **26**, 1671 (1957).

[b] The constants s and β defined in Eqs. (2) and (3a) were computed with the molecular constants given in G. Herzberg, *Spectra of Diatomic Molecules* (D. Van Nostrand Company, Inc., Princeton, New Jersey, 1950), 2nd ed.

[c] We have employed the same value of β for both HCl and DCl.

is expanded in terms of the entire set of vibrational wave functions, with coefficients given by the matrix elements of the dipole moment. This approach, termed by them the "wave function approximation," has been compared with the more conventional polynomial approximation for the dipole moment function for a number of cases.

It is interesting to note that in the same way that it is possible to construct a vibrational potential energy function from measurements of line positions, it is possible to construct a dipole moment function for a molecule from measurements of line and band intensities. This procedure is, of course, predicated on the availability of an adequate set of vibrational wave functions. In this paper we wish to exploit certain very useful relations that exist among matrix elements and which follow from the basic treatment given by Trischka and Salwen. In addition, we discuss in this paper some of the consequences that arise from taking into account the vibration-rotation interaction.

II. THEORY

A. Matrix Elements Ignoring Rotation Effects

Following the treatment of Trischka and Salwen, we ignore at first the influence of rotation. For purposes of illustration we assume that the diatomic molecule can be represented adequately by a Morse[2] oscillator and later by a Pekeris[3] oscillator. As has been pointed out[1] the quantity $M(z)R_0(z)$, for example, can be represented as

$$M(z)R_0(z)=\sum_i \mathfrak{M}_0^i R_i(z), \tag{1}$$

where the Hamiltonian for the Morse oscillator is given by

$$H=-(\hbar^2/2m)(\partial^2/\partial r^2)+D_e\{1-\exp[-\beta(r-r_e)]\}^2, \tag{2}$$

and where

$$z=2d_0\exp[-\beta(r-r_e)], \tag{3}$$

with

$$s=2\epsilon^2/\gamma, \tag{3a}$$

$$\epsilon=1/\beta r_e, \tag{3b}$$

and

$$\gamma=2B_e/\omega_e. \tag{3c}$$

The normalized radial wave function $R_i(z)$ for the state i is given by

$$R_i(z)=N_i e^{-z/2}z^{b/2}\,{}_1F_1(-i,b+1;z), \tag{4}$$

where

$$b=s-2i-1, \tag{4a}$$

and where the normalization constant N_i is

$$N_i=\beta^{\frac{1}{2}}[\Gamma(b)]^{-\frac{1}{2}}\left[\binom{i+b}{i}\right]^{\frac{1}{2}}. \tag{4b}$$

It follows from the orthogonality of the radial wave functions that the quantities M_0^i are the matrix elements of the dipole moment, i.e.,

$$\mathfrak{M}_0^i=(0\mid M(z)\mid i)=\int_0^\infty R_0(z)M(z)R_i(z)dz/z. \tag{5}$$

Since $R_0(z)$ has the particularly simple form

$$R_0(z)=N_0e^{-z/2}z^{(s-1)/2}, \tag{6}$$

we obtain the following expression for $M(z)$ from Eq. (1):

$$M(r)=\sum_i (N_i/N_0)\mathfrak{M}_0^i z^{-i}\,{}_1F_1(-i,b+1;z). \tag{7}$$

This relation is useful in correlating intensity measurements for bands other than the $0-i$. For example, if we use Eq. (7) in the expression for $\mathfrak{M}_v^{v'}$ we obtain the following relation between $\mathfrak{M}_v^{v'}$ and the $\mathfrak{M}_0^i$'s, which for Morse wave functions involve a relatively small number of the $\mathfrak{M}_0^i$:

$$\mathfrak{M}_v^{v'}=\sum_{i=v'-v}^{v'+v}(N_i/N_0)\mathfrak{M}_0^i\int_0^\infty R_v(z)R_{v'}(z)z^{-i}\times{}_1F_1(-i,b+1;z)dz/z,\quad v'>v. \tag{8}$$

The justification for the limits placed on the sum and the values of the integrals are discussed in Appendix A. In using Eq. (7) or (8) it should be remembered that only the absolute values of the matrix elements $\mathfrak{M}_0^i$ or $\mathfrak{M}_v^{v'}$ can be determined experimentally. Thus Eq. (8) is useful in the determination of the relative signs of the $\mathfrak{M}_0^i$. As an example of the application of Eq. (8) we have determined the numerical relation among $\mathfrak{M}_1^2$ and $\mathfrak{M}_0^1$, $\mathfrak{M}_0^2$, and $\mathfrak{M}_0^3$ for the HCl molecule. The necessary numerical data are given in Table I. For the

[2] P. M. Morse, Phys. Rev. **34**, 57 (1929).
[3] C. L. Pekeris, Phys. Rev. **45**, 98 (1934).

1–2 transition the relation among the foregoing matrix elements is

$$\mathfrak{M}_1^2=[\sqrt{2}(s-2)^{\frac{1}{2}}/(s-5)^{\frac{1}{2}}(s-4)]\mathfrak{M}_0^1 +[8(s-3)^{\frac{1}{2}}/(s-4)(s-6)]\mathfrak{M}_0^2 +[\sqrt{3}(s-2)(s-3)/(s-5)^{\frac{1}{2}}(s-6)(s-7)^{\frac{1}{2}}]\mathfrak{M}_0^3. \quad (9)$$

For the HCl molecule we have from Eq. (9) and Table I

$$\mathfrak{M}_1^2=1.525\mathfrak{M}_0^1+1.276\mathfrak{M}_0^2+2.020\mathfrak{M}_0^3, \quad (10)$$

or

$$(\pm)9.71\times10^{-2}=(\pm)10.18\times10^{-2}+(\pm)0.90\times10^{-2} +(\pm)0.10\times10^{-2}\text{ debye},$$

where 1 debye $=10^{-18}$ esu. Thus it appears very likely that $\mathfrak{M}_0^1$ and $\mathfrak{M}_0^2$ have opposite signs while the relative sign of $\mathfrak{M}_0^3$ is indeterminate because of the relatively small value of the $\mathfrak{M}_0^3$ term in Eq. (10).

Since we assume that the dipole moment and potential functions for DCl may be taken as identical with those of HCl, it is possible to evaluate the matrix elements of the dipole moment for DCl using the intensity data for HCl. From Eq. (3) we note an expression relating the coordinate z_H for HCl and z_D for DCl, namely:

$$z_H=(s_H/s_D)z_D=\zeta z_D. \quad (11)$$

As an illustration we calculate the 0–1 matrix element for DCl, $\mathfrak{M}_0^1(D)$, according to the following expression:

$$\mathfrak{M}_0^1(D)=\sum_i[N_i(H)/N_0(H)]\mathfrak{M}_0^i(H)\int_0^\infty R_0(z_D) \times R_1(z_D)\zeta^{-i}z_D^{-i}\,{}_1F_1(-i, s_H-2i; \zeta z_D)dz_D/z_D. \quad (12)$$

A straightforward procedure shows that the main contribution to $\mathfrak{M}_0^1(D)$ in Eq. (12) comes from the term involving $\mathfrak{M}_0^1(H)$. The contribution from $\mathfrak{M}_0^2(H)$ is about 4% of the leading term and it is expected that higher terms will contribute even less. We obtain the result

$$\mathfrak{M}_0^1(D)=\zeta^{-1}\left(\frac{s_H-2}{s_D-2}\right)\left(\frac{s_H-3}{s_D-3}\right)^{\frac{1}{2}}\mathfrak{M}_0^1(H) +\frac{4\sqrt{2}}{\zeta^2}\left(1-\frac{1}{\zeta}\right)\left(\frac{s_H-3}{s_D-2}\right)\left(\frac{s_H-2}{s_D-4}\right)\left(\frac{s_H-5}{s_H-4}\right)^{\frac{1}{2}}\frac{\mathfrak{M}_0^2(H)}{(s_D-3)^{\frac{1}{2}}}+\cdots \cong(\pm)5.48\times10^{-2}-(\pm)0.20\times10^{-2}\text{ debye} \quad (13a)$$

which is in good agreement with the experimental value 5.63×10^{-2} debye. We note that, as in the case of Eq. (10) for the relation among $\mathfrak{M}_1^2(H)$ and $\mathfrak{M}_0^1(H)$, $\mathfrak{M}_0^2(H)$, and $\mathfrak{M}_0^3(H)$, the closest agreement between the predicted and experimental values in Eq. (13a) is obtained if the HCl matrix elements, $\mathfrak{M}_0^1(H)$ and $\mathfrak{M}_0^2(H)$, have opposite signs.

It is interesting to compare the representation for tne dipole moment function given in Eq. (7) with a Taylor series expansion

$$M(r)=\sum_i M_i(r-r_e)^i \quad (14)$$

where

$$M_i=(1/i!)(d^iM(r)/dr^i)_{r=r_e}. \quad (14a)$$

In Appendix B we obtain from Eq. (7) an expression for $M(r)$ through terms in $\mathfrak{M}_0^3$, from which are derived M_0, M_1, and M_2 as defined in Eq. (14a). Using these results for the case of HCl, we obtain

$$M_0=\mathfrak{M}_0^0-0.275\mathfrak{M}_0^1-0.499\mathfrak{M}_0^2+0.590\mathfrak{M}_0^3\text{ debye},$$

$$M_1=12.52\times10^{+8}\mathfrak{M}_0^1-9.41\times10^{+8}\mathfrak{M}_0^2 +5.31\times10^{+8}\mathfrak{M}_0^3\text{ debye cm}^{-1}, \quad (15)$$

and

$$M_2=11.9\times10^{16}\mathfrak{M}_0^1-94\times10^{16}\mathfrak{M}_0^2 +146\times10^{16}\mathfrak{M}_0^3\text{ debye cm}^{-2}.$$

Using the values of the $\mathfrak{M}_0^i$ in Table I we then have

$$M_0=[\mathfrak{M}_0^0-(\pm)0.0184-(\pm)0.0035 +(\pm)0.0003]\text{ debye},$$

$$M_1=[(\pm)0.840-(\pm)0.066+(\pm)0.003] \times10^8\text{ debye cm}^{-1}, \quad (16)$$

and

$$M_2=[(\pm)0.80+(\pm)0.66-(\pm)0.08] \times10^{16}\text{ debye cm}^{-2}.$$

It is noteworthy in Eqs. (16) that although the coefficients of $\mathfrak{M}_0^3$ in Eqs. (15) are not small, the products of these coefficients with $\mathfrak{M}_0^3$ yield relatively small contributions to M_0, M_1, and M_2.

B. Influence of Vibration-Rotation Interaction

In similar fashion, we shall now indicate how the effect of the vibration-rotation interaction can be incorporated into the wave function approximation. Corresponding to Eq. (1) we now have a set of similar relations with one for each rotational state, namely,[4]

$$M(r)R_{0,J}(z_J)=\sum_i\mathfrak{M}_{0,J}{}^{i,J\pm1}R_{i,J\pm1}(z_{J\pm1}), \quad (17)$$

where

$$z_J=2d_J\exp[-\beta(r-r_e)], \quad (17a)$$

and

$$2d_J=s\{1+\tfrac{1}{2}\gamma^2\epsilon^{-1}(3\epsilon-1)J(J+1)\}. \quad (17b)$$

The J-dependent wave functions are

$$R_{i,J}(z_J)=N_{i,J}e^{-z_J/2}z_J{}^{b_{i,J}/2}\,{}_1F_1(-i, b_{i,J}+1; z_J), \quad (18)$$

[4] Except for the subscripts on z and b, the notation which we use here for the wavefunctions is that used in R. Herman and R. J. Rubin, Astrophys. J. **121**, 533 (1955).

where

$$N_{i,J}=\beta^{\frac{1}{2}}[\Gamma(b_{i,J})]^{-\frac{1}{2}}\left[\binom{i+b_{i,J}}{i}\right]^{\frac{1}{2}},$$

and where

$$b_{i,J}=s\{1+\tfrac{3}{2}\gamma^2\epsilon^{-1}(\epsilon-1)\,J(J+1)\}-2i-1. \quad (18a)$$

The quantities defined in Eqs. (17b), (18), and (18a) are correct to the first order in the rotational perturbation.[4]

For the following development we wish to choose a "basic" set of matrix elements which we arbitrarily take to be the set $\{\mathfrak{M}_{0,0}^{i,1}\}$, $i=0, 1, \cdots$. The matrix element $\mathfrak{M}_{v,J}^{v',J\pm1}$ can then be expressed in terms of the set of $\mathfrak{M}_{0,0}^{i,1}$'s simply from the definition

$$\mathfrak{M}_{v,J}^{v',J\pm1}$$

$$=(v,\,J\,|\,\sum_i \mathfrak{M}_{0,0}^{i,1}[R_{i,1}(z_1)/R_{0,0}(z_0)]\,|\,v',\,J\pm1). \quad (19)$$

As an example of the application of Eq. (19), we obtain the following expression for $\mathfrak{M}_{0,J}^{1,J\pm1}$

$$\mathfrak{M}_{0,J}^{1,J\pm1}=\sum_i (N_{0,J}/N_{0,0})[(s+\xi_J)^{(s+\eta_J-1)/2}/s^{(s-1)/2}]\mathfrak{M}_{0,0}^{i,1}$$

$$\times\int_0^\infty e^{-\xi_J y/2}y^{\eta_J/2}R_{i,1}[(s+\xi_1)y]R_{1,J\pm1}[(s+\xi_{J\pm1})y]dy/y \quad (20)$$

where

$$y=\exp[-\beta(r-r_e)]$$

$$\xi_J=\tfrac{1}{2}s\gamma^2\epsilon^{-1}(3\epsilon-1)\,J(J+1),$$

and

$$\eta_J=\tfrac{3}{2}s\gamma^2\epsilon^{-1}(\epsilon-1)\,J(J+1).$$

Convenient methods for the numerical evaluation of the integrals appearing in Eq. (2) have been outlined by Herman *et al.*[5] Except for the small rotational-dependent correction terms in these integrals, the vibrational wave functions are orthonormal with respect to the weight factor $(1/y)$. Thus the principal contribution to $\mathfrak{M}_{0,J}^{1,J\pm1}$ comes, as one should expect, from the term involving $\mathfrak{M}_{0,0}^{1,1}$; and the other terms on the right-hand side of Eq. (20) constitute the rotational correction. An order of magnitude calculation shows that in the case of HCl and DCl the major part of the correction comes from the $\mathfrak{M}_{0,0}^{0,1}$ term.

ACKNOWLEDGMENT

We wish to thank Professor John Trischka for his kindness in sending us a copy of his manuscript concerning the "wave function approximation."

APPENDIX A

Evaluation of the Matrix Element $\mathfrak{M}_v^{v'}$

We wish to evaluate the integral which appears in Eq. (8), namely,

$$I_v^{v'}(i)=\int_0^\infty R_v(z)\,R_{v'}(z)z^{-1}\,{}_1F_1(-i,\,b+1;\,z)dz/z. \quad (A1)$$

If we introduce into Eq. (A1) the $R_i(z)$ from Eq. (4) and replace ${}_1F_1$ by the polynomial form

$${}_1F_1(-i,\,b+1;\,z)=\sum_{n=0}^{i}[(-i)_n/n!][z^n/(b+1)_n], \quad (A2)$$

where the symbol $(b)_n$ denotes $b(b+1)\cdots(b+n-1)$, we obtain for $I_v^{v'}(i)$ the following:

$$I_v^{v'}(i)=N_vN_{v'}\Gamma(s-1-v-v'-i)\sum_{l=0}^{v}\sum_{m=0}^{v'}\sum_{n=0}^{i}[(-v)_l/l!][(-v')_m/m!][(-i)_n/n!]\frac{(s-1-v-v'-i)_{l+m+n}}{(s-2v)_l(s-2v')_m(s-2i)_n}. \quad (A3)$$

By performing the sum on n in Eq. (A3) with the aid of Gauss's theorem,[6] we obtain

$$I_v^{v'}(i)=N_vN_{v'}\frac{\Gamma(s-1-v-v'-i)}{(s-2i)_i}\sum_{l=0}^{v}\sum_{m=0}^{v'}[(-v)_l/l!][(-v')_m/m!]\frac{(s-1-v-v'-i)_{l+m}}{(s-2v)_l(s-2v')_m}(1+v+v'-i-l-m)_i. \quad (A4)$$

The factor $(1+v+v'-i-l-m)_i$ has the property that it contains the factor zero if $i>v+v'$. Thus

$$I_v^{v'}(i)=0, \qquad i>v+v'.$$

Furthermore without loss of generality we can assume that $v\leq v'$. If instead of performing the summation on n, we first sum over m, then we obtain the analogous expression

$$I_v^{v'}(i)=N_vN_{v'}\frac{\Gamma(s-1-v-v'-i)}{(s-2v')_{v'}}\sum_{l=0}^{v}\sum_{n=0}^{i}[(-v)_l/l!][(-i)_n/n!]\frac{(s-1-v-v'-i)_{l+n}}{(s-2v)_l(s-2i)_n}. \quad (A5)$$

In Eq. (A5) the factor $(1+v+i-v'-l-n)_{v'}$ is zero if $v+i-v'<0$ or $i<v'-v$. Thus $\mathfrak{M}_v^{v'}$ is expressible as a linear combination of those $\mathfrak{M}_0^{i}$'s for which $v'-v\leq i\leq v'+v$.

[5] R. Herman, R. J. Rubin, and R. W. Rothery, J. Mol. Spectroscopy **2**, 369 (1958).

[6] W. N. Bailey, *Generalized Hypergeometric Series* (Cambridge University Press, New York, 1935). Gauss's theorem is used repeatedly in reference 5, e.g., to obtain Eq. (16) of that reference.

APPENDIX B

Taylor Expansion Coefficients for $M(r)$

In order to obtain the coefficients of the Taylor expansion for $M(r)$ we first write the wave function approximation for $M(r)$ explicitly as a function of r through terms in $\mathfrak{M}_0^3$:

$$M(r)=\mathfrak{M}_0^0+[(s-2)_2]^{\frac{1}{2}}[s-2]^{\frac{1}{2}}s^{-1}\{\exp[\beta(r-r_e)]-[s/(s-2)]\}\mathfrak{M}_0^1$$
$$+[(s-2)_4]^{\frac{1}{2}}s^{-2}[\tfrac{1}{2}(s-3)_2]^{\frac{1}{2}}\{\exp[2\beta(r-r_e)]-[2s/(s-4)]\exp[\beta(r-r_e)]+[s^2/(s-4)(s-3)]\}\mathfrak{M}_0^2$$
$$+[(s-2)_6]^{\frac{1}{2}}s^{-3}[\tfrac{1}{6}(s-4)_3]^{\frac{1}{2}}\{e^{3\beta(r-r_e)}-[3s/(s-6)]e^{2\beta(r-r_e)}$$
$$+[3s^2e^{\beta(r-r_e)}/(s-6)(s-5)]-[s^3/(s-6)(s-5)(s-4)]\}\mathfrak{M}_0^3. \quad \text{(B1)}$$

It follows from Eq. (B1) that M_0 is given by

$$M_0=\mathfrak{M}_0^0-(2/s)(s-3)^{\frac{1}{2}}\mathfrak{M}_0^1-[(s-12)/s^2][(s-5)(s-2)/2]^{\frac{1}{2}}\mathfrak{M}_0^2+[(14s-120)/s^3][(s-7)(s-3)(s-2)/6]^{\frac{1}{2}}\mathfrak{M}_0^3. \quad \text{(B2)}$$

We also have

$$M_1=\beta\left\{\frac{(s-3)^{\frac{1}{2}}(s-2)}{s}\mathfrak{M}_0^1-\frac{4\sqrt{2}(s-5)^{\frac{1}{2}}(s-3)(s-2)^{\frac{1}{2}}}{s^2}\mathfrak{M}_0^2-\frac{\sqrt{3}}{2}\frac{(s-30)[(s-7)(s-3)(s-2)]^{\frac{1}{2}}(s-4)}{s^3}\mathfrak{M}_0^3\right\}, \quad \text{(B3)}$$

and

$$M_2=\frac{\beta^2}{2}\left\{\frac{(s-3)^{\frac{1}{2}}(s-2)}{s}\mathfrak{M}_0^1+\sqrt{2}\frac{(s-5)^{\frac{1}{2}}(s-2)^{\frac{1}{2}}(s-8)(s-3)}{s^2}\mathfrak{M}_0^2-\frac{39s-270}{6^{\frac{1}{2}}s^3}[(s-7)(s-3)(s-2)]^{\frac{1}{2}}(s-4)\mathfrak{M}_0^3\right\}. \quad \text{(B4)}$$

Application of Least-Squares Method to Density-Intensity Calibration in Electron Diffraction Studies*

KATSUMI KIMURA† AND MASAO KIMURA

Department of Chemistry, Nagoya University, Nagoya, Japan

(Received October 29, 1959)

A new method based on the principle of least squares is proposed for the calibration of the characteristics of photographic emulsion employed in electron diffraction studies. The calibration procedure consists of two steps. First, a function having three parameters was found which represents the relation between the optical density and exposure. Secondly, the most probable values of the parameters and their standard errors were determined in a straightforward way by the method of least squares. An application of this method to the diffraction patterns of benzene is described. The standard errors of final relative intensities were evaluated over the entire observed range of optical densities.

I. INTRODUCTION

RECENTLY, molecular structures in the gaseous state have been investigated by a sector-microphotometer technique of electron diffraction. The analysis of a diffraction photograph requires the construction of a calibration curve by which the optical density of the diffraction pattern can be converted into the relative intensity of electron scattering.

Several attempts have been made to obtain a calibration curve from two diffraction photographs of different exposure.[1,2] In these procedures, it is assumed that the amount of exposure to fast electrons is given by the product of the time and intensity. Karle and Karle[1] have devised a calibration method based on the additional assumption that the optical density is proportional to the exposure, for low exposures, to fast electrons. Their procedure seems to be adequate for the purpose of determining molecular dimensions. However, the main disadvantage of this method is that errors introduced in the course of calibration procedure might accumulate as the optical density increases. At least, an error is present in the proportionality constant of the optical density to the exposure. Moreover, the effect of these errors on the molecular structure that is finally determined can hardly be estimated. A closely related but more improved method has been proposed by Bartell and Brockway,[2] in order to average out errors involved in the calibration curve, but they have given no method of estimation of the errors of the relative intensities evaluated from the optical densities.

In the present paper, a new calibration method is proposed which is based on the principle of least squares, and an application of the method to the diffraction patterns of benzene is described as an example.

II. LEAST SQUARES METHOD

For two diffraction photographs taken under identical conditions except for exposure time, the following relation must be satisfied between the two patterns, A and B:

$$I^A = kI^B, \tag{1}$$

where I is the relative intensity and k is a proportionality constant. In general, I may be expressed by a certain function of the optical density,

$$I = f(D, X_1, X_2, \cdots, X_{m-1}), \tag{2}$$

including $m-1$ parameters, $X_1, X_2, \cdots$etc., to be determined. Substitution of Eq. (2) into Eq. (1) gives

$$\begin{aligned} I_i^A - kI_i^B &= f(D_i^A, X_1, X_2, \cdots, X_{m-1}) \\ &\quad - kf(D_i^B, X_1, X_2, \cdots, X_{m-1}) \\ &= F(D_i^A, D_i^B, X_1, X_2, \cdots, X_m) = 0, \\ &\quad i = 1, 2, 3, \cdots, n, \end{aligned} \tag{3}$$

where k is replaced by the mth parameter X_m, n is the number of independent observation equations, and m ($<n$) the number of independent unknown parameters to be determined. If a set of good approximate values $X_1', X_2', \cdots, X_m'$ is known, the corrections $x_1 = X_1' - X_1$, $x_2 = X_2' - X_2, \cdots$etc., are required to reduce the approximate values to the most probable values. The Taylor expansion of Eq. (3), retaining only the first powers of the corrections, gives

$$\mathbf{Ax} = \mathbf{L},$$

where $\mathbf{x}$ is a column matrix, the elements of which are corrections to be sought, $\mathbf{A}$, an m-column, n-row matrix having the partial derivatives of F with respect to X as its elements, and $\mathbf{L}$, a column matrix whose elements are constant terms. The quantity $\mathbf{L}$ cannot be observed directly in experiment, but can be determined from the observed quantities and the approximate values of these parameters.

* A part of this work has been reported at the twelfth annual meeting of the Chemical Society of Japan held April, 1959.

† Present address: The Institute for Solid State Physics, The University of Tokyo, Komaba-cho, Meguro-ku, Tokyo, Japan.

[1] J. Karle and I. L. Karle, J. Chem. Phys. **18**, 957 (1950).

[2] L. S. Bartell and L. O. Brockway, J. Appl. Phys. **24**, 656 (1953).

Since all the observation equations are not of the same weight, they must be reduced to ones of the same weight by multiplying each by the square root of its weight. With an appropriate weighting matrix $\mathbf{P}$, the normal equation can be set up in the form

$$\mathbf{A^*PAx}=\mathbf{A^*PL} \quad \text{or} \quad \mathbf{x}=\mathbf{B^{-1}A^*PL}, \tag{4}$$

where $\mathbf{B}=\mathbf{A^*PA}$ and an asterisk indicates the corresponding transposed matrix. Thus, the correction $\mathbf{x}$ can be calculated by Eq. (4).

Standard Errors of the Parameters

The standard error σ_i of the ith parameter x_i can be evaluated by means of the equation

$$\sigma(x_i)^2=(B^{-1})_{ii}\sigma_0^2=(B^{-1})_{ii}(\mathbf{V^*PV})/(n-m), \tag{5}$$

where σ_0 is the standard error of a single observation, $(\mathbf{V^*PV})$ being the sum of the weighted squares of the residuals.

Standard Errors of the Relative Intensities

Equation (2) is reduced to a linear form by use of Eq. (4),

$$\Delta I=c_0\Delta D+\mathbf{c^*x}=c_0\Delta D+\mathbf{c^*B^{-1}A^*PL},$$

where $c_0=(\partial I/\partial D)$, and c is a column matrix whose elements, $c_1, c_2, \cdots, c_{m-1}$ are the partial derivatives of I with respect to $X_1, X_2, \cdots, X_{m-1}$, respectively, c_m being equal to zero. The second term on the right-hand side is associated with the conversion of density into intensity, and the first term is with the observed density at an arbitrary position. Then the standard error, $\sigma(I)$, of the relative intensity can be, to a good approximation, given by

$$\sigma(I)^2=c_0^2\sigma(D)^2+(\mathbf{c^*B^{-1}c})\sigma_0^2. \tag{6}$$

Standard Errors of the Optical Densities

In order to estimate the errors of the relative intensities obtained by the least squares method, it is necessary to consider uncertainties introduced in the optical densities measured with a microphotometer trace shown in Fig. 1. The optical density D is given by the definition

$$D=\log_{10}[(y_D-y_B)/(y_D-y)],$$

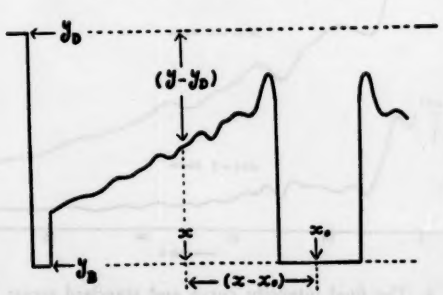

FIG. 1. The microphotometer trace of diffraction pattern.

with an error

$$\Delta D=(\log_{10}e)\{[(y_D-y_B)^{-1}-(y_D-y)^{-1}]\Delta y_D + (y_D-y_B)^{-1}\Delta y_B+(y_D-y)^{-1}\Delta y\},$$

where y_D denotes the position of a dark line, y_B the position of the base line, y the coordinate of a point of the curve, and Δ denotes errors in reading the corresponding y positions.

Since all y's in the foregoing equation are independent of each other, the standard error of D may be expressed in terms of the standard error of y as follows:

$$\sigma(D)=(\log_{10}e)\{[(y_D-y_B)^{-1}-(y_D-y)^{-1}]^2\sigma(y_D)^2 + (y_D-y_B)^{-2}\sigma(y_B)^2+(y_D-y)^{-2}\sigma(y)^2\}^{\frac{1}{2}}, \tag{7}$$

where σ represents the standard error of the corresponding y. In addition, an error introduced in reading y is given by $\Delta y=\Delta y_R+(\partial y/\partial x)\Delta x_0+(\partial y/\partial x)\Delta x$. Consequently, the standard error of y is given by the form

$$\sigma(y)^2=\sigma(y_R)^2+(\partial y/\partial x)^2\sigma(x_0)^2+(\partial y/\partial x)^2\sigma(x)^2, \tag{8}$$

where Δy_R is an error in reading the position of a point of the curve; Δx_0 and Δx are errors in determining the positions of the center of patterns and of the x scale, respectively, and σ denotes the corresponding standard error. In Eqs. (5) and (6), standard errors $\sigma(y_D)$, $\sigma(y_B)$, $\sigma(x_0)$, and $\sigma(x)$ are due to systematic errors.

III. EXAMPLE

The observed densities of two diffraction photographs of benzene[3] were $D^A=0.14\sim0.74$ and $D^B=0.11\sim0.63$, leading to k equal to about 1.2. As described in the preceding section, it is required that the relative intensity be expressed in advance by an analytic function of the optical density. The first problem is to find the type of function representing the characteristics of the emulsion of these photographs. The second is to determine the unknown parameters involved in the function from observed densities in accordance with the procedure explained in the foregoing.

Determination of a Calibration Function

In the first place, a calibration curve was obtained graphically using Karle's method.[1] To check the general

[3] Electron diffraction photographs of benzene were taken through an r^3 sector at a camera length of 12 cm and with a wavelength of 0.052 A. The diffraction patterns covering the region of $s=5.35\sim30.05$ were taken on Fuji Process Hard Plates, and scanned with a Riken B-type recording microphotometer to measure the optical density as a function of radius [$s=(4\pi/\lambda)\sin\theta$, where 2θ is scattering angle and λ wavelength]. In order to average over the grains of emulsion, the photographic plates were rotated rapidly about the center of the diffraction pattern while being scanned. Regarding the apparatus used here and the experimental procedure, see also M. Iwasaki, Bull. Chem. Soc. Japan **32**, 205 (1959); K. Kimura and M. Kubo, J. Chem. Phys. **30**, 151 (1959).

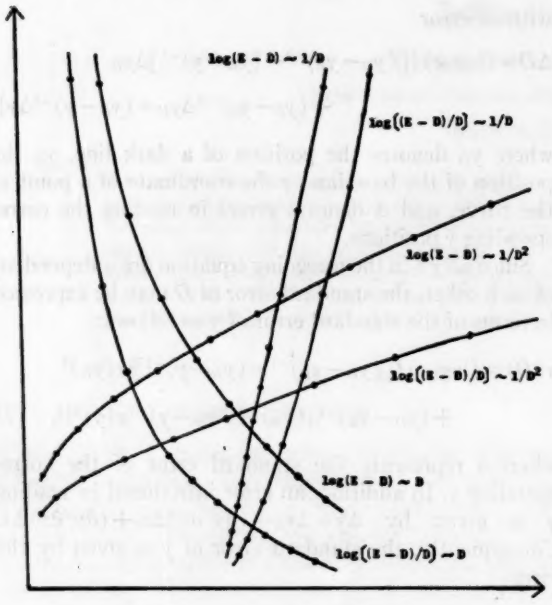

FIG. 2. Plots of the logarithms of $(I'-D)$ and $(I'-D)/D$ versus D, $1/D$, and $1/D^2$. The scales of the abscissa and ordinate are arbitrary.

feature of the curve (I') thus obtained, the following six plots were made:[4]

(1) $\log(I'-D)$ vs D, (2) $\log[(I'-D)/D]$ vs D,

(3) $\log(I'-D)$ vs $1/D$, (4) $\log[(I'-D)/D]$ vs $1/D$,

(5) $\log(I'-D)$ vs $1/D^2$, (6) $\log[(I'-D)/D]$ vs $1/D^2$.

As seen in Fig. 2, it was found that the values of $\log(I'-D)$ plotted against $1/D$ lie on a straight line when densities are less than 0.6. The curve of plot 3 is the straightest one of the six curves. This fact indicates that the calibration curve may be expressed by a function of the type $I=D+10^{-\phi}$, where $\phi=a+b/D$ for $D<0.6$ and the constants a and b are positive. By fitting this function to curve 3, it was found that $a=0.65$ and $b=0.43$. Accordingly $k=1.193$. For densities greater than 0.6, the deviation of curve 3 from linearity was corrected to a good approximation by giving an additional term, cD^p, to the foregoing function ϕ. By using the data of $D>0.6$, a simple calculation gave $c=-0.50$ and $p=5.7$. Thus, for the whole range of observed densities, the following analytic function was found to represent the characteristics of the emulsion of these photographs:

$$I=D+10^{-\phi}, \qquad \phi=a+b/D+cD^6. \tag{9}$$

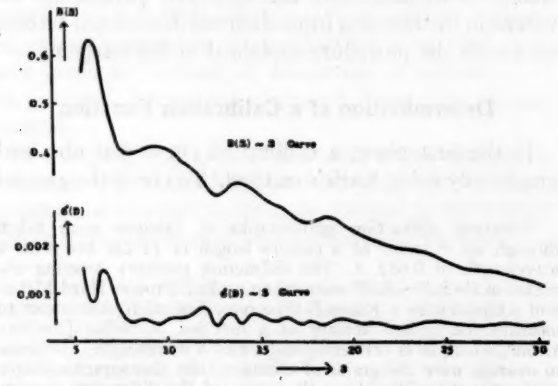

FIG. 3. Plots of D^4 and $\sigma(D^4)$ against s.

[4] For convenience in the calculation, common logarithms were used.

TABLE I. The results of least squares refinements for the density-intensity calibration.

	Trial value	First refinement	Standard error	Second refinement	Standard error
a	0.650	0.743	0.035	0.717	0.021
b	0.430	0.415	0.016	0.419	0.009
c	−0.500	−0.467	0.049	−0.491	0.029
k	1.193_0	1.185_1	0.002_3	1.187_0	0.001_4

Weighting Factors and Standard Errors of Observed Densities

The number of optical densities observed for each photograph was about 40. Since the observed values have different degrees of uncertainty at each point of s, weighting factors P_i, which are inversely proportional to $\sigma(D_i^A)^2$, were used in the least squares refinements; namely,

$$P_i=\sigma_{\min}^2/\sigma(D_i^A)^2, \tag{10}$$

where $\sigma(D_i^A)^2$ was evaluated from Eq. (5) with $\sigma(y_D)\simeq\sigma(y_B)\simeq\sigma(y_R)\simeq 0.01$ mm, $\sigma(x_0)\simeq 0.014$ mm, and $\sigma(x)\simeq 0.0005(x-x_0)$ mm. Fig. 3 shows the plot of $\sigma(D^4)$ mm. Fig. 3 shows the plot of $\sigma(D^4)$ against s together

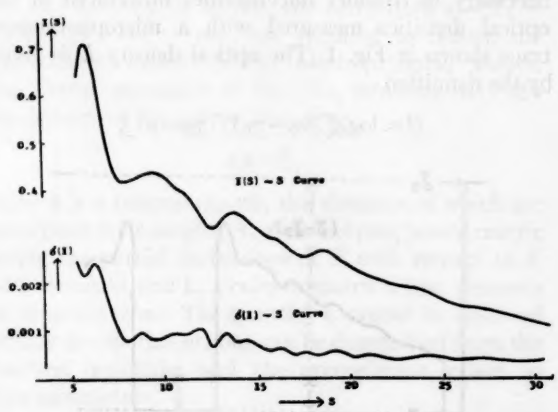

FIG. 4. The final intensity curve and standard errors plotted against s.

with the curve of the optical density for the diffraction pattern A.[5]

Results of Least Squares Treatment

The parameter values obtained in the preceding section were used as trial values for the first least squares treatment with the weighting factor estimated in the last section (see the first column in Table I). Two successive refinements were made. Table I lists the most probable values of the parameters and their standard errors obtained in the first and second refinements. The final parameter values with standard errors are $a=0.717\pm0.021$, $b=0.419\pm0.009$, $c=-0.491\pm0.029$, and $k=1.187_0\pm0.001_4$.

The calibration function used here has no theoretical basis. As shown in Table I, however, the standard errors converge rapidly after very few successive approximations. It seems that the type of calibration function is satisfactory for the region of densities covered by the present experiment and that three parameters are sufficient to specify the calibration function. Further, it must be mentioned that the shape of the foregoing calibration function is in good agreement with that obtained from our previous studies.

Fig. 4 shows the final intensity curve and the curve which exhibits the standard errors. The standard errors for several s values are listed in Table II together with the corresponding values of D, I, and $\sigma(D)$. It shows that $\sigma(I)$ is due mainly to $\sigma(D)$, as expected, except in the inner part of s. This also indicates that the contribution of the second term of Eq. (6) to $\sigma(I)$ is considerably smaller than that of the first term. Therefore the use of additional parameters is not required.

TABLE II. The standard errors, $\sigma(D)$ and $\sigma(I)$, of D and I.

s	D	I	$\sigma(D)$	$\sigma(I)$
5.5	0.68	0.72	0.0015	0.0028
10	0.40	0.44	0.0005	0.0010
20	0.25	0.26	0.0004	0.0005
30	0.14	0.14	0.0004	0.0004

IV. CONCLUSION

The least squares procedure may be satisfactorily applied to the cailbration of photographic emulsion. Once a good trial function is found, the least squares method enables us to obtain the most probable calibration function. Practically, the procedure consists of two steps. The first is to find the type of analytic function representing the characteristics of photographic emulsion, and the second is to determine the most probable function by the least squares method. The main advantages of the application of the least squares method are that uncertainties introduced into the calibration are averaged out and that errors due to the uncertainties can be estimated. It should be noted that the calibration method proposed in the present paper does not require an assumption that the optical density is proportional to the relative intensity for low optical densities, but it requires the use of a certain type of analytic function which covers only the range of optical densities under investigation.

ACKNOWLEDGMENT

The authors wish to express our thanks to Professor M. Kubo for his advice and encouragment.

[5] Although D^A and D^B are observed independently of one another with the different standard errors $\sigma(D^A)$ and $\sigma(D^B)$, the two series of the observed densities have the degree of precision nearly proportional to one another at the same values of s.

Simple Configuration-Interaction Wave Functions. I. Two-Electron Ions: A Numerical Study*

J. N. SILVERMAN, O. PLATAS, AND F. A. MATSEN

Departments of Chemistry and Physics, The University of Texas, Austin, Texas

(Received September 11, 1959)

The ground state energies of the two-electron ions from H^- to Ne^{8+} are calculated for the simple wave function $(1s1s')+\lambda(2p)^2$ with optimized orbital exponents. The use of the difference between the calculated energy and the experimental energy as a function of the atomic number for accurate extrapolation is explored. The expectation values of the operators $r^n(n \geq -2)$, $\delta^{(3)}(\mathbf{r}_1)$, and $\delta^{(3)}(\mathbf{r}_{12})$ are compared with those obtained from more accurate wave functions.

I. INTRODUCTION

QUITE exact wave functions for two-electron systems[1-3] and relatively exact wave functions for three-electron systems[4] are available. These are functions of the Hylleraas[5] type which explicitly introduce the interelectronic distance and normally contain many terms.

There is real need for approximate wave functions which, on the one hand, yield reasonably accurate values of the properties of polyelectronic atomic and simple molecular systems and, on the other hand, are of sufficiently simple form so that the calculations remain tractable.

One purpose of this series is to investigate the properties of several such simple functions in detail. Expectation values derived from these simple functions are compared with corresponding data from experiment and more elaborate wave functions to establish a criterion of accuracy. The helium-like ions from H^- to Ne^{8+} have been selected for the present calculations because there is a large amount of material available for comparison.

A second purpose is the development of extrapolation procedures employing the difference between observed and approximately calculated quantities to obtain improved estimates of quantities not experimentally determined.

As a starting point in the selection of suitable wave functions, we note that a *single* open-shell[6] or DODE (different orbitals for different electrons) configuration has been found to give good results in a particularly simple manner for the energy[5,7-10] and other physical properties[11,12] of 2- to 4-electron atomic systems. DODE functions permit some radial correlation although r_{ij} is not explicitly introduced. Recently, these DODE calculations have been successfully extended to the 5-electron atomic case[13] and simple molecular systems.[14] This demonstrates the general applicability of such functions.

In 2-electron calculations, the $(1s1s')$ configuration (Hylleraas[5]-Eckart[7] symmetrized exponential) is the appropriate choice because this simple function, which represents a specialized superposition of radial configurations,[8] gives a variational ground state energy for helium which is 0.003 atomic unit above the estimated radial limit[15,16] and 0.014 atomic unit below the Hartree-Fock value.[17] Some angular correlation can be introduced by the addition of one or more angular configurations. In paper II of this series, a method of analysis is presented which may be used to make an estimate of the energy improvement to be expected from each configuration added.[18] The $(2p)^2$ configuration alone has been selected because it has been found to make the major angular contribution to the ground state energy of helium in expansions of this type.[19,20]

* This research was supported by the Robert A. Welch Foundation of Houston, Texas, and the Office of Ordnance Research, U.S. Army.

[1] E. A. Hylleraas and J. Midtdal, Phys. Rev. **103**, 829 (1956); **109**, 1013 (1958).
[2] T. Kinoshita, Phys. Rev. **105**, 1490 (1957).
[3] C. L. Pekeris, Phys. Rev. **112**, 1649 (1958); **115**, 1216 (1959).
[4] H. M. James and A. S. Coolidge, Phys. Rev. **49**, 688 (1936).
[5] E. A. Hylleraas, Z. Physik **54**, 347 (1929).
[6] R. S. Mulliken, Proc. Natl. Acad. Sci. U.S. **38**, 160 (1952).
[7] C. Eckart, Phys. Rev. **36**, 878 (1930).
[8] H. Shull and P.-O. Löwdin, J. Chem. Phys. **25**, 1035 (1956).
[9] R. P. Hurst, J. D. Gray, G. H. Brigman, and F. A. Matsen, Mol. Phys. **1**, 189 (1958).
[10] G. H. Brigman and F. A. Matsen, J. Chem. Phys. **27**, 829 (1957); E. A. Burke and J. F. Mulligan, *ibid.* **28**, 995 (1958); G. H. Brigman, R. P. Hurst, J. D. Gray, and F. A. Matsen, *ibid.* **29**, 251 (1958).
[11] R. P. Hurst, J. Miller, and F. A. Matsen, Acta Cryst. **11**, 320 (1958); R. P. Hurst and F. A. Matsen, Acta Cryst. **12**, 7 (1959).
[12] F. T. Ormand and F. A. Matsen, J. Chem. Phys. **30**, 368 (1959).
[13] G. H. Brigman, J. N. Silverman, and F. A. Matsen (to be published).
[14] P. Csavinszky, J. Chem. Phys. **31**, 178 (1959); W. W. Robinson, J. D. Stuart, and F. A. Matsen, Bull. Am. Phys. Soc. Ser. II **4**, 105 (1959); G. H. Brigman, S. J. Brient, and F. A. Matsen (to be published); O. Platas, P. N. Reagan, J. D. Stuart, and F. A. Matsen (to be published).
[15] L. C. Green, M. N. Lewis, M. M. Mulder, C. W. Wyeth, and J. W. Woll, Jr., Phys. Rev. **93**, 273 (1954).
[16] H. Shull and P.-O. Löwdin, J. Chem. Phys. **30**, 617 (1959).
[17] L. C. Green, M. M. Mulder, M. N. Lewis, and J. W. Woll, Jr., Phys. Rev. **93**, 757 (1954).
[18] C. W. Scherr and J. N. Silverman, J. Chem. Phys. **32**, 1407 (1960), this issue.
[19] G. R. Taylor and R. G. Parr, Proc. Natl. Acad. Sci. U.S. **38**, 154 (1952).
[20] L. C. Green, M. M. Mulder, C. W. Ufford, E. Slaymaker, E. Krawitz, and R. T. Mertz, Phys. Rev. **85**, 65 (1952).

TABLE I. Wave function parameters.

Function	$(1s1s')$		Eq. (1)			
Z	a	b	a	b	g	$-\lambda$
1	1.039230	0.2832215	1.03556	0.323563	0.998054	0.112426
2	2.183171	1.188530	2.17621	1.20152	2.47547	0.0617557
3	3.294909	2.078981	3.28975	2.08734	3.93732	0.0407435
4	4.389731	2.984717	4.38638	2.99095	5.39864	0.0303173
5	5.473412	3.901259	5.47076	3.90515	6.86000	0.0241219
6	6.549100	4.825682	6.54625	4.82894	8.32799	0.0200115
7	7.618701	5.756144	7.60546	5.76892	9.79802	0.0170967
8	8.683481	6.691402	8.68290	6.69260	11.2391	0.0149483
9	9.744315	7.630595	9.74370	7.63261	12.7350	0.0132339
10	10.80184	8.573085	10.8018	8.57309	14.1850	0.0119038
50	52.18575	47.18925	52.1857	47.1892	72.7577	0.00235451

TABLE II. Computed ground state energies[a] for heliumlike ions in atomic units.

Function	$-E$				$-\Delta E$		
Z	$(1s)^2$	$(1s1s')$	Eq. (1)	Pekeris[a]	Radial[b]	Angular[c]	Pekeris[d]
1	0.47265625	0.51330289	0.52457430	0.52775097	0.040647	0.011271	0.003177
2	2.8476562	2.8756614	2.8952278	2.9037244	0.028005	0.019566	0.008497
3	7.2226562	7.2487480	7.2697616	7.2799133	0.026092	0.021014	0.010152
4	13.597656	13.622965	13.644592	13.655566	0.025309	0.021627	0.010974
5	21.972656	21.997539	22.019506	22.030972	0.024883	0.021967	0.011466
6	32.347656	32.372268	32.394456	32.406247	0.024612	0.022188	0.011791
7	44.722656	44.747087	44.769414	44.781445	0.024431	0.022327	0.012031
8	59.097656	59.121946	59.144399	59.156595	0.024290	0.022453	0.012196
9	75.472656	75.496843	75.519383	75.531712	0.024187	0.022540	0.012329
10	93.847656	93.871769	93.894367	93.906806	0.024113	0.022598	0.012439
50	2468.8477	2468.8713	2468.8945		0.0236	0.0232	

[a] Nonrelativistic energies; footnote 3.
[b] $E_{(1s1s')}-E_{(1s)^2}$.
[c] $E_{[\text{Eq.(1)}]}-E_{(1s1s')}$.
[d] $E_{\text{Pekeris}}-E_{[\text{Eq.(1)}]}$.

By neglecting the antisymmetric spin function, the ^1S normalized wave function may be written as

$$\psi=(1+\lambda^2)^{-\frac{1}{2}}\{N[1s(1)1s'(2)+1s'(1)1s(2)] + (\lambda/\sqrt{3})[2p_0(1)2p_0(2)+2p_+(1)2p_-(2) +2p_-(1)2p_+(2)]\}, \quad (1)$$

where N is the normalization constant for the $(1s1s')$ function and λ is a variational parameter. Wave function (1) was constructed with hydrogen-like atomic orbitals.[21] The normalized radial portions of these are

$$R_{10}=2a^{\frac{3}{2}}\exp-ar, \quad (2.1)$$

$$R_{10}'=2b^{\frac{3}{2}}\exp-br, \quad (2.2)$$

$$R_{21}=(2/\sqrt{3})g^{5/2}r\exp-gr, \quad (2.3)$$

where a, b, and g are the variationally determined orbital exponents. Such a function has previously been employed by Taylor and Parr[19] for energy calculations of helium alone without completely optimizing the parameters.

[21] Our selection of the ^1S function of $(2p)^2$ corresponds to a normalization of the spherical harmonics for which $Y^*_{l,m}(\theta,\phi)=Y_{l,-m}(\theta,\phi)$. See C. W. Ufford and G. H. Shortley, Phys. Rev. **42**, 167 (1932).

II. CALCULATIONS

A. Energy

The optimum parameters of Eq. (1) for $1\leq Z\leq 10$ and $Z=50$[22] were determined by an iterative process described elsewhere.[9] These parameters as well as the optimum orbital exponents of $(1s1s')$,[23] taken as a single configuration, are presented in Table I. The angularly correlated energies from (1) are given in Table II where they are compared with the results of three other approximations, namely, $(1s)^2$, $(1s1s')$ and the function of Pekeris.[3] All energies are in atomic units.[24]

B. Expectation Values of Other Operators

The operators considered here are $r^n=(r_1^n+r_2^n)$, $(n\geq -2)$; $\delta^{(3)}(\mathbf{r}_1)$, and $\delta^{(3)}(\mathbf{r}_{12})$.[25] The angularly

[22] The case of $Z=50$ was included in the calculations as a numerical check on the analytically derived optimized parameters and energy for large Z discussed in reference 18.

[23] The optimum $(1s1s')$ orbital exponents were refined by a more sensitive numerical method to greater accuracy than values reported in references 8 and 9.

[24] As the atomic unit of energy, we have used $2hcR_M$, where R_M is the Rydberg of the atom or ion in question.

[25] See H. A. Bethe and E. E. Salpeter, *Handbuch der Physik* (Springer-Verlag, Berlin, 1957), Vol. 35, Part 1, p. 248 ff.

TABLE III. Expectation values of r^{-2} in atomic units.

Z	$(1s)^2$	$(1s1s')$	Eq. (3)
1	1.8906	2.1868	2.1947
2	11.391	11.930	11.916
3	28.891	29.676	29.659
4	54.391	55.424	55.419
5	87.891	89.173	89.152
6	129.39	130.92	130.89
7	178.89	180.67	180.57
8	236.39	238.42	238.40
9	301.89	304.17	304.18
10	375.39	377.92	377.88
50	9875.4	9887.9	9887.9

TABLE IV. Expectation values of r^{-1} in atomic units.

Z	$(1s)^2$	$(1s1s')$	Eq. (3)
1	1.3750	1.3225	1.3546
2	3.3750	3.3717	3.3743
3	5.3750	5.3739	5.3747
4	7.3750	7.3744	7.3755
5	9.3750	9.3747	9.3744
6	11.375	11.375	11.374
7	13.375	13.375	13.373
8	15.375	15.375	15.375
9	17.375	17.375	17.376
10	19.375	19.375	19.374
50	99.375	99.375	99.375

TABLE V. Expectation values of r in atomic units.

Z	$(1s)^2$	$(1s1s')$	Eq. (3)
1	4.3636	6.2247	5.6152
2	1.7778	1.8758	1.8681
3	1.1163	1.1490	1.1477
4	0.81356	0.82979	0.82930
5	0.64000	0.64968	0.64955
6	0.52747	0.53390	0.53385
7	0.44860	0.45317	0.45307
8	0.39024	0.39366	0.39365
9	0.34532	0.34798	0.34795
10	0.30968	0.31180	0.31180
50	0.60377×10^{-1}	0.60454×10^{-1}	0.60454×10^{-1}

TABLE VI. Expectation values of r^2 in atomic units.

Z	$(1s)^2$	$(1s1s')$	Eq. (3)
1	12.694	33.993	26.209
2	2.1070	2.4757	2.4470
3	0.83072	0.90623	0.90323
4	0.44125	0.46830	0.46754
5	0.27307	0.28569	0.28551
6	0.18548	0.19236	0.19231
7	0.13416	0.13831	0.13821
8	0.10153	0.10423	0.10421
9	0.79499×10^{-1}	0.81350×10^{-1}	0.81333×10^{-1}
10	0.63933×10^{-1}	0.65257×10^{-1}	0.65259×10^{-1}
50	0.24303×10^{-2}	0.24396×10^{-2}	0.24396×10^{-2}

TABLE VII. Expectation values of r^4 in atomic units.

Z	$(1s)^2$	$(1s1s')$	Eq. (3)
1	201.43	2749.2	1541.1
2	5.5493	9.3729	9.0585
3	0.86262	1.1503	1.1387
4	0.24338	0.29657	0.29516
5	0.93207×10^{-1}	0.10833	0.10812
6	0.43006×10^{-1}	0.48552×10^{-1}	0.48499×10^{-1}
7	0.22499×10^{-1}	0.24905×10^{-1}	0.24835×10^{-1}
8	0.12885×10^{-1}	0.14062×10^{-1}	0.14057×10^{-1}
9	0.79001×10^{-2}	0.85300×10^{-2}	0.85254×10^{-2}
10	0.51094×10^{-2}	0.54707×10^{-2}	0.54707×10^{-2}
50	0.73828×10^{-5}	0.74774×10^{-5}	0.74774×10^{-5}

TABLE VIII. Expectation values of r^8 in atomic units.

Z	$(1s)^2$	$(1s1s')$	Eq. (3)
1	2840.2×10^2	1312.7×10^5	4224.7×10^4
2	215.56	1112.5	1019.4
3	5.2088	13.632	13.246
4	0.41464	0.81690	0.80579
5	0.60812×10^{-1}	0.10257	0.10195
6	0.12946×10^{-1}	0.19802×10^{-1}	0.19730×10^{-1}
7	0.35433×10^{-2}	0.50679×10^{-2}	0.50176×10^{-2}
8	0.11621×10^{-2}	0.15828×10^{-2}	0.15812×10^{-2}
9	0.43688×10^{-3}	0.57335×10^{-3}	0.57250×10^{-3}
10	0.18274×10^{-3}	0.23292×10^{-3}	0.23290×10^{-3}
50	0.38155×10^{-9}	0.39938×10^{-9}	0.39938×10^{-9}

TABLE IX. Expectation values of $\delta^{(3)}(\mathbf{r}_1)$ in atomic units.

Z	$(1s)^2$	$(1s1s')$	Eq. (4)	Pekeris[a]
1	0.10344	0.16116	0.15742	0.1645
2	1.5296	1.7512	1.7430	1.8104
3	6.1787	6.6863	6.6744	6.8519
4	15.960	16.874	16.864	17.198
5	32.785	34.224	34.204	34.758
6	58.562	60.645	60.612	61.443
7	95.201	98.048	97.928	99.162
8	144.61	148.34	148.32	149.82
9	208.71	213.44	213.44	215.34
10	289.39	295.25	295.20	297.62
50	39047.	39196.	39196.	

[a] See footnote 3.

TABLE X. Expectation values of $\delta^{(3)}(\mathbf{r}_{12})$ in atomic units.

Z	$(1s)^2$	$(1s1s')$	Eq. (5)	Pekeris[a]
1	0.12929×10^{-1}	0.53780×10^{-2}	0.49191×10^{-2}	0.2742×10^{-2}
2	0.19120	0.16477	0.14462	0.10641
3	0.77233	0.71114	0.65251	0.53389
4	1.9951	1.8841	1.7683	1.5232
5	4.0981	3.9224	3.7285	3.3128
6	7.3202	7.0649	6.7737	6.1415
7	11.900	11.550	11.149	10.248
8	18.077	17.617	17.076	15.871
9	26.088	25.504	24.812	23.249
10	36.174	35.451	34.578	32.622
50	4880.9	4862.4	4838.9	

[a] See footnote 3.

TABLE XI. Various expectation values in atomic units for ^1S He.

Function or method	Hartree-Fock	$(1s)^2$	Perturbation[d] procedure	$(1s1s')$	Eq. (1)	Correlated[e] configuration-interaction	Hylleraas-type	Exptl.
$-E=-\langle H\rangle$	2.8617[a]	2.8477		2.8757	2.8952	2.90228	2.90372[f]	2.90372[f]
$\langle r^{-1}\rangle$		3.375	3.375	3.372	3.374		3.376,[g] 3.377[h]	
$\langle r\rangle$	1.860[b]	1.778		1.876	1.868	1.794	1.859[h]	
$\langle r^2\rangle$	2.386[b]	2.107	2.309	2.476	2.447	2.282	2.37[i], 2.387[h]	2.439[j]
$\langle r^3\rangle$	3.888[b]	3.121		4.299	4.206	3.802		
$\langle\delta^{(3)}(\mathbf{r}_1)\rangle$	1.798[c]	1.530	1.849	1.751	1.743		1.810[h]	
$\langle\delta^{(3)}(\mathbf{r}_{12})\rangle$	0.188[c]	0.1912		0.1648	0.1446		0.1064[h]	

[a] Computed with an analytic SCF function; see footnote 17.
[b] Computed with an analytic SCF function; see footnote 26.
[c] See footnote 25.
[d] See footnote 27.
[e] See footnote 26.
[f] Computed nonrelativistic energy; see footnote 3.
[g] See footnote 28.
[h] See footnote 3.
[i] See footnote 27(b).
[j] See footnote 29.

correlated expectation values in atomic units are found to be

$$\langle r^n\rangle=\langle r_1^n\rangle+\langle r_2^n\rangle=(1+\lambda^2)^{-1}\{N^2(n+2)![(2a)^{-n}+(2b)^{-n}+(a+b)^{-n}2S^2(a,b)]+\lambda^2[(n+4)!/12](2g)^{-n}\};\quad n\geq -2, \tag{3}$$

$$\langle\delta^{(3)}(\mathbf{r}_1)\rangle=(1+\lambda^2)^{-1}(N^2/4\pi)[4a^3+4b^3+(a+b)^3S^2(a,b)], \tag{4}$$

$$\langle\delta^{(3)}(\mathbf{r}_{12})\rangle=(1+\lambda^2)^{-1}(1/\pi)\{4N^2[ab/(a+b)]^3+128\sqrt{3}N\lambda(ab)^{\frac{3}{2}}[g/(a+b+2g)]^5+\tfrac{15}{256}\lambda^2g^3\}, \tag{5}$$

where

$$N=[2+2S^2(a,b)]^{-\frac{1}{2}} \tag{6}$$

and

$$S(a,b)=\int 1s1s'd\tau=8[(ab)^{\frac{3}{2}}/(a+b)^3]. \tag{7}$$

Equations (3)–(5) reduce to the corresponding open-shell form for $\lambda=0$ and further to the closed-shell expression for $a=(Z-\frac{5}{16})=b$. The angularly correlated, open-shell, and closed-shell values of $\langle r^n\rangle$ for $n=-2$, -1, 1, 2, 4, and 8 are presented in Tables III to VIII, $\langle\delta^{(3)}(\mathbf{r}_1)\rangle$ in Table IX, and $\langle\delta^{(3)}(\mathbf{r}_{12})\rangle$ in Table X. As a guide in estimating the accuracy of these results, we have included the values of $\langle\delta^{(3)}(\mathbf{r}_1)\rangle$ and $\langle\delta^{(3)}(\mathbf{r}_{12})\rangle$ computed by Pekeris[3] in Tables IX and X, respectively, and have collected in Table XI some calculated[17,26–28] and experimental[29] expectation values for the helium atom.

In addition, x-ray atomic scattering factors calculated with (1) have been presented and will be published elsewhere.[30]

C. Extrapolation Procedure

Numerous attempts have been made to extrapolate experimentally obtained energies of isoelectronic series to systems for which accurate experimental measurements are not available.[31] For this purpose, a series in descending powers of Z has usually been employed as the semiempirical extrapolation function.[32] The electron affinities of negative ions found in this manner are estimated to be too low, the error increasing with atomic number.[31] The relatively small differences between experimental energies and computed nonrelativistic energies from an approximate wave function suggest that greater accuracy might be obtained by extrapolating these differences rather than the experimental energies themselves. On testing this procedure with helium-like ions, this was found to be the case with the best results being given by an extrapolation function

[26] P.-O. Löwdin and L. Redei, Phys. Rev. **114**, 752 (1959).
[27] (a) C. Schwarz, Ann. Phys. **6**, 170 (1959); (b) *ibid.*, footnote 2.
[28] E. Hylleraas and S. Skavlem, Phys. Rev. **79**, 117 (1950).
[29] G. G. Havens, Phys. Rev. **43**, 992 (1933); A. Dalgarno and N. Lynn, Proc. Phys. Soc. (London) **A70**, 802 (1957). See also A. P. Wills and L. G. Hector, Phys. Rev. **23**, 209; **24**, 418 (1924) for an earlier determination of $\langle r^2\rangle$.
[30] J. N. Silverman, O. Platas, R. D. McIver, and F. A. Matsen, Bull. Am. Phys. Soc. Ser. II **4**, 105 (1959); Acta Cryst. (to be published).
[31] See, for example, H. S. W. Massey, *Negative Ions* (Cambridge University Press, New York, 1950).
[32] Such a series was first employed by E. A. Hylleraas, Z. Physik **65**, 209 (1930) for perturbation-variation energy calculations. See also reference 25, pp. 214 and 237 ff for a discussion of the theoretical justification of this series.

TABLE XII. Extrapolated and experimental[a] ground state energies for some helium-like ions.

Wave function	$-E_{\text{calc}}$ $(1s)^2$		$(1s1s')$		Eq. (1)		
Z	R[b] $\mathcal{E}$	$\mathcal{E}/Z$	$\mathcal{E}$	$\mathcal{E}/Z$	$\mathcal{E}$	$\mathcal{E}/Z$[d]	$-E_{\text{exptl}}$[a]
1	0.50929	0.49162	0.53180	0.52272	0.53007	0.52756	0.52774
2	2.8999	2.8921	2.9031	2.8987	2.9038	2.9027	2.9038
10	94.011	94.039	94.010	94.015	94.009	94.011	94.009
σ[c]	0.0060	0.0153	0.0013	0.0030	0.0007	0.0009	

[a] The computed energies of reference 3, including mass polarization, relativistic, and Lamb shift corrections, were used as the experimental energies in obtaining the least-squares fit.
[b] See Eq. (8) and text.
[c] Root-mean square deviation over range $1 \leq Z \leq 10$.
[d] The least-squares parameters used here are: $C_1 = -0.00471967$, $C_2 = 0.00208884$, $C_3 = -0.0003$, $89210C_4 = 0.0000319548$, $C_5 = -0.00000103732$.

of the form[33]

$$R_j = \sum_{i=1}^{n} C_i Z_j^i; \quad C_0 = 0, \tag{8}$$

where we have taken R_j as $\mathcal{E}_j = (E_j \text{ exptl.} - E_j \text{ calc})$ and also as $\mathcal{E}_j/Z_j$. By using five parameters and fitting intermediate values $(3 \leq Z \leq 9)$ by the method of least squares, extrapolated values of the energy for $Z = 1$, 2, and 10 were obtained for the three approximations: $(1s)^2$, $(1s1s')$, and Eq. (1). These results are presented in Table XII where they are compared with experimental values.

III. DISCUSSION

The asymptotic behavior of the variational parameters and energy for large Z is discussed elsewhere.[18] From Table II, it is seen that with increasing nuclear charge, the magitudes of the radial- and angular-correlation energy increments approach their limiting values from above and below, respectively, while their sum remains approximately constant. This behavior closely parallels that found by Green *et al.*,[15] who expanded Hylleraas-type functions for H^-, He, and Li^+ in terms of radial and angular orthogonal functions. Function (1) gives energies which differ from those obtained from the elaborate Pekeris[3] function by only about 0.010 to 0.012 atomic unit for $Z \geq 3$ and by a smaller amount for $Z < 3$. The data in Tables III through IX show that in general the angularly correlated expectation values of r^n and $\delta^{(3)}(\mathbf{r}_1)$ are intermediate to the corresponding closed- and open-shell values and approach the latter with increasing Z. For small Z and large n, the expectation values of r^n obtained from these three approximations differ widely (e.g., see Tables VII and VIII). From Table XI it is seen that $\langle r^{-1} \rangle$, which gives the nuclear diamagnetic shielding,[12] is relatively insensitive to the choice of wave function as all calculated values are in good agreement. There is a greater variation in the calculated values of $\langle r^2 \rangle$, the atomic diamagnetism. In fact, the value of $\langle r^2 \rangle$ calculated with (1) is in better agreement with the most recent experimental result[29] than that calculated with Kinoshita's[2,27] or Pekeris'[3] wave function (see Table XI). An experimental redetermination of this quantity would be of interest. $\langle \delta^{(3)}(\mathbf{r}_1) \rangle$ and $\langle \delta^{(3)}(\mathbf{r}_{12}) \rangle$ are relativistic corrections which afford some measure of electronic correlation. Values of these quantities computed with (1) are in reasonably good agreement with the results obtained by Pekeris[3] (see Tables IX and X). In particular, our computed values of $\langle \delta^{(3)}(\mathbf{r}_{12}) \rangle$ are in much better agreement than the Hartree-Fock, closed- and open-shell values (see Table XI).

In most cases, the expectation values calculated with (1) are surprisingly close to those obtained for the more accurate wave functions. There is, in these results, the implication that functions of the simplicity of (1) may be able to give good approximations to the properties of more complex systems.

It appears that the expectation values calculated with simple functions are quite useful for the accurate extrapolation of the observables from an isoelectronic series. In general, at least one significant figure is gained by extrapolating the difference between the experimental energies and those calculated with $(1s)^2$, $(1s1s')$, and Eq. (1) (see Tables II and XII). While (1) gives the best results, the extrapolation in terms of $(1s1s')$ also is quite good.

[33] For this purpose, an extrapolation function in ascending powers of Z seems preferable to the Hylleraas-type series of reference 32 because the relativistic corrections depend upon higher powers of Z. See the relativistic corrections in reference 3 and the discussion in A. Fröman, Phys. Rev. **112**, 870 (1958).

Simple Configuration-Interaction Wave Functions. II. Two-Electron Ions: An Analytic Study*†

CHARLES W. SCHERR, *Department of Physics, The University of Texas, Austin, Texas*
AND
JEREMIAH N. SILVERMAN, *Department of Chemistry, The University of Texas, Austin, Texas*

(Received September 11, 1959)

An analytical study of the ^1S ground state of helium-like ions employing the open-shell function $(1s1s')$ and the angularly correlated configuration-interaction function $(1s1s')+\lambda(2p)^2$ has been made. Expressions for the wave function parameters, energy values, and certain other expectation values in terms of the nuclear charge Z have been obtained. These are asymptotic expressions for large Z, but they reproduce numerically obtained results for small Z with sufficient accuracy to be useful for many purposes.

INTRODUCTION

IN the first paper of the present series[1] Silverman, Platas, and Matsen have considered in numerical detail ground state wave functions for two-electron atomic systems of the form

$$(1+\lambda^2)^{-\frac{1}{2}}\{N[1s(1)1s'(2)+1s'(1)1s(2)] + (\lambda/\sqrt{3})[2p_0(1)2p_0(2) + 2p_+(1)2p_-(2)+2p_-(1)2p_+(2)]\} \quad (1)$$

about a nucleus of charge Z. The N is a normalization factor for the first term in the braces, and λ is a variation parameter. Their purpose was the practical one of making parameters and results available to facilitate estimations of atomic properties, as well as to study the behavior of configuration-interaction in this simple case. In the present paper certain of their numerical results are reproduced by purely analytic means.

NOTATION

We work throughout in atomic units[2] so that the Hamiltonian for the two-electron atom of nuclear charge Z is

$$-\tfrac{1}{2}\nabla_1^2-\tfrac{1}{2}\nabla_2^2-(Z/r_1)-(Z/r_2)+(1/r_{12}). \quad (2)$$

Our wave function, Eq. (1), is constructed from hydrogen-like atomic orbitals. The normalized radial portions are defined as follows:

$$R_{10}=2\zeta^{\frac{3}{2}}(1+x)^{\frac{1}{2}}\exp[-\zeta(1+x)r], \quad (3.1)$$

$$R_{10}'=2\zeta^{\frac{3}{2}}(1-x)^{\frac{1}{2}}\exp[-\zeta(1-x)r], \quad (3.1')$$

$$R_{21}=\tfrac{2}{3}\sqrt{3}(\zeta y)^{5/2}r\exp[-\zeta yr]. \quad (3.2)$$

The relevant integrals were evaluated by standard methods.[3] Equation numbers followed by an asterisk indicate that the corresponding equations are the basis of a columnar entry in one of the tables. Exact equalities are indicated by an ordinary equals sign, and approximations by the usual symbol. The subscript c refers to closed-shell values; the subscript o refers to open-shell values; the subscript a refers to angularly correlated values. The use of these subscripts indicates specifically an optimized quantity.

CLOSED SHELL $(1s)^2$

Here $x=0$ and $\lambda=0$. We state the well-known results for optimum energy,

$$\zeta_c=(Z-\tfrac{5}{16}), \quad (4)$$

$$E_c=-(Z-\tfrac{5}{16})^2. \quad (5)$$

OPEN SHELL N$(1s1s'+1s'1s)$

Here $\lambda=0$. An explicit expression for the unoptimized energy as a function of the parameters has been given by Shull and Löwdin.[4] They performed their optimization numerically, however, and for a limited range of Z. This numerical approach obscured certain interesting points. In our notation the energy is given by

$$E=(1-x^2)\zeta^2+(\tfrac{5}{8}-2Z)\zeta+\frac{16\zeta^2-(6-x^2)\zeta}{8[1+(1-x^2)^{\frac{1}{2}}]}x^2. \quad (6)$$

One may immediately minimize with respect to ζ to obtain

$$\zeta_o(x^2,Z)=\frac{(16Z-5)[1+(1-x^2)^{\frac{1}{2}}]+(6-x^2)x^2}{16\{(1-x^2)[1+(1-x^2)^{\frac{1}{2}}]+2x^2\}}. \quad (7)$$

Resubstitution into Eq. (6) gives

$$E_o(x^2,Z)=-\zeta_o^2(x^2,Z)\frac{(1-x^2)[1+(1-x^2)^{\frac{1}{2}}]+2x^2}{1+(1-x^2)^{\frac{1}{2}}}. \quad (8)$$

* This research was supported in part by the Robert A. Welch Foundation of Houston, Texas.

† Briefly reported on at the Boulder Conference, Boulder, Colorado (June, 1959).

[1] J. N. Silverman, O. Platas, and F. A. Matsen, J. Chem. Phys. 32, 1402 (1960), this issue.

[2] Unit of length is a_0, the Bohr radius; unit of energy is $2hcR_M$.

[3] C. C. J. Roothaan, J. Chem. Phys. 19, 1445 (1951), for example.

[4] H. Shull and P.-O. Löwdin, J. Chem. Phys. 25, 1035 (1956); also cf. R. P. Hurst, J. D. Gray, G. H. Brigman, and F. A. Matsen, Mol. Phys. 1, 189 (1958).

TABLE I. Wave-function parameters and energies.[a]

Z		2	3	4	10	50
ζ_0	Computed[b]	1.685851	2.686945	3.687224	9.687464	49.68750
ζ_a	Computed	1.688865	2.688547	3.688663	9.687436	49.68750
x_0^2	Eq. (10)	0.0652174	0.0428571	0.0319149	0.0126050	0.00250417
	Quadratic[c]	0.0962698	0.0524520	0.0367033	0.0132498	0.00252804
	Computed	0.0870230	0.0511963	0.0362996	0.0132326	0.00252800
x_a^2	Computed	0.0832705	0.0500046	0.0357782	0.0132320	0.00252800
$\zeta_0(1+x_0)$	Eq. (12)	2.1875	3.2999	4.3946	10.806	52.188
	Computed	2.1832	3.2949	4.3897	10.802	52.186
$\zeta_a(1+x_a)$	Computed	2.1762	3.2898	4.3864	10.802	52.186
$\zeta_0(1-x_0)$	Eq. (12)	1.1875	2.0751	2.9804	8.5695	47.188
	Computed	1.1885	2.0790	2.9847	8.5731	47.189
$\zeta_a(1-x_a)$	Computed	1.20152	2.0873	2.9909	8.5731	47.189
y_a	Computed	1.46576	1.46448	1.46358	1.46427	1.46431
$-\lambda$	Eq. (27)	0.06951	0.04366	0.03182	0.01212	0.002362
	Computed	0.06176	0.04074	0.03032	0.01190	0.002355
$-E_0$	Eq. (15)	2.8710938	7.2460938	13.621094	93.871094	2468.8711
	Computed	2.8756614	7.2487480	13.622965	93.871769	2468.8713
$-E_a$	Eq. (26)	2.8945415	7.2695415	13.644541	93.894541	2468.8945
	Computed	2.8952278	7.2697616	13.644592	93.894367	2468.8945

[a] Atomic units.
[b] Computed refers throughout to the numerical calculations of footnote 1.
[c] Calculated with the quadratic approximation to Eq. (9).

The energy in Eq. (8) is next optimized with respect to x^2. After some manipulation one obtains

$$16Zx_0^2(24-90x_0^2+169x_0^4-201x_0^6+162x_0^8-91x_0^{10}+36x_0^{12}-9x_0^{14}+x_0^{16})=48+32x_0^2-414x_0^4+1013x_0^6-1388x_0^8+1188x_0^{10}-644x_0^{12}+224x_0^{14}-48x_0^{16}+5x_0^{18}. \quad (9)$$

Now x_0^2 is a small quantity (cf. Table I). Thus, we solve for x_0^2 retaining only first-order terms and obtain

$$x_0^2\approx 3/(24Z-2). \quad (10)^*$$

If one is interested in a particular ion, it is worthwhile to expand to second order in x_0^2 and solve the resulting quadratic equation.[5] The degree of accuracy so obtained is indicated in Table I. As a further approximation when Z is large, we may write

$$x_0^2\approx 1/8Z. \quad (10')$$

When Eq. (7) is expanded to the second order in x^2, and then has x^2 substituted for according to Eq. (10), we obtain

$$\zeta_0\approx Z-\tfrac{5}{16}+O(1/Z^2), \quad (11)$$

i.e., essentially ζ_c. By dropping the term in Z^{-2}, we obtain from Eqs. (11) and (10) that

$$x_0\zeta_0\approx x_0\zeta_c\approx (Z-\tfrac{5}{16})[3/(24Z-2)]^{\frac{1}{2}}.$$

We expand the square root in powers of Z^{-1} and obtain

$$x_0\zeta_0\approx \tfrac{1}{4}(2Z)^{\frac{1}{2}}(1-13/48Z),$$

so that finally the orbital exponents for (3.1) and (3.1′) are, respectively,

$$\zeta_0(1+x_0)\approx Z+\tfrac{1}{4}(2Z)^{\frac{1}{2}}-\tfrac{5}{16},$$
$$\zeta_0(1-x_0)\approx Z-\tfrac{1}{4}(2Z)^{\frac{1}{2}}-\tfrac{5}{16}. \quad (12)^*$$

If we expand Eq. (8) to second order in x^2, we obtain

$$E_0(x^2, Z)\approx -\zeta_0^2(x^2, Z)(1+\tfrac{3}{2}x^4)$$

or, putting in the optimized values,

$$E_0\approx E_c(1+\tfrac{3}{2}x_0^4). \quad (13)$$

By substituting Eq. (10) and expanding the denominator in powers of Z^{-1} [or from Eq. (10′) directly], we obtain

$$E_0\approx E_c(1+3/128Z^2+1/256Z^3+\cdots), \quad (14)$$

or

$$E_0-E_c\approx 3E_c/128Z^2=-3(Z-\tfrac{5}{16})^2/128Z^2,$$

so that

$$E_0-E_c\approx -3/128. \quad (15)^*$$

[5] In this paper, we are only concerned with the root of Eq. (9) corresponding to the ground state. This root, which must be less than unity, is given to the first order by Eq. (10). For $Z=1$, the extraneous roots were found to be 0.880382 (which corresponds to an energy maximum), unity (which corresponds to the energy of a hydrogen atom plus a just ionized electron), two roots greater than unity and four complex roots.

That is, the energies of the closed-shell and open-shell configurations differ by a constant amount for large enough Z. This result is contrary to previous speculation.[4]

ANGULAR CORRELATION: ADDITION OF $(2p)^2$

In this case we obtain a secular determinant

$$\begin{vmatrix} H_{11}-E & H_{12} \\ H_{12} & H_{22}-E \end{vmatrix} = 0, \tag{16}$$

where H_{11} is given by the E of Eq. (6). In addition, we have

$$H_{12}=\frac{4(6)^{\frac{1}{2}}y^5[7(1+y)^2-3x^2](1-x^2)^{\frac{1}{2}}\zeta}{3(1+y)^5[1+(1-x^2)^3]^{\frac{1}{2}}[(1+y)^2-x^2]^2}, \tag{17}$$

and

$$H_{22}=y^2\zeta^2-(Z-111/256)y\zeta. \tag{18}$$

Since the problem now has three parameters (two of them nonlinear), we cannot give quite so exhaustive a discussion as in the previous sections. Thus, in order to proceed, we assume that for large Z the addition of the $(2p)^2$ does not appreciably affect the optimized values of the open-shell parameters so that

$$x_a^2\approx x_o^2; \qquad \zeta_a\approx\zeta_o. \tag{19}$$

Actually, due to the very small mixing coefficient, the assumption is excellent even for $Z=2$, as may be seen in Table I. Since x_a^2 is a small quantity for large Z, it should negligibly affect the limiting values of λ_a and y_a. Thus, to determine these quantities, we may write

$$H_{11}/\zeta^2\approx -1 \tag{20}$$

and

$$H_{12}/\zeta\approx 28y^5/\sqrt{3}(1+y)^7. \tag{21}$$

For large Z,

$$H_{22}/\zeta^2\approx y^2-y. \tag{22}$$

The second-order perturbation energy approximation to the solution of Eq. (16) is given by

$$E\approx E_o+\epsilon_2$$

where

$$\epsilon_2=H_{12}^2/(H_{11}-H_{22})$$
$$\approx -[784y^{10}/3(1+y)^{14}(y^2-y+1)]. \tag{23}$$

We maximize the magnitude of this quantity with respect to y. This procedure leads to a cubic equation for y_a which has only one real foot,

$$y_a\approx 1.4643059. \tag{24}*$$

This value should be compared with the computed values listed in Table I, where it is seen that the convergence is rapid. We now use this value to find ϵ_{2a};

$$\epsilon_{2a}=-0.023147736. \tag{25}$$

Now

$$E_a\approx E_o+\epsilon_{2a}$$
$$\approx E_c-(3/128)+\epsilon_{2a}.$$

Therefore

$$E_a\approx E_c-0.046585236. \tag{26}*$$

That is, the wave function of Eq. (1) gives an energy which differs by a constant amount from the simple open-shell configuration result for large enough Z,[6] and this constant difference is very nearly equal to a similar constant difference between E_0 and E_c [Eq. (15)], despite the fact that the mixing coefficient becomes quite small for large Z. We obtain the mixing coefficient from Eq. (16) by using Eqs. (21), (24), and (25).

$$\lambda=-0.11738547/\zeta_a. \tag{27}*$$

ζ_a may be replaced by ζ_o in Eq. (27).

One may also obtain immediately the values for a wave function of the form

$$(1s)^2+\lambda(2p)^2 \tag{28}$$

by replacing the appropriate quantities in Eqs. (26) and (27) by the closed-shell values. Thus, the optimum energy for the wave function (28) is

$$E_{\rm opt}\approx E_c-0.023147736. \tag{29}$$

MEAN VALUE OF r^n AND OTHER OPERATORS

One finds easily for the simple open-shell wave function that to first order in x^2

$$\langle r^n\rangle_o=\langle r_1^n\rangle_o+\langle r_2^n\rangle_o$$
$$\approx[(n+2)!/(2\zeta_o)^n][1+n(n+1)x_o^2/4]; \quad n\geq -2 \tag{30}$$

and[7]

$$\langle\delta^{(3)}(\mathbf{r}_1)\rangle_o=\langle\delta^{(3)}(\mathbf{r}_2)\rangle_o\approx\zeta_o^3(1+\tfrac{3}{2}x_o^2)/\pi, \tag{31}$$

$$\langle\delta^{(3)}(\mathbf{r}_{12})\rangle_o\approx\zeta_o^3(1-\tfrac{3}{2}x_o^2)/8\pi. \tag{32}$$

Equations (30)–(32) reduce to the equivalent closed-shell expressions for $x^2=0$. One may consult the first paper of this series for the exact expressions of the angularly correlated expectation values from which approximations similar to Eqs. (30)–(32) may be obtained.

---

[6] The perturbation series expansion of the energy of two-electron ions may be written as

$$E=-Z^2+(5/8)Z+E_2(Z).$$

Hylleraas and Midtdal [E. A. Hylleraas and J. Midtdal, Phys. Rev. **103**, 829 (1956); **109**, 1013 (1958)] find $E_2(\infty)=-0.157657_8$; our best approximation to this quantity, computed with equations (5) and (26), is -0.14424149.

[7] See, for example, H. A. Bethe and E. E. Salpeter, *Handbuch der Physik* (Springer-Verlag, Berlin, 1957), Vol. 35, Part 1, p. 248 ff.

Effect of Metal Atom Perturbations on the Luminescent Spectra of Porphyrins*

JEAN B. ALLISON† AND RALPH S. BECKER

Department of Chemistry, University of Houston, Houston, Texas

(Received August 11, 1959)

The low-temperature emission spectra of the dimethyl ester of mesoporphyrin IX and its divalent derivatives of cobalt, nickel, copper, zinc, palladium, cadmium, and barium have been obtained. Magnesium etioporphyrin(II) and zinc phthalocyanine were also investigated. The divalent silver mesoporphyrin was also studied, but no luminescence was obtained for this compound. Considerations of the relative lifetimes of fluorescence and phosphorescence of the various derivatives permit qualitative deductions to be made regarding magnetic susceptibility. Certain qualitative information on metal-porphyrin bonding is presented based on the comparative intensities of fluorescence and phosphorescence. Anomolous emission characteristics of several of the metallo-porphyrins are tentatively interpreted in terms of crossing of a first excited state and the ground state.

INTRODUCTION

IN the present investigation, the low-temperature electronic emission spectra of the dimethyl ester of mesoprophyrin IX and several of its metallo derivatives as well as that of magnesium etioporphyrin II and zinc phthalocyanine are reported. By considering the types of emission obtained (i.e., fluorescence and phosphorescence) together with their relative intensities and lifetimes, certain deductions are made regarding the nature of the metal-porphyrin bonding and the magnetic character of the central metal ion for these molecules.

Relatively few papers have appeared in which the emission spectra of metallo-porphyrins have been investigated. The most complete study, to the present time, concerning the effect of metal substituents on the emission spectra of one of the mesoporphyrins was carried out by Haurowitz.[1] He observed that all the diamagnetic metal complexes possessed fluorescent bands, while the paramagnetic derivatives had no such emission. Since no fluorescent bands were found for the nickel complex, it was included in the latter group. However, later magnetic susceptibility measurements[2] revealed that the metal ion in nickel porphyrins was actually diamagnetic. Another group of investigators[3,4] reported that the nickel, as well as the paramagnetic silver, derivative of a tetraphenylporphine, displayed weak fluorescent bands in the same region as those found for the uncomplexed tetraphenylporphine. Becker and Kasha[5] were the first to report a solely phosphorescent emission for nickel etioporphrin II in a region clearly discernible from that of the metal-free porphyrin.

Numerous investigators have studied the effects of various divalent metal ions upon the absorption spectra of porphyrins.[6–9] Dorough and co-workers actually attempted to correlate the changes in the absorption bands with the nature of the metal-nitrogen bonding present in these metallo-porphyrins. While all these studies are interesting and important, it should be pointed out that, so far, absorption spectral studies have been incapable of indicating any of the intricate differences that exist between the metal derivatives of the porphyrins. For example, the absorption spectra of copper and zinc porphyrin are very similar, yet the magnetic character of these two metal ions is entirely different (i.e., copper is paramagnetic whereas zinc is diamagnetic). In addition to this, the absorption spectral studies have been incapable of predicting certain unusual spectral emission properties often encountered in the metallo-porphyrins.

Normally, extensive x-ray and infrared analyses are carried out in order to ascertain the molecular geometry of a molecule. Although such studies do yield quantitative data, it will be shown that certain valuable qualitative information can be gained in a much shorter time from electronic spectral emission studies. Moreover, although quantitative susceptibilities can be obtained by means of a Gouy balance, qualitative data can be obtained from electronic spectral considerations in less time and with much less sample. It should be obvious that such information gained from emission spectral studies should not necessarily be limited to the prophyrin-like molecules, but could be extended to any number of metallo-organic molecules.

* This research was supported by a grant from the Robert A. Welch Foundation.

† Abstracted in part from a thesis submitted in partial fulfillment for the degree of Master of Science, University of Houston (1958).

[1] F. Haurowitz, Ber. deut. chem. Ges. **68**, 1795 (1935).

[2] F. Haurowitz and W. Klemm, Ber. deut. chem. Ges. **68**, 2312 (1935).

[3] H. V. Knorr and V. M. Albers, Phys. Rev. **57**, 347 (1940).

[4] V. M. Albers, H. V. Knorr, and D. L. Fry, J. Chem. Phys. **10**, 700 (1942).

[5] R. S. Becker and M. Kasha, J. Am. Chem. Soc. **77**, 3669 (1953).

[6] G. D. Dorough, J. R. Miller, and F. M. Huennekens, J. Am. Chem. Soc. **73**, 4315 (1951).

[7] R. J. P. Williams, Chem. Revs. **56**, 299 (1956).

[8] M. Gouterman, Ph.D. dissertation, University of Chicago, (1958); J. Chem. Phys. **30**, 1139 (1959).

[9] D. W. Thomas and A. E. Martell, Arch. Biochem. Biophys. **76**, 286 (1958).

TABLE I. Luminescence and lifetime data of metalloporphyrins.

Compound	Fluorescence		Phosphorescence		
	Position of 1st band–cm^{-1}	Relative intensity[a]	Position of 1st band–cm^{-1}	Relative intensity[a]	Estimated lifetime of triplet state
Mesoporphyrin IX, dimethyl ester	16 196	vs	13 310	vw	$\geq 5\times10^{-4}$ sec
Co(II) mesoporphyrin IX, dimethyl ester	None	...	14 908	vw	$<5\times10^{-4}$ sec
Ni(II) mesoporphyrin IX, dimethyl ester	None	...	14 680	vw	$\geq 5\times10^{-4}$ sec
Cu(II) mesoporphyrin IX, dimethyl ester	None	...	14 665	vs	$<5\times10^{-4}$ sec
Zn(II) mesoporphyrin IX, dimethyl ester	17 492	m	14 260	m	$\geq 5\times10^{-4}$ sec
Pd(II) mesoporphyrin IX, dimethyl ester	None	...	15 200	vs	$\geq 5\times10^{-4}$ sec
Ag(II) mesoporphyrin IX, dimethyl ester	Not observed	...	Not observed	...	...
Cd(II) mesoporphyrin IX, dimethyl ester	17 185	w	13 772	vs	$\geq 5\times10^{-4}$ sec
Ba(II) mesoporphyrin IX, dimethyl ester	16 780	vw	13 345	vs	$\geq 5\times10^{-4}$ sec
Mg(II) etioporphyrin II	16 972	s	13 439	w	$\geq 5\times10^{-4}$ sec
Zn(II) phthalocyanine	14 876	...	Not observed	...	...

[a] vs=very strong; s=strong; m=moderate; w=weak; vw=very weak.

EXPERIMENTAL

All absorption spectra were recorded on a Beckman model DK-1 spectrophotometer. Two instruments were employed for the emission spectral studies: (1) a Steinheil 3-prism spectrograph, model GH and (2) a Hilger medium (infrared) glass 1-prism spectrograph. The exciting light was supplied by a 1-kw Hanovia Xe-Hg compact arc lamp. The wavelength of this source was selectively controlled either by use of a combination of solution and glass filters or by a Bausch and Lomb grating monochromator. A modified Becquerel phosphorscope was used in conjunction with the spectrograph for obtaining solely phosphorescent emissions of the compounds whose lifetimes were sufficiently long, *ca.* 5×10^{-4} sec or longer. The emission spectra were determined at liquid nitrogen temperature in either of two solvent systems which formed a clear glass at 77°K: (1) EPA, 2 parts absolute ethanol, 5 parts ether, and 5 parts isopentane; or (2) EPAF, 3 parts absolute ethanol, 0.5 parts *N*,*N*-dimethylformamide, 6 parts ether, and 5 parts isopentane. The isopentane (Phillips instrument grade) and ether were purified by fractional distillation over calcium hydride. In addition, the isopentane was chromatographed by passing it through an activated silica gel column. The pure absolute ethanol and spectro grade *N*,*N*-dimethylformamide were used without further purification.

The absorption spectra of the compounds not prepared in our laboratory gave no indication of band characteristic of the parent porphyrin; however, subsequent investigation of their emission spectra disclosed trace amounts of the metal-free parent porphyrin in the cobalt, nickel, and palladium derivatives. Recrystallization from a methanol-chloroform[10] mixture failed to remove the contaminant completely. The purification process described by Erdman and coworkers[11] proved to be the most satisfactory. According to this method the metallo-porphyrin is first extracted with formic acid and then chromatographed on a calcium carbonate column. The acid extraction was eliminated for the cobalt derivative due to the extreme instability of this compound in an acid medium. Following this procedure, the emission spectra showed either no trace of parent porphyrin or exhibited these bands only upon extremely long exposure.

The divalent cadmium, silver, and barium mesoporphyrin were prepared by a modification of that described by Dorough, *et al.*[6] The conversion of the dimethyl ester of mesoporphyrin IX to the metalloporphyrin was carried out in a solvent medium which could be diluted with the appropriate solvents to form an EPAF glass. A 10^{-4} molar solution of the parent porphyrin in 0.6 ml of dimethylformamide was added to 1.0 ml of absolute ethanol saturated with the metal salt [e.g., $Cd(C_2H_3O_2)_2$, $Ag(C_2H_3O_2)$, or $Ba(OH)_2$]. The transformation to the metallo-porphyrin was approximately quantitative for the silver derivative if the reaction was greatly refluxed for several minutes.

The barium derivative was found to be unstable in solution; therefore, special precautions were observed when preparing this compound. In this case, the reaction was allowed to proceed at room temperature in the

[10] A. H. Corwin and J. G. Erdman, J. Am. Chem. Soc. **68**, 2473 (1946).

[11] J. G. Erdman, V. G. Ramsey, N. K. Kalenda, and W. E. Hanson, J. Am. Chem. Soc. **78**, 5844 (1956).

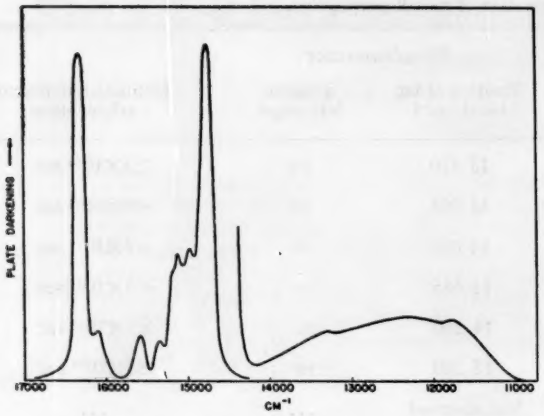

FIG. 1. Fluorescent and phosphorescent spectra of the dimethyl ester of mesoporphyrin IX in EPAF glass.

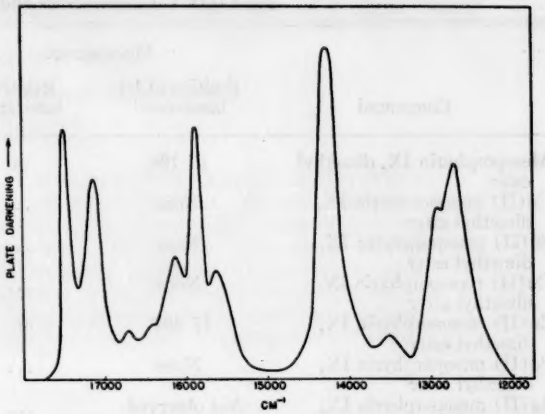

FIG. 3. Fluorescent and phosphorescent spectra of the dimethyl ester of zinc mesoporphyrin IX in EPA glass.

absence of light. After several minutes the mixture was diluted with the solvents necessary to form an EPAF glass (i.e., 2 ml. absolute ethanol, 6 ml of ether, and 5 ml of isopentane) and immediately cooled to 77°K. The absorption spectrum of barium mesoporphyrin indicated that 70–85% of the parent had been converted to the metal derivative. This procedure is exceptionally valuable in all those cases where the metal complex is unstable, such as the barium prophyrin. The concentration of all solutions was approximately $10^{-5}M$. Moreover, in the regions of excitation the integrated absorption areas were approximately equal.

RESULTS

All experimental results are summarized in Table I. The origin of the fluorescence and phosphorescence is given as well as an estimate of the lifetime associated with the triplet state. Figures 1–10 are densitometer tracings of the emission spectra of the compounds investigated (see Fig. 11 for formulas). Only the first fluorescent bands are shown for the barium and cadmium prophyrins due to the interference of the fluorescent spectrum of the parent compound present as an impurity. The emission spectra for the cobalt, palladium, and barium derivatives are reported and have not appeared in the literature previous to this investigation.

This investigation parallels the earlier work of Becker and Kasha[5] in which they reported what appeared to be a totally phosphorescent emission from nickel etioporphyrin II. No fluorescence was observed for the nickel or silver mesoporphyrins contrary to that reported for the corresponding tetraphenylporphines.[3,4] Thus, it is concluded that the reported fluorescent emission[3,4] was just that of the parent porphyrin present as an impurity.

DISCUSSION

The metallo derivatives of meosporphyrin provide an excellent series of compounds to illustrate the effect of increased spin-orbital interaction on the emission spectra. The parent meosporphyrin exhibits an emission spectrum consisting of very intense fluorescent bands

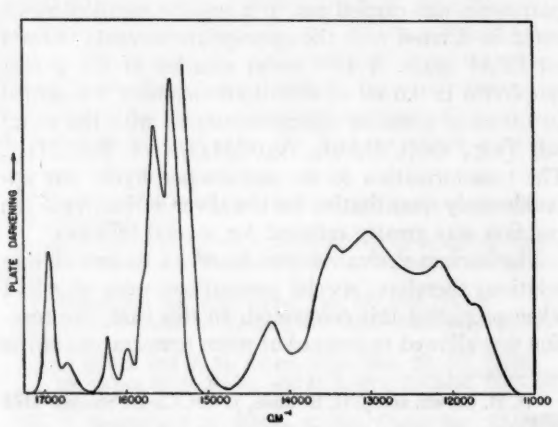

FIG. 2. Fluorescent and phosphorescent spectra of magnesium etioporphyrin II in EPA glass.

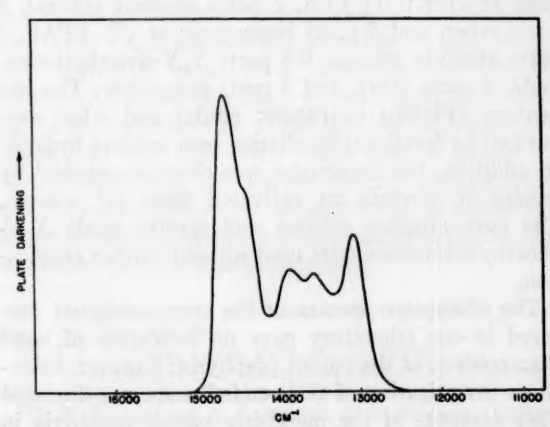

FIG. 4. Phosphorescent spectra of the dimethyl ester of copper mesoporphyrin IX in EPAF glass.

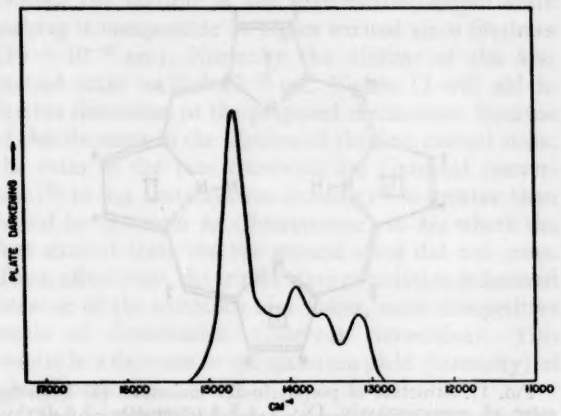

FIG. 5. Phosphorescent spectrum of the dimethyl ester of nickel mesoporphyrin IX in EPAF glass.

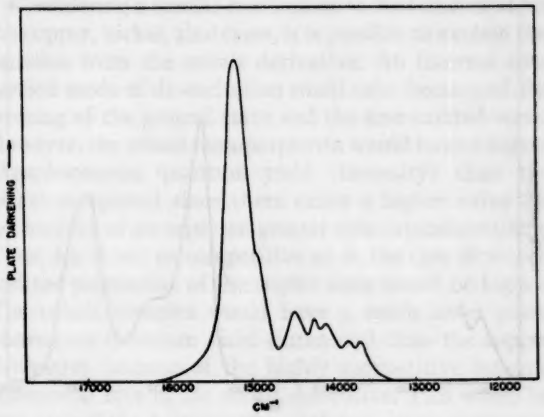

FIG. 7. Phosphorescent spectrum of the dimethyl ester of palladium mesoporphyrin IX in EPAF glass.

and weak phosphorescent bands (Fig. 1). A decided increase in the phosphorescent intensity with a corresponding decrease in fluorescent intensity occurs when magnesium is complexed with this compound. This can be attributed to the atomic number (Z) effect on spin-orbital interaction. Replacement of magnesium ($Z=12$) by zinc ($Z=30$) results in even further enhancement of the phosphorescent intensity and a decrease in the fluorescent intensity. Complexing a paramagnetic metal ion, like copper, with the porphyrin molecule causes a high degree of spin-orbital coupling to occur in the molecular system. As a result, there is total quenching of fluorescence and an increase in phosphorescent intensity with considerable shortening of the lifetime associated with the triplet state (Fig. 4 and Table I). Although these cases behave as expected, several of the cases to be considered do not behave in accordance with expectation.

The divalent metallo-porphyrins are normally considered to exhibit dsp^2 square planar bonding between the central metal ion and the four pyrrole nitrogens. This bonding scheme requires the divalent nickel ion to have an electronic configuration similar to that for the zinc ion (i.e., no unpaired electrons). Complexing the nickel ion via dsp^2 square planar bonding with the parent porphyrin should then have much the same effect on the emission spectrum as did the introduction of the zinc ion. Since the emission spectrum of the latter contains both fluorescence and phosphorescence, and since the atomic number of nickel is even less than that of zinc, the nickel derivative would be expected to contain fluorescent bands in addition to phosphorescent bands. Contrary to this prediction, the nickel mesoporphyrin is solely phosphorescent (Fig. 5) and has a lifetime $\geq 5\times10^{-4}$ sec.

If the metal ion in nickel mesoporphyrin is considered paramagnetic, then this solely phosphorescent emission would be expected. However, the lifetime of the triplet state for the nickel complex is too long and the emission too weak when compared to a porphyrin known to contain a paramagnetic metal ion—the copper complex (Table I). Thus, it is concluded that the nickel ion is diamagnetic.

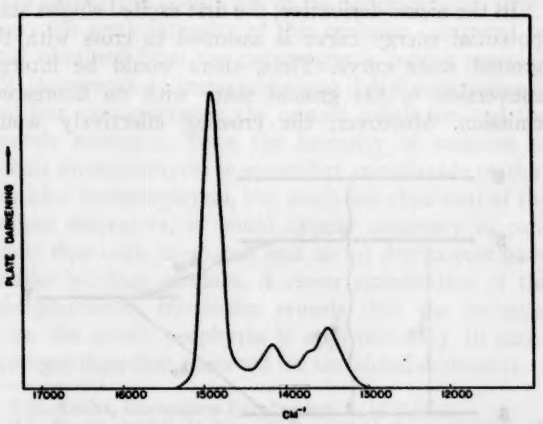

FIG. 6. Phosphorescent spectrum of the dimethyl ester of cobalt mesoporphyrin IX in EPAF glass.

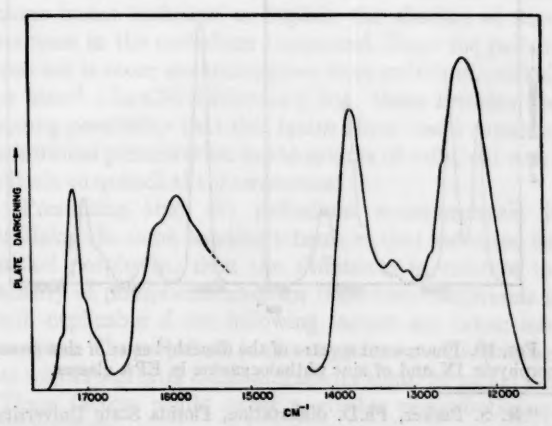

FIG. 8. Fluorescent and phosphorescent spectra of the dimethyl ester of cadmium mesoporphyrin IX in EPA glass.

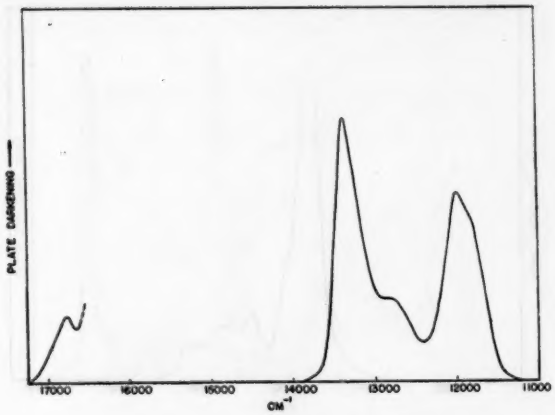

FIG. 9. Fluorescent and phosphorescent spectra of the dimethyl ester of barium mesoporphyrin IX in EPAF glass.

Earlier work by Becker[12] on nickel etioporphyrin II gave results similar to those reported herein. On the basis of the emission spectral considerations and comparisons, Becker concluded that the metal-porphyrin bonding in the nickel derivative was unusual; that is, different from the other metalloporphyrins normally considered coplanar. One of the bonding schemes suggested was a distorted tetrahedron. Further investigation by the present authors, including the lifetime of a nickel porphyrin (from which the magnetic susceptibility can be inferred), has led to a similar, but more definite conclusion—irregular tetragonal bonding.

A recent x-ray investigation of nickel etioporphyrin II[13,14] indicates that while the central metal ion is in the plane of the molecule as a whole (nickel atom plus the four methine carbon atoms), the four pyrrole rings may be displaced slightly above and below this plane in an alternating manner. The metal-

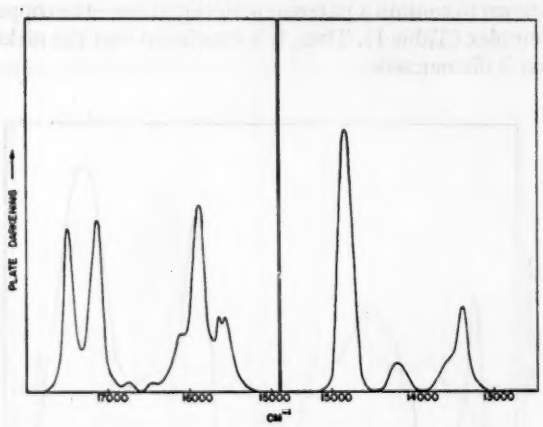

FIG. 10. Fluorescent spectra of the dimethyl ester of zinc mesoporphyrin IX and of zinc phthalocyanine in EPA glasses.

[12] R. S. Becker, Ph.D. dissertation, Florida State University (1955).
[13] M. Crute (personal communication).
[14] M. Crute, Acta Cryst. **12**, 24 (1959).

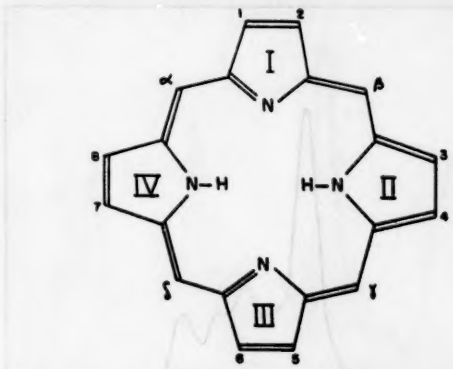

FIG. 11. Structure of porphyrin-like molecules. (1) Dimethyl ester of mesoporphyrin IX: 1,3,5,8-tetramethyl-2,4-diethyl-6,7-di-(methylpropionate)-porphin; (2) etioporphyrin II: 1,4,5,8-tetramethyl-2,3,6,7-tetraethyl-porphin; (3) phthalocyanine: α, β,γ,δ aza-1,2,3,4,5,6,7,8-phenyl porphin; (4) metallo-derivatives: a divalent metal atom replaces the two central H atoms forming coordinate-covalent bonds with the four pyrrole nitrogens.

porphyrin geometry of such a system would indicate that the bonding is that of an irregular tetragon (dp^3 or dsp^2).

A more quantitative relative comparison of the intensity of phosphorescence of nickel and copper mesoporphyrin shows the copper derivative to be 300–600 times greater in intensity than the nickel derivative. This could, perhaps, be accounted for in terms of the difference in the magnetic susceptibility (thus affecting the spin-orbital coupling) of the metal ions involved. However, since the nickel derivative does not have fluorescence, it is not possible to account for the missing quanta via this mechanism as could be possible, for instance, in the zinc derivative which does exhibit fluorescence and is also diamagnetic. In view of these and other considerations, the following mechanism and a preferred subsequent one satisfactorily accounts for the above results and for those of another derivative which will be considered shortly.

GEOMETRIC CONSIDERATIONS

In the nickel derivative, the first excited singlet state potential energy curve is assumed to cross with the ground state curve. Thus, there would be internal conversion to the ground state with no fluorescent emission. Moreover, the crossing effectively would

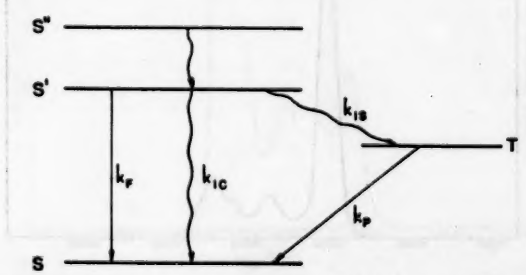

FIG. 12. Energy level diagram relating rate constants for transitions.

shorten the lifetime of the first excited singlet state making it comparable to higher excited state lifetimes (10^{-10}–10^{-12} sec). Normally the lifetime of the first excited state is 10^{-8}–10^{-10} sec. Figure 12 will aid in further discussion of the proposed mechanism. Because of this decrease in the lifetime of the first excited state, the ratio of the rate constants k_{IC} (internal conversion)[15] to k_{IS} (intersystem crossing)[15] is greater than would be the ratio k_F (fluorescence) to k_{IS} where the first excited state the the ground state did not cross. Thus, effectively, the triplet state population is lowered because of the existence of a faster, more competitive mode of deexcitation (internal conversion). This results in a decrease in the quantum yield (intensity) of phosphorescence.

The preceding development has further verification when the zinc derivative is considered. The relative intensities of the phosphorescence of the metallo derivatives are approximately Zn/Ni = 60 and Cu/Zn = 5–10. In the copper-zinc case, even though the phosphorescence of the copper complex is greater than that of the zinc complex, the zinc derivative has fluorescence making the total quantum yields comparable. However, in the zinc-nickel case, it can be seen that despite the fact they are both diamagnetic and differ in atomic number by only two, the zinc phosphorescence and total quantum yield are considerably greater. This is satisfactorily accounted for on the basis of the mechanism proposed in the foregoing. The cause of these differences is attributed in total or in part to the nature of the metal-porphyrin bonding as previously discussed.

The emission spectrum of cobalt mesoporphyrin consists solely of phosphorescence. Moreover, the lifetime of the phosphorescence is less than 10^{-4} sec. These factors are attributed to strong spin-orbital coupling resulting from a paramagnetic ion, namely the cobalt ion. The paramagnetic susceptibility is expected whether the cobalt ion is involved in dsp^2 square planar bonding or an odd type of bonding such as that exhibited by the nickel derivative. Earlier workers[16] also have shown the cobalt ion to be paramagnetic. However, the weak intensity of this emission compared to that obtained from the paramagnetic copper complex (50 times weaker) seems surprising if dsp^2 square planar bonding exists between the central cobalt ion and the pyrrole nitrogens. Since the intensity of emission of cobalt mesoporphyrin is somewhat comparable to that of nickel mesoporphyrin, but much less than that of the copper derivative, it would appear necessary to conclude that both the cobalt and nickel derivatives have similar bonding schemes. A closer examination of the phosphorescent intensities reveals that the emission from the cobalt porphyrin is approximately 10 times stronger than that observed for the nickel derivative.

Considering a similar mechanism to that discussed for the copper, nickel, zinc cases, it is possible to explain the emission from the cobalt derivative. An internal conversion mode of de-excitation could exist because of the crossing of the ground state and the first excited state. However, the cobalt mesoporphyrin would have a higher phosphorescent quantum yield (intensity) than the nickel compound since there exists a higher value for k_{IS} because of an expected greater spin-orbital coupling. Thus, k_{IC} is not as competitive as in the case of nickel, and the population of the triplet state would be higher. The cobalt complex would have a much lower phosphorescent quantum yield (intensity) than the copper derivative because of the highly competitive internal conversion rate in the cobalt derivative. This would be true even if the k_{IS} values for each were comparable and large as in the copper porphyrin.

Palladium mesoporphyrin, like the nickel analog, has an emission consisting solely of phosphorescence (Fig. 7). The intensity of this emission appears to be at least equal to that of the copper complex. This would imply that the k_{IS} is equal to or greater than that of the copper derivative. However, the lifetime of the triplet state is much longer in the palladium compound than that in the copper porphyrin. The lifetime is equal to or greater than 5×10^{-4} sec. The difference in lifetimes of the copper and palladium porphyrins strongly supports the conclusion that the palladium ion is diamagnetic.

Since the metal ion in the palladium porphyrin is diamagnetic, the solely phosphorescent emission might be attributed to an increase in spin-orbital coupling resulting from the high atomic number of the metal ion. However, this explanation is ruled out when the emission spectrum of the cadmium complex is examined. The cadmium ion is not only diamagnetic, but its atomic number is also two units higher than that of the palladium ion. The spectrum of the cadmium compound still contains weak fluorescence in addition to the intense phosphorescence (Fig. 8). Furthermore, the lifetime of the triplet state of cadmium mesoporphyrin is $\geq 5\times10^{-4}$ sec. Thus, the atomic number effect alone is not sufficient to explain the absence of fluorescence in the palladium compound. Since the palladium ion is more electronegative than cadmium, nickel, or zinc[17] ($Zn < Ni < Pd \gg Cd \leq Zn$), there remains the strong possibility that this factor alone could cause an additional perturbation to the system of sufficient magnitude to quench the fluorescence.

Presuming that the palladium mesoporphyrin is utilizing the same bonding scheme as that indicated for nickel porphyrin, then the difference in relative intensity of phosphorescence for these two compounds is still explicable if the following factors are taken into account. The palladium ion has a greater atomic number as well as a greater electronegativity than the nickel ion. These factors would cause a greater perturbation to

[15] M. Kasha, Discussions Faraday Soc. 9, 14 (1950).

[16] L. Pauling and C. D. Coryell, Proc. Natl. Acad. Sci. U.S. 22, 159 (1936).

[17] W. Gordy and W. J. O. Thomas, J. Chem. Phys. 24, 439 (1956).

the optical electron system. In addition, the palladium ion has a larger diameter than the nickel ion. As a result, there should be greater overlap between the pyrrole nitrogen orbitals and those of the metal ion. This would tend to perturb the charge cloud even more with a consequent increase in spin-orbital perturbation (r effect). These factors also could be operative in the case where the palladium bonding scheme was that considered normal, that is, square coplanar.

Considering the intense phosphorescent emission of the copper complex, it would seem logical to suppose that when any other paramagnetic metal of this same periodic group is complexed with the mesoporphyrin, the intensity of the resulting phosphorescent emission should be equal to or greater than that of copper porphyrin. However, no emission bands for the silver II porphyrin could be located up to 9000 A even with long periods of exposure. If this divalent silver ion possesses electronic excitation levels lower than the triplet level of the mesoporphyrin complex, it is possible that all excitation energy could be transferred to these atomic levels. In this case the emission could occur farther into the infrared than the photographic plates used could detect. (For an example of this type of energy transfer see Weissman[18] and Crosby and Kasha.[19]) On the other hand, there are several other plausible explanations for this lack of expected emission. For instance, the divalent silver ion represents an oxidation state for this metal which is uncommon. As a result, the divalent metal ion is much more electronegative (3.2)[20] than if it were in the univalent state (1.8),[20] and moreover, more electronegative than divalent copper (2.3).[17,20] Owing to the paramagnetic and more electronegative character of the metal ion, an internal degradation mechanism could exist which would allow drain off of excitation energy in a radiationless manner. Moreover, the type and geometry of the bonding with the pyrrole nitrogen atoms could be different than in the divalent copper case due to the expected more electronegative nature of the divalent silver ion. In order to test these hypotheses, a more comprehensive study of silver(II) porphyrin seems necessary.

The barium porphyrin exhibits very weak fluorescence in addition to its intense phosphorescence (Fig. 9). The decrease in fluorescent intensity between the cadmium ($Z=48$) and barium ($Z=56$) derivatives is much larger (approximately 200 times) than the decrease occurring between the zinc ($Z=30$) and cadmium ($Z=48$) complexes. This decrease in fluorescent intensity is considerably larger (2000 times) than can be accounted for by atomic number effect alone. However, the change in radius of these metals could be one factor explaining this difference (ionic radius of $Ba^{2+}=1.43$ A, $Cd^{2+}=1.03$ A, and $Zn^{2+}=0.83$ A.[21]) Because of the large size of barium, the central metal ion may no longer assume a normal position in the center of the ring. This could provide an additional perturbation which could increase the spin-orbital coupling to an even greater degree than that due to just a change in atomic number. In addition, the barium ion is highly electropositive (the same as the sodium ion).[17] This factor certainly causes an appreciable alteration in the nature of the metal porphyrin bonding. The effect is manifested by the high degree of instability of the barium derivative. Thus, the relative decrease in fluorescent intensity as noted previously appears to be a complex function of atomic number, ionic radius, planarity, and electronegativity effects.

LIGAND FIELD CONSIDERATIONS

Because of the fact that the total quantum yield of luminescence was low for the nickel(II) and cobalt(II) porphyrins, special spectroscopic investigation was performed on these derivatives. The investigation centered on the possibility of the introduction of new levels resulting from ligand field splitting of the d levels in these transition metal ions (for example, see J. F. Gibson *et al.*[22] and Griffith[23]). Thus, if low-lying levels existed, intramolecular energy transfer could have occurred to these levels with a consequent lower energy emission. The emission spectrum of each of the derivatives was studied using photographic plates to approximately 11 400 A ($\bar{\nu}\sim8770$ cm^{-1}). No definitive emission characteristic of the metallo-porphyrins was found.

The introduction of levels resulting from ligand field splitting could provide a modification of part or all of the mechanisms proposed herein. The absence of fluorescence and low quantum yield (intensity) of phosphorescence could be caused by internal conversion among the level which is normally the first excited level (also normally the fluorescence level, S^1 Fig. 11), the new level (s) resulting from ligand field splitting, and the ground level.

The comparison of the emission spectra of the nickel(II) and zinc(II) derivatives provides the knowledge of a rather high intrinsic spin-orbital coupling perturbation by zinc because of the nearly equal intensity of the phosphorescence and fluorescence of the metallo-porphyrin. The difference in the nickel(II) and zinc(II) is $2Z$ units and unfilled d orbitals for the nickel(II). It is entirely unreasonable that the change in the Z factor could be responsible for the low phosphorescence intensity of the nickel derivative. Moreover, fluorescence is entirely quenched. Thus, the

[18] S. I. Weissman, J. Chem. Phys. **10**, 214 (1942).
[19] G. A. Crosby and M. Kasha, Spectrochim. Acta **10**, 377 (1958).
[20] E. G. Rochow, D. T. Hurda, and R. N. Lewis, *The Chemistry of Organometallic Compounds* (John Wiley & Sons, Inc., New York, 1957), p. 17.
[21] T. Moeller, *Inorganic Chemistry* (John Wiley & Sons, Inc., New York, 1956), pp. 140–141.
[22] J. F. Gibson, D. J. Ingram, and D. Schonland, Discussions Faraday Soc. **26**, 72 (1958).
[23] J. S. Griffith, Discussions Faraday Soc. **26**, 81 (1958).

difference in these ions of great importance is the *d* electron configuration. These and other factors provide evidence that the mechanism proposed in the preceding paragraph is the operative one in the cases of the nickel and cobalt derivatives.

BONDING CONSIDERATIONS

An estimation of the quantum yield of fluorescence for zinc phthalocyanine compared to zinc mesoporphyrin presents a means to determine the structural similarity between these molecules. In order to make this estimation as quantitative as possible, both metallo compounds were studied in the same solvent system (EPA). The concentration of each sample was adjusted so that equal integrated absorption areas were present in the regions excited. Approximately twice the intensity of exciting light was used to irradiate the mesoporphyrin derivative as that for the corresponding phthalocyanine.

A consideration of all factors, including plate sensitivity, shows that the intensity of fluorescence in the zinc phthalocyanine is approximately twice that of the zinc porphyrin despite the excitation intensity difference. This would indicate that the quantum yield of phosphorescence for zinc phthalocyanine would be approximately one-half as great as that for the zinc mesoporphyrin. This difference in quantum yield (intensity) of fluorescence is related to the amount of spin-orbital interaction present in these metallo compounds. The implied greater intensity of phosphorescence for zinc mesoporphyrin indicates a greater degree of spin-orbital interaction. This could be accounted for by the difference in the expected electron density in the vicinity of the pyrrole nitrogens for these two compounds. In the case of the phthalocyanine, there would be a fairly uniform distribution of electron density on all of the skeletal nitrogens. The porphyrin, on the other hand, no longer has this uniform distribution since the four methine carbon atoms have replaced the nitrogens joining the pyrrole rings. Moreover, the electron density on the pyrrole nitrogens in the porphyrin is increased because of the difference in electronegativity of the nitrogen compared to the methine carbon. This would enable the central metal ion (in the porphyrin) to have a greater degree of orbital overlap with the pyrrole nitrogen orbitals. As a result, the bond distance between the metal ion and the four pyrrole nitrogens could be shorter than those in the metallo-phthalocyanine molecule. The effect of this would be an increase in the spin-orbital perturbation caused by the metal ion (r effect) with a consequent decrease in the quantum yield (intensity) of fluorescence. Thus, it appears that the pyrrole rings in the zinc porphyrin molecule would be moved in closer toward the center of the ring system than in the corresponding phthalocyanine molecule.

The use of electronic emission spectral data for the prediction of magnetic susceptibility and certain structrual and bonding characteristics appears to have qualitative validity. It is obviously important to have actual lifetime data and, in addition, have such data on more compounds before conclusive validity and limits can be established. Moreover, more quantitative intensity data would be desirable. These and other considerations are under investigation.

ACKNOWLEDGMENT

We wish to thank the Monadnock Research Institute, Antrim, New Hampshire, for supplying some of the metallo-porphyrins utilized in this investigation.

Effect of Pressure on the Spectra of Color Centers*

R. A. EPPLER AND H. G. DRICKAMER

Department of Chemistry and Chemical Engineering, University of Illinois, Urbana, Illinois

(Received October 20, 1959)

The effect of pressure on the spectra of certain color centers produced in the alkali halides by x irradiation has been measured to pressures as high as 166 000 atm.

For the *F* center a shift to higher energies with increasing pressure is observed. The slope of the shift versus density is at least twice the value that would be predicted from Ivey's relation at low pressure, and decreases with increasing pressure. This indicates that the compressibility in the neighborhood of the *F* center is greater than in the bulk crystal, particularly at low pressure.

For the *M* center in LiCl a shift to higher energy with increasing pressure is observed, about one-fifth as great as the shift observed for the *F* center.

INTRODUCTION

THE effect of pressure on the spectra of certain color centers in alkali halide lattices produced by ionizing radiation has been studied to as high as 166 000 atm.

There have been three previous investigations of the effect of pressure on color centers in alkali halides. Burstein *et al.*[1] measured the shift of the *F*-band peak frequency to 2000 atm in three alkali halides. Jacobs[2] measured the effect of pressure on the peak frequency of the *F* band to as high as 8000 atm in seven alkali halides. Maisch and Drickamer[3] studied the effect of pressure on the spectra of the *F* band in six alkali halides and the *M* band in one other alkali halide to 50 000 atm.

They found that, in general, a shift to higher energy occurred for all bands with pressure as long as no phase transition occurred. Maisch and Drickamer[3] also found that in some alkali halides, there appears at higher pressures a new band on the high energy side of the *F* band which they called the K^1 band.

EXPERIMENTAL PROCEDURE

The types of crystals and color centers studied, the techniques used to introduce the centers, and the pressure ranges involved are summarized in Table I.

The crystals to be x irradiated were cleaved to about $2\frac{1}{2}\times5\times\frac{1}{2}$ mm and exposed at a distance of one inch for times ranging from one to twenty-five hours to an x-ray tube with a tungsten target and beryllium windows operated at 40 kv and 15 ma. The crystals were stored in the dark until used. They were loaded into the bomb in a very dim red light. This procedure was found by Maisch and Drickamer[3] to give results identical to those obtained with additively colored crystals.

The crystals to be bleached were exposed from 5–10 min at a distance of 2–3 in. to the radiation from a Hanovia type 16 200 mercury lamp, then used immediately.

The high-pressure optical system and techniques have been described previously.[4]

RESULTS AND DISCUSSION

A. *F* Center in the fcc Structure

The primary result of x irradiation of a pure alkali halide crystal is the introduction of a band in the visible called the *F* center. The commonly accepted model of the defect, due to deBoer,[5] is that of an electron trapped at a negative ion vacancy. The shift of this peak with pressure is shown in Figs. 1 to 6 for six alkali halide crystals which have the fcc (NaCl) structure, at least at atmospheric pressure. The maximum scatter in the data is ±300 cm^{-1}. Figures 7 to 10 show typical spectra for KCl, KBr, and KI.[6]

It was first suggested by Burstein and Oberly[7] that the *F* center could, to the zeroth order, be treated as a particle trapped in a box. One of the important conclusions of this model is that $E\propto(1/l)^2$ where l is the box diameter. Thus

$$\nu_m = E/h \propto (1/A_0^2)\alpha\rho^{\frac{1}{3}}$$

where A_0 is the lattice parameter and ϵ is the density.

Mollwo,[8] using data at one atmosphere and 25°C for several alkali halides having the fcc structure, showed that $\nu_m A_0^2$ is essentially constant. Later Ivey[9] correlated the data and found that

$$E_m A_0^{1.84} = 1.76\times10^{-19}\ \text{v m}^2.$$

The density of certain alkali halides has been measured as a function of pressure to 100 000 kg/cm^2 by

* This work was supported in part by U. S. Atomic Energy Commission contract, Chemical Engineering Project 5.

[1] E. Burstein, J. J. Oberly, and J. W. Davisson, Phys. Rev. **85**, 729 (1952).

[2] I. S. Jacobs, Phys. Rev. **93**, 993 (1954).

[3] W. G. Maisch and H. G. Drickamer, J. Phys. Chem. Solids **5**, 328 (1958).

[4] R. A. Fitch, T. E. Slykhouse, and H. G. Drickamer, J. Opt. Soc. Am. **47**, 1015 (1957).

[5] J. H. deBoer, Rec. trav. chim. **56**, 301 (1937).

[6] It may be noted that the half-widths do not agree particularly well with other published values.

[7] E. Burstein and J. J. Oberly, Natl. Bur. Standards Circ. No. 5109, 285 (1952).

[8] E. Mollwo, Nachr. Ges. Wiss. Göttingen, Math. phys. Kl. 97 (1931).

[9] H. F. Ivey, Phys. Rev. **72**, 341 (1947).

TABLE I. Preparation of color centers in alkali halides.

Study of	Starting material	Source	Preparation	Maximum pressure (atm)
F center in NaCl	Single crystal NaCl	Harshaw Chemical Company	x irradiation	166 000
F center in NaBr	Single crystal NaBr	Single Crystal Corporation	x irradiation	150 500
F center in KCl	Single crystal KCl	Harshaw Chemical Company	x irradiation	137 500
F center in KBr	Single crystal KBr	Harshaw Chemical Company	x irradiation	152 000
F center in KI	Single crystal KI	Harshaw Chemical Company	x irradiation	104 000
F center in LiCl	Single crystal LiCl	Semi-Elements Inc.	x irradiation	106 000
M center in LiCl	Single crystal LiCl	Semi-Elements, Inc.	x irradiation; bleaching	50 000

Bridgman.[10] Figures 10 to 14 are plots of $\log(\nu/\nu_0)_m$ vs $\log(\rho/\rho_0)$. If the compressibility in the neighborhood of the *F* center were the same as the bulk compressibility one should obtain a slope of $\frac{2}{3}$ (or 06.13 assuming the Ivey relation). Actually the slope is at least twice this at low pressures, but decreases rapidly with pressure in the low pressure region. At higher pressures the slope is constant at a value somewhat above $\frac{2}{3}$. The situation in KBr and KI is complicated by the presence of the *K'* and other bands. The results are generally quite consistent with the vacancy mechanism since the absence of the nuclear repulsive force should lead to a greater local compressibility than is exhibited by the bulk crystal.

The data also permit the evaluation of Jacob's function $f_T=\partial \ln R/\partial \ln A)$ where *R* is the lattice constant in the neighborhood of the *F* center, if one accepts the validity of the Ivey relation as applied to the *F* center. By using this assumption, $\partial \ln R/\partial P$ can be calculated from the experimental data (Figs. 10–14) and converted to $\partial \ln R/\partial A$ using Bridgman's data. The values of f_T shown are based on the data in the region 0–20 000 atm. Table II compares the experimental values with Jacob's calculations.

The agreement is reasonably good considering the simplicity of the model.

The effect of pressure on the density of LiCl has not been measured directly. It can be estimated from the effect of pressure on the *F* center ν_m and the atmospheric lattice constant, assuming ν_m has a density dependence similar to the other chlorides. Results are listed in Table III.

B. Growth of the *K'* Band

Maisch and Drickamer[3] found that in KBr, KI, CsCl, CsBr a new band appeared on the high energy

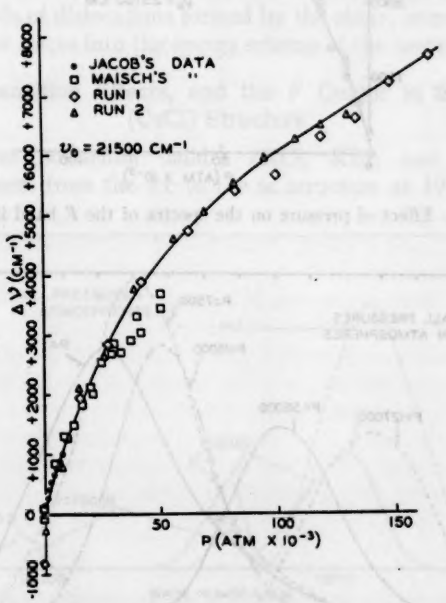

FIG. 1. Effect of pressure on the spectra of the *F* band in NaCl.

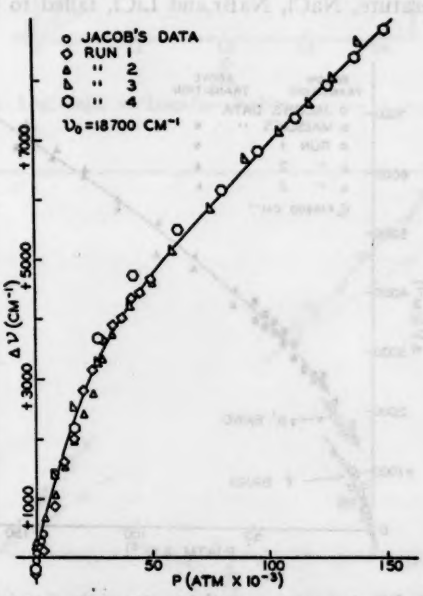

FIG. 2. Effect of pressure on the spectra of the *F* band in NaBr.

[10] P. W. Bridgman, Proc. Am. Acad. Arts Sci. 76, 1 (1945).

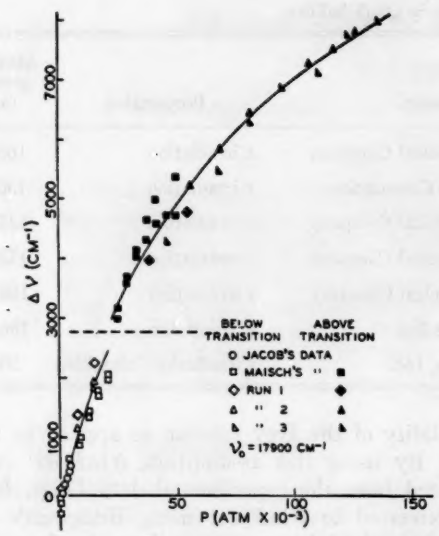

FIG. 3. Effect of pressure on the spectra of the F band in KCl.

side of the F band under pressure. They made an extensive investigation of its characteristics which can be summarized as follows:

(1) The K' band grows with increasing pressure at the expense of the F band.

(2) Transition between the two bands is reversible.

(3) Bleaching with light of the frequency of one band bleaches both bands.

As a result of the further measurements presented in this paper the following additional observations can be made:

(a) Measurements on three alkali halides which do not undergo phase transition at any known pressure or temperature, NaCl, NaBr,and LiCl, failed to produce

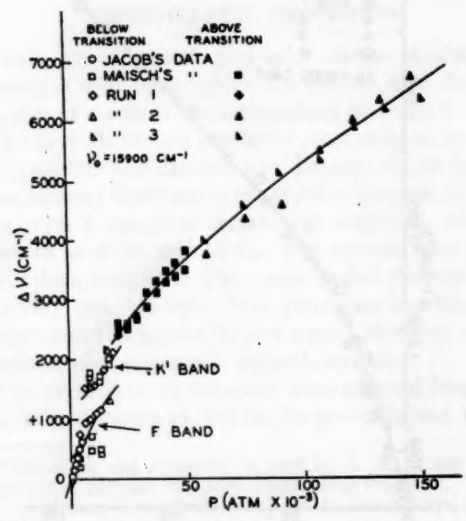

FIG. 4. Effect of pressure on the spectra of the F and K' bands in KBr.

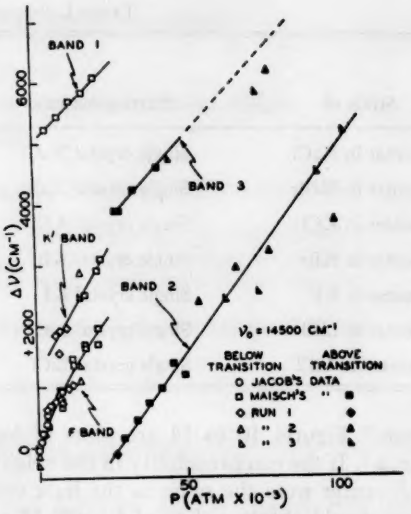

FIG. 5. Effect of pressure on the spectra of color centers in KI.

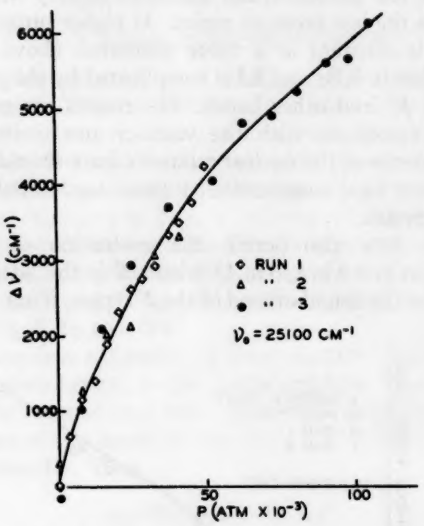

FIG. 6. Effect of pressure on the spectra of the F band in LiCl.

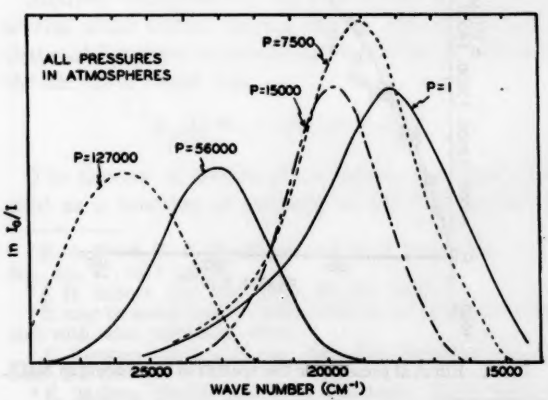

FIG. 7. F center spectra at various pressures—KCl.

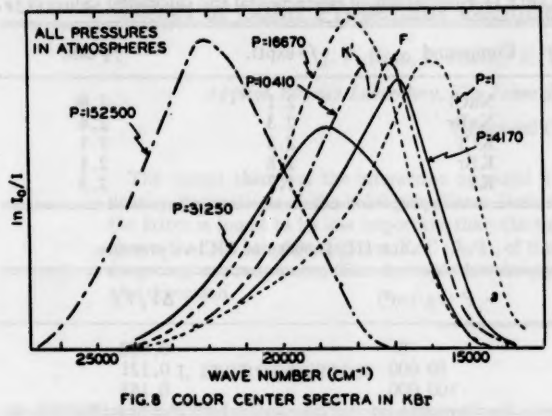

FIG. 8. Color center spectra at various pressures—KBr.

the K' band in any case. This indicates that the formation of the K' band is related in some way to the transition between the two alkali halide structures.

(b) The paper by Lazarus[11] shows that the shear constant of sodium chloride is relatively high and is relatively independent of pressure, while the shear constant of potassium chloride is not only much lower at one atmosphere, but decreases with increasing pressure.

(c) Wiederhorn[12] has shown that the transmittance of the potassium halides decreases by a factor of over 10^{-3} before the pressure induced phase transition is more than 10% complete.

The preceding indicate that the K' band growth may possibly by connected with the propagation of shear through the lattice, causing a disruption in the structure of the F center. It is possible that the defect ties down the ends of dislocations formed by the shear, introducing new forces into the energy scheme of the center.

C. Transition Effects, and the F Center in the sc (CsCl) Structure

Three potassium halides (KCl, KBr, and KI) transform from the fcc to the sc structure at 19 000–

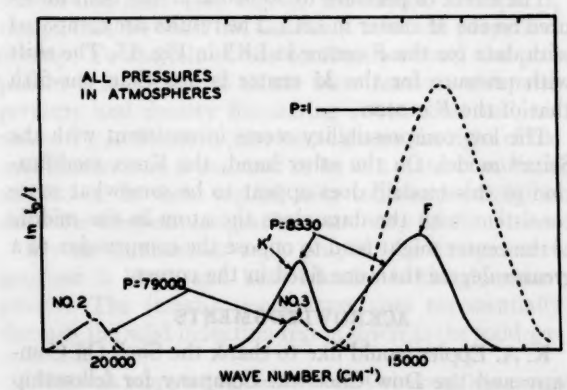

FIG. 9. Color center spectra at various pressures—KI.

[11] D. Lazarus, Phys. Rev. 76, 545 (1949).
[12] S. Wiederhorn (private communication).

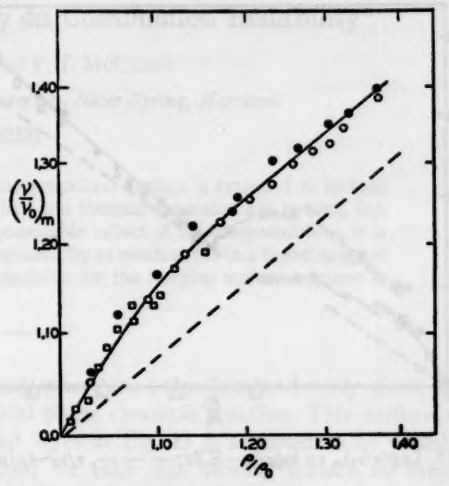

FIG. 10. $\text{Log}(\nu/\nu_0)_m$ vs $\log\rho/\rho_0$—NaCl; — — —, $\nu/\nu_0 \sim (\rho/\rho)^{2/3}$.

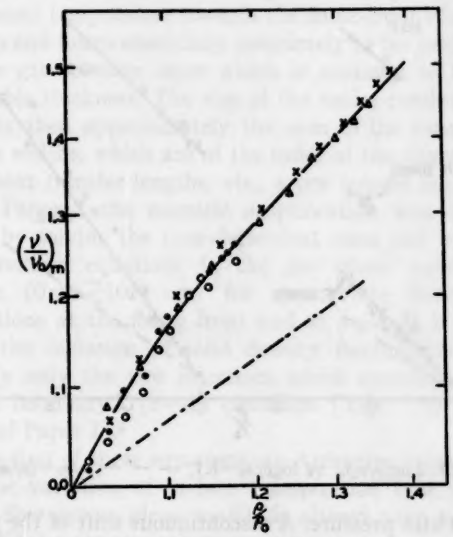

FIG. 11. $\text{Log}(\nu/\nu_0)_m$ vs $\text{Log}\rho/\rho_0$—NaBr; — — — — —, $\nu/\nu_0 \sim \rho/\rho_0)^{2/3}$.

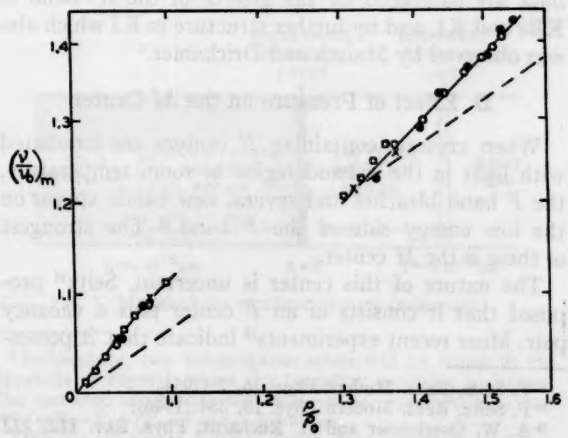

FIG. 12. $\text{Log}(\nu/\nu_0)_m$ vs $\log\rho/\rho_0$—KCl; — — —, $\nu/\nu_0 \sim (\rho/\rho_0)^{2/3}$.

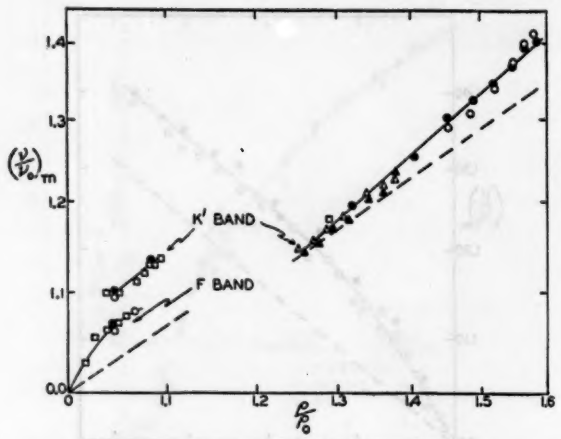

FIG. 13. $\text{Log}(\nu/\nu_0)_m$ vs $\log\rho/\rho_0$—KBr; — — —, $\nu/\nu_0 \sim (\rho/\rho_0)^{2/3}$.

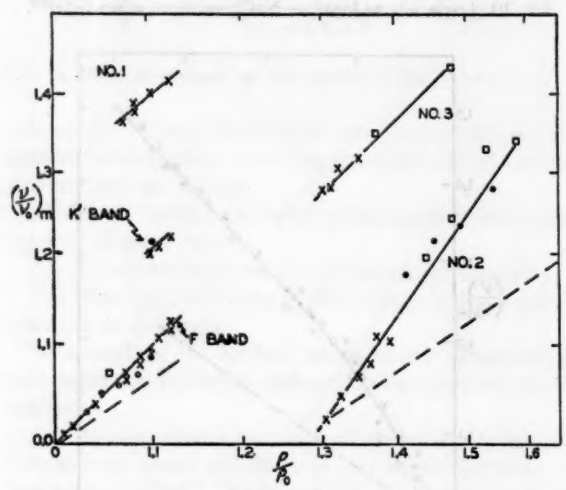

FIG. 14. $\text{Log}(\nu/\nu_0)_m$ vs $\log\rho/\rho_0$—KI; — — —, $\nu/\nu_0 \sim (\rho/\rho_0)^{2/3}$.

20 000 atm pressure. A discontinuous shift of the peak frequency to higher energies is observed at the transition (see Figs. 3–5 and 12–14). Interpretation of these data are hampered by the growth of the K' band in KBr and KI, and by further structure in KI which also was observed by Maisch and Drickamer.[3]

D. Effect of Pressure on the *M* Center

When crystals containing F centers are irradiated with light in the F-band region at room temperature, the F band bleaches and several new bands appear on the low energy side of the F band.[13] The strongest of these is the M center.

The nature of this center is uncertain. Seitz[14] proposed that it consists of an F center plus a vacancy pair. More recent experiments[15] indicate that it possesses a higher degree of symmetry than Seitz' model would indicate. Knox[16] proposed a modification of Seitz' model which possesses this higher symmetry, wherein a positive ion and an electron occupy a vacancy aggregation consisting of two negative ion vacancies and two positive ion vacancies.

The effect of pressure to 50 000 atm has been measured on the M center in LiCl. The results are compared with data for the F center in LiCl in Fig. 15. The shift with pressure for the M center is less than one-fifth that of the F center.

The low compressibility seems inconsistent with the Seitz[14] model. On the other hand, the Knox modification to this model[16] does appear to be somewhat more consistent with the data since the atom in the middle of the center might tend to oppose the compression to a greater degree than one fixed in the corner.

TABLE II. Comparison of experimental and calculated values of f_T.

Compound	f_T exptl.	f_T calc
NaCl	2.1	2.9
NaBr	2.3	2.4
KCl	2.3	2.1
KBr	1.8	2.1
KI	1.7	2.3

TABLE III. Density of LiCl vs pressure.

P (kg/cm²)	$\Delta V/V_0$
0	0.000
50 000	0.121
100 000	0.183

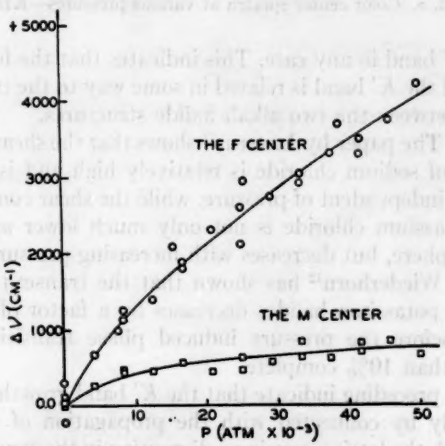

FIG. 15. Effect of pressure on the spectra of the F and M centers in LiCl.

ACKNOWLEDGMENTS

R. A. Eppler would like to thank the Shell Oil Company and the Dow Chemical Company for fellowship support.

[13] F. Seitz, Revs. Modern Phys. **26**, 7 (1954).
[14] F. Seitz, Revs. Modern Phys. **18**, 384 (1946).
[15] A. W. Overhauser and H. Ruchardt, Phys. Rev. **112**, 722 (1958).
[16] R. S. Knox, Phys. Rev. Letters **2**, 87 (1959).

Effect of Solid Propellant Compressibility on Combustion Instability*

J. F. Bird, L. Haar,† R. W. Hart, and F. T. McClure

Applied Physics Laboratory, The Johns Hopkins University, Silver Spring, Maryland

(Received October 2, 1959)

The recent theory of the interaction of sound with a burning propellant surface is extended to include density fluctuations of the solid propellant. Both compressibility and thermal expansion are treated, but the latter is found to be less important than the former. For reasonable values of the compressibility, it is shown that the acoustic response, Real $(\bar{\mu}_1/\bar{\epsilon})$, of the surface is reduced by as much as 0.1 in a broad range of frequency around several Kc. A simple low-frequency approximation for the burning surface response is also discussed.

I. INTRODUCTION

A FUNDAMENTAL theoretical treatment[1] of the interaction of a sound wave with a burning propellant surface has shown that, even in the absence of time lags in the chemical processes of combustion, the time dependent transport of heat and mass in the combustion zone can lead to acoustic amplification. This was shown to occur over a broad frequency range for many typical sets of values of the physicochemical constants of a propellant.

One simplification employed in that study was in the treatment of heat transfer in the solid—the density of the solid was treated as constant (i.e., the effects of compressibility and thermal expansion were omitted). However, typical solid propellants are relatively compressible, so it is desirable to calculate the effect of propellant density fluctuations on the acoustic amplification.

The object of the present work is then to extend the calculation of Paper I to include compressibility and thermal expansion of the solid propellant. To this end we treat in detail the (one-dimensional) problem of heat transfer in the solid in the presence of acoustic oscillations.

II. STATEMENT OF THE PROBLEM

Our calculation will be based on the model of the combustion zone (see Fig. 1) introduced in Paper I, except that we shall not assume a constant propellant density. To the left of the combustion zone, the propellant is in a state of elastic wave motion, with temperature and density fluctuating about their ambient values T_c, ρ_c. Similarly, the burnt gas on the right of the combustion zone is assumed to be in a state of acoustic oscillation. In these regions heat transfer is negligible since the temperature gradients are very small.

In the combustion zone proper, the temperature gradient is large, and heat transfer is the dominant process. The (mean) temperature rises exponentially through the solid induction region towards the solid-gas interface, where the propellant undergoes phase change and solid phase chemical reaction. This surface region (shaded layer in Fig. 1) is assumed to be vanishingly thin, and we take this moving surface as origin for our one-dimensional coordinate system. In the gas induction region, the evolved gas rises exponentially in (mean) temperature towards the flame-front where it ignites and burns essentially completely to its products in the gas reaction layer which is assumed to be of ignorable thickness. The size of the entire combustion zone is then approximately the sum of the induction region widths, which are of the order of the characteristic heat transfer lengths, viz., a few tens of microns.

In Paper I the acoustic amplification was calculated by solving the time-dependent mass and energy conservation equations in the gas phase induction region ($0<x\lesssim 10^{-3}$ cm) for appropriate boundary conditions at the flame front and at $x=0$. It is clear that the inclusion of solid density fluctuations will modify only the two equations which constitute the "cold boundary" ($x=0$) condition [Eqs. (3b) and (6a) of Paper I].[2]

The first of these equations, an Arrhenius expression for the variation of surface transpiration rate ($m_0=$ mass flow across plane $x=0$), is altered very simply by solid density variations:

$$\delta m_0/\bar{m}_0 \cong \beta(\delta T_0/\bar{T}_0) - (\delta G_0/\bar{G}_0) + (\delta\rho_0/\bar{\rho}_0), \quad (1)^3$$

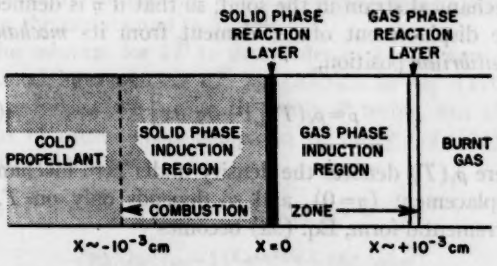

FIG. 1. Model of the combustion zone (schematic).

* This work supported by the Bureau of Ordnance, Department of the Navy.

† Now with Physics Section, Convair, San Diego, California.

[1] R. W. Hart and F. T. McClure, J. Chem. Phys. **30**, 1501 (1959) hereafter referred to as Paper I.

[2] Incidentally, two transcription errors will be found in the Appendix of Paper I, where this boundary condition is derived. The corrected expressions read $y_0=-\bar{m}l/\rho_s-(m_0-\bar{m})/i\omega\rho_s$, and $e^{i\omega t_0'}=T_0-\bar{T}_0+(\bar{T}_0-T_s)(m_0-\bar{m})/\bar{m}i\omega\tau_s$.

[3] We use the bar to indicate steady-state quantities, and δ to indicate an infinitesimal fluctuation.

in the symbols of reference 1. $\delta\rho_0$ is related [Eq. (12)] to variations of surface temperature and pressure.

The second cold-boundary equation is derived by first writing down the equation of (instantaneous) heat balance across the solid phase reaction layer. Since the layer is very thin, this balance is the same as in Paper I; for infinitesimal fluctuations it reads

$$\lambda\delta G_0-\lambda_s\delta G_{0s}=\bar{m}(C_p-C_s)\delta T_0+[h_v+(C_p-C_s)\bar{T}_0]\delta m_0. \tag{2}$$

Then the temperature gradient on the solid side of the reaction layer, G_{0s}, is found in terms of other surface fluctuations [Eq. (16)]. Combining this with Eq. (2) gives the second cold-boundary equation [Eq. (17)] as a relation between G_0, m_0, T_0 and the surface pressure p_0. (Note that in Paper I none of the cold-boundary equations involved p_0 explicitly, since the solid was incompressible.)

Our main concern in the following work, then, is to calculate G_{0s} by finding the temperature distribution in the solid induction region ($-10^{-3}\lesssim x<0$), taking account of the thermal and mechanical density fluctuations of the solid propellant.

III. BASIC EQUATIONS IN SOLID INDUCTION REGION

The energy and mass conservation equations in the x-coordinate system of Fig. 1 are[4]

$$C_v[\partial(\rho T)/\partial t]=(\partial/\partial x)[\lambda_s(\partial T/\partial x)]-C_v[\partial(mT)/\partial x]+(\theta T/k\rho)[(\partial\rho/\partial t)+v(\partial\rho/\partial x)], \tag{3}$$

$$\partial\rho/\partial t=-\partial m/\partial x, \tag{4}$$

where $v=m/\rho$ is particle velocity, C_v is constant volume specific heat, θ is thermal expansion coefficient, k is compressibility, and the other symbols are as in Paper I. Equations (3) and (4) relate the three variables m, T, and ρ. ρ is related to T and to the mechanical strain in the solid, so that if η is defined as the displacement of an element from its *mechanical equilibrium* position,

$$\rho=\rho_e(T)[1+\partial\eta/\partial x]^{-1}. \tag{5a}$$

Here $\rho_e(T)$ denotes the density under zero mechanical displacement ($\eta=0$), and so depends only on T. In incremental form, Eq. (5a) becomes

$$d\ln\rho=-\theta dT-d\ln(1+\partial\eta/\partial x), \tag{5b}$$

since $\theta=-\rho^{-1}(\partial\rho/\partial T)_{\partial\eta/\partial x}$.

[4] Equation (3) may be derived from the first law of thermodynamics with the aid of M. W. Zemansky, *Heat and Thermodynamics* (McGraw-Hill Book Company, Inc., New York, 1943), p. 226.

It is convenient to rewrite the energy equation (3), with the aid of (4) and (5b), in the form

$$C_s\rho(\partial T/\partial t)=(\partial/\partial x)[\lambda_s(\partial T/\partial x)]-C_s m(\partial T/\partial x)-(\theta T/k)[(\partial/\partial t)+v(\partial/\partial x)]\ln(1+\partial\eta/\partial x), \tag{6}$$

where $C_s\equiv C_v+\theta^2T/k\rho$ is the constant pressure specific heat of the propellant.

Equations (4), (5), and (6) give the variation of T in terms of the strain $\partial\eta/\partial x$. η could be found by solving the momentum equation in the combustion zone and matching it to the acoustic displacements in the cold solid and the burnt gas (cf. Fig. 1), but this would be extremely difficult since the combustion zone is inhomogeneous. However, since the combustion zone thickness ($\sim10^{-3}$ cm) is very small compared to sound wavelength ($\gtrsim1$ cm), $\partial\eta/\partial x$ may be taken as constant over the zone.[5] Its value we then obtain by matching normal force in the solid to the fluctuation in gas pressure on the transpiring surface, $\delta p_0\equiv\epsilon(t)\bar{p}$. Thus we replace $\partial\eta/\partial x$ in Eqs. (5), and (6) according to

$$\partial\eta/\partial x\rightarrow-k_1\bar{p}\epsilon, \tag{7}$$

where $k_1\equiv(\lambda+2\mu)^{-1}$, and where λ, μ are the usual Lamé elastic moduli; k_1 may be thought of as a "one-dimensional" compressibility.[6]

The set of Eqs. (4)–(7) is now sufficient to determine the temperature distribution in the solid induction region in terms of $\epsilon(t)$, as well as in terms of the other boundary conditions to be applied to the solution.

IV. BOUNDARY CONDITIONS

It is clear that the solution $T(x, t)$ of Eqs. (4)–(7) will involve the fractional surface pressure variation, $\epsilon(t)$. In addition, there will be three arbitrary constants in the solution, arising from the x integration of Eqs. (4) and (6). Two of these may be evaluated in terms of T_0 and m_0, the temperature and mass flow at $x=0$. The remaining integration constant is fixed by matching the temperature fluctuation at the cold end of the solid induction region to the temperature variation associated with the acoustic disturbance in the cold propellant (Fig. 1). For such a disturbance we may neglect heat conduction ($\lambda_s=0$) and then, from Eq. (6), the boundary condition is (to first order in ϵ),

$$T\rightarrow T_c+\epsilon r_s T_c, \tag{8}$$

where $r_s\equiv\theta k_1\bar{p}/\rho_c kC_s$.

[5] This generally introduces $\sim0.1\%$ error in the compressibility effect, which itself only contributes a small part to the amplification, so our approximation is excellent. It is true that when the transpiring surface approaches very near a pressure node for the solid-gas system, the effect of nonconstant $\partial\eta/\partial x$ becomes large compared even to incompressible effects. However, in this limit the amplification vanishes anyway and there is never any significant error arising from our approximation.

[6] For simplicity, we regard C_s, λ_s, θ, k, and k_1 as absolutely constant in all the rest of this work.

We will have finally a temperature distribution depending parametrically on T_0, m_0, and ϵ, from which we will find G_{0s} as a function of T_0, m_0, ϵ.

V. LINEARIZED EQUATIONS FOR TEMPERATURE DISTRIBUTION

Since the pressure disturbance will be assumed very small ($\epsilon \ll 1$), we shall consider only first-order fluctuations about steady-state values. This allows us to linearize Eqs. (4) to (7), and reduce them to a single equation for δT.

Considering first the steady-state (time-independent in x frame), we have from (4) that $\bar{m}=$constant, so that the $\bar{p}$ and $\bar{T}$ equations (4) and (6) are

$$\partial \ln\bar{p}/\partial x = -\theta \partial \bar{T}/\partial x; \qquad \lambda_s \partial^2 \bar{T}/\partial x^2 = C_s \bar{m} \partial \bar{T}/\partial x. \quad (9)$$

From (9) the characteristic heat transfer length is $\lambda_s/\bar{m}C_s \sim 10^{-3}$ cm for a typical propellant ($\lambda_s = 7\times10^{-4}$ cal/cm sec °K, $C_s = \frac{1}{3}$ cal/g °K, $\bar{m}=2$ g/cm² sec). Introducing the dimensionless coordinate $y \equiv \bar{m}C_s x/\lambda_s$, the steady-state solutions are

$$\bar{T} = T_c + \Delta e^{y}, \qquad \Delta \equiv \bar{T}_0 - T_c, \quad (10a)$$

and

$$\bar{p} = \rho_c \exp[-\theta \Delta e^{y}]. \quad (10b)$$

We shall assume harmonic time dependence for the fluctuations, so $\epsilon = \mathrm{Re}[\tilde{\epsilon}\exp(i\omega t)]$, $\delta T = \mathrm{Re}[\delta\tilde{T}\exp(i\omega t)]$, etc. Then, from Eqs. (6), (7), and (10), the first-order temperature perturbation satisfies

$$(\bar{p}/\rho_c) i\omega\tau_s (\delta\tilde{T}) = [d^2(\delta\tilde{T})/dy^2] - [d(\delta\tilde{T})/dy] - \tilde{\mu}\Delta e^{y} + i\omega\tau_s r_s (T_c + \Delta e^{y})\tilde{\epsilon}. \quad (11a)$$

Here we have introduced the characteristic time $\tau_s \equiv \lambda_s \rho_c/\bar{m}^2 C_s \sim 10^{-3}/v_c \sim 10^{-3}$ sec, since $v_c = \bar{m}/\rho_c \sim 1$ cm/sec. The fractional increment of mass flux in the solid $\mathrm{Re}[\tilde{\mu}\exp(i\omega t)] \equiv \mu \equiv \delta m/\bar{m}$) is given in terms of its value at the surface by integrating the perturbed continuity equation (4):

$$\tilde{\mu} = \tilde{\mu}_0 + i\omega\tau_s \int_0^y dy (\bar{p}/\rho_c)[\theta(\delta\tilde{T}) - k_1 \bar{p}\tilde{\epsilon}]. \quad (11b)$$

We have used here the density perturbation found from Eqs. (5a) and (7) [noting that $\bar{p} = \rho_c(\bar{T})$],

$$\delta\rho = -\bar{p}(\theta\delta T - k_1\bar{p}\epsilon). \quad (12)$$

The pair of Eqs. (11) form an integro-differential equation for the fluctuation δT in terms of μ_0 and ϵ.

VI. TEMPERATURE DISTRIBUTION IN SOLID INDUCTION REGION

We shall now obtain the temperature perturbation δT, up to and including terms linear in θ, by an iteration procedure. This approach makes the Eqs. (11) tractable and is justified by the fact that thermal expansion effects have little importance in our results, as we shall see.

The magnitude of the effect of solid density fluctuations contained in Eqs. (11) is governed by the sizes of θ and $k_1(\sim k)$. For our one-dimensional treatment, θ is the linear coefficient of thermal expansion, while k_1 is related to the velocity of longitudinal ("dilational") waves in the solid by $k_1 = 1/\rho c_d^2$. For typical propellants we may assume celluloidlike values, viz., $\theta \sim 10^{-4}$/°K, and $k_1 \sim 4\times10^{-4}$/atm ($\rho \sim 1.6$ gm/cc, $c_d \sim 4\times10$ cm/sec), for approximately room temperature. For the higher temperatures of the combustion zone ($T_0 \sim 600$°K), θ is probably not much different, but it is possible that k_1 is several times larger. In the following work we shall adopt as plausible estimates

$$\theta \sim 10^{-4}/\text{°K}, \qquad k_1 \sim 10^{-3}/\text{atm}$$

As we shall show in detail later, one may gauge the importance of thermal and mechanical density variations from the sizes of $\theta\Delta$, r_s, and $k_1\bar{p}$ compared to unity. For $\Delta \sim 300$°K and $\bar{p}=60$ atm, we have

$$\theta\Delta \sim 3\times10^{-2}, \qquad r_s \sim 3\times10^{-4}, \qquad k_1\bar{p} \sim 6\times10^{-2} \text{ or larger.} \quad (13)$$

From (13) one may anticipate that thermal expansion effects will be secondary in importance to compressibility effects.

For the case of zero θ, the temperature perturbation satisfying Eqs. (11) and the boundary conditions (Sec. IV) is readily found to be

$$(\delta\tilde{T})_{\theta=0} = (\delta\tilde{T}_0)_{\theta=0} e^{\alpha y} + [\Delta/\alpha(\alpha-1)](\tilde{\mu}_0 - k_1\bar{p}\tilde{\epsilon})(e^{\alpha y} - e^{y}) + \Delta k_1 \bar{p}\tilde{\epsilon} y e^{y}, \quad (14)$$

where $\alpha \equiv \frac{1}{2} + \frac{1}{2}(1+4i\omega\tau_s)^{\frac{1}{2}}$. The *form* of this solution differs from that of the incompressible case (Paper I) by the last term in (14). The amplitude of this term is largest at $y=-1$, and is opposite in phase to the pressure oscillation. To understand this behavior, we note that a positive pressure fluctuation produces a positive density fluctuation which means that the mass flow toward $x=0$ increases linearly with distance below the solid-gas interface. This net mass flow from lower to higher temperature regions then produces a negative temperature fluctuation, which is proportional to depth below the surface and to $\partial\bar{T}/\partial y$.

The solution for $\delta\tilde{T}$ to first order in θ may now be obtained by replacing $\delta\tilde{T}$ by $(\delta\tilde{T})_{\theta=0}$ in Eq. (11b). For simplicity we neglect not only θ^2 terms, but also terms of order $k_1\bar{p}\theta\Delta$ compared to unity [cf. (13)]. We then find

$$\begin{aligned}\delta\tilde{T} = \delta\tilde{T}_0 \{ &[1 + (\theta\Delta/2\alpha)(\alpha^2 - 2\alpha - 1)] e^{\alpha y} \\ &- (\theta\Delta/2\alpha)(\alpha-1)^2 e^{(\alpha+1)y} + (\theta\Delta/\alpha) e^{y}\} \\ &+ \tilde{\mu}_0 [\Delta/\alpha(\alpha-1)] \{ [1 + (\theta\Delta/2\alpha)(\alpha^2-1)] e^{\alpha y} \\ &- (\theta\Delta/2\alpha)(\alpha-1)^2 e^{(\alpha+1)y} - [1 + (\theta\Delta/\alpha)(\alpha-1)] e^{y}\} \\ &- \tilde{\epsilon}[k_1\bar{p}\Delta/\alpha(\alpha-1)] \{ e^{\alpha y} - e^{y} - \alpha(\alpha-1) y e^{y}\} \\ &- \tilde{\epsilon} r_s \{ \bar{T}_0 e^{\alpha y} - \Delta e^{y} - T_c \}. \end{aligned} \quad (15)$$

Finally, from Eq. (15), we have for the fluctuation in temperature gradient at the solid side of the surface $x=0$:

$$(\lambda_s/\bar{m}C_s)\delta\bar{G}_{0s}=\delta\bar{T}_0\alpha\{1-\theta\Delta[(\alpha^2-1)/2\alpha^2]\}+\tilde{\mu}_0(\Delta/\alpha)\{1+\theta\Delta[(\alpha-1)/2\alpha]\}+\tilde{\epsilon}k_1\bar{p}\Delta[(\alpha-1)/\alpha]-\tilde{\epsilon}r_s(\alpha\bar{T}_0-\Delta) \quad (16)$$

VII. ACOUSTIC AMPLIFICATION BY COMBUSTION ZONE

We can now present the modified form of the second "cold-boundary" equation (Sec. II), and the consequent changes in the response functions[7] $\tilde{\mu}_0/\tilde{\epsilon}$, $\tilde{\mu}_1/\tilde{\epsilon}$. From Eqs. (1), (2), and (16) [with (12)] the desired equation is

$$\lambda G_0=m_0(h+C_p\bar{T}_0)+\bar{m}\mu_0 J_+(\omega)+\bar{m}\epsilon K(\omega), \quad (17)$$

where

$$J_+=C_s\Delta[(1-\alpha)/\alpha][1-(\theta\Delta/2\alpha)]+C_s\bar{T}_0(\alpha-1)\{1-\tfrac{1}{2}(\theta\Delta)[(\alpha+1)/\alpha]\}$$
$$\times\frac{2(h+C_p\bar{T}_0)-C_s\Delta[(\alpha-1)/\alpha][1-(\theta\Delta/2\alpha)]}{(\beta-\theta\bar{T}_0)(h+C_p\bar{T}_0)-C_p\bar{T}_0-C_s\bar{T}_0(\alpha-1)\{1-\tfrac{1}{2}(\theta\Delta)[(\alpha+1)/\alpha]\}}, \quad (18a)$$

and

$$K=C_s\Delta\{[(\alpha-1)/\alpha]k_1\bar{p}-[\alpha(\bar{T}_0/\Delta)-1]r_s\}+C_s\bar{T}_0(\alpha-1)\{1-\tfrac{1}{2}(\theta\Delta)[(\alpha+1)/\alpha]\}$$
$$\times\frac{C_s\Delta\{[(\alpha-1)/\alpha]k_1\bar{p}-[\alpha(\bar{T}_0/\Delta)-1]r_s\}-(h+C_p\bar{T}_0)k_1\bar{p}}{(\beta-\theta\bar{T}_0)(h+C_p\bar{T}_0)-C_p\bar{T}_0-C_s\bar{T}_0(\alpha-1)\{1-\tfrac{1}{2}(\theta\Delta)[(\alpha+1)/\alpha]\}}. \quad (18b)$$

Now, in view of the order of magnitude estimates (13), as well as the fact that, typically, $\beta\sim40$, we shall in all the following neglect terms of relative order r_s, $\theta\Delta/\beta$, and $k_1\bar{p}/\beta$, with consequent error less than 0.1%. In this approximation, Eqs. (18) simplify to

$$J_+(\omega)\approx J(\omega)+C_s\Delta[(\alpha-1)/2\alpha^2]\theta\Delta, \quad (19a)$$

$$K(\omega)\approx C_s\Delta[(\alpha-1)/\alpha]k_1\bar{p}, \quad (19b)$$

with $J(\omega)$ given by Eq. (6b) of Paper I.

Equations (17) [with (19)] and (1) are the appropriate modification of the "cold-boundary" condition for the effects of solid density variations. It is now straightforward, though extremely arduous, to obtain the altered $\tilde{\mu}_0$ and $\tilde{\mu}_1$ by the procedure of Paper I. We find[8] (omitting the bars on steady-state quantities from now on)

$$\tilde{\mu}_0/\tilde{\epsilon}=[1+(J_+/2h)(1-\Gamma_0)]^{-1}\Big\{1-[(\gamma-1)/\gamma]\tfrac{1}{2}(1+\Gamma_0)$$
$$-(b_1/D_\nu^+)-(K/h)\tfrac{1}{2}(1-\Gamma_0)$$
$$-\frac{(a_1+a_2+a_K)}{D_\nu^+}(1-\Gamma_0^2)\left[T_\nu\frac{dP_\nu}{d\Gamma}\Big|_{\Gamma_0}-S_\nu\frac{dQ_\nu}{d\Gamma}\Big|_{\Gamma_0}\right]\Big\}, \quad (20)$$

$$\frac{\tilde{\mu}_1}{\tilde{\epsilon}}=2\left(\frac{1-\Gamma_1}{1+\Gamma_1}\right)\Big\{(1-\Gamma_1)^{-i}-\left(\frac{\gamma-1}{2\gamma}\right)\left(\frac{1+\Gamma_1}{1-\Gamma_1}\right)-\frac{\tilde{\mu}_0}{2\tilde{\epsilon}}\left(1+\frac{J_+}{h}\right)$$
$$+\frac{i\omega\tau_0}{(1-\Gamma_1)D_\nu^+}(a_1+a_2+a_K)-\frac{i\omega\tau_0}{2\gamma}\ln\left(\frac{1-\Gamma_0}{1-\Gamma_1}\right)$$
$$+\frac{(1+\Gamma_1)}{D_\nu^+}b_1\left[V_\nu^+\frac{dP_\nu}{d\Gamma}\Big|_{\Gamma_1}-W_\nu^+\frac{dQ_\nu}{d\Gamma}\Big|_{\Gamma_1}\right]-\frac{K}{2h}\Big\}. \quad (21)$$

[7] We recall (Paper I) that the combustion zone amplifies if $\mathrm{Re}(\tilde{\mu}_1/\tilde{\epsilon})>1/\gamma$, where γ is specific heat ratio of the burnt gas.

[8] We make one further change, unrelated to solid density fluctuations, in the treatment of Paper I, in order to include the effect mentioned in the footnote to Eq. (18) in Paper I. Thus we replace T_0 by $\bar{T}_0$ in that equation, so $\bar{x}(T)$ is exactly time independent for fixed T, but Eq. (19c) of Paper I is changed to $\Phi(T_0, l)=-\lambda\delta T_0/m(h+C_pT_0)$.

Here P_ν, Q_ν are Legendre functions, $D_\nu^+=W_\nu^+T_\nu-V_\nu^+S_\nu$, S_ν, T_ν are given in Paper I,

$$W_\nu^+=P_\nu(\Gamma_0)+\left(\frac{dP_\nu}{d\Gamma}\Big|_{\Gamma_0}\right)\frac{(1-\Gamma_0^2)}{i\omega\tau_0[1+(J_+/2h)(1-\Gamma_0)]}$$
$$\times\left\{\frac{J_+}{2h}-\frac{i\omega\tau_0}{\beta-(1+\Gamma_0)/2}\times\left[1+\frac{J}{4h}(1-\Gamma_0)\right]\right\}, \quad (22a)$$

V_ν^+ similar but with $P_\nu\to Q_\nu$, τ_0 is a characteristic response time for the gas, and

$$b_1=\frac{1-a-b}{1-\Gamma_1}+\frac{\gamma-1}{\gamma}\left[-\frac{1}{1-\Gamma_1}+\frac{b}{2}\frac{1+\Gamma_1}{1-\Gamma_1}+\frac{i\omega\tau_0}{2}\right], \quad (22b)$$

$$a_1=\frac{\gamma-1}{2\gamma}[1-(i\omega\tau_0)^{-1}]$$
$$\cdot+\frac{J_+}{2h\gamma i\omega\tau_0}\frac{[1+\frac{1}{2}(\gamma-1)(1-\Gamma_0)]}{[1+(J_+/2h)(1-\Gamma_0)]} \quad (22c)$$

$$a_2=-\frac{1}{\gamma}\frac{[1+\frac{1}{2}(\gamma-1)(1-\Gamma_0)][1+(J/4h)(1-\Gamma_0)]}{[\beta-\frac{1}{2}(1+\Gamma_0)][1+(J/2h)(1-\Gamma_0)]}, \quad (22d)$$

$$a_K=(K/2hi\omega\tau_0)[1+(J/2h)(1-\Gamma_0)]^{-1} \quad (22e)$$

with a, b of Eq. (22b) given in Paper I.

The mass flux response functions (20) and (21) differ from those of Paper I by the modifications J_+-J, and K, which arise from the solid thermal expansion and compressibility, respectively. A further difference, arising from the change mentioned in the last footnote, appears in the terms $\propto a_2$ as well as in $W_\nu^+-W_\nu$, $V_\nu^+-V_\nu$ and $D_\nu^+-D_\nu$ (cf. Paper I).

VIII. AMPLIFICATION FOR AUDIO FREQUENCIES

Before presenting numerical calculations of the response function, we shall first consider the simple limiting case that exists when the gas induction region

TABLE I. Summary of numerical results.

Case[a] number	n^a	j^a	Δ^a/T_c	$\bar{p}^a$ (atm)	τ_c^a (10^{-3} sec)	τ_0^a (10^{-6} sec)	Maximum value of δ^b	Frequency at which δ is max	Frequency range (sec^{-1}) over which $\delta \gtrsim 1/2\,\delta_{max}$	f_0 (sec^{-1})[c]
1	0	1.0	1.00	50.0	0.6	2.2	+0.051	2 500 sec^{-1}	500–9 500	900
2	0.5	1.0	1.00	50.0	0.6	2.2	+0.062	2 200 sec^{-1}	500–7 600	4 600
3	0.5	0.75	1.00	50.0	0.6	2.2	+0.044	2 800 sec^{-1}	400–12 700	5 300
4	0.5	0.5	1.00	50.0	0.6	2.2	+0.026	3 600 sec^{-1}	400–31 000	8 600
5	0.5	0	1.00	50.0	0.6	2.2	+0.006	100 000 sec^{-1}	25 000–>100 000	20 000
6	0.54	0.45	1.94	50.2	0.403	1.25	+0.082	5 000 sec^{-1}	800–28 000	9 000
7	0.54	0.45	1.42	69.0	0.239	1.20	+0.052	9 300 sec^{-1}	1 000–66 000	20 000
8	0.54	0.45	1.24	65.5	0.251	1.29	+0.041	9 900 sec^{-1}	800–77 000	24 000
9	0.18	0.39	2.09	70.5	0.669	1.41	+0.086	4 900 sec^{-1}	600–32 000	7 400
10	0.18	0.39	1.42	66.7	0.563	1.36	+0.040	6 500 sec^{-1}	500–73 000	20 000
11	0.18	0.39	1.20	85.5	0.478	1.64	+0.040	8 800 sec^{-1}	500–87 000	22 000
12	0.54	0.45	1.24	65.5	0.502	1.29	+0.042	6 200 sec^{-1}	400–71 000	19 000
13	0.54	0.45	1.24	65.5	0.126	1.29	+0.038	12 300 sec^{-1}	1 600–99 000	32 000
14	0.54	0.45	1.21	69.0	0.239	1.20	+0.041	8 500 sec^{-1}	900–66 000	20 000

[a] Consult reference 1, Table I, where values of the other parameters are given.
[b] $\delta \equiv [\mathrm{Re}(\tilde{p}_1/\tilde{\epsilon})]_{\theta=0,k_1=0} - [\mathrm{Re}(\tilde{p}_1/\tilde{\epsilon})]_{\theta=10^{-4}/°K;\ k_1=1/1200/\mathrm{atm}}$.
[c] $f_0 \equiv$ frequency above which adiabatic approximation [Eq. (26)] is in error by >0.1.

responds adiabatically to the pressure fluctuation, i.e., when its response time τ_0 is small compared to the period of the oscillating disturbance. For typical values, $\tau_0 \sim 10^{-5}$ sec, we do not expect errors arising from this assumption to be *large* so long as $\omega \lesssim 10^5$ sec^{-1} (cf. Paper I, especially Fig. 6). Thus, the great amount of labor saved by the assumption is paid for by limiting its applicability at the interesting high frequencies.

Rather than obtaining the desired limit by setting $\omega\tau_0 \to 0$ in Eqs. (20) and (21), it is simpler to use adiabaticity from the start in order to see first, that by the continuity equation we have $\mu_1 = \mu_0$, and second, that the relationship between m_0, ϵ and the temperature gradient on the gas side of $x=0$ is

$$\delta G_0/\bar{G}_0 = a_0\mu_0 + b_0\epsilon, \tag{23}$$

where a_0, b_0 are to be determined from the steady-state relation between $\bar{G}_0$, $\bar{m}$, $\bar{p}$. We use the empirical burning rate law of Paper I $\bar{m} \propto \bar{p}^n T_c^j$, together with the steady-state forms of Eqs. (1) and (8) of Paper I to find

$$a_0 = \frac{h + C_p T_0[1 + (\beta - \theta T_0)^{-1}] - (C_s T_c/j)}{h + C_p T_0[1 - (\beta - \theta T_0)^{-1}]}, \tag{24a}$$

$$b_0 = \frac{(n/j)\,C_s T_c - C_p T_0[k_1\bar{p}/(\beta - \theta T_0)]}{h + C_p T_0[1 - (\beta - \theta T_0)^{-1}]}. \tag{24b}$$

On solving Eqs. (23) and (17) [using also (1)] we find the response function is simply

$$\frac{\tilde{p}_1}{\tilde{\epsilon}} = \frac{\tilde{\mu}_1}{\tilde{\epsilon}} = \frac{n - j(K/C_s T_c)}{1 + j(J_+/C_s T_c)}. \tag{25}$$

Now because $1/\beta$ and $\theta\Delta$ are ordinarily only a few percent, while $k_1\bar{p}$ may be considerably larger, let us consider the case of dominant compressibility effects. Thus, in Eqs. (19), we neglect $1/\beta$ and $\theta\Delta$, so that $J_+ \approx -C_s\Delta(\alpha-1)/\alpha$ and Eq. (25) is approximately

$$\frac{\tilde{p}_1}{\tilde{\epsilon}} = \frac{\tilde{\mu}_0}{\tilde{\epsilon}} \approx \frac{n - k_1\bar{p}j(\Delta/T_c)(\alpha-1)/\alpha}{1 - j(\Delta/T_c)(\alpha-1)/\alpha}. \tag{26}$$[9]

From (26) we can now see that in this low-frequency regime the effect of compressibility on the amplification criterion [Eq. (32) of Paper I] is equivalent to the simple modification

$$n \to n - k_1\bar{p}, \qquad 1/\gamma \to 1/\gamma - k_1\bar{p}, \tag{27}$$

in the results of the incompressible case (Paper I). As such, the effect is inessential, unless $k_1\bar{p}$ is abnormally large.

IX. NUMERICAL RESULTS

The response function $\tilde{p}_1/\tilde{\epsilon}$ given by Eqs. (21) and (22) has been computed as a function of frequency for the following values of θ, k_1:

$$\theta = \tfrac{1}{3}\times 10^{-4};\ 10^{-4};\ 3\times 10^{-4}\ (\text{in } °\text{K}^{-1}):$$

$$k_1 = 1/1200;\ 1/600;\ 1/120\ (\text{in atm}^{-1}). \tag{28}$$

For other parameters involved we have restricted ourselves to the 14 sets of values displayed in Table I of Paper I.

For all the cases considered, the computation shows that the effect of solid density fluctuations is to *de-*

[9] The sensitivity of the response (26) to values of the parameter group $j\Delta/T_c$ near unity is associated with an inherent instability of the type mentioned in Paper I. We shall not discuss this aspect further here.

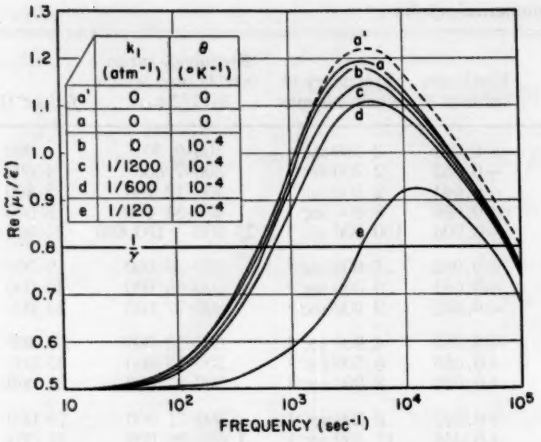

FIG. 2. Response vs frequency in case 2 of Table I, for varying compressibility (k_1) and thermal expansion (θ). (For explanation of curve a' see text.)

crease[10] Re($\tilde{\mu}_1/\tilde{\epsilon}$) and consequently lower the amplification. This decrease is generally largest around frequencies $\sim 10^3$ to 10^4 sec^{-1}, and extends over a fairly broad frequency interval. As an example, we present in Table I of this report the main features of the results for $\theta = 10^{-4}$/°K, $k_1 = 1/1200$/atm. We see that the decrease is $\sim 5\%$ to 10% (relative to $1/\gamma = 0.8$), the largest effects occurring when Δ/T_c is largest. [Case 5 is unusual, both in that the effect is small, and restricted to the high frequency region. This is probably because $j = 0$ here, (cf. Eq. (26)].

The calculations for other values of θ, k_1[Eq. (28)] show that the thermal expansion effects are secondary in importance to the compressibility effects. In fact,

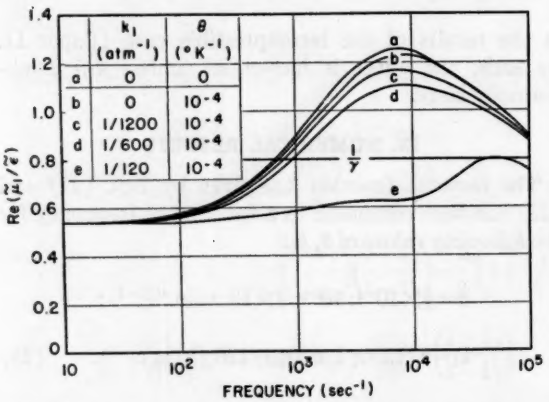

FIG. 3. Response curves in case 6 of Table I, as functions of compressibility (k_1) and thermal expansion (θ). Note for very large k_1 there is no amplification (curve e).

[10] This seems plausible, since compressibility contributes a temperature fluctuation in the solid induction region which is opposite in phase to ϵ (cf. Sec. VI). For this leads to an in-phase fluctuation of G_{0s}, which in turn produces an in-phase variation of heat loss from the surface reaction layer. Consequently, there results a transpiration rate fluctuation which is 180° out of phase with the pressure oscillation ϵ.

the decrease in the response function for the *largest* value of θ in (28) (with $k_1 = 0$) is at most only about as much as for the *smallest* value of k_1 in (28) (with $\theta = 0$). The compressibility effect for $k_1 = 1/600$/atm is roughly twice as large as for $k_1 = 1/1200$/atm. For the largest value of k_1 considered $k_1 = 1/120$/atm, the decrease in the response function is drastic, however, as might be expected since here $k_1\bar{p} \sim 1$. As discussed above (Sec. VI), reasonable values of θ and k_1 are probably $\theta = 10^{-4}$/°K, $k_1 = 1/1200$/atm to 1/600/atm.

In Figs. 2–4 we display the calculated response function *vs* frequency for the cases 2, 6, and 9 of Table I. These exhibit the general feature of decrease of the response function in the frequency region 10^3–10^4 cps. In addition, they show the amount of decrease for various values of θ and k_1.[11]

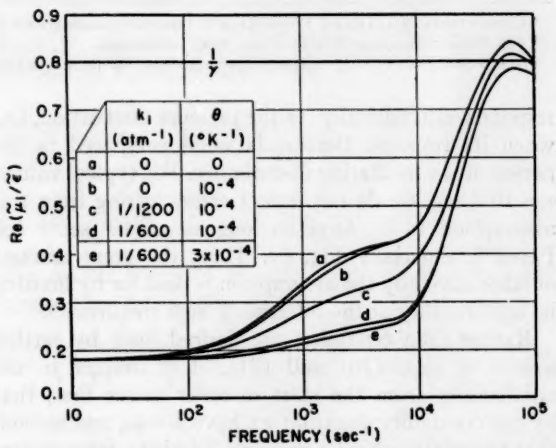

FIG. 4. Response curves in case 9 of Table I, for several values of compressibility (k_1) and thermal expansion (θ).

We have also computed the response function from the approximation (26). On comparing the results to the exact calculation for the 14 cases considered we find, as expected, that the adiabatic approximation is frequently adequate ($\sim 10\%$ accuracy) up to frequencies $f_0 \sim 10^4$ sec^{-1}. This is shown in Table I. Note that case 1, however, is exceptional in that the limiting frequency is much lower. This uniqueness is presumably associated with the fact that in this case the pressure exponent n is 0.

X. CONCLUSIONS

We first recall the approximations made in getting to the results of Sec. IX. In addition to neglecting the combustion zone thickness compared to sound wavelength (Sec. III), we have dropped terms of relative order $(\theta\Delta)^2$, $(k_1\bar{p}\theta\Delta)$, r_s, $\theta\Delta/\beta$, and $k_1\bar{p}/\beta$. None of these

[11] Of all the curves, only a' (Fig. 2) does not include the effect of the correction mentioned in the footnote preceding Eq. (20). Comparing a' to a in Fig. 2, we see that this correction reduces the response by ~ 0.04, mostly at frequencies $\lesssim 5000$ sec^{-1}. For other cases of Table I, the effect is similar.

approximations should introduce error >1%. For a discussion of the adequacy of the combustion model we used, see reference 1, Sec. VI.

It seems safe to conclude from our results that, insofar as the parameter values we have considered are typical:

(a) The adiabatic-gas approximation is usually adequate (~10% accuracy) for frequencies below 10^4 sec^{-1}, though not always;

(b) the solid density fluctuations which arise from thermal expansion (θ) generally have only a small effect (~0.01) on the response function;

(c) the solid density fluctuations induced mechanically via propellant compressibility (k_1) tend to decrease the response moderately (~0.1) at frequencies $\sim 10^3 - 10^4$ sec^{-1}. The effect seems largest for large Δ/T_c and/or j. For extremely compressible propellants (i.e., small elastic constants and sound velocity in the solid) the decrease may sometimes be sufficient to render the combustion zone nonamplifying.

In general, it is seen that the results of Paper I are not changed qualitatively by the introduction of solid density fluctuations. In an exact treatment these fluctuations would have to be included. However, such a treatment would also have to handle appropriately the large number of chemical reactions involved in both the gas and solid in the real combustion process. If any of these have rates such that they contribute significantly to the phase and amplitude relationships at the burning surface, they may produce even larger effects (both positive and negative) on the response function. This may be expected particularly at high frequencies, of course, but even at frequencies ~10^4 sec^{-1}, the residual influence of chemical reaction time lags sometimes may be considerable.

ACKNOWLEDGMENT

The authors wish to thank Mrs. M. E. Lynam, who skillfully programmed the equations for computation on the Univac-Scientific.

Equilibrium and Transport Properties of the Carbon Tetrachloride-Methylene Chloride System

CHARLES R. MUELLER AND ALBERT J. IGNATOWSKI

Chemistry Department, Purdue University, Lafayette, Indiana

(Received July 6, 1959)

Liquid densities of solutions of CCl_4 and CH_2Cl_2 have been measured at 20°C, and the excess volume has been obtained. Liquid-vapor equilibrium studies have been made at 30°, 35°, and 39°C, and the excess free energy of mixing has been deduced. Liquid viscosities have been measured at 20°C. The excess free energy of activation for viscous flow has been calculated. Vapor viscosity measurements have been made on the same system at 20°, 80°, and 140°C, as an adjunct to the theory to calculate the parameters in the Lennard-Jones potential.

INTRODUCTION

As a continuation of the experimental and theoretical program of this laboratory on the liquid state,[1,2] we have undertaken to measure the equilibrium and transport properties of a nonelectrolyte system exhibiting only slight deviations from ideality. The carbon tetrachloride-methylene chloride system fulfills the requirements by having only a slight deviation from Raoult's law. Of the equilibrium properties, we were interested in the volume change on mixing and the activity coefficients at several temperatures. Of the transport properties, we were interested in the liquid and gaseous viscosity. From the latter we obtained the six interaction parameters of the Lennard-Jones potentials.

PURIFICATION OF MATERIALS

Solvent grade CCl_4 was twice refluxed for 16 hr over clean mercury. After shaking with concentrated sulfuric acid and washing with water, the material was refluxed for about 24 hr with 10% NaOH—10% $KMnO_4$ aqueous solution. Finally, the CCl_4 was distilled from P_2O_5 through a 5-ft column filled with glass helices. The middle cut was stored over CaH_2. The refractive index was $n_D=1.46026$ at 20.00°C. Cooling curve analysis[3] indicated an impurity of 0.015 mole%.

Eastman Organic Chemical's methylene chloride was refluxed over mercury for 25 hr. Shaking with concentrated sulfuric acid produced a distinct amber coloration of the acid layer. This step was repeated with fresh acid until no further coloration was noticed. This material was washed with a 5% aqueous solution of Na_2CO_3 and water. The material was distilled from the same column used in the foregoing, and stored over CaH_2. The final material had a refractive index of $n_D=1.42347$ at 20.00°C. Cooling curve analysis showed no detectable impurity so that the material is at least 99.99 mole % CH_2Cl_2.

[1] C. R. Mueller and J. E. Lewis, J. Chem. Phys. **26**, 286 (1957).
[2] C. R. Mueller and E. R. Kearns, J. Phys. Chem. **62**, 1441 (1958).
[3] K. L. Nelson, Anal. Chem. **29**, 512 (1957).

VOLUME CHANGE ON MIXING

The densities of various mixtures of CCl_4 and CH_2Cl_2 were measured at 20.00°C. A bicapillary pycnometer[4] was used for these measurements due to the high volatility of CH_2Cl_2. The device was calibrated with standard water,[5] and all weighings were reduced to vacuo. The isothermal bath temperature was measured with a platinum resistance thermometer and could be maintained to ±0.004°C.

Table I gives the results of these measurements along with the percentage volume change on mixing.

TABLE I. Densities and excess volumes for solutions of carbon tetrachloride and methylene chloride at 20.00°C.

Mole fraction CCl_4	Density (g/ml)	$(V^E/V^0)100$
0	1.3252	0
0.1001	1.3620	0.129
0.1938	1.3933	0.233
0.2746	1.4188	0.279
0.4035	1.4559	0.328
0.5051	1.4830	0.328
0.7020	1.5312	0.227
0.7677	1.5458	0.196
0.9026	1.5745	0.080
1	1.5937	0

VAPOR PRESSURE MEASUREMENTS

The Scatchard equilibrium still[6] as modified by Lewis[1] was used in the vapor pressure measurements. This device was coupled with a precision manometer-cathetometer system. Full manometric corrections were applied as recommended by Beattie and co-workers.[7] The temperature in the equilibrium still was measured by a platinum resistance thermometer and a Leeds

[4] *ASTM Standards* (1952), Part 5, ASTM Designation: D 941-49, p. 400.
[5] *Technique of Organic Chemistry*, edited by A. Weisberger (Interscience Publishers, Inc., New York, 1959), Vol. I, *Physical Methods*, Part 1, 3rd ed., p. 256.
[6] G. Scatchard, C. L. Raymond, and H. H. Gilmann, J. Am. Chem. Soc. **60**, 1275 (1938).
[7] J. A. Beattie, M. Benedict, and B. E. Blaisdell, Proc. Am. Acad. Arts Sci. **74**, 327, 343, 371 (1941).

TABLE II. Vapor pressures of pure carbon tetrachloride and pure methylene chloride at various temperatures.

Temp. °C	CCl_4 mm Hg±0.02	CH_2Cl_2 mm Hg±0.02
29.993	141.59	529.02
34.993	174.44	638.87
38.993	...	739.34
39.993	213.35	765.94
49.992	311.89	...
69.992	617.31	...

and Northrup Mueller bridge arrangement. The thermometer was recalibrated prior to starting the measurements.

Vapor pressure measurements were made on pure carbon tetrachloride near 30°, 35°, 40°, 50°, and 70°C. Methylene chloride was measured at 30°, 35°, 39°, and 40°C. The measurements on CCl_4 served as a satisfactory check on the apparatus and technique since several workers have made measurements on CCl_4 with a corresponding degree of precision, including the work of Scatchard *et al.*,[8] who used essentially the same apparatus. The excellent agreement attests to the consistency of the method employed. Table II gives the vapor pressures of CCl_4 and CH_2Cl_2 in standard mm of mercury, taking 0°C=273.150° K according to the Tenth General Conference on Weights and Measures (1954).

The phase diagrams are for temperatures of 30°, 35°, and 39° C. Because of the great difference in liquid and vapor composition, equilibrium is quite difficult to attain in this region, and the actual measurements were made at slightly different temperatures. These results have been corrected by use of a concentration-dependent form of the Clausius-Clapeyron equation. The heat of mixing data of Cheesman and Whitaker[9] was used for this correction.

Tables III to V give a summary of the liquid-vapor equilibrium data for the system near 30°, 35°, and 39° C, respectively. The composition of the liquid phase is given under x_{CCl_4}, while the vapor-phase composition is given under y_{CCl_4}. Figure 1 is the phase diagram at 29.99°C and is representative of the others.

TABLE III. Vapor pressure data at 30°C.

x_{CCl_4}	y_{CCl_4}	$p(t)$ ±0.02	t, °C	$p(29.993)$ ±0.02
0.9507	0.785	173.46	29.993	173.46
0.8251	0.551	234.83	29.993	234.83
0.7290	0.396	283.28	29.993	283.28
0.5188	0.226	367.80	30.035	367.19
0.3933	0.166	411.07	30.035	410.39
0.2599	0.107	451.19	29.966	451.66

TABLE IV. Vapor pressure data at 35°C.

x_{CCl_4}	y_{CCl_4}	$p(t)$ ±0.02	t, °C	$p(35.000)$ ±0.02
0.9613	0.860	198.08	34.992	198.14
0.8529	0.597	270.43	34.987	270.57
0.8111	0.516	292.67	34.989	292.80
0.7190	0.384	344.47	35.003	344.43
0.6034	0.286	406.29	35.041	405.64
0.4679	0.198	469.03	34.969	469.59
0.3510	0.150	513.09	34.980	513.48
0.2915	0.127	532.84	35.012	532.60

A few remarks are, perhaps, in order about the accuracy of the measurements reported in the various tables. The behavior of the free energy plot leads one to suspect that there is a disparity between accuracy and precision. By means of density measurements we can, for example, measure the trap concentration quite precisely, but in the subsequent calculations we assume that this measures the equilibrium vapor concentration. We do not yet know to what extent this is true, and we do not know how many significant figures should really be reported.

Similar remarks should also apply to the parameters calculated, later in the paper, from vapor viscosity data.

LIQUID VISCOSITY

Measurements of the liquid viscosity of solutions of CCl_4 and CH_2Cl_2 were made at 20°C using a Cannon-Fenske viscometer (No. 50).

The viscometer was calibrated with the same standard water used in the density calibration. The kinematic viscosity (η/d) of water at 20.00°C was taken as 1.0038 centistokes.[10]

The results of the liquid viscosity measurements at 20.00°C are shown in Table VI. The column headed η/d gives the kinematic viscosity in centistokes (cm^2/sec), while the column headed η gives the dynamic viscosity in centipoise (g/cm sec).

TABLE V. Vapor pressure data at 39°C.

x_{CCl_4}	y_{CCl_4}	$p(t)$ ±0.02	t, °C	$p(38.993)$ ±0.02
0.9025	0.676	278.90	38.993	278.90
0.7994	0.483	353.73	38.998	353.66
0.5923	0.269	483.19	38.980	483.43
0.5035	0.225	524.17	39.010	523.84
0.3172	0.135	607.15	38.966	607.75
0.2313	0.0953	643.92	39.043	642.51

[8] G. Scatchard, S. E. Wood, and J. M. Mochel, J. Am. Chem. Soc. **61**, 3206 (1939).

[9] G. H. Cheesman and A. M. B. Whitaker, Proc. Roy. Soc. (London) **A212**, 406 (1952).

[10] J. F. Swindler, J. R. Coe, Jr., and T. B. Godfrey, J. Research Natl. Bur. Standards **48**, 1 (1952).

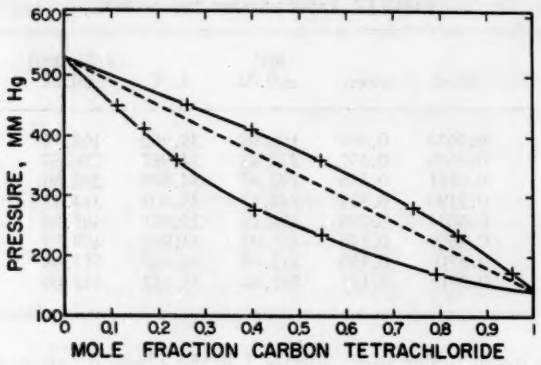

FIG. 1. Phase diagram, 29.99°C.

VAPOR VISCOSITY

The viscosity of the vapors of this system were measured by observing the damping produced by the vapors on the oscillatory vibrations of a freely suspended set of disks, moving parallel to, and between, a fixed set. The method is similar to that originally described by Maxwell.[11]

Details of construction are given by Lewis.[12] Only slight modifications were made to extend the temperature range of operation and to increase the ease of making the visual observations.

This form of viscosity apparatus serves as a fairly good manometer at low pressures. In order to obtain a value of the wire constant, the system must be pumped and degassed. It was found necessary to close off all mercury manometers from the system. After an extended period of pumping, the wire constant dropped by a factor of fifteen, and remained constant.

The low value of the logarithmic decrement of the suspension was confirmed by making some approximate theoretical calculations based on the internal friction of metals.[13] The empirical value lies between the extremes set by two different approaches.

TABLE VI. Coefficient of liquid viscosity for solutions of carbon tetrachloride and methylene chloride at 20.00°C.

mole fraction CCl_4	η/d centistokes	η centipoise
0	0.3356	0.4447
0.1001	0.3437	0.4681
0.1938	0.3544	0.4939
0.2746	0.3665	0.5200
0.4035	0.3903	0.5683
0.5051	0.4125	0.6117
0.6023	0.4381	0.6605
0.7020	0.4668	0.7147
0.7677	0.4894	0.7564
0.9026	0.5494	0.8651
1	0.6038	0.9623

[11] *The Scientific Papers of James Clerk Maxwell*, edited by W. D. Niven (Libraire Scientifique, J. Hermann, Paris), Vol. II, pp. 1–25.

[12] J. E. Lewis, Ph.D. thesis, Purdue University (1956).

[13] A. Gemant, *Frictional Phenomena* (Chemical Publishing Company, Inc., Brooklyn, 1950).

The apparatus constant was determined at each of the temperatures studied using filtered, dried, and CO_2-free air, taking the value $\eta_{23}° = 1830.0_6 \times 10^{-7}$ poise as suggested by Hopper and Laby.[14] The viscosity at other temperatures was calculated by means of the Sutherland equation taking $C = 117$.

The results of the vapor viscosity measurements are given in Table VII. The precision values give the deviation from the mean of the separate determinations. The measurements at 80.10°C are inexplicably erratic and were used only as a rough check.

TABLE VII. Coefficient of viscosity for vapors of carbon tetrachloride and methylene chloride.

Mole fraction CCl_4	$\eta \times 10^7$ poise
19.99°C	
0	1024.8±3.2
0.1575	1020.7±1.2
0.3015	1015.9±1.1
0.4986	1012.7±0.4
0.6886	999.8±0.3
0.8516	991.2±2.1
1	982.1±1.5
80.10°C	
0	1202±26
0.3261	1212± 1
0.6351	1192±37
1	1160±38
140.27°C	
0	1426.6±1.6
0.1515	1424.6±2.5
0.2882	1402.9±8.7
0.4738	1410.8±2.7
0.7096	1382.4±0.6
0.8739	1368.3±5.4
1	1362.6±0.9

DISCUSSION

From the viscosity at two temperatures, the parameters ϵ and σ in the Lennard-Jones (6–12) potential may be determined. For this purpose it is convenient to use the tables of Hirschfelder *et al.*[15] In the case of the pure components, the parameters were easily extracted. Considerably more difficulty was encountered in the case of the 1–2 interaction parameters. Normal methods failed to give physically acceptable values. The A_{12}^* collision integral was fixed by a stochastic method which finally resulted in excellent reproducibility of the viscosity data. The values of the parameters obtained are given in Table VIII. The Sutherland constants for the pure components are also included.

[14] V. D. Hopper and T. H. Laby, Proc. Roy. Soc. (London) **A178**, 243 (1941).

[15] J. O. Hirschfelder, C. F. Curtiss, and R. B. Bird, *Molecular Theory of Gases and Liquids* (John Wiley & Sons, Inc., New York, 1954).

TABLE VIII. Lennard-Jones parameters and Sutherland constants.

	CCl_4	CH_2Cl_2	1–2
ϵ/k, °K±5%	264	276	244
σ, Å±1%	6.19	5.16	5.79
C, °K	287.4	298.9	

TABLE IX. Virial coefficients (cc/mole).

	29.993°C	35.000°C	38.993
B_{CCl_4}±5%	−595	−578	−565
$B_{CH_2Cl_2}$±5%	−375	−364	−356
B_{AB}±5%	−422	−410	−400

TABLE X. Fugacities, activity coefficients and excess free energies at 29.993°C.

x_{CCl_4}	f_{CCl_4}	$f_{CH_2Cl_2}$	γ_{CCl_4}	$\gamma_{CH_2Cl_2}$	g^E
1	140.9	0	1	...	0
0.9507	135.4	37.14	1.011	1.440	17.1
0.8251	128.6	104.8	1.105	1.145	64.2
0.7290	111.2	170.1	1.082	1.199	64.7
0.5188	82.2	282.0	1.124	1.119	69.5
0.3933	67.4	339.4	1.216	1.068	70.2
0.2599	47.9	399.5	1.308	1.031	55.9
0	0	523.5	...	1	0

TABLE XI. Fugacities, activity coefficients, and excess free energies at 35.000°C.

x_{CCl_4}	f_{CCl_4}	$f_{CH_2Cl_2}$	γ_{CCl_4}	$\gamma_{CH_2Cl_2}$	g^E
1	173.5	0	1	...	0
0.9613	169.3	27.67	1.015	1.133	11.9
0.8529	160.3	108.4	1.083	1.168	55.9
0.8111	150.0	140.8	1.065	1.181	50.9
0.7190	131.2	210.6	1.052	1.187	51.9
0.6034	114.8	287.3	1.097	1.147	67.8
0.4679	91.8	373.2	1.131	1.111	69.9
0.3510	76.2	431.9	1.252	1.054	68.6
0.2915	66.7	460.2	1.320	1.029	62.1
0	0	631.1	...	1	0

TABLE XII. Fugacities, activity coefficients, and excess free energies at 38.993°C.

x_{CCl_4}	f_{CCl_4}	$f_{CH_2Cl_2}$	γ_{CCl_4}	γ_{CH_2Cl}	g^E±1 cal
1	203.8	0	1	...	0
0.9025	187.3	89.7	1.018	1.262	24.1[a]
0.7994	169.2	181.6	1.038	1.241	45.8[a]
0.5923	128.8	349.9	1.067	1.176	65.0
0.5035	116.3	402.1	1.133	1.110	71.4
0.3172	80.8	519.9	1.250	1.043	62.2
0.2313	60.3	574.4	1.279	1.024	46.9
0	0	729.4	...	1	0

[a] Note remarks in text on accuracy.

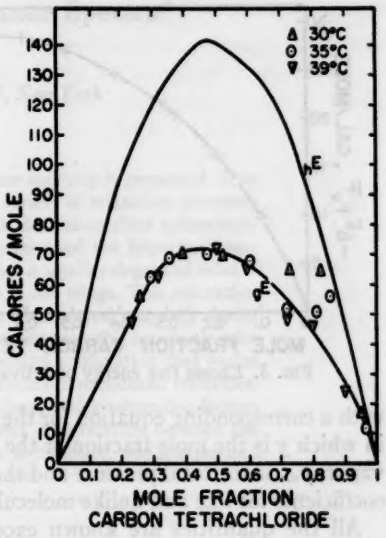

FIG. 2. Excess free energy and enthalpy.

Once all the parameters have been obtained, a theoretical equation for the viscosity of a gaseous binary mixture can be derived from Eq. (8.2-22) of Hirschfelder *et al.*,[15] of the form

$$\eta_{mix}(\text{poise}) = (1+a+bx_1x_2+cx_2^2)/(dx_1^2+ex_1x_2+fx_2^2). \quad (1)$$

There is considerable uncertainty in the values of the 1–2 interaction potentials. These values must be known quite accurately if they are to be of use in comparison of theories of solution, and it seems probable that measurements of the diffusion coefficient or use of the molecular beam technique will be required.

The parameters ϵ and σ are used to calculate the degree of gaseous imperfection. Guggenheim[16] gives the fugacity of a component in a slightly imperfect binary gaseous mixture,

$$f_A = y_A p_{tot} \exp\{(p_{tot}/RT)[B_{AA} + y_B^2(2B_{AB}-B_{AA}-B_{BB})]\} \quad (2)$$

TABLE XIII. Free energies of activation for viscous flow at 20.00°C.

Mole fraction CCl_4	$\Delta F_v^{\ddagger}$ cal/mole	$\Delta^E F_v^{\ddagger}$ cal/mole
0	5169	0
0.1001	5229	−9.4
0.1938	5286	−16.5
0.2746	5338	−20.5
0.4035	5422	−24.7
0.5051	5490	−27.3
0.6023	5556	−27.4
0.7020	5624	−28.3
0.7677	5671	−26.6
0.9026	5777	−13.9
1	5857	0

[16] E. A. Guggenheim, *Mixtures* (Clarendon Press, Oxford, England, 1952), p. 153.

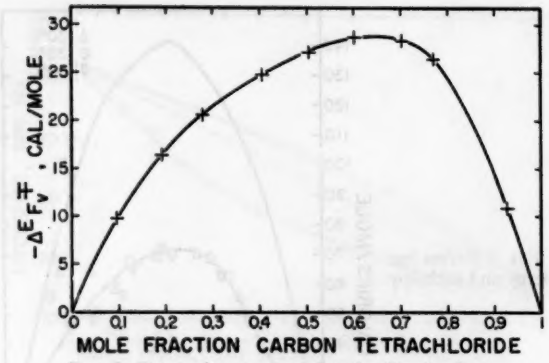

FIG. 3. Excess free energy of activation for flow.

with a corresponding equation for the other component, in which y is the mole fraction of the component in the vapor, p_{tot} is the total pressure and the B's are the virial coefficients for like and unlike molecular interactions.

All the quantities are known except the virial coefficients. These may be calculated by the methods of statistical mechanics. Assuming the Lennard-Jones (6–12) potential for the form of the interaction potential, the second virial coefficient can be expressed in terms of σ and the reduced temperature, $T^*=kT/\epsilon$. The computations are facilitated by the table of coefficients given in Hirschfelder *et al.*[15] Table IX is a summary of the calculated virial coefficients.

Tables X–XII summarize the fugacities and activity coefficients at the temperatures 30°, 35°, and 39°C, respectively. In addition, the excess free energies at each temperature are included.

However, the excess entropy and enthalpy, requiring a knowledge of the temperature derivative of the activity coefficient, could not be obtained. In the case of this system, the free energy is so weakly dependent on the temperature that the entropy is masked by the experimental fluctuations.

Fortunately, this same system of $CCl_4-CH_2Cl_2$ has been studied by Chessman and Whitaker.[9] They have measured the enthalpy at various compositions and several temperatures, taking the often neglected precaution of eliminating the vapor space in the design of their apparatus. The enthalpy was observed to be a contrast over the temperature range studied. With this knowledge, the entropy may be obtained from the familiar formula

$$Ts^E=h^E-g^E. \tag{3}$$

Figure 2 shows the concentration dependence of the excess free energy along with the enthalpy of Cheesman and Whitaker. The smooth symmetry of the enthalpy curve contrasts the rather uncertain shape of the free energy curve. We would like to reserve judgement as to the final shape of the free energy curve until after making a more critical investigation of vapor pressure measurements as a technique of obtaining the thermodynamics of solutions.

The scattering of the free energy data in the region of 0.60 to 0.85 mole fraction CCl_4 is a reflection of the difficulty experienced in this region in the operation of the equilibrium still. There is in this region almost a factor of two in the concentrations of gaseous and liquid states. In order to make the measurements in this region, one must start with different concentrations in the various boilers and traps. While the pressure composition curves are smooth, the scatter in the free energy curve probably reflects the inability of the apparatus to reach equilibrium. Further, the inability to obtain the temperature derivative of the activity coefficients points up the limitation of the vapor pressure device used.

The theory of absolute reaction rates of Eyring[17] has been applied to the viscous flow of a liquid. A relationship is obtained between the viscosity and the free energy of activation for the viscous flow process:

$$\eta/d=(hN/M)\exp(\Delta F_v^{\ddagger}/RT). \tag{4}$$

Table XIII gives these free energies of activation for various solutions of CCl_4 and CH_2Cl_2. In addition, the excess free energy of activation for flow, $\Delta^E F_v^{\ddagger}$, are calculated. These excess quantities are also tabulated in Table XIV.

Figure 3 is a curve of the excess free energy of activation for flow versus the mole fraction of CCl_4 in the CCl_4—CH_2Cl_2 solutions. This curve shows the characteristic parabolic shape of the excess solution functions. In this case, however, the asymmetry is rather pronounced. The maximum occurs at about 0.65 mole fraction CCl_4 with about -27.5 cal/mole excess free energy of activation. The shift of the maximum to a higher CCl_4 concentration is similar to the situation in the CCl_4–$CHCl_3$ system.[18]

The excess free energy of activation and the excess free energy of mixing as obtained from the vapor pressure work are related. An empirical correlation has been obtained by Powell *et al.*[19] It was found that the ratio of the excess free energy of mixing and the excess free energy of viscosity is approximately equal to 2.45. This same relation appears between $\Delta F_v^{\ddagger}$ and the energy of vaporization or the energy required for hole formation. The ratio $g^E/\Delta F_v^{\ddagger E}$ was examined at integral tenths of mole fraction CCl_4. The value of this ratio ranged from 2.88 to 2.00 with a value of 2.57 at 0.5 mole fraction. However, the average for the 9 ratios was 2.43.

ACKNOWLEDGMENTS

We are indebted to the Purdue Research Foundation and the Research Corporation for support, and to the Ethyl Corporation, who sponsored a fellowship for Mr. Ignatowski.

[17] S. Glasstone, K. J. Laidler, and H. Eyring, *The Theory of Rate Processes* (McGraw-Hill Book Company, Inc., New York, 1941), p. 477 ff.

[18] T. A. Bak and K. Andersen, Acta Chem. Scand. **12**, 1367 (1958).

[19] R. E. Powell, W. C. Roseveare, and H. Eyring, Ind. Eng. Chem. **33**, 430 (1941).

Theory of Saturation in Electron Spin Resonance Spectra*

MICHAEL J. STEPHEN AND GEORGE K. FRAENKEL
Department of Chemistry, Columbia University, New York 27, New York

(Received September 4, 1959)

A theory of saturation in electron spin resonance spectra exhibiting hyperfine splitting is presented. This theory is used to study the saturation of free radical spectra in solution, and a variety of relaxation processes are investigated. It is shown that motional modulation of the intramolecular electron-nuclear anisotropic dipole–dipole interaction introduces a relation between the saturation parameters and the hyperfine components that varies symmetrically about the center of the spectrum and causes a smaller degree of relaxation for the components in the central portion of the spectrum than for those in the wings. This relaxation mechanism introduces a greater dependence on nuclear spin state for radicals with several magnetic nuclei than for radicals with only one such nucleus. It is also shown that a cross term between this intramolecular dipolar interaction and motional modulation of the anisotropic g tensor introduces a relaxation that varies linearly from one side of the spectrum to the other. Numerical values of the relaxation-induced transition probabilities are estimated for the benzene negative ion, and tables are given from which saturation factors can be computed for a variety of conditions for several different spin systems. The relation between the spin-lattice relaxation time T_1 and the parameters which determine saturation is discussed, and it is pointed out that these quantities are not equivalent in systems exhibiting cross relaxation.

I. INTRODUCTION

EXPERIMENTAL studies of the electron resonance of solutions of free radicals have shown that the spectra are partially saturated at typical levels of microwave power and that the individual hyperfine components saturate to varying degrees.[1] In many spectra, the intensities (areas) and heights of maximum absorption of the hyperfine components are quantitatively not in the ratio of the relative degeneracies of the components, and the line widths vary from one component to another. Furthermore, the relative intensities, peak heights, and widths vary with the degree of saturation.

In the present discussion, we examine the theory of saturation in complex multilevel systems, extending the work of Lloyd and Pake,[2] and calculate the effects of a variety of relaxation mechanisms. Our primary objective has been to investigate a mechanism which would affect the relaxation of the different hyperfine components to varying degrees. To agree with the experimental observations,[1] the mechanism would have to explain a greater degree of saturation for the central components of the spectrum than for the wings, and would have to produce an effect which was essentially symmetric about the center of the spectrum. It is shown in the following that a symmetrical saturation of this type can arise from motional modulation of the intramolecular anisotropic dipole-dipole interaction between the unpaired electron and the magnetic nuclei in a free radical.[3] McConnell[4] has shown that anisotropy in the spectroscopic-splitting tensor (g tensor) can cause a systematic variation of the line widths among the different hyperfine components from one end of the spectrum to the other, and the influence of this mechanism on the saturation behavior is also included in the present calculation. These two mechanisms, anisotropic intramolecular electron-nuclear dipolar interaction and g-factor anisotropy, are the only types of relaxation considered which give rise to differences in behavior among the different hyperfine components. Nuclear electric quadrupole relaxation (for nuclear spins with $I>\frac{1}{2}$), and modulation of the isotropic hyperfine interaction[5] also may relax different hyperfine components differently.

A large variety of mechanisms can cause relaxation of the electron spin without affecting the nuclear-spin states. One contribution to these effects is the interaction between the electron and the fluctuating magnetic fields arising from the motion of charged particles in the solution. The intramolecular part is the spin-rotational interaction. For molecules with electron spin greater than one-half ($S>\frac{1}{2}$), motional modulation of the zero-field splitting (analogous to crystal-field splitting) can give rise to another type of intramolecular relaxation which does not depend on the nuclei. The significant intermolecular relaxation mechanisms which affect the electron also cause a nuclear-spin-state independent relaxation. Of these, probably the most important in free-radical spectra arise from dipole-dipole interaction between the unpaired electron and the nuclear moments in the solvent; from dipole-dipole and exchange interactions between different radicals and between radicals and paramagnetic impurities; and from chemical reactions which destroy the radical species. In the present calculation, explicit estimates

* This research was supported in part by the United States Air Force through the Office of Scientific Research.

[1] J. W. H. Schreurs, G. E. Blomgren, and G. K. Fraenkel J. Chem. Phys. (to be published).

[2] J. P. Lloyd and G. E. Pake, Phys. Rev. 94, 579 (1954).

[3] We are indebted to Professor N. Bloembergen for suggesting this mechanism.

[4] H. M. McConnell, J. Chem. Phys. 25, 709 (1956).

[5] A. Abragam and J. Combrisson, Nuovo cimento 6, Suppl. No. 3, 1197 (1957).

are made of the effects of the spin-rotational interaction and of the dipolar interactions.

A complete study of the effect of relaxation mechanisms on the characteristics of electron resonance spectra in solutions would include a calculation of the widths of the hyperfine components. Such a calculation is most suitably performed by use of a theory similar to that developed by Kubo and Tomita,[6] and is being carried out by Kivelson.[7]

In Sec. II of the present paper, the equations which relate the steady-state populations of the nuclear- and electron-spin energy levels to the intensity of the applied radiation field are formulated. A simple procedure is given for obtaining from these equations the parameters which determine the saturation in terms of the transition probabilities arising from relaxation. In Sec. III, explicit calculation is made of the transition probabilities induced by relaxation mechanisms. Section IV is concerned with a brief discussion of the relation of the spin-lattice relaxation time (T_1) to the transition probabilities causing relaxation and of limitations on the use of T_1 as a parameter to describe saturation behavior in complex multilevel systems. The final results are described in Sec. V.

II. GENERAL THEORY OF SATURATION

In this section we discuss the saturation behavior of a dilute solution of molecules consisting of an unpaired electron (i.e., $S=\frac{1}{2}$) interacting with a number of equivalent nuclear spins. Two nuclei are considered equivalent in the present treatment if they consist of the same isotopic species and their positions can be interchanged by the symmetry operations under which the molecular properties are invariant. The molecules will be assumed to be rapidly tumbling in the solution. In the presence of a strong static magnetic field H_0 in the z direction, the spin energy levels of a molecule are given by[8,9]

$$E(m_s, m_J)=g_s\beta_s H_0 m_s-g_I\beta_I H_0 m_J+hAm_s m_J. \quad (2.1)$$

In this expression, β_s and β_I are the Bohr and nuclear magnetons, respectively, and g_I is the nuclear g factor. The electronic g factor g_s is the motionally averaged value of the spectroscopic splitting factor tensor, and is given by

$$g_s=\tfrac{1}{3}(g_1+g_2+g_3) \quad (2.2)$$

where g_1, g_2, and g_3 are the principal values of the g tensor of the molecule. The coupling parameter A is the motionally averaged value of the hyperfine interaction and therefore consists primarily of the Fermi contact interaction. The eigenvalue of the z component of the electron spin angular momentum (in units of $\hbar$) is given by m_s, and m_J is the eigenvalue of the total z component of the nuclear spin. Thus, if m_i is the z component of the ith nuclear spin,

$$m_J=\sum_{i=1}^{J} m_i,$$

where n is the number of (equivalent) nuclei in the molecule. The energy levels have a degeneracy which will be denoted by $D(n, I, m_J)$ where I is the spin of the nuclei. For a single nucleus, $D(1, I, m_J)=1$, and for nuclei with spin of one-half (e.g., protons),

$$D(n, \tfrac{1}{2}, m_J)=n!/[(\tfrac{1}{2}n-m_J)!(\tfrac{1}{2}n+m_J)!]. \quad (2.3)$$

If $I>\frac{1}{2}$, expressions for $D(n, I, m_J)$ are also easily obtained.

In an electron resonance experiment, the laboratory radiation field induces transitions $(m_s, m_J)\rightarrow(m_s\pm1, m_J)$, and in the presence of a given radiation field and a fixed static field (slow passage), a stationary spin population will ultimately result in which the radio-frequency absorption is just balanced by the energy carried to the lattice through relaxation processes. The rate P at which energy is absorbed from the radiation field is proportional to the population difference between the two levels.[2,10] For convenience in the following, we frequently replace the (m_s, m_J) notation to designate an energy level by a single index, say k, and designate a particular one of the $D_k=D(n, I, m_J)$ degenerate states belonging to the kth energy level by the index u.[11] Let the probability of finding the system in the state ku be Q_{ku}, and let the probability distribution for a system at equilibrium, namely, the Boltzmann distribution, be denoted by Q_{ku}^0. The Q_{ku} are independent of the particular degenerate state, and we can write Q_k, the probability of finding the system in the kth energy level, as

$$Q_k=D_kQ_{ku}. \quad (2.4)$$

It is useful, following Lloyd and Pake,[2] to express the steady-state difference in relative populations when an rf field is present, $Q_\alpha-Q_\beta$, in terms of the relative population difference at equilibrium, $Q_\alpha^0-Q_\beta^0$, by introducing a saturation factor defined as

$$Z_{\alpha\beta}=(Q_\alpha-Q_\beta)/(Q_\alpha^0-Q_\beta^0). \quad (2.5)$$

As shown by Lloyd and Pake and also in the following, the saturation factor always may be written in the form

$$Z_{\alpha\beta}=(1+2V_{\alpha\beta}\Omega_{\alpha\beta})^{-1} \quad (2.6)$$

where $\Omega_{\alpha\beta}$ takes the place of the spin lattice relaxation time T_1 appropriate for the description of saturation for a two-level spin system as used by Bloembergen *et al.*[10]

[6] R. Kubo and K. Tomita, J. Phys. Soc. Japan **9**, 888 (1954).
[7] D. Kivelson (private communication).
[8] B. Venkataraman and G. K. Fraenkel, J. Am. Chem. Soc. **77**, 2707 (1955).
[9] S. I. Weissman, J. Chem. Phys. **22**, 1378 (1954).
[10] N. Bloembergen, E. M. Purcell, and R. V. Pound, Phys. Rev. **73**, 679 (1948).
[11] We use α, β to denote a particular pair of energy levels between which radiation-induced transitions are occurring and j, k to denote any pair of levels.

and by Bloch.[12] $V_{\alpha\beta}$ is the probability of the transition (α, β) induced by the radiation. For a system with $S=\frac{1}{2}$, we have[13]

$$V_{\alpha\beta}=\sum_{u,u'}V_{\alpha u,\beta u'}=\tfrac{1}{4}\hbar^{-2}g_s^2\beta_s^2H_1^2g_{\alpha\beta}(\nu-|\nu_{\alpha\beta}|)D_\alpha, \quad (2.7)$$

where $2H_1$ is the amplitude of the applied radiation field perpendicular to the static field, and $g_{\alpha\beta}(\nu-|\nu_{\alpha\beta}|)$ is a line-shape factor for the (α,β) transition. In obtaining Eq. (2.7), use has been made of the equality of the degeneracy of the two levels involved in the transition $(D_\alpha=D_\beta)$. The parameter $\Omega_{\alpha\beta}$ is related to what Lloyd and Pake call the relaxation probability, $(W_R)_{\alpha\beta}$, by

$$\Omega_{\alpha\beta}=[2(W_R)_{\alpha\beta}]^{-1}. \quad (2.8)$$

From Eq. (2.6) it will be observed that the saturation factor is a function of the particular transition (α, β) through the dependence of $V_{\alpha\beta}$ on the line-shape function $g_{\alpha\beta}$ and the degeneracy D_α as well as through the saturation parameter $\Omega_{\alpha\beta}$.

It can be shown from Eqs. (2.6) and (2.7)[12,14] that the imaginary part of the magnetic susceptibility associated with the transition (α, β) is given by

$$\chi_{\alpha\beta}''=\tfrac{1}{2}\chi_0\,|\,\omega_{\alpha\beta}\,|\,[D_\alpha/\sum_a D_a]\cdot\left[\frac{g_{\alpha\beta}(\nu-|\,\nu_{\alpha\beta}\,|)}{1+\frac{1}{2}\hbar^{-2}g^2\beta_s^2H_1^2g_{\alpha\beta}(\nu-|\,\nu_{\alpha\beta}\,|)D_\alpha\Omega_{\alpha\beta}}\right]. \quad (2.9)$$

Equation (2.9), in which χ_0 is the static electron-spin susceptibility of the radical, is a well-known result for nondegenerate systems; it has been given here only to indicate how to take proper account of the degeneracy.

The remainder of this section is concerned with the evaluation of the saturation factors $Z_{\alpha\beta}$ in terms of the transition probabilities induced by relaxation mechanisms. Under conditions of a steady-state distribution of populations, the Q_{ku} satisfy the well-known system of equations[2]

$$\dot{Q}_{ju'}=\sum_{k,u}{}'Q_{ku}W_{ku,ju'}-Q_{ju'}\sum_{k,u}{}'W_{ju',ku}=0 \quad (2.10)$$

where $W_{ku,ju'}$ is the total transition probability from state k, u to state j, u' including that induced by both the lattice and the radiation field. The prime on the summation is to indicate that the term $ku=ju'$ is excluded. Equation (2.10) also contains terms arising out of a reshuffling among the degenerate states. These terms are not important and drop out in Eq. (2.13). The Q_{ku} also must satisfy the normalizing condition

$$\sum_{k,u}Q_{ku}=1. \quad (2.11)$$

In writing Eq. (2.10) we are making the random phase approximation, i.e., assuming all off-diagonal elements of the density matrix are zero. By introducing the total transition probability from energy level k to level j, W_{kj},

$$W_{kj}=\sum_{u,u'}W_{ku,ju'}, \quad (2.12)$$

and adding together all equations belonging to the same j, these equations can be expressed in terms of the Q_k:

$$\sum_k{}'Q_kD_k^{-1}W_{kj}-Q_jD_j^{-1}\sum_k{}'W_{jk}=0, \quad (2.13)$$

$$\sum_k Q_k=1. \quad (2.14)$$

Written in matrix form, Eq. (2.13) is

$$\mathbf{AQ}=0 \quad (2.15)$$

where $\mathbf{A}$ is a singular matrix having elements

$$A_{jk}=W_{kj}D_k^{-1} \qquad (j\neq k)$$

$$A_{jj}=-\sum_k{}'W_{jk}D_j^{-1}. \quad (2.16)$$

A solution of Eq. (2.15) is proportional to any column of the matrix adjoint to $\mathbf{A}$ and the constant of proportionality is determined by the condition Eq. (2.14) When the rank of $\mathbf{A}$ is $r-1$ (where r is the order of $\mathbf{A}$), the solution is unique and is proportional to the sum of all the columns of Adj $\mathbf{A}$. Thus, using Eq. (2.14),

$$Q_i=\sum_j B_{ji}/\sum_{jk}B_{jk} \quad (2.17)$$

where B_{ij} is the cofactor of A_{ij} in $\mathbf{A}$ and the jith element of Adj $\mathbf{A}$. The results also may be expressed in terms of diagonal cofactors only. Since $\sum_j B_{ji}$ is just $|\,\mathbf{A}\,|$ with the ith column replaced by a column in which each element is unity, we may add all rows to row i in this determinant to obtain

$$\sum_j B_{ji}=rB_{ii}.$$

By using this result in Eq. (2.17), we obtain

$$Q_i=B_{ii}/\sum_k B_{kk}. \quad (2.18)$$

For a lattice in thermal equilibrium, the lattice-induced transition probabilities, W'_{kj}, are related by[15]

$$W'_{kj}=W'_{jk}\exp(\hbar\beta\omega_{kj}). \quad (2.19)$$

Substitution of Eq. (2.19) into Eq. (2.18) may be shown to lead to a Boltzmann distribution in the Q_i.

Suppose now that a radiation field induces transitions between levels α and β with transition probability

[12] F. Bloch, Phys. Rev. **70**, 460 (1946).
[13] G. E. Pake, *Solid State Physics* (Academic Press, Inc., New York, 1956), Vol. 2, p. 13.
[14] E. R. Andrew, *Nuclear Magnetic Resonance* (University Press, Cambridge, England, 1955).
[15] Y. Ayant, J. phys. radium **16**, 411 (1955); F. Bloch, Phys. Rev. **102**, 104 (1956).

$V_{\alpha\beta}=V_{\beta\alpha}$ as given by Eq. (2.7). Then,

$$W_{\alpha\beta}=W'_{\alpha\beta}+V_{\alpha\beta}$$
$$W_{\beta\alpha}=W'_{\beta\alpha}+V_{\alpha\beta}$$
$$W_{ij}=W'_{ij}, \qquad (ij\neq\alpha\beta,\beta\alpha). \quad (2.20)$$

Consider the matrix $\mathbf{A}'$ obtained from $\mathbf{A}$ by setting all the degeneracies $D_k=1$ and replacing the W_{ij} by the W'_{ij}. Let C_{ij} be the cofactor of A'_{ij} and $C_{ij,ij}$ the determinant obtained from A'_{ij} by crossing out rows i and j and columns i and j. By using an expansion on diagonal elements and Eq. (2.20), it is readily seen that

$$B_{\alpha\alpha}=(D_\alpha/D)[C_{\alpha\alpha}-V_{\alpha\beta}C_{\alpha\beta,\alpha\beta}]$$
$$B_{\beta\beta}=(D_\beta/D)[C_{\beta\beta}-V_{\alpha\beta}C_{\alpha\beta,\alpha\beta}] \quad (2.21)$$

where

$$D=\prod_k D_k \quad (2.22)$$

is the product of all the degeneracies. By using Eqs. (2.21) and (2.18) in Eq. (2.5) for the saturation factor, one obtains, since $D_\alpha=D_\beta$,

$$Z_{\alpha\beta}=\frac{Q_\alpha-Q_\beta}{Q_\alpha^{(0)}-Q_\beta^{(0)}}=\frac{\sum_k B_{kk}(0)}{\sum_k B_{kk}(V_{\alpha\beta})} \quad (2.23)$$

where we have indicated explicitly that B_{kk} in the numerator is calculated when there is no rf field while in the denominator it is calculated when the field-induced transition probability is $V_{\alpha\beta}$.

At temperatures high enough to allow the approximation $\exp(\beta_l\hbar\omega_{kj})\cong 1$, we can use Eq. (2.19) to write

$$W'_{ij}=W'_{ji} \quad (2.24)$$

and Eq. (2.23) can be simplified. By using Eq. (2.24) one can show that

$$[B_{ii}(V_{\alpha\beta})]_{\beta_l=0}=(D_i/D)[\tilde{C}_{\alpha\alpha}-V_{\alpha\beta}\tilde{C}_{\alpha\beta,\alpha\beta}] \quad (2.25)$$

where the tildes over the C's, $(\tilde{C})$ indicate this is the high-temperature approximation. By putting $V_{\alpha\beta}=0$, it is seen from Eq. (2.25) that all the diagonal cofactors $\tilde{C}_{\alpha\alpha}$ are equal. Substitution of Eq. (2.25) in Eq. (2.23) leads to the very simple formula for the saturation factor:

$$Z_{\alpha\beta}=[1-V_{\alpha\beta}(\tilde{C}_{\alpha\beta,\alpha\beta}/\tilde{C}_{\alpha\alpha})]^{-1}. \quad (2.26)$$

The relaxation parameter $\Omega_{\alpha\beta}$ is therefore

$$\Omega_{\alpha\beta}=[2(W_R)_{\alpha\beta}]^{-1}=-\tilde{C}_{\alpha\beta,\alpha\beta}/2C_{\alpha\alpha}. \quad (2.27)$$

For a two-level system we must take

$$\tilde{C}_{\alpha\beta,\alpha\beta}=1.$$

The order r of $\mathbf{A}$ is even and it may be shown[16] that $\tilde{C}_{\alpha\beta,\alpha\beta}$ is always positive and $\tilde{C}_{\alpha\alpha}$ negative so that $\Omega_{\alpha\beta}$ in Eq. (2.27) is positive.

[16] W. Ledermann, Proc. Cambridge Phil. Soc. 46, 581 (1950).

III. TRANSITION PROBABILITIES EFFECTING RELAXATION

The transition probability per unit time induced between states j and k by a perturbation H' acting on the spin system may be calculated from the result

$$W'_{jk}=2\hbar^{-2}\sum_q \frac{\tau_{cq}}{1+\omega_{jk}^2\tau_{cq}^2}\langle|F^{(q)}(0)|^2\rangle\sum_{u,u'}|(ju|A^{(q)}|ku')|^2 \quad (3.1)$$

where the perturbation has been written as

$$H'=\sum_q F^{(-q)}(t)A^{(q)}. \quad (3.2)$$

In Eq. (3.2), the $F^{(q)}(t)$ are randomly varying functions of the lattice coordinates and the $A^{(q)}$ are operators in spin space. The quantity τ_{cq} is the correlation time associated with the function $F^{(q)}$. The large angular brackets in Eq. (3.1) indicate a classical average over all configurations of the system, and the summation u,u' is over all degenerate states. W'_{jk} may be shown to be independent of the particular choice of degenerate states, i.e., W'_{jk} is invariant under a unitary transformation among the u, u'.

The relaxation mechanisms that can induce transitions may be conveniently divided into intramolecular and intermolecular contributions, and only intramolecular mechanisms will lead to relaxation effects that vary from one hyperfine component to another. In free radicals, the most important effects that cause a dependence on the hyperfine component arise from motional modulation of the electron-nuclear anisotropic dipole-dipole interaction and of the anisotropic g tensor. Other effects causing relaxation which is dependent on the nuclear-spin state (all probably small and not included in the present calculation) would arise from quadrupole coupling ($I>\frac{1}{2}$), nuclear spin-spin coupling, and modulation of the isotropic hyperfine coupling constant A of Eq. (2.1). In addition to these effects, there will be a number of sources of relaxation, both inter- and intramolecular, that relax the electron spin independently of the nuclei, and which will all be included together in terms of a single parameter.

A detailed examination of the electron-nuclear dipole-dipole interaction and of the anisotropy in the g tensor shows that the lattice-induced transition probabilities may be written in the form

$$W'(m_s, m_J; m_s\pm 1, m_J)$$
$$=(Km_J^2+Lm_J+M)D(n, I, m_J) \quad (3.3)$$

$$W'(m_s, m_J; m_s\pm 1, m_J\pm 1)$$
$$=6W'(m_s, m_J; m_s\mp 1, m_J\pm 1)$$
$$=4(1+\omega^2\tau_c^2)^{-1}W'(m_s, m_J; m_s, m_J\pm 1)$$
$$=nK\sum_{m=-I}^{I}(I\mp m)(I\pm m+1)D(n-1, I, m_J-m). \quad (3.4)$$

Here n is the number of equivalent nuclei in the radical and $D(n, I, m_I)$ is the degeneracy of the level (m_s, m_I), as for example, in Eq. (2.3). For a single nucleus, the last line in Eq. (3.4) should be replaced by

$$K(I\mp m_I)(I\pm m_I+1).$$

For simplicity, a single correlation time τ_c has been assumed for the dipole-dipole and g-tensor interactions. In Eqs. (3.3) and (3.4), the ω_{jk} of Eq. (3.1) have been replaced by $\omega=\hbar^{-1}g_s\beta_sH_0$, the mean angular frequency of the spectrum, for all transitions in which $\Delta m_s=\pm1$, so that differences in frequency between different hyperfine components in the electron resonance spectrum have been neglected. For the nuclear transitions ($\Delta m_s=0$, $\Delta m_I=\pm1$), the ω_{jk} have been taken to be zero, i.e., it is assumed for these transitions that $\omega\tau_c\ll1$.

The parameter K in these equations arises from the effects of the intramolecular dipole-dipole interaction and L arises from a cross term between the effects of this dipolar interaction and the anisotropy of the g tensor. In the vertical transitions ($\Delta m_s=\pm1$, $\Delta m_I=0$) with probabilities given by Eq. (3.3), K affects the relaxation symmetrically about the center of the spectrum, causing a greater relaxation for large m_I than for small m_I, while L introduces an asymmetric effect that varies linearly from the low-field side of the spectrum to the high-field side. M includes all the effects that relax the electron spin without influencing the nuclei, and produces a relaxation that is independent of m_I. Only K affects the cross relaxations ($\Delta m_s=0, \pm1$; $\Delta m_I=\pm1$), with probabilities given by Eqs. (3.4), and again the relaxation is symmetric about the center of the spectrum. This symmetry can be seen as follows. That part of the determinant A'_{ij} [see discussion following Eq. (2.20)] which depends on K is both symmetric and centrosymmetric, i.e., $A'_{ij}=A'_{r+1-j,r+1-i}$, where r is the order of the determinant and where the rows and columns are labeled so as to progress uniformly from low m_I to high m_I. Thus, by interchanging rows and columns, one can show for the K-dependent part that

$$\tilde{C}_{\alpha\beta,\alpha\beta}=\tilde{C}_{\beta\alpha,\beta\alpha}=\tilde{C}_{r+1-\alpha,r+1-\beta;r+1-\alpha,\,r+1-\beta},$$

and since $\tilde{C}_{\alpha\alpha}$ is independent of α [see Eq. (2.25)], the saturation parameter can be written as

$$\Omega_{\alpha\beta}=\Omega_{r+1-\alpha,r+1-\beta}.$$

In other words, that part of the saturation which depends on the intramolecular dipolar interaction (K) is symmetric about the center of the spectrum.

The calculation of the transition probabilities from Eq. (3.1) is quite standard.[4,10] The explicit expressions for the parameters K and L are

$$K=\tfrac{3}{5}\frac{\tau_c}{1+\omega^2\tau_c^2}g_s^2\beta_s^2\gamma_I^2[|\,a\,|^2+2\,|\,b\,|^2+2\,|\,c\,|^2] \tag{3.5}$$

$$L=\tfrac{1}{5}\frac{\tau_c}{1+\omega^2\tau_c^2}g_s\beta_s^2\hbar^{-1}\gamma_IH_0\{(\tfrac{3}{2})^{\frac{1}{2}}(g_1-g_2)(c+c^*)+[2g_3-(g_1+g_2)]a\} \tag{3.6}$$

where

$$a=(\tfrac{1}{4}\pi)^{\frac{1}{2}}\langle r'^{-3}Y_{20}(\theta',\phi')\rangle$$
$$b=(\tfrac{1}{4}\pi)^{\frac{1}{2}}\langle r'^{-3}Y_{21}(\theta',\phi')\rangle$$
$$c=(\tfrac{1}{4}\pi)^{\frac{1}{2}}\langle r'^{-3}Y_{22}(\theta',\phi')\rangle \tag{3.7}$$

and where g_1, g_2, and g_3 are the principal values of the g tensor along molecule-fixed axes x', y', and z', respectively. In Eq. (3.7), the angular brackets signify an average over the electronic wave function of the unpaired electron, and the spherical harmonics $Y_{mn}(\theta',\phi')$ are referred to the molecule-fixed principal axes x', y', z' of the g tensor.

The parameter M may arise from a number of different effects some of which we now consider.

(a) The g-factor anisotropy also leads to a nuclear-spin independent relaxation of electron spins. The contribution calculated using Eq. (3.1) is

$$M_0=\frac{1}{30}\frac{\tau_c}{1+\omega^2\tau_c^2}\beta_s^2H_0^2\hbar^{-2}(3g:g-9g_s^2) \tag{3.8}$$

where

$$g:g=g_1^2+g_2^2+g_3^2.$$

(b) Relaxation is caused by dipole-dipole interactions between the electron spin and other magnetic spins, either nuclear or electronic, in the solution. The contribution from solvent nuclei may be estimated by a modified version[6,17] of the arguments of Bloembergen *et al.*[10] to be

$$M_{solv}=[8\pi^2\eta N^s/3kT][rr^s/(r+r^s)^2]g_s^2\beta_s^2(\gamma_I^s)^2I^s(I^s+1) \tag{3.9}$$

Here r is the effective radius of the free radical, r^s is the effective radius of the solvent molecules, η is the viscosity of the solvent, N^s is the number of solvent nuclei per cubic centimeter of spin I^s with gyromagnetic ratio γ_I^s, and T is the absolute temperature. In obtaining Eq. (3.9), relative rotational motion of interacting molecules is neglected, and it is assumed that the translational correlation time τ_0 is so short that $\omega\tau_0\ll1$. Both of these assumptions may be questionable in the present application. The contribution of paramagnetic species in the solution with magnetic moments different from that of the free radical giving rise to the spin resonance spectrum also may be estimated from Eq. (3.19) if the magnetic moment of the paramagnetic species μ is substituted for $\hbar\gamma_I^s[I^s(I^s+1)]^{\frac{1}{2}}$. It is as-

[17] I. Solomon, Phys. Rev. 99, 559 (1955).

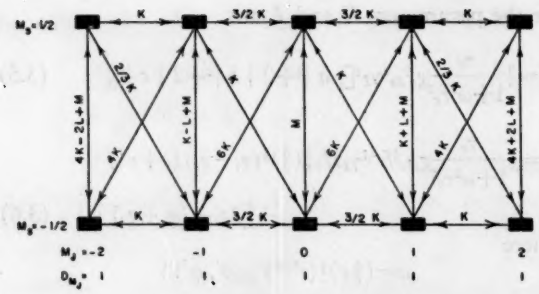

FIG. 1. Relaxation probabilities for spin system with $S=\frac{1}{2}$ and one nucleus with $I=2$. Energy levels, indicated by filled rectangles are labeled by M_s, M_J. The possible relaxations calculated from Eqs. (3.3) and (3.4) for extreme motional narrowing are shown by arrows. The degeneracies are indicated by D_{M_J}.

sumed that the concentration of these other paramagnetic species is so low that exchange effects can be neglected. A modification of Eq. (3.19) also can be used to estimate the effects of dipolar interaction between the free radicals themselves. Again, assuming the concentration of the primary species N^0 (in molecules per cm^3) is low enough to allow neglect of exchange, one obtains[6,10,17]

$$M_{\text{rad-rad}}=3\pi^2\eta N^0(g_e\beta_e)^4\hbar^{-2}/4kT. \qquad (3.10)$$

(c) The interaction between the electron spin and the fluctuating magnetic fields arising from the relative motion of the electron and charged particles also may contribute to the relaxation parameter M. Let us assume that the magnetic field is of intramolecular origin and of magnitude $H(t)$ so that the interaction with the electron is $g_e\beta_e\mathbf{S}\cdot\mathbf{H}(t)$. The contribution to the transition probability of this spin-rotational interaction is then

$$M_H=\tfrac{1}{3}g_e^2\beta_e^2\hbar^{-2}\langle|H(t)|^2\rangle[\tau_c'/(1+\omega^2\tau_c'^2)] \qquad (3.11)$$

where the angular brackets signify an average over all configurations of the system, and the correlation time is denoted by τ_c' in Eq. (3.11) to indicate that it is different from the correlation time τ_c used previously for the dipolar and g-factor interactions in Eqs. (3.4)–(3.18). A similar mechanism has been proposed by Landesman.[18]

These three mechanisms of relaxation of the electron spin are probably the most important for dilute solutions of free radicals but do not form a comprehensive list of possible mechanisms. In much of what follows, relaxations represented by M will be treated as an adjustable parameter.

In the way of an example, we attempt to make order of magnitude estimates of the parameters K, L, and M for the benzene negative ion. The magnitude of the intramolecular electron-nuclear dipolar interaction can be estimated from the calculation of McConnell and Strathdee[19] for a —CH fragment. Adapting their results to the parameters a, b, and c in Eq. (3.7), one obtains,

$$g_e\beta_e\hbar\gamma_I a=(2.5/6)\text{ Mc/sec}$$
$$g_e\beta_e\hbar\gamma_I b=0$$
$$g_e\beta_e\hbar\gamma_I c=(-16.7/6)\text{ Mc/sec} \qquad (3.12)$$

where the factor of six arises from the division of the unpaired electron among six nuclei. It is assumed that the electron is equally distributed over the six nuclei, and contributions from carbon atoms which are not nearest neighbors are neglected. The anisotropy of the g tensor was estimated as follows. The isotropic g factors, g_s, of free radicals are typically in the range from 2.004 to 2.005,[20–22] so that the departure from the free-electron value of $g_0=2.0023$ is about $g_s-g_0=0.002$. Assume the odd electron in the benzene negative ion is in an orbitally nondegenerate state in an axially symmetric field. When the external magnetic field is oriented perpendicular to the plane of the molecule, the g value will be the free-electron g value, g_0. From Eq. (2.2) we therefore obtain, since $g_1=g_2$,

$$g_1-g_3=g_2-g_3=(\tfrac{3}{2})(g_s-g_0)=0.003. \qquad (3.13)$$

In evaluating the contributions of g-tensor anisotropy, the external field was taken to be $H_0=3\times10^3$ gauss. The solvent was assumed to be water at room temperature (300°K.) with viscosity $\eta=1.02$ centipoises. For the effective radii of solvent and solute we have put $rr^s/(r+r^s)^2$ equal to its maximum value of $\frac{1}{4}$.

The quantity $H(t)$ in Eq. (3.11) is more difficult to estimate than the other parameters. Let us assume $H(t)$ to arise out of spin-rotational interaction and take $H(t)$ proportional to the rotational angular momentum J, i.e., $H(t)=A_0J$ where A_0 is a constant. Taking the average indicated in Eq. (3.11), assuming a Boltzmann distribution of rotational states, one obtains

$$\langle|H(t)|^2\rangle=A_0^2(2I_0kT/\hbar^2), \qquad (3.14)$$

where I_0 is the average moment of inertia of the molecule. For benzene, $I_0\cong2\times10^{-38}$ g-cm^2. A_0 is difficult to estimate, but rotational magnetic moments are of the order of a nuclear magneton, and if we take the distance between the rotational axis and the electron spin to be 2 A, the value of A_0 is of the order of (one nuclear magneton)/(8 A^3), i.e., $A_0\cong0.6$. By using Eq. (3.14), the mean square field becomes $\langle|H(t)|^2\rangle\cong5.4\times10^2$ (gauss)^2. Comparison of Eq. (3.11) with Eq. (2.7) shows that an external radiation field of amplitude

[8] A. Landesman (private communication from Professor A. Abragam).

[19] H. M. McConnell and J. Strathdee, J. Mol. Phys. **2**, 129 (1959).

[20] M. Adams, M. S. Blois, and R. H. Sands, J. Chem. Phys. **28**, 774 (1958).

[21] J. Wertz, Chem. Rev. **55**, 829 (1953).

[22] B. Venkataraman, B. G. Segal, and G. K. Fraenkel, J. Chem. Phys. **30**, 1006 (1959).

$2H_1$ produces an intensity of transition equal to that induced by the spin-rotational field $H(t)$ if

$$H_1 \cong H(t)[4\tau_c'/3g(\nu)]^{\frac{1}{2}} \cong 27[\tau_c'/g(\nu)]^{\frac{1}{2}}. \quad (3.15)$$

Substitution of the preceding numerical values for the benzene negative ion in Eqs. (3.5), (3.6), (3.8), (3.9), and (3.11) gives

$$K = 3.8\times10^{14}\tau_c(1+\omega^2\tau_c^2)^{-1}\ \text{sec}^{-1}$$

$$L = -0.8\times10^{14}\tau_c(1+\omega^2\tau_c^2)^{-1}\ \text{sec}^{-1}$$

$$M_0 = 4.2\times10^{14}\tau_c(1+\omega^2\tau_c^2)^{-1}\ \text{sec}^{-1}$$

$$M_{\omega 1\nu} = 2.0\times10^{4}\ \text{sec}^{-1}$$

$$M_H = 5\times10^{16}\tau_c'(1+\omega^2\tau_c'^2)^{-1}\ \text{sec}^{-1}. \quad (3.16)$$

For typical free radicals, the rotational correlation time τ_c is the time in which a molecule undergoes an appreciable change in orientation. It is undoubtedly greater than 10^{-11} sec, and values from 10^{-9} to 10^{-11} sec are not unreasonable. The correlation time τ_c' appropriate for the spin-rotational interaction may be thought of as the time that the rotational magnetic moment of a molecule maintains its orientation in space. In a liquid, any small collision will generally be sufficient to change the orientation of the magnetic moment, and thus τ_c' will be several orders of magnitude smaller than τ_c. As a result, the quantity M_H is probably not as important as the other terms in Eq. (3.16), although for a molecule in the gas phase, the interaction between the electron spin and the rotational motion is in general the largest term.

It is instructive to examine an energy-level diagram showing the different transitions effecting relaxation. In Fig. 1, the transitions are shown in terms of the parameters K, L, and M for a single electron interacting with a nucleus of spin $I=2$, and in Fig. 2 the transitions are shown for the interaction of a single electron with four equivalent nuclei of spin $I=\frac{1}{2}$. In the diagrams, each horizontal bar represents an energy level determined by m_s and m_J; those for $m_s=+\frac{1}{2}$ are in the top row, and the values of m_J increase from left to right.

Differences in the transitions from one level to another exist in both diagrams, but there is a much more marked variation among the levels in Fig. 2 than in Fig. 1. In other words, the intramolecular dipolar interactions exhibit a greater effect when several nuclei are present than when only a single nucleus interacts with the electron. The increase in these effects when several nuclei are present may be explained very simply. Since the transition probabilities W_{ij}' involve sums over degenerate states that are independent of the particular choice of degenerate functions, the nuclear spin states can be described by a coupled representation. In the case of four nuclei of spin $I=\frac{1}{2}$, the possible values of the total nuclear spin angular momentum $\mathbf{J}=\sum_i \mathbf{I}_i$ are $J=2$, 1^3, 0^2, where the exponent indicates the number

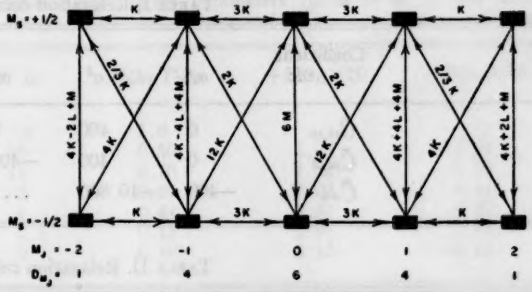

FIG. 2. Relaxation probabilities for spin system with $S=\frac{1}{2}$ and four equivalent nuclei with $I=\frac{1}{2}$. Energy levels, indicated by filled rectangles are labeled by M_s, M_J. The possible relaxations calculated from Eqs. (3.3) and (3.4) for extreme motional narrowing are shown by arrows. The degeneracies are indicated by D_{MJ}.

of states with this particular value of J. When all the nuclei are equivalent, the dipolar mechanism cannot connect states of different J, and therefore the cross-relaxation terms are just the superposition of the relaxations for the individual values of J. The pattern in Fig. 2, for example, is just the pattern that would be obtained by superimposing the cross relaxation from a single nucleus with spin $I=2$, three nuclei with spin $I=1$, and two nuclei with zero spin.

IV. SPIN-LATTICE RELAXATION TIME

The spin-lattice, or longitudinal, relaxation time T_1 was introduced by Bloch as a parameter to measure the presumed exponential decay of the component of the macroscopic magnetization parallel to the externally applied field.[12] This parameter was then calculated by Bloembergen *et al.*[10] from the transition probabilities causing relaxation in a two-level system. This spin-lattice relaxation time for a two-level system determines both the saturation behavior and the decay of the field-direction component of the magnetization. It also can be shown that there is an exponential decay of this component of the magnetization in such a system which is describable by a single relaxation time.[17] A multilevel equally spaced system such as a nuclear spin with $I>\frac{1}{2}$ also behaves in many respects like a two-level system. The decay of the field-direction component of the magnetization in complex systems of the type considered in the present discussion may not, however, be determined by a single relaxation time; and the saturation parameters Ω of Sec. II are, in general, not simply related to a parameter that can be identified with T_1.

Nevertheless, even in a complex system, there is a simple relation between T_1 as defined, for example, by Kubo and Tomita,[6] and the transition probabilities induced by relaxation. By assuming that the approach to equilibrium is governed by an exponential law, i.e., $\exp(-t/T_1)$, it is readily shown that

$$T_1^{-1} = \tfrac{1}{2}\hbar^2\Big(\sum_{jk} W_{jk}'\omega_{jk}^2 / \sum_j D_j E_j^2\Big), \quad (4.1)$$

TABLE I. Relaxation cofactors; one nucleus, spin $I=1$.

Coefficient of:	α_1^3	α_1^2	α_2^2	$\alpha_1\alpha_2$	α_1	α_2	α^0
$\bar{C}_{12,12}$	0	400	0	−400	6900	−3000	29 025
$\bar{C}_{34,34}$	0	400	−400	0	7800	0	38 025
$\bar{C}_{aa}$	−400	−10 800	...	...	−96 075	...	−280 800

TABLE II. Relaxation cofactors; two nuclei, spin $I=\frac{1}{2}$.

Coefficient of:	α_1^3	α_1^2	α_2^2	$\alpha_1\alpha_2$	α_1	α_2	α^0
$\bar{C}_{12,12}$	0	800	0	−800	10 800	−3000	29 025
$\bar{C}_{34,34}$	0	400	−400	0	7800	0	38 025
$\bar{C}_{aa}$	−800	−18 600	...	...	−134 100	...	−280 800

TABLE III. Relaxation cofactors; four nuclei, spin $I=\frac{1}{2}$.

Coefficient of:	α_1^5	α_1^4	α_2^4	$\alpha_1^3\alpha_2$	$\alpha_1^2\alpha_2^2$	$\alpha_1\alpha_2^3$	α_1^3	$\alpha_1^2\alpha_2$
$10^{-6}\,\bar{C}_{12,12}$	0	22.118	0	−44.237	−44.237	44.237	1459.8	−1526.2
$10^{-6}\,\bar{C}_{34,34}$	0	5.5296	0	−5.5296	−22.118	22.118	464.49	−389.84
$10^{-6}\,\bar{C}_{56,56}$	0	3.6864	14.7456	0	−18.432	0	331.78	0
$10^{-6}\,\bar{C}_{aa}$	−22.1184	−2156.5	...	...	...	...	−78469	...

Coefficient of:	$\alpha_1\alpha_2^2$	α_2^3	α_1^2	$\alpha_1\alpha_2$	α_2^2	α_1	α_2	α^0
$10^{-6}\,\bar{C}_{12,12}$	−862.62	331.78	32 497	−12348	−5225.5	296 359	−59 552	935 221
$10^{-6}\,\bar{C}_{34,34}$	−464.49	165.89	13 355	−8105.7	−2220.8	150 078	−41 197	550 169
$10^{-6}\,\bar{C}_{56,56}$	−630.37	0	10 596	0	−6353.5	140 901	0	664 877
$10^{-6}\,\bar{C}_{aa}$	...	...	−1 319 376	...	...	−1 026 105×10¹	...	−294 202×10²

where the summation extends over all spin energy levels [the degeneracy already having been included, see Eq. (2.12)], and where the origin of the energy has been taken at the center of gravity of the energy-level system.

Application of Eq. (4.1) to the transition probabilities given by Eqs. (3.3) and (3.4) is performed by summing over m_s and m_J. After some manipulation it can be shown that the T_1 appropriate for energy transfer to the lattice from a spin system consisting of an unpaired electron and n equivalent nuclei of spin I is

$$T_1^{-1}=(20/9)I(I+1)K+2M. \tag{4.2}$$

In obtaining Eq. (4.2), the system is assumed to be at high fields, and the only mechanisms assumed to cause relaxation are those considered in Sec. III.

In concluding this section, we would like to emphasize the distinction between T_1 and the saturation parameter Ω. For a complex system, T_1 may not have meaning unless it can be shown that the field-direction component of the magnetization decays exponentially with a single relaxation time, and it is possible that in different spectral regions the magnetization may decay at different rates. Furthermore, in steady-state magnetic resonance experiments, such as are typically performed for electron resonance at microwave frequencies, T_1 is not an experimental parameter, while the saturation parameters Ω are directly amenable to experimental determination. On the other hand, suppose a system consisting of an unpaired electron ($S=\frac{1}{2}$) interacting with a number of nuclei undergoes relaxation through mechanisms which are predominantly independent of the nuclear spin states. Such a system reduces effectively to a set of two-level systems, one for each value of m_J. Under these conditions, the only important transition probability is the term in M in Eq. (3.3), and from Eq. (4.2), $T_1^{-1}=2M$. Also, it can be readily seen from Eq. (2.27) that $D_\alpha\Omega_{\alpha\beta}=(2M)^{-1}$, and therefore $D_\alpha\Omega_{\alpha\beta}=T_1$. By substituting this value in Eq. (2.6) and using Eq. (2.7), one obtains

$$Z_{\alpha\beta}=[1+(\tfrac{1}{2})g_s^2\beta_s^2\hbar^{-2}H_1^2g_{\alpha\beta}T_1]^{-1}, \tag{4.3}$$

which is the usual expression for the saturation factor for a two-level system.[14]

V. RESULTS

In this section we give the results of the calculation of the saturation parameters Ω for spin systems consisting of an unpaired electron, $S=\frac{1}{2}$, interacting with three different collections of nuclei: (1) one nucleus with spin $I=1$; (2) two equivalent nuclei with spin $I=\frac{1}{2}$; and (3) four equivalent nuclei with spin $I=\frac{1}{2}$.

The transition probabilities are taken to be of the form given in Eqs. (3.3) and (3.4), so that the mechanisms of relaxation considered are confined to those discussed in Sec. III. We assume for simplicity that $\omega\tau_c \ll 1$ (extreme motional narrowing) even though for electron resonance experiments performed at 9000 Mc/sec this condition is not met unless $\tau_c < 10^{-11}$. When extreme narrowing does not occur, terms in the intramolecular dipolar interaction (K) involving transitions among nuclear levels which do not change the spin of the electron ($\Delta m_s=0$, $\Delta m_J=\pm 1$), and terms depending on translational relaxation such as M_{solv}, show a different dependence on τ_c than the other transition probabilities.

By using the assumption of extreme narrowing, three parameters, K, L, and M, determine the transition probabilities in Eqs. (3.3) and (3.4), and by forming ratios we may calculate the saturation factors for the various transitions as a function of two parameters. These parameters are taken to be

$$\alpha_1 = 6M/K$$
$$\alpha_2 = 6L/K. \qquad (5.1)$$

The cofactors occurring in Eq. (2.27) may now be expanded as polynomials in α_1 and α_2, and the coefficients of the various powers of $\alpha_1\alpha_2$ for the preceding spin systems are tabulated in Tables I to III. (In Tables I and II $\tilde{C}_{56,56}$ is obtained from $\tilde{C}_{12,12}$ by changing the sign of α_2. In Table III $\tilde{C}_{78,78}$ and $\tilde{C}_{9,10;9,10}$ are obtained from $\tilde{C}_{34,34}$ and $\tilde{C}_{12,12}$, respectively, by changing the sign of α_2.) A simple method exists for evaluating the cofactors using relaxation diagrams of the type shown in Figs. 1 and 2. This method will be described elsewhere.[23] In the Tables, energy levels have been labeled in order of decreasing values of m_J and odd numbers correspond to $m_s=+\frac{1}{2}$ and even numbers to $m_s=-\frac{1}{2}$. Thus $1\equiv(m_s=\frac{1}{2}, m_J=nI)$, $2\equiv(m_s=-\frac{1}{2}, m_J=nI)$, $3\equiv(m_s=\frac{1}{2}, m_J=nI-1)$, etc. By using Eq. (5.1), each of the cofactors is expressed in units of $(K/6)^p$ where p is the order of the cofactor.

TABLE IV. Saturation parameters (units of K^{-1}); one nucleus, spin $I=1$.

α_1	$D_1\Omega_{12}/D_5\Omega_{34}$	$+D_1\Omega_{12}\times 10$	$+D_5\Omega_{34}\times 10$
∞	1.0	...	...
20	0.92	1.01	1.09
10	0.89	1.52	1.72
5	0.85	2.04	2.45
1	0.79	2.81	3.57
0.5	0.77$_5$	2.95	3.80
0	0.76	3.10	4.06

TABLE V. Saturation parameters (units of K^{-1}); two nuclei, spin $I=\frac{1}{2}$.

α_1	$D_1\Omega_{12}/D_5\Omega_{34}$	$+D_1\Omega_{12}\times 10$	$+D_5\Omega_{34}\times 10$
∞	1.0	...	...
20	0.80	1.01	1.26
10	0.70	1.52	2.19
5	0.59	2.04	3.44
1	0.44	2.81	6.39
0.5	0.41	2.95	7.14
0	0.38	3.10	8.13

Limiting values (for H_1 large) of the ratios of peak heights for different components can be obtained [see Eq. (2.9)] by computing ratios of the $\Omega_{\alpha\beta}$, and since the $\tilde{C}_{\alpha\alpha}$ are independent of α [see Eq. (2.25)], ratios of $\Omega_{\alpha\beta}$ can be obtained from ratios of the $\tilde{C}_{\alpha\beta,\alpha\beta}$. For simplicity, therefore, the $\tilde{C}_{\alpha\alpha}$ required to obtain the absolute magnitude of the saturation are tabulated only for the case $\alpha_2=0$, corresponding to absence of the asymmetric feature of the saturation arising from the cross term between the intramolecular dipolar interaction and the g-tensor anisotropy.

The variation of the ratio of the saturation parameters for different hyperfine components is illustrated (for the case $\alpha_2=0$) by allowing α_1 to vary from 0 to ∞, and ratios of the factor $D_\alpha\Omega_{\alpha\beta}$ for the outer lines to the central line are tabulated for the preceding spin systems in Tables IV to VI.

The absolute magnitude of $D_\alpha\Omega_{\alpha\beta}$ is also given in Tables IV to VI in units of K^{-1}. Values of $D_\alpha\Omega_{\alpha\beta}$ in seconds are obtained by multiplying the numbers in the tables by K^{-1} where K is expressed in sec^{-1}.

The anisotropy of the spectrum depends on the magnitude and sign of α_2. To illustrate the type of anisotropy to be expected when saturation is taking place, we have arbitrarily set $\alpha_1=10$ and varied α_2 over the range 0 to 10 for the spin system (2) in the foregoing, i.e., $S=\frac{1}{2}$ and two equivalent nuclei with $I=\frac{1}{2}$. The results are shown in Table VII. Further values may be readily calculated from the results in Tables I to III.

In actual application of these results a spectrum that is symmetrical about its center is determined by values of Ω which depend on only one parameter. If this parameter is fixed by one ratio, it will be possible to make definite predictions about the other lines of the spectrum. If the spectrum shows a variation from low field to high field, there are still only two parameters, and it will again be possible to compare theory and experiment directly for any spectrum with more than three components. An evaluation of the parameters α_1 and α_2 from experiment would enable us to

[23] M. J. Stephen (to be published).

TABLE VI. Saturation parameters (units of K^{-1}); four nuclei, spin $I=\frac{1}{2}$.

α_1	$D_1\Omega_{12}/D_1\Omega_{56}$	$D_3\Omega_{34}/D_5\Omega_{56}$	$+D_1\Omega_{12}\times10$	$+D_3\Omega_{34}\times10$	$+D_5\Omega_{56}\times10$
∞	1.0	1.0	...	...	...
100	0.82	0.95	0.23	0.26_5	0.28
50	0.70_5	0.90_5	0.37	0.47	0.52
30	0.61	0.86	0.49	0.69	0.80
20	0.53	0.82	0.58	0.90	1.09
10	0.42	0.74	0.72	1.28	1.72
5	0.34	0.67	0.82	1.63	2.42
1	0.26	0.58	0.92	2.08_5	3.58
0.5	0.25	0.57	0.94	2.16	3.81
0	0.234	0.55	0.95	2.24	4.07

draw conclusions about the relative importance of the intramolecular dipolar relaxation, the g-tensor anisotropy relaxation, and those mechanisms which relax the electron without influencing the nuclear states.

When α_1 is large, there is no appreciable cross relaxation, and the system behaves as a number of two-level systems, one for each value of m_J. Replacing the notation $\alpha\beta$ for a transition with the notation m_J, it is easy to show that

$$D_{m_J}\Omega_{m_J}=(2M)^{-1}. \tag{5.3}$$

As mentioned in Sec. IV, in the special case that there is no cross relaxation, the spin-lattice relaxation time T_1 and the quantity $D_\alpha\Omega_{\alpha\beta}$ become equal.

When α_1 is large, and Eq. (5.3) holds, systems with $S=\frac{1}{2}$ and either (i) n equivalent nuclei of spin I, or (ii) one nucleus of spin nI, behave identically with respect to saturation. On the other hand, when α_1 is not large, corresponding to appreciable relaxation through the intramolecular dipolar interaction, there is no simple relaxation between the one-nucleus and the many-nuclei problems, and there is no simple relation between the $D_\alpha\Omega_{\alpha\beta}$ and the spin-lattice relaxation time.

TABLE VII. Anisotropy in saturation parameters; two nuclei, spin $I=\frac{1}{2}$ ($\alpha_1=10$).

α_2	$D_1\Omega_{12}/D_3\Omega_{34}$	$D_2\Omega_{56}/D_3\Omega_{34}$
10	0.46	1.41
5	0.55	0.93
1	0.66	0.73
0	0.70	0.70

The sign of the anisotropy introduced by the cross-term between the intramolecular and g tensor-induced relaxation is also of interest. If the sign of the term which governs this anisotropy, the parameter L of Eq. (3.18), is negative, as it is estimated to be for the benzene negative ion, components with negative values of m_J relax more rapidly than components with positive values of m_J. For the benzene negative ion, in which the hyperfine splitting arises from an indirect mechanism involving configuration interaction, McConnell has predicted that the isotropic proton hyperfine interaction constant A should be negative, and recent experimental results on malonic acid radicals trapped in malonic acid single crystals confirm this prediction.[24,25] As a result, high-field components correspond to positive values of m_J. The low-field components should therefore relax more rapidly than high-field components, and the high-field components should be narrower and should saturate more rapidly than the low-field components. For other free radicals, detailed examination of the g-tensor anisotropy and of the anisotropic dipolar interaction must be made to determine the sign of L, and other types of isotropic hyperfine interaction exist for which A is not necessarily negative.

VI. ACKNOWLEDGMENTS

We would like to acknowledge numerous helpful discussions of relaxation problems with Professor D. Kivelson and Professor N. Bloembergen.

[24] H. M. McConnell and D. B. Chesnut, J. Chem. Phys. **28**, 107 (1958).
[25] H. M. McConnell (private communication).

Electronic Interaction in the Free-Electron Network Model for Conjugated Systems. III. Spectra of Hydrocarbons Other Than Even Alternants

NORMAN S. HAM

Division of Chemical Physics, C.S.I.R.O. Chemical Research Laboratories, Melbourne, Australia

(Received December 7, 1959)

The effects on spectral calculations of including interaction between the ground and lower excited states are investigated by the free-electron model for some hydrocarbons in which such interaction should occur in principle, viz., phenanthrene, perinaphthenylium cation, and azulene. The resultant lowering of the ground state energy is less than 150 cm^{-1} when the ground and excited states have equal charge densities. For azulene, with unequal charge densities, the interaction is about 4000 cm^{-1}, and the agreement with experiment for the two lower singlet levels is considerably improved. The free-electron calculations for the nonalternant ions $C_5H_5^-$ and $C_7H_7^+$ are also reported.

RECENT semiempirical theories of the π-electronic spectra of even alternant hydrocarbons, with explicit inclusion of the effects of π-electron repulsion, have met with considerable quantitative success.[1-5] One of the reasons for this success is that for even alternants, the excited states have charge densities (uniform) equal to that of the ground state,[6] and this equality gives considerable self-consistency to the spectral calculations for these molecules. For odd alternants, and for even and odd nonalternants, the equality of charge densities may not hold and in this circumstance there results a larger interaction between the lower excited states and the ground state. It is the purpose of this note to examine quantitatively by the free-electron model[4,5] the effects of this type of interaction on spectral calculations for some representative molecules and ions, viz., phenanthrene (even alternant), the highly symmetric nonalternant ions $C_5H_5^-$ and $C_7H_7^+$, the perinaphthenylium cation $C_{13}H_9^+$ (odd alternant), and azulene, an even nonalternant.

I. PHENANTHRENE

Phenanthrene and the polyacenes are similar in being even alternants (with equal charge densities in the ground and excited states), but they differ in that the four lower excited states of the polyacenes (^1B_a, ^1B_b, ^1L_a, ^1L_b)[7] are not totally symmetric and cannot interact with the ground state, whereas in phenanthrene, two of these states (^1B_b, ^1L_b) are of the correct symmetry to interact with the ground state. For the B_b state the interaction almost cancels, but for the L_b state it lowers the ground state by 134 cm^{-1}. This interaction does nothing toward removing the 3200 cm^{-1} discrepancy between the calculated and observed ^1L_b level (see Fig. 1), but it suggests that in other less symmetrical even alternants, e.g., the polyacene isomers, the lower energy levels will be only very slightly affected by such interaction.[8]

II. IONS $C_5H_5^-$ AND $C_7H_7^+$

The high symmetry (D_{5h}, D_{7h}) of these nonalternant ions (iso-π-electronic with benzene) determines the orbitals and state functions and since these are already self-consistent, the excited states do not interact with the ground state. These ions have been treated by Longuet-Higgins and collaborators[9] using the Pariser-Parr LCAO method.[10]

The separations between the excited states are formally the same in the free-electron model as in the LCAO method.[11] The major difference between the two calculations lies in the equation used to obtain the orbital energies, which difference places the centers of gravity of the transitions differently.[12] For $C_7H_7^+$

[1] J. A. Pople, Trans. Faraday Soc. **49**, 1375 (1953).
[2] W. Moffitt, J. Chem. Phys. **22**, 320 (1954).
[3] R. Pariser, J. Chem. Phys. **24**, 250 (1956).
[4] N. S. Ham and K. Ruedenberg, J. Chem. Phys. **25**, 1 (1956); **29**, 237 (1958).
[5] N. S. Ham and K. Ruedenberg, J. Chem. Phys. **25**, 13 (1956).
[6] W. Moffitt, J. Chem. Phys. **22**, 1820 (1954); M. J. S. Dewar and H. C. Longuet-Higgins, Proc. Phys. Soc. (London) **A67**, 795 (1954); and footnotes 3–5.
[7] The state notation is that of J. R. Platt, J. Chem. Phys. **17**, 484 (1949) with the modifications discussed in Part II (footnote 5).
[8] This conclusion, for the FE method, is in keeping with Pariser's finding for the LCAO method that the ground states of the polyacenes were depressed by less than 0.05 ev (400 cm^{-1}) following the interaction of a large number of singly excited configurations formed with Hückel orbitals (see footnote 3).
[9] J. N. Murrell and H. C. Longuet-Higgins, J. Chem. Phys. **23**, 2347 (1955); H. C. Longuet-Higgins and K. L. McEwen, J. Chem. Phys. **26**, 719 (1957).
[10] R. Pariser and R. G. Parr, J. Chem. Phys. **21**, 767 (1953).
[11] The theoretical separations (s_i) in terms of the orbital energies ϵ_n and electron interaction function G_J are as follows:

$C_5H_5^-$: $s_0=\epsilon_c-\epsilon_b-0.2000G_1+0.3236G_2-0.1236G_3$
$s_1=0.4000G_1-0.2472G_2-0.6472G_3$
$s_3=\delta_3=0.4000G_1-0.6472G_2+0.2472G_3$
$s_2\equiv 0.$

$C_7H_7^+$: $s_0=\epsilon_c-\epsilon_b-0.1429G_1+0.2574G_2-0.1781G_3+0.0636G_4$
$s_1=0.2857G_1+0.3563G_2-0.1272G_3-0.5148G_4$
$s_3=\delta_3=0.2857G_1-0.5148G_2+0.3563G_3-0.1272G_4$
$s_2\equiv 0.$

For definition of symbols s_i, ϵ_n, and G_J, see Part I[4]. For the LCAO separations the G_J's are replaced by Coulomb integrals $(11\,|\,JJ)$ between the $2p\pi$ atomic orbitals.
[12] The FE formula of Part II[5] for the orbital excitation energies $\epsilon_c-\epsilon_b$ gives 55 700 cm^{-1} ($C_5H_5^-$) and 28 420 cm^{-1} ($C_7H_7^+$), whereas the LCAO formula of Pariser and Parr[10] gives the values 43 120 cm^{-1} and 32 630 cm^{-1}, respectively.

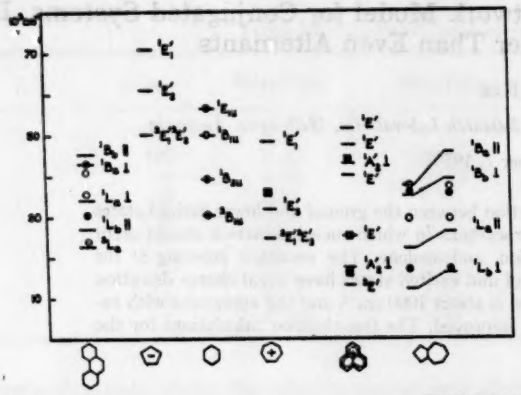

FIG. 1. Theoretical and experimental energy levels for phenanthrene, cyclopentadienyl anion, benzene, tropylium cation, perinaphthenylium cation, and azulene. Theoretical levels are indicated by lines and experimental levels for phenanthrene, benzene, and azulene by circles (a levels, hollow circles; b levels, solid circles), and for tropylium and perinaphthenylium cations by solid squares. The theoretical polarizations are indicated by: ||, parallel to long axis; ⊥, perpendicular to long axis, except for the perinaphthenylium cationwhere || and ⊥ are referred to one of the bonds to the central atom. For azulene, the left-hand column is obtained if the interaction between ^1B_a level and the ground state is neglected; the interaction is included for the right-hand column.

both methods agree about equally well with the single experimental point,[13] but the free-electron results for $C_5H_5^-$ are much higher than the LCAO ones. Unfortunately no experimental data for $C_6H_6^-$ seem to be available to check the predictions here.

III. PERINAPHTHENYLIUM CATION $C_{13}H_9^+$

This odd alternant ion (symmetry D_{3h}) does not have uniform charge density in its ground state[14]; in the lower excited states, some have the ground state charge distribution and some do not.

The orbitals of the perinaphthene nucleus can be related nodally to those of the cyclic polyene $C_{12}H_{12}$ (symmetry D_{12h}) and can be labeled as in Fig. 2. As to the orbital labeled r_2, it is not possible to classify it according to its number of nodes around the C_{12} perimeter: it is the orbital introduced by the atom in the center of the framework. Since the molecule is an odd alternant, it has one nonbonding orbital ($\sin 3\phi$).

The ground state of the ion has 12 π electrons assigned to the orbitals as shown in Fig. 2 and the lower excited states (symmetry E', A_1', A_2' in D_{3h}) result from the orbital excitations shown. The energies and other properties of the excited states are summarized in Table I. Three E' states and one A_2' state have charge distributions which are different from that of the ground state, but none of these states is of the correct symmetry to interact with the ground state. On the other hand, the two A_1' states, with ground state charge distributions, interact only very weakly with the ground state. With the effects of the charge of the ion thus minimized, the calculated spectrum might be expected to be free from serious quantitative error.

The reported spectrum consists of a strong band at 25 000 cm^{-1} ($\log \epsilon_{max}$ 4.67) and another band at 44 250 cm^{-1} ($\log \epsilon_{max}$ 4.51).[15] The lowest transition is calculated to lie at 25 300 cm^{-1} and two allowed and one forbidden transitions are calculated to occur between 40 000 and 47 500 cm^{-1}. The calculations also predict a forbidden transition at about 17 400 cm^{-1} and it seems likely that the cation has a weak band close to 16 000 cm^{-1}.[16] These results are summarized in Fig. 1.

The general agreement is extremely good but part of this must be attributed to the high symmetry of the perinaphthene nucleus. For less symmetrical molecules containing this nucleus, the free-electron calculations should be equally successful provided that their orbitals can be related to those of the perinaphthene nucleus itself and the excited states are formed from excitations corresponding to those used in Table I. In this way the reduced symmetry, with its attendant interaction between the ground state and excited states, will be minimized.

IV. AZULENE

For the molecules considered so far, the interaction of the ground state with the lower excited states has either been small (equal charge densities) or zero (symmetry forbidden). For the nonalternant azulene, which is polar in its ground state and has different nonuniform charge distributions in each of the four lower

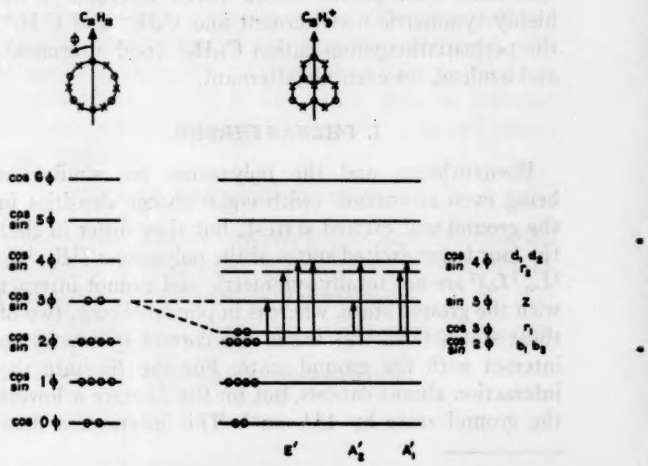

FIG. 2. Nodal properties of orbitals of the cyclic polyene $C_{12}H_{12}$ and the perinaphthene framework. For the perinaphthenylium cation, the orbital excitations, indicated by arrows, result in states belonging to the representations of D_{3h} as shown.

[13] W. E. von Doering and L. H. Knox, J. Am. Chem. Soc. **76**, 3203 (1954); M. J. S. Dewar and R. Pettit, J. Chem. Soc. **1956**, 2021.

[14] H. C. Longuet-Higgins, J. Chem. Phys. **18**, 265 (1950).

[15] R. Pettit, Chem. and Ind. **1956**, 1306.

[16] Dr. D. H. Reid reports (private communication) that 1,4,7-trimethyl perinaphthenylium perchlorate shows a weak band ($\log \epsilon_{max}$ 2.98) at 15 430 cm^{-1}. Indeno [2,1-a] perinaphthene in 77% (w/w) H_2SO_4 has a band at 16 130 cm^{-1} ($\log \epsilon_{max}$ 3.22) which most probably arises within the perinaphthene framework; see I. M. Aitken and D. H. Reid, J. Chem. Soc. **1956**, 3487.

TABLE I. Properties of lower excited states for the perinaphthenylium cation $C_{13}H_9^+$.

Two electron function ($b_i d_j$) corresponding to orbital excitation $b_i \rightarrow d_j$	Nodal classification of excitation	Behavior of state function on reflection at symmetry plane	Representation of state in D_{3h}	State charge density compared with that of ground state	Interaction with ground state	State energy before configuration interaction {singlet / triplet cm^{-1}}	Orbital transition moment (in units 1.4 A)	State energy after configuration interaction[a] {singlet / triplet cm^{-1}}	Oscillator strength of singlet transition
$(b_1 z)$ $(b_2 z)$	2→3	−1 1	E'	unequal	symmetry forbidden	28 640 13 770	0.8540	25 290 13 200	1.72
$(b_2 r_2)$ $(b_1 r_2)$	3→?	−1 1	E'	unequal	symmetry forbidden	39 750 32 860	0.5365	40 000 31 030	1.92
$(r_1 d_2)$ $(r_1 d_1)$	3→4	−1 1	E'	unequal	symmetry forbidden	48 450 41 570	0.5365	51 630 43 620	2.42
$2^{-\frac{1}{2}}(b_1 d_2 + b_2 d_1)$ $2^{-\frac{1}{2}}(b_1 d_1 - b_2 d_2)$	2→4	−1 1	E'	equal	symmetry forbidden	47 620 39 330	0.1585	47 530 39 690	0.66
$r_1 z$	3→3	−1	A_2'	unequal	symmetry forbidden	18 120 17 180	0.0000	17 420 16 500	
$2^{-\frac{1}{2}}(b_1 d_2 - b_2 d_1)$	2→4	−1	A_2'	equal	symmetry forbidden	42 340 42 340	0.0000	43 040 43 030	
$r_1 r_2$	3→?	1	A_1'	equal	25 cm^{-1}	48 860 31 110	0.0000		
$2^{-\frac{1}{2}}(b_1 d_1 + b_2 d_2)$	2→4	1	A_1'	equal	60 cm^{-1}	49 010 36 320	0.0000		
Ground state $(b_i b_i)$		1	A_1'			0		0	

[a] These energies are referred to the ground state represented by the single configuration $(b_i b_i)$.

excited states (^1B_a, ^1B_b, ^1L_a, ^1L_b)[7], the interaction is considerable. Here the interaction occurs with the a states: it almost cancels for the ^1L_a state but it reinforces for the ^1B_a state to lower the ground state by 4073 cm^{-1}.[17]

The new energy levels referred to the ground state are plotted in Fig. 1, together with the previous energy levels obtained without interaction.[5] The agreement with experiment for the two lower levels is greatly improved by including the interaction, but the two higher levels are pushed too high.

[17] This lowering is larger than that found by Pariser (2412 cm^{-1}) in his LCAO calculations on azulene, J. Chem. Phys. **25**, 1112 (1956).

V. CONCLUSIONS

From the foregoing results it seems that the criterion used previously to limit the amount of configuration interaction included in the free-electron calculations,[5] viz., to include only those configurations (a) which would be degenerate in the perimeter model (catacondensed hydrocarbons) or (b) which involve an increase of one in the number of angular nodes of the orbitals (pericondensed hydrocarbons), remains a good compromise between accuracy and ease of computation, even in cases where the model does not attain the same self-consistency that it does for even alternant hydrocarbons.

THE JOURNAL OF CHEMICAL PHYSICS VOLUME 32, NUMBER 5 MAY, 1960

Nuclear Magnetic Resonance Study of Polycrystalline NH_4ClO_4

JAMES A. IBERS

Shell Development Company, Emeryville, California

(Received December 30, 1959)

The second moments of the proton resonance absorption line in polycrystalline NH_4ClO_4 are found to be 1.27 ± 0.02 gauss^2 at 70°K and 1.18 ± 0.01 gauss^2 at 298°K; these results are interpreted in terms of reorientation of the ammonium ion about random or nearly random axes. Spin-lattice relaxation times for polycrystalline NH_4ClO_4 have been measured between 77° and 298°K by the progressive saturation method. These relaxation times are consistent with a barrier hindering reorientation of 2.0 ± 0.6 kcal.

RECENTLY Smith and Levy[1] reported that reasonable agreement could be obtained with their room-temperature neutron diffraction data for NH_4ClO_4 if a theoretical model were assumed in which the ammonium ion was freely rotating.[2] Here, as the result of a nuclear magnetic resonance study of polycrystalline NH_4ClO_4,[3] we present additional information on the motion of the ammonium ion in NH_4ClO_4.

The measured second moments[4] of the proton resonance absorption line in polycrystalline NH_4ClO_4 are 1.18 ± 0.01 gauss^2 at 298°K and 1.27 ± 0.02 gauss^2 at 70°K. (The limits of error are obtained from a comparison of two independently recorded and measured sets of data.) The corresponding line widths are 2.7 and 3.3 gauss, respectively. The proton second moment from a rigid NH_4ClO_4 lattice should be about 40 gauss^2; on the other hand, if the ammonium ions are reorienting about random axes at frequencies greater than about 10^5 cps (the inverse, proton spin-spin interaction time), then the contributions to the second moment of the intramolecular H–H interactions will average to zero,[5] and only the intermolecular H–H contributions will remain. We have followed Andrew and Eades[6] and have considered the calculation of such intermolecular contributions to the second moment under the assumptions (1) that the protons are smeared out over spheres of radius a (the N–H distance) separated by R(the N–N distance), and (2) that the angular terms in the second moment expression are unaffected by motion. We obtain, using the crystallographic data of Smith and Levy,[7] a second moment of 1.34 gauss^2. (The H–N and H–Cl interactions contribute less than 2% to this value.) We estimate that inclusion of the effects of motion on the angular terms will reduce this value by at most 40%, and probably by about 10 to 20%. An exact calculation of this reduction did not seem

[1] H. G. Smith and H. A. Levy, Abstract K-6, American Crystallographic Association Annual Meeting, Cornell University, Ithaca, New York (July, 1959).

[2] But see K. Venkatesan [Proc. Indian Acad. Sci. **46A**, 134 (1957)] for less convincing evidence that the hydrogen atoms occupy ordered positions at room temperature.

[3] G. Frederick Smith Chemical Company ammonium perchlorate, reagent grade, was used without further purification in this study.

[4] We measure the central portion of the resonance line, and calculate a second moment from this portion. The weak side bands, which are produced by motion and which when added to this central portion preserve the invariance of the total second moment to such motion [E. R. Andrew and R. A. Newing, Proc. Phys. Soc. (London) **72**, 959 (1958)], are not observed and measured here.

[5] H. S. Gutowsky, G. E. Pake, and R. Bersohn, J. Chem. Phys. **22**, 643 (1954).

[6] E. R. Andrew and R. G. Eades, Proc. Roy. Soc. (London) **A216**, 398 (1953).

[7] H. G. Smith and H. A. Levy (private communication).

warranted in view of our lack of knowledge of the N–H distance and of the effects of zero-point motion of the hydrogen atoms. Moreover, the reasonable agreement of the calculated and experimental values is taken as ample evidence that the motion of the ammonium ion is such as to average the intramolecular contributions to the second moment to zero, or nearly to zero. Whether such an average is truly zero, or whether there is a small residual contribution of the intramolecular terms (owing, for example, to departures from randomness of the reorientation axes) cannot be determined. The small difference between the measured values of the second moments at 298° and 70°K is significant, and is presumably the result of small contractions (perhaps 1%) of the crystal lattice as the temperature is lowered.

In an attempt to determine the barrier hindering reorientation, measurements of the spin-lattice relaxation time T_1 were made. The progressive saturation method was used. A previous calibration of the rf field meter on our apparatus allowed us to obtain the following absolute values of T_1: 77°K, 0.0059±0.0017 sec; 102°K, 0.083±0.027 sec; 112°K, 0.133±0.053 sec; 147°K, 0.143±0.062 sec; 298°K, 0.154±0.025 sec. We interpret these data in the following way. There are two relaxation processes: one is temperature insensitive; the other is temperature dependent and is the result of reorientation of the ammonium ion. The temperature insensitive process, with $T_1 = T_1$ (298°K), is perhaps the result of coupling of lattice vibrational modes with the quadrupole moments of the nitrogen or chlorine atoms, or perhaps with paramagnetic impurities. The T_1's of the reorientation process follow the high-temperature region ($\omega\tau_c \ll 1$) of the Kubo and Tomita[8] relation which connects T_1 with the assumed single correlation time τ_c. If we assume that the reorientation process is an activated one, then the foregoing data lead to a barrier of 2.0±0.6 kcal. With a suitable assumption concerning the minimum value of T_1 for the reorientation process the foregoing data lead to an entropy for the reorientation process of about 3 eu. This result is subject to large uncertainties because the minimum T_1 is not observed, and because of uncertainties in the data. Nevertheless, since we expect an entropy near zero (there is little possibility for cooperative motion among the widely separated ammonium groups), the derived value of the entropy at least is indicative of self-consistency in the interpretation of the data. This interpretation also leads us to expect broadening of the resonance line at between 45° and 55°K.

The measured barrier of 2.0±0.6 kcal may be compared with the following results for the ammonium halides[5]: NH_4Cl, 4.7; NH_4Br, 3.3; NH_4I, 2.9 kcal. In these compounds the ammonium ion is reorienting randomly at room temperature; the line-width transitions are at somewhat higher temperatures than that predicted for NH_4ClO_4. In the ammonium halides the ammonium ion can form four linear N—H—X bonds; in NH_4ClO_4, if the ammonium tetrahedron is to remain even approximately regular, more than two short, linear N—H—O bonds cannot be formed. It is possible then that the order of energies found in the ammonium halides and in NH_4ClO_4 represents a decreasing tendency to form hydrogen bonds.

Pendred and Richards[9] have studied the proton and fluorine resonances in NH_4BF_4 at 20°K. (NH_4BF_4 and NH_4ClO_4 are isostructural.) They find that at 20°K the ammonium ion is not reorienting about random axes, but rather about a single C_2 axis. Their interpretation is certainly not inconsistent with ours for NH_4ClO_4. It seems reasonable to expect that the frequency of interchange of axes of reorientation in NH_4ClO_4 will decrease with decreasing temperature, until there will arise, from the point of view of the resonance experiment, a principal reorientation process around a particular axis or axes.

I am grateful to C. H. Holm for help with the experimental work as well as for fruitful discussions of theory. I am also grateful to D. P. Stevenson for a helpful discussion.

[8] R. Kubo and K. Tomita, J. Phys. Soc. Japan 9, 888 (1954).

[9] D. Pendred and R. E. Richards, Trans. Faraday Soc. 51, 468 (1955).

Some Notes on Molecular Complexes between Iodine and Polynuclear Aromatic Hydrocarbons

MIHIR CHOWDHURY AND SADHAN BASU

Department of Chemistry, University College of Science, Calcutta 9, India

(Received October 22, 1959)

It has been observed that when iodine concentration is high in a mixture of iodine and polynuclear aromatic hydrocarbon in carbon tetrachloride, the spectral data may be interpreted on the assumption of 2:1 molecular complex formation between iodine and aromatic hydrocarbon. The equilibrium constants for 2:1 complexes were, however, found to be much higher than those of the corresponding 1:1 complexes and they were further found to be independent of the nature of the hydrocarbon. Interpretation of the experimental data based on contact charge transfer appears to be much more reasonable in the present case.

IN a previous communication[1] using high hydrocarbon but low iodine concentration in carbon tetrachloride solution, it has been shown by Bhattacharya and Basu that there is formation of 1:1 molecular complexes of charge transfer type in these systems. The equilibrium constant for complex forming reaction was found to increase with the lowering of the ionization potential of the aromatic hydrocarbons. If, however, the iodine concentration is increased much above that of the hydrocarbon concentration, two different types of interaction may take place. Since the hydrocarbons are undoubtedly π donors, the possibility of one hydrocarbon molecule complexing with two iodine molecules, in which iodine occupies two equivalent positions above and below the plane of the hydrocarbon molecule, exists. On the other hand, if there is any contact charge transfer effect present in iodine-hydrocarbon system, then this effect may become predominant at higher iodine concentration. In order to see if this could be settled experimentally, the spectrophotometric investigations were repeated with high iodine but low aromatic hydrocarbon concentration, the results of which are reported herein.

In order to estimate the equilibrium constant from the measurement of optical densities of mixtures of iodine and aromatic hydrocarbons, Benesi-Hildebrand type of relations[2] may be deduced for 1:1 and 2:1 complexes as follows. Let us assume that the equilibrium may be represented as

$$A+I_2 \rightleftharpoons AI_2 \qquad K_1=[AI_2]/[A][I_2] \qquad (1)$$

and

$$A+2I_2 \rightleftharpoons A(I_2)_2 \quad K_2=[A(I_2)_2]/[A][I_2]^2. \qquad (2)$$

In these equations A and I_2 represent aromatic hydrocarbon and iodine, respectively. The optical density of a solution containing the molecular species (1) and (2) is given by

$$\text{O.D.}=l\bar{\epsilon}[A]_0=l[\epsilon_0[A]+\epsilon_1[AI_2]+\epsilon_2[A(I_2)_2]\}, \qquad (3)$$

provided the absorption due to iodine is negligible at the wavelength where O.D. measurements are made. The ϵ_i's are the appropriate molar extinction coefficients. Combining (1)–(3) with the equation representing the conservation of hydrocarbon,

$$[A]_0=[A]\{1+K_1[I_2]+K_2[I_2]^2\}, \qquad (4)$$

one obtains

$$[I_2]/(\bar{\epsilon}-\epsilon_0)=\frac{1+K_1[I_2]+K_2[I_2]^2}{(\epsilon_1-\epsilon_0)K_1+(\epsilon_2-\epsilon_0)K_2[I_2]} \qquad (5)$$

if $[I_2]\gg[A]$. In these expressions $\bar{\epsilon}$ is the formal extinction coefficient of a solution containing an initial concentration of hydrocarbon $[A]_0$ moles/liter= O.D./$[A]_0$ l, ϵ_0=molar extinction coefficient of the hydrocarbon at the same wavelength and ϵ_1 and ϵ_2 are the molar extinction coefficients of 1:1 and 2:1 complex, respectively. If there is only 1:1 complex formation, then the relation (5) shows that a plot of $(\bar{\epsilon}-\epsilon_0)^{-1}$ against $1/[I_2]$ should be linear, from the slope and intercept of which the equilibrium constant K_1 and molar extinction coeficient ϵ_1 can be calculated. On the other hand, for 2:1 complex a plot of $(\bar{\epsilon}-\epsilon_0)^{-1}$ against $1/[I_2]^2$ should be linear, the slope and the intercept of which will similarly give K_2 and ϵ_2. It may be observed that for 1:1 complex the relation (5) reduces effectively to Benesi-Hildebrand equation. On the other hand, if the interaction be predominantly of contact type, then Benesi-Hildebrand plot will give a straight line of zero intercept.

EXPERIMENTAL

The method of purification of the hydrocarbons has been described in greater detail in the previous communication.[1] As iodine concentrations used in the present study were several hundred times those used in the previous communication, the solvent was carefully purified in order to eliminate the formation of I_3^- ion as much as possible. O.D. measurements were made in Beckman spectrophotometer model DU using 1-cm silica cells. In the range of 340 mμ to 430 mμ the absorption due to iodine was low compared to hydrocarbons and the complexes. The small amount of ab-

[1] Bhattacharya and Basu, Trans. Faraday Soc. **54**, 1286 (1958).
[2] Benesi and Hildebrand, J. Am. Chem. Soc. **71**, 2703 (1949).

TABLE I. Spectral data for I_2-hydrocarbon mixtures.

Hydrocarbons	Concentration of hydrocarbon (moles/liter)	$1/[I_2]$	$1/[I_2]^2$	$1/(\bar{\epsilon}-\epsilon_0)$	ϵ_2	$K_2\times10^{-2}$
Naphthalene	0.001806	17.1	292	0.00972	181	3.82
		19.6	384	0.01095		
$\lambda_{max}=363$ mμ		22.8	521	0.01369		
		27.4	751	0.01632		
Anthracene	0.001000	12.5	156	0.00579	227	4.10
		14.4	204	0.00651		
$\lambda_{max}=430$ mμ		16.7	279	0.00738		
		20.0	400	0.00816		
		25.0	625	0.01132		
Pyrene	0.001695	13.2	173	0.00663	200	4.00
		14.8	219	0.00764		
$\lambda_{max}=425$ mμ		18.9	359	0.00957		
		19.8	392	0.01004		
		26.3	694	0.01344		
Phenanthrene	0.002517	14.7	215	0.00769	175	5.43
		18.9	357	0.00952		
$\lambda_{max}=367$ mμ		22.1	487	0.01077		
		26.4	699	0.01281		
Chrysene	0.000639	14.1	200	0.00486	185	4.00
		16.2	262	0.00586		
$\lambda_{max}=388$ mμ		18.9	357	0.00667		
		22.6	511	0.00779		
Stilbene	0.001097	14.7	215	0.00599	238	4.70
		18.9	357	0.00738		
$\lambda_{max}=372$ mμ		22.1	488	0.00835		
		26.4	699	0.01027		

sorption due to iodine was eliminated by balancing the mixture against a solution of iodine having the same concentration as the mixture.

RESULTS

The first step in the execution of the proposed scheme of work was to locate the characteristic absorption band of the complex for each hydrocarbon. It was observed that when the iodine concentration was high and the hydrocarbon concentration was a tenth (or less) of the iodine concentration, the characteristic absorption maximum came out at about the same position as that previously reported with high hydrocarbon and low iodine concentration. The characteristic λ_{max} are recorded in the Table I. The O.D. values of a number of mixtures of constant but low hydrocarbon and different but high iodine concentrations were measured at the characteristic λ_{max}. The relevant data are summarized in Table I and $1/(\bar{\epsilon}-\epsilon_0)$ vs $1/[I_2]$ and $1/[I_2]^2$ plots are given in Figs. 1 and 2.

DISCUSSION

It may be observed from the Figs. 1 and 2 that a plot of $(\bar{\epsilon}-\epsilon_0)^{-1}$ against $1/[I_2]$ as well as against $1/[I_2]^2$ is linear, but the first plot gives a straight line having zero intercept, in almost all cases, on the $(\bar{\epsilon}-\epsilon_0)^{-1}$ axis, which is a physically impossible result on the basis of complex formation—stable or otherwise. The equilibrium (1) is therefore of negligible im, portance in these systems. The second plot, however-gives a straight line with a positive slope and a positive intercept, from which the equilibrium constant for 2:1 complex formation was calculated by the relation (5) and is listed in the Table I. It appears that the equilibrium constant is independent of the nature of the hydrocarbon and is practically constant. Further the absolute value of the equilibrium constant is much larger for 2:1 than for 1:1 molecular complexes.

We are thus faced with a number of problems. First, why does the characteristic absorption band for 2:1 complex appears at about the same position as that of the 1:1 complex: Secondly, why is the equilibrium constant for 2:1 complex so much larger than that for 1:1 complex, and why is it independent of the nature of the hydrocarbon?

No satisfactory answer can be given to any of these questions, which makes the very existence of 2:1 molecular complexes in these systems rather doubtful. The fact that $(\bar{\epsilon}-\epsilon_0)^{-1}$ is linear with respect to $1/[I_2]$ and $1/[I_2]^2$, suggests that the system probably is concentration-dependent in a more complicated way, and the two types of equilibrium cannot be distinguished, with the experimental data in the concentration range over which the measurement was extended.

If, however, we assume that the charge transfer is of a contact type, then the linear $(\bar{\epsilon}-\epsilon_0)^{-1}$ vs $1/[I_2]$ plot with zero intercept is understandable from the con-

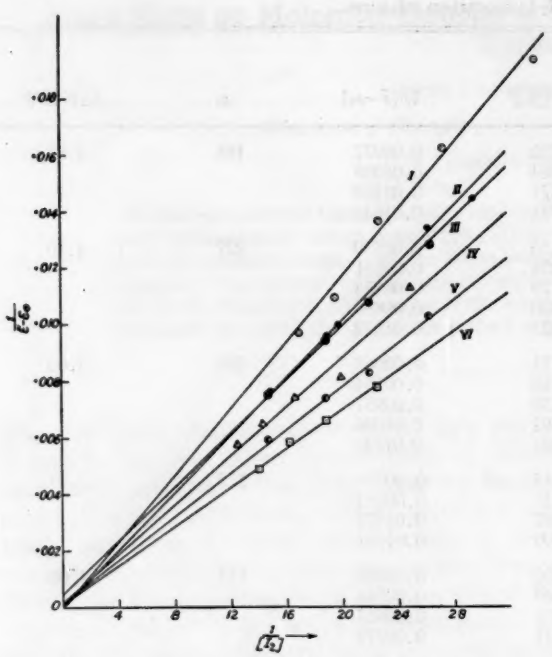

FIG. 1. Plot for 1:1 complexes. Curve I, naphthalene; II, pyrene; III, phenanthrene; IV, anthracene; V, stilbene; VI, chrysene.

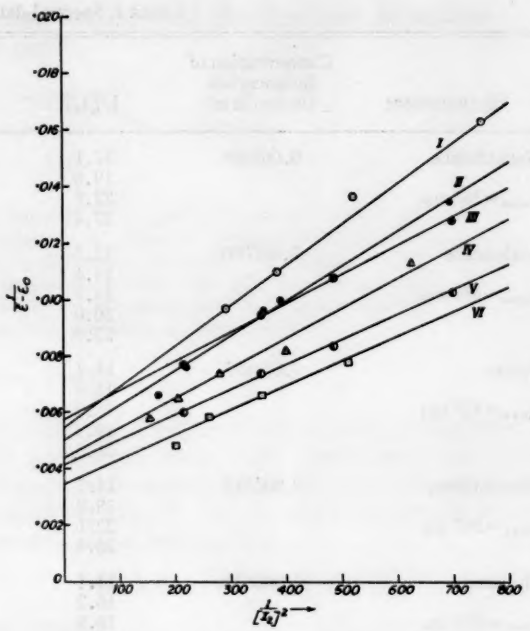

FIG. 2. Plot for 2:1 complex formation. Curve I, naphthalene, II, pyrene; III, phenanthrene; IV, anthracene; V, stilbene; VI, chrysene.

sideration of Orgel and Mulliken's analysis.[3] We may suggest that in hydrocarbons-I_2 systems the charge transfer is due both to 1:1 complex formation and to molecular contact. At low iodine concentration the absorption due to 1:1 complex is more important, while at high iodine concentration, as each hydrocarbon molecule makes many more contacts with iodine, the contact charge transfer becomes predominant.

Thanks are due to Council of Scientific and Industrial Research, India, for a Junior Research Fellowship to one of us (M.C.).

[3] Orgel and Mulliken, J. Am. Chem. Soc. **79**, 4839 (1957).

Potential Energy Curves for Lithium Hydride*

ROBERT J. FALLON, JOSEPH T. VANDERSLICE, AND EDWARD A. MASON

Institute for Molecular Physics, University of Maryland, College Park, Maryland

(Received November 9, 1959)

Potential energy curves for the $X\,^1\Sigma^+$, $A\,^1\Sigma^+$, and $B\,^1\Pi$ states of LiH have been calculated by the Rydberg-Klein-Rees method. The results are in agreement with curves previously obtained by Crawford and Jorgensen and by Rosenbaum using different methods. As a check, the somewhat peculiar curve for the $A\,^1\Sigma^+$ state has also been calculated for LiD, and agrees with the LiH curve to about one percent. The curves obtained theoretically by Karo and Olson for the $X\,^1\Sigma^+$ and $A\,^1\Sigma^+$ states are only in fair agreement with the experimental results.

INTRODUCTION

RECENTLY, there has been a great deal of interest in calculating potential energy curves for the ground and excited states of simple systems over a large range of internuclear distances. Since LiH is a relatively simple molecule and has been the subject of many theoretical calculations,[1] it would be interesting to have experimental potential curves for this system with which to compare those calculated by standard quantum-mechanical procedures. The Rydberg-Klein-Rees (RKR) method[2–5] affords a simple and reliable procedure for obtaining potential curves directly from spectroscopic data. We have applied this method to the $X\,^1\Sigma^+$, $A\,^1\Sigma^+$, and $B\,^1\Pi$ states of LiH and the $A\,^1\Sigma^+$ state of LiD. In the case of the $A\,^1\Sigma^+$ states, the vibrational energy levels vary in a peculiar manner with v, the vibrational quantum number, so that the original analytical formulation of Rees[4,5] has to be modified.

The results obtained from the RKR procedures can be compared with the results obtained by Rosenbaum[6] for the $A\,^1\Sigma^+$ state using the older graphical procedures of Rydberg[2] and Klein.[3] The results can also be compared with potential curves given by Crawford and Jorgensen[7] for the $X\,^1\Sigma^+$ and $A\,^1\Sigma^+$ states. These were were obtained by a Dunham[8] procedure and hence should be reliable near the minimum. However, the $A\,^1\Sigma^+$ state is somewhat peculiar, and the results obtained by Crawford and Jorgensen for LiH and LiD agree at best only to about four percent. The potential curve for the $A\,^1\Sigma^+$ state of LiD was therefore calculated by the RKR method as a check. Finally, the results can be compared with the work of Karo and Olson[1a,b] who have made extensive quantum-mechanical calculations on the LiH molecule and have obtained potential curves for the $X\,^1\Sigma^+$ and $A\,^1\Sigma^+$ states.

RYDBERG-KLEIN-REES METHOD

The RKR method is a semiclassical procedure for obtaining the classical turning points, $r_{\max}$ and $r_{\min}$, of the vibrational motion. These turning points are given in terms of functions f and g as follows:

$$r_{\max}=[(f/g)+f^2]^{\frac{1}{2}}+f,$$
$$r_{\min}=[(f/g)+f^2]^{\frac{1}{2}}-f. \quad (1)$$

The functions f and g, in turn, are given in terms of an auxiliary function S, defined by

$$S(U,\kappa)=(2\pi^2\mu)^{-\frac{1}{2}}\int_0^{I'}[U-E(I,\kappa)]^{\frac{1}{2}}dI \quad (2)$$

where U is the constant total energy, μ is the reduced mass, $I=h(v+\frac{1}{2})$, $\kappa=(8\pi^2\mu/h^2)^{-1}J(J+1)$, and $E(I,\kappa)$ is the vibrational-rotational energy expressed in terms of the vibrational and rotational quantum numbers v and J. The upper limit I' of the integral is the value of I for which $E(I,\kappa)=U$. The expressions for f and g are then

$$f=(\partial S/\partial U)_\kappa, \qquad g=-(\partial S/\partial\kappa)_U. \quad (3)$$

Rees[4] has pointed out that an analytical formulation of the method can be given if $E(I,\kappa)$ can be expressed as a quadratic in I,

$$E(I,\kappa)=\omega(v+\tfrac{1}{2})-\omega x(v+\tfrac{1}{2})^2-\alpha(v+\tfrac{1}{2})J(J+1)$$
$$+BJ(J+1)+DJ^2(J+1)^2+\cdots, \quad (4)$$

where ω, ωx, α, B, D,$\cdots$ are constants. In this case, the expressions for f and g become

$$f=(8\pi^2\mu)^{-\frac{1}{2}}\int_0^{I'}[U-E(I,\kappa)]^{-\frac{1}{2}}dI, \quad (5)$$

$$g=(8\pi^2\mu/h^4)^{\frac{1}{2}}[B+2D\kappa(8\pi^2\mu/h^2)]\int_0^{I'}[U-E(I,\kappa)]^{-\frac{1}{2}}dI$$
$$-\alpha(8\pi^2\mu/h^6)^{\frac{1}{2}}\int_0^{I'}[U-E(I,\kappa)]^{-\frac{1}{2}}IdI. \quad (6)$$

* This research was supported in part by the National Aeronautics and Space Administration.

[1] (a) A. M. Karo and A. R. Olson, J. Chem. Phys. **30**, 1232 (1959); (b) A. M. Karo, J. Chem. Phys. **30**, 1241 (1959); (c) O. Platas and F. A. Matsen, J. Chem. Phys. **29**, 965 (1958); (d) references to earlier work as contained in references 1(a)–(c).

[2] R. Rydberg, Z. Physik **73**, 376 (1931); **80**, 514 (1933).

[3] O. Klein, Z. Physik **76**, 226 (1932).

[4] A. L. G. Rees, Proc. Phys. Soc. (London) **59**, 998 (1947).

[5] Vanderslice, Mason, Maisch, and Lippincott, J. Mol. Spectroscopy **3**, 17 (1959).

[6] E. J. Rosenbaum, J. Chem. Phys. **6**, 16 (1938).

[7] F. H. Crawford and T. Jorgensen, Phys. Rev. **49**, 745 (1936).

[8] J. L. Dunham, Phys. Rev. **41**, 721 (1932).

TABLE I. Potential energy of the $X\ ^1\Sigma^+$ state of LiH.

v	$V(\text{cm}^{-1})$	r_{max} (A)	r_{min} (A)	V (ev)
0	698	1.779	1.447	0.0864
1	2058	1.938	1.354	0.2549
2	3376	2.061	1.297	0.4179
3	4643	2.173	1.255	0.5754

These integrals are readily evaluated[4] to give simple expressions for f and g. The method then becomes rapid and accurate, and has been applied to a number of cases. The details of the procedure have been given in previous papers.[4,5] We have applied the method straightforwardly to the $X\ ^1\Sigma^+$ and $B\ ^1\Pi$ states of LiH, and the results are given in Tables I and II. The data used were obtained from the work of Crawford and Jorgensen[9] and of Velasco.[10]

In all cases considered so far, the constant ωx in Eq. (4) has been positive. For the $A\ ^1\Sigma^+$ states of LiH and LiD, however, ωx is negative and the resulting integrations of Eqs. (5) and (6) carried out by Rees have to be performed differently. For ωx negative the expressions for f and g are readily found for the rotationless ($J=0$) state to be:

$$f=[8\pi^2\mu c(-\omega x)/h]^{-\frac{1}{2}}\{(\pi/2) - \arcsin[1+4U(-\omega x)\omega^{-2}]^{-\frac{1}{2}}\}, \quad (7)$$

$$g=(8\pi^2\mu c/h)^{\frac{1}{2}}(-\omega x)^{-\frac{1}{2}}[B+\tfrac{1}{2}\alpha\omega/(-\omega x)]\{(\pi/2) - \arcsin[1+4U(-\omega x)\omega^{-2}]^{-\frac{1}{2}}\} - (8\pi^2\mu c/h)^{\frac{1}{2}}[\alpha U^{\frac{1}{2}}/(-\omega x)], \quad (8)$$

where c is the velocity of light, so that f is in cm and g, U, ω, ωx, α, and B are in cm^{-1}. Usually $E(I,\ \kappa)$ cannot be represented over the whole experimental range by a quadratic, but it can be represented by a quadratic over different regions, so that the entire range can be covered by a series of quadratics. In such a case, the method is easily extended[4,5] to give the following expressions for f and g:

$$f=(8\pi^2\mu c/h)^{-\frac{1}{2}}\sum_{i=1}^{n}(-\omega x)_i^{-\frac{1}{2}}Y_i, \quad (9)$$

$$g=(8\pi^2\mu c/h)^{\frac{1}{2}}\sum_{i=1}^{n}\{(-\omega x)_i^{-\frac{1}{2}}[B_i+\tfrac{1}{2}\alpha_i\omega_i(-\omega x)_i^{-1}]Y_i - \alpha_i(-\omega x)_i^{-1}[U_i^{\frac{1}{2}}-U_{i-1}^{\frac{1}{2}}]\}, \quad (10)$$

TABLE II. Potential energy of the $B\ ^1\Pi$ state of LiH.

v	$V(\text{cm}^{-1})$	V(ev)	r_{max} (A)	r_{min} (A)	T_e+V(ev)[a]
0	101	0.0125	2.998	2.076	4.1794
1	231.7	0.0287	4.105	2.034	4.1956

[a] T_e is the energy difference between the bottom of the potential curve for the state in question and the bottom of the curve for the $X\ ^1\Sigma^+$ state.

[9] F. H. Crawford and T. Jorgensen, Phys. Rev. **47**, 932 (1935).
[10] R. Velasco, Can. J. Phys. **35**, 1204 (1957).

TABLE III. Potential energy of the $A\ ^1\Sigma^+$ state of LiH.

v	$V(\text{cm}^{-1})$	V(ev)	r_{max} (A)	r_{min} (A)	T_e+V(ev)
0	131	0.0162	3.005	2.240	3.3021
1	412.0	0.0511	3.290	2.028	3.3380
2	724.9	0.0899	3.483	1.908	3.3768
3	1061	0.1315	3.642	1.822	3.4184
4	1413	0.1752	3.787	1.754	3.4621
5	1779	0.2206	3.909	1.699	3.5075
6	2155	0.2671	4.031	1.651	3.5540
7	2538	0.3146	4.148	1.611	3.6015
8	2925	0.3626	4.262	1.575	3.6495
9	3316	0.4109	4.375	1.543	3.6978
10	3707	0.4593	4.485	1.512	3.7462
11	4098	0.5080	4.598	1.486	3.7949
12	4487	0.5563	4.711	1.462	3.8432
13	4873	0.6041	4.827	1.440	3.8910

where

$$Y_i=\arcsin[1+4U_{i-1}(-\omega x)_i\omega_i^{-2}]^{-\frac{1}{2}} - \arcsin[1+4U_i(-\omega x)_i\omega_i^{-2}]^{-\frac{1}{2}}.$$

In Eqs. (9) and (10), the index i runs over all the vibrational levels. The values of r_{max} and r_{min} as a function of U for the $A\ ^1\Sigma^+$ state of LiH and LiD were calculated from Eqs. (9) and (10) in the regions where ωx is negative, and from the previously derived[5] expressions in the regions where ωx is positive. The results are given in Tables III and IV. The data of Crawford and Jorgensen[9,11] were used.

DISCUSSION

The potential curves calculated by the RKR method for the $X\ ^1\Sigma^+$, $A\ ^1\Sigma^+$, and $B\ ^1\Pi$ states of LiH are shown as solid lines in Fig. 1. The $A\ ^1\Sigma^+$ states of LiH and LiD agree to about one percent, which is a good check on the accuracy of the RKR method as well as on the consistency of the data used. The other states of LiD are in obvious agreement with those of LiH, and have

TABLE IV. Potential energy of the $A\ ^1\Sigma^+$ state of LiD.

v	$V(\text{cm}^{-1})$	V(ev)	r_{max} (A)	r_{min} (A)	T_e+V(ev)
0	94.6	0.0117	2.941	2.276	3.2986
1	300.6	0.0373	3.195	2.086	3.3242
2	525.2	0.0651	3.364	1.975	3.3520
3	765.2	0.0949	3.500	1.894	3.3818
4	1017	0.1261	3.618	1.830	3.4130
5	1279	0.1586	3.725	1.776	3.4455
6	1550	0.1921	3.824	1.731	3.4790
7	1826	0.2264	3.919	1.691	3.5133
8	2108	0.2614	4.009	1.656	3.5483
9	2394	0.2969	4.097	1.625	3.5838
10	2684	0.3327	4.184	1.597	3.6196
11	2975	0.3689	4.268	1.571	3.6558
12	3268	0.4052	4.354	1.548	3.6921
13	3562	0.4416	4.427	1.514	3.7285
14	3856	0.4781	4.509	1.493	3.7650
15	4149	0.5144	4.595	1.474	3.8013
16	4442	0.5506	4.680	1.456	3.8375
17	4732	0.5867	4.767	1.440	3.8736

[11] F. H. Crawford and T. Jorgensen, Phys. Rev. **47**, 358 (1935).

not been explicitly calculated. The circles are the results obtained by Rosenbaum[6] for the $A\ ^1\Sigma^+$ state of LiH using the graphical procedures of Rydberg[2] and Klein.[3] The agreement with our results is within the error inherent in the graphical method, which is about five percent. The potentials for the $X\ ^1\Sigma^+$ and $A\ ^1\Sigma^+$ states were also compared around the minimum with the potentials obtained by Crawford and Jorgensen[7] using the Dunham[8] method. The agreement is well within the expected uncertainty of the two methods for the $X\ ^1\Sigma^+$ state. The differences appear to be a few parts in the last figures for r_{max} and r_{min} in Table I. This corresponds to energy differences of less than two percent. In the case of the $A\ ^1\Sigma^+$ states for LiH and LiD, the agreement of the Dunham potentials with the RKR results is as good as the agreement between the two Dunham potentials.

The dashed lines in Fig. 1 are the curves calculated by Karo and Olson[1a,b] for the $X\ ^1\Sigma^+$ and $A\ ^1\Sigma^+$ states of LiH using valence-bond and molecular-orbital methods which included configuration interaction. It is disappointing that the results are not in better agreement with the experimental curves. The probable reason for this is that Karo and Olson did not include enough configuration interaction in their treatment. It was originally hoped that a correction for this lack of enough configuration interaction (or electron correlation) could be made empirically and would be nearly independent of internuclear distance. Thus a correction might be applied to Karo and Olson's calculated values which would make the agreement with the experimental curves good over the whole range of internuclear distance.[12] That this is not the case can be seen from Fig. 1, where the shapes of the $A\ ^1\Sigma^+$ curves obtained by Karo and Olson and by us are different. It may well be that a more elaborate treatment, including a larger amount of electron correlation, would show a relatively

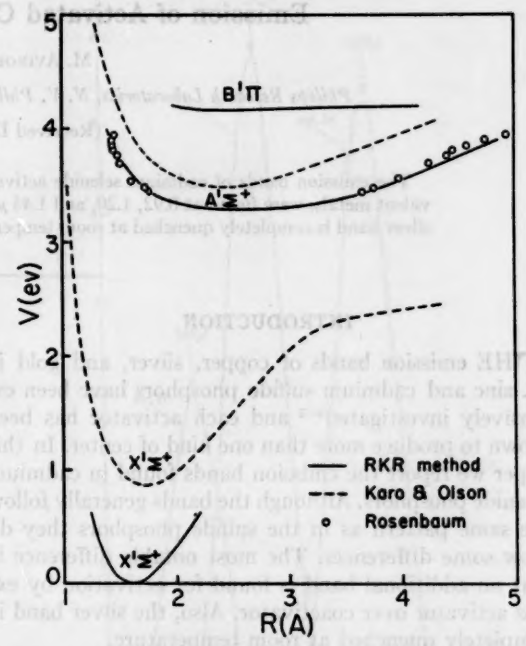

FIG. 1. Potential energy curves for the $X\ ^1\Sigma^+$, $A\ ^1\Sigma^+$, and $B\ ^1\Pi$ states of LiH. The solid curves are the RKR results. The circles are the values obtained by Rosenbaum. The dashed lines are the curves calculated by Karo and Olson.

constant difference with respect to the true energy.[13] It appears, therefore, that still further effort must go into the *ab initio* calculations of potential curves for simple systems, such as LiH, before one can hope to obtain reliable potential curves for more complicated systems such as N_2, O_2, and NO.

Finally, it might be mentioned that the slope of the attractive portion of the $A\ ^1\Sigma^+$ state is not as large as first proposed by Mulliken on the basis that this state is largely ionic in character.[14] This point has been previously noted by Karo.[15]

[12] Professor Sahni (private communication) had previously found this to be the case in his calculations on the $X\ ^1\Sigma_g^+$ ground state of N_2. Professor Matsen (private communication) has also informed us that he has successfully applied such a procedure to the ground state of HeH^+.

[13] We are grateful to the referee for pointing this out.

[14] R. S. Mulliken, Phys. Rev. **50**, 1017, 1028 (1936).

[15] A. M. Karo (private communication).

Emission of Activated Cadmium Selenide Phosphors

M. AVINOR* AND G. MEIJER

Philips Research Laboratories, N. V. Philips Gloeilampenfabrieken, Eindhoven, Netherlands

(Received December 14, 1959)

The emission bands of cadmium selenide activated by silver, copper, and gold, and coactivated by trivalent metals, were found at 0.92, 1.20, and 1.45 μ, respectively, at the temperature of liquid nitrogen. The silver band is completely quenched at room temperature. A near edge emission of CdSe was found at 0.72 μ.

INTRODUCTION

THE emission bands of copper, silver, and gold in zinc and cadmium sulfide phosphors have been extensively investigated[1–5] and each activator has been shown to produce more than one kind of center. In this paper we report the emission bands found in cadmium selenide phosphors. Although the bands generally follow the same pattern as in the sulfide phosphors they do show some differences. The most notable difference is that no additional band is found for activation by excess activator over coactivator. Also, the silver band is completely quenched at room temperature.

EXPERIMENTAL

The starting material was CdSe prepared by hydrazine reduction of cadmium selenite (Merck electronic grade CdSe) and spectrographic check showed the presence of traces of both silver and copper. The activators and coactivators were added as a solution of the sulfate or nitrate, except gold, which was added as a solution of the chloride. The powders were dried at 120°C and fired for 1 hr at 1000°C in an atmosphere of hydrogen and hydrogen selenide. This gas mixture was prepared by passing hydrogen over hot selenium (500°C). The powders were then ground and refired under the same conditions for another hour. The spectra were measured by a Perkin-Elmer 12C monochromator equipped with a quartz prism and a thermocouple detector. The light beam entering the monochromator was chopped and the signal was amplified, rectified synchronously, and fed into a chart recorder. Excitation was by radiation of a high-pressure mercury lamp filtered through a copper sulfate solution contained in a quartz cell. This filter stopped all radiation of wavelengths longer than the yellow mercury lines. Corrections were applied for the dispersion of the prism to obtain equal energy spectra. All the spectra are drawn to the same scale and give a true relative measure of the emission intensities.

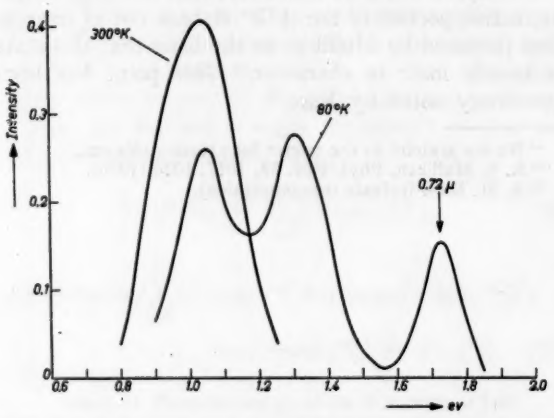

FIG. 1. Emission of CdSe starting material after firing in H_2+H_2Se.

RESULTS

Because the starting material was not very pure the bands of both copper and silver appeared in the fired undoped powder (Fig. 1) and the near edge emission at 0.72 μ was rather weak. When only a coactivator is added the intensity of the impurity bands grows (Fig. 2) and by comparing it to the intensity of the bands when a known amount of activator is added an estimate of the residual impurities can be made. Such an estimate is very rough because the intensity does not grow linearly with concentration, but we can see that the concentration of both copper and silver in the starting material is of the order of 10^{-5} atom/mole. By adding an activator concentration of 2.10^{-4} atom/mole the intensity of the undesired impurity band becomes rather low and the skirts of the curves can easily be corrected to obtain the pure activator bands. The results are shown in Figs. 3 and 4. We see that the silver band appears only at low temperatures. The gold band shifts a little to longer wavelengths on cooling in the same way as it does in CdS (Fig. 7). The same emissions appear when gallium or aluminum are used as coactivators and the emission intensities vary by less than a factor of two. The highest intensity is obtained with aluminum. When we used an excess of activator (5.10^{-4} atom/mole) over coactivator (2.10^{-4} atom/mole) no new emission band appeared with silver activation. In the case of copper the conclusion is less definite because of interference from the silver band,

* On leave of absence from the Scientific Department, Ministry of Defence, Israel.

[1] S. Rothschild, Trans. Faraday Soc. **42**, 635 (1946).

[2] H. W. Leverenz, *An Introduction to the Luminescence of Solids* (John Wiley & Sons, Inc., New York, 1950), pp. 196–211.

[3] F. A. Kröger and J. Dikhoff, Physica **16**, 297 (1950).

[4] E. Grillot and P. Guintini, Compt. rend. **239**, 418 (1954).

[5] W. van Gool, Philips Research Repts. **13**, 157 (1958).

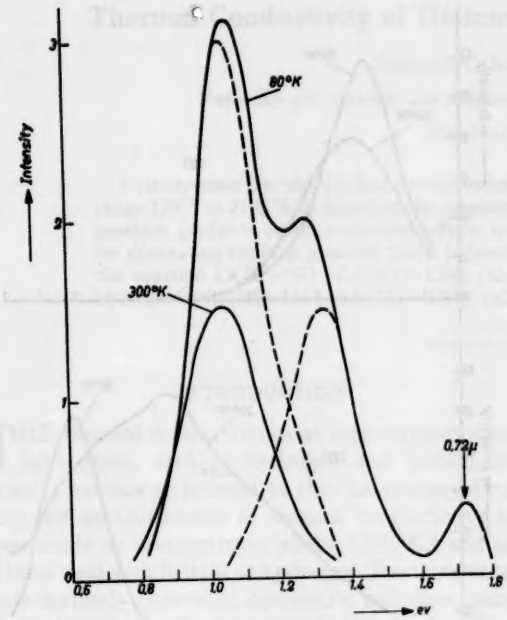

FIG. 2. Emission of CdSe starting material doped with indium (2.10^{-4} atom/mole).

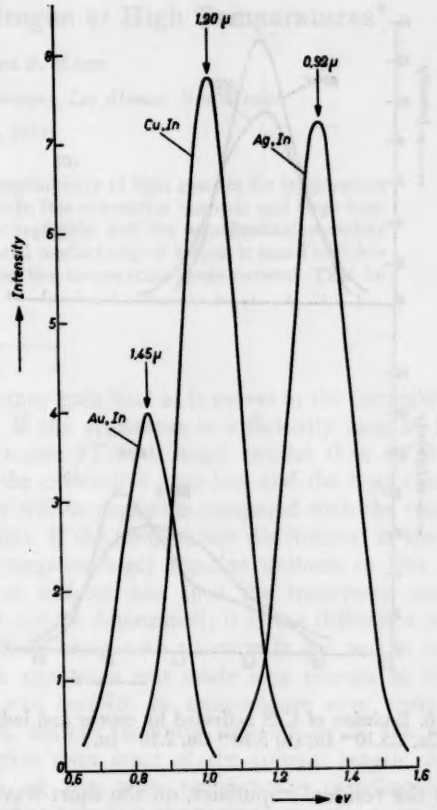

FIG. 4. Emission bands of CdSe activated by equal amounts of activator and coactivator (2.10^{-4} atom/mole) at the temperature of liquid nitrogen.

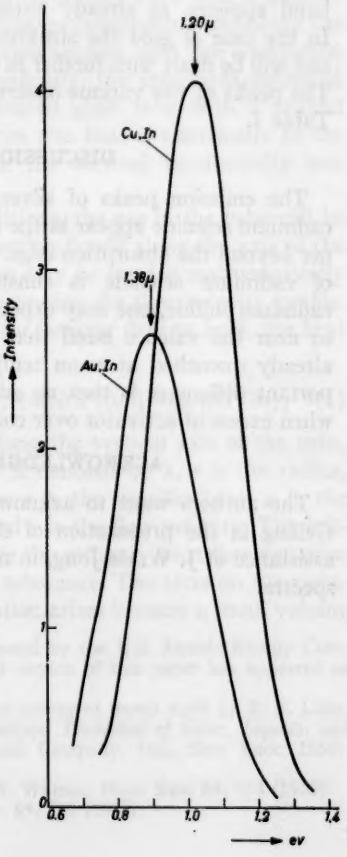

FIG. 3. Emission bands of CdSe activated by equal amounts of activator and coactivator (2.10^{-4} atom/mole) at room temperature.

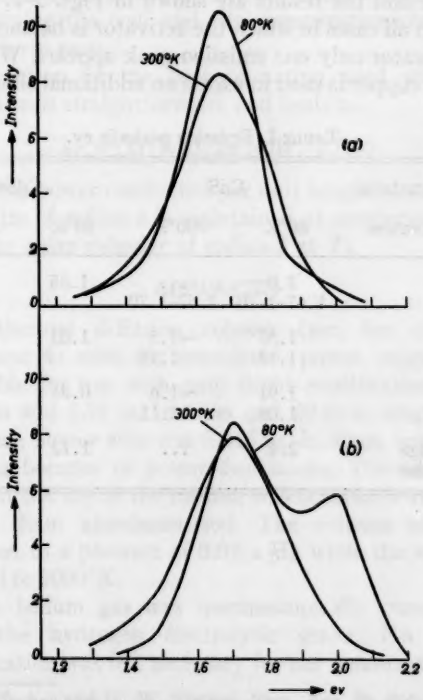

FIG. 5. Emission of CdS activated by silver and indium (a) 2.10^{-4} Ag, $2.5.10^{-4}$ In; (b) 3.10^{-4} Ag, 2.10^{-4} In.

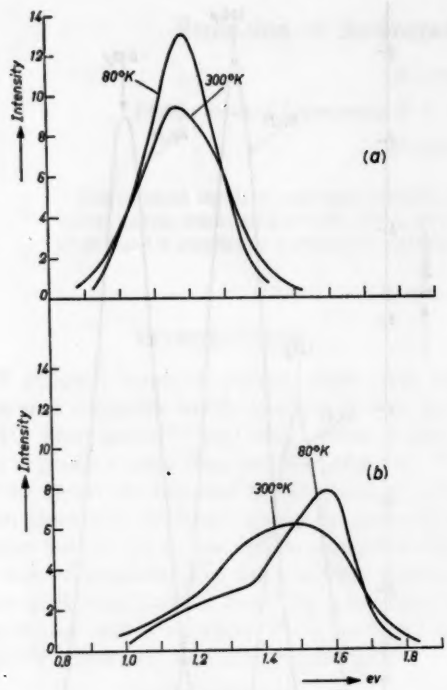

FIG. 6. Emission of CdS activated by copper and indium (a) 2.10^{-4} Cu, $2.5.10^{-4}$ In; (b) 5.10^{-4} Cu, 2.10^{-4} In.

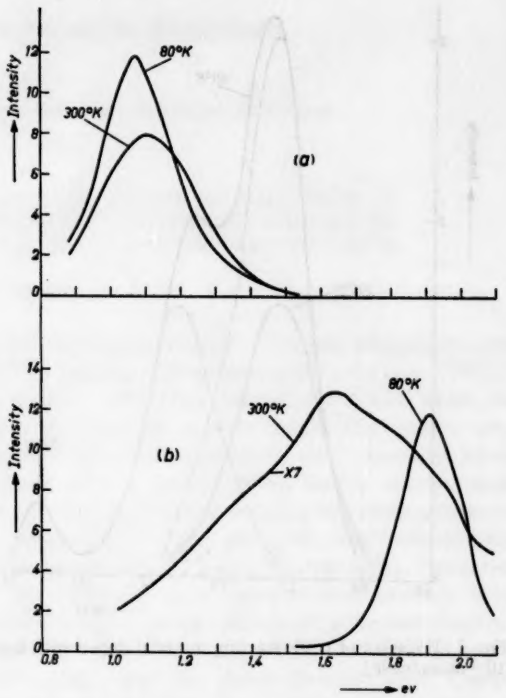

FIG. 7. Emission of CdS activated by gold and indium (a) 2.10^{-4} Au, 2.10^{-4} In; (b) 4.10^{-4} Au.

due to the residual impurities, on the short-wave side. However, no positive indication of a short-wave band was found. For comparison we measured also the emission spectra of silver, copper, and gold in cadmium sulfide and the results are shown in Figs. 5–7. We see that in all cases in which the activator is balanced by a coactivator only one emission peak appears. When silver or copper is used in excess an additional short-wave band appears, as already found by other workers.[4,5] In the case of gold the situation is more complicated and will be dealt with further in a separate publication. The peaks of the various observed bands are listed in Table I.

TABLE I. Emission peaks in ev.

Base material	CdS		CdSe	
Activators	80°K	300°K	80°K	300°K
Ag, In	2.0 1.67–1.70	... 1.67–1.70	1.35	...
Cu, In	1.57 1.18	~1.5 1.18	1.03	1.03
Au Au, In	1.91 1.08	~1.6 1.11	0.85	0.90
Near edge emission	2.4	...	1.72	...

DISCUSSION

The emission peaks of silver, copper, and gold in cadmium selenide appear in the regular, expected manner beyond the absorption edge. Because the band gap of cadmium selenide is considerably smaller than cadmium sulfide, one may expect the silver level to be so near the valence band that the silver emission is already quenched at room temperature. Another important difference is that no additional band appears when excess of activator over coactivator is used.

ACKNOWLEDGMENT

The authors want to acknowledge the help of W. Gelling in the preparation of the phosphors and the assistance of J. W. de Jong, in measuring the emission spectra.

Thermal Conductivity of Helium and Hydrogen at High Temperatures*

NORMAND C. BLAIS AND JOSEPH B. MANN

University of California, Los Alamos Scientific Laboratory, Los Alamos, New Mexico

(Received December 14, 1959)

A steady-state hot wire method for measuring the thermal conductivity of light gases in the temperature range 1200° to 2100°K is described. In contrast to other methods, free convection currents and large temperature gradients occur; convection effects are shown to be negligible, and the experimental procedure for eliminating the large gradient effects is described. The thermal conductivity of helium is found to follow the equation $\lambda\times10^4=991+0.678(T-1200)$ cal/sec cm deg over the temperature range covered. That for hydrogen is $\lambda\times10^4=1434+1.257(T-1200)$ cal/sec cm deg.

INTRODUCTION

THE thermal conductivities at high temperatures of light gases, such as hydrogen and helium, have recently become of interest to this Laboratory. Only a very few measurements of thermal conductivity have been made at temperatures above 1200°K,[1] and none of these deal with helium or hydrogen. The usual steady-state methods (hot wire, concentric cylinders, parallel plates) employ temperature gradients of a few degrees per cm. These methods are not amenable to extension to high temperatures; bath temperature fluctuations, as compared to the applied temperature difference, as well as deterioration of thermal and electrical insulation, cause serious difficulties.

The method employed in this work was a steady-state method in which large temperature gradients (as high as 10^4 deg/cm) were applied, and free convection currents allowed. Specifically, the apparatus consisted of a vertical, water-cooled glass tube with a coaxial tungsten wire. The wire was heated electrically to the temperature at which the thermal conductivity was desired.

Under certain conditions, the gas in the tube will be in laminar, free-convection flow[2,3] along the axis of the tube. This type of flow may be treated mathematically (see Appendix) to determine the flow velocity profile. Assuming conditions for laminar flow to hold, the heat flow equation becomes

$$r^{-1}(\partial/\partial r)\lambda r(\partial T/\partial r)+\lambda(\partial^2T/\partial z^2)=c\rho v(\partial T/\partial z), \quad (1)$$

where the z axis is along the vertical axis of the tube, thermal conductivity is denoted by λ, r is the radius, T is the temperature, c is the specific heat, ρ is the density of the gas, and v is the flow velocity. The left-hand side is seen to be the ordinary heat flow equation through an isotropic substance. The term on the right-hand side of the equation arises because a small volume of gas may gain heat as it moves in the convective flow cycle. If the apparatus is sufficiently long so that in some region $\partial T/\partial z$ is much smaller than $\partial T/\partial r$, then both the convective heat loss and the heat conducted axially will be negligible compared with the transverse heat flux. If the temperature distribution of the source (the tungsten wire) remains uniform in this region, with or without gas, then the transverse conducted power can be determined; it is the difference between the ohmic losses with the wire in gas and in vacuum.

The apparatus was made long enough so that the wire was uniform in temperature over most of its length, thereby assuring that $\partial T/\partial z$ in the gas was negligible over most of the column length. A crude model of the wire temperature distribution then sufficed to calculate the power losses due to radial conduction.

The virtue of our method lies chiefly in the fact that no special materials are required for insulation and that maintaining the wall and wire temperatures constant is relatively easy.

Derivation of the basic equation used with the apparatus is straightforward, and leads to

$$\lambda_{T_a}=[\ln(b/a)/2\pi](dW_c/dT_a). \quad (2)$$

W_c is the power conducted per unit length of the wire. The wire of radius a is maintained at temperature T_a, and the outer cylinder of radius b at T_b.

APPARATUS

A thermal diffusion column (see, for example, reference 4) with its associated power supply was available for use with only slight modifications. The column was 1.22 in. in diam and 20 ft in length. The tungsten heater wire was 0.015 in. in diam, but only 8 ft long because of power limitations. The remaining 12 ft at the top of the column was accurately centered, $\frac{5}{16}$-in. diam aluminum rod. The column could be pumped to a pressure of 0.02 μ Hg while the wire was heated to 2000°K.

The helium gas was spectroscopically pure grade, and the hydrogen electrolytic grade. No further purification was felt necessary for our measurements.

* This work was sponsored by the U.S. Atomic Energy Commission. A more detailed version of this paper has appeared as LA-2316.

[1] See the comprehensive survey of recent work by P. E. Liley, *Thermodynamic and Transport Properties of Gases, Liquids, and Solids* (McGraw-Hill Book Company, Inc., New York, 1959), pp. 40–69.

[2] L. Onsager and W. W. Watson, Phys. Rev. 56, 474 (1939).

[3] R. Simon, Phys. Rev. 69, 596 (1946).

[4] A. Zucker and W. W. Watson, Phys. Rev. 80, 966 (1950).

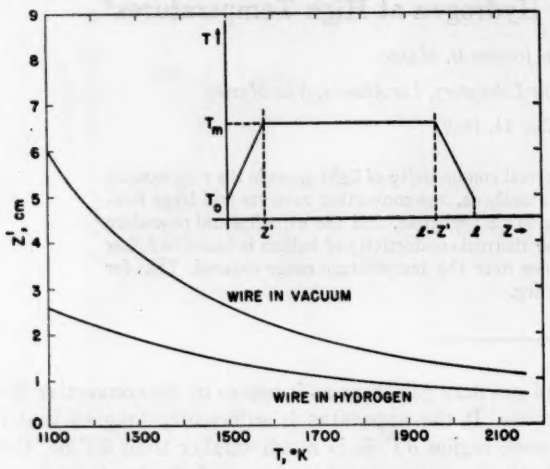

FIG. 1. Wire length in which temperature is nonuniform; inset shows model of temperature variation for calculation of maximum resistance.

A 5-kw amplidyne generator was the source of dc power for the wire. A negative feedback system in the generator field windings gave about 0.1% voltage regulation, with an ac component less than 1% of the direct current.

A Leeds and Northrup portable pyrometer was used to measure the wire temperature midway along the wire length. A previous calibration of the pyrometer was made against two secondary standard lamps. The effective wavelength of this pyrometer may be taken as 0.653 μ.[5]

The potential across the tungsten wire was measured with a calibrated 0–150/300-v dc meter. The current was determined by measuring the potential drop across a 0.01-ohm series precision resistor with a Rubicon portable potentiometer.

Throughout the experiment, the length of the tungsten wire was measured. On installation, the initial length was measured with a steel tape. Subsequent changes in length were measured with a cathetometer.

PROCEDURE

The operating procedure for a typical gas run was as follows: Power dissipation measurements were made at approximately 100° intervals in the temperature range 1100° to 2100°K. At each point the readings taken were current I, voltage E, wire length l, and the temperature. For these points the gas pressure was maintained at 61 cm Hg. In addition, the variation of power dissipation with pressure (from 61 to 10 cm Hg) was determined at approximately 200° temperature intervals. For these points the ratio E/I was kept constant in order to maintain approximately constant wire temperature.

At every temperature, a visual estimate was made of the wire length at each end which was not at maximum temperature. This length was called z' and is shown in Fig. 1.

TREATMENT OF DATA

The wire resistance per unit length in the region of maximum temperature T_m is given by

$$R_m=[(E/I)-r]/l_{eff}, \tag{3}$$

where r is any circuit resistance exclusive of the tungsten wire, and l_{eff} is called the effective length of the wire.

The wire temperature, as determined by the averaged resistance per unit length, and by resistivity tables,[6] agreed with the pyrometer temperature to within 15° to 20°K. At most, 5% of the length of the wire was nonuniform in temperature. Therefore, the simple model shown in Fig. 1 for the temperature distribution of the wire was sufficient to find l_{eff}.

$$l_{eff}\cong l-2z'\{1-[2.195(1-\theta)]^{-1}\} \tag{4}$$

where $\theta=T_0/T_m$, and the proper temperature dependence[6] for resistance is included. T_0 was chosen as 350°K, but the results are insensitive to this value if $T_0\ll T_m$. Similarly, the actual temperature distribution in the region of z' was not important since l_{eff} was generally only 1% less than the total length.

The power loss per unit length was then given by I^2R_m. This method was preferred over the use of re-

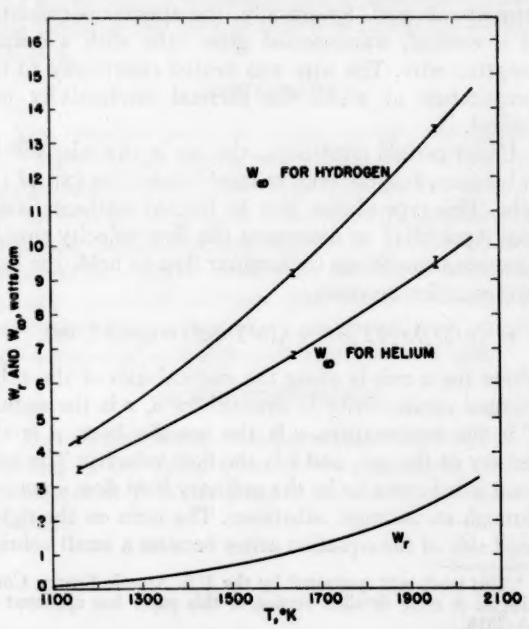

FIG. 2. Radiated power W_r and gas-conducted power W_∞ per unit length of wire. Standard deviations are indicated.

[5] K. A. Walch and R. C. Stroud, *Manufacture of L. and N. Pyrometers* (Leeds and Northrup Company, Philadelphia, Pennsylvania).

[6] C. J. Smithells, *Tungsten* (Chemical Publishing Company, Inc., New York, 1953), Table XXVIII, pp. 177–180.

sistivity tables, as a measure of either T_m or of R_m, because correction for change in the cross-sectional area of the wire due to thermal expansion, or to stretching, was unnecessary.

As mentioned earlier, the brightness temperature of the wire was measured with a pyrometer. To find the true temperature, it is necessary to know the emissivity of the tungsten wire and the transmission of the water jacket. Table values of emissivity[7] were corrected to wire emissivity by multiplying by 1.028.[8] The transmission (0.844) was measured by observing a tungsten ribbon in an evacuated bulb both inside and outside the column at several different temperatures.

The radiated power W_r was obtained as a function of temperature from runs made with the column evacuated, and agreed very well with the theoretical relation

$$W_r=2\pi a\epsilon\sigma(T^4-T_0^4). \quad (5)$$

These data are shown in Fig. 2. The gas-conducted power W_c was obtained by subtracting W_r from the total dissipated power. Power lost by free convection of the gas in the column is treated in the Appendix, and was found to be negligible.

The experiments showed that W_c depended on the pressure as well as the temperature, as shown in Figs. 3 and 4 for helium and hydrogen, respectively. These figures are typical plots of $1/W_c$ vs $1/p$. The extrapolation of the straight line portion of the data points to $1/p=0$ yields a value of conducted power called W_∞.

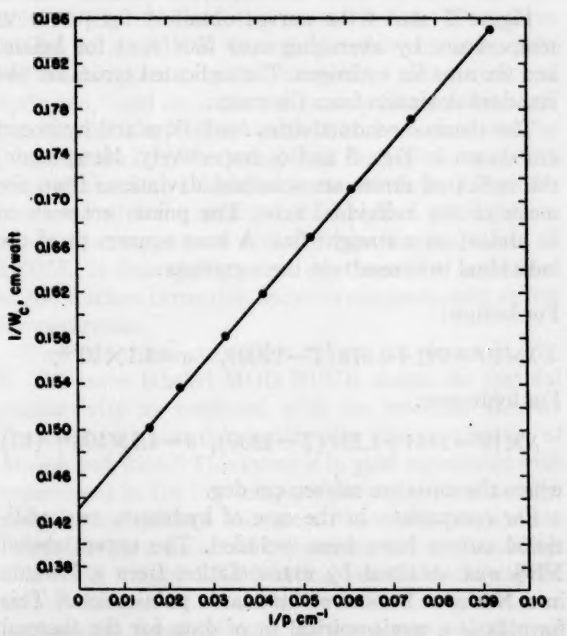

FIG. 3. Helium: reciprocal of the conducted power W_c vs reciprocal pressure.

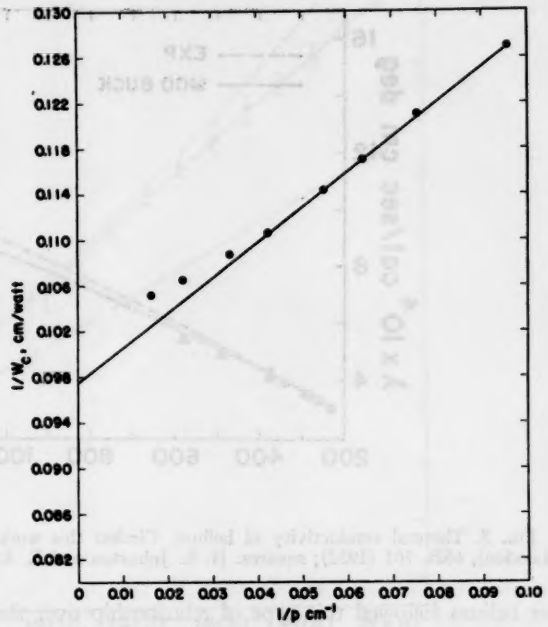

FIG. 4. Hydrogen: reciprocal of the conducted power W_c vs reciprocal pressure.

For helium, the variation of W_c with p is consistent with that obtained from the so-called temperature jump,[9] which occurs between a surface (in this case, the hot wire) and an unequally heated gas. In this region, the molecular nature of the gas is emphasized, because the temperature change in a mean free path is significant, and the accommodation coefficient for collisions with tungsten can be small.[10]

The magnitude of this temperature jump is given by

$$\Delta T=-g(dT/dr) \quad (6)$$

where g is the "temperature jump distance," which varies inversely with pressure. The temperature gradient is evaluated near the wire. Then

$$W_c=\frac{2\pi}{\ln(b/a)}\int_{T_b}^{T_a-\Delta T}\lambda dT$$

$$=W_\infty+\frac{2\pi}{\ln(b/a)}(\lambda A/p)(dT/dr), \quad (7)$$

where A/p has been substituted for g.

Since, to a good approximation,

$$2\pi a\lambda(dT/dr)=W_c, \quad (8)$$

then

$$1/W_c=(1/W_\infty)+(B/p) \quad (9)$$

where B is a function of temperature, the accommodation coefficient, and other constants. The data points

[7] *Handbook of Chemistry and Physics* (Chemical Rubber Publishing Company, Cleveland, Ohio, 1958), p. 2955.
[8] See p. 181 of work cited in footnote 6.
[9] E. H. Kennard, *Kinetic Theory of Gases* (McGraw-Hill Book Company, Inc., New York, 1953), pp. 311–315.
[10] K. B. Blodgett and I. Langmuir, Phys. Rev. **40**, 78 (1932).

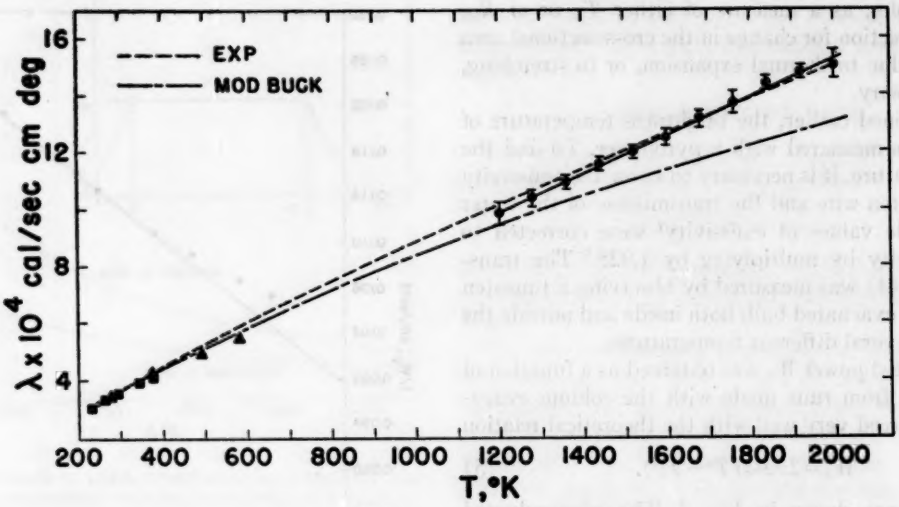

FIG. 5. Thermal conductivity of helium. Circles: this work; triangles: W. G. Kannuluik and E. H. Carman, Proc. Phys. Soc. (London), **65B**, 701 (1952); squares: H. L. Johnston and E. R. Grilly, J. Chem. Phys. **14**, 233 (1946).

for helium followed this type of relationship over the complete range of temperatures and pressures and incidentally verified that the gas flow was laminar rather than turbulent.

Some difficulty was encountered in the case of hydrogen. At the lowest temperature points (1100° to 1300°K), curves similar to those for helium were obtained, but as the temperature was increased, departures from linearity were found (see Fig. 4). For pressures less than 30 cm Hg, the points could be connected by a straight line, but higher pressure points deviated sharply from this line. The magnitude of this deviation increased slowly with temperature, but no significant temperature-pressure relation at which deviation started was evident.

Our conclusion about hydrogen is that the apparent change in thermal conductivity with pressure is caused by a change in the accommodation coefficient. A small amount of impurity, or hydrogen reaction, can change the surface conditions on the wire drastically, although no mechanism has yet been found to account for the strong pressure dependence. Our extrapolation procedure implies that we are taking the accommodation coefficient to be constant where the points lie on the straight line, and that it decreases in the higher pressure region where the points lie above the line. The slopes of the $1/W_e$ vs $1/p$ lines for both helium and hydrogen indicate accommodation coefficients in the range 0.10 to 0.16.

For those temperatures at which the pressure was not varied, the correction factor W_∞/W_e (W_e at 61 cm Hg) was obtained from a plot of the correction factor vs temperature.

As indicated earlier, in Eq. (2), the thermal conductivity at any temperature is directly proportional to the derivative of the conducted power vs temperature curve. The derivatives were found by numerical differentiation based on Stirling's interpolation formula.[11] Five points, at 40° intervals, were used for each derivative. The points were read from the smoothed curve drawn through the W_∞ points for each run.

RESULTS AND DISCUSSION

Results

Figure 2 shows the curves obtained for power vs temperature by averaging over four runs for helium and six runs for hydrogen. The indicated errors are the standard deviation from the mean.

The thermal conductivities for helium and hydrogen are shown in Figs. 5 and 6, respectively. Here, again, the indicated errors are standard deviations from the mean of the individual runs. The points are seen to lie almost on a straight line. A least squares fit of the individual runs results in the equations:

For helium:

$$\lambda\times10^6=991+0.678(T-1200), \quad \sigma=3.1\times10^{-5};$$

For hydrogen:

$$\lambda\times10^6=1434+1.257(T-1200), \quad \sigma=4.5\times10^{-5}; \quad (10)$$

where the units are cal/sec cm deg.

For comparison in the case of hydrogen, two additional curves have been included. The curve labeled NBS was obtained by extrapolation from a formula in a National Bureau of Standards publication.[12] This formula is a semiempirical fit of data for the thermal conductivity of hydrogen for temperatures ranging

[11] J. B. Scarborough, *Numerical Mathematical Analysis* (Johns Hopkins Press, Baltimore, 1955), 3rd ed., p. 70.

[12] Joseph Hilsenrath *et al.*, *Tables of Thermal Properties of Gases*, Natl. Bur. Standards Circ. No. 564 (1955).

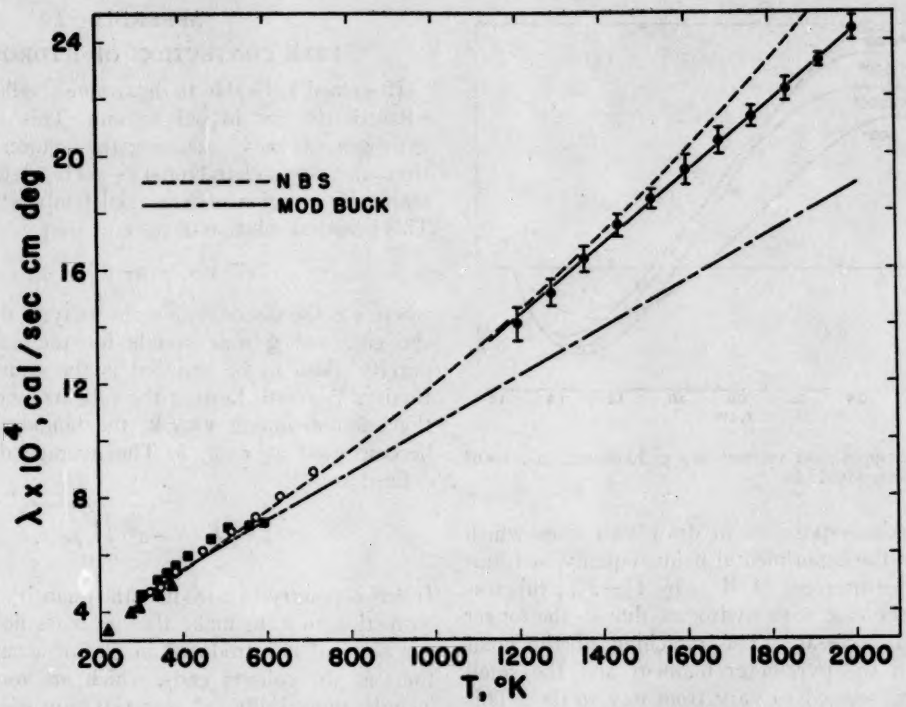

FIG. 6. Thermal conductivity of hydrogen. Closed circles: this work; squares: H. S. Gregory, Proc. Roy. Soc. (London) **149A**, 35 (1935); open circles: N. B. Vargaftik and I. D. Parfenov, J. Exptl. Theoret. Phys. (U.S.S.R.) **8**, 189 (1946); triangles: H. L. Johnston and E. R. Grilly, J. Chem. Phys. **14**, 233 (1946).

only up to 700°K. A previous publication[13] gave quite similar results, although the form of the equation differed slightly from the one used here. The curve labeled MOD BUCK was calculated by using a modified Buckingham (exp-6) potential for the viscosity of hydrogen,[14] and an improved Eucken factor as outlined by Hirschfelder.[15] The curve has been included to illustrate the large deviation from the high-temperature data of the best calculated curve to date. Viscosities predicted with the modified Buckingham potential are in excellent agreement with the experimental[14] data to 1100°K; it thus appears that the theoretical treatment of the Eucken correction factor is adequate only at low temperatures.

Two additional curves for helium are shown in Fig. 5. The curve labeled MOD BUCK shows the thermal conductivity as predicted with the modified (exp-6) Buckingham potential, again with the parameters of Mason and Rice.[14] This curve is in good agreement with experiment in the low temperature region, but at high temperatures shows the error that can result from extrapolating a potential beyond its region of validity. The curve labeled EXP was the best fit to the experimental data, as calculated with collision integrals for an exponential potential such as $\phi=\phi_0\exp(-\alpha r/2)$; an additional requirement was that the predicted value of the conductivity at 0°C should be 342.5×10^{-7} cal/sec cm deg. The parameters that give this curve are $\phi_0=366\times10^{-12}$ erg, $\alpha=8.5$, with r in A. The exponential potential thus found is in good agreement with the potential given by Amdur[16] for high energies, and with that of Mason and Rice at low energies. The exponential potential parameters suggested by Amdur lead to a thermal conductivity curve that fits our data almost as well as the EXP curve, but gives a slightly higher value (351×10^{-7}) at room temperature.

The calculations of the collision integrals and of the auxiliary factors for the third approximation to the transport properties were carried out using an IBM 704 calculator; this work, along with further discussion of its application to helium and hydrogen, is reported elsewhere.[17]

Errors

The variation between pyrometer readings of the wire at constant temperature rarely exceeded 10°K. Also, the measured power W_e was accurate to within $\pm\frac{1}{2}\%$. In view of these reproducibilities, the standard deviations from the mean shown in Figs. 2, 5, and 6 may seem large. Two factors have contributed most to these deviations. In the process of extrapolation to find W_{∞}

[13] H. W. Woolley, R. B. Scott, and F. G. Brickwedde, J. Research Natl. Bur. Standards **41**, 379 (1948), p. 447.
[14] E. A. Mason and W. E. Rice, J. Chem. Phys. **22**, 522 (1954).
[15] J. O. Hirschfelder, J. Chem. Phys. **26**, 282 (1957).
[16] I. Amdur and E. A. Mason, Phys. Fluids **1**, 370 (1958).
[17] J. B. Mann, Los Alamos Scientific Laboratory Report LA-2383 (Office of Technical Services, U.S. Department of Commerce, Washington 25, D. C., 1960).

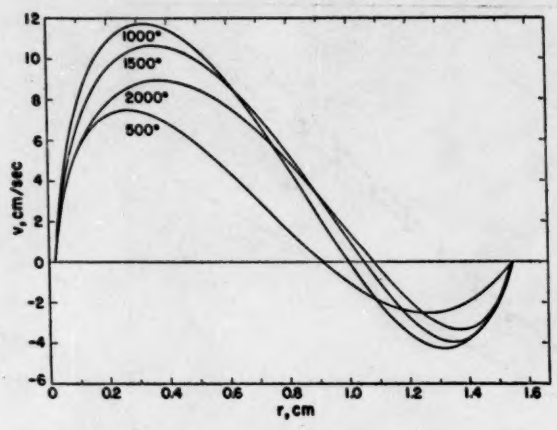

FIG. 7. Speed profile for vertical flow of hydrogen gas; $p=61$ cm Hg, wire diam=0.015 in.

it was sometimes possible to draw two lines which seemed to fit the experimental points equally well, but differed at the intercept $(1/W_\infty)$ by $1\frac{1}{2}-2\%$; this was more often the case with hydrogen, due to the longer extrapolation necessary. The matching of the color brightness of the pyrometer filament and the small tungsten wire seemed to vary from day to day. This type of subjective phenomenon seems to defy analysis. These two sources of error are not, strictly speaking, random. Nevertheless, they were treated as such.

Calculations of magnitudes of some of the more obvious systematic errors were made, and found either to be unlikely or insignificant compared to the standard deviations. For example, a difference of 6% would have been necessary between the literature value of emissivity and the actual value for a 10° error at 2000°K. A wire that was off-axis by one or two wire diameters would have given too large a value of λ by less than 0.005%.

In summary, the observed thermal conductivities for hydrogen and helium are given by Eq. (10). The random errors [σ of Eq. (10)] amount to 3%, or less, of the thermal conductivity values. Such errors as pyrometer instability and uncertainty in extrapolation of conducted power to infinite pressure are included in this figure. We feel that any systematic errors which might be present could cause at most an additional uncertainty of 1%.

ACKNOWLEDGMENTS

We wish to thank Eugene S. Robinson for bringing this problem to our attention. We are certainly indebted to B. B. McInteer for pointing out that laminar convective flow disturbs the temperature distribution only at the ends of the apparatus. We are grateful to Don L. Bunker for instruction in programing convection calculations for the IBM 704 data processing machine.

APPENDIX

FREE CONVECTION OF HYDROGEN

It seemed advisable to determine the flow characteristics of the gas in our column. This was done for hydrogen gas only, assuming the column long enough that the flow characteristics were determined primarily by a region of zero axial temperature gradient. This involved solution of the equation

$$\nabla\eta\nabla\cdot\mathbf{v}=-(\rho-\bar{\rho}+\rho^*)\mathbf{g}, \qquad \text{(A-1)}$$

where η is the viscosity, ρ the density, $\mathbf{v}$ the velocity of the gas, and $\mathbf{g}$ now stands for the acceleration of gravity. Also to be satisfied is the equation of continuity, $\nabla\cdot\rho\mathbf{v}=0$. Letting the tube axis be the z direction, and assuming $\mathbf{v}=v_z\mathbf{k}$, the boundary conditions become $v=0$ at $r=a$, b. The average density, $\bar{\rho}$, is defined as

$$\bar{\rho}=[2/(b^2-a^2)]\int_a^b \rho r dr. \qquad \text{(A-2)}$$

It was necessary to introduce the quantity ρ^* as a small correction to $\bar{\rho}$, to make the net mass flow, $\int\rho v r dr$, of gas zero; ρ^* is introduced in lieu of accurate calculations at the column ends, which are too difficult to include analytically. ρ^* was typically of the order of one-tenth of $\bar{\rho}$.

Integration of Eq. (A-1) gives

$$v=g\int_a^r (dr'/\eta r')\int_a^{r'}(\rho-\bar{\rho}+\rho^*)r dr+C\int_a^r (dr/\eta r), \qquad \text{(A-3)}$$

where C is a constant determined by the condition $v=0$, $r=b$. The problem was programed for the IBM 704 machine, and run at various wire temperatures, pressures, wire radii, etc. The temperature distribution, neglecting "temperature jump" effects, in the gas depends on the thermal conductivity; this was assumed to vary linearly with temperature, from 0.00042 at 300°K to 0.0024 at 2000°K. The temperature dependence of the viscosity was taken from the literature[12]; the density was not assumed to be constant, but was varied inversely with temperature.

Figure 7 is a plot of the axial velocity vs r for several values of T_a. The heat carried by the flowing gas, in excess of the room temperature enthalpy, was found by numerical integration of the integral

$$\int_a^r \rho v r\int_{286}^{T_r} c_p dT dr.$$

At a wire temperature of 2000°K the heat flowing upwards amounted to only 0.60 w; the downward flow was 0.13 w. These heat flows are negligible compared to the total power input to the apparatus of about 4000 w.

With the foregoing results it is now possible to estimate the disturbed length in the gas at the ends of

the column, that is, the distance along z in the gas in which $\partial T/\partial z$ is not negligibly small.

It can be shown on the simple model depicted in Fig. 7 that the convection term of Eq. (1) can be neglected for hydrogen. It leads to a relaxation length of the order of

$$l_1 = b^2\rho v c_p/\lambda \cong 0.1 \text{ cm}. \quad \text{(A-4)}$$

On the other hand, the remainder of Eq. (1) can be solved approximately at the ends of the tube, and leads to a relaxation length of

$$l_2 \cong b = 1.6 \text{ cm}. \quad \text{(A-5)}$$

This indicates that $\partial T/\partial z$ becomes very small in a distance of 10 to 15 cm from either end. A column 30 cm long would have been sufficiently long to fulfill those requirements discussed in the introduction. However, more care would have been necessary in calculating R_m from the wire temperature distribution.

THE JOURNAL OF CHEMICAL PHYSICS VOLUME 32, NUMBER 5 MAY, 1960

Triplet-Singlet Emission Spectra of Xylenes in Crystalline State at 4.2° and 77°K, and in EPA at 77°K*

LAWRENCE A. BLACKWELL,† YOSHIYA KANDA,‡ AND H. SPONER

Department of Physics, Duke University, Durham, North Carolina

(Received November 27, 1959)

The triplet-singlet emission spectra of xylenes in the crystalline state at 4.2° and 77°K and in a rigid glass at 77°K have been photographed and analyzed. The samples were obtained from the National Bureau of Standards. They were kept sealed under an oxygen-free atmosphere of helium gas throughout the experiments. Large well-formed crystals were grown from the vapor on a surface cooled by liquid nitrogen, and some were grown from the melt. At 4.2°K *o*-xylene produced two sharp spectra similar in structure and separated by 370 cm^{-1} from each other. These spectra are ascribed to two distinct crystalline phases. At 77°K *o*-xylene did not produce a significant phosphorescence. The spectrum of *m*-xylene at 4.2°K consisted of a strong diffuse spectrum and a weak sharp spectrum toward shorter wavelengths. The diffuse spectrum appeared to be associated with the amorphous phase. At 77°K a broad spectrum appeared which was found to be characteristic of an aldehyde. At 4.2°K *p*-xylene showed a sharp spectrum beginning at 25 254 cm^{-1}. It differs in vibrational structure from the spectrum of this compound in a rigid glass. A vibrational analysis indicated that the carrier of this spectrum is *p*-methylbenzaldehyde. With crystals of the *p*-xylene grown from the melt the genuine spectrum due to *p*-xylene was observed between 28 246 and 25 416 cm^{-1}, overlapped by the spectrum of *p*-methylbenzaldehyde in the longer wavelength region. These results suggest a temperature-activated sensitization which had been first observed in toluene.

INTRODUCTION

THE first genuine phosphorescence spectra of the xylenes were those observed by von Kowalski[1] in 1911 between 350 and 430 mμ. In 1949 Dikun and Sveshnikov[2] studied the phosphorescence spectra of *o*-, *m*-, and *p*-xylenes in ethanol at 90°K and analyzed them in detail. Lifetime measurements made by Dikun, Petrov, and Sveshnikov[3] in 1951 gave 5.6 sec for *o*-xylene, 8.1 sec for *m*-xylene, and 8.4 sec for *p*-xylene. The phosphorescence spectra of xylene crystals were first reported by Pesteil and Zmerli[4] at 20°K in 1955. We have studied the triplet-singlet emission spectra of *o*-, *m*-, and *p*-xylene crystals at 4.2° and 77°K, and the xylenes in EPA at 77°K using great care to avoid contamination of the spectra by impurities.

EXPERIMENTAL

Samples of the three isomeric xylenes were obtained from the National Bureau of Standards. These samples were reported to have the following purities: the ortho derivative, 0.010±0.007 mole percent impurity; the meta sample, 0.17±0.07 mole percent impurity; and the para, 0.04±0.02 mole percent impurity. The degree of purity of these standard samples had been evaluated from measurements of freezing points. Each sample was supplied sealed under vacuum. The phosphorescence cell was carefully loaded to eliminate contamination by oxygen. This was performed by sealing the thoroughly cleaned cell onto a high vacuum system to

* Based in part on a thesis submitted by L. A. Blackwell to the Graduate School of Arts and Sciences, Duke University, in partial fulfillment of the requirements for the degree of Doctor of Philosophy. Supported by the National Science Foundation.

† Present address: Texas Instruments Inc., Dallas, Texas.

‡ Present address: Department of Chemistry, Faculty of Science, Kyushu University, Fukuoka, Japan.

[1] J. von Kowalski, Physik Z. **12**, 956 (1911).

[2] P. P. Dikun and B. Ya. Sveshnikov, Zhur. Eksptl. i. Teoret. Fiz. **19**, 1000 (1949).

[3] P. P. Dikun, A. A. Petrov, and B. Ya. Sveshnikov, Zhur. Eksptl. i. Teoret. Fiz. **21**, 150 (1951).

[4] P. Pesteil and A. Zmerli, Ann. phys. **10**, 1077 (1955).

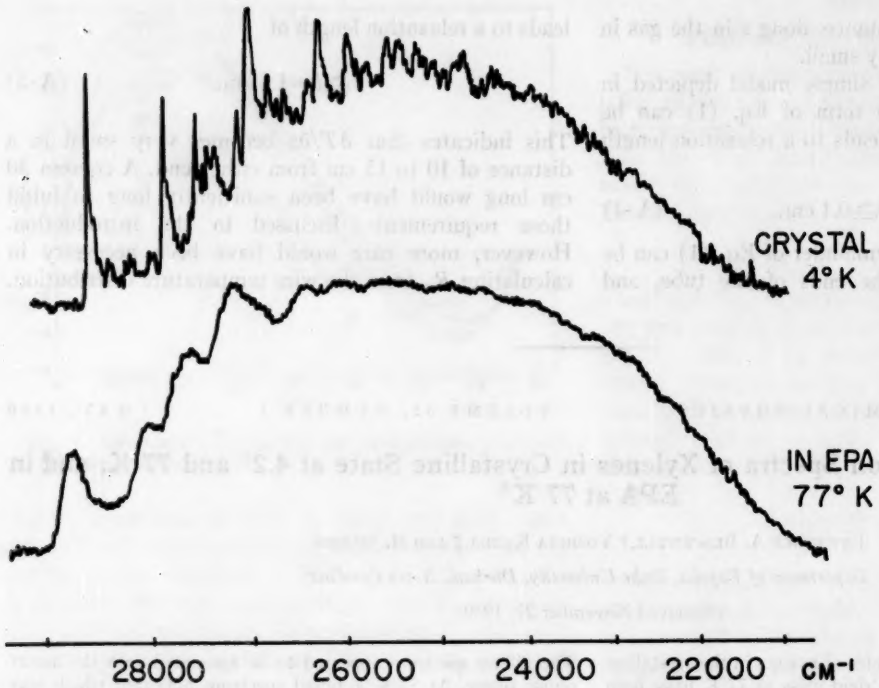

FIG. 1. Phosphorescence spectra of *o*-xylene in the crystalline state at 4.2°K, and in EPA at 77°K.

which was connected the sample contained in a break-seal ampoule. After the system was completely evacuated down to about 10^{-6} mm Hg, the break seal was broken. The xylene vapor was then condensed on a cold sodium mirror, and the sample was allowed to warm to remove any trace of water. The sample was finally distilled off over the sodium and the middle fraction was collected in the cell. Then the stopcock between the cell and the pump was closed and the cell was warmed up, allowing any trapped gas to escape. The sample was then refrozen and pumped down again, and this procedure was repeated several times. Finally, the cell was filled to a pressure of about one-half atmosphere with oxygen-free helium gas. The helium had been purified by passing it over a red-hot mirror of calcium. The sample cell was then sealed off from the vacuum system. Helium gas above the sample was found necessary to maintain good thermal conductivity between the walls of the cell and the emitting surface. In preliminary experiments it was found that a crystal sealed under high vacuum would not produce a low-temperature spectrum in this arrangement because of the low thermal conductivity of the crystal at these temperatures.

The melting points of *o*-, *m*-, and *p*-xylenes are, respectively, 247.82°, 225.27°, and 286.39°K. Crystals were grown directly from the melt by cooling the sample near the surface of liquid nitrogen. In the case of *p*-xylene usable crystals were produced in this way because of its higher symmetry. With the other two isomers it is difficult to prevent supercooling, and the consequential almost instantaneous freezing of the sample. When this happened, a conglomerate of very small crystals and of regions of amorphous material was formed. In order to avoid these effects as much as possible, crystals were grown from the vapor. In this method the xylene was first condensed on the wall of the cell. The base of the cell was then cooled by immersion in liquid nitrogen, and the crystals were allowed to form on this cold surface. In this way crystals could be grown to over a centimeter in length within about 20 min. While sizable crystals of *p*-xylene were easily obtained, crystallization of *o*- and *m*-xylene proved to be rather difficult to initiate and was extremely sensitive to cooling rate and vapor pressure. For purpose of comparison the emission spectra of the xylenes were also photographed in a rigid solution of EPA. Since the purity required in solution work is much less than that necessary for crystal spectra, commercial samples of the xylenes were used here. The *o*- and *p*-xylenes were Eastman Distillation Products white label grade and the *m*-xylene was an Eimer and Amend sample of cp grade. The materials were subjected to a vacuum distillation immediately before use.

The optical setup used was essentially the same as reported previously.[5,6] The sample was cooled with liquid nitrogen or liquid helium and excited with a high pressure mercury arc lamp of General Electric type AH-6 filtered with a Corning 9863 Red Purple Corex filter. A Bausch and Lomb quartz spectrograph of medium dispersion was used throughout the work. Exposure times ranged from 30 min to 2 hr on Eastman

[5] R. C. Heckman, J. Mol. Spectroscopy **2**, 27 (1958).
[6] Y. Kanda and H. Sponer, J. Chem. Phys. **28**, 798 (1958).

Kodak 103a-O plates with a slit width of 50 μ for the crystal spectra and 100 μ for the EPA spectra. Wavelengths and intensities of spectral bands were measured with a Jarrell-Ash recording microphotometer. The maximum precision of measurements was ± 3 cm^{-1} for sharp bands. For broad bands in the EPA spectra the maximum accuracy was not greater than ± 30 cm^{-1}.

RESULTS AND DISCUSSION

(a) *o*-Xylene

The triplet-singlet emission spectrum of *o*-xylene was observed in the crystalline state at 4.2°K and in EPA at 77°K. The microphotometer tracing curves are shown in Fig. 1, and the spectral data are listed in Tables I and IV. The general appearance of the spectrum of *o*-xylene crystal is quite different from that of either *m*- or *p*-xylene. Its over-all structure resembles that of the EPA spectrum. The 0,0 band lies at 28 607 cm^{-1} which is about 163 cm^{-1} toward the red from the corresponding band in the EPA medium. It may be seen by examination of the spectrum shown in Fig. 1 that a rather weak band lies to the shorter wavelength side of the band assigned to the 0,0 transition. The origin of the band was at first quite puzzling since, if the band at 28 607 cm^{-1} is truly the 0,0 band, this weak band would necessarily correspond to a transition from a vibrational level of the triplet to the vibrationless ground state. While the band is only 25 cm^{-1} in energy from the 0,0 band and is undoubtedly a lattice vibration, for this vibrational mode to be excited with any appreciable population it would require a temperature considerably higher than 4°K. This same phenomenon had been encountered in the spectrum of toluene crystal at low temperatures and in order to clear up this point spectra were photographed with a layer of liquid helium over and in contact with the emitting surface of the crystal.[6] Under these conditions bands to the shorter wavelength side of the 0,0 band disappeared. The presence of these bands, then, does seem to indicate that at least part of the crystals in these experiments were at a temperature somewhat greater than 4°K during exposure. This is not hard to understand if we remember that these crystals are extremely poor conductors of heat and that they are exposed to rather intense irradiation which is absorbed within a few microns of the surface. The same lattice mode of 25 cm^{-1} not only appears in combination with the 0,0 band but is also barely resolvable from several more of the stronger bands throughout the spectrum.

TABLE I. Phosphorescence spectrum of *o*-xylene in EPA at 77°K.

Wave number	Relative intensity	$\nu_0-\nu$	Assignment
28 760	1	0	0, 0
28 040	2	720	$0-733(a_1)$
27 640	3	1120	$0-1117(a_1)$
27 190	4	1570	$0-1584(a_1)$
26 920	3	1840	0−733−1117
26 500	4	2260	0−1584−733
26 100	4	2660	0−1584−1117
25 600	4	3160	0−1584×2
24 940	4	3820	0−1584−733
24 550	4	4210	0−1584×2−1117
24 040	3	4720	0−1584×3

The next prominent band, which is also the second strongest in the spectrum, is 740 cm^{-1} from the 0,0 band and may be unequivocally assigned to the 733 cm^{-1} Raman vibration. This is the strongest line in the Raman spectrum, and Pitzer and Scott[7] assigned it to the totally symmetrical breathing vibration of the ring having a value of 992 cm^{-1} in benzene. This vibration also occurs in overtones up to the fourth and in combination with the main progression of 1586 cm^{-1}.

Turning for the moment to the EPA spectrum of *o*-xylene shown in Fig. 1, the similarity of its vibrational structure to that of the crystal spectrum is immediately apparent. The separation of the band at 28 043 cm^{-1} from the 0,0 band is 717 cm^{-1} which is in good agreement with the Raman value of 733. (Table I contains rounded-off values.) The third band at 27 639 cm^{-1}, however, is separated from the 0,0 band by an interval of 1121 cm^{-1}. Dikun and Sveshnikov[2] in their work on the xylene phosphorescence in supercooled alcoholic solutions assigned this to the weak

TABLE II. Phosphorescence spectrum of *m*-xylene in EPA at 77°K.

Wave number	Relative intensity	$\nu_0-\nu$	Assignment
28 120	1	0	0, 0
27 430	1	690	$0-724(a_1)$
27 200	2	920	$0-998(a_1)$
26 550	3	1570	$0-1592(a_1)$
25 650	3	2470	0−1592−998
24 940	3	3180	0−1592×2
24 130	3	3990	0−1592×2−998
23 350		4770	0−1592×3
23 010	3	5110	
22 450	3	5670	0−159×3−998

TABLE III. Phosphorescence spectrum of *p*-xylene in EPA at 77°K.

Wave number	Relative intensity	$\nu_0-\nu$	Assignment
28 145	3	0	0, 0
27 840	1	305	$0-313(b_{2g})$
27 315	4	830	$0-826(a_1)$
26 965	4	1180	$0-1182(a_1)$
26 550	7	1590	$0-1616(a_1)$
25 720	7	2425	0−1616−826
25 380	7	2765	0−1616−1182
24 960	7	3185	0−1616×2
24 580	6	3565	0−1616−1182−826
24 170	6	3975	0−1616×2−826
23 810	5	4335	0−1616×2−1182
23 440	5	4705	0−1616×3
22 660	4	5485	0−1616×3−826

[7] K. S. Pitzer and D. W. Scott, J. Am. Chem. Soc. 65, 803 (1943).

TABLE IV. Phosphorescence spectrum of crystalline *o*-xylene at 4.2°K.

Wave number	Relative intensity	$\nu_{0,0}-\nu$	$\nu_{0,0}^*-\nu$	Assignment I	Assignment II
28 632	2	−25		0+25	
28 607	10	0		0, 0	
28 573	4	34		0−34	
28 543	4	64		0−34×2	
28 482	1	125		0−125	
28 407	1	200		0−200	
28 377	1	230		0−200−34	
28 284	1	323		0−200−125	
28 242	2	365	0		0, 0*
28 203	2	404	39	0−200×2	0*−39
28 163	1	444	79		0*−39×2
28 098	1	509	144	0−509	0*−144
28 021	2	586	221	0−586	0*−221
27 969	2		273		0*−144×2
27 894	2	713		0−740+25	
27 880	1	727	362		0*−221−144
27 867	7	740		0−740	
27 836	3	771		0−740−34	
27 800	2	807	442	0−740−34×2	0*−221×2
27 676	1	931		0−740−200	
27 616	1	991	626	0−991	
27 584	1	1023		0−740−200×2	
				0−2×509	
27 555	4	1051		0−1051	
27 517	1		725		0*−725
27 488	2	1119		0−1119	
27 453	2	1154		0−1154	
27 431	1	1176	811	0−1176	
27 360	2	1247		0−1247	
27 157	3	1450		0−1247−200	
				0−740×2+25	
27 129	4	1478		0−740×2	
27 111	1		1121		0*−1121
27 052	3	1555		0−1586+25	
27 021	7	1586		0−1586	
27 000	6	1607	1242	0−1607	0*−1242
26 972	1	1635		0−1247−200×2	
26 845	1	1762		0−740−1051+25	
26 813	3	1794		0−740−1051	
				0−1586−200	
26 793	1	1814	1449	0−1607−200	0*−725×2
26 718	1	1889		0−740−1154	
26 651	2		1591		0*−1591
26 620	2	1987	1622	0−1247−740	0*−1591−39
				0−740−1051−200	
				0−1586−200×2	
26 601	1	2006		0−1607−200×2	
26 578	1		1664		0*−1591−39×2
26 504	1		1738		0*−1591−144
26 426	1	2181	1816	0−1247−740−200	0*−1591−221
				0−740−1051−200×2	
				0−1586−200×3	
26 392	2	2215		0−740×3	
26 359	1	2248		0−1119×2	
26 315	2	2292		0−1247−1051	
				0−1586−740+25	
26 286	4	2321		0−1586−740	
26 263	3	2344	1979	0−1607−740	0*−1242−725
26 199	1		2043		0*−1591−221×2
26 081	1	2526	2161	0−1607−740−200	0*−725×3
26 011	1	2596		0−1586−1051+25	
25 985	3	2622		0−1586−1051	
25 956	1		2286		0*−1591−221×3
25 873	1	2734		0−1586−1154	
25 799	1	2808		0−1586−1247	
25 761	1		2481		0*−1242×2
25 661	1	2946		0−740×4	0*−1591−990
25 584	1	3023		0−1586−740×2+25	
25 558	2	3049		0−1586−740×2	
25 530	1	3077			
25 450	1	3157		0−1586×2	

TABLE IV. (Continued)

Wave number	Relative intensity	$\nu_{0,0}-\nu$	$\nu_{0,0}^*-\nu$	Assignment I	Assignment II
25 357	1		2885		0*−725×4
25 235	2		3007		
25 058	1		3184		0*−1591×2
24 934	1	3673		0−740×5	
24 835	1		3407		0*−1591×2−221
24 758	1	3849			
24 725	2	3882		0−1586−1247−1051	
				0−1586×2−740	
24 660	1		3582		
24 510	1		3732		0*−1242×3
24 403	2	4204		0−1586×2−1051	
24 336	1	4271	3906	0−1586×2−1119	0*−1591×2−725
24 306	1	4301		0−1586×2−1154	
23 980	1	4627		0−1586×2−740×2	

Raman vibration at 1117 cm^{-1}. In the spectrum of the crystal there is a weak band at a separation from the 0,0 band of 1119 cm^{-1} which may be assigned to this vibration. The crystal spectrum shows that what appears to be a single vibration in the solution spectrum is really a group of bands, the strongest of which is at 1051 cm^{-1} from the 0,0. The third strongest band in the Raman spectrum has a value of 1051 cm^{-1} and has been assigned to the totally symmetrical wagging vibration of the methyl groups. Presumably this vibration is either shifted to a slightly higher value or is weakened in the EPA spectrum because of the greater hindrance by the amorphous xylene glass.

The xylene vibration at 1154 cm^{-1} in the crystal is assigned to the totally symmetrical Raman line of medium intensity at 1156 cm^{-1}. The vibration of 1247 cm^{-1} in the crystal is ascribed to the second strongest Raman line representing the totally symmetrical vibration 1233 cm^{-1}. The strongest band in the phosphorescence spectrum of the crystal at 1586 cm^{-1} is assigned to the Raman and infrared active 1584 cm^{-1} (a_1) vibration. This vibration forms the main progression of the spectrum both in EPA and in the crystalline state. The second member of this progression shows a slight anharmonicity and is separated from the first by 1571 cm^{-1}. A frequency of 1607 cm^{-1} may possibly also occur in the crystal and should then be correlated with the b_1 vibration 1606 cm^{-1}. However, the last assignment is not entirely conclusive since this band and its combination bands are overlapped accidentally by bands in another system as will be described in detail in the following. The assignments of the main bands of the crystal confirm generally the assignments by Dikun and Sveshnikov.

There seemed to be several bands throughout the spectrum of the crystal which had no counterpart in the EPA spectrum. The appearance of the weak band at 28 242 cm^{-1} was especially puzzling. There is neither Raman nor infrared vibration for *o*-xylene which would correspond to the 365 cm^{-1} separation of this band from the 0,0 band. It was observed also that the intensity of this band varied from plate to plate but the band was never completely absent from the spectrum. This led to the assumption that this band may be characteristic of another phase present in the crystal, whose concentration depended on the conditions of crystal growth. To examine this possibility more fully, crystals were grown from the melt and their spectrum (called II) was compared to the spectrum (I) which belonged to crystals from the vapor. It was found that the crystals grown from the melt gave a spectrum shifted by 370 cm^{-1} toward the red from the 0,0 band of the latter spectrum (I). The structures of these two spectra were found to be identical. The greater richness in bands apparent in the spectrum from crystals obtained from the vapor is explained by the fact that this spectrum (I) is actually the superposition of two spectra. The main bands in the second spectrum may be picked out from among the weaker bands in the first spectrum clearing up, therefore, many of the difficulties in the assignment of the weaker bands.

These findings suggest that the two spectra arise from two distinct phases present within the crystal. If a phase transition occurred between the melting point at 248° and 77°K, a crystal grown from the melt by the methods used here could quite conceivably have a nonequilibrium phase "frozen in." On the other hand, a crystal grown from the vapor would be expected to exhibit predominantly the lower temperature structure. Pitzer and Scott, however, who measured the specific heats of the xylenes down to 77°K failed to find any evidence for such a transition in *o*-xylene.[7]

In examining the second, longer wavelength spectrum more closely it was found that nearly all of the strong bands exhibit a "splitting" of about 40 cm^{-1}. The weaker of the two components is toward longer wavelengths and is about one half as intense as the other. It is suggested that this "splitting" is the result of a strong vibrational coupling with a lattice mode of the crystal. This is supported by the evidence on a few plates of a two-membered progression of this vibration. If this is the correct explanation, then there are two crystalline

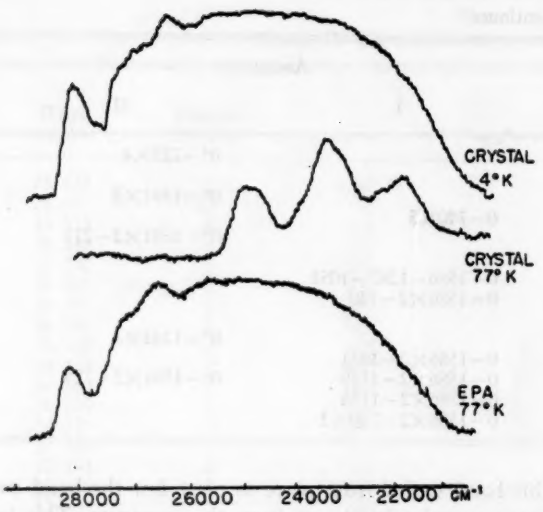

FIG. 2. Phosphorescence spectra of *m*-xylene in the crystalline state at 4.2° and 77°K, and in EPA at 77°K.

phases present since a lattice frequency of 40 cm^{-1} is not found in the first spectrum. No data were found in the literature on the Raman spectra of any of the xylenes in the crystalline state, so that the question of whether these small frequencies may be properly assigned to lattice vibrations is an open one.

It is interesting to compare the results reported here with those of other workers. Kronenberger[8] in his excellent paper on the absorption and luminescence of benzene and some of its derivatives at low temperatures has given measurements of the phosphorescence spectra of the xylenes in the crystal at liquid air and liquid hydrogen temperatures, and in alcoholic solution at liquid air temperature. No analyses were made nor any reproductions given of the spectra. According to these tabular data the spectrum of *o*-xylene begins with a weak band at 28 100 cm^{-1} and extends well into the visible to 17 630 cm^{-1}. The spectrum is not the same as obtained here, and there is no coincidence of even a single band between the two spectra. Actually, the spectrum reported by Kronenberger seems to be the superposition of two spectra, one of which is strong and diffuse and extends into the visible with a prominent 1700 cm^{-1} progression. The other spectral data on the phosphorescence of the xylenes at low temperatures that could be found in the literature are those given by Pesteil and Zmerli.[4] Their work was performed using liquid hydrogen as the refrigerant and observation was without a phosphorescope. The authors report twenty-nine sharp bands in the spectrum of *o*-xylene beginning at 28 242 cm^{-1}. The analysis of the *o*-xylene spectrum by Pesteil and Zmerli was done in analogy to that proposed by them for the triplet-singlet emission of benzene in the same paper. They consider that since the ${}^1A_{1g}-{}^3B_{2u}$ benzene transition is forbidden by symmetry and spin multiplicity, the 0,0 band should not be observed. Consequently they interpret the first band as the combination of the 992 and the 606 cm^{-1} frequencies to give a 1606 cm^{-1} vibration of e_{2g} symmetry which makes the transition allowed. The stronger bands of the spectrum are built on this vibration while many of the weaker bands are assigned to, at best, rather awkward combinations. It should be added that the symmetry of the lowest triplet state in benzene is generally agreed to be B_{1u} rather than B_{2u}, which also gives a forbidden transition.

Many of the difficulties of their interpretation are resolved if we compare their results with the spectrum reported here. Their first band at 28 242 cm^{-1} is coincident with the first band of the "second" spectrum as reported in Table IV. In fact, we see that every strong band in their spectrum has been assigned here to the weak second spectrum. Similarly, except for the 0,0 band, the stronger bands of the first spectrum appear in their spectrum as weak ones. Clearly then what they have found is actually a superposition of two spectra, and this may, as suggested here, be evidence for two crystalline phases. It should be noted also that the 40 cm^{-1} interval is prominent in their spectrum.

In the "second" spectrum (II) frequencies 725, 1121, 1242, and 1591 cm^{-1} are found and these are seen to associate with the frequencies 740, 1119, 1247, and 1586 cm^{-1}, respectively, in the "first" spectrum (I). The frequencies 1051 and 1154 cm^{-1} in spectrum I have no counterparts in II.

A frequency of 200 cm^{-1} is found in the "first" and one of 221 cm^{-1} in the "second" spectrum. One of the difficulties in the analyses of the *o*-xylene spectra is that these frequencies have no corresponding lines in the Raman spectrum. Pesteil and Zmerli in their analysis tried to account for this fact by assigning a vibrational combination to this band as they had done for a 225 cm^{-1} separation in the benzene crystal spectrum. We have observed the same band in benzene at 4°K but it is discussed as a crystal vibration.[9] Consequently, the 200/221 is here also considered to be typical of the crystal. That it is different in spectrum I and spectrum II supports the assumption of two crystalline phases in *o*-xylene.

The lowest excited singlet state of point group C_{2v} is of A_1 symmetry. Therefore, the lowest triplet of *o*-xylene is a B_1 level and the triplet-singlet emission has a transition moment along the *y* axis. The transition ${}^3B_1 \rightarrow {}^1A_1$ is then allowed by symmetry but forbidden by spin multiplicity. The vibrational analyses of spectra I and II conform to these symmetry properties.

At the beginning of this investigation it was hoped that by eliminating any trace of oxygen in the samples used for these experiments, photooxidation could be avoided and that it would be possible to obtain spectra

[8] A. Kronenberger, Z. Physik **63**, 494 (1930).

[9] H. Sponer, Y. Kanda, and L. A. Blackwell, presented at the Symposium on Molecular Structure and Spectroscopy at Columbus, Ohio (June 11–15, 1956, to be published).

TABLE V. Phosphorescence spectrum of crystalline *m*-xylene at 4.2°K.

Wave number	Intensity	$\nu_0-\nu$	$\nu_0^*-\nu$	Assignment
28 301	s	0		0, 0
28 257	s	44		0−44
28 133	s	168		0−168
28 080		221	0	0−221 0*
27 920			160	0*−160
27 350			730	0*−730
27 060			1020	0*−998
26 500			1580	0*−1580
25 770			2310	0*−1580−730
25 470			2610	0*−1580−1020
25 081	s			impurity
24 984	s			impurity
24 890			3190	0*−1580×2
24 040			4040	0*−1580×2−730
23 379	s			impurity
23 295	s			impurity
23 280			4800	0*−1580×3
22 190			5890	0*−1580×3−1020
21 770			6310	0*−1580×4

of these crystals at 77°K uncontaminated by impurities. In the case of *o*-xylene, at least, only a limited success was realized. No detectable light was registered on photographic plates in spite of wide slit opening and long exposures. Nor was there any light observed visually from *o*-xylene crystals at 77°K. This leads to the conclusion that a nonradiative process becomes quite efficient at this temperature. This process could be one in which the excitation energy is used for a chemical rearrangement.

(b) *m*-Xylene

The triplet-single emission spectra of *m*-xylene were observed in the crystalline state at 4.2° and 77°K and in EPA at 77°K. The microphotometer tracing curves are shown in Fig. 2 and the spectral data are listed in Tables II, and V–VII. The general spectral appearance of *m*-xylene in EPA is similar to that of the other isomers although the bands seem to be somewhat broader and not as well resolved as either in the ortho or para compound. There are three prominent vibrational frequencies built on the 0,0 band at 28 120 cm^{-1}. Three members of the 1570 cm^{-1} frequency forming the main progression may be seen. This vibrational interval is assigned to the totally symmetric Raman frequency at 1592 cm^{-1}. A separation of 690 cm^{-1} may be barely resolved and is assigned to the Raman line at 724 cm^{-1} (a_1). A separation of 920 cm^{-1} appears in combination with the 0,0 band and with the 1570 cm^{-1} frequency throughout the spectrum. Dikun and Sveshnikov[9] assigned it to the 945 cm^{-1} (b_1) vibration. Although this is a possible interpretation, we have correlated the 920 with the strong Raman line of 998 cm^{-1} since this vibration is present in the crystal spectrum at 4°K (Table V).

It was hoped that a sharp crystal spectrum would remove some of the doubt connected with these assignments. Actually the spectrum of the crystal was only slightly better resolved than the EPA spectrum, but in general it confirmed the assignments made in the foregoing. The *m*-xylene crystal spectrum at 4.2°K shown in Fig. 2 is, in its over-all appearance, very much like the EPA spectrum. This is one of the few compounds studied in this laboratory which have given a crystal spectrum predominantly composed of broad bands.[10] The suspicion, therefore, arose that the spectrum represented the amorphous phase of this substance rather than the crystalline. Every care was exercised in the growing of these crystals to avoid supercooling of the sample. The conditions of crystalli-

TABLE VI. Phosphorescence spectrum of crystalline *m*-xylene at 77°K.

Wave number	Relative intensity	$\nu_0-\nu$	Assignment
24 960	3	0	0, 0
24 680	2	280	0−280
23 880	4	1080	0−1080
23 330	6	1630	0−1630
23 000	5	1960	0−1630−280
22 270	6	2690	0−1630−1080
21 710	7	3270	0−1630×2
21 350	6	3610	0−1630×2−280

TABLE VII. Impurity bands in the phosphorescence spectrum of *m*-xylene at 4.2°K.

Wave number	Relative intensity	$\nu_0-\nu$	$\nu_0^*-\nu$	Assignment
25 081		0		0, 0
24 984			0	0*, 0
23 379		1702		0, 1702
23 295			1689	0*−1689

[10] It is of interest that the vapor spectrum of *m*-xylene has also broad bands in absorption [C. D. Cooper and H. Sponer, J. Chem. Phys. **20**, 1248 (1952)] and in fluorescence [V. Ramakrishna Rao and Mantrala L. N. Sastri, J. Chem. Phys. **20**, 1552 (1952)]. The diffuseness was ascribed partly to internal rotation of the CH_3 groups.

TABLE VIII. Phosphorescence spectrum (b) from crystalline *p*-xylene at 4.2°K.

Wave number	Relative intensity	$\nu_0-\nu$	Assignment
25 254	10	0	0, 0
25 196	3	58	0−58
25 158	1	96	0−96
25 122	4	132	0−132
25 044	8	210	0−210
24 993	1	261	0−210−58
24 960	2	294	0−294
24 914	2	340	0−340
24 842	5	412	0−412
			0−210×2
24 773	2	481	0−481
24 709	1	545	0−340−210
24 648	2	606	0−606
			0−210×3
24 556	6	698	0−698
24 501	2	753	0−753
24 451	6	803	0−412×2
24 413	4	841	0−841
24 312	4	942	0−606−340
24 257	9	997	0−997
24 206	2	1048	0−1048
			0−997−58
24 083	8	1171	0−1171
24 040	4	1214	0−1214
23 996	1	1258	0−841−412
			0−1171−96
23 949	2	1305	0−1305
23 869	3	1385	0−1385
23 833	1	1421	0−1421
23 747	2	1507	0−1507
23 649	9	1605	0−1605
23 538	9	1716	0−1716
23 489	1	1765	0−1716−58
23 446	1	1808	0−1716−96
23 410	4	1844	0−1716−132
23 332	5	1922	0−1716−210
23 261	3	1993	0−1716−210−58
23 207	1	2047	0−1716−340
23 128	3	2126	0−1716−412
23 090	2	2164	
23 061	2	2193	0−1716−481
22 916	1	2338	0−1605−740
22 838	3	2416	0−1716−698
22 729	3	2525	0−1716−412×2
22 694	1	2560	0−1716−841
22 654	2	2600	0−1605−997
			0−1305×2
22 591	1	2663	0−1605−1048
			0−1716−340−606
22 543	6	2711	0−1716−997
22 481	2	2773	0−1716−1048
22 369	4	2885	0−1716−1171
22 338	1	2916	0−1716−1214
22 269	1	2985	0−1605−1385
22 169	1	3085	0−1716−1385
22 041	1	3213	0−1605×2
21 933	5	3321	0−1716−1605
21 851	7	3403	0−1716×2
21 734	2	3520	0−1716−1605−210
21 595	2	3659	0−1716−1605−340
21 562	1	3692	0−1716×2−294
21 442	1	3812	0−1716×2−412
21 371	1	3883	0−1716×2−481
20 842	1	4412	0−1716×2−997

zation were varied within practical limits, but in all cases the spectrum was characterized by a diffuse system of bands. There are, however, three weak bands at the beginning of the spectrum which are sharp. The appearance of these sharp bands toward shorter wavelengths and the definite crystalline appearance of the sample suggest that they belong to the crystal and that the "amorphous spectrum" may have been sensitized by the crystalline phase. In the absorption spectra of *m*-xylene reported by Kronenberger[8] we find support for this conclusion. He photographed the spectrum of the amorphous and the crystalline state at −260°C. Only the absorption spectrum of the crystal at the lowest temperature was sharp.

As was mentioned, in emission there were found only three sharp and weak bands preceding the system of broad bands. Only these weak bands are here assigned to the crystal, so that actually two phases must be present in the solid. The first band of the sharp series appears at 38 301 cm^{-1} and may be seen in Fig. 2. The next two bands are found at a separation from the first of 44 cm^{-1} and of 168 cm^{-1}. The fourth band, the first of the diffuse system, is taken as the 0,0 band of that system (Table V). A three-member progression of 1580 cm^{-1} forms the backbone of the spectrum. A frequency interval of 730 cm^{-1} appears in combination with the first two members of this progression confirming the EPA assignment of this vibration to the 724 cm^{-1} Raman frequency. A separation of 1020 cm^{-1} appears in combination with the 0,0 band and with the first member, at least, of the 1580 cm^{-1} progression. This is 100 cm^{-1} removed from the 920 cm^{-1} interval found in the EPA spectrum but nevertheless is assigned to the 998 cm^{-1} (a_1) mode. It has been found that usually vibrations in the crystal are energetically higher because of the hindrance produced by lattice neighbors. This seems to be especially true for "breathing" type vibrations. A shift, therefore, of 20 cm^{-1} does not make the assignment untenable. According to Kanda and Shimada,[11] frequencies of 700, 995, and 1600 cm^{-1} were obtained in the phosphorescence spectrum of *m*-xylene in a matrix of cyclohexane. The spectrum was comparatively sharp and measurement was easy. It is obvious that the mentioned frequencies are to be assigned to the totally symmetrical vibrations of 724, 998, and 1592 cm^{-1}, respectively. Since the structure of *m*-xylene belongs to point group C_{2v}, the lowest triplet has A_1 symmetry and the transition $^3A_1 \rightarrow {}^1A_1$ of *m*-xylene is allowed by symmetry but forbidden by spin multiplicity. The transition moment is along the *y* axis.

In addition to the sharp bands at the beginning of the spectrum there are two sharp doublets lying toward longer wavelengths and beginning around 25 000

[11] Y. Kanda and R. Shimada (to be published).

cm^{-1}. These bands can not be made to fit in any reasonable way into the analysis of the diffuse system nor can they be combined with the three sharp bands at the beginning at 28 301 cm^{-1}. Considering the most recent results in toluene,[6] a spectrum in this region suggests that an $n-\pi$ transition may be involved. This suspicion was confirmed when the separation between the first bands of each doublet was measured and found to be 1702 cm^{-1} as shown in Table VII. This frequency is nearly always associated with the stretching vibration of the carbonyl group. In most cases where it has been observed it was associated with band systems found in benzaldehyde derivatives. If a comparison is made between these bands and the spectrum of *p*-xylene in Table VIII which will be shown to be due to an impurity of *p*-methylbenzaldehyde, a striking similarity is seen. The spectrum is shifted 173 cm^{-1} toward longer wavelength in the *m*-xylene with respect to *p*-xylene, but this shift is not unusually large for a solvent shift. In spite of the similarities between the two spectra, they are not identical. Therefore, it seems more reasonable to assign these bands to an impurity of *m*-methylbenzaldehyde. Because of the weakness of this system this assignment remains open to question.

Kronenberger[8] lists six bands in the phosphorescence spectrum of *m*-xylene at −260°C beginning with a band at 27 870 cm^{-1}. His results agree with the measurements given here within the limits of accuracy. Pesteil and Zmerli[4] obtained quite different results in their study of xylenes. They found a sharp spectrum consisting of sixteen bands in the ultraviolet between 31 660 and 29 760 cm^{-1}. No picture nor tracing is given but from the band intensities it appears that the first band is one of the weakest in the spectrum and the last is the strongest. This is unusual. No vibrational intervals characteristic of *m*-xylene could be found in the spectrum.

The spectrum obtained when *m*-xylene was photographed at 77°K is also shown in Fig. 2. A broad system of eight bands beginning at 24 960 cm^{-1} was observed and separations of 280, 1080, and 1630 cm^{-1} were measured as shown in Table VI. These values may be in error by as much as fifty wave numbers because of the broadness of these bands. There is a close resemblance of this spectrum in position and in structure to the spectrum of toluene at 77°K observed by Kanda and Sponer.[6] This spectrum was ascribed by them to a temperature-activated sensitization of a benzaldehyde impurity produced by photooxidation of the toluene. They found that from about 25°K on the low-temperature spectrum characteristic of toluene is quenched and a new spectrum appears. This spectrum shows the characteristic 1700 cm^{-1} separation which is associated with the carbonyl group. The spectrum obtained for *m*-xylene under similar conditions has an apparent lifetime of only a few tenths of a second compared with a lifetime of at least five seconds for the crystal at 4.2°K. Although the bands are so diffuse that an identification based on vibrational frequencies is impossible, the spectrum obtained here is considered to be that of *m*-methylbenzaldehyde.

Another possibility is suggested by an interesting idea put forth by Nauman.[12] He assumes that upon irradiation alkylbenzenes break down forming the benzal radical to which he attributes the diffuse spectra exhibited by these compounds at 77°K.

(c) *p*-Xylene

The triplet-singlet emission spectrum of *p*-xylene was investigated in the crystalline state at 4.2° and 77°K, and in EPA at 77°K. The microphotometer tracing curves of the spectra are shown in Figs. 3 and 4, and the spectral data are listed in Tables III, VIII, and IX. The spectrum of *p*-xylene in EPA extends from 3500 to 4500 A and consists of thirteen resolvable bands. The structure is very much like that of the other xylenes. Frequencies of 305, 830, 1180, and 1590 cm^{-1} are found and assigned to Raman frequencies of 313(b_{3g}), 826(a_g), 1182(a_g), and 1616(a_g). Dikun and Sveshnikov[3] reported frequencies of 322, 793, 1173, 1578, and 1616 cm^{-1}. Their analysis was complicated and had no analogy to the analyses for the other isomers, whereas the analysis shown in Table III is simple and is similar to the analyses of the EPA spectra of *o*- and *m*-xylenes. The frequency of 1590 cm^{-1} obtained in this experiment can not be ascribed to the b_{3g} vibration of 1575 cm^{-1} contrary to the assignment by Dikun and Sveshnikov, because the 1590 cm^{-1} progression has no appreciable intensity alternations.

The spectrum of *p*-xylene crystal at 4.2°K represented in Fig. 3 is entirely different from the EPA spectrum. Fifty-eight bands in all have been measured and are tabulated with the analysis in Table VIII. The fact that the spectrum is shifted from the EPA spectrum toward longer wavelengths by about 3000 cm^{-1} suggests that *p*-xylene is not the carrier of this spectrum. This hypothesis is strengthened when one compares the vibrational structure of the spectrum with that of the solution spectrum. Any attempt to analyze this spectrum in terms of fundamentals or combinations of *p*-xylene vibrations proves futile. The most prominent separation found in the spectrum is at 1716 cm^{-1}. This vibration occurs in a short progression built on the 0,0 band at 25 254 cm^{-1}. Its second member is found at 1687 cm^{-1} from the first. Because of the similarity to the spectrum of benzaldehyde found in toluene crystals by Kanda and Sponer,[6] it seemed reasonable to attempt an analysis based on the Raman data of *p*-methylbenzaldehyde which would, of course, be the principal product of the oxidation of *p*-xylene. It is remarkable that so many vibrational modes may be found in the spectrum. Frequencies of 210, 294, 340,

[12] S. S. Mims and R. V. Nauman, reported at the Southeastern Regional Meeting of the American Chemical Society, Durham, North Carolina (November, 1957).

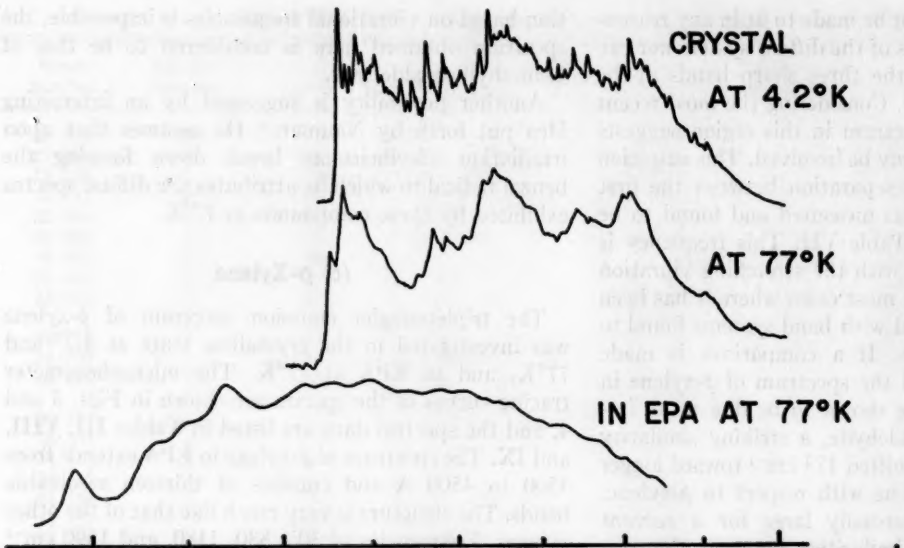

FIG. 3. Phosphorescence spectra of *p*-xylene in the crystalline state at 4.2° and 77°K (*p*-methylbenzaldehyde), and in EPA at 77°K.

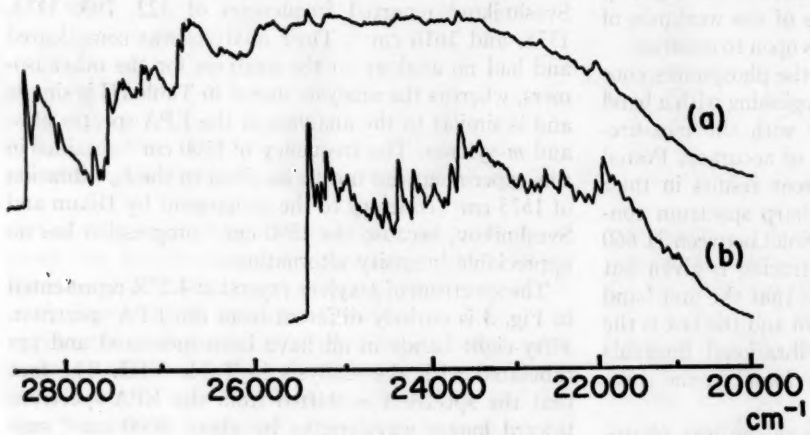

FIG. 4. Phosphorescence spectra of *p*-xylene and of *p*-methylbenzaldehyde in the crystalline state at 4.2°K.

412, 481, 606, 698, 753, 841, 997, 1048, 1171, 1214, 1305, 1385, 1507, 1605, and 1716 cm^{-1} in the phosphorescence spectrum are assigned to those of 220, 304, 347, 406, 470, 593, 700, 750, 840, 996, 1044, 1161, 1203, 1301, 1376, 1505, 1601, and 1689 cm^{-1}, respectively, in the Raman spectrum of *p*-methylbenzaldehyde.[13] Usually aldehyde spectra show predominantly the frequency connected with the carbonyl vibration in $n-\pi$ transitions because of the localized character of the nonbonding orbital.

The phosphorescence spectrum of the crystal at 77°K is pictured in the same figure. Although it is generally more diffuse than the 4°K spectrum, it is much sharper than the spectrum of *m*-xylene at this temperature. Kasha[14] has pointed out that while $n-\pi$ transitions give sharp spectra in the vapor that even in hydrocarbon solvents the solution spectra are extremely broad and show little vibrational structure owing to the strong perturbations of the nonbonding orbitals by the solvent. The possibility of complex formation involving hydrogen bonding has been considered as a factor contributing to this unusual behavior. This diffuse structure has been confirmed in this laboratory in the spectra of benzaldehyde in EPA and in the crystalline phase as well as when produced photochemically in toluene.[6] If we assume that the *p*-methylbenzaldehyde was not present initially, one explanation for the sharp spectrum of *p*-methylbenzaldehyde offered here is the possibility that in *p*-xylene we may have an example of a case of photooxidation by interstitial oxygen within the lattice giving a true mixed crystal of *p*-xylene and *p*-methylbenzaldehyde. If, in the case of the toluene phosphorescence reported by Kanda and Sponer, benzaldehyde had been present initially instead of being photochemically produced, it would find itself ran-

[13] Landolt-Börnstein, *Zahlenwerte und Funktionen* (Springer-Verlag, Berlin, 1951), Teil 2, S. 536.
[14] M. Kasha, Discussions Faraday Soc. 9, 14 (1950).

TABLE IX. Phosphorescence spectrum (a) of crystalline *p*-xylene at 4.2°K.

Wave number	Relative intensity	$\nu_0-\nu$	Assignment	Wave number	Relative intensity	$\nu_0-\nu$	Assignment
28 246	6	0	0, 0	26 664	6	1582	0−1582
28 188	4	58	0−58	26 624	7	1622	0−1622
28 149	5	97	0−97	26 592	7	1654	0−830×2
28 113	6	133	0−133	26 571	7	1675	0−1622−58
28 068	4	178	0−178	26 532	7	1714	0−1622−97
27 998	3	248	0−133×2	26 490	7	1756	0−1622−133
27 930	3	316	0−316	26 448	7	1798	0−1622−178
27 795	2	451	0−316−133	26 406	6	1840	0−1212−316×2
27 770	2	476	0−476				0−1212−639
27 667	1	579	0−316−133×2	26 348	6	1898	0−1212−690
27 607	2	639	0−316×2	26 308	6	1938	0−1622−316
			0−639	26 277	6	1969	0−830×2−316
27 556	1	690	0−690	26 228	6	2018	0−1190−830
27 480	2	766	0−316×2−133	26 208	6	2038	0−1212−830
27 438	3	808	0−808	26 159	6	2087	0−1622−476
27 416	6	830	0−830	26 104	6	2142	0−830×2−316−178
27 367	4	879	0−830−58	26 028	6	2218	0−1212−830−178
27 318	4	928	0−830−97	25 987	6	2259	0−1622−639
27 277	4	969	0−830−133				0−1622−312×2
27 238	4	1008	0−830−178	25 907	6	2339	0−1212−830−312
27 207	4	1039		25 846	7	2400	0−1582−830
27 100	4	1146	0−830−316	25 806	7	2440	0−1622−830
27 056	5	1190	0−1190	25 716	7	2530	0−1582−830−133
27 034	5	1212	0−1212	25 667	7	2579	0−1622−830−133
26 961	4	1285	0−1190−97	25 614	7	2632	0−1582−830−133×2
26 922	5	1324	0−1190−134	25 585	7	2661	0−1622−830−133×2
26 860	4	1386	0−1212−178	25 441	7	2805	0−1622−1190
26 778	4	1468	0−830−316×2	25 419	7	2827	0−1622×2
26 723	4	1523	0−1212−316				

domly oriented in the toluene lattice and produce a somewhat broadened spectrum because of nonuniform interactions with the lattice.

Since the spectrum of *p*-methylbenzaldehyde quenches so completely the emission of *p*-xylene, though ostensibly present to no more than a few parts per million, the efficiency of the sensitization process appears to be quite high.

Kronenberger[8] obtained eighteen bands in the spectrum of *p*-xylene at −260°C beginning at 25 240 cm^{-1} and extending to 17 630 cm^{-1}. This spectrum appears to contain an impurity responsible for the longer wavelength portion of the spectrum as also in the case of *o*-xylene since several of the long wavelength bands coincide in both spectra. A few vibrational separations may be found in this spectrum which match those in the spectrum of *p*-methylbenzaldehyde reported here, and it is quite probable that the spectra are the same.

At the beginning of this investigation we used samples of *p*-xylene crystallized by freezing. No genuine spectrum of *p*-xylene crystal was obtained but that of *p*-methylbenzaldehyde was observed. However, the *p*-xylene spectrum did appear when we introduced helium gas into the phosphorescence cell. The spectrum labeled (a) in Fig. 4 was thus obtained after the spectrum (b) in the same figure came out as the result of incomplete cooling. It is seen in the figure that the spectrum (a) consists of two regions, i.e., between 28 246 and 25 419 cm^{-1} and between 25 254 and 20 842 cm^{-1}. The latter is idential with that of the spectrum (b) due to *p*-methylbenzaldehyde. In other words, spectrum (a) is the superposition of the spectrum of *p*-xylene crystal and that of *p*-methylbenzaldehyde in *p*-xylene crystal.

The band at 28 246 cm^{-1} is assigned to the 0,0 band of the spectrum of *p*-xylene crystal. The separations at 58, 97, and 178 cm^{-1} from the 0,0 band are ascribed to lattice vibrations although no Raman data of *p*-xylene crystal have been reported. A frequency of 133 cm^{-1} is seen to form progressions and may also be assigned to a lattice vibration. However, the 133 cm^{-1} band is comparatively strong in intensity and it acts in the progressions as a totally symmetrical vibration. It is tentatively assumed that the frequency 133 cm^{-1} occurs in the spectrum of *p*-xylene crystal at low temperature in analogy to the 226 cm^{-1} band of benzene crystal and the 200 and 221 cm^{-1} bands of *o*-xylene crystal. The prominent band at 830 cm^{-1} from the 0,0 band is attributed to the strong symmetric Raman vibration 826 cm^{-1}. It is found in overtones and frequently in combination bands. The bands at separations 476, 1190, 1212, and 1622 cm^{-1} from the 0,0 band are assigned to the totally symmetrical vibrations 460, 1182, 1204, and 1616 cm^{-1}, respectively. The frequency 1622 cm^{-1} is seen to represent the principal vibration of the spectrum although it is somewhat concealed by the superposition of the spectrum of *p*-methylbenzaldehyde from 25 254 cm^{-1} to lower wave numbers. The bands at 316, 639, 690, 808, and 1582 cm^{-1} from the 0,0 band are attributed to the Raman

frequencies of 313(b_{3g}), 313×2(a_g), or 644(b_{3g}), 697(b_{2g}), 811(b_{1g}), and 1575(b_{3g}), respectively. These bands have weak intensity compared with bands of a_g symmetry. The frequency 1582 cm^{-1} does not form a progression and this agrees with the interpretation given to the EPA spectrum of *p*-xylene. According to Kanda and Shimada,[11] frequencies of 815, 1180, and 1595 cm^{-1} were found in the phosphorescence spectrum of *p*-xylene in the matrix of cyclohexane. This spectrum was fairly sharp and its measurement was easy. The mentioned frequencies were assigned to the totally symmetrical vibrations of 826, 1182, and 1616 cm^{-1}, respectively. A frequency of 305 cm^{-1} was interpreted as a b_{3g} vibration (313 cm^{-1}), but it was not well resolved from the 0,0 band at 28 135 cm^{-1}.

Pesteil and Zmerli[4] reported that the spectrum of *p*-xylene crystal at 20°K extended from 27 422 to 25 843 cm^{-1}. If we compare their $\Delta\tilde{\nu}$ values, taken from their shortest wavelength band at 27 422 cm^{-1}, with those shown in Table IX, it may be assumed that the frequencies of 123, 311, 640, 1181, 1224, and 1579 cm^{-1} in their spectrum correspond to those of 133, 316, 639, 1190, 1212, and 1582 cm^{-1} in our spectrum, respectively. This could suggest that the two spectra belong to two different crystal phases. The magnitude of the shift is too large, however. Moreover, we should mention that in our experiments with *p*-xylene crystals no bands were found between 27 500 and 25 800 cm^{-1} above 4°K. We think, therefore, that the bands observed by Pesteil and Zmerli must be of different origin.

ACKNOWLEDGMENTS

The authors would like to acknowledge stimulating discussions with other members of the spectroscopy group of the Duke Physics Department. Special thanks are also due William Fairbank and the members of the low-temperature physics group both for the supply of liquid helium and for their valuable assistance and advice. One of the authors (L.A.B.) is grateful to the Du Pont Company for support through the Du Pont Teaching Assistantship for one year.

Thermal Decomposition of Niobium and Tantalum Monocarbides

CHARLES P. KEMPTER AND M. R. NADLER

University of California, Los Alamos Scientific Laboratory, Los Alamos, New Mexico

(Received October 29, 1959)

The thermal decomposition of polycrystalline NbC was investigated from 2000° to 3200°C, and TaC from 1890° to 3320°C in the presence of one atmosphere of helium. It was found that both compounds lose carbon preferentially, and that the final carbon/metal molar ratio obtained may be represented by an equation of the form $C/M=A-B\exp(\lambda t)$, where t is the maximum temperature of heating for a constant time (30 min in both cases). Similarly the resultant lattice constant may be expressed as $a_0=A'-B'\exp(\lambda' t)$, where a_0 is in A at 25°C. For a maximum temperature of 3000°C and heating times of 30 min to 12 hr, $a_0=4.459084+0.0093071\exp(-0.18916\,\tau)$ for NbC, where τ is the time in hours. It was found that $a_0=4.414712+0.056862$ (C/Nb) for the C/Nb range 0.885 to 0.981 and that $a_0=4.385779+0.070204$ (C/Ta) for the C/Ta range 0.906 to 0.996. By extrapolation, the lattice constants of stoichiometric NbC and TaC should be 4.47157±0.00012 A at 25°C and 4.45598±0.00038 A at 25°C, respectively.

IT is well known that the transition metal carbides exhibit varying ranges of homogeneity.[1] The homogeneity ranges for NbC and TaC were most recently investigated by Brauer and Lesser[2,3] who reported a C/Nb molar ratio range of 0.70 to 0.91 and C/Ta range of 0.74 to 1.00. The crystal structure of NbC was first reported by Becker and Ebert,[4] and by van Arkel[5] for TaC, who found a NaCl-type structure for both compounds. As the amount of carbon decreases in the cubic lattices, the lattice constants decrease accordingly. Thus, in speaking of the properties of "niobium or tantalum monocarbides" such as lattice constant, density, and free energy of formation, one must define the composition of the materials. If stoichiometric NbC or TaC exist, they are only special cases of the NbC or TaC phases. Robbins[6] reported that the maximum C/Ta ratio which can exist is 0.96. No studies of the thermal decomposition of NbC could be found in the literature; however, Storms and Krikorian[7] recently studied the variation of lattice parameter with C/Nb molar ratio for NbC. These investigators prepared their specimens by combination of the elements *in vacuo*. Hoch[8] and co-workers have measured the vapor pressure of carbon over TaC from 1962° to 2492°C.

In view of the foregoing considerations, it was decided to investigate the thermal stability of NbC and TaC and to correlate the temperatures and times used with the compositions and lattice constants obtained.

EXPERIMENTAL

The NbC and TaC used in this investigation were Fansteel Metallurgical Corporation high purity columbium carbide powder and standard grade tantalum carbide. The spectrographic analysis results (based on the sample as Nb_2O_5 and Ta_2O_5 are shown in Tables I and II.

The chemical analyses are shown in Tables III and IV. The metals and total carbon were determined by combustion and the free carbon and nitrogen by chemical methods.[9] The amount of oxygen reported is that extracted at 2000°C.

If one assumes that all of the Nb or Ta is combined with the total C minus the free C, the resultant empirical formulas are $NbC_{0.9698}$ and $TaC_{0.9548}$. Examination by the x-ray powder camera technique showed only lines of well-crystallized cubic NbC and TaC.

The specimens for thermal decomposition studies were prepared by pressing the material into cylinders at 10 000 psi without binder. The NbC cylinders were $\frac{5}{8}$ in. in diam by $\frac{7}{32}$ in. high and weighed 7.0 g, and the TaC cylinders were $\frac{5}{8}$ in. in diam by $\frac{29}{64}$ in. high and weighed 17.0 g. Two holes 0.043 in. in diam and $\frac{1}{8}$ in. in depth, one in the center and the other near the edge of the cylinder top, were drilled for temperature measurements. All specimens were inductively heated in one atmosphere of helium by means of a Lepel 20-kw radio-frequency induction heater, and were supported on NbC and TaC cylinders, respectively. The cylindrical concentrator was $\frac{3}{4}$ in. in diameter and $\frac{3}{4}$ in. high. An analysis of the helium gas used showed less than 10 ppm water and less than 5 ppm oxygen. The temperature was read with an optical pyrometer in both sight holes, and the average of these two readings was corrected for absorption of a window and prism.

After a specimen had cooled, it was pulverized in a Plattner mortar to −100 mesh, cleaned of possible steel

[1] P. Schwarzkopf and R. Kieffer, *Refractory Hard Metals* (The Macmillan Company, New York, 1953).
[2] G. Brauer and R. Lesser, Z. Metallkunde **50**, 8 (1959).
[3] R. Lesser and G. Brauer, Z. Metallkunde **49**, 622 (1958).
[4] K. Becker and F. Ebert, Z. Physik **31**, 268 (1925).
[5] A. E. van Arkel, Physica **4**, 286 (1924).
[6] D. A. Robbins, *The Physical Chemistry of Metallic Solutions and Intermetallic Compounds*, Paper 7B (Her Majesty's Stationery Office, London, 1959).
[7] E. K. Storms and N. H. Krikorian, J. Phys. Chem. **63**, 1747 (1959).
[8] M. Hoch, P. E. Blackburn, D. P. Dingledy, and H. L. Johnston, J. Phys. Chem. **59**, 97 (1955).
[9] O. H. Kriege, Los Alamos Scientific Laboratory Report LA-2306 (March, 1959).

TABLE I. Spectrographic analysis results for NbC.

Composition ppm	Elements
Major	Nb
<500	Zn
<100	Ti, Mo
<50	V
30	Al
<30	K, Sr
20	B, Ba
<20	Co, Sn, Bi
10	Si, Cr, Fe, Cu
<10	Ni, Pb
5 or less	Li, Be, Na, Mg, Ca, Mn, Ag

(mortar fragment) contamination with a magnet, and thoroughly mixed with a spatula. A very small −325 mesh sample was taken for x-ray examination and the remainder was analyzed for niobium or tantalum, total carbon, and free carbon.[9] All x-ray diffraction studies were carried out on a Norelco unit using cobalt radiation (iron filtered) and the sample temperature controlled at 25.0±0.5°C. The use of a cobalt target gave high angle diffraction lines for subsequent precision lattice constant calculations. For each specimen, a 114.59-mm diam Debye-Scherrer camera was used for phase identification, and a 120-mm symmetrical back-reflection focusing camera was used for the lattice constant determination. Only the inner emulsion of the back-reflection films was used and the shrinkage was measured by reference to six pairs of fiducial marks. The films were measured at constant temperature by three different readers. The lattice constants were determined from the (331), (420), and (422) $K\alpha_1$ and $K\alpha_2$ lines, assuming the systematic errors in $\Delta a_0/a_0$ directly proportional to $\phi \tan\phi$ (where a_0 is the "true" lattice constant uncorrected for refraction, and ϕ is the complement of the Bragg angle). These constants and their standard deviations were calculated on an IBM 704 computer using the method of Vogel and Kempter.[10] All the lattice constants in this paper

TABLE II. Spectrographic analysis results for TaC.

Composition ppm	Elements
Major	Ta
<3000	W
1000	Nb
<300	Zn
200	Fe
100	Ti, Zr
60	Si
50	Mo
<50	Co, Ni
30	Al
<30	K, V, Sr, Sn, Pb, Bi
10	Na, Ca, Cr, Mn
<10	B, Ag, Ba
5 or less	Li, Be, Mg, Cu

[10] R. E. Vogel and C. P. Kempter, Los Alamos Scientific Laboratory Report LA-2317 (April, 1959).

TABLE III. Chemical analysis results for NbC.

Composition wt %	Element
88.22	Nb
11.22	Total C
0.16	Free C
0.25	N
0.28	O

were corrected for refraction in Co$K\alpha$ radiation by adding 0.000135 A for NbC, and 0.000228 A for TaC to the IBM 704 result.

RESULTS AND DISCUSSION

The combined analytical and x-ray results for NbC and TaC cylinders heated for 30 min at maximum temperatures of 1890° to 3320°C are shown in Tables V and VI, in comparison with the results on the unheated material. The wt % carbon reported is total carbon; free carbon was not detectable in any of the heated samples. The Debye-Scherrer films showed only the lines of NbC and TaC. Temperatures were measured with a Pyro microoptical pyrometer or, where noted in Table VI, by a Leeds and Northrup optical pyrometer. Both instruments had been checked against an NBS-calibrated Leeds and Northrup optical pyrometer.

From these data, it can be seen that the carbon/metal molar ratio and the lattice constant generally decrease with increasing temperature of heat treatment. The lattice constant is of course the much more precise measurement; however, it is sensitive to the oxygen and nitrogen present in the unheated material.

The plots of C/Nb, C/Ta, and of the NbC and TaC lattice constants vs maximum temperature of heating (30 min at temperature) all have the appearance of exponential decay curves. The equations of the curves were determined on an IBM 704 computer by the iterative least squares technique of Moore and Zeigler.[11] The equations were:

For NbC:

$$C/Nb = 0.9614 - 4.024\times10^{-8}\exp(0.004521t) \quad (1)$$

$$a_0 = 4.469377 - 1.577\times10^{-9}\exp(0.004643t); \quad (2)$$

TABLE IV. Chemical analysis results for TaC

Composition wt %	Element
93.72	Ta
6.04	Total C
0.10	Free C
0.07	N
0.18	O

[11] R. H. Moore and R. K. Zeigler, Trans. Am. Nuclear Soc. **1** [2], 128 (1958).

TABLE V. Analytical and x-ray results on NbC for 30-min specimens.

Maximum temp. of heating, °C	Wt % Nb	Wt % C	Total Nb+C	C/Nb Molar ratio	Lattice constant A, at 25°C
Not heated	88.22	11.22	99.44	0.970	4.47023±0.00005
2000	88.91	11.07	99.98	0.963	4.46933±0.00003
2200	88.96	11.01	99.97	0.957	4.46928±0.00003
2400	88.96	11.02	99.98	0.958	4.46925±0.00004
2600	89.00	11.00	100.00	0.956	4.46916±0.00003
2800	88.96	11.00	99.96	0.956	4.46883±0.00003
3000	89.30	10.68	99.98	0.925	4.46748±0.00007
3200	89.72	10.26	99.98	0.885	4.46494±0.00012[a]

[a] (422) $K\alpha_2$ line not readable.

TABLE VI. Analytical and x-ray results on TaC for 30-min specimens.

Maximum temp. of heating, °C	Wt % Ta	Wt % C	Total Ta+C	C/Ta Molar ratio	Lattice constant A, at 25°C
Not heated	93.72	6.04	99.76	0.955	4.45568±0.00002
1890	94.04	5.93	99.97	0.950	4.45214±0.00002
1950	94.06	5.94	100.00	0.951	4.45209±0.00003
2115	94.07	5.94	100.01	0.951	4.45225±0.00004
2270	94.03	5.94	99.97	0.952	4.45210±0.00002
2525	94.04	5.93	99.97	0.950	4.45222±0.00003
2715	94.05	5.92	99.97	0.948	4.45219±0.00003
2900[a]	94.08	5.85	99.93	0.937	4.45172±0.00004
3100[b]	94.30± 0.08	5.81± 0.09	100.11	0.928± 0.015	4.45139
3320[a]	94.48	5.68	100.16	0.906	4.44910±0.00005

[a] Last three readings with a cross-calibrated L and N pyrometer.
[b] Average results for two specimens heated at 3100°C; the two lattice constant values were 4.45133±0.00006 A and 4.45145±0.00005 A.
[c] (422) $K\alpha_2$ line not readable.

TABLE VII. Analytical and x-ray results on NbC for 3000°C specimens.

Heating time at 3000°C	Wt % Nb	Wt % C	Total Nb+C	C/Nb molar ratio	Lattice constant A, at 25°C
0 hr 30 min	89.30	10.68	99.98	0.925	4.46748±0.00007[a]
2 0	89.43	10.56	99.99	0.913	4.46580±0.00009
4 0	89.65	10.31	99.96	0.890	4.46292±0.00006
8 0	90.24	9.81	100.05	0.841	4.46159±0.00017
12 0	90.13	9.82	99.95	0.843	4.45985±0.00026

[a] (422) $K\alpha_2$ line readable only for this specimen.

TABLE VIII. Analytical and x-ray results on TaC for 3000°C specimens.

Heating time at 3000°C	Wt % Ta	Wt % C	Total Ta+C	C/Ta molar ratio	Lattice constant[a] A, at 25°C
2 hr 0 min	94.22	5.83	100.05	0.932	4.45121±0.00004
4 0	94.38	5.66	100.04	0.903	4.45069±0.00007
8 0	94.38	5.65	100.03	0.902	4.44858±0.00013

[a] (422) $K\alpha_2$ line not readable.

TABLE IX. Data for high C/Nb molar ratio specimens.

Starting material								
Wt NbC (g)	Wt C (g)	Heating time, (hr)	Wt % Nb	Wt % C	Total Nb+C	Wt % Free C	C/Nb Molar ratio	Lattice constant A, at 25°C
7.000	0.112	4.0	86.98	12.98	99.96	1.95	0.981	4.47031±0.00004
7.000	0.112	0.5	87.44	12.49	99.93	1.46	0.976	4.47040±0.00003

TABLE X. Data for high C/Ta molar ratio specimens.

Starting material								
Wt TaC (g)	Wt C (g)	Heating time, (hr)	Wt % Ta	Wt % C	Total Ta+C	Wt % Free C	C/Ta Molar ratio	Lattice constant A, at 25°C
17.00	0.288	0.5	92.36	7.63	99.99	1.53	0.995	4.45585±0.00002
17.00	0.192	0.5	92.98	7.01	99.99	0.95	0.982	4.45584±0.00003
17.00	0.096	0.5	93.44	6.54	99.98	0.36	0.996	4.45555±0.00003

For TaC:

$$C/Ta = 0.9525 - 1.693\times10^{-6}\exp(0.003081t) \quad (3)$$

$$a_0 = 4.452166 - 1.1004\times10^{-11}\exp(0.005856t). \quad (4)$$

These equations fit the data very well, but it must be emphasized that their validity applies only to the range and conditions specified. Further investigations will determine whether or not an exponential decay curve has general applicability to the thermal decomposition of nonstoichiometric binary systems such as Nb—C and Ta—C. The effect of time on thermal stability was next investigated for a constant maximum heating temperature—3000°C. Temperature measurements were made with a Leeds and Northrup optical pyrometer which had been checked against an NBS-calibrated L and N pyrometer. The combined analytical and x-ray results for these specimens are shown in Tables VII and VIII in comparison with the previous 30 min results. Free carbon was not detectable in any of these samples. The Debye-Scherrer films showed only the lines of NbC and TaC.

From these data, it can be seen that the carbon-to-metal molar ratio and the lattice constant generally decrease with increasing time. The plot of lattice constant vs time for NbC (at 3000°C) is shown in Fig. 1. Again, the equation of the curve was determined on an IBM 704 computer by an iterative least squares technique.[11]

The equation obtained was

$$a_0 = 4.459084 + 0.0093071\exp(-0.18916\tau) \quad (5)$$

where τ is in hours and 4.459084 A is the asymptote.

In order to correlate carbon-to-metal molar ratios with the precision lattice constants, it was decided also to prepare NbC and TaC specimens with high carbon-to-metal ratios, thus obviating long extrapolations to the lattice constants corresponding to the stoichiometric compounds. For each carbide, the specimens were prepared by heating mixtures of the starting material and spectro grade graphite at ca 2500°C. The mixtures were pressed into cylinders as previously described and inductively heated in one atmosphere of helium. The specimen descriptions and results are shown in Tables IX and X. The Debye-Scherrer films showed only the lines of NbC and TaC.

The plot of lattice constant vs carbon-to-metal molar ratios for these specimens plus the heated specimens of Tables V and VI are shown in Figs. 2 and 3. The data for the specimens in Tables VII and VIII heated longer than 30 min were not plotted because of the diffuseness of the lines; the (422) $K\alpha_2$ line was not readable on these films. The data of Brauer and Lesser[2,3] and of Robbins[6] for carbon-to-metal ratios in the same range are shown for comparison. It should be noted that the former investigators calculated (total C)/M ratios.

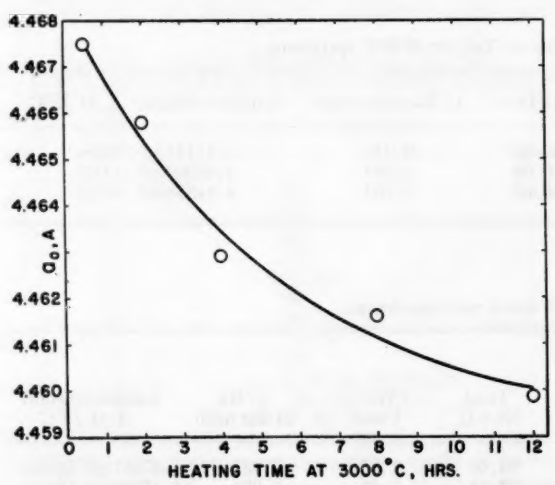

FIG. 1. NbC lattice constant vs heating time at 3000°C.

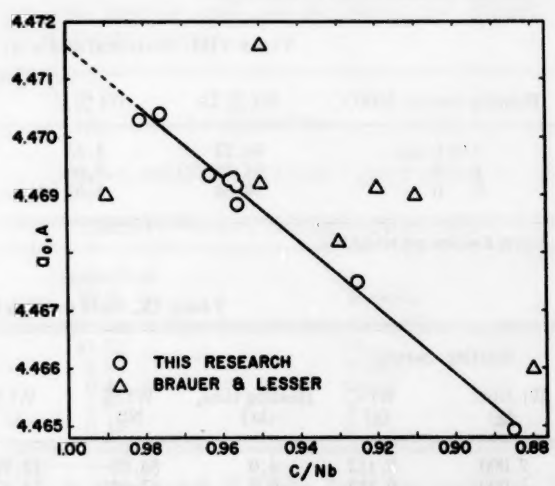

FIG. 2. NbC lattice constant vs C/Nb molar ratio.

The IBM 704 least squares equations obtained were

$$a_0 = 4.414712 + 0.056862\ (C/Nb) \quad (6)$$

and

$$a_0 = 4.385779 + 0.070204\ (C/Ta). \quad (7)$$

The standard deviation of the fit (sigma) was 1.78×10^{-4} for NbC and 6.45×10^{-4} for TaC. These linear fits were selected because their standard deviations were slightly lower than for quadratic or cubic polynomial fits. Attempts to fit a quadratic curve maximizing at C/M=1 resulted in larger standard deviations. It should be noted that the foregoing equations are empirical fits for high C/M ratios. It is not known at this time whether one or more theoretical functions are needed to express the relationship for the entire phase range. Thus if one could prepare stoichiometric compounds, the lattice constants at 25°C should be 4.47157±0.00012 A for NbC and 4.45598±0.00038 A for TaC. Therefore, the theoretical densities are 7.793 g/cc and 14.483 g/cc and the metal-carbon bond distances for coordination number 6 are 2.2358 A and 2.2280 A for NbC and TaC, respectively.

Equations (6) and (7) may be rewritten in terms of carbon-to-metal ratios to give

$$C/Nb = 17.5864 a_0 - 77.6391 \quad (8)$$

and

$$C/Ta = 14.2443 a_0 - 62.4724. \quad (9)$$

It should be noted that the summations of metal plus carbon for all the heated samples are nearly equal to 100%. The arithmetic means of these summations are 99.98% and 100.01% for the NbC and TaC specimens, respectively. Although the size of the heated samples did not permit determination of oxygen and nitrogen, these data indicate that the level of such impurities was very low.

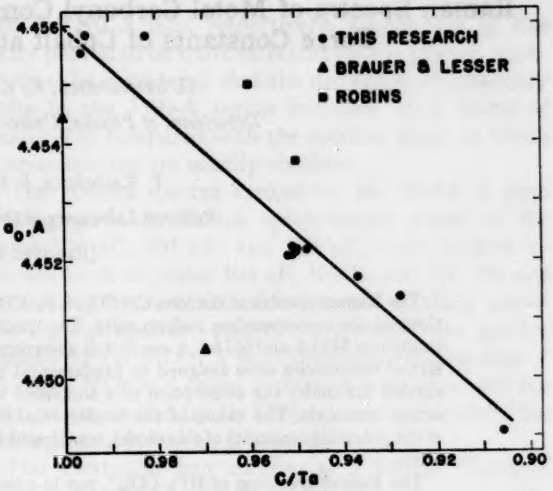

FIG. 3. TaC lattice constant vs C/Ta molar ratio.

ACKNOWLEDGMENTS

The authors are especially grateful to R. H. Moore for his advice on the application of the iterative least squares technique. Also they wish to thank R. E. Vogel and Dorothy L. Cooper for their assistance with the IBM 704 calculations, O. H. Kriege, E. Van Kooten, G. C. Heasley, O. R. Simi, and L. A. Gritzo for their analytical assistance and D. D. Crecelius for his film reading assistance.

Raman Spectra of Metal Carbonyl Compounds. II. Raman Spectra, Structure, and Force Constants of Cobalt and Iron Tetracarbonylate Anions

H. STAMMREICH, K. KAWAI,* AND YARA TAVARES

Department of Physics, University of São Paulo, São Paulo, Brazil

AND

P. KRUMHOLZ, J. BEHMOIRAS, AND S. BRIL

Research Laboratory of Orquima S.A., São Paulo, Brazil

(Received October 6, 1959)

The Raman spectra of the ions $Co(CO)_4^-$, $Fe(CO)_4^{2-}$, and $HFe(CO)_4^-$ have been studied in aqueous solutions of the corresponding sodium salts. The spectra of $Co(CO)_4^-$ and $Fe(CO)_4^{2-}$, excited by the helium radiations 5875.6 and 6678.1 A are in full agreement with the expected T_d symmetry of these ions; all observed frequencies were assigned to fundamental vibrational modes. A normal coordinate treatment was carried out under the assumption of a simplified valence force field model making use of only two interaction constants. The values of the fundamental frequencies of the tetrahedral ions, calculated by means of the potential constants of this model, were found to be in satisfactory agreement with the observed Raman shifts.

The Raman spectrum of $HFe(CO)_4^-$, put in correlation with that of $Fe(CO)_4^{2-}$, points strongly to a C_{3v} symmetry of the former ion.

INTRODUCTION

THE present paper deals with the Raman spectra of the tetracarbonylate anions $Co(CO)_4^-$, $Fe(CO)_4^{2-}$, and $HFe(CO)_4^-$. It seems that no vibrational spectral data on the iron carbonylate ions have been reported previously; an investigation of the ir absorption spectrum of the cobalt carbonylate ion has been carried out by Friedel *et al.*[1] using a solution of dicobalt octacarbonyl in pyridine where the $(Co(Pyr)_6)^{2+}$ cation and $Co(CO)_4^-$ anion are formed. Only two absorption bands were found, namely, 555 and 1883 cm^{-1}, the latter being assigned to a carbonyl stretching mode. A systematic investigation of the position of the infrared-active C–O stretching vibrations of various cobalt carbonyl derivatives has been reported by Vohler[2] who observed in all compounds containing the $Co(CO)_4^-$ anion an absorption band at approximately 1900 cm^{-1}, whereas the corresponding frequencies of the nonionic species were found between 2000 and 2100 cm^{-1}.

An additional interest of the present study is provided by the fact that $Co(CO)_4^-$ and $Fe(CO)_4^{2-}$ are isoelectronic with nickel tetracarbonyl, whereas $HFe(CO)_4^-$ is isoelectronic with cobalt hydrocarbonyl. The vibrational spectra of these neutral molecules have been the object of numerous investigations, especially in the ir, but until now the interpretation of the experimental results proved to be difficult and not thoroughly satisfactory. Because of the selection rules governing the activities of the vibrational modes of tetrahedral molecules belonging to the T_d point group, it is expected to obtain more direct information from Raman than from ir spectra. Hence, the results here reported may possibly contribute toward a fuller understanding of the vibrational spectra of nickel carbonyl and cobalt hydrocarbonyl and, eventually, to the elucidation of some questions concerning the chemical bonding in these molecules.

EXPERIMENTAL

Preparation of Samples

Aqueous solutions of the sodium salts of metal carbonyl hydrides were prepared by making use of a technique previously described by one of us and Stettiner.[3] All operations had to be performed under nitrogen absolutely free from oxygen and, owing to the photosensitivity of the compounds, especially of $NaHFe(CO)_4$, in dim red light. The Raman tubes were sealed beforehand to the apparatus and the solutions were filtered from the reaction vessel into the tubes through dense sintered glass filters at very low speed.

Sodium cobalt carbonylate $NaCo(CO)_4$ was prepared according to Hieber and co-workers[4,5] from $Hg(Co(CO)_4)_2$ and Na_2S. The mercury salt was purified and brought into a finely divided and reactive form by dissolving it in a tenfold quantity of methanol, and subsequent filtering and precipitating by addition of an equal amount of water. The purified mercury cobalt carbonylate was shaken during 12 hr with 10% less than the theoretical quantity of a 0.15*M* solution of sodium sulfide. The pale yellow solution of $NaCo(CO)_4$ was separated from the excess of the original material and from the formed mercury sulfide

* Fellow of the University of São Paulo; permanent address: Osaka Municipal Technical Research Institute, Osaka, Japan.

[1] R. A. Friedel, I. Wender, S. L. Shufler, and H. W. Sternberg, J. Am. Chem. Soc. **77**, 3951 (1955).

[2] A. Vohler, Chem. Ber. **91**, 1161, 1235 (1958).

[3] P. Krumholz and H. M. A. Stettiner, J. Am. Chem. Soc. **71**, 3035 (1949).

[4] W. Hieber, E. O. Fischer, and E. Boeckly, Z. anorg. u. allgem. Chem. **269**, 308 (1952).

[5] W. Hieber and R. Breu, Chem. Ber. **90**, 1259, 1270 (1957).

by careful filtering. The samples used in the spectroscopic work were 0.28*M*.

Solutions of the monobasic salt $NaHFe(CO)_4$ were prepared[5] by shaking iron pentacarbonyl for 4 hr with equimolecular amounts of barium hydroxide and sodium hydroxide of a total normality 0.9. The solutions, filtered from the formed barium carbonate, were 0.28*M* in $NaHFe(CO)_4$ and 0.01–0.015*M* in $Na_2Fe(CO)_4$, as determined by the reaction with $HgCl_2$.[5] The pale yellow or slightly pinkish solutions are very sensitive to radiations below 5500 or 5000 A; exposed to daylight they rapidly turn dark red. When kept at room temperature in the dark and, naturally, under complete absence of oxygen, the samples showed no appreciable change of color for several days or even weeks, and the Raman spectra of freshly prepared and of older solutions were found to be identical. The dimerization to binuclear carbonyl derivatives, recently reported by Sternberg *et al.*,[6] seems thus to be a photochemical reaction.

The spectroscopic study of $Na_2Fe(CO)_4$ in solutions of stoichiometric composition appeared inadvisable since iron tetracarbonyl hydride is a very weak bibasic acid ($K_2 \simeq 4 \cdot 10^{-14}$) and its bibasic salts are strongly hydrolyzed. In order to limit the hydrolysis to about 10% or less, we prepared samples containing an excess of about 1 mole NaOH per liter. To that purpose 0.03 mole of $Fe(CO)_5$ were shaken for 4 hr with 50 ml 0.6*M* barium hydroxide and 25 ml 6.0*M* NaOH. The solution of barium hydroxide was prepared at 50°C and cooled to room temperature before the addition of the iron pentacarbonyl. The filtered solutions were pale yellow and contained 0.38 mole per liter of $Na_2Fe(CO)_4$; they were found to be much less photosensitive than the solutions of the monobasic salt.

Spectroscopic Technique

The photosensitivity of the three investigated species of sodium salts of metal carbonyl hydrides in aqueous solution prevented the excitation of the Raman spectra in the conventional way through mercury radiations of 4358 A, or even 5461 A. We found, however, that spectra of good quality could be obtained in the red region of the spectrum by excitation with He 5875.6 and 6678.1 A. In order to avoid the incidence of radiations of shorter wavelengths on the samples, filters possessing a sharp spectral cutoff had to be used.

The technique of exitation of Raman spectra in the red and near infrared region has been described previously by one of us[7] and details can be omitted here.

The Raman spectrograph was provided with a Bausch & Lomb 600 grooves/mm plane grating blazed in the first order for 7500 A. The spectra were photographically recorded with cameras having apertures 1:1.9 and 1:2.8 corresponding to reciprocal dispersions of about 110 and 70 A/mm, respectively. Dispersions of this order proved to be quite sufficient for the present work. It must be considered that the dispersion in frequency units in the 7500-A region increases by a factor of nearly 3 as compared with the spectral range in which Raman spectra are usually obtained.

The Raman spectra excited by He 5875.6 A were photographed on Kodak spectroscopic plates of the types 103 aC, 103 aE, and 103 aF, those excited by He 6678.1 A on plates 103 aF, 103 U, and IN, the last type being hypersensitized before use. Making use of the highest aperture camera we recorded the spectra excited by He 5875.6 A with exposures ranging from 5 to about 80 min. Longer exposures were necessary for the spectra excited by He 6678.1 A and particularly for those photographed on IN plates.

Our excitation unit consists of a helium discharge tube helicoidally wound around the Raman tube. The direction of incidence of the exciting radiation is, therefore, not sufficiently defined to carry out correct quantitative measurements of the state of polarization of the Raman shifts and to distinguish weakly polarized from depolarized lines. The arrangement enables us, however, to identify with certainty depolarization factors <0.5 or 0.4; such strongly polarized shifts are indicated in the following by *P*. Consequently, the Raman lines without indication may be depolarized or weakly polarized.

THE RAMAN SPECTRA

About one hundred spectra of the three molecular species studied in this work were recorded; the frequencies, estimated intensities, and further characteristics of the observed shifts are the following:

$NaCo(CO)_4$: 90 (30) *b*; 439 (15) *P*; 532 (8); 619 (2.5); 715 (4); 1883 (2); 1918 (10).

The strong Raman line 1918 cm^{-1} is probably weakly polarized; a definite result could not be obtained due to the experimental difficulties mentioned in the foregoing.

$Na_2Fe(CO)_4$: 85–100 (50) *vb*; 464 (20) *P*; 550 (6); 644 (4); 785 (1) *b*, *d*; 1788 (10) *vb*.

The weak Raman line 785 cm^{-1}, marked *d*, was observed only in overexposed spectra and must be regarded as questionable. In such prolonged exposures appears the emission spectrum of the He_2 molecule with band systems interfering with the observation of weak Raman shifts in this spectral range. Comparative measurements of intensities indicated, however, that the 785-cm^{-1} shift is probably genuine.

The strong Raman line found at 1788 cm^{-1} is very broad; with increasing exposure it enlarges asymmetrically, and its center is shifted by about 7 cm^{-1} toward lower wave numbers, thus indicating the presence of two components, a stronger one at about 1790 cm^{-1} and a weaker one at perhaps 1783 cm^{-1}. Our attempts at resolving this shift clearly into two components were not successful.

[6] H. W. Sternberg, R. Markby, and I. Wender, J. Am. Chem. Soc. 79, 6116 (1957).

[7] H. Stammreich, Spectrochim. Acta 8, 41 (1956).

$NaHFe(CO)_4$: 80–95 (50) *vb*; 451 (20) *P*; 518 (3); 539 (6); 598 (2) *sh*; 610 (5); 708 (0) *d*; 780 (0) *b*, *d*; 1768 (3); 1835 (10) *P*; 1895 (10).

The Raman line 598 cm^{-1} appears as a shoulder incompletely resolved from the main shift 610 cm^{-1}. The genuineness of the faint lines 708 and 780 cm^{-1} is questionable due to the same circumstances that difficulted the observation of the Raman band 785 cm^{-1} of $Na_2Fe(CO)_4$.

ASSIGNMENT OF FREQUENCIES OF THE TETRAHEDRAL IONS

It will be seen that the Raman spectra of $NaCo(CO)_4$ and $Na_2Fe(CO)_4$ are fully consistent with those which would be expected regular tetrahedral $A(BC)_4$ molecules. Hence, the observed frequencies have to be attributed to the isolated ions $Co(CO)_4^-$ and $Fe(CO)_4^{2-}$, respectively, and will be assigned under the point group T_d.

The nine fundamental modes of vibration of such molecules belong to the species A_1 (2), E (2), F_2 (4) and F_1 (1). All of them, except the F_1 species, are Raman active whereas only the F_2 modes are allowed in absorption. The approximate forms of the normal vibrations are shown by Crawford and Cross.[8] However, their numbering of the fundamentals differs slightly from ours in the present work, which is the same as that used by Jones[9] and by Murata and one of us.[10] These papers refer to the vibrational spectrum of nickel carbonyl.

The fundamental modes may be described as C—O stretching vibrations (1 A_1; 1 F_2) expected to be found around 2000 cm^{-1}, as M–(CO) stretching modes (1 A_1; 1 F_2) and M–C–O bending modes (1 E; 1 F_2; 1 F_1) to be observed in the middle-frequency region extending from about 400 cm^{-1} to perhaps as high as 785 cm^{-1}, and as (CO)–M–(CO) bending motions (1 E; 1 F_2) with frequencies around 100 cm^{-1} or lower. needless to say, such descriptions (in which the group (CO) is considered as a rigid unit) must be regarded as being only roughly approximate. Especially in the middle-frequency region different vibrational motions are expected to couple.

Before discussing in detail the assignment of the observed frequencies to the fundamental modes of vibration of the two investigated species of tetrahedral metal carbonylate ions, we must point out that the Raman spectra of $Co(CO)_4^-$ were of exceptionally good quality, all shifts being of high or at least reasonable intensity. Even strongly overexposed spectra were obtained without any interfering background, and no additional Raman lines were found in such prolonged exposures. Since the number of the observed shifts is fully consistent with the theoretical expectancy, we feel justified in assigning all observed frequencies to fundamental modes.

C—O Stretching Vibrations

Friedel *et al.*[1] found in the ir spectrum of the $Co(CO)_4^-$ ion a strong absorption band at 1883 cm^{-1} in exact agreement with our Raman shift. Thus this frequency is readily assigned to the F_2 mode ν_5, whereas 1918 cm^{-1} must be attributed to the symmetric C–O stretching vibration ν_1. As mentioned in the foregoing, we did not succeed in resolving the broad band 1788 cm^{-1} in the spectrum of the $Fe(CO)_4^{2-}$ ion into two components, but we obtained indications of a separation of the symmetric and antisymmetric C–O stretching modes by about 7 cm^{-1}.

(CO)—M—(CO) Bending Vibrations

In the low-frequency region two modes, ν_4 and ν_8, belonging to species E and F_2, respectively, are expected. In the spectra of both ions only one large band was observed whose frequency had to be assigned to the two species. An identical situation was found in the Raman spectrum of nickel carbonyl by Duncan and Murray[11] and Crawford and Horwitz.[12]

M—(CO) Stretching and M—C—O Bending Vibrations

The very intense and strongly polarized Raman shifts 439 and 464 cm^{-1} of $Co(CO)_4^-$ and $Fe(CO)_4^{2-}$, respectively, are immediately assigned to the symmetric metal-carbon stretching mode $\nu_2(A_1)$.

The ir absorption band 555 cm^{-1} observed by Friedel *et al.*[1] in the spectrum of $(Co\ Pyr_6)^{2+}(Co(CO)_4^-)_2$, attributed to the $Co(CO)_4^-$ anion, differs appreciably from our Raman shift 532 cm^{-1}. Nevertheless, in the absence of another coincidence we must assign this Raman line to an F_2 mode. Since further ir data on the two ions are not available we depend on other evidence for the assignment of the remaining fundamentals in the middle-frequency region.

The results of a normal coordinate treatment of the vibrational spectrum of $Ni(CO)_4$, recently carried out by Murata and Kawai[10] under the assumption of a Urey-Bradley force field, show that one should expect to find $\nu_3(E) > \nu_6(F_2) > \nu_7(F_2)$. We arrived at the same conclusion through a normal coordinate analysis, to be discussed in the following, which is based on a valence force model. It will be shown, also, that a reasonable correlation between the spectra of the ions $Fe(CO)_4^{2-}$ and $HFe(CO)_4^-$ can be established when the foregoing order is assumed. Furthermore, a comparative study of all available Raman data on metal carbonyl compounds leads to the purely qualitative conclusion that

[8] B. L. Crawford and P. C. Cross, J. Chem. Phys. **6**, 525 (1938).
[9] L. H. Jones, J. Chem. Phys. **28**, 1215 (1958).
[10] H. Murata and K. Kawai, J. Chem. Phys. **26**, 1355 (1957).
[11] A. B. F. Duncan and J. W. Murray, J. Chem. Phys. **2**, 636 (1934).
[12] B. L. Crawford and W. Horwitz, J. Chem. Phys. **16**, 147 (1948).

TABLE I. Raman spectra of metal carbonylate ions, assignments of frequencies, and tentative scheme of correlation.

Approximate description of modes		Point group T_d			Point group C_{3v}		
	ν_i	Species	$Co(CO)_4^-$	$Fe(CO)_4^{2-}$	$HFe(CO)_4^-$	Species	ν_i
ν_{C-O}	1	A_1	1918	1788	1895	A_1	1
$\nu_{M-(CO)}$	2	A_1	439	464	451	A_1	2
δ_{M-C-O}	3	E	715	785	780 or 708	E	3
$\delta_{(CO)-M-(CO)}$	4	E	90	85–100	80–95	E	4
ν_{C-O}	5	F_2	1883	1788	1835	A_1	5_a
					1768	E	5_e
δ_{M-C-O}	6	F_2	619	644	610	A_1	6_a
					598	E	6_e
$\nu_{M-(CO)}$	7	F_2	532	550	539	A_1	7_a
					518	E	7_e
$\delta_{(CO)-M-(CO)}$	8	F_2	90	85–100	80–95	A_1	8_a
					80–95	E	8_e
δ_{M-C-O}	9	F_1	*i.a.*	*i.a.*	*i.a.*	A_2	9_a
					708 or 780?	E	9_e
H ‖ to C_3 axis	...	...	...	...	See discussion	A_1	10
H ⊥ to C_3 axis	...	...	...	...	See discussion	E	11

the shifts corresponding to M–(CO) stretching motions appear with higher intensities and at lower frequencies than those of the M–C–O bending modes.

With these indications pointing to identical conclusions we assign the frequencies 715 and 785 cm^{-1} of $Co(CO)_4^-$ and $Fe(CO)_4^{2-}$, respectively, to the bending mode $\nu_3(E)$, 619 and 644 cm^{-1} to the bending mode $\nu_6(F_2)$ and 532 and 550 cm^{-1} to the stretching mode $\nu_7(F_2)$.

The resulting vibrational assignments for $Co(CO)_4^-$ and $Fe(CO)_4^{2-}$ are shown in the first columns of Table I.

STRUCTURE AND FREQUENCY ASSIGNMENT OF $HFe(CO_4)^-$

The $HFe(CO)_4^-$ ion is isoelectronic with cobalt hydrocarbonyl. Sternberg *et al.*,[13] Friedel *et al.*,[1] and Edgell *et al.*[14] have reported ir absorption measurements on the latter compound and have found the spectrum to be consistent with a C_{3v} structure of the molecule. Edgell *et al.*[14] and Edgell and Gallup[15] proposed a particular "bridge model" of C_{3v} symmetry for cobalt hydrocarbonyl in which the hydrogen atom is located symmetrically between three CO groups at a distance of about 2.0 A from the cobalt atom. Bonding is primarily to the CO groups and to a lesser extent only to the cobalt atom. Cotton,[16] however, considers the contribution of the Co–H overlap to the bonding of the hydrogen atom as being quite important and arrives at a probable Co–H distance of about 1.2 A. It thus appears to be justified to consider the proton, as proposed by Cotton and Wilkinson,[17] as being buried in the electron density of the metal atom. This picture is rather close to the conception of a "pseudo-nickel" atom, CoH, previously advanced by Hieber.[18]

An uncommon type of bonding of the hydrogen to the metal carbonyl skeleton is suggested, also, by the results of NMR measurements on $HCo(CO)_4$,[19] $H_2Fe(CO)_4$,[17] and $HMn(CO)_5$,[20] showing much larger negative proton resonance shifts as found when hydrogen is bound in the ordinary way to oxygen or carbon atoms.

However, the ir absorption spectra of $HCo(CO)_4$ mentioned in the foregoing offer no conclusive evidence for the C_{3v} structure of the molecule. The transition from T_d to C_{3v} symmetry, brought up by the hydrogen atom, is expected to cause a splitting of the triply degenerate vibrations of the regular tetrahedron into two modes belonging to species A_1 (or A_2) and E, respectively. All fundamentals of the C_{3v} model are active in Raman and in the ir, except one A_2 mode which is forbidden in both. The ir spectrum of cobalt carbonyl hydride indicates that the selection rules of the C_{3v} point group are indeed operative, however, the expected splitting was observed only for the antisymmetric C–O stretching vibration, but not for the two F_2 modes of the middle-frequency region. Edgell and co-workers[14] believe that the slight perturbation of the tetrahedral skeleton, produced by the hydrogen atom, is just sufficient to make the selection rules of the C_{3v} point group operative, but not large enough to cause an observable splitting of the F modes of lower fre-

[13] H. W. Sternberg, I. Wender, R. A. Friedel, and M. Orchin, J. Am. Chem. Soc. **75**, 2717 (1953).
[14] W. F. Edgell, Ch. Magee, and G. Gallup, J. Am. Chem. Soc. **78**, 4185 (1956).
[15] W. F. Edgell and G. Gallup, J. Am. Chem. Soc. **78**, 4188 (1956).
[16] F. A. Cotton, J. Am. Chem. Soc. **80**, 4425 (1958).
[17] F. A. Cotton and G. Wilkinson, Chem. & Ind. (London) **1956**, 1305.
[18] W. Hieber, Chemie Die **55**, 24 (1942).
[19] H. S. Gutowsky, quoted in references 1 and 14.
[20] F. A. Cotton, J. L. Down, and G. Wilkinson, J. Chem. Soc. **1959**, 833.

quency into A and E species. That would mean that the intrinsically degenerated modes of the T_d model become in part accidentally degenerated ones in the C_{3v} model. Hence, the spectroscopic evidence for the C_{3v} structure of $HCo(CO)_4$ rests essentially on the assignment of the C–O stretching modes. The spectrum observed in the 2000-cm^{-1} region is certainly not inconsistent with the given assignment but cannot be said to require it, owing to the presence of numerous further bands in this range.

Therefore, it is particularly interesting that the splitting pattern, expected for the transition from T_d to C_{3v} symmetry, becomes clearly evident in the Raman spectrum of $HFe(CO)_4^-$, not only in the high- but also in the middle-frequency region. The observed splittings have to be interpreted as the result of a considerable disturbance of the tetrahedral symmetry of the $Fe(CO)_4$ skeleton. The correlation between the spectra of the ions belonging to the T_d point group and of $HFe(CO)_4^-$, assigned under C_{3v} symmetry, is shown in Table I. The components belonging to species A and E originating from the triply degenerate species of the undisturbed tetrahedron are indicated by subscripts a and e, respectively. The observed frequencies have been assigned to these components under the criterion that the A_1 modes appear usually with higher intensities in Raman spectra than the E modes. Also in relation to some other details the correlation scheme of Table I must be regarded as tentative.

In the high-frequency region we found three Raman shifts, one of them (1835 cm^{-1}), being strongly polarized. This frequency has been assigned to the A_1 mode ν_{5a}; the assignment to ν_1 would be possible too. The shift of lowest intensity has been attributed to the E mode ν_{5e} according to the foregoing criterion.

In the middle-frequency region we have two pairs of Raman lines, namely 610/598 and 539/519 cm^{-1}, which are readily assigned to the A_1 and E modes produced by the splitting of the F_2 species ν_6 and ν_7, respectively. The strongly polarized and very intense Raman shift 451 cm^{-1} corresponds without doubt to the symmetric M–(CO) stretching mode that was observed in the spectra of the undisturbed tetrahedral species $Co(CO)_4^-$ and $Fe(CO)_4^{2-}$ at 439 and 464 cm^{-1}, respectively. There remain the weak Raman lines 780 and 708 cm^{-1} whose genuineness is not absolutely certain. They have been assigned in a purely tentative way to the E modes ν_3 and ν_{9e}. The latter is expected to arise from the splitting of the inactive species F_1 into an A_2 and an E mode, the A_2 species being inactive both in Raman and in the ir.

In addition to the vibrational modes of the disturbed tetrahedral carbonyl skeleton we have to expect in the spectra of $HCo(CO)_4$ and $HFe(CO)_4^-$, assuming a C_{3v} symmetry, two more fundamentals which may be described, in zero approximation, as motions of the hydrogen atom parallel and perpendicular to the principal axis. They belong to species A_1 (ν_{10}) and E (ν_{11}), respectively. Since the bonding of the H atom to the skeleton is certainly of an unusual kind, the frequencies of such vibrations cannot be foreseen. In the foregoing assignment we attributed all observed Raman shifts of $HFe(CO)_4^-$ to the fundamental modes of the $Fe(CO)_4$ skeleton, the number of them being exactly that which must be expected for a disturbed tetrahedron with C_{3v} symmetry. Now, we shall discuss briefly an alternative assignment of one or two of the observed frequencies to motions involving the hydrogen atom.

The most reliable evidence of a hydrogen stretching vibration in metal hydrocarbonyls has been recently obtained from the ir spectra of $HMn(CO)_5$ and $DMn(CO)_5$ as reported by Wilson,[21] Cotton *et al.*,[20] and by Edgell and co-workers,[22] whose measurements are in excellent agreement. The value of the hydrogen stretching frequency in $HMn(CO)_5$ was found to be 1782 cm^{-1}.

Earlier, Edgell *et al.*[14] had assigned a strong absorption band of $HCo(CO)_4$, observed at 703 cm^{-1}, to a hydrogen stretching mode, arguing that no skeletal vibration of so high a frequency (except the C–O stretching modes) can be expected. In our opinion, the weight of this argument is impaired by the fact that we found in the spectra of $Co(CO)_4^-$, $Fe(CO)_4^{2-}$, and $Fe(CO)_5$[23] Raman lines at 715, 785, and 753 cm^{-1}, respectively, which must be attributed to fundamental skeletal vibrations.

Taking into account the foregoing observations on related metal hydrocarbonyl compounds, we cannot exclude the possibility that one of the high-frequency shifts, observed in the $HFe(CO)_4^-$ spectrum, or one of the weak lines in the 700- to 800-cm^{-1} region belongs to the ν_{10} or ν_{11} mode. The latter hypothesis is consistent with the results of a normal coordinate analysis, referring to the tetrahedral ions, which will be discussed later. We calculated the frequencies of the inactive F_1 species of $Co(CO)_4^-$ and $Fe(CO)_4^{2-}$ to be 489 and 459 cm^{-1}, respectively. Since the ν_{9e} mode of $HFe(CO)_4^-$ has its origin in the F_1 species of the undisurbed skeleton one should expect for this fundamental a frequency considerably lower than 708 or 780 cm^{-1}. The Raman spectrum of the isotopic species $NaDFe(CO)_4$ in a heavy water solution should be helpful in order to reach an unambiguous decision of the question.

POTENTIAL FUNCTION AND FORCE CONSTANTS OF $Co(CO)_4^-$ AND $Fe(CO)_4^{2-}$

A normal coordinate analysis of the tetrahedral ions $Co(CO)_4^-$ and $Fe(CO)_4^{2-}$ was carried out making use of Wilson's **FG** matrix method. It was less our aim to reproduce the observed frequencies with the highest

[21] W. Wilson, Z. Naturforsch. **13b**, 349 (1958).
[22] W. F. Edgell, G. Asato, W. Wilson, and C. Angell, J. Am. Chem. Soc. **81**, 2022 (1959).
[23] H. Stammreich, O. Sala, and Y. Tavares, J. Chem. Phys. **30**, 856 (1959).

possible accuracy than to introduce a simple but adequate force field in order to obtain the values of the more significant potential constants which could be compared with the corresponding force constants of related molecules. Furthermore, the results of the analysis have to be regarded as a test of the reasonableness of our frequency assignment.

Similar treatments for nickel carbonyl have been recently reported by Murata and Kawai[10] and by Jones.[9] The former authors have made use of a Urey-Bradley force field model whereas Jones assumed as a starting point a most general quadratic valence force potential function, resorting subsequently to the assumption of certain values for many of the involved constants. Jones has pointed out that for the treatment of metal carbonyl compounds the valence force model seems to be more promising than the Urey-Bradley field, since the latter model neglects resonance interactions which are probably quite important in these molecules; particularly, it is to be expected that a significant C–O stretching interaction will arise from the change of the structure of this bond during distortion.

In agreement with Jones's point of view, we used in the present analysis the following simplified quadratic valence force potential function:

$$2V=\sum_{i=1}^{4}[f_{(C-O)}(\Delta R_i)^2+f_{(M-C)}(\Delta r_i)^2]$$
$$+\sum_{i<j=1}^{4}f_{(C-M-C)}(r\Delta\alpha_{ij})^2$$
$$+\sum_{i=1}^{4}\sum_{k=a}^{b}f_{(M-C-O)}[(rR)^{\frac{1}{2}}\Delta\pi_{ik}]^2$$
$$+2\sum_{i<j=1}^{4}f_{(C-O)(C-O)}(\Delta R_i)(\Delta R_j)$$
$$+2\sum_{i<j=1}^{4}\sum_{l,k=a}^{b}f_{(M-C-O)(M-C-O)}[(rR)^{\frac{1}{2}}\Delta\pi_{il}][(rR)^{\frac{1}{2}}\Delta\pi_{jk}].$$

Here R and r are, respectively, the equilibrium values of the C–O and M–C bond lengths; the other symbols in the foregoing expressions correspond to those used by Murata and Kawai[10] in the setting up of the internal coordinates. It is seen that only two cross terms, referring to C–O stretching and M–C–O bending interactions, have been considered, the different interactions of the latter kind were assumed to be equal.

TABLE II. Valence force constants of tetrahedral metal carbonylate ions.

Force constant	$Co(CO)_4^-$ md/A	$Fe(CO)_4^{2-}$ md/A
$f_{(C-O)}$	13.22	11.40
$f_{(M-C)}$	3.55	4.06
$f_{(M-C-O)}$	0.45	0.48
$f_{(C-M-C)}$	0.09	0.09
$f_{(C-O)(C-O)}$	0.14	0.05
$f_{(M-C-O)(M-C-O)}$	0.06	0.09

TABLE III. Observed and calculated frequencies of tetrahedral ions.

Species	i	$Co(CO)_4^-$ obs	$Co(CO)_4^-$ calc	$Fe(CO)_4^{2-}$ obs	$Fe(CO)_4^{2-}$ calc
A_1	1	1918	1918	1788	1792
A_1	2	439	444	464	468
E	3	715	712	785	772
E	4	90	88	85–100	88
F_2	5	1883	1885	1788	1785
F_2	6	619	626	644	648
F_2	7	532	523	550	537
F_2	8	90	93	85–100	93
F_1	9	*i.a.*	489	*i.a.*	459

For the calculation of valence force constants we used the G matrix elements given by the forenamed authors; the M–C and C–O equilibrium distances which are 1.83 and 1.15 A, respectively, in $Ni(CO)_4$ were assumed to be 1.82 and 1.18 A in the $Co(CO)_4^-$ ion and 1.82 and 1.19 A in the $Fe(CO)_4^{2-}$ ion. These values of the bond lengths were estimated from the alternation of the frequencies of the corresponding totally symmetric stretching modes in going from $Ni(CO)_4$ by $Co(CO)_4^-$ to $Fe(CO)_4^{2-}$. It must be pointed out, however, that the numerical values of the valence force constants, as given in Table II, are but little affected by small changes of the assumed bond distances.

By using the potential constants given in Table II we calculated the frequencies of the normal modes of the two ions, including the inactive F_1 species. The results as compared with the observed values are shown in Table III.

From the satisfactory agreement between observed and calculated values one may conclude that the simplified force field, as assumed in our treatment, describes in a good approximation the vibrational properties of the two tetrahedral metal carbonylate ions. The results of the present work suggested also the convenience of a reexamination of the Raman spectrum of nickel tetracarbonyl and of the vibrational analytical data on this molecule as reported in previous publications. This work will be described in a subsequent paper, together with a comparative study of spectral data, force constants, and bond properties of the three isoelectronic species.

ACKNOWLEDGMENTS

The writers are indebted to Professor W. Hieber of Munich, Germany, who placed at their disposal the necessary quantity of mercury cobalt carbonylate to carry out this work. They are grateful to Professor F. A. Cotton and Professor W. F. Edgell for stimulating discussions and to the Conselho Nacional de Pesquísas, Rio de Janeiro, for having supported this work.

Spin Densities in Dimesitylmethyl

A. D. McLACHLAN*

Gates and Crellin Laboratories of Chemistry,† California Institute of Technology, Pasadena, California

(Received December 15, 1959)

A simple valence bond calculation indicates that if the dimesitylmethyl radical were planar large unpaired spin densities would appear on the ring methyl groups giving a spectrum about 130 gauss wide. A perturbation calculation, assuming that the molecule is very twisted, gives spin densities $\rho_1=1.000$, $\rho_2=-0.069$, $\rho_3=0.054$, $\rho_4=-0.040$, $\rho_5=0.043$ on the carbon atoms, numbered from the center outwards.

INTRODUCTION

NOW that something is known about the negative spin densities[1,2] and the hyperconjugation between methyl groups and the odd electron in aromatic radicals,[3,4] it is interesting to see whether these ideas can explain the complex electron resonance spectrum of dimesitylmethyl[5]:

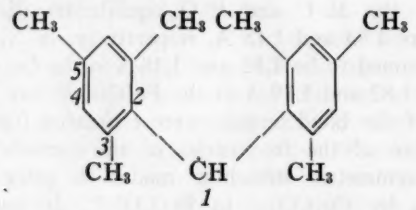

Jarrett and Sloan's spectrum has over 60 closely spaced lines, with a total width of 51 gauss, which fall into two main groups 24 gauss apart. The large number of lines makes it certain that methyl protons interact with the odd electron, and the 24 gauss splitting is attributed to the central proton. According to current theoretical ideas the hyperfine splittings a_H are connected with the π electron spin densities ρ on the ring carbon atoms by the equation

$$a_H=Q\rho, \tag{1}$$

with $Q=-23$ gauss for ring protons[6] and $Q=+25$ for freely rotating methyl ones.[4] We therefore estimate that $\rho_1=1$ at the center, and $\rho\simeq 0.05$ on the ring carbons. Triphenylmethyl, which has a similar ring arrangement, has much larger unpaired spin densities on the rings and a smaller one at the center.[7] The spectrum therefore suggests that the ortho methyl groups prevent the dimesitylmethyl radical from lying in one plane, and reduce the delocalization of the unpaired spin.

CONVENTIONAL VALENCE BOND CALCULATION

We calculated the spin density first by conventional valence bond methods, neglecting any effect the methyl groups or the twisting might have on the π electrons. We used nearest neighbor exchange integrals only, and neglected all but the Kekulé structures. These are $\phi_1\cdots\phi_4$; $\theta_1\cdots\theta_4$; and $\chi_1\cdots\chi_8$; where the unpaired electron is, respectively, on the central, para, or ortho positions. The ground state wave function is then of the form

$$\Psi=a\Phi+b\Theta+c\mathrm{X}, \tag{2}$$

where Φ, Θ, X are the normalized sums of the ϕ's, θ's, and χ's. After taking J for the exchange integral between ring carbon atoms, K for that between the rings and the center, and Q for the Coulomb integral, one obtains by standard methods[8] the secular determinant

$$\begin{vmatrix} (180x-25E) & (76x+10y-10E) & (180x+25y-25E) \\ (76x+10y-10E) & (128x+24y-22E) & (170x+30y-25E) \\ (180x+25y-25E) & (170x+30y-25E) & (390x+75y-62\tfrac{1}{2}E) \end{vmatrix}=0. \tag{3}$$

Here $E=W-Q+6J+K$, $x=\frac{3}{2}J$, and $y=\frac{3}{2}K$.

In a planar molecule with $J=K$ the ground state calculated from (3) is

$$\Psi=0.411\Phi+0.265\Theta+0.489\mathrm{X}; \qquad E=11.641J, \tag{4}$$

which leads to spin densities of $\rho_1=+.605$ (center), $\rho_2=-0.263$, $\rho_3=+0.243$ (ortho), $\rho_4=-0.128$ (meta), and $\rho_5=+0.230$ (para). These are clearly too large on the ring, so that we must allow for some twisting

* Harkness Fellow of the Commonwealth Fund, 1959–1961.

† Contribution No. 2534.

[1] H. M. McConnell and D. B. Chesnut, J. Chem. Phys. **27**, 984 (1957); P. Brovetto and S. Ferroni, Nuovo cimento **5**, 142 (1957).

[2] H. M. McConnell and H. H. Dearman, J. Chem. Phys. **28**, 51 (1958).

[3] R. Bersohn, J. Chem. Phys. **24**, 1066 (1956).

[4] A. D. McLachlan, Mol. Phys. **1**, 233 (1958).

[5] H. S. Jarrett and G. J. Sloan, J. Chem. Phys. **22**, 1783 (1954).

[6] H. M. McConnell and D. B. Chesnut, J. Chem. Phys. **28**, 107 (1958).

[7] F. C. Adam and S. I. Weissman, J. Am. Chem. Soc. **80**, 2057 (1958).

[8] H. Eyring, J. Walter, and G. E. Kimball, *Quantum Chemistry* (John Wiley & Sons, Inc., New York, 1944), p. 232.

and set $K \ll J$. Serious difficulties now arise, for as $K \to 0$ the ground state given by (3) tends, not to Φ, which is the correct limit for three separated systems, but to $\Psi' = 0.974\Phi + 0.122\Theta - 0.049X$! The anomaly comes because the canonical structures ϕ, θ, χ are not a complete set, and are only appropriate when $J \simeq K$. In particular the Θ's contain components corresponding to Dewar structures of the mesitylene rings, which combine with the ϕ's even if K vanishes.

LIMIT OF WEAK COUPLING

Instead we use an entirely different approach, building up the ground state of the radical from states of three fragments—two benzene rings (mesitylene) A, B and an isolated carbon atom C—and treating the exchange integral K as a small perturbation. A doublet state of ABC can be broken down into combinations of the following states:

$$\begin{aligned} &\text{(i)} \quad C\alpha \cdot AB \text{ singlet}, \\ &\text{(ii)} \quad C\alpha \cdot AB \text{ triplet}, \ S_z = 0, \\ &\text{(iii)} \quad C\beta \cdot AB \text{ triplet}, \ S_z = 1. \end{aligned} \tag{5}$$

In the allyl radical, for example, the two canonical structures with $S = S_z = \frac{1}{2}$ are

$$\begin{aligned} \psi_1 &= a\!=\!b\!-\!c\uparrow = (1/\sqrt{2})(\alpha\beta\alpha - \beta\alpha\alpha), \\ \psi_2 &= \uparrow a\!-\!b\!=\!c = (1/\sqrt{2})(\alpha\alpha\beta - \alpha\beta\alpha), \end{aligned} \tag{6}$$

while the structures (5) for the separated systems ab and c are

$$\begin{aligned} V_1 &= a\!=\!b\cdot c\uparrow = (1/\sqrt{2})(\alpha\beta\alpha - \beta\alpha\alpha) \\ V_2 &= a\vdots b\cdot c\uparrow = (1/\sqrt{2})(\alpha\beta\alpha + \beta\alpha\alpha) \\ V_3 &= \uparrow a\vdots b\uparrow \cdot c\downarrow = \alpha\alpha\beta. \end{aligned} \tag{7}$$

We see that $\psi_1 = V_1$, and $\psi_2 = \frac{1}{2}(V_1 + V_2) - 1/\sqrt{2}V_3$. An extension of this argument shows that unpaired spin density on the benzene rings A, B comes from states like [5(ii)] in which one ring is excited to a triplet state. For small values of K one may treat each ring separately, and use perturbation theory, taking the perturbation energy to be

$$H' = -\tfrac{1}{2}K.(1 + \sigma_1 \cdot \sigma_2). \tag{8}$$

The spin density ρ_r at any atom on the ring is then found to be

$$\rho_r = \sum_{n \neq 0} \frac{\langle 0 \mid K\sigma_{z2} \mid n \rangle \langle n \mid \sigma_{zr} \mid 0 \rangle}{E_n - E_0}. \tag{9}$$

We evaluated this expression taking ψ_0 to be the exact valence bond ground singlet state of benzene, including the Dewar structures, and ψ_n to be the nine excited triplets. They have been calculated by Hückel,[9] or can be found by writing down canonical structures and matrix elements according to rules similar to those which apply to singlet states. The spin densities are $-0.504 \cdot K/J$, $+0.388 \cdot K/J$, $-0.292 \cdot K/J$, and $+0.312 \cdot K/J$, at positions 2, 3, 4, 5. To fit the observed width of the electron resonance spectrum one must set $K/J = 0.137$, so that the spin densities and splitting constants are found to be

$$\begin{aligned} &\rho_1 = 1.000 \ (24 \text{ gauss}) \qquad \rho_3 = 0.054 \ (1.3 \text{ gauss}) \\ &\rho_2 = -0.069 \qquad \rho_4 = -0.040 \ (1.0 \text{ gauss}) \\ &\rho_5 = 0.043 \ (1.1 \text{ gauss}). \end{aligned}$$

These values seem to account roughly for the observed spectrum, whose details will vary considerably with the precise ratio of ρ_3: ρ_4: ρ_5. Our calculations indicate that this radical is twisted out of plane, and if one assumes that $K = J \cos^2\alpha$, the angle of twist α should be about 60–70°.

We thank Professor H. C. Longuet-Higgins and Dr. L. E. Orgel for helping to show why the conventional valence bond theory breaks down.

[9] E. Hückel, Z. Physik **70**, 204–86 (1931).

Variational Principles for Chemical Equilibrium

W. S. Dorn

IBM Research Center, Yorktown Heights, New York

(Received November 27, 1959)

Two variational principles for the chemical equilibrium of a gaseous mixture are formulated. These provide a means for calculating upper and lower bounds to the energy of the equilibrium mixture.

INTRODUCTION

In a recent paper,[1] a dual problem for a class of nonlinear programing problems was formulated and a duality theorem relating the problem and its dual was proved. In the following note this theorem will be employed to construct from a previously known principle a new variational principle for the chemical equilibrium of a gaseous mixture. The two principles may then be coupled to produce a computational method of solution. Moreover, they provide upper and lower bounds to the Gibbs free energy of the equilibrium mixture.

FIRST VARIATIONAL PRINCIPLE: MINIMUM FREE ENERGY

Consider the problem of determining the equilibrium configuration of a mixture of gases under conditions of constant pressure and temperature. It will be assumed that the gases obey the ideal gas law for all values which the variables may take on in the process. The Gibbs free energy function F, is defined by $F=H-TS$ where H is the enthalpy, T the temperature and S the entropy.

Under conditions of constant pressure and temperature, the total Gibbs free energy of the system is a minimum at equilibrium.[2]

The differential of F_j, the Gibbs free energy per mole of the jth gas, is given by

$$dF_j=RT(dP_j/P_j)$$

where P_j is the partial pressure of the jth gas and R is the universal gas constant.

After integration this becomes

$$F_j/RT=\log P_j+(F_j^\circ/RT)$$

where F_j° is the Gibbs function per mole of the jth gas at a temperature T and 1 atm of pressure.

From Dalton's law of partial pressures

$$P_j=(x_j/\sum_i x_i)\,P$$

where x_j is the number of moles of the jth gas in the mixture. Thus, the total free energy of the system in dimensionless form is

$$F/RT=\sum_j(x_jF_j/RT)=\sum_j c_jx_j+\sum_j x_j\log(x_j/\sum_i x_i) \tag{1}$$

where

$$c_j=(F_j^\circ/RT)+\log P. \tag{2}$$

At equilibrium the Gibbs free energy F, expressed here as a function of the mole numbers x_j, must be a minimum. The mole numbers are not arbitrary, but must be nonnegative and satisfy the mass balance equations. A set of mole numbers x_j will be called *allowable* if they satisfy these requirements.

The following variational principle for the equilibrium problem posed in the first paragraph of this section may be stated: *Of all allowable mole numbers x_j, those which minimize the total Gibbs free energy of the system (1), correspond to the equilibrium mole numbers.*

If there are n gases involving m elements in the mixture, this may be phrased:

Minimize

$$\sum_{j=1}^n c_jx_j+\sum_{j=1}^n x_j\log(x_j/x^*) \tag{3}$$

where

$$\sum_{j=1}^n a_{ij}x_j=b_i, \qquad (i=1,2,\cdots,m) \tag{4}$$

$$x_j\geq 0 \tag{5}$$

where x^* is defined by

$$x^*=\sum_{j=1}^n x_j \tag{6}$$

and where the c_j are given by (2), a_{ij} represents the number of atoms of the ith element in a molecule of the jth gas, b_i is the number of moles of the ith element in the total mixture and x_j is the number of moles of the jth gas.

This formulation was made previously by Dantzig *et al.*[3,4] where the functional (3) was shown to be convex. Two methods of solution may be found in these

[1] W. S. Dorn, AEC Report NYO-2878 (August, 1959).

[2] See, for example, Mark W. Zemansky, *Heat and Thermodynamics* (McGraw-Hill Book Company, Inc., New York, 1951), pp. 388–390.

[3] G. Dantzig, S. Johnson, and W. White, Measurement Sci. **5**, 38 (1958).

[4] G. Dantzig, S. Johnson, and W. White, J. Chem. Phys. **28**, 751 (1958).

references. Other methods of solution of the general convex programing problem have also been proposed.[5-9]

SECOND VARIATIONAL PRINCIPLE: MAXIMUM ENERGY CONTRIBUTION

The dual programing problem to the one phrased in (3)-(6) may be written:

$$\text{Maximize} \sum_{i=1}^{m} b_i u_i \tag{7}$$

subject to

$$\sum_{i=1}^{m} a_{ij} u_i \leq \log(x_j/x^*) + c_j \qquad (j=1, 2, \cdots, n) \tag{8}$$

and the duality theorem[1] insures the existence of a solution to this problem.

This implies that there is an energy associated with each element. The variable u_i represents this energy (in dimensionless form) and is the energy contributed by the ith element to the reaction. A set of energies $u_i (i=1, 2, \cdots, m)$ will be called *admissible* if the total energy contribution of all of the atoms in a molecule to that molecule does not exceed the Gibbs free energy of the molecule, i.e., the inequalities (8) are satisfied.

The dual problem then gives rise to the following variational principle:

Of all admissible energies u_i, those which maximize the total energy contribution of all of the atoms in the system correspond to the equilibrium energies.

The duality theorem also requires that at equilibrium the total energy contribution of all of the elements be equal to the total Gibbs free energy of all of the gases. That is to say, for the equilibrium values of x_j and u_i

$$\sum_{i=1}^{m} b_i u_i = \sum_{j=1}^{n} c_j x_j + \sum_{j=1}^{n} x_j \log(x_j/x^*). \tag{9}$$

COMPUTATIONAL METHOD

The two variational principles give rise to a method for computing the equilibrium mole numbers. Notice first that by virtue of (4)

$$\sum_{j=1}^{n} x_j \Big[c_j + \log(x_j/x^*) - \sum_{i=1}^{m} a_{ij} u_i\Big]$$

$$= \sum_{j=1}^{n} x_j [c_j + \log(x_j/x^*)] - \sum_{i=1}^{m} b_i u_i.$$

From (9), however, the right-hand member vanishes for the equilibrium values of x_j and u_i. Now (6) and (8) require that each term in the summation over j in the left-hand member be nonnegative. Since the sum vanishes, this requires that each term in the sum vanish, i.e.,

$$x_j(c_j + \log(x_j/x^*) - \sum_{i=1}^{m} a_{ij} u_i) = 0 \qquad (j=1, 2, \cdots, n).$$

If the n compounds are chosen so that $x_j \neq 0$ then it follows that

$$\sum_{i=1}^{m} a_{ij} u_i = \log(x_j/x^*) + c_j \qquad (j=1, 2, \cdots, n). \tag{10}$$

Thus the inequalities (8) may be replaced by the equalities (10).

Consider now a set of u_i and x_j which simultaneously satisfy (4)-(6) and (10). It follows that

$$\sum_{i=1}^{m} b_i u_i = \sum_{i=1}^{m} \sum_{j=1}^{n} a_{ij} x_j u_i = \sum_{j=1}^{n} x_j \log(x_j/x^*) + \sum_{j=1}^{n} x_j c_j$$

and (9) implies that this is an equilibrium set of energy values. This set of equations is, indeed, that to which an approximate solution is found in reference 4 by iteration.

More important, however, the second variational principle provides a measure of the closeness of an approximation to the equilibrium mole numbers. From any set of approximate values of x_j a set of energies u_i satisfying (8) can be constructed. The value of (7) for these u_i is then a lower bound to the Gibbs free energy, while the value of (3) is an upper bound. The best lower bound is obtained by solving the linear programing problem posed by (7) and (8) where the x_j are regarded as fixed. In practice a good lower bound is obtained by inspection.

NUMERICAL EXAMPLE

Consider the example of reference 4, i.e., the combustion of a stoichiometric mixture of hydrazine and oxygen at 3500°K and a pressure of 750 psi. Table I gives the values of c_j, a_{ij}, and b_i together with the approximation

TABLE I.

			a_{ij}				
		$i=$	1	2	3		
j	Gas	c_j	H	N	O	x_j	F_j
1	H	−6.089	1			0.040668	−9.785056
2	H_2	−17.164	2			0.147730	−19.570111
3	H_2O	−34.054	2		1	0.783153	−34.792172
4	N	−5.914		1		0.001414	−12.969076
5	N_2	−24.721		2		0.485247	−25.937840
6	NH	−14.986	1	1		0.000693	−22.754224
7	NO	−24.100		1	1	0.027399	−28.190991
8	O	−10.708			1	0.017947	−15.222075
9	O_2	−26.662			2	0.037314	−30.444129
10	OH	−22.179	1		1	0.096872	−25.007108
		$b_i=$	2	1	1		
						$x^*=1.638437$	
						$F=\Sigma_j x_j F_j=-47.761067$	

[1] E. M. L. Beale, J. Roy. Stat. Soc. **17B**, 173 (1955).
[5] A. Charnes and C. E. Lemke, Am. Math. Soc. Meeting, 1958.
[7] J. E. Kelley, RAND Symposium Math. Programing, 1959.
[8] J. B. Rosen, Shell Development Report P-749.
[9] D. A. D'Esopo, Naval Research Log. Quart. 6, 33 (1959).

to the mole numbers x_j, computed in reference 4, and the associated molal Gibbs free energy functions, F_j.

The value of F is an upper bound to the total Gibbs free energy of the system.

By using equalities in (8) for $j=1, 6, 8$ (corresponding to the gases H, NH, and O) the values of the contributing energies are

$$u_1=-9.785056,$$
$$u_2=-12.969168,$$
$$u_3=-15.222075,$$

for the elements H, N, and O, respectively. These values of the u_i satisfy all of the inequalities (8). Had the x_j been exact equilibrium mole numbers, equality would hold in all of (8).

The value of F corresponding to these u_i is -47.761355 which is a lower bound. Thus the true value of F at equilibrium is

$$F=-47.761211\pm0.000144.$$

REMARKS

It should be noted that the first variational principle has been formulated in terms of "extensive variables," the mole numbers x_j. On the other hand, its dual, the second variational principle is cast in terms of "intensive variables," i.e., the energy contributions u_i, and the molal Gibbs free energies F_j.

Finally, it has been pointed out[4] that similar results are available for constant volume rather than constant pressure problems. In this case, however, the Helmholtz function $A=F-PV$ is a minimum at equilibrium.

THE JOURNAL OF CHEMICAL PHYSICS VOLUME 32, NUMBER 5 MAY, 1960

Diffusion of Cadmium in Pure and Cadmium Doped AgBr*

J. E. HANLON†‡

Department of Physics and The Institute for the Study of Metals, University of Chicago, Chicago 37, Illinois

(Received March 25, 1959)

The diffusion of Cd in pure AgBr and dilute AgBr-$CdBr_2$ solid solutions was measured by a tracer technique using carrier-free Cd^{109}. It was necessary to use the extremely high specific activity carrier-free isotope because the diffusion of Cd in AgBr depends sensitively on impurity concentration. The data support Lidiard's theory for the diffusion of divalent impurities in monovalent ionic crystals. From the diffusion rates in the pure material, it is possible to calculate the association energy ΔG of $Cd^{++}Ag$ vacancy complexes. The value of ΔG extrapolated to 0°K is estimated to be 0.21 ± 0.04 ev. The observed concentration dependence of Cd diffusion in doped samples can be explained only if the mobility of complexes is assumed to have a strong concentration dependence. This interpretation suggests that a reappraisal of the analysis of previous electrical conductivity and thermoelectric power doping experiments, in which the mobility was assumed to be concentration independent, would be desirable.

I. INTRODUCTION

A KNOWLEDGE of the concentration and mobility of point defects in ionic crystals[1] is essential for an understanding of many of their physical properties. In a pure crystal electrical neutrality requires that these imperfections occur in oppositely charged pairs; e.g., a positive interstitial associated with a vacancy in the cation sublattice (Frenkel defect), or the simultaneous occurrence of a vacancy on both the cation and anion sublattices (Shottky defect). To separate the mobilities of the individual imperfections, it is necessary to study a transport phenomenon controlled primarily by a known density of imperfections of one sign. Wagner[2] suggested that solid solutions of a divalent salt in a monovalent host might provide a suitable medium for such studies because each divalent ion in solution replaces two monovalent ions substitutionally, creating one lattice vacancy.

Subsequent studies supported Wagner's model, so this technique has been exploited in studies on a number of ionic crystals.[3] In the quantitative interpretation of doping experiments, it has been necessary to assume that imperfection mobilities are concentration independent and that the degree of association between divalent impurity ions and vacancies is either negligible or can be derived using a highly doubtful analysis. In

* Submitted to the University of Chicago in partial fulfillment for the degree of Doctor of Philosophy.

† Present address: Engineering Research Laboratory, Engineering Department, E. I. du Pont de Nemours and Company, Inc., Wilmington 98, Delaware.

‡ Standard Oil Company of Indiana Fellow, 1956, Shell Oil Company Foundation Fellow, 1957.

[1] For a thorough review of transport properties of ionic crystals, see A. B. Lidiard, *Handbuch der Physik* (Springer-Verlag, Berlin, 1957), Vol. XX, p. 246 ff.

[2] E. Koch and C. Wagner, Z. physik. Chem. **B38**, 295 (1937).

[3] See Lidiard,[1] p. 285 ff.

view of these weak assumptions, it is not surprising that previous workers have often arrived at contradictory conclusions.

In a monovalent ionic lattice, a substitutional divalent cation impurity and a cation vacancy have effective charges of +1 and −1 electron units, respectively. When the impurity and vacancy are nearest neighbors they form a complex with a positive association energy arising primarily from their electrostatic mutual attraction. The vacancy in a complex is presumed to be so tightly bound that it is unable to contribute to the electrical conductivity. Although the electrostatic interaction is not strongly shielded at an impurity-vacancy distance of a few lattice spaces, it is customarily assumed that the motion of the vacancy is unaffected by the impurity when they are not nearest neighbors. Thus the impurities and vacancies are considered to be present in two forms, as complexes and as unassociated charges, whose relative concentrations are derived from a chemical equilibrium equation.

A recent theoretical treatment by Lidiard[4] suggests that a divalent impurity ion in an ionic crystal moves primarily by jumping into a nearest neighbor vacancy. Thus the diffusion of divalent impurities should be proportional to the relative concentration of complexes. Because the degree of association can be varied by changing either the temperature or impurity concentration, the association energy and its concentration dependence may in principle be obtained. With a more complete picture of the association phenomena, the validity of the other assumptions involved in the doping technique may be evaluated.

The experiments reported here represent an effort to test Lidiard's theory by a study of the diffusion of Cd into AgBr doped with varying amounts of $CdBr_2$. The choice of this system was dictated by a number of considerations:

(1) Since $CdBr_2$ is soluble up to several percent in AgBr at elevated temperatures, a wide range of concentrations can be used in the association study.

(2) Pure AgBr has such a large concentration of intrinsic defects that reliable values of impurity diffusion can be obtained over a wide temperature range.

(3) Suitable Cd isotopes are available.

(4) Considerable information is available concerning the preparation of pure AgBr single crystals.

Prior to this experiment, several properties of AgBr had been measured as a function of temperature. These measurements included specific heat,[5] thermal expansion coefficient,[6] elastic constants,[7] electrical conductivity,[8,9] diffusion coefficients of Ag[10,11] and Br,[12] dielectric constant,[13] dielectric relaxation,[14] optical absorption,[15] creep,[16] nuclear magnetic resonance,[17] surface polarization effects,[18] thermoelectric power,[19,20] thermal diffusivity,[21] electronic[22] and photochemical properties,[23] and the effect of plastic deformation on electrical conductivity.[24] Many of these properties have been studied as a function of Cd^{++} concentration, and some have been measured as a function of pressure. Qualitatively, the experiments agree with a model in which Frenkel disorder is dominant in the temperature range 175° to 350°C. The origin of the abnormal behavior above 350°C is still in dispute. The values quoted for the parameters controlling the Frenkel defects vary. The discrepancies arise principally from theoretical interpretation rather than experimental uncertainty. In particular, the doping experiments require a knowlege of the association energy of Cd^{++}Ag vacancy complexes. This energy is variously estimated as 0.16 ev[18] and 0.3 ev[25] from conductivity studies. The association of Cd^{++} ions and Ag vacancies has also been observed in the study of the Br NMR line[17] in doped AgBr.

In the ensuing sections, we will (1) give a brief description of the association and diffusion theories, (2) describe diffusion experiments which establish the probable validity of the diffusion mechanism suggested by Lidiard, (3) derive a value for the association energy of Cd^{++}Ag vacancy complexes, (4) demonstrate that the mobility of complexes is a function of Cd concentration, (5) estimate the effect of Debye-Hückel interactions, (6) describe supporting experiments, and (7) discuss the modifications required by these results in the interpretation of previous experiments. The experimental techniques and results are described in Sec. II. The theoretical analysis and discussion are given in Sec. III. In Sec. IV, we discuss the conclusions which may be drawn from this work.

[4] A. B. Lidiard, Phil. Mag. **46**, 815, 1218 (1955).
[5] R. W. Christy and A. W. Lawson, J. Chem. Phys. **19**, 517 (1951).
[6] W. Zieten, Z. Phys. **145**, 128 (1956).
[7] D. S. Tannhauser, L. J. Bruner, and A. W. Lawson, Phys. Rev. **102**, 1275 (1956).
[8] J. Teltow, Ann. Phys. **5**, 63 (1950).
[9] S. Kurnick, J. Chem. Phys. **20**, 218 (1952).
[10] R. J. Friauf, Phys. Rev. **105**, 843 (1957).
[11] A. S. Miller and R. J. Maurer, J. Phys. Chem. Solids **4**, 196 (1958).
[12] D. S. Tannhauser, J. Phys. Chem. Solids **5**, 224 (1958).
[13] G. Smith, G. Everett, and A. W. Lawson (private communication).
[14] J. Teltow and G. Wilke, Naturwissenschaften **41**, 423 (1954).
[15] R. Matejee, Z. Phys. **147**, 593 (1957).
[16] R. W. Christy, Acta Met. **2**, 284 (1954).
[17] F. Reif and M. H. Cohen, *Solid State Physics* (Academic Press, Inc., New York 1957), Vol. 5, p. 422 ff.
[18] R. J. Friauf, J. Chem. Phys. **22**, 1329 (1954).
[19] L. Patrick and A. W. Lawson, J. Chem. Phys. **22**, 1492 (1954).
[20] R. W. Christy, E. Fukushima, and H. T. Li, J. Chem. Phys. **30**, 136 (1959).
[21] T. E. Pochapsky, J. Chem. Phys. **21**, 1539 (1953).
[22] L. M. Shamouskii, A. A. Dunina, and M. I. Gustever, Soviet Phys. Doklady **1**, 124 (1956).
[23] J. W. Mitchell, *Chemistry of the Solid State* (Academic Press, Inc., New York, 1955), p. 311.
[24] W. G. Johnston, Phys. Rev. **98**, 1777 (1955).
[25] See reference 1, p. 308.

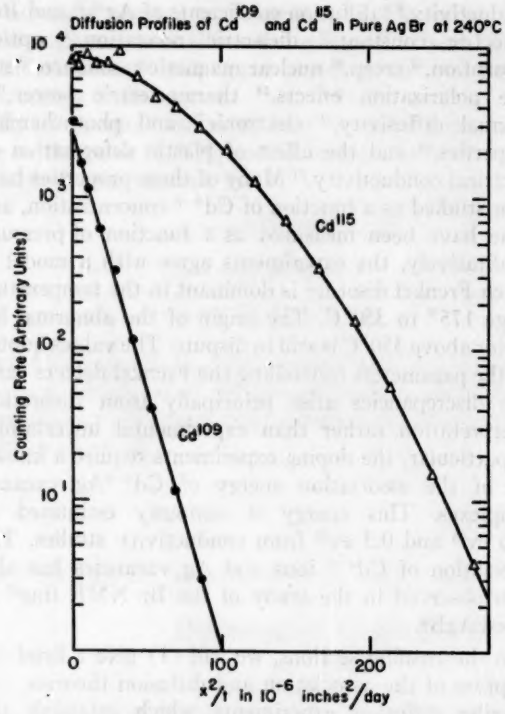
Diffusion Profiles of Cd109 and Cd115 in Pure AgBr at 240°C
Counting Rate (Arbitrary Units)
Cd115
Cd109
x²/t in 10⁻⁶ inches²/day

FIG. 1. Diffusion profiles of Cd^{109} and Cd^{115} in pure AgBr at 240°C.

II. EXPERIMENTAL PROCEDURES AND RESULTS

The diffusion of Cd into AgBr was measured by observing the penetration of radioactive Cd^{109} or Cd^{115} contained initially in a thin film of $CdBr_2$ deposited on the sample surface by evaporation from an aqueous solution. The activity per unit distance C, found in the sample at a depth x below the surface plane after a time t, is given by[26]

$$C=C_0/(\pi Dt)^{\frac{1}{2}}\exp(-x^2/4Dt) \qquad (1)$$

provided that the diffusion coefficient D is independent of the tracer concentration. In this case $-1/4Dt$ is the slope of the straight line obtained by plotting $\ln C$ vs x^2 in the usual way.

The AgBr was prepared from reagent grade AgNO and HBr. Single crystals were grown from the melt by the Czochralski method at a rate of $\frac{1}{2}$ to 1 in. per hr. For the doped samples, cp $CdBr_2$ was added to the melt. The ingots were rough cut with a jeweler's saw and machined to the form of right circular cylinders on a lathe using a stainless steel bit. Spectrographic analysis of the pure AgBr samples showed they contained about 20 ppm metallic impurities, principally Mg and Fe.

Since the diffusion of Cd in AgBr is strongly concentration dependent, it is essential to use high specific activity isotopes. Early work using 2.3-day half-life Cd^{115} yielded unsatisfactory profiles in pure AgBr at temperatures below 300°C. Later, carrier-free 470-day half-life Cd^{109} was used. Cd^{109} gave completely satisfactory profiles in pure AgBr at temperatures as low as 192°C, where the intrinsic vacancy concentration is 50 ppm. In Fig. 1, profiles are shown for Cd^{115} and Cd^{109} diffusion in pure AgBr at 240°C clearly exhibiting the superiority of the Cd^{109} data.

Before each experiment, the diffusion samples were annealed for from 3 to 60 hr at temperatures ranging from the diffusion temperature to 404°C. The diffusion anneals were from 50 min to one week in duration at temperatures ranging from 186° to 404°C. Thermal equilibrium was achieved in about 10 min after which the temperature was held constant to $\pm\frac{1}{2}$%°C by a proportional controller. Although the time average relative temperature was obtained to $\pm\frac{1}{4}$°C, the absolute temperature, measured by a Pt-Pt 10% Rh thermocouple calibrated against the melting points of Pb and Sn, was known to about $\pm\frac{1}{2}$°C corresponding to an uncertainty in the diffusion coefficient of $\pm 2\%$.

After the diffusion anneal the samples were aligned on a lathe so that the active surface was parallel to the cross feed within 0.05°, and about a dozen slices were turned off, each of thickness 1 to 4 mils. The thickness of each slice was determined to $\pm 5\%$ using a dial gauge and later checked to $\pm 1\%$ by weighing on a microbalance. The total distance removed was determined from the dial gauge settings and the relative weight of the first slice. This value checked to $\pm 1\%$ with that obtained from the difference in the sample weight before and after the experiment. The uncertainty in x^2 is therefore about $\pm 2\%$. The misalignment and slice thickness corrections amounted to less than 1%. The turnings were collected in 1-dram glass bottles for counting.

The 0.087- and 0.35-Mev γ's of Cd^{109} and Cd^{115}, respectively, were detected by a scintillation counter using a Tl-activated NaI crystal shaped like a well to obtain approximately 4π solid angle counting. The activity on the slices was corrected for background and counting efficiency fluctuations. The scatter of the points on the penetration plot from the best straight line average $\pm 5\%$, allowing D to be determined to $\pm 3\%$. Part of the scatter is caused by the fact that the counting efficiency of the weak Cd^{109} γ's varied with the arrangement of the active turnings. When the turnings were distributed evenly at the bottom of their containers the count obtained was up to 20% higher than when they were all in one corner. For this reason considerable care was exercised in reproducing the geometry for all slices.

The percentage of Cd in the doped samples was determined by separating the Ag using controlled potential electrolysis[27] and analyzing the residual Cd

[26] W. Jost, *Diffusion* (Academic Press, Inc., New York, 1952), p. 19.

[27] J. J. Lingane, *Electroanalytical Chemistry* (Interscience Publishers, Inc., New York, 1953).

concentration polarographically.[28] Typically, 250 mg of doped AgBr was dissolved in 125 ml of 0.1*M* KCN. During the electrolysis, the temperature was maintained above 65°C to avoid anodic deposition of Ag_2O_2. At the beginning of the electrolysis, the voltage of the cathode was held at −0.7 v with respect to a saturated calomel reference electrode. When the plating current decreased to its background value, the cathode voltage was reduced first to −0.8 v and finally to −0.9. After 2½ hr the amount of Ag remaining in solution was less than 2 mg, which did not interfere with the subsequent Cd determination. Spectrographic analysis of the Ag deposit showed that less than 1% of the Cd had coplated.

When the electrolysis was completed, the cyanide was driven off by acidifying with HCl and evaporating to dryness. The residual salts were then dissolved in distilled H_2O and an aliquot was polarographed. The Cd concentration was determined by comparing the wave height with that of previously run standards. The uncertainty of the Cd concentration was about ±8% for sample concentrations of less than 1% and ±5% for higher sample concentrations.

The values for the diffusion coefficients of Cd into pure AgBr at various temperatures together with their estimated uncertainties are given in Table I. All of the data in Table I were measured with Cd^{109} except the 339.7°C point for which Cd^{115} was used. The measurements of the temperature and the penetration plot slope are the largest sources of error. The data have not been corrected for thermal expansion; so when necessary in the analysis to follow, this effect is included using the values of Zieten.[6] This systematic correction amounts to +4% at 403°C and +2% at 300°C. Figure 2 illustrates the temperature dependence of Cd diffusion in pure and 3.30 atomic % Cd doped AgBr. The activation enthalpy for diffusion is 0.55±0.02 ev in the heavily doped sample and 0.95±0.02 ev in pure AgBr at the lower temperatures.

TABLE I. Diffusion coefficients of Cd in pure AgBr.

Sample	Temp °C	Diffusion coefficient cm²/sec
31	192.4±½°C	$3.30\pm0.16\times10^{-11}$
31	204.2	$5.70\pm0.3\times10^{-11}$
37	219.9	$1.20\pm0.06\times10^{-10}$
37	240.4	$2.38\pm0.12\times10^{-10}$
31	264.9	$6.70\pm0.3\times10^{-10}$
37	290.4	$1.71\pm0.08\times10^{-9}$
37	317.9	$5.20\pm0.3\times10^{-9}$
37	333.7	$1.06\pm0.05\times10^{-8}$
27	339.7	$1.38\pm0.11\times10^{-8}$
37	360.7	$2.46\pm0.15\times10^{-8}$
31	367.9	$3.72\pm0.22\times10^{-8}$
31	378.6	$7.00\pm0.42\times10^{-8}$
37	403.2	$1.76\pm0.11\times10^{-7}$

[28] I. M. Kolthoff and J. J. Lingane, *Polarography* (Interscience Publishers, Inc., New York, 1952), 2nd ed.

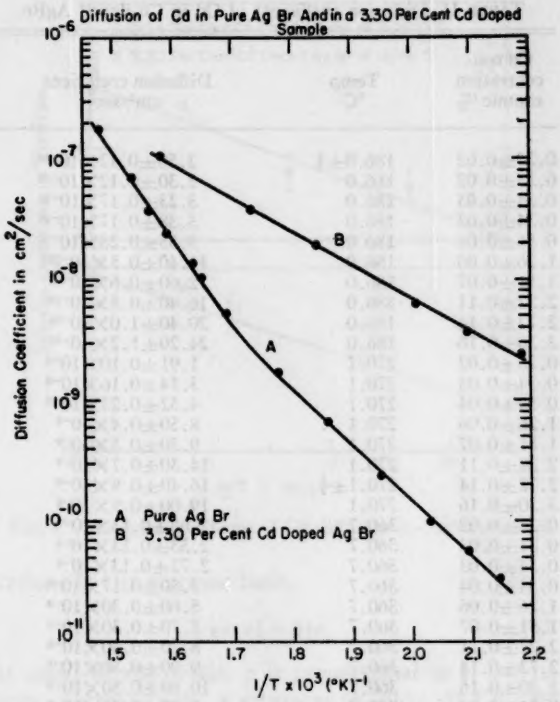

FIG. 2. Diffusion of Cd in pure AgBr and in a 3.3% Cd doped sample.

The doped sample diffusion data measured at atmospheric pressure are recorded in Table II. Three isothermal curves of $\log_{10} D$ vs Cd concentration are plotted in Fig. 3 to illustrate the concentration dependence. The doped sample results presented here differ by a factor of 3 on the average from the data given by Schone *et al.*[29] They measured the diffusion coefficient of Cd in AgBr by placing two samples with different Cd concentrations face to face in a furnace. After the diffusion anneal, they separated and homogenized the samples. They then measured the electrical conductivity to determine how much Cd was transferred from the high concentration to the low concentration sample. Because of the strong dependence of the Cd diffusion coefficient on concentration, the theoretical framework on which the analysis of the experiment is based is not valid.

The technique used in the high-pressure experiments has been described by Nachtrieb.[30] The pressure apparatus was heated by a snug-fitting furnace with warmup and cooldown times of 3 and 2 hr, respectively. Since the heating and cooling time amounted to from 30 to 50% of the diffusion duration, a quite large systematic correction is necessary, resulting in a large uncertainty of about ±12% in the measured values of *D*. The pressure experiments were carried out early in

[29] E. Schone, O. Stasiw, and J. Teltow, Z. physik. Chem. **197**, 10 (1951).

[30] N. H. Nachtrieb, J. A. Weil, E. Catalano, and A. W. Lawson, J. Chem. Phys. **20**, 1189 (1952).

TABLE II. Diffusion coefficient of Cd in Cd doped AgBr.

Cd concentration atomic %	Temp °C	Diffusion coefficient cm^2/sec
0.23±0.02	186.0±½	$2.50\pm0.12\times10^{-10}$
0.23±0.02	186.0	$2.30\pm0.12\times10^{-10}$
0.34±0.03	186.0	$3.23\pm0.17\times10^{-10}$
0.34±0.03	186.0	$3.38\pm0.17\times10^{-10}$
0.54±0.04	186.0	$5.55\pm0.28\times10^{-10}$
1.26±0.06	186.0	$11.40\pm0.5\times10^{-10}$
1.51±0.07	186.0	$12.60\pm0.6\times10^{-10}$
2.22±0.11	186.0	$16.40\pm0.8\times10^{-10}$
2.72±0.14	186.0	$20.40\pm1.0\times10^{-10}$
3.30±0.16	186.0	$24.20\pm1.2\times10^{-10}$
0.23±0.02	270.1	$1.91\pm0.10\times10^{-9}$
0.34±0.03	270.1	$3.14\pm0.16\times10^{-9}$
0.54±0.04	270.1	$4.52\pm0.23\times10^{-9}$
1.26±0.06	270.1	$8.50\pm0.4\times10^{-9}$
1.51±0.07	270.1	$9.30\pm0.5\times10^{-9}$
2.22±0.11	270.1	$14.30\pm0.7\times10^{-9}$
2.72±0.14	270.1±½	$16.40\pm0.8\times10^{-9}$
3.30±0.16	270.1	$19.00\pm0.9\times10^{-9}$
0.23±0.02	360.7	$2.68\pm0.13\times10^{-8}$
0.34±0.03	360.7	$2.53\pm0.13\times10^{-8}$
0.34±0.03	360.7	$2.72\pm0.13\times10^{-8}$
0.54±0.04	360.7	$3.50\pm0.17\times10^{-8}$
1.26±0.06	360.7	$5.60\pm0.30\times10^{-8}$
1.51±0.07	360.7	$5.70\pm0.30\times10^{-8}$
2.22±0.11	360.7	$8.70\pm0.40\times10^{-8}$
2.72±0.14	360.7	$9.00\pm0.50\times10^{-8}$
3.30±0.16	360.7	$10.60\pm0.50\times10^{-8}$
0.54±0.04	225.7	$1.57\pm0.09\times10^{-9}$
3.30±0.16	204.0	$3.70\pm0.3\times10^{-9}$
3.30±0.16	224.0	$6.30\pm0.4\times10^{-9}$
3.30±0.16	305.9	$3.80\pm0.2\times10^{-8}$

this work using Cd^{115}. Although the high-pressure data are not of high precision, they suffice for the peripheral role they play in the present work. The high-pressure data are presented in Table III and graphed in Fig. 4.

The distribution coefficient f of Cd in AgBr is approximately given by the ratio of Cd concentration in the ingot to that in the melt. From the analysis of the samples and the original amount of Cd in the melt, f was found to vary between 1.6 and 2.2. Using this value for f, we can estimate the Cd concentration gradient in the ingot to be about 5%/cm. Since the analysis samples were obtained from within a few mm of the sample surface and the total thickness removed from any sample was of the same magnitude, it is concluded that the concentration gradients existing in the samples were not significant.

The limit of solubility of $CdBr_2$ in AgBr according to Teltow[8] is 7% at the lowest temperature used in the present work, 186°C. To check this value, we obtained the heat of solution of $CdBr_2$ in AgBr by measuring the electrical conductivity of a 0.96±0.08% Cd doped sample from room temperature to 350°C. The ac electrical resistance of the sample with Pt electrodes was determined at 1000 cps using a Beco model 250 impedance bridge and a General Radio type 1231B amplifier and null detector. The sample capacitance was balanced out by an external capacitor placed across the appropriate bridge arm. In Fig. 5 the conductivity data are plotted against $1/T$ together with Teltow's data for a 1.0% Cd doped sample. The graph shows the following features: From room temperature to 117°C the conductivity is limited by the amount of Cd in solution. In the range 117° to 300°C the conductivity is proportional to the total Cd concentration and the Ag vacancy mobility. Above 300°C, the intrinsic vacancy concentration begins to play a role. Teltow's values for the electrical conductivity are lower in the mobility limited range, and the intrinsic defects begin playing a role at a lower temperature than in the present sample. Thus his sample may have contained somewhat less than 1.0 at % Cd.

According to Lidiard,[31] the heat of solution ΔH_s for $CdBr_2$ in AgBr should be approximately equal to twice the difference between the activation energies for electrical conductivity in the solubility limited and extrinsic regions. Using this analysis, we find $\Delta H_s=0.76\pm0.04$ ev which corresponds to a solubility limit of approximately 6% $CdBr_2$ at the lowest temperature used in the diffusion work. The fact that the samples were always transparent when first removed from the furnace after diffusion anneal also leads us to conclude that the sample concentration never exceeded the solubility limit at temperature.

III. THEORETICAL ANALYSIS AND DISCUSSION

There are at least three possible mechanisms for the diffusion of Cd in AgBr: (1) mobile Cd interstitials, (2) direct or ring interchange, and (3) mobile complexes.

Because the formation of a Cd interstitial requires the simultaneous formation of an Ag vacancy, Cd dop-

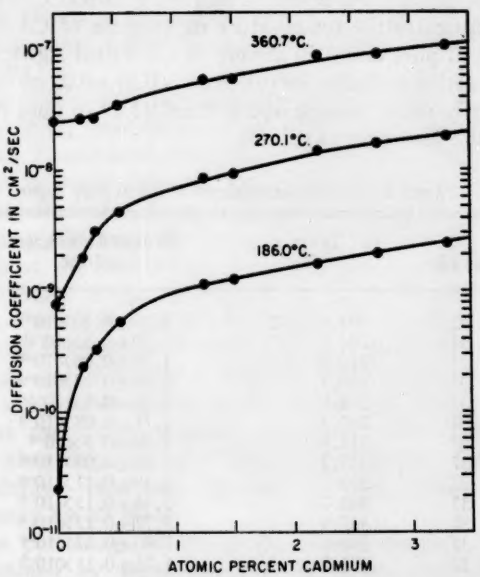

FIG. 3. Diffusion of Cd in AgBr as a function of Cd concentration.

[31] See Lidiard,[1] p. 294.

ing should decrease the impurity diffusion; however, experimentally, it increases markedly. Further, the activation volume of the impurity diffusion should be greater than that for the formation of Frenkel defects, which, according to Kurnick,[9] is 16 cm³/mole. The activation volume for Cd diffusion in AgBr is determined using the relation[30]

$$\Delta V^* = -\partial \ln D(c)/\partial P \qquad (2)$$

in which ΔV^* is the activation volume, $D(c)$ is the diffusion coefficient of Cd concentration c and P the pressure. From the pressure data illustrated in Fig. 4, we obtain $\Delta V^* = 9.8 \pm 1.0$ cm³/mole for the 0.54% Cd doped sample at 224°C and $\Delta V^* = 8.1 \pm 1.0$ cm³/mole for the 3.30% Cd doped sample at 306°C. Thus the observed activation volume is too small for diffusion by interstitials to be the dominant mechanism.

TABLE III. High pressure diffusion coefficients of Cd in doped AgBr.

Cd concentration atomic %	Temp °C	Pressure bars	Diffusion coefficient cm²/sec
0.54±0.04	224½±½	0	$1.53 \pm 0.09 \times 10^{-9}$
0.54±0.04	224½±2	150	$1.80 \pm 0.2 \times 10^{-9}$
0.54±0.04	224½±2	5000	$8.30 \pm 1.0 \times 10^{-10}$
0.54±0.04	224½±2	8000	$7.30 \pm 0.9 \times 10^{-10}$
3.30±0.16	306±½	0	$3.80 \pm 0.2 \times 10^{-8}$
3.30±0.16	306±2	4000	$2.72 \pm 0.33 \times 10^{-8}$
3.30±0.16	306±2	8000	$1.92 \pm 0.23 \times 10^{-8}$

Diffusion by direct or ring interchange should be relatively insensitive to the presence of small amounts of doping because the only effect of impurities would be to slightly alter the mobility of the ions. At low concentrations, it is difficult to envisage a sufficient change in mobility with doping to explain the sharp rise observed in the diffusion rate. It is even more difficult to explain the saturation effects at the larger doping concentrations. We therefore discard the interchange mechanism as a predominant factor in impurity diffusion.

On the other hand, diffusion by mobile complexes qualitatively agrees with the data very well. In this model, Cd^{++} ions are mobile only when they form nearest neighbor complexes with Ag vacancies. The diffusion of Cd should then be proportional to the fraction p of Cd^{++} ions which have Ag vacancies as nearest neighbors. The degree of association p is given by the chemical equilibrium equation[8]

$$p/(1-p) = (12v/N^+) \exp(\Delta G/kT) \qquad (3)$$

in which v is the concentration of unassociated vacancies, N^+ is the concentration of positive ion sites, ΔG is the association energy, k is Boltzmann's constant, and T is the absolute temperature. In the limit of low Cd concentration, $v = v_0$, the intrinsic vacancy concentration. In the extrinsic limit,

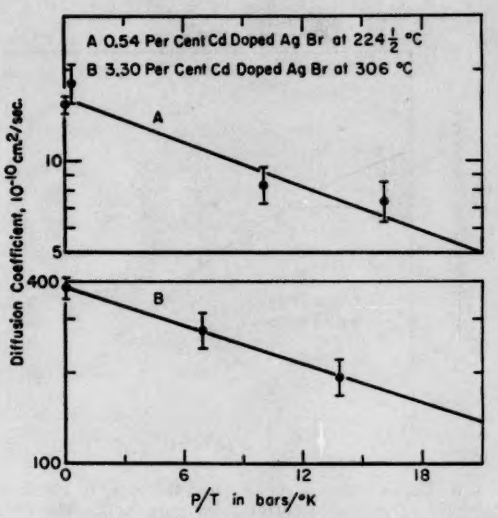

FIG. 4. Pressure dependence of Cd diffusion in doped samples.

$$v = (1-p)c. \qquad (4)$$

At small doping levels, p is proportional to c, but at large concentrations, p saturates to unity. If Cd ions diffuse as complexes, the diffusion rate should at first increase very rapidly with doping concentration and then saturate as association becomes complete. This is the observed behavior at 186.0° and 270.1°C. The very

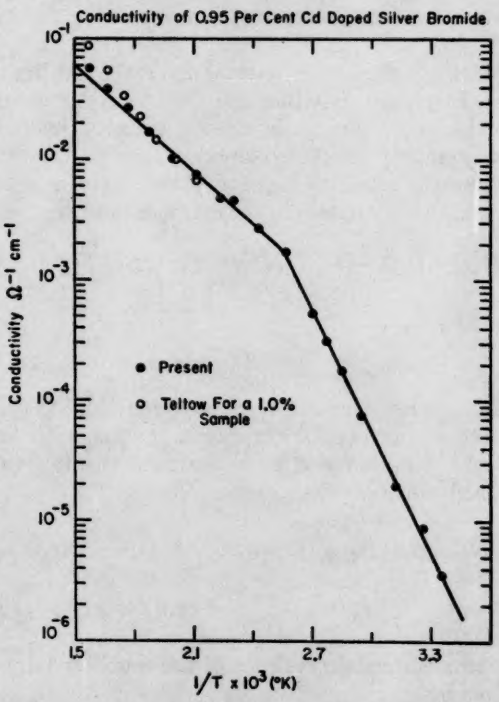

FIG. 5. Conductivity of 0.95% Cd doped AgBr as a function of temperature.

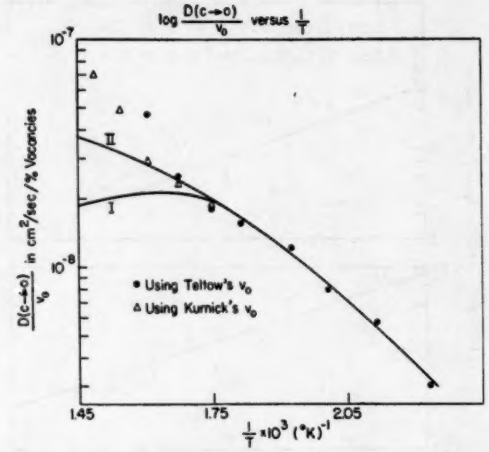

FIG. 6. Temperature dependence of the ratio of Cd diffusion to intrinsic vacancy concentration in pure AgBr. The dots are experimental points using Teltow's v_0 values. The triangles are experimental points using v_0 values reported by Kurnick.

low initial variation of D with c at 360.7°C is in agreement with the large value of v_0 at that temperature. Thus the present data strongly suggest that Cd^{++} ions diffuse in AgBr principally in the form of mobile complexes.

We shall now examine how well the theory of diffusion by complexes agrees quantitatively with the present data. According to Lidiard,[4] the diffusion of Cd in the form of complexes should be governed by

$$D(c)=(a^2\nu/3)(d/dc)(pc) \tag{5}$$

in which a is the lattice constant and ν, the rate limiting jump frequency, is either the Cd^{++} ion-Ag vacancy interchange frequency or the Ag vacancy jump frequency among complexed sites.

Using the relations between p and c given in Eqs. (3) and (4), we obtain in the extrinsic limit,

$$D(c)=D_0(1-[1+(48c/N^+)\exp(\Delta G/kT)]^{-1}) \tag{6}$$

in which

$$D_0=a^2\nu/3. \tag{7}$$

At small concentrations, $D(c)$ is proportional to c, but at large doping levels the bracketed term becomes large and the diffusion coefficient saturates to the value D_0. In the intrinsic limit, $c \ll v_0$,

$$D(c\to 0)=D_0(12v_0/N^+)\exp(\Delta G/kT)[1+(12v_0/N^+)+\exp(\Delta G/kT)]^{-1}. \tag{8}$$

The temperature dependence of the mobility term D_0 is given by

$$D_0=D_{00}\exp(-U_0/kT) \tag{9}$$

in which U_0 is the mobility activation energy. At low temperatures the bracketed term in Eq. (8) is nearly unity, and

$$\log_e[D(c\to 0)/v_0]=-(U_0/kT)+(\Delta G/kT)+\log_e(12D_{00}/N^+). \tag{10}$$

From the slope of the plot of $\log_e D(c\to 0)/v_0$ vs $1/T$, we may obtain the enthalpy of association, ΔH_a, if we know U_0;

$$\Delta G=\Delta H_a-T\Delta S_a, \tag{11}$$

in which ΔS_a is the entropy of association. Assuming that the Cd^{++} ions in the 3.30% Cd doped sample are nearly completely associated throughout the temperature range measured, we may obtain U_0.

ΔG may be estimated from ΔH_a using an empirical relation of Keyes[32] and Lawson,[33]

$$\Delta G=\Delta H_a(1-4\eta T), \tag{12}$$

in which η is the volume coefficient of expansion. From the data of Zieten,[6] $\eta=1.08\times10^{-4}$/°C in the low temperature region. At 500°K, $\Delta G=0.77\ \Delta H_a$. The best fit to the diffusion data in pure AgBr was obtained for $\Delta H_a=0.21\pm0.04$ ev using either Teltow's[8] or Kurnick's[9] values for v_0 in the low temperature region. Thus, ΔG at 500°K is 0.16±0.04 ev. The theoretical curve derived using Eq. (8) is curve I in Fig. 6. It may be seen that the saturation in the value of $D(c\to 0)/v_0$ at $1/T=1.75\times10^{-3}$ is found, but the sharp rise at higher temperatures is not. The scatter in the low temperature region is essentially that of the v_0 values.

ΔH_a should nearly be ΔG at $T=0$°K. It is suggestive that ΔH_a is only about 25% lower than $e^2/\sqrt{2}\epsilon a$ which would be the association energy at 0°K if only Coulombic interactions were operating (ϵ is the dielectric constant). In the analysis described in the preceding, ΔG was assumed to depend on temperature only because of the entropy term. Since ϵ exhibits a considerable temperature dependence in AgBr, it is of interest to

TABLE IV. Temperature dependence of the dielectric constant in pure AgBr.

Temp °C	Dielectric constant
175	15.8
186	16.0
200	16.2
225	16.4
250	17.4
270	17.8
275	18.0
300	19.0
325	20.1
350	20.6
361	19.2
375	19.0
400	19.7

[32] R. W. Keyes, J. Chem. Phys. **29**, 467 (1958).
[33] A. W. Lawson, J. Chem. Phys. Solids **3**, 250 (1957).

check whether the disagreement between experiment and theory at high temperatures may be due to this factor. Assuming that coulombic interactions are principally responsible for the association energy of a complex, we would expect ΔG to be proportional to ϵ^{-1}. Using this hypothesis, we find that an analysis of the data by a technique analogous to that described above yields ΔH_a (500°K) $=0.16\pm0.04$ ev and ΔG (500°K) $=0.12\pm0.04$ ev. The fit with the data is illustrated by curve II of Fig. 6. The theoretical curve is in close agreement with the experimental results below 350°C. The microwave dielectric constants of Smith *et al.*[13] used in the calculation are recorded in Table IV. When the dielectric constant data is extrapolated to 0°K, we find $\epsilon=11\frac{1}{2}$ and $\Delta G(0°K)=0.22\pm0.04$ ev, in good agreement with the previous estimate. Although curve II fits the data somewhat better at high temperatures than curve I, it is not felt that this is conclusive evidence that ΔG is proportional to ϵ^{-1}.

Including Debye-Hückel interactions in the manner of Lidiard[34] has little effect upon the analysis of the pure sample data. The ΔG and ΔH_a values obtained differ by less than 0.01 ev, well within experimental error.

We may conclude that the data for diffusion of Cd in pure AgBr agree well with Lidiard's association model using $\Delta G(0°K)=0.21\pm0.04$ ev. The deviation of the experimental results from theory at temperatures above 350°C may arise in the v_0 values, which are obtained from an analysis of the electrical conductivity data which is doubtful in this temperature range.

In deriving an association energy value, we have assumed that the activation energy for diffusion in the 3.30% Cd doped sample is the mobility activation energy. For this assumption to be valid, the degree of association in the heavily doped sample should not depend too markedly on temperature and the mobility activation energy should not be a strong function of cadmium concentration. The effect of the temperature variation of association in the heavily doped sample estimated using Eq. (6) is negligible. Since the activation energy for diffusion in all of the samples doped with more than $\frac{1}{2}$% Cd are within about 0.02 ev of each other, the variation of the mobility activation energy with Cd concentration is less than 0.01 ev/% Cd.

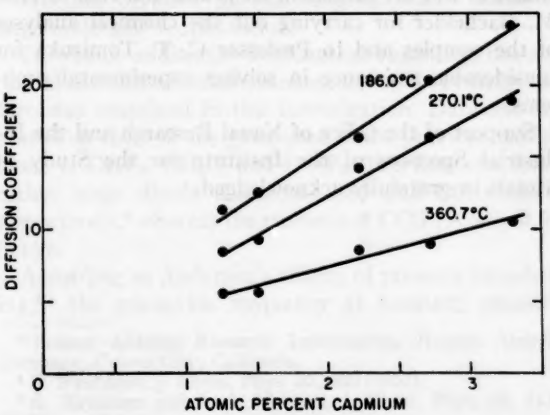

FIG. 7. The diffusion of Cd in AgBr at high doping levels. The units are 10^{-10} cm²/sec for the 186.0°C data, 10^{-9} cm²/sec for the 270.1°C data, and 10^{-8} cm²/sec for the 360.7°C data.

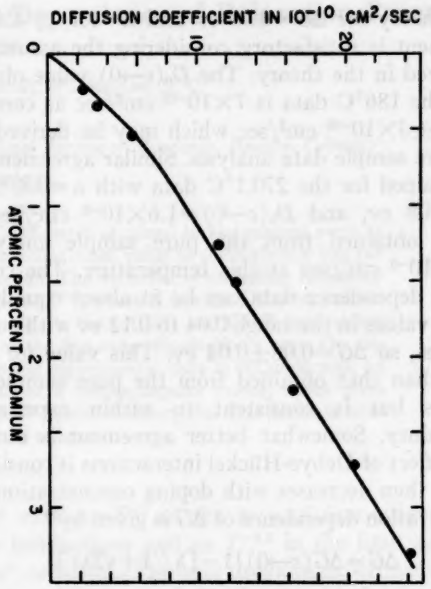

FIG. 8. Comparison of the 186.0°C experimental data with the theory assuming $\Delta G=0.08$ ev and $\alpha=1.1$/% Cd.

At large doping concentrations, the diffusion of Cd saturates as may be seen from Fig. 3. However, the Cd diffusion rate does not approach a limiting value but rather continuously increases with concentration. This behavior suggests that the mobility varies with Cd concentration. For the high Cd concentrations, association should be nearly saturated so the dependence of Cd diffusion upon concentration should be principally due to the mobility variation. In Fig. 7 the diffusion data for the samples doped with more than 1% Cd are plotted on a linear scale. It may be seen that the concentration dependence is satisfied reasonably well by a linear relation in this concentration range.

We may estimate from Fig. 7 that the mobility of complexes increases by a factor of 2 for 1% of Cd doping. Because of this very large concentration dependence of the mobility, it is difficult to rigorously test the form of Lidiard's expression for the dependence of the diffusion rate on the degree of association. Assuming a linear dependence of D_{00} on c,

$$D_{00}(c)=D_{00}(c\to0)(1+\alpha c), \qquad (13)$$

we can examine how well the diffusion results agree with Eq. (6). In Fig. 8, the data at 186°C are compared

[34] A. B. Lidiard, Phys. Rev. 94, 29 (1954).

with theory for $\Delta G=0.08$ ev and $\alpha=1.1/\%$ Cd. The agreement is satisfactory considering the assumptions employed in the theory. The $D_0(c\rightarrow 0)$ value obtained from the 186°C data is 7×10^{-10} cm²/sec as compared with $5\pm3\times10^{-10}$ cm²/sec which may be derived from the pure sample data analysis. Similar agreement may be obtained for the 270.1°C data with $\alpha=0.8/\%$ Cd, $\Delta G=0.08$ ev, and $D_0(c\rightarrow 0)=1.6\times10^{-9}$ cm²/sec. $D_0(c\rightarrow 0)$ obtained from the pure sample analysis is $2\pm1\times10^{-9}$ cm²/sec at this temperature. The concentration dependence data can be fit about equally well for ΔG values in the range 0.04 to 0.12 ev with suitable α values, so $\Delta G=0.08\pm0.04$ ev. This value for ΔG is lower than that obtained from the pure sample data analysis but is consistent to within experimental uncertainty. Somewhat better agreement is obtained if the effect of Debye-Hückel interactions is considered, for ΔG then decreases with doping concentration. The concentration dependence of ΔG is given by[34]

$$\Delta G=\Delta G(c\rightarrow 0)\{1-[\lambda/(1+\sqrt{2}\lambda)]\} \qquad (14)$$

in which

$$\lambda=(2\pi\sqrt{2})^{\frac{1}{2}}(e^2/\sqrt{2}\epsilon akT)^{\frac{1}{2}}[(1-p)c]^{\frac{1}{2}}. \qquad (15)$$

For $c\approx1\%$, ΔG is about 70% of the zero concentration value. If we consider the value obtained for ΔG as an average over the concentration range measured, we may predict $\Delta G(c\rightarrow 0)\approx0.11\pm0.05$ ev in better agreement with the pure data analysis. However, the large mobility effect masks the details of the association process to such an extent that it is not possible to obtain a precise value for ΔG or to determine with certainty its concentration dependence. We may conclude that the quantitative agreement of the concentration dependence of Cd diffusion with Lidiard's theory is satisfactory only if there is a large variation of mobility with doping concentration. The value of ΔG obtained from the doped analysis is consistent with that obtained from the pure data analysis.

It is possible that the high temperature anomaly in the electrical conductivity of pure AgBr is related to the dependence of mobility upon doping concentration discussed previously. Near the melting point, AgBr contains a few percent of ionic imperfections which may increase the mobility as much as would a similar impurity concentration. If the mobility of complexes increased by a factor of 2 for 1% Ag vacancy concentration, the agreement between the data for Cd diffusion in pure AgBr and the theory would be much better in the high-temperature range. An increase in the Ag vacancy mobility of about the same magnitude would also resolve the high-temperature electrical conductivity anomaly.

IV. CONCLUSIONS

Using Lidiard's theory for the diffusion of complexes, we have derived a value for the association energy ΔG of Cd^{++}-Ag vacancy complexes in AgBr from the measured rate of Cd diffusion in pure AgBr, the observed activation enthalpy for the diffusion of Cd in a heavily doped sample, and the previously measured intrinsic vacancy concentration. The value of ΔG extrapolated to 0°K is estimated to be 0.21 ± 0.04 ev. Although Lidiard's theory is qualitatively consistent with the concentration dependence of Cd diffusion, the detailed dependence can be explained quantitatively only by introducing a very large dependence of mobility upon doping concentration. It is necessary to assume that the mobility of complexes increases by a factor of about 2 upon doping AgBr with 1% $CdBr_2$. Assuming that the mobility of complexes varies linearly with doping concentration, we obtained a value for ΔG from the concentration dependence of Cd diffusion which is consistent with that obtained from the pure sample data analysis. Better agreement is obtained if the effect of Debye-Hückel interactions is included in the analysis of the doped sample data.

ACKNOWLEDGMENTS

The author wishes to express his particular gratitude to Professor A. W. Lawson for his continued interest, encouragement, and valuable suggestions during the course of this investigation. He is also indebted to Miss M. Bachelder for carrying out the chemical analyses of the samples and to Professor C. T. Tomizuka for considerable assistance in solving experimental problems.

Support of the Office of Naval Research and the Industrial Sponsors of the Institute for the Study of Metals in gratefully acknowledged.

Nonresonant Absorption in Symmetric-Top Gases: Dependence of Relaxation Frequency on Temperature

A. A. MARYOTT, *National Bureau of Standards, Washington, D. C.*

AND

A. ESTIN AND G. BIRNBAUM,* *Boulder Laboratories of the National Bureau of Standards, Boulder, Colorado*

(Received December 7, 1959)

The nonresonant absorption spectra of CHF_3, CH_3F, and $CClF_3$ were obtained in the gaseous state at various temperatures in the range 230° to 360°K. In all cases the maximum value of the dielectric loss per unit pressure varies as T^{-2}, in accordance with the Debye equation. The variation of relaxation frequency (line width) with pressure and temperature is represented by $\Delta\nu \propto pT^{-m}$, where m has the following values: 1.59 ± 0.03 for CHF_3, 1.60 ± 0.02 for CH_3F, and 1.27 ± 0.02 for $CClF_3$, Since CHF_3 and CH_3F have rather large dipole moments, the predominant interaction should be of the first-order dipole-dipole type. On this basis Anderson's theory predicts $m=1$. Closer agreement with the experimental data is obtained with an expression derived essentially from dimensional considerations of a torque-impulse model, which gives $m=1.5$. In the case of $CClF_3$, which has a comparatively small dipole moment, the data indicate that molecular reorientation is governed primarily by forces of shorter range.

INTRODUCTION

IN a preceding paper[1] the nonresonant, or Debye-like, absorption spectra of a number of symmetric-top molecules were studied in the vapor phase in order to obtain the detailed shape of these spectra and the relaxation times for molecular reorientation. When the dipole moment is small, substantially less than one debye unit, the Debye line shape is found to represent accurately the experimental data. For gases with larger dipole moments, there are small but definite deviations from the Debye shape which are indicative of a distribution of relaxation times. For pressures up to at least several atmospheres, the relaxation frequency, or line width, increases in proportion to the pressure. This dependence on pressure shows that only binary collisions are important in the relaxation mechanism. It was also shown[2] that the relaxation frequencies for the various gases with large dipole moments could be correlated on the basis that the first order dipole-dipole interaction between the colliding molecules causes a large molecular reorientation.

To obtain additional information regarding the nature of the relaxation mechanism, the effect of temperature was examined in this investigation. Data are reported on three of the gases used in the previous study, namely, CHF_3, CH_3F, and $CClF_3$. The first two have rather large dipole moments, 1.81 and 1.64 debyes, respectively,[3] whereas the moment of $CClF_3$ is only 0.50 debye.

According to Anderson's theory of pressure broadening,[4,5] the relaxation frequency at constant pressure should vary as T^{-1} in the case of first-order dipole-dipole interactions and as $T^{-0.5}$ in the limit of "hard sphere" collisions. The only previous experimental data appear to be those of Krishnaji and Srivistava[6] on CH_3Cl. Their results are consistent with Anderson's theory within the assigned limits of error ($T^{-1.2\pm0.3}$), but the large uncertainty precludes a definitive test. The present results, on the other hand, clearly show that the effect of temperature is well outside the limits set by Anderson's theory.

EXPERIMENTAL

The apparatus and resonant-cavity technique used to measure the dielectric loss in compressed gases have been described previously.[7] The present measurements were made at a frequency of 1190 Mc (0.0398 cm^{-1}) with a TM_{01} hybrid mode cavity having a loaded Q in the neighborhood of 3000.

The gases were portions of the samples previously used. The temperature of the cavity was regulated with an air bath that was heated electrically or cooled with dry ice. The temperature was measured with a thermocouple, one junction of which was mounted on the cavity. Pressures were determined with a mercury manometer.

METHOD OF ANALYZING THE DATA

The frequency and the range of pressures employed are sufficiently low so that the resonant absorption associated with the pure rotational spectrum makes a negligible contribution to the observed loss. Also, the relaxation frequency may be assumed to be simply proportional to the pressure and deviations from the ideal gas density are small. For this case the procedures used to evaluate the parameters characterizing the non-

* Present address: Research Laboratories, Hughes Aircraft Company, Culver City, California.

[1] G. Birnbaum, J. Chem. Phys. **27**, 360 (1957).

[2] G. Birnbaum and A. A. Maryott, J. Chem. Phys. **29**, 1422 (1958).

[3] A. A. Maryott and F. Buckley, *Table of Dielectric Constants and Electric Dipole Moments of Substances in the Gaseous State*, Natl. Bur. Standards Circ. No. 537 (1953).

[4] P. W. Anderson, Phys. Rev. **76**, 647 (1949).

[5] Townes and Schawlow, *Microwave Spectroscopy* (McGraw-Hill Book Company, Inc., New York, 1955), Chap. 13.

[6] Krishnaji and G. P. Srivistava, Phys. Rev. **109**, 1562 (1958).

[7] A. A. Maryott and G. Birnbaum, J. Chem. Phys. **24**, 1022 (1956); H. E. Bussey and G. Birnbaum, Rev. Sci. Instr. **30**, 800 (1959).

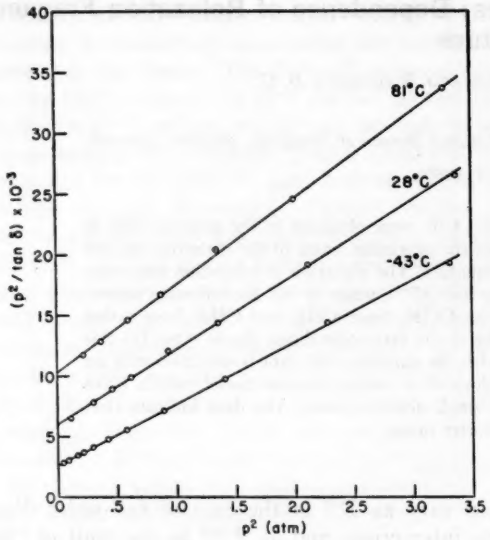

FIG. 1. Representative data for $CClF_3$. Plots of $p^2/\tan\delta$ as a function of p^2 at several temperatures.

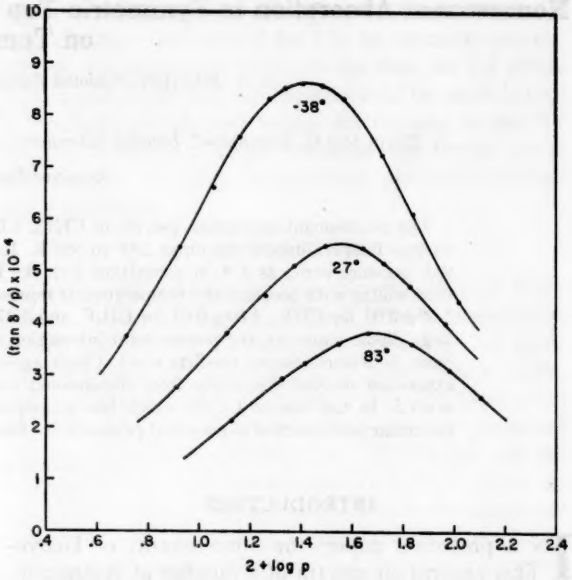

FIG. 2. Representative data for CH_3F. Plots of $\tan\delta/p$ as a function of $\log p$ at several temperatures.

resonant loss have already been discussed[1,7] and will be reviewed only briefly.

When the loss is governed by a single relaxation frequency,

$$\tan\delta/p = 2\,(\tan\delta/p)_{\max}[\nu\Delta\nu/(\Delta\nu^2+\nu^2)], \qquad (1)$$

where ν and $\Delta\nu$ are the applied frequency and the relaxation frequency, respectively. Since $\Delta\nu \propto p$, it is convenient to express the loss tangent as a function of pressure in the form,

$$p^2/\tan\delta = a + bp^2. \qquad (2)$$

The relaxation frequency parameter is then given by

$$\Delta\nu/p = (b/a)^{\frac{1}{2}}, \qquad (3)$$

and the maximum value of the loss tangent per unit pressure (occurring when the relaxation frequency and and the applied frequency are equal) by

$$(\tan\delta/p)_{\max} = (4ab)^{-\frac{1}{2}}$$
$$= [2\pi(N/p)\mu^2/3kT]\textstyle\sum_{JK} f_{JK}K^2/(J^2+J), \qquad (4)$$

where μ is the dipole moment and f_{JK} is the fractional number of molecules in the rotational state designated by the quantum numbers J and K.

Data that are not adequately represented by a single relaxation frequency parameter [Eq. (2)] can be represented by plots of $\tan\delta/p$ as a function of $\log p$. The bell-shape curve will be somewhat broader than the Debye curve for a single relaxation frequency, and the value of $(\tan\delta/p)_{\max}$ will be less than that computed from the right-hand side of Eq. (4). The relaxation frequency parameter is then some average value, and $\tan\delta/p$ has its maximum value when $\langle\Delta\nu\rangle = \nu$.

TABLE I. Parameters for the nonresonant absorption of $CClF_3$ at various temperatures.

T (°K)	$\Delta\nu/p$ cm^{-1} atm^{-1}	$(\tan\delta/p)_{\max}$ atm^{-1}
230.0	0.0557	1.38×10^{-4}
240.8	0.0525	1.28
253.7	0.0487	1.13
270.6	0.0454	0.995
301.5	0.0397	0.807
315.6	0.0373	0.706
329.2	0.0342	0.654
343.6	0.0330	0.623
354.2	0.0328	0.582

RESULTS

The data for $CClF_3$ are accurately represented at all temperatures by Eq. (2). There is no evidence of a distribution of relaxation frequencies. Representative plots of $p^2/\tan\delta$ with respect to p^2 are shown in Fig. 1. The values of $(\tan\delta/p)_{\max}$ and $\Delta\nu/p$ obtained from these and similar plots at the other temperatures are summarized in Table I.

TABLE II. Parameters for the nonresonant absorption of CHF_3 at various temperatures.

T (°K)	$\langle\Delta\nu\rangle/p$ cm^{-1} atm^{-1}	$(\tan\delta/p)_{\max}$ atm^{-1}
238.8	0.0733	20.7×10^{-4}
256.8	0.0659	18.5
273.2	0.0582	16.6
296.1	0.0518	13.0
319.8	0.0459	12.2
330.9	0.0436	11.0
359.6	0.0385	9.27

TABLE III. Parameters for the nonresonant absorption of CH_3F at various temperatures.

T (°K)	$\langle\Delta\nu\rangle/p$ cm^{-1} atm^{-1}	$(\tan\delta/p)_{max}$ atm^{-1}
231.2	0.165	9.54×10^{-4}
234.6	0.148	8.65
258.1	0.141	7.49
271.4	0.130	6.80
299.4	0.111	5.42
318.3	0.103	4.95
330.6	0.0938	4.48
356.1	0.0830	3.87

The shapes of the loss curves for CHF_3 and CH_3F are somewhat broader than those for the Debye case, so the characteristic parameters were evaluated from plots of $\tan\delta/p$ with respect to $\log p$, as illustrated in Fig. 2 for CH_3F. Values of $(\tan\delta/p)_{max}$ and $\langle\Delta\nu\rangle/p$ are listed for CHF_3 and CH_3F in Tables II and III, respectively.

DISCUSSION

(A) Dependence of $(\tan\delta/p)_{max}$ on Temperature

It is apparent from Eq. (4) that $(\tan\delta/p)_{max}$ should vary as the inverse square of the absolute temperature in cases where there is a single relaxation time, provided the small deviations from the ideal gas law are neglected so that $(N/p)\propto T^{-1}$. A least-squares analysis of the data for $CClF_3$, as plotted in Fig. 3, gives $(\tan\delta/p)_{max}\propto T^{-2.03\pm0.02}$; the uncertainty expressed in the exponent being the probable error. These data show no significant departure from the expected dependence on temperature.

Similar plots for the two more polar gases, CHF_3 and CH_3F, are shown in Fig. 4. These give $T^{-2.02\pm0.06}$ and $T^{-2.02\pm0.04}$, respectively, for CHF_3 and CH_3F.

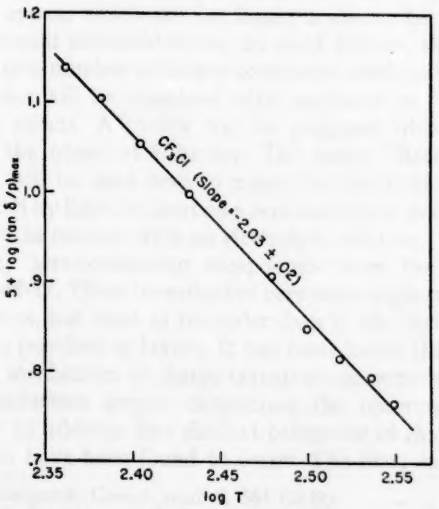

FIG. 3. Variation of $(\tan\delta/p)_{max}$ with temperature for $CClF_3$. Plot of $\log(\tan\delta/p)_{max}$ as a function of $\log T$.

Since there is a distribution of relxation frequencies, causing a deviation from the Debye shape in these cases, good agreement with the T^{-2} law indicates that the breadth of the distribution is not sensitive to temperature. For CHF_3, this distribution lowers the value of $(\tan\delta/p)_{max}$ by about 12%. Similar departures from the simple Debye shape occur in many polar liquids and solutions.[8] In contrast to the behavior of the foregoing gases, the breadth of the distribution of relaxation frequencies in liquids usually depends strongly on

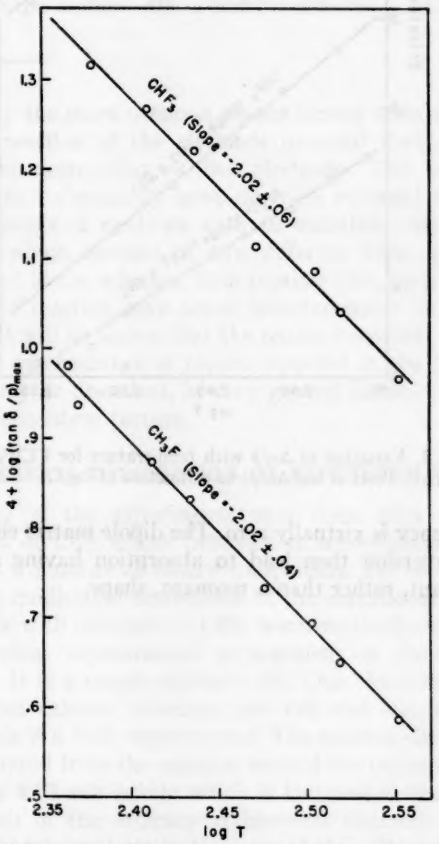

FIG. 4. Variation of $(\tan\delta/p)_{max}$ with temperature for CHF_3 and CH_3F. Plots of $\log(\tan\delta/p)_{max}$ as a function of $\log T$.

temperature, and the loss curves rapidly approach the Debye shape at higher temperatures.

(B) Dependence of $\Delta\nu/p$ on Temperature

Anderson's theory of pressure broadening has been notably successful in predicting the line widths and their dependence on temperature in the case of the resonant inversion spectrum of ammonia. The theory might also be considered applicable to the more general case of the symmetric-top molecule, where the inversion

[8] F. Buckley and A. A. Maryott, *Tables of Dielectric Dispersion Data for Pure Liquids and Dilute Solutions*, Natl. Bur. Standards Circ. No. 589 (1959).

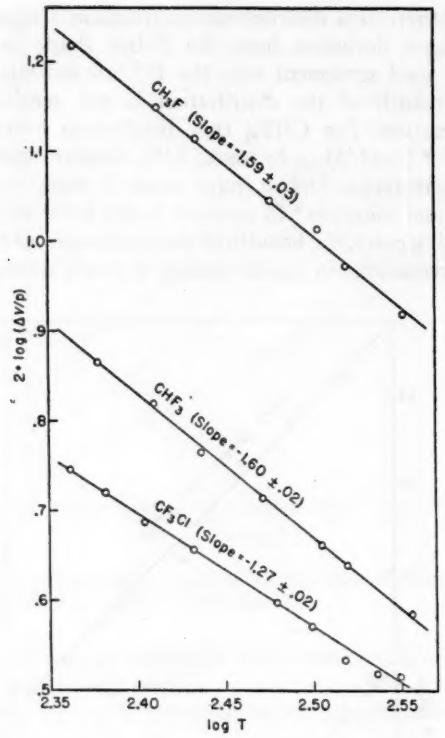

FIG. 5. Variation of $\Delta\nu/p$ with temperature for $CClF_3$, CHF_3, and CH_3F. Plots of $\log(\Delta\nu/p)$ as a function of $\log T$.

frequency is virtually zero. The dipole matrix elements for inversion then lead to absorption having a nonresonant, rather than a resonant, shape.

With the intermolecular potential of the form A/b^n, Anderson's theory gives

$$\Delta\nu/p \propto T^{-m} \text{ and } m=(n+1)/(2n-2), \quad (5)$$

where T is the absolute temperature. Since $n=3$ for the first order dipole-dipole interactions and $n\rightarrow\infty$ in the limit of "hard-sphere" collisions, the exponent, m, is restricted to values in the range 1 to 0.5.

The experimental results are shown in Fig. 5, where $\log(\Delta\nu/p)$ is plotted as a function of $\log T$. These plots appear linear, in accordance with Eq. (5), but the values of the exponent m lie well outside of the limits of Anderson's theory, being 1.59 ± 0.03 for CHF_3, 1.60 ± 0.02 for CHF_3, and 1.27 ± 0.02 for $CClF_3$.

Better agreement is obtained with an expression which we employed previously[2] to correlate the magnitude of the relaxation frequencies for a variety of symmetric-top molecules. This relation, based on dimensional considerations of an idealized torque-impulse model of collisions, leads to a temperature dependence of the form,

$$\Delta\nu/p \propto T^{-(n+3)(2n-2)}. \quad (6)$$

For dipole-dipole interactions, $\Delta\nu/p$ is then proportional to $T^{-1.5}$, in reasonably good agreement with the data for the two more polar gases. The lesser dependence on temperature in the case of $CClF_3$ is in qualitative accord with the fact that the dipole moment is small, so that shorter-range interactions should be more important. At the present time, however, there appears to be no complete and satisfactory theory relating nonresonant relaxation to molecular properties.

Becquerel Photovoltaic Effect in Binary Compounds

RICHARD WILLIAMS
RCA Laboratories, Princeton, New Jersey

(Received December 10, 1959)

An experimental study has been made of photovoltaic effects which occur at semiconductor-electrolyte interfaces. Single crystal specimens of CdS and several other compounds were used. It was found that in a number of cases the photovoltaic effect results from a chemical reaction of the electrode materials. In such cases the observations may be explained by a simple mechanism which relates the sign of the photo-emf to the conductivity type of the semiconductor and to the chemical reaction which is occurring. The reaction may be predicted using readily available thermodynamic data. A different process occurs when the electrode material is GaAs. It acts as an inert electrode which exchanges electrons with an oxidation-reduction couple in the solution.

BECQUEREL observed the first photovoltaic effect in 1839.[1] He used an electrode consisting of a sheet of platinum covered with a thin layer of silver chloride. The nature of the second electrode is not entirely clear from his account, but it was probably a sheet of platinum. These dipped into an electrolyte solution and, when the silver chloride electrode was illuminated, an electric current resulted. He was able to demonstrate that the current was not due to a heating effect, and obtained a rough spectral response curve by means of color filters placed between the electrode and the light source, which was the sun. In addition, he postulated that the current resulted from a chemical reaction at the electrode and gave the correct reaction. A number of similar experiments have been reported since, but no modern interpretation of a general nature has emerged. Very recently, some important contributions to understanding of the photovoltaic effect in semiconductor-electrolyte systems have appeared in studies of the electrode properties of elemental semiconductors.[2,3] When the electrode is made of a binary compound semiconductor, several features of its behavior appear which are not found in electrodes made of elemental semiconductors. In what follows, the behavior of a number of binary compound semiconductor electrodes will be examined with emphasis on photovoltaic effects. A theory will be proposed which explains the observed behavior. The name "Becquerel effect" will be used here to mean the electrical effect produced by light incident on a semiconductor electrode which is in contact with an electrolyte solution.

Many semiconducting compounds show the Becquerel effect. Those investigated here were single crystal specimens, but most of the older data in the literature refer to powders or layers. It has been found that the special mechanism of charge transport characteristic of semiconductors largely determines the observed behavior. In addition two distinct categories of electrode reaction have been found to occur. The first, and apparently the more common among binary compounds, is the reaction of the electrode material itself, with eventual destruction of the electrode. The second occurs in a chemically inert electrode material and is an exchange of electrons with an oxidation-reduction couple which consists of two different ionic species dissolved in the solution. It is possible that both categories of reaction may occur simultaneously in some cases. It will be shown that the results from this work, as well as a number of results reported in the literature, may be described, in their general features, by a simple consistent picture.

GENERAL DESCRIPTION OF EXPERIMENTS

Many of the experiments were done with single crystals of CdS whose behavior is representative of that of a number of binary compounds. For convenience, a qualitative description of the experiments will be made with reference to CdS. A schematic drawing of the typical experimental arrangement is shown in Fig. 1. It is a simple galvanic cell. One electrode is a saturated calomel reference half cell and the second electrode is a CdS single crystal. The calomel electrode is separated from the solution around the crystal by a built-in KCl salt bridge which is included in the construction of the ordinary commercial electrode. The CdS crystals used are in the form of thin plates about 10 x 2 x 0.1 mm in their dimensions. They were grown in this laboratory by Charles Busanovich. They are clear yellow in color with strong light absorption occurring for wavelengths less than about 5150 A and high transparency for longer wavelengths. Because of the presence of small amounts of chlorine incorporated during their growth, they are highly conducting. Their dark resistivities are around 10 ohm cm. An ohmic indium dot contact[4] is made to the upper end of the crystal and led to an electrometer as illustrated. The crystal is then mounted so that its bottom half is immersed in the electrolyte solution and its upper half remains dry. A tungsten lamp is mounted so that its light is incident on the broad face of the crystal. When

[1] E. Becquerel, Compt. rend. **9**, 561 (1839).
[2] W. H. Brattain and C. G. B. Garrett, Bell System Tech. J. **34**, 129 (1955).
[3] H. Gobrecht, R. Kuhnkies, and A. Tausend, Z. Elektrochem. **63**, 541 (1959).
[4] R. W. Smith, Phys. Rev. **97**, 1525 (1955).

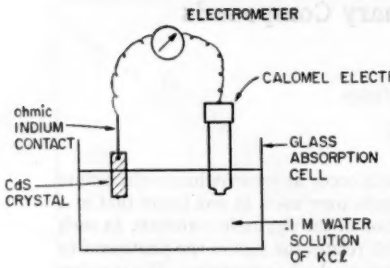

FIG. 1. Schematic drawing of apparatus for observing the Becquerel effect.

the crystal is illuminated, an emf of about 0.6 v develops immediately. The crystal is the negative terminal. Short circuit currents of about 100 μA are produced under bright illumination. The current and voltage in the dark are negligible compared to their values in the light. The short circuit current is proportional to light intensity at low intensities and reaches a saturation value at high intensities. The emf is a complicated but monotonic function of light intensity, very roughly logarithmic. If the cell is short-circuited and illuminated for a period of several hours, a layer of a pale yellow solid forms on that face of the crystal on which the light is incident, but not on the face farthest from the lamp. This solid is soluble in cyclohexane and the ultraviolet spectrum of the dissolved product agrees very well with the spectrum which has been reported for sulfur.[5] It is concluded that this material is free sulfur which has been formed by the chemical decomposition of the crystal of CdS under the influence of light. The preceding characteristics are representative of cases where the Becquerel effect is demonstrably (or very likely) the result of a chemical reaction which consumes the electrode material.

By the following experiment it may be shown that the driving force for the photo-emf is inherent in the crystal and is not provided by the reference electrode. The reference electrode may be replaced by a CdS crystal so there is a symmetrical system with two identical CdS crystals forming the two electrodes. An emf is now observed if one crystal is illuminated and the other is kept dark. Whichever crystal is illuminated becomes negative and the direction of current flow may be reversed at any time by switching the light beam from one crystal to the other.

EXPERIMENTAL DETAILS

The actual experimental apparatus was quite similar to the schematic arrangement shown in Fig. 1. A glass absorption cell was used with inside dimensions of 5×5×5 cm and optically finished windows. The cell was placed inside a small brass box which was covered and provided with a small window through which the crystal could be illuminated. A tungsten microscope lamp was used where monochromatic light was not required. The flux of radiation of the focused lamp was measured and found to be 0.6 w/cm². The highest values of light intensity shown in Figs. 2, 3, and 10 refer to this value. Considering the errors involved, the above figure for the absolute intensity is believed to be accurate to within 50%. The relative intensity values are believed to be accurate to within 10%. Various known relative intensities of light were obtained by interposing calibrated wire screens between the lamp and the absorption cell. Monochromatic light was obtained from a Bausch and Lomb grating monochromator fitted with a tungsten lamp source. This was calibrated to give the relative number of photons/sec at the exit slit for various wavelengths. Current and emf were measured with a Keithley Model 610 electrometer. For emf measurements the input impedance of the instrument could be varied by factors of ten up to a maximum of 10^{14} ohms. It was found that with most crystals the observed emf was independent of input resistance of the electrometer in the range of 10^{6} to 10^{14} ohm for the input resistance. Most emf measurements were therefore made with the highest input impedance to minimize the amount of chemical reaction at the crystal. In some crystals a small and unreproducible dark emf was observed for the highest values of input impedance but was absent for input impedances below 10^{9} ohm. To eliminate this extraneous emf an input impedance of 10^{8} was used for some of the measurements of emf. It was found that stirring the solution of bubbling nitrogen through it during the measurements did not significantly affect the results. Some measurements were made of the current as a function of externally applied voltage with various incident light intensities. Known voltages were applied by means of a Helipot potentiometer and attached voltmeter. All measurements were made at 25°C. Deionized water and analytical grade reagents were used in the preparation of solutions.

RESULTS WITH CdS CRYSTALS

A typical curve of emf vs light intensity is given in Fig. 2. It can be seen that the emf increases very slowly as the light intensity increases. The emf for a given light intensity is steady over operating periods of

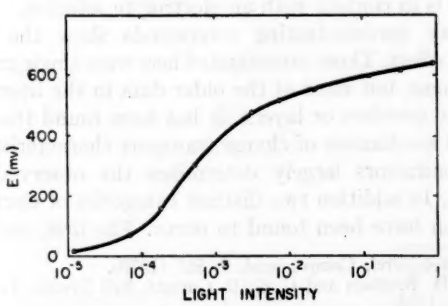

FIG. 2. Photo-emf at various light intensities for CdS. Crystal becomes negative terminal on illumination.

[5] J. E. Baer and M. Carmack, J. Am. Chem. Soc. **71**, 1214 (1949).

hours and is reproducible from crystal to crystal to within about 10% (more than ten crystals were tested). A log-log plot of short circuit current vs light intensity is shown in Fig. 3. At low light intensity the slope of the line is unity showing a direct proportionality between current and light intensity. At high light intensity a saturation current is reached. The spectral response curve in Fig. 4 shows the short-circuit current per unit light intensity (quanta per second) as a function of wavelength. The absorption spectrum of the CdS is shown in the same drawing and the position of the optical band edge[6] is shown.

As will be discussed thoroughly in the next section, the probable reaction occurring at the CdS electrode is the solution of a Cd^{++} ion. A negatively charged S^{--} ion is left behind on the crystal and the removal of electrons from this completes the electrode reaction. If the electrode does, indeed, involve a cadmium ion

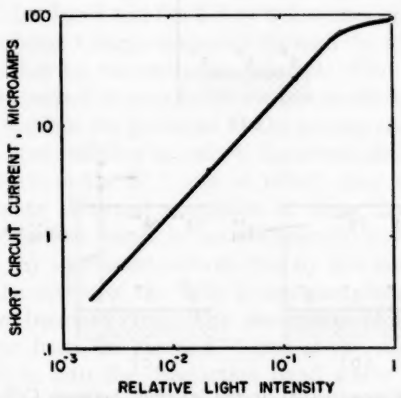

FIG. 3. Current at various light intensities for CdS vs calomel electrode in 0.1 *M* KCl.

going into solution then there should be an effect on the emf if cadmium ions are present in the solution. For the electrode reaction,

$$CdS \rightarrow Cd_{aq}^{++} + S + 2e,$$

the relation between the potential, E, of the half cell in which the reaction is occurring, and the activity, $a_{Cd^{++}}$, of the cadmium ion in solution is given by the Nernst equation,[7]

$$E = E_0 - (RT/2F) \ln a_{Cd^{++}}.$$

(The definition of E_0 now differs from the usual definition in that it must include the light intensity.) Thus, the observed emf, which is the sum of this half cell potential and the half cell potential of the calomel reference electrode, should decrease as the concentration of cadmium ions in the solution increases. It is unlikely that the CdS electrode is reversible, which is necessary

[6] R. H. Bube, Proc. I. R. E. **43**, 1836 (1955).
[7] W. M. Latimer, *Oxidation Potentials* (Prentice-Hall, Inc., Englewood Cliffs, New Jersey, 1952), 2nd ed.

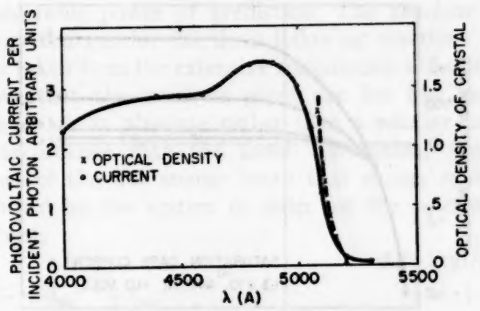

FIG. 4. Spectral response of photovoltaic effect compared with optical density of CdS crystal. Photovoltaic current units on left ordinate; optical density units on right ordinate. Crystal thickness ca 0.1 mm.

for quantitative use of the Nernst equation, but the qualitative relation between electrode potential and cadmium ion concentration should still hold. Figure 5 shows the emf at constant light intensity of the cell in which the CdS electrode is in solutions containing various concentrations of $CdCl_2$. In addition there are shown the emf values for cells in which the CdS electrode is in various concentrations of a solution of an inert salt, KCl. Changes in the concentration of the cadmium salt clearly have a larger influence on the emf than do changes in the concentration of KCl, showing that it is not simply an ionic strength effect which is involved. The change in emf with cadmium ion concentration is in the direction and of the order of magnitude which the Nernst equation predicts. No attempt has been made to fit the data quantitatively to the Nernst equation because $CdCl_2$ solutions contain several ionic species in equilibrium, and not enough data are available to determine the Cd^{++} activity at the several ionic strengths employed here.

An important consideration in understanding the photovoltaic effects is the mechanism of charge transport across the interface between crystal and solution. To throw some light on this question measurements were made of current as a function of externally applied voltage with various intensities of light incident on the

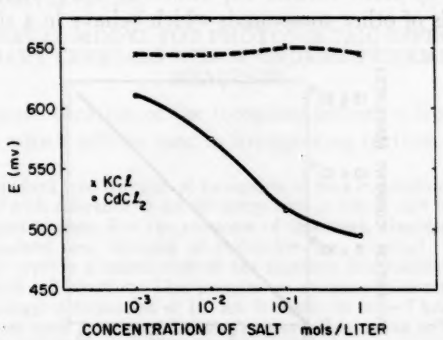

FIG. 5. Effect of added salts to the photo-emf of the CdS electrode under constant illumination. Dashed curve, KCl; solid curve, $CdCl_2$.

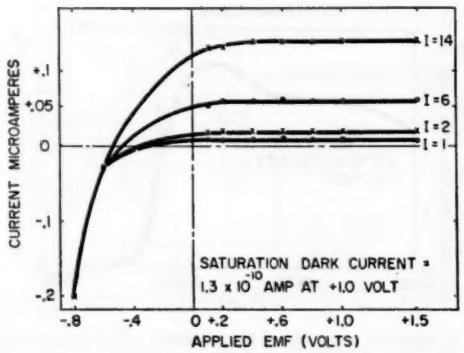

FIG. 6. Current as a function of externally applied voltage for CdS electrode at several light intensities. Sign of applied voltage taken as positive when positive terminal of external emf goes to CdS crystal. I is the relative light intensity.

crystal. The cell consisted of a CdS crystal in 0.1M KCl solution together with the saturated calomel electrode. For the small current densities employed here the potential drop across the reference electrode should be independent of current, and the ohmic drops in the crystal and solution are negligible. Hence differences in applied voltage appear as differences at the CdS-electrolyte junction. Results are shown in Fig. 6. It is seen that when the crystal is made positive a saturation current is reached after which further increases in applied voltage have almost no effect on the current. The saturation value of current is directly proportional to light intensity as shown by Fig. 7. If the current is allowed to flow for an hour or so in this direction a yellow deposit of sulfur forms on the surface of the crystal. When the crystal is made negative the current reaches large values which are independent of light intensity and rather unsteady. If the voltage is raised to several volts in this direction the current rises and a black deposit of cadmium metal forms on the surface of the crystal. When the crystal is made positive, on the other hand, voltages of 120 v may be applied without catastrophic breakdown of the crystal and no evidence of electrolysis of the solution. An analysis of these experiments will now be given, followed by some further experimental observations on crystals of other compounds which behave in a similar way.

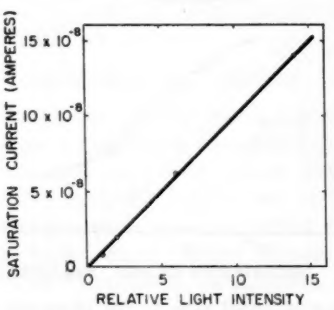

FIG. 7. Saturation current through CdS electrode as a function of relative light intensity.

INTERPRETATION OF EXPERIMENTS ON CdS

The first consideration in understanding the CdS electrode is the mechanism of conductivity within the crystal. It has been demonstrated by Hall effect measurements that CdS is an n-type semiconductor.[6] As mentioned in the foregoing, the crystals used here contained chlorine which forms a shallow donor level lying 0.04 ev below the conduction band.[6] These donor ions are completely ionized at room temperature and the electrons are free to move in the conduction band of the crystal.

It has been demonstrated that the photo-emf observed with CdS is accompanied by chemical reaction of the crystal. Since the crystal becomes negative on illumination the simplest reaction to assume is that Cd^{++} ions from the crystal go into solution leaving

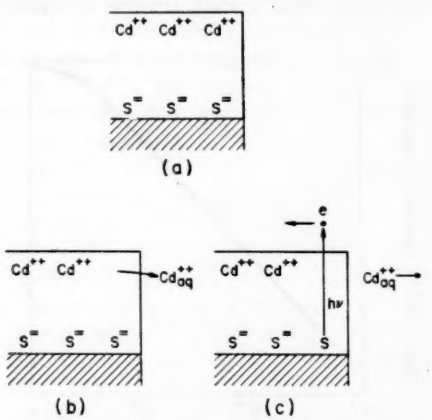

FIG. 8. Energy bands at the interface between CdS and an electrolyte solution. (a) Before any solution occurs. Empty conduction band is associated with Cd^{++} ions. Filled valence band is associated with S^{--} ions. (b) Cd^{++} ion goes into solution leaving behind negative charge bound to S^{--} ion. (c) Light liberates electron into conduction band.

behind excess S^{--} ions. Evidence to support this idea is given in Fig. 5 in which the data suggest that Cd^{++} participates in the electrode reaction. The excess charge on the crystal is bound to the S^{--} ions and unless it can be transported out of the crystal into the external circuit a potential difference between crystal and solution would quickly build up and prevent further solution of Cd^{++} ions. To visualize the relation between the bound charge and the band structure of the crystal we adopt a point of view which has been extensively employed in the discussion of alkali halide crystals. This is that in an ionic lattice the electrons bound to the negative ions are at the energy level of the highest filled band (valence band). The conduction band corresponds to the energy which an electron would have if it were associated with a positive ion.[8] This is illustrated for CdS in Fig. 8(a) using the con-

[8] N. F. Mott and R. W. Gurney, *Electronic Processes in Ionic Crystals* (Oxford University Press, New York, 1948), 2nd ed., p. 69–74.

ventional one-dimensional band picture. The allowed energy bands are shown with their respective ions and the boundary between crystal and solution is at the right hand edge. The position indicated for the S^{--} ions means that if an electron is removed from the S^{--} ion to a state of higher energy its energy in the initial state lies somewhere in the range of energies covered by the highest filled band. The position of the Cd^{++} ions means that if an electron leaves a state of some lower energy and is brought to a state in which it is associated with a cadmium ion, the final state lies in the range of energies covered by the conduction band. It is understood that a metal connection to the external circuit makes ohmic contact to the crystal, but this is omitted from the figure for simplicity. The transfer of a cadmium ion from the crystal into the solution is shown in Fig. 8(b). It is seen that the extra electrons left behind on the sulfide ion are not free to move out of the crystal since their energy level is that of the filled band and lies 2.5 ev below that of the conduction band. Charge transport through the filled band is forbidden by the exclusion principle. The electrons from the ionized donor centers are free to move through the crystal but the potential at the surface can be prevented from building up only if the excess electrons are removed from the S^{--} ions at which they originally accumulate. Thermal excitation of these electrons to the conduction band is not sufficiently probable to permit any significant current flow by this mechanism. Thus the action of the light in assisting the electrode reaction becomes clear. The absorption of light lifts electrons from the excess S^{--} ions at the surface and puts them into the conduction band where they are free to move through the crystal into the external circuit as shown in Fig. 8(c). From here they go to the other electrode where an electron-consuming reaction is occurring. The surface returns toward over-all electrical neutrality and further Cd^{++} ions can go into the solution. The sulfur deposit which accumulates on the surface of the crystal as time goes on provides evidence in support of this picture. In Fig. 4 it is seen that the spectral response of the photovoltaic current coincides with the onset of strong fundamental absorption in the crystal. This absorption would release electrons from the highest filled band into the conduction band as postulated. It is important to note that if CdS were a *p*-type semiconductor there would be no photovoltaic effect. In this case the excess charge left behind on the S^{--} could be neutralized by transport of holes through the valence band and there would be no need for light to assist the electrode reaction. The reaction would proceed in the dark if it were thermodynamically favored.

It remains to be shown why Cd^{++} ions should go into solution from CdS rather than S^{--} ions or both together. Simple considerations using readily available thermodynamic data may be used to rationalize this finding and these considerations will be shown to have considerable power of prediction. The absolute free energy changes for the three following reactions have been taken from the extensive compilation of Latimer.[7] (Note that the numbers given are for free energy changes on an absolute rather than a relative basis.[9] In accordance with the usual convention, positive values of the free energy mean that energy must be absorbed by the system in order for the reaction to proceed;

	ΔF° kcal/mole
$CdS \rightarrow Cd_{aq}^{++} + S_{aq}^{--}$	+37.1
$CdS \rightarrow Cd_{aq}^{++} + S + 2e$	+20.
$CdS + 2e \rightarrow Cd + S_{aq}^{--}$	+55.7.

The first equation represents the ordinary process of solution with over-all electrical neutrality. The second and third equations are typical electrode reactions. These free energy values refer to solutions in which the ionic species are at unit activity. In cases where the ionic species in solution are very dilute (such as the foregoing experiments) all the reactions would have lower free energy values due to the effect of dilution on free energy. The relative values would be unchanged, however. It is seen that the second reaction is favored on thermodynamic grounds since it has the lowest free energy change. This gives a simple rule which will be applied to a number of other data in what follows. The rule is: *When an ionic crystal is in contact with water, the reaction which occurs is that having the lowest free energy change.* (Only the three types mentioned before are considered.) If a compound is highly insoluble, it follows that the free energy change for the first process has a high positive value and it is in such compounds that the second and third types of process are likely to dominate.

To summarize the interpretation of the Becquerel effect in the CdS-electrolyte system, it has been shown that the effect is accompanied by a reaction in which Cd^{++} ions go into solution and free sulfur is left behind on the crystal. The function of light is to permit the negative charge on the crystal to be conducted into the external circuit.

A GENERAL MODEL FOR PHOTOVOLTAIC EFFECTS IN BINARY CRYSTALS WHICH UNDERGO CHEMICAL REACTION

A generalization of the foregoing picture will now be made which will be used in interpreting further experi-

[9] Standard free energies of formation of ions in solution are reported with reference to an arbitrary zero in which ΔF^0 for H^+ is set equal to zero. For the purposes of this work absolute values of standard free energies of formation are required. Latimer (p. 22) reports a calculation of the absolute free energy change of a half cell reaction. This permits an estimate of the absolute free energy of formation of H^+ ion in water to be +5 kcal/mole. This was used to correct Latimer's reported values of ΔF^0 of ions to absolute values. For positive ions the absolute value is obtained by adding 5 kcal/mole to Latimer's reported value of ΔF^0. For negative ions 5 kcal is subtracted from Latimer's value. For neutral species no change is required.

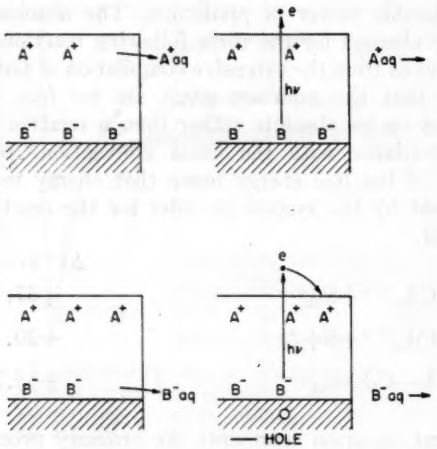

FIG. 9. Generalization of process shown in Fig. 8. (Top) type I reaction with positive ion going into solution leaving excess negative charge on crystal. (Bottom) type II reaction with negative ion going into solution leaving excess positive charge on crystal.

ments in this work and some data from the literature. The kind of analysis made in Fig. 8 is now given in Fig. 9. In the upper half of the drawing the general reaction of the type occurring in CdS is shown and this reaction with the positive ion going into solution will be referred to as "type I reaction." When this reaction occurs there can be a photovoltaic effect only if the compound AB is an *n*-type semiconductor, and the sign of the photo-emf must be negative. As mentioned before, if a type I reaction is favored, and if AB is a *p*-type semiconductor the reaction will go on in the dark and no photovoltaic effect should be observed. In some compounds such as CuI the thermodynamically favored process is the preferential solution of the negative ion. This is shown in the lower half of Fig. 9 and will be given the name "type II reaction." Here the excess charge on the crystal resides on the A^+ ion and this must be neutralized for the reaction to proceed. If AB is an *n*-type semiconductor these ions may be readily neutralized by electrons moving through the conduction band from the external circuit. No light is required and no photovoltaic effect should be observed in this case. If AB is a *p*-type semiconductor, charge moves only in the valence band and the assistance of a light quantum would be required to place an electron on an A^+ ion. Thus, for a reaction of type II, only a *p*-type semiconductor should show a photovoltaic effect and the sign of the photo-emf must be positive. The choice between whether a type I reaction or a type II reaction should occur for any given compound may be decided by the rule that the reaction with the lowest free energy change is the most likely to occur.

EXPERIMENTS WITH OTHER COMPOUNDS

Experiments similar to those described for CdS were carried out for several other compounds though these were not studied in as much detail. Emf values were measured for cells consisting of the crystal in contact with 0.1*M* KCl solution and a calomel electrode as in Fig. 1. Some of the results of these experiments are tabulated in Table I along with a number of results which have been reported in the literature. The data taken from the literature include all the binary compounds for which clearcut experimental data were found on a routine survey of the literature. The table gives the thermodynamic data for the two simplest types of reaction mentioned before, wherever these data are available in Latimer's book. The table also gives the conductivity type of the semiconductor (*n* or *p*) where this is known, the sign of the photo-emf as predicted by the mechanism outlined in the last section, and the sign of the photo-emf actually observed.

Cadmium Selenide

These crystals had about the same resistivity as the CdS crystals. The conductivity was due to incorporated iodine. CdSe has *n*-type conductivity and has an optical band gap of 1.70 ev.[10] The free energy of formation of CdSe has not been reported but the values for the Cd^{++} ions and the Se^{--} ions are both known and this is enough to show that the standard free energy change of the type I reaction is smaller by 52 kcal/mole than the standard free energy change of the type II reaction. Thus according to the rule given above the type I reaction should occur since it has the lowest standard free energy change. For an *n*-type semiconductor this can give rise to a photo-emf in which the crystal becomes negative on being illuminated. This was found to be the case. There was no emf in the dark and on being illuminated the crystal became negative and an emf of 490 mv was reached at high light intensity. Similar results were found with three different crystals. The dependence of emf on light intensity was much like that found with CdS. The spectral response curve given in Fig. 10 shows the effect to have a long wavelength threshold approximately coinciding with the optical band edge.

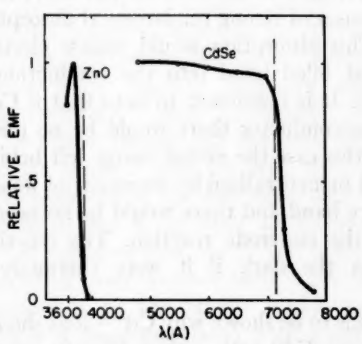

FIG. 10. Relative values of emf at various wavelengths for CdSe and ZnO. The optical band edge for each compound is shown by a vertical dashed line.

[10] R. H. Bube, Phys. Rev. **98**, 431 (1955).

TABLE I.

Compound[a]	Type I reaction $\Delta F_I°$ kcal/mole $AB \rightarrow A_{aq}^{+}+B+e$	Type II reaction $\Delta F_{II}°$ kcal/mole $AB+e \rightarrow A+B_{aq}^{-}$	Conductivity type	Predicted sign of photo-emf	Observed sign of photo-emf and reference
CdS	+20.0	+50.7	*n*	−	−[b]
CdSe	...	...	*n*	−	−[b]
ZnS	+17.2	+64.5	*n*	−	−[b]
ZnO	...	...	*n*	−	−[b]
CuI	+33.6	−0.8	*p*	+	+[b]
ZnTe	$\Delta F_I° < \Delta F_{II}°$		*p*	0	0,[b]
AgCl	+49.6	−10.2	...	+	+[d]
AgBr	+46.3	−6.7	*p*	+	+[e]
AgI	+49.2	−1.6	...	+	+[f]
Hg_2Cl_2	+91.8	−22.4	...	+	+[g]
Hg_2Br_2	+84.1	−16.5	...	+	+[g]
Hg_2I_2	+68.0	−8.2	...	+	+[g]
HgS	+55.4	+28.1	...	+	−[g]
Cu_2O	...	...	*p*	+	+[h]

[a] For all the sulfides the negative ion species in solution is taken to be S^{--}. For the mercurous salts the positive ion in solution is taken to be Hg_2^{++}, and for HgS the positive ion is taken to be Hg^{++}.
[b] This work.
[c] No photo-emf; emf in dark predicted and observed.
[d] E. Becquerel, Compt. Rend. 9, 561 (1839).
[e] B. Vanselow and S. E. Sheppard, Sci. Abstracts 34, 4037 (1931).
[f] A. L. Hughes and L. A. DuBridge, *Photoelectric Phenomena* (McGraw-Hill Book Company, Inc., New York, 1932), p. 356.
[g] G. Athanasiu, Compt. rend. 175, 214 (1922).
[h] V. P. Barton, Phys. Rev. 23, 337 (1924).

Cuprous Iodide

This compound provides an interesting comparison with the previous results. It is a *p*-type semiconductor[11] and the type II reaction is the thermodynamically favored one. Thus it can show a photo-emf in which the crystal becomes positive on illumination. A conducting crystal was used. A positive photo-emf was found which reached 68 mv at high light intensity.

Zinc Oxide

It is not easy to pick any simple reactions here for comparison as was done previously, since the oxide ion does not exist in water solution. However, ZnO is an *n*-type semiconductor[12] and according to the foregoing reasoning only a negative photo-emf can be observed in *n*-type semiconductors if any occurs at all. Hence if a photo-emf occurs in ZnO it must be negative. Two crystals of conducting ZnO were provided by the New Jersey Zinc Company. These had resistances of around 500 ohms. A negative photo-emf was found ranging up to 195 mv in bright light. The dependence of emf on light intensity was again similar to that shown by CdS. Figure 9 shows the spectral response and again the long wavelength threshold lies close to the optical band edge.

Zinc Sulfide

Crystals of ZnS were in the form of thin plates. Their resistance in the light of the focused microscope lamp was about 5×10^9 ohms and their dark resistance was much higher. A type I reaction is favored thermodynamically and ZnS shows *n*-type conductivity.[6] A negative photo-emf was found for each of two crystals with a maximum of 415 mv in bright light.

Zinc Telluride

ZnTe is a *p*-type semiconductor.[6] The thermodynamic data show that the standard free energy change of the type I reaction is 77 kcal/mole less than that for the type II reaction. For a *p*-type semiconductor and type I reaction, however, the reaction should occur in the dark and no photo-emf should be observed. This is what was found. A conducting crystal of *p*-type ZnTe, in combination with the calomel electrode, gave an emf in the dark of 72 mv in which the crystal was negative. Bright light on the crystal caused no observable change in this emf.

[11] R. J. Maurer, J. Appl. Phys. **16**, 563 (1945).
[12] *American Institute of Physics Handbook* (McGraw-Hill Book Company, Inc., New York, 1957).

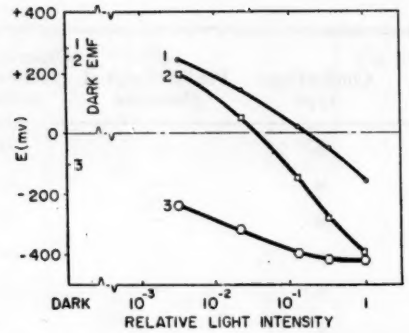

FIG. 11. Emf vs light intensity for *n*-type GaAs electrode in solutions containing three different oxidation-reduction couples. (1) 1:1 Fe^{++}/Fe^{+++}. (2) Quinhydrone in 1*M* HCl. (3) 1:1 Sn^{++}/Sn^{4+}, solutions 1 and 3 also contain 1*M* HCl.

DISCUSSION OF RESULTS

It can be seen that the simple model proposed in the preceding is capable of interpreting the general features of the Becquerel photovoltaic effect in binary compounds. The thermodynamic data and information on the conductivity type are available for many binary compounds and their use in connection with the model is unambiguous. All the types of behavior predicted by the model have been observed. It is not suggested that the mechanism of any of the electrode reactions can be completely represented by the equations which we have labeled type I and type II. The reactions are undoubtedly more complicated. To the extent that it permits of reliable prediction, however, the classification introduced here may be regarded as a useful point of view.

ELECTRODE PROPERTIES OF CdS WITH EXTERNALLY APPLIED VOLTAGE

The current-voltage curve in Fig. 6 may be understood using the concepts introduced before. A similar result has been reported by Brattain and Garrett for an electrode of *n*-type germanium in KOH solution.[2] In that case, however, the dark current was of the same order of magnitude as the current carried by the illuminated electrode. The simplest interpretation of the electrode process represented by the data in Fig. 6 is the following. Current flows between the crystal and the external circuit by motion of electrons through the conduction band of the crystal and into the adjoining metal contact. At the boundary between the crystal and solution the mechanism of conductivity changes and the current across the boundary is carried by ions of the appropriate sign which leave the crystal. Cd^{++} ions leave the crystal when the current is flowing in one direction and S^{--} ions leave the crystal when the current is flowing in the other direction. No ions from the solution are discharged in either case. Neutralization of an ion of opposite sign is necessary after a given ion has left the crystal. This requires light if the S^{--} ion on the crystal must be neutralized and a current independent of voltage but proportional to light intensity is observed when the polarity is such that this process occurs. On the other hand, the Cd^{++} ion on the crystal may be neutralized by motion of electrons through the conduction band from the external circuit and a current increasing rapidly with voltage but independent of light intensity is observed when this process is occurring.

Brattain and Garrett[2] suggested that, as the applied voltage is changed, at a semiconductor electrode, the change in voltage occurs mainly in the space charge layer of the semiconductor rather than in the solution or at the surface double layer. The results with the CdS electrode confirm this idea completely. Since an applied voltage of 120 v (positive terminal to CdS) causes no electrolysis of the solution it suggests the potential drop within the solution is only a small fraction of the total. At the same time there is a shift in the optical absorption edge of the crystal, indicating the existence within the crystal, itself, of electric fields of 10^5 v/cm or greater.[13] Both these observations indicate that the potential drop in the system is mainly within the space charge region of the crystal near the interface with the electrolyte.

EXPERIMENTS WITH GaAs

Some experiments will now be discussed in which photovoltaic effects were observed in GaAs crystals which were in contact with electrolyte solutions. These experiments are still in progress but some preliminary results will help to round out the picture presented in the foregoing. Samples of *N*-type GaAs were used which had a resistivity of 0.0057 ohm cm and contained 5.5×10^{17} carriers/cc. These were cut in pieces $10\times5\times1$ mm and mounted as in Fig. 1. Results using 0.10*M* KCl solution as the electrolyte were somewhat erratic and though currents were of the same order as those found with CdS there was no evidence of extensive chemical reaction of the GaAs itself, even after prolonged current flow. This is entirely reasonable since GaAs is quite inert chemically. It seemed likely that current flow was the result of reaction with an oxidation-reduction couple in the solution. Solutions were made up of several common oxidation reduction couples having widely different oxidation potentials. These were then used in place of the KCl solution. All experiments were performed without externally applied voltage. The experiments with the solution containing Sn^{++} and Sn^{4+} were performed with the cell under a nitrogen atmosphere. Results are given in Fig. 11. Emf values are given for the cell in which the GaAs is in the solution containing the ions of the oxidation-reduction couple and the calomel half cell is the second electrode. The emf is plotted as a function of light intensity for cells having different oxidation-reduction systems in the solution. One of these systems is a mixture of ferrous and ferric ions in equal propor-

[13] R. Williams, Phys. Rev. (to be published).

tions dissolved in 1.0*M* HCl. The second is a saturated quinhydrone solution in 1.0*M* HCl and the third is an equimolar mixture of Sn^{++} and Sn^{4+} ions in 1.0*M* HCl. The sign of the emf is taken as the sign acquired by the GaAs crystal when the cell is operating.

There is a dark emf in every case whose magnitude is indicated at the left along the ordinate. This dark emf is reproducible to within 3% as measurements at widely different times are made on the same crystal sample. It was reproducible to within 10% among different crystal samples. The order of the dark emf values for the several different solutions is the same as the order of the oxidation potentials for the same solutions as shown in Table II. Naturally the comparison of the present data with the standard oxidation potential data requires considerable caution since the standard oxidation potentials are obtained for reactions at a platinum electrode which may behave quite differently from the GaAs electrode for these reactions. The correlation between oxidation potentials and the results with a GaAs electrode leads us to propose that the dark reaction is simply the reaction of electrons from the crystal with the appropriate ion of the oxidation-reduction couple. This will be discussed in more detail in what follows. When light is incident on the crystal the initially positive emf values become smaller, finally changing sign at high light intensity so that the crystal has now become the negative terminal of the cell. A spectral response measurement shows that the photo-emf occurs only for wavelengths less than that corresponding to the band gap in GaAs (1.4 ev) showing that light absorbed by the crystal is responsible for the effect.

Table II.

Oxidation-reduction couple in solution	Dark emf mv	Oxidation potential of couple vs calomel electrode mv	Observed photo-emf at high light intensity
1:1 Fe^{++}/Fe^{+++}	+285	+510	−470
1:1 Sn^{++}/Sn^{4+}	−100	−110	−320
Quinhydrone in 1.0 *M* HCl	+260	+440	−660

DISCUSSION OF RESULTS OBTAINED WITH GaAs ELECTRODE

For simplicity, the results will be discussed using the data obtained with the 1:1 Fe^{++}/Fe^{+++} solution. These data will then be compared with those obtained with the other solutions.

Though the conduction of electricity in electrolyte solutions is entirely by ions, it is convenient for simple oxidation-reduction systems such as the Fe^{++}/Fe^{+++} system to regard these ions as carriers of electrons (or holes) which are exchanged with the electrode.[14] For instance, when an electrode in such a solution is passing electrons to the Fe^{+++} ion;

$$Fe^{+++}+e\rightarrow Fe^{++},$$

the electron is retained on an ion which remains in the solution and which may migrate to another electrode and give up the electron. Hence, in a very real sense, the ions act as carriers of electrons and may be regarded as an electronic state which may be occupied or unoccupied. The Fe^{++} ion is the occupied state and the Fe^{+++} ion is the unoccupied state. On an energy level diagram both would lie at the same level since an electron may be taken from a Fe^{++} ion to a Fe^{+++} ion without expenditure of energy. The relative numbers of occupied and unoccupied levels may be varied within wide limits by varying the relative concentrations of the two ions in solution. It is clear that this point of view would not be appropriate to other ions such as the hydrogen ion where the reaction of the ion at an electrode results in the separation of a product in a gaseous or solid phase.

We consider now the results obtained with the GaAs electrode in the 1:1 Fe^{++}/Fe^{+++} solution. Figure 12 shows the energy band diagram at the interface between the crystal and the solution. The majority carriers, electrons, are indicated by solid black circles in the conduction band while holes are indicated by open circles in the valence band. Holes are in negligible concentrations except when the crystal is illuminated. The energy levels of the electrons on the Fe^{++} and Fe^{+++} ions in solution are indicated by horizontal lines. Fe^{+++} ions are shown with an open circle indicating that they are unoccupied levels with respect to electrons while Fe^{++} ions are shown with solid circles to indicate that they are occupied. Since the electrode reaction in the dark is the passage of electrons from the crystal into the solution it is likely that the Fe^{++}/Fe^{+++} ion level lies well below that of the conduction band. Thus some electrons would be transferred from the crystal to the solution at the instant of contact with the solution, leading to a typical double layer at the interface. The space charge layer in the crystal resulting from this charge transfer is indicated by the upward curvature of the bands at the interface. For simplicity, no indication is made of the corresponding space charge region in the solution. The dark reaction is shown as a transfer of electrons from the conduction band of the crystal to the unoccupied levels of the solution with the result that the crystal becomes the positive terminal of the cell. In the light the motion of electrons is from the occupied levels of the solution to the holes in the valence band which are produced by light and move readily through the space charge region of the crystal to the surface.

Since the dark emf and the photo-emf act in opposite directions the total value of the photo emf is obtained

[14] N. B. Hannay, *Semiconductors* (Reinhold Publishing Corporation, New York, 1959); see Chap. 17 by J. F. Dewald.

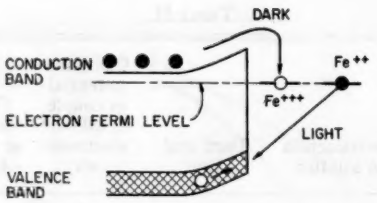

FIG. 12. Configuration of GaAs bands at interface with solution containing ions of oxidation-reduction couple.

by adding the absolute values of the observed photo-emf and the dark emf. This has been done, using the data in Fig. 11 and the results are shown in the last column of Table II. (For the Sn^{++}/Sn^{4+} solution the dark emf and photo-emf are in the same direction and photo-emf is obtained by subtracting the dark emf from the total emf observed in the light.) The net result is a transfer of electrons from solution to crystal so the crystal becomes the negative terminal of the cell.

For the Sn^{++}/Sn^{4+} couple the energy level of the ions in solution should lie roughly 0.6 ev above that of the ions in the 1:1 Fe^{++}/Fe^{+++} couple. It is seen that the dark current is such that electrons flow from the solution into the crystal indicating that this energy level is, indeed, considerably higher than that of the Fe^{++}/Fe^{+++} system. Again the photo-emf is negative indicating that electrons are entering the crystal.

This purely qualitative interpretation is seen to explain the general features of the electrode behavior. It is hoped that the accumulation of more data will permit a quantitative formulation of the behavior at this kind of interface and permit the integration of extensive information which is available for both semiconductors and electrolyte solutions.

CONCLUSIONS

An experimental investigation has been made of the Becquerel effect in a variety of binary compounds. Two different over-all processes have been observed. In one of these the photovoltaic effect results from a chemical reaction in which the material of the electrode itself is consumed. An analysis of the detailed mechanism of the effect results in two generalizations which apply in this case and are in good agreement with experiment:

1. For a reacting electrode of a binary compound, if the compound is an *n*-type semiconductor it can show only a negative photo-emf. A *p*-type semiconductor can show only a positive photo-emf.

2. The over-all chemistry at the electrode may be inferred from readily available thermodynamic data and, together with knowledge of the conductivity type may be used to predict whether a given compound will show a photo-emf or react in the dark.

In the second type of over-all process the reaction is predominantly an exchange of electrons with an oxidation-reduction couple in the solution. Both a dark current and a photocurrent are observed which may be of the same or opposite signs. Results may be understood on the assumption that, in the dark, electrons may leave the conduction band of *n*-type GaAs for ions in the solution. In the light, electrons leave ions in the solution to enter the valence band of the GaAs.

ACKNOWLEDGMENT

The author wishes to acknowledge the valuable contribution to this work made by Albert Rose who first brought the problem to the author's attention and gave generously of his time in discussions.

Polarized Octahedra in Barium Tetratitanate

DAVID H. TEMPLETON AND CAROL H. DAUBEN

Department of Chemistry and Lawrence Radiation Laboratory, University of California, Berkeley, California

(Received November 6, 1959)

Single-crystal x-ray diffraction studies show that $BaTi_4O_9$ is orthorhombic, space group $Pmmn$, with $a=14.53\pm0.02$, $b=3.79\pm0.01$, and $c=6.29\pm0.01$ A, with two formula units per unit cell and calculated density 4.54 g cm^{-3}. Each barium atom has four oxygen neighbors at 2.81 A, two at 2.96, and four at 3.09, at the corners of a pentagonal prism. Titanium atoms are in distorted octahedra of oxygen atoms. The Ti–O distances range from 1.77 to 2.32 A, with standard deviations of 0.03 A or less. Titanium atoms occur at points 0.30 and 0.21 A from the centers of gravity of the oxygen atoms of the two kinds of octahedra. This polarization of the two octahedra is similar to or greater in magnitude than that observed in the ferroelectric phases of $BaTiO_3$ and $PbTiO_3$.

INTRODUCTION

BARIUM tetratitanate, $BaTi_4O_9$ or $BaO\cdot4TiO_2$, is one of several compounds which occur in the BaO–TiO_2 system.[1–5] Its crystal structure has attracted attention in several laboratories. The orthorhombic unit cell was reported by Lukazewicz and Trzebiatowski[6] and by Harrison.[7] The atomic positions were determined by Lukaszewicz.[8] We were also investigating its structure prior to these reports. In this paper we describe our results, which agree with those mentioned in the preceding except for minor details. An interesting feature of this structure is that it contains polarized octahedra, somewhat like those found in the ferroelectric phases of $BaTiO_3$, but in a centric symmetry.

UNIT CELL AND SPACE GROUP

Single crystals were prepared by Dr. L. K. Templeton by heating stoichiometric proportions of $BaCO_3$ and TiO_2 (rutile) to about 1450°C.[9] The dimensions of the orthorhombic unit cell are listed in Table I. We determined a and c from a quartz-calibrated[10] zero-layer Weissenberg pattern, and b from a rotation pattern using the other axes as a secondary calibration. The radiation used was Cu$K\alpha$, with $\lambda=1.5405$ A for the $K\alpha_1$ component. Our results are in excellent agreement with the published values, with one exception.[11]

The density calculated from our cell dimensions, with two formula units per cell, is 4.54 g cm^{-3}. The measured density is reported by Rase and Roy[5] to be 4.6 g cm^{-3}.

The systematic absences and diffraction symmetry correspond to space groups $Pmmn$, $P2_1mn$, and $Pm2_1n$. Weissenberg photographs taken with Mo$K\alpha$ radiation showed that the intensities for a given hl depend only on whether k is even or odd, up to $k=4$; thus the atoms lie in (or at least very near to) planes half a cell apart and perpendicular to b. If the atoms are exactly in these planes, the symmetry includes mirror planes in this orientation. A structure was easily found which ultimately gave good agreement with the data when the higher symmetry $Pmmn$ was assumed. This agreement gives good support for the assumption of mirror planes perpendicular to a. The present x-ray data are not sensitive to small deviations from the mirror plane perpendicular to b. Probably the best evidence against such deviations is the normal dielectric behavior observed by Skanavi.[2] A polar structure which deviated slightly in that way from the structure reported here would be expected to be ferroelectric.

TABLE I. Unit cell dimensions of $BaTi_4O_9$.

Authors	a, A	b, A	c, A
This work	14.53±0.02	3.79±0.01	6.29±0.01
Lukaszewicz and Trzebiatowski[a]	14.53±0.02	3.79±0.01[b]	6.30±0.01
Harrison[c]	14.51±0.04	3.79±0.01	6.30±0.02

[a] References 6 and 8.
[b] See reference 11.
[c] Reference 7.

ATOMIC COORDINATES

Barium atoms are located in twofold special positions on the intersections of the mirror planes; they may be designated

$$2(b): \pm(\tfrac{1}{4}, \tfrac{3}{4}, z).$$

Oxygen atoms, designed O_b, are in the other twofold set,

$$2(a): \pm(\tfrac{1}{4}, \tfrac{1}{4}, z).$$

[1] E. N. Bunting, G. R. Shelton, and A. S. Creamer, J. Am. Ceram. Soc. **30**, 114 (1947).
[2] G. I. Skanavi, Doklady Akad. Nauk S.S.S.R. **59**, 41 (1948).
[3] W. O. Statton, J. Chem. Phys. **19**, 33 (1951).
[4] W. Trzebiatowski, M. Drys, and J. Berak, Roczniki Chem. **28**, 21 (1954).
[5] D. E. Rase and R. Roy, J. Am. Ceram. Soc. **38**, 102 (1955).
[6] K. Lukaszewicz and W. Trzebiatowski, Roczniki Chem. **29**, 943 (1955).
[7] F. W. Harrison, Acta Cryst. **9**, 198 (1956).
[8] K. Lukaszewicz, Roczniki Chem. **31**, 1111 (1957).
[9] L. K. Templeton and J. A. Pask, J. Am. Ceram. Soc. **42**, 212 (1959).
[10] A. Pabst, Am. Mineral **42**, 664 (1957).
[11] The b axis is given as 3.75 A in the English summary of the article by Lukaszewicz,[8] and this value is repeated in Acta Cryst. **10**, 792 (1957). This value seems to be a misprint, since 3.79 A appears elsewhere in reference 8, as well as in reference 6.

TABLE II. Atomic coordinates, standard deviations, and temperature factors for $BaTi_4O_9$.

Atom	x	y	z	$\sigma(x)$	$\sigma(z)$	B, A²
Ba	¼	¾	0.7076 (0.709)[a]		0.0005	2.6
Ti_1	0.0363 (0.035)[a]	¼	0.807 (0.807)	0.0005	0.001	1.7
Ti_2	0.1298 (0.126)	¼	0.248 (0.250)	0.0005	0.001	1.7
O_1	0.514 (0.510)	¼	0.158 (0.140)	0.002	0.004	2.8
O_2	0.604 (0.592)	¼	0.740 (0.733)	0.002	0.003	2.3
O_3	0.155 (0.154)	¼	0.952 (0.958)	0.002	0.004	2.9
O_4	0.095 (0.100)	¼	0.560 (0.550)	0.002	0.004	3.1
O_5	¼	¼	0.346 (0.340)		0.006	2.8

[a] Values in parentheses are those of Lukaszewicz, reference 8.

Two fourfold sets of titanium atoms and four fourfold sets of oxygen atoms are distributed in positions

$$4(f): \pm(x, \tfrac{1}{4}, z; \quad \tfrac{1}{2}-x, \tfrac{1}{4}, z).$$

Fourier methods were used to derive an approximate structure. At an early stage of our work, before any correction was made for absorption, we obtained atomic parameters that were not greatly different from our final values, but the unreliability index

$$R_1 = \sum || F_0 | - | F_c || / \sum | F_0 |$$

could not be reduced below 0.35. The intensity data came from a crystal in the form of an asymmetric but approximately circular prism, of diameter large enough to be quite opaque to the Cu$K\alpha$ radiation. The zero-layer data ($k=0$) were corrected laboriously by a method which took account of this irregular shape, as measured with the graduated objective of a microscope. The first-layer data were corrected for absorption with the assumption that the crystal was a circular cylinder, with results not substantially worse than for the zero layer.

Our final atomic parameters were derived by least-squares refinement with the IBM 650 computer and the program known as LSII.[12] Throughout these calculation, atomic form factors from *International Tables*[13] were used for Ti^{4+} and O^{2-}. Form factors for Ba^{2+} were estimated from the values[13] for Ba, with 2.1 electrons subtracted for the real dispersion effect.[14] Because no y parameters were refined, we used only the data for $k=0$ and 1, corrected for absorption as described before. In the last cycles, the weighting of strong, weak, and undetected reflections was as described for the last cycles of choline chloride.[15] The final atomic coordinates, their standard deviations, and individual isotropic temperature factors are listed in Table II. For comparison, the values obtained by Lukaszewicz[8] by Fourier methods are given in parentheses. It is apparent that the structures are substantially the same, but the parameters differ by more than the accuracy claimed for this work. The largest discrepancies of

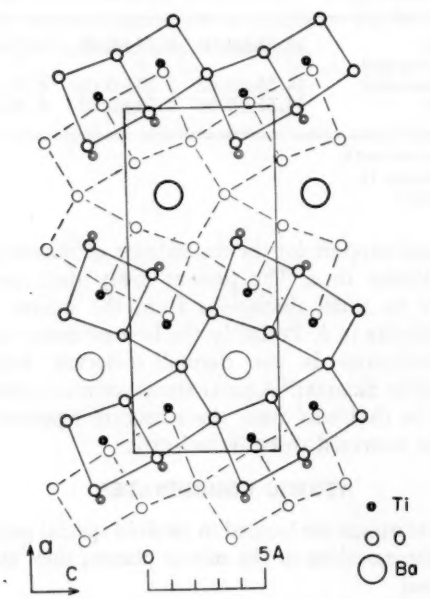

FIG. 1. Crystal structure of $BaTi_4O_9$. The rectangle outlines one unit cell. The atoms at $y=\frac{1}{4}$ are drawn more heavily than those at $y=\frac{3}{4}$. Lines join oxygen atoms to show the linking of the octahedra in each layer. Each octahedron also shares edges with octahedra in adjacent layers.

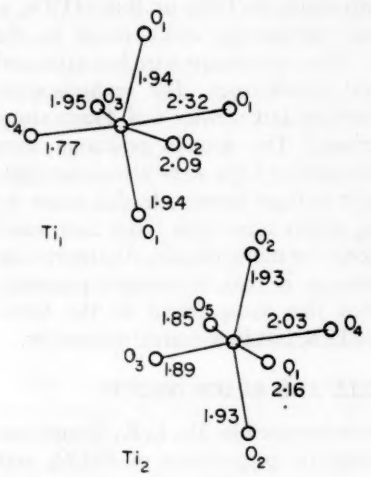

FIG. 2. Ti–O distances (in angstrom units) in the two kinds of octahedra in $BaTi_4O_9$.

[12] M. E. Senko, Acta Cryst. **10**, 385 (1957).
[13] *Internationale Tabellen zur Bestimmung von Kristallstrukturen* (Borntraeger, Berlin, 1935), Vol. II.
[14] C. H. Dauben and D. H. Templeton, Acta Cryst. **8**, 841 (1955).
[15] M. E. Senko and D. H. Templeton, Acta Cryst. (to be published).

TABLE III. Observed and calculated structure factors, $BaTi_4O_9$.

Values marked with asterisk (*) are the estimated limit of detection for undetected reflections; the letter "X" marks four strong reflections which seem to be affected by extinction and which were omitted from the final cycles of refinement.

h	k	l	F_o	F_c	h	k	l	F_o	F_c	h	k	l	F_o	F_c	h	k	l	F_o	F_c
2	0	0	11	15-	11	0	3	41	32	7	0	7	5	2-	6	1	3	24	26-
4	0	0	33	43	12	0	3	48	43	8	0	7	26	19	7	1	3	10	13-
6	0	0	55	62-	13	0	3	43	33-	9	0	7	33	29	8	1	3	43	59
8	0	0	103	122	14	0	3	4*	3-	0	0	8	12	10-	9	1	3	28	38
10	0	0	70	72-	15	0	3	25	15	1	0	8	19	16	10	1	3	24	31-
12	0	0	6*	1	16	0	3	32	26	2	0	8	5	5-	11	1	3	8	7-
14	0	0	67	51-	0	0	4	67	75						12	1	3	11	13
16	0	0	30	17	1	0	4	38	36	3	1	0	81X	146-	13	1	3	15	18
18	0	0	49	35-	2	0	4	25	25-	5	1	0	99	80	14	1	3	3*	5
0	0	1	12	7	3	0	4	69	76-	7	1	0	94	77-	15	1	3	24	22-
1	0	1	37	43	4	0	4	36	31-	9	1	0	25	14-	16	1	3	25	31
2	0	1	44	50	5	0	4	11	7-	11	1	0	48	50-	0	1	4	72	71-
3	0	1	62	88-	6	0	4	23	21-	13	1	0	46	52	1	1	4	5*	3
4	0	1	4*	5-	7	0	4	53	56-	15	1	0	15	14-	2	1	4	16	15
5	0	1	98X	165	8	0	4	44	43	17	1	0	16	16	3	1	4	44	45-
6	0	1	60	69	9	0	4	16	12	0	1	1	88	77-	4	1	4	51	60-
7	0	1	36	33	10	0	4	28	21-	1	1	1	42	28-	5	1	4	39	45
8	0	1	14	17-	11	0	4	49	46-	2	1	1	71X	130	6	1	4	39	49
9	0	1	52	61	12	0	4	16	11-	3	1	1	24	19	7	1	4	18	21-
10	0	1	8	7-	13	0	4	14	9	4	1	1	43	41-	8	1	4	14	21-
11	0	1	44	38-	14	0	4	18	8-	5	1	1	6*	5-	9	1	4	12	13-
12	0	1	23	20-	15	0	4	16	12-	6	1	1	42	47	10	1	4	28	37
13	0	1	62	60	16	0	4	18	16	7	1	1	16	15-	11	1	4	19	23-
14	0	1	11	7	0	0	5	6*	7-	8	1	1	97	106-	12	1	4	3*	4-
15	0	1	20	15-	1	0	5	6*	5-	9	1	1	34	31-	13	1	4	30	30
16	0	1	17	13-	2	0	5	65	68	10	1	1	39	41	14	1	4	37	39
17	0	1	6	5-	3	0	5	38	36-	11	1	1	14	13	15	1	4	8	7-
18	0	1	7	3	4	0	5	25	21-	12	1	1	37	35-	0	1	5	12	13-
0	0	2	119X	179-	5	0	5	27	21	13	1	1	5*	1-	1	1	5	48	47-
1	0	2	17	19-	6	0	5	41	41	14	1	1	4*	7-	2	1	5	15	10
2	0	2	21	24	7	0	5	5*	1-	15	1	1	7	8	3	1	5	13	14
3	0	2	41	48	8	0	5	41	34-	16	1	1	51	58-	4	1	5	13	9
4	0	2	50	52-	9	0	5	16	16-	17	1	1	2*	2	5	1	5	46	53-
5	0	2	5*	2-	10	0	5	15	12	18	1	1	14	18	6	1	5	2*	0
6	0	2	50	51	11	0	5	33	27-	0	1	2	78	58	7	1	5	10	11
7	0	2	57	69	12	0	5	42	38-	1	1	2	50	48-	8	1	5	16	18-
8	0	2	72	88-	13	0	5	26	19	2	1	2	43	41-	9	1	5	38	43-
9	0	2	17	15	14	0	5	5	3	3	1	2	82	79	10	1	5	18	19
10	0	2	53	53	0	0	6	19	12-	4	1	2	51	51	11	1	5	12	10
11	0	2	31	29	1	0	6	28	26-	5	1	2	46	48-	12	1	5	23	22
12	0	2	22	16	2	0	6	13	13	6	1	2	25	25-	13	1	5	21	20-
13	0	2	14	8-	3	0	6	46	41	7	1	2	51	65	0	1	6	47	46
14	0	2	49	37	4	0	6	49	44	8	1	2	14	15	1	1	6	11	12
15	0	2	15	11	5	0	6	20	16-	9	1	2	17	15	2	1	6	10	13-
16	0	2	12	26-	6	0	6	7	4	10	1	2	44	51-	3	1	6	10	7
17	0	2	19	14-	7	0	6	51	46	11	1	2	44	51	4	1	6	44	41
18	0	2	32	27	8	0	6	34	19-	12	1	2	5*	2	5	1	6	28	27-
0	0	3	5*	3	9	0	6	10	8-	13	1	2	43	52-	6	1	6	13	13-
1	0	3	14	10	10	0	6	9	5-	14	1	2	29	28-	7	1	6	17	16-
2	0	3	90	115-	11	0	6	30	24	15	1	2	7	6	8	1	6	19	16
3	0	3	81	94	12	0	6	14	8	16	1	2	3*	1	9	1	6	9	8
4	0	3	7	12	0	0	7	18	13	17	1	2	5	3-	10	1	6	26	32-
5	0	3	94	103-	1	0	7	33	29	0	1	3	76	72	0	1	7	28	25
6	0	3	56	53-	2	0	7	30	25-	1	1	3	47	44	1	1	7	28	27
7	0	3	24	14-	3	0	7	28	22	2	1	3	63	67-	2	1	7	17	16
8	0	3	39	38	4	0	7	18	15	3	1	3	5*	9-	3	1	7	17	14-
9	0	3	27	20-	5	0	7	4	2	4	1	3	25	19-	4	1	7	20	17-
10	0	3	32	24-	6	0	7	27	22-	5	1	3	52	65	5	1	7	28	27

TABLE IV. Titanium-oxygen distances in $BaTi_4O_9$.

Atoms	Distance, A	Atoms	Distance, A
Ti_1—O_1	2.32±0.03	Ti_2—O_1	2.16±0.03
—O_1[a]	1.94±0.01	—O_2[a]	1.93±0.01
—O_2	2.09±0.03	—O_3	1.89±0.03
—O_3	1.95±0.03	—O_4	2.03±0.03
—O_4	1.77±0.03	—O_5	1.85±0.02

[a] Two neighbors at this distance.

atomic position are 0.18 A for O_2, 0.12 A for O_1, and 0.10 A for O_4.

Observed structure factors and those calculated for the parameters listed in Table II are compared in Table III. For these data, R_1 is 0.154 and R_3, defined as $(\sum w(|F_0|-|F_c|)^2/\sum wF_0^2)^{\frac{1}{2}}$, is 0.179. It is believed that errors in the absorption correction are the limiting factor in the agreement.

DISCUSSION OF STRUCTURE

The structure is shown in Fig. 1. Barium atoms are packed among the oxygen atoms, with ten oxygen neighbors at the corners of a pentagonal prism. Four oxygen atoms (O_3) are at 2.81±0.02 A, four (O_4) are at 3.09±0.02 A, and two (O_5) are at 2.96±0.03 A. Titanium atoms are in oxygen octahedra which share edges and corners in a three-dimensional array. These octahedra are considerably distorted, as can be seen in Fig. 1, and the lengths of their edges (oxygen-oxygen distances) range from 2.62 to 3.11 A, with standard deviations of about 0.05 A.

Titanium-oxygen distances are listed in Table IV, and their configurations in the two kind of octahedra are shown in Fig. 2. The titanium atoms are significantly displaced from the centers of these octahedra in much the same way as in the ferroelectric perovskite phases, $BaTiO_3$[16,17] and $PbTiO_3$.[18] Similar displacements occur in the structure of low Ti_3O_5,[19] which like that of $BaTi_4O_9$ is centric rather than polar. We have calculated, as a parameter for comparison of the extents of polarization of these octahedra, the displacement of the titanium atom from the center of gravity of the six oxygen atoms of each octahedron. Values of this parameter are listed in Table V. It may be noted that for $BaTi_4O_9$ our values for this polarization parameter are in excellent agreement with those calculated from the coordinates of Lukaszewicz,[8] even though the agreement is not this good for coordinates of certain oxygen atoms. The polarization in the centric phases exceeds that observed in both $TaBiO_3$ phases, and in one case is as great as that in $PbTiO_3$.

TABLE V. Displacement of titanium atom from center of gravity of six oxygen atoms in various structures.

Structure		Displacement, A
$BaTi_4O_9$,	Ti_1	0.30 (0.28)[a]
	Ti_2	0.21 (0.19)[a]
Ti_3O_5 (low),[b]	Ti_1	0.25
	Ti_2	0.24
	Ti_3	0.18
$BaTiO_3$ (orthorhombic)[c]		0.13
$BaTiO_3$ (tetragonal)[d]		0.13
$PbTiO_3$ (tetragonal)[e]		0.29

[a] Lukaszewicz, reference 8.
[b] Asbrink and Magnéli, reference 19.
[c] Shirane *et al.*, reference 16.
[d] Frazer *et al.*, reference 17.
[e] Shirane *et al.*, reference 18.

These results show that the phenomenon of ferroelectricity is not a necessary companion of the polarization of titanium-oxygen octahedra, though the interactions responsible for this polarization must be essentially the same in the centric phases as in the polar ones. These centric structures are not examples of antiferroelectricity as that term is defined by Megaw,[20] since small shifts of atoms cannot lead to higher symmetry by a "pseudosymmetric transition."

ACKNOWLEDGMENT

We thank Dr. Lieselotte Templeton for providing the crystals used in this study. This research was performed under the auspices of the U.S. Atomic Energy Commission.

[16] G. Shirane, H. Danner, and R. Pepinsky, Phys. Rev. **105**, 856 (1957).
[17] B. C. Frazer, H. R. Danner, and R. Pepinsky, Phys. Rev. **100**, 745 (1955).
[18] G. Shirane, R. Pepinsky, and B. C. Frazer, Phys. Rev. **97**, 1179 (1955).
[19] S. Asbrink and A. Magnéli, Acta Cryst. **12**, 575 (1959).
[20] H. D. Megaw, *Ferroelectricity in Crystals* (Methuen and Company, London, 1957).

Vibrational Frequencies of Alkali Halide Dimers. II. Bending, Symmetric Stretch, and B_{1g} Modes*

JOSEPH BERKOWITZ†

Argonne National Laboratory, Lemont, Illinois

(Received November 30, 1959)

Three of the normal vibrational frequencies of alkali halide dimers are calculated on the basis of the potential function for an ionic model. The results indicate that the out-of-plane bending mode may have a frequency almost as high as the in-plane stretching frequencies. A summary of the results of calculations for the six normal modes is presented.

I. INTRODUCTION

In a previous publication[1] the molecular configuration and more specifically the normal modes of vibration of alkali halide dimer molecules were studied by making use of the approximation that the molecule was an assemblage of positive and negative ions. At that time, there was considerable interest in two of these vibrations, the B_{2u} and B_{3u} modes, because theory required that they give rise to an infrared spectrum, and yet none had been observed.[2] It was thought that the other infrared-active vibrational mode, the out-of-plane bending frequency or B_{1u}, would have too low a frequency to be observable, because a planar ionic system was believed to have a very small restoring force for out-of-plane motions. As a result, the earlier calculation[1] concerned itself primarily with an estimate of the B_{2u} and B_{3u} vibrational frequencies of alkali halide dimers, and incidentally also with the symmetric in-plane bending or A_g'.

Since that time, several factors have arisen which make desirable a reexamination and extension of the previous calculations. These factors may be summarized as follows:

(1) Considerable recent activity is evidence of continuing interest in the magnitude of bending vibrations in highly ionic systems. Experimental evidence[3] and calculations[4–6] have indicated that the linear[7] triatomic halides of the alkaline earths possess a much higher bending frequency than had generally been assumed.[8,9] The philosophy of these calculations[4–6] could be adapted to the out-of-plane bending frequencies of alkali halide dimers.

(2) Klemperer[10] has recently reported the observation of two infrared absorption bands for each of the lithium halide dimers. Since no absolute assignment to normal modes could be made, he considered the possibility that the out-of-plane bending frequency might be contributing one of these absorptions. An ionic-model calculation could conceivably aid in the assignment of bands to the three possible infrared-active vibrational modes.

(3) If a calculation based on an ionic model can give reasonable agreement with experiment for allowed transitions, it may be used to estimate those other frequencies not easily accessible to experiment. This in turn would assist greatly in comparing the heats of sublimation and the dimerization energies arrived at by experiments based on absolute pressure (third law) with the values obtained from the measured variation of partial pressure with temperature (second law).

(4) A further application would be to compare calculated and experimental binding energies for these ionic systems. Since experiments involving alkali halide dimers have generally been performed at ca 1000°K and calculations of energy are based on the vibrationless state, an accurate comparison of the two must take into account the hitherto unknown vibrational energy.

II. CALCULATION OF THE OUT-OF-PLANE (B_{1u}) MODE

A planar rhombic model is assumed[1] as shown in Fig. 1. Metal ions m^+ are located on the Y axis, halide ions x^- on the X axis. Conservation of linear momentum requires

$$\theta_x/\theta_m = aM_m/bM_x. \tag{1}$$

The symmetry coordinate $S_{B_{1u}}$ is related to the internal coordinates by the relation

$$S_{B_{1u}} = \tfrac{1}{2}(\Delta_m - \Delta_x), \tag{2}$$

where

$$\Delta_m = a\theta_m$$

$$\Delta_x = b\theta_x.$$

* Work performed under the auspices of the U.S. Atomic Energy Commission.

† Presently on leave of absence at the University of Illinois, Urbana, Illinois.

[1] J. Berkowitz, J. Chem. Phys. **29**, 1386 (1958).
[2] W. Klemperer and S. A. Rice, J. Chem. Phys. **26**, 618 (1957).
[3] A. Büchler and W. Klemperer, J. Chem. Phys. **29**, 121 (1958).
[4] R. S. Berry, J. Chem. Phys. **30**, 286 (1959).
[5] W. Klemperer, J. Chem. Phys. **30**, 594 (1959).
[6] R. G. Pearson, J. Chem. Phys. **30**, 1537 (1959).
[7] P. A. Akishin and V. P. Spiridonov, Kristallografiya **2**, 475 (1957).
[8] G. Herzberg, *Infrared and Raman Spectra* (D. Van Nostrand Company, Inc., Princeton, New Jersey, 1945), p. 161.
[9] E. B. Wilson, J. Decius, and P. C. Cross, *Molecular Vibrations* (McGraw-Hill Book Company, Inc., New York, 1955), p. 174.
[10] W. Klemperer, paper presented before the American Chemical Society's High Temperature Symposium, Boston, Massachusetts (April 8, 1959).

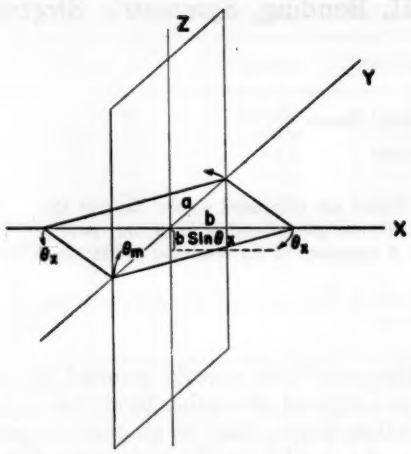

FIG. 1. The out-of-plane bending mode B_{1u}.

Hence

$$\partial\theta_m/\partial S_{B_{1u}}=2M_x/a(M_x-M_m). \tag{3}$$

In the same notation as used previously[1] the force constant matrix $|F|$ is given by

$$\partial^2V/\partial S_{B_{1u}}{}^2 \quad \text{or} \quad \partial/\partial S_{B_{1u}}(\partial V/\partial S_{B_{1u}}), \tag{4}$$

where

$$\partial V/\partial S_{B_{1u}}=(\partial V/\partial\theta_m)(\partial\theta_m/\partial S_{B_{1u}})$$

$$\partial V/\partial\theta_m=(\partial V/\partial s)\cdot(\partial s/\partial\theta_m)+(\partial V/\partial t)\cdot(\partial t/\partial\theta_m)$$
$$+(\partial V/\partial r)\cdot(\partial r/\partial\theta_m), \tag{5}$$

and V=potential energy of system, s=distance between halide ions, t=distance between alkali ions, r=distance between alkali and halide ions. It can be shown readily that

$$\partial s/\partial\theta_m=-(2a^2/b)(M_m/M_x)^2\theta_m, \tag{6}$$

$$\partial t/\partial\theta_m=-2b\theta_m, \tag{7}$$

$$\partial r/\partial\theta_m=(2a^2/r)(M_m/M_x)\theta_m. \tag{8}$$

TABLE I. Calculated frequencies of vibration of alkali halide dimers, in cm^{-1}.

	A_g	A_g'	B_{1g}	B_{1u}	B_{2u}	B_{3u}
Li_2F_2	465	365	407	385	441	448
Li_2Cl_2	330	296	385	356	375	412
Li_2Br_2	202	203	353	327	329	365
Li_2I_2	166	160	383	310	323	395
Na_2F_2	350	209	270	201	294	313
Na_2Cl_2	265	159	226	155	222	260
Na_2Br_2	182	120	207	134	188	228
Na_2I_2	143	100	202	127	173	215
K_2F_2	273	150	235	150	255	258
K_2Cl_2	219	108	180	104	184	206
K_2Br_2	159	84	153	84	148	169
K_2I_2	...	68	...	90	131	157
Rb_2Cl_2	169	79	148	83	156	170
Cs_2Cl_2	140	67	141	76	151	156

At this point V is identified with the potential derived from an ionic model,[1] so

$$V=e^2[(1/s)+(1/t)-(4/r)]-e\alpha_1E_1[(2t/r^3)-(2/t^2)]$$
$$-e\alpha_3E_3[(2s/r^3)-(2/s^2)]-3(\alpha_1E_1)(\alpha_3E_3)(st/r^5)$$
$$+[2(\alpha_1E_1)^2/t^3]+[2(\alpha_3E_3)^2/s^3]+\alpha_1E_1{}^2+\alpha_3E_3{}^2$$
$$+4Ae^{-r/\rho}-(4C_{+-}/r^6)-(C_{--}/s^6). \tag{9}$$

The partial derivatives $\partial V/\partial s$, $\partial V/\partial t$, and $\partial V/\partial r$ can readily be evaluated from Eq. (9). All the partial derivatives involved in Eq. (5) have now been evaluated, and hence $\partial V/\partial\theta_m$ can be computed. All the terms of this expression have a factor θ_m. To obtain $\partial^2V/\partial\theta_m{}^2$ the chain rule is employed again.

To terms of second order in θ_m, the result is

$$\partial^2V/\partial\theta_m{}^2$$
$$=(2a^2/r)(M_m/M_x)\{(4e^2/r^2)+[(6e\alpha_1E_1t+6e\alpha_3E_3s)/r^4]+[15(\alpha_1E_1)(\alpha_3E_3)st/r^6]-(4A/\rho)e^{-r/\rho}+(24C_{+-}/r^7)\}$$
$$+(2a^2/b)(M_m/M_x)^2\{(e^2/s^2)+(2e\alpha_3E_3/r^3)+(4e\alpha_3E_3/s^3)+3(\alpha_1E_1)(\alpha_3E_3)(t/r^5)+[5(\alpha_3E_3)^2/s^4]-(6c_{--}s^7)\}$$
$$+2b\{(e^2/t^2)+(2e\alpha_1E_1/e^3)+(4e\alpha_1E_1/t^3)+3(\alpha_1E_1)(\alpha_3E_3)(s/r^5)+[6(\alpha_1E_1)^2/t^4]\}. \tag{10}$$

Equation (4) may be expanded

$$\partial^2V/\partial S_{B_{1u}}{}^2=[(\partial/\partial\theta_m)(\partial V/\partial\theta_m)(\partial\theta_m/\partial S_{B_{1u}})]$$
$$\times(\partial\theta_m/\partial S_{B_{1u}})+(\partial V/\partial\theta_m)(\partial/\partial S_{B_{1u}})(\partial\theta_m/\partial S_{B_{1u}}).$$

Since $\partial\theta_m/\partial S_{B_{1u}}$ is a constant, the second term vanishes. Hence,

$$F=(\partial^2V/\partial\theta_m{}^2)(\partial\theta_m/\partial S_{B_{1u}})^2.$$

To evaluate the element of the G matrix, write

$$2T=2[M_m(d\Delta_m/d\tau)^2+M_x(d\Delta_x/d\tau)^2].$$

The geometric relations between Δ_m, Δ_x, θ_m, and $S_{B_{1u}}$ lead readily to

$$2T=\frac{8M_mM_x(M_m+M_x)}{(M_x-M_m)^2}\left(\frac{\partial S_{B_{1u}}}{\partial\tau}\right)^2$$

and therefore

$$|G|=\frac{(M_x-M_m)^2}{8M_mM_x(M_m+M_x)}. \tag{11}$$

Since $|F|\cdot|G|=\lambda=4\pi^2\omega^2c^2$ and our choice of symmetry coordinates has assured a 1×1 matrix, the frequency in wave numbers is readily computed. The results are compiled in Table I, together with the values for the previously calculated frequencies[1] B_{2u}, B_{3u}, A_g', and the two to be evaluated subsequently, A_g and B_{1g}.

III. SYMMETRIC STRETCH A_g

Figure 2 defines the coordinates for this mode. The relations

$$\partial^2V/\partial S^2_{A_g}=(\partial^2V/\partial V_m^2)(\partial\Delta_m/\partial S_{A_g})^2$$

and

$$\partial\Delta_m/\partial S_{A_g}=a/(a+b)$$

are readily proved.

The procedure for evaluating $\partial^2V/\partial\Delta_m^2$ in terms of the potential coordinates r_i, s and t is directly analogous to the method used for the B_{1u} mode (Sec. II) and need not be repeated.

Similarly, the G-matrix element follows from the formal method used for B_{1u}, and yields the expression

$$|G|_{A_g}=\frac{(a+b)^2}{2(a^2M_m+b^2M_x)}. \tag{12}$$

IV. IN-PLANE MODE B_{1g}

Referring to the coordinates in Fig. 3, we once again obtain

$$\partial^2V/\partial^2B_{1g}=(\partial^2V/\partial\Delta_m^2)(\partial\Delta_m/\partial S_{B_{1g}})^2$$

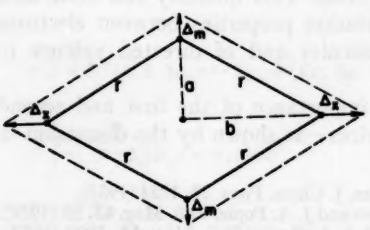

FIG. 2. The symmetric stretch A_g.

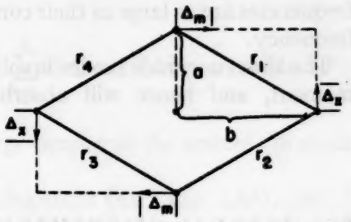

FIG. 3. The plane mode B_{1g}.

and

$$\partial\Delta_m/\partial S_{B_{1g}}=bM_x/(aM_m+bM_x).$$

As in the previous calculations, $\partial^2V/\partial\Delta_m^2$ is found by application of the chain rule for differentiation in terms of the coordinates r_i, s and t.

The G matrix becomes

$$|G|_{B_{1g}}=\frac{(bM_x+aM_m)^2}{2M_mM_x(b^2M_x+a^2M_m)}. \tag{13}$$

V. DISCUSSION

The frequencies compiled in Table I are certainly no more reliable than the potential function from whence they are derived. It was estimated earlier[1] that this accuracy was of the order of 15–20%. The parameters (α, c, A, ρ) employed in the potential function are based upon experimental data (binding energies, vibration frequencies, internuclear distances) obtained from crystalline and diatomic alkali halides. The parameters to which the potential function is most sensitive are the repulsion constants A and ρ. The exponential constant ρ has been shown to be very nearly the same for the various alkali halides, in both the crystalline and diatomic form. The preexponential A does change with the state of aggregation of the atoms in the molecule. The value of A employed in these calculations was based upon the dissociation energy of the diatomic molecule, and hence is expected to contribute the major source of error. As dimerization energies for alkali halides are more precisely evaluated experimentally, it should be possible to fit a value of A to match the dimerization energy, and employ this revised potential function to calculate a better set of vibrational frequencies, as well as more accurate bond distances and angles for the rhombic dimers.

Until these better values are available, one may employ the computed geometries[1] and frequencies of Table I to obtain a provisional set of third law entropies for the dimers.

A surprising consequence of these calculations is the similarity in absolute value of the wave numbers for the various vibrational modes listed in Table I. The in-plane bending mode A_g' and the out-of-plane vibration B_{1u} have somewhat lower frequencies, on the average, but the difference is not striking. None of the dimer

frequencies are as large as their corresponding monomer frequency.

The three ungerade modes involve a change of dipole moment, and hence will absorb infrared radiation. Although the bending mode B_{1u} is definitely of lower frequency than the others, the separation may not be sufficient to eliminate this vibration in assigning the dimer absorption frequencies observed by Klemperer.[10]

THE JOURNAL OF CHEMICAL PHYSICS VOLUME 32, NUMBER 5 MAY, 1960

Some Properties of First Order Density Matrices with Special Application to Many-Electron Atoms*

WERNER A. BINGEL

Department of Chemistry, Carnegie Institute of Technology, Pittsburgh, Pennsylvania

(Received June 17, 1959)

Properties of the first order density matrix $\gamma(\mathbf{x}' \mid \mathbf{x})$ of an N-electron system are discussed, including the relation between $\gamma(\mathbf{x}' \mid \mathbf{x})$ and the spinless first order density matrix $\gamma(\mathbf{r}' \mid \mathbf{r})$ and those symmetry properties of the total electronic charge density $\gamma(\mathbf{r}) \equiv \gamma(\mathbf{r} \mid \mathbf{r})$ which result from the corresponding properties of the total wave function with special reference to many-electron atoms. General formulas are given for the evaluation of $\gamma(\mathbf{r})$ of many-electron atoms in the orbital approximation and for its decomposition into terms of different angular symmetry. These formulas are applied to all terms of the electron configurations $s^n p^m$ and the results collected in tables.

I. INTRODUCTION

DENSITY matrices were introduced by von Neumann[1] and Dirac[2] and their use in atomic calculations investigated by Fock[3] and Lennard-Jones.[4] These early treatments were mainly concerned with the description of N-electron systems in the Hartree-Fock scheme, where the total wave function is approximated by a single Slater determinant made up from one-electron orbitals. This is a special case of what is usually called the orbital approximation. As was shown by Löwdin[5] the definition and use of these quantities can be generalized to include the treatment of approximate or exact wave functions of *arbitrary* forms. These generalized density matrices have played an increasingly important role in the modern development of approximate treatments of many electron systems.[6–13]

The calculation of most properties of an N-electron system does not require a complete knowledge of the total wave function (defined in $4N$-dimensional space, when the spin is included); only the first and second order density matrices with their usually much lower dimensionalities need to be known.[2,5] The reason for this is that the quantum mechanical operators associated with these properties are generally sums of terms depending only on one or two electrons at a time.

Furthermore, the first and second order density matrices have a simpler and more direct meaning than the wave function itself: the diagonal element of the first order density matrix gives the probability of finding a particle within the volume dv_1 around the point $\mathbf{r}_1$ having the spin s_1 when all other particles have arbitrary spins and positions; integration of this quantity over s_1 then gives the total charge density $\gamma(\mathbf{r})$ of the state considered. The diagonal element of the second order density matrix gives the probability of finding a *pair* of particles, one in volume dv_1 around $\mathbf{r}_1$ with spin s_1, and the other in volume dv_2 around $\mathbf{r}_2$ with spin s_2, irrespective of the positions and spins of the remaining particles. This quantity has been used in discussing correlation properties between electrons in atoms and molecules and of directed valence in molecules.[14–16]

In view of the importance of the first and second order density matrices—as shown by the discussion in

* Research supported by a grant from the Alfred P. Sloan Foundation to Carnegie Institute of Technology.

[1] J. von Neumann, Nachr. Akad. Wiss. Göttingen, Math.-physik. Kl. Math. physik. chem. Abt. **1927**, 245; *Mathematische Grundlagen der Quantenmechanik* (Berlin, 1932).

[2] P. A. M. Dirac, Proc. Cambridge Phil. Soc. **25**, 62 (1929); **26**, 376 (1930); **27**, 240 (1930).

[3] V. Fock, Z. Physik **61**, 126 (1930).

[4] J. E. Lennard-Jones, Proc. Cambridge Phil. Soc. **27**, 469 (1931).

[5] P. O. Löwdin, Phys. Rev. **97**, 1474, 1490, 1509 (1955).

[6] K. Husimi, Proc. Physico-Math. Soc. Japan **22**, 264 (1940).

[7] J. E. Mayer, Phys. Rev. **100**, 1579 (1955).

[8] R. McWeeny, Proc. Roy. Soc. (London) **A232**, 114 (1955); **A235**, 496 (1956); **A237**, 355 (1956); **A241**, 239 (1957).

[9] U. Fano, Revs. Modern Phys. **29**, 74 (1957).

[10] B. H. Chirgwin, Phys. Rev. **107**, 1013 (1957).

[11] R. H. Tredgold, Phys. Rev. **105**, 1421 (1957).

[12] N. H. March and W. H. Young, Proc. Phys. Soc. (London) **A72**, 182 (1958).

[13] R. U. Ayres, Phys. Rev. **111**, 1453 (1958).

[14] J. E. Lennard-Jones, J. Chem. Phys. **20**, 1024 (1952).

[15] J. E. Lennard-Jones and J. A. Pople, Phil. Mag. **43**, 58 (1952).

[16] A. Brickstock and J. A. Pople, Phil. Mag. **43**, 1090 (1952); **44**, 697, 705 (1953).

the previous paragraph—a study of their properties in general and also for specific N-electron systems should be valuable. In this paper such a study is carried out for the first order density matrix $\gamma(\mathbf{x}' \mid \mathbf{x})$. The following points are discussed: Sec. (II) the dependence of γ on the spin variables, (Sec. III) the symmetry properties of the charge density $\gamma(\mathbf{r})$ resulting from a given behavior of the total wave function Φ under symmetry operations, (Sec. IV) applications of Sec. III to many electron atoms, and (Sec. V) the orbital approximation as applied to Sec. IV.

II. DEFINITION AND SPIN DEPENDENCE OF THE FIRST ORDER DENSITY MATRIX

In the following we use the convention of combining the spatial coordinate $\mathbf{r}_i$ and the spin coordinate s_i of the ith particle in the common symbol $\mathbf{x}_i$. The total wave function Φ of an N-particle system is then a function of all $\mathbf{x}_i$ ($i=1, 2, \cdots N$), and for electrons it fulfills the antisymmetry condition

$$P\Phi(\mathbf{x}_1, \mathbf{x}_2, \cdots \mathbf{x}_N) = (-1)^P \Phi(\mathbf{x}_1, \mathbf{x}_2, \cdots \mathbf{x}_N), \quad (1)$$

where P is a permutation applied to the indices of the N coordinates and $(-1)^P = \pm 1$ depending on whether P is an even or odd permutation.

The generalized first order density matrix can be defined by[5]

$$\gamma(\mathbf{x}' \mid \mathbf{x}) = N \int \Phi^*(\mathbf{x}', \mathbf{x}_2, \cdots \mathbf{x}_N) \Phi(\mathbf{x}, \mathbf{x}_2, \cdots \mathbf{x}_N) (d\mathbf{x})^{N-1} \quad (2)$$

where the integration is performed over all coordinates except those of the first particle. Because of Eq. (1), *any* particle number i could have been chosen without changing the result. For the diagonal element the alternative definition

$$\gamma(\mathbf{x}) \equiv \gamma(\mathbf{x} \mid \mathbf{x}) = \langle \Phi \mid \sum_{i=1}^{N} \delta(\mathbf{x}_i - \mathbf{x}) \mid \Phi \rangle \quad (2')$$

in terms of the expectation value of an operator made up from a sum of δ functions can also be used.[17] The corresponding spinless quantities are then given by

$$\gamma(\mathbf{r}' \mid \mathbf{r}) = N \int \Phi^*(\mathbf{r}'s, \mathbf{x}_2, \cdots \mathbf{x}_N) \Phi(\mathbf{r}s, \mathbf{x}_2, \cdots \mathbf{x}_N) (d\mathbf{x})^{N-1} ds = \int \gamma(\mathbf{x}' \mid \mathbf{x}) \delta(s'-s) ds ds' \quad (3)$$

and

$$\gamma(\mathbf{r}) \equiv \gamma(\mathbf{r} \mid \mathbf{r}) = \langle \Phi \mid \sum_{i=1}^{N} \delta(\mathbf{r}_i - \mathbf{r}) \mid \Phi \rangle = \int \gamma(\mathbf{x}) ds. \quad (3')$$

$\gamma(\mathbf{r})$ is the total charge density of the system (in units of $-e$).

It is shown in the Appendix [e.g., Eqs. (A6), (A8)] that the following relation holds between $\gamma(\mathbf{x}' \mid \mathbf{x})$ and its spinless counterpart $\gamma(\mathbf{r}' \mid \mathbf{r})$:

$$\gamma(\mathbf{x}' \mid \mathbf{x}) = \gamma_+(\mathbf{r}' \mid \mathbf{r}) \cdot \alpha(s')\alpha(s) + \gamma_-(\mathbf{r}' \mid \mathbf{r}) \cdot \beta(s')\beta(s) \quad (4)$$

where

$$\gamma(\mathbf{r}' \mid \mathbf{r}) = \gamma_+(\mathbf{r}' \mid \mathbf{r}) + \gamma_-(\mathbf{r}' \mid \mathbf{r}). \quad (5)$$

It should be noted that Eq. (4) *does not contain any cross terms with spin parts* $\alpha(s')\beta(s)$ *and* $\beta(s')\alpha(s)$.

Equations (4) and (5) have been derived under the assumption that Φ is an eigenfunction of S^2 and S_z and that it can be expressed as a sum of products of space and spin functions as in Eq. (A1).

This behavior has a parallel in the *orbital* treatment. Here $\gamma(\mathbf{x}' \mid \mathbf{x})$ can be written as[5]

$$\gamma(\mathbf{x}' \mid \mathbf{x}) = \sum_{k,l} \psi_k^*(\mathbf{x}') \psi_l(\mathbf{x}) \gamma(l \mid k), \quad (6)$$

i.e., as an expansion in products of a complete set of spin orbitals. Since each ψ_k is the product of an orbital part ϕ_k with either of the two spin functions α and β, occurrence of nondiagonal elements ($k \neq l$) means that Eq. (6) will in general contain cross terms. Transformation to a new basis of *natural spin orbitals* χ_k brings the matrix $\gamma(l \mid k)$ to diagonal form and reduces Eq. (6) to a single sum

$$\gamma(\mathbf{x}' \mid \mathbf{x}) = \sum_k \chi_k^*(\mathbf{x}') \chi_k(\mathbf{x}) n_k. \quad (7)$$

Thus no cross terms $\alpha \cdot \beta$ or $\beta \cdot \alpha$ occur, if the spin factor of χ_k is pure α *or* β.

The foregoing suggests *that the use of natural spin orbitals in the orbital approximation corresponds to the special choice of spin functions constructed according to the branching rule of Eq.* (A2).

For the *diagonal* elements, Eqs. (4) and (5) give

$$\gamma(\mathbf{x}) = \gamma_+(\mathbf{r}) \cdot \alpha^2(s) + \gamma_-(\mathbf{r}) \cdot \beta^2(s), \quad (4')$$

where

$$\gamma(\mathbf{r}) = \gamma_+(\mathbf{r}) + \gamma_-(\mathbf{r}). \quad (5')$$

Integration of (4') over the spin variable s just gives (5') according to (3'); integration over the space

[17] H. C. Longuet-Higgins, Proc. Roy. Soc. (London) **A235**, 537 (1956).

variable $\mathbf{r}$ gives

$$\int\gamma(\mathbf{x})d\mathbf{r}=N_+\cdot\alpha^2(s)+N_-\cdot\beta^2(s),$$

where

$$N_\pm=\int\gamma_\pm(\mathbf{r})d\mathbf{r} \tag{8}$$

and a succeeding spin integration gives

$$\int\gamma(\mathbf{x})d\mathbf{x}=\int\gamma(\mathbf{r})d\mathbf{r}=N=N_++N_-. \tag{9}$$

N_+ and N_- are equal to the number of electrons with plus and minus spin, respectively. From their definition as the space integrals of $\gamma_\pm(\mathbf{r})$ and Eq. (A7) for these functions, one obtains

$$N_\pm=\int\gamma_\pm(\mathbf{r})d\mathbf{r}=N/2\pm M, \tag{10}$$

where the explicit formula for $f_S{}^N$—the number of times the multiplicity $2S+1$ occurs—has been used to get the simple and well-known result for $N_\pm$.

As is shown in the Appendix the quantities $\gamma_\pm(\mathbf{r}'\mid\mathbf{r})$ can be expressed in terms of the total wave function Φ. For the diagonal elements, there results the simple formula

$$\gamma_\pm(\mathbf{r})=\langle\Phi\mid\sum_{i=1}^{N}\delta(\mathbf{r}_i-\mathbf{r})\,(\tfrac{1}{2}\pm S_{zi})\mid\Phi\rangle \tag{A12}$$

which expresses the *partial* densities $\gamma_\pm(\mathbf{r})$ as the expectation value of an operator. Taking $\frac{1}{2}$ times the difference of these two quantities, one gets the so-called *spin density*[18]

$$\gamma_S(\mathbf{r})=\tfrac{1}{2}(\gamma_+(\mathbf{r})-\gamma_-(\mathbf{r}))=\langle\Phi\mid\sum_{i=1}^{N}\delta(\mathbf{r}_i-\mathbf{r})\,S_{zi}\mid\Phi\rangle. \tag{11}$$

$\hbar\gamma_S$ gives the density of spin angular momentum (erg sec/cm^3) at the point $\mathbf{r}$. This quantity occurs in the theory of electron-coupled nuclear spin interactions and of proton isotropic hyperfine splittings of electron magnetic resonance spectra of π-electron radicals.

III. SYMMETRY PROPERTIES OF CHARGE AND TRANSITION DENSITIES

Extending the definition of Eq. (3′) we consider here the *transition density* between two *different* electronic states, i.e.,

$$\gamma_{m,n}(\mathbf{r})=\langle\Phi_m\mid\sum_{i=1}^{N}\delta(\mathbf{r}_i-\mathbf{r})\mid\Phi_n\rangle. \tag{12}$$

[18] H. M. McConnell, J. Chem. Phys. **28**, 1188 (1958).

Because of the orthogonality of the wave functions Φ_m,

$$\int\gamma_{m,n}(\mathbf{r})d\mathbf{r}=N\cdot\delta_{m,n}. \tag{13}$$

Let R be a symmetry operation applied to the point $\mathbf{r}$ and $\mathfrak{R}$ the same symmetry operation acting on all the $\mathbf{r}_i$.

N.B. Simultaneous application of R and $\mathfrak{R}$ to $\sum\delta(\mathbf{r}_i-\mathbf{r})$ leaves this quantity invariant, since only the differences $\mathbf{r}_i-\mathbf{r}$ occur as arguments. That is,

$$\mathfrak{R}R\sum_i\delta(\mathbf{r}_i-\mathbf{r})=\sum_i\delta(\mathbf{r}_i-\mathbf{r})$$

or

$$R\sum_i\delta(\mathbf{r}_i-\mathbf{r})=\mathfrak{R}^{-1}\sum_i\delta(\mathbf{r}_i-\mathbf{r}). \tag{14}$$

Then

$$\begin{aligned}R\gamma_{m,n}(\mathbf{r})&=\int\Phi_m{}^*\Phi_nR\sum_i\delta(\mathbf{r}_i-\mathbf{r})\,(d\mathbf{r})^N\\&=\int\Phi_m{}^*\Phi_n\mathfrak{R}^{-1}\sum_i\delta(\mathbf{r}_i-\mathbf{r})\,(d\mathbf{r})^N\\&=\int(\mathfrak{R}\Phi_m{}^*\Phi_n)\sum_i\delta(\mathbf{r}_i-\mathbf{r})\,(d\mathbf{r})^N.\end{aligned} \tag{15}$$

If the operator $\mathfrak{R}$ obeys the "product law," $\mathfrak{R}(\phi\psi)=(\mathfrak{R}\phi)\,(\mathfrak{R}\psi)$, then

$$R\gamma_{m,n}(\mathbf{r})=\int(\mathfrak{R}\Phi_m{}^*)\,(\mathfrak{R}\Phi_n)\sum_i\delta(\mathbf{r}_i-\mathbf{r})\,(d\mathbf{r})^N. \tag{16}$$

This is valid if $\mathfrak{R}$ is any point transformation, or any permutation of the indices of $\mathbf{r}_1$, $\mathbf{r}_2$, $\cdots\mathbf{r}_N$. In general it will not hold for differential operators like L_z, S_z, L^2, S^2.

Now let $\Phi_m{}^*$ and Φ_n, respectively, belong to the irreducable representations Γ and Γ' with dimensions g and g' of the symmetry group, of which $\mathfrak{R}$ is one element. Then

$$\begin{aligned}R\gamma_{m,n}(\mathbf{r})&=\sum_{m'}\sum_{n'}\Gamma_{m'm}\Gamma'_{n'n}\int\Phi_{m'}{}^*\Phi_{n'}\cdot\sum_i\delta(\mathbf{r}_i-\mathbf{r})\,(d\mathbf{r})^N\\&=\sum_{m'}\sum_{n'}\Gamma_{m'm}\Gamma'_{n'n}\cdot\gamma_{m'n'}(\mathbf{r}).\end{aligned} \tag{17}$$

This means *that $\gamma_{m,n}$ belongs to the representation $\Gamma\times\Gamma'$ of the direct product of the representations of the wave functions. The direct product representation has the dimension $g\cdot g'$ if all the $g\cdot g'$ products $\Phi_m{}^*\Phi_n$ are linearly independent.*[19]

[19] For $\Gamma'=\Gamma$ two cases have to be distinguished: (1) The two sets of functions $\Phi_m{}^*$ $(m=1,\,2,\cdots g)$ and Φ_n $(n=1,\,2,\cdots g)$ are *different*, that is, the operations $\mathfrak{R}$ transform the $\Phi_m{}^*$ and Φ_n among themselves, but do not transform a $\Phi_m{}^*$ into a linear combination of Φ_n's and vice versa. Here the above statement holds without any change. (2) The two sets are *identical*. Now there will be only $g(g+1)/2$ linearly independent products, which then span a representation given by the symmetric direct product $[\Gamma^2]$. See H. Weyl, *The Theory of Groups and Quantum Mechanics* (Dover Publishers, New York, p. 124.

In both cases the representation to which the $\gamma_{m,n}$ belong may be reduced, and its irreducible components $\Gamma^{(\alpha)}$ noted. Then each $\gamma_{m,n}$ can be decomposed into terms of different symmetry type:

$$\gamma_{m,n}(\mathbf{r})=\sum_{\alpha,i}c_{\alpha,i}{}^{m,n}\gamma_{\alpha,i}(\mathbf{r}), \tag{18}$$

where $\gamma_{\alpha,i}(\mathbf{r})$ is a function belonging to the ith row of the αth irreducible representation. Now

$$\int\gamma_{\alpha,i}(\mathbf{r})d\mathbf{r}=\begin{cases}N \text{ for the unit representation}\\ 0 \text{ for all other representations}\end{cases}. \tag{19}$$

The second statement is true because the integral over all space of any nontotally symmetric function must be zero; for the totally symmetric or unit representation the first row of Eq. (19) assumes normalization of $\gamma_{0,0}$. Equations (13), (18), and (19) then give $c_{0,0}{}^{m,n}=\delta_{m,n}$. From this it follows that the charge density of any state $(m=n)$ always contains the identity representation. Furthermore, the transition density between two states belonging to the *same* nondegenerate irreducible representation is always totally symmetric.

Let us now assume that the states m and n correspond to definite quantum numbers S, M_S and S', $M_{S'}$ of the total spin and its z component, respectively, $(m=\nu,\ S,\ M_S$ and $n=\nu',\ S',\ M_{S'}$, where ν and ν' designate any additional quantum numbers necessary for a complete description of these states). Then

$$\gamma_{\nu,S,M_S;\nu',S',M_{S'}}(\mathbf{r})=\delta_{S,S'}\delta_{M_S,M_{S'}}\cdot\gamma_{\nu,S,0;\nu',S,0}(\mathbf{r}). \tag{20}$$

This means that the transition density is different from zero only for states with the same values of the total spin and its z component, and that it has the same value for all values of M_S. This follows from the invariance of the operator in Eq. (12) defining $\gamma_{m,n}$ under any permutation of the electrons.[20]

IV. SYMMETRY PROPERTIES OF CHARGE AND TRANSITION DENSITIES FOR MANY-ELECTRON ATOMS

If spin-orbit interaction terms in the atomic Hamiltonian are neglected, the wave functions Φ_n can be chosen to be eigenfunctions of the operators $S,^2S_z$, L^2, L_z. Any state n can then be characterized by the quantum numbers ν, S, M_S, L, and M_L, where ν represents the eigenvalues of a set of observables which commute with S^2, S_z, L^2, L_z. The dependence of the transition density $\gamma_{m,n}$ on S, M_S is given by Eq. (20). The existence of quantum numbers L, M_L means that Φ_n belongs to an irreducible representation Γ_L of the 3-dimensional rotation group. The general expansion of Eq. (18) then takes the form $(\alpha\rightarrow L,\ i\rightarrow M_L)$

$$\gamma_{\nu'S'M_{S'}L'M_{L'},\nu''S''M_{S''}L''M_{L''}}=\delta_{S',S''}\delta_{M_{S'},M_{S''}}\cdot\sum_{L=|L'-L''|}^{L'+L''}\sum_{M=-L}^{+L}c_{L,M_L}{}^{*}\gamma_{L,M_L}. \tag{21}$$

The limits in the L summation follow from the rule for the direct product of the irreducible representations of the 3-dimensional rotation group

$$\Gamma_{L'}\times\Gamma_{L''}=\sum_{L=|L'-L''|}^{L'+L''}\Gamma_L. \tag{22}$$

If the operator R in Eq. (16) is taken to be the inversion, it follows that the parity of $\gamma_{m,n}$ must be equal to the product of the parities of the wave functions, or $(-1)^L=(-1)^{L'}\cdot(-1)^{L''}$. This restricts the permissible L values in Eqs. (21) and (22) to the series $L=L'+L'',\ L'+L''-2,\cdots\mid L'-L''\mid$. This restriction applies to the L summation in all the following formulas. It reduces the dimension of the reducible representation Γ of the $\gamma_{m,n}$ from $(2L'+1)\cdot(2L''+1)$ to $(L'+1)\cdot(2L''+1)$ with $L'\leq L''$. For $L'=L''$ this is equivalent to the use of the representation $[\Gamma^2]$ [see the discussion following Eq. (17)].

The angular dependence of $\gamma_{L,M_L}(r,\theta,\phi)$ is fixed by the requirement that this quantity should be an eigenfunction of L^2 and L_z,

$$\gamma_{L,M_L}(r,\theta,\phi)=\exp(-iM_L\phi)\cdot P_L{}^{|M_L|}(\cos\theta)\times(\text{function of } r). \tag{23}$$

Then Eq. (21) takes the form

$$\gamma_{\nu'S'M_{S'}L'M_{L'},\nu''S''M_{S''}L''M_{L''}}=\delta_{S',S''}\delta_{M_{S'},M_{S''}}\cdot\sum_{L}\sum_{M=-L}^{+L}r^L R_{L,M}(r)\cdot P_L{}^{|M|}(\cos\theta)\exp(iM\phi) \tag{24}$$

where the coefficient c_{L,M_L} has been incorporated in R_{L,M_L}. The radial factor must have the special form used in Eq. (24) for $\gamma(r,\theta,\phi)$ to be well behaved at the origin.

Finally it may be shown that in the sum over M in (24) only *one* term $(M=M_{L'}-M_{L''})$ is different from zero.

N. B. From

$$L_z=(1/i)\sum_{k=1}^{N}[x_k(\partial/\partial y_k)-y_k(\partial/\partial x_k)]$$

the following product law [see the discussion following Eq. (16)] can be inferred

$$L_z(\phi^*\psi)=\phi^*(L_z\psi)+(L_z\phi^*)\psi.$$

[20] E. Wigner, *Gruppentheorie* (1931), p. 125.

TABLE I. Coefficients $c_{n,l,m}$ in the expansion of the charge density [Eq. (27)].

Configuration	State	M_L[a]	$\|s\|^2$	$\|p_+\|^2$	$\|p_0\|^2$	$\|p_-\|^2$[b]
s	^2S	0	1			
s^2	^1S	0	2			
p	^2P	1		1		
		0			1	
p^2	^3P	1		1	1	
		0		1		1
	^1D	2		2		
		1		1	1	
		0		1/3	4/3	1/3
	^1S	0		2/3	2/3	2/3
sp	$^{1,3}P$	1	1	1		
		0	1		1	
p^3	^2D	2		2	1	
		1		3/2	1	1/2
		0		1	1	1
	^2P	1		3/2	1	1/2
		0		1	1	1
	^4S	0		1	1	1
sp^2	$^{2,4}P$	1	1	1	1	
		0	1	1		1
	^2D	2	1	2		
		1	1	1	1	
		0	1	1/3	4/3	1/3
	^2S	0	1	2/3	2/3	2/3
p^4	^3P	1		2	1	1
		0		1	2	1
	^1D	2		2	2	
		1		2	1	1
		0		5/3	2/3	5/3
	^1S	0		4/3	4/3	4/3
sp^3	$^{3,5}S$	0	1	1	1	1
	$^{1,3}P$	2	1	2	1	0
		1	1	3/2	1	1/2
		0	1	1	1	1
	$^{1,3}P$	1	1	3/2	1	1/2
		0	1	1	1	1
p^5	^2P	1		2	2	1
		0		2	1	2
sp^4	$^{2,4}P$	1	1	2	1	1
		0	1	1	2	1
	^2D	2	1	2	2	
		1	1	2	1	1
		0	1	5/3	2/3	5/3
	^2S	0	1	4/3	4/3	4/3
p^6	^1S	0		2	2	2
sp^5	$^{1,3}P$	1	1	2	2	1
		0	1	2	1	2

[a] Only values of $M_L \geq 0$ are included, for $M_L < 0$ the entries for the row corresponding to $|M_L| > 0$ apply with the coefficients for p_+ and p_- interchanged.
[b] Empty places stand for the value zero of the corresponding coefficient.

If $L_z\Phi_n = M_{L''}\Phi_n$ and $L_z\Phi_m = M_{L'}\Phi_m$, or $L_z^*\Phi_m^* = M_{L'}\Phi_m^* = -L_z\Phi_m^*$ then $L_z(\Phi_m^*\Phi_n) = (M_{L''} - M_{L'}) \times \Phi_m^*\Phi_n$. This together with Eq. (15) gives

$$L_z\gamma_{m,n}(r,\theta,\phi) = (1/i)(\partial/\partial\phi)\gamma_{m,n}(r,\theta,\phi)$$
$$= (M_{L''} - M_{L'})\gamma_{m,n}(r,\theta,\phi)$$

or

$$\gamma_{m,n}(r,\theta,\phi) = \exp[-i(M_{L'} - M_{L''})\phi]\cdot\gamma_{m,n}(r,\theta,0).$$

Combining this with Eq. (24) gives the final formula

$$\gamma_{\nu'S'M_{S'}L'M_{L'},\nu''S''M_{S''}L''M_{L''}}(r,\theta,\phi) = \delta_{S',S''}\delta_{M_{S'},M_{S''}}$$
$$\cdot\sum_L \frac{(L-|M|)!}{(L+|M|)!}\frac{2L+1}{4\pi}P_L^{|M|}(\cos\theta)e^{-iM\phi}\cdot r^L\rho_{L,M}(r) \tag{25}$$

with $M = M_{L'} - M_{L''}$. The numerical factors in Eq. (25) correspond to choice as follows of the multipole coefficients ($S' = S''$, $M_{S'} = M_{S''}$):

$$r^L\rho_{L,M}(r)$$
$$= \int \gamma(r,\theta,\phi)\,P_L^{|M|}(\cos\theta)\exp(+iM\phi)\,d\phi\,d(\cos\theta). \tag{26}$$

Equation (24) can be derived more directly by noting that the functions $P_L^{|M|}(\cos\theta)e^{-iM\phi}$ form a complete system for the angle variables, therefore any function of (r, θ, ϕ) must be expressible as a series in them with coefficients depending on r.[21] The derivation given in the preceding serves rather as an illustration for the general expansion of Eq. (18) and in addition leads to the restrictions on the M and L values in such a series characteristic for the transition densities for atoms.

V. CHARGE DENSITIES OF MANY-ELECTRON ATOMS IN THE ORBITAL APPROXIMATION

The results of Sec. IV are valid not only for exact wave functions but also for approximate wave functions of correct symmetry. This section is devoted to the illustration of these results with the approximate wave functions of Slater's theory of complex atoms. Here the wave functions are built from Slater determinants made up from one-electron orbitals. A recent paper on atomic valence states by Companion and

[21] W. A. Bingel, J. Chem. Phys. **30**, 1250, 1254 (1959) where some of the results of this paper were given without proof. The following misprints should be corrected: left side of Eq. (16a) on p. 1252 should read $f_k(s,t)$, the integrand in Eq. (17) is $r^{L+2}\rho_{L|0}(r)\times$, line 7 from bottom of left column of p. 1252 should read $R_aZ_a = R_bZ_b$, Eq. (18a) should read $R_a = RZ_b/Z_u$, the second term in Eq. (19) should be E_1R; the caption of Fig. 3 on p. 1257 should read NH_3 instead of CH_3.

Ellison[22] contains tables for all states arising from the electron configurations $s^n p^m$, giving the coefficients in the expansion of the approximate wave functions in terms of Slater determinants. Using these tables the charge density $\gamma(\mathbf{r})$ for any state turns out to have the form [see Eqs. (6) and (7)]

$$\gamma(\mathbf{r}) = \sum_{n,l,m} c_{n,l,m} \, | \, \phi_{n,l,m}(\mathbf{r}) \, |^2 \qquad (27)$$

with the atomic orbitals given by

$$\phi_{n,l,m}(\mathbf{r}) = R_{nl}(r) \Pi_l^{|m|}(\cos\theta) [\exp(im\phi)/(2\pi)^{\frac{1}{2}}]. \qquad (28)$$

The coefficients $c_{n,l,m}$ for all states arising from the electron configurations $s^n p^m$ are collected in Table I. They fulfill the obvious relations

$$\sum_{n,l,m} c_{n,l,m} = N, \qquad \sum_{m} c_{n,l,m} = N_{nl}. \qquad (29a, b)$$

Here N is the total number of electrons and N_{nl} is the number of electrons in the subshell nl. The first of these two equations follows from integration of Eq. (27) according to Eq. (9), the second holds only in the orbital approximation. Substitution of Eq. (28) into Eq. (27) gives

$$\gamma(\mathbf{r}) = \sum_{n,l,m} c_{n,l,m} R_{nl}^2(r) \cdot [\Pi_l^{|m|}(\cos\theta)]^2 \cdot (2\pi)^{-1} \qquad (30)$$

which is independent of the angle ϕ.

The decomposition (25) of the charge density $\gamma(\mathbf{r})$ into terms of different angular symmetry proceeds as follows. From Eq. (26) and (30)

$$r^L \rho_{L,M}(r) = \sum_{n,l,m} c_{n,l,m} [R_{nl}(r)]^2 \cdot \int [\Pi_l^{|m|}(\cos\theta)]^2 P_L^{|M|}(\cos\theta) \, d(\cos\theta) \cdot \int (e^{iM\phi}/2\pi) \, d\phi$$

$$= \delta_{M,0} \cdot \sum_{n,l} [R_{nl}(r)]^2 \cdot \sum_{m} c_{n,l,m} c^L(lm, lm) \qquad (31)$$

TABLE II. The Condon-Shortley coefficients for s and p electrons.

	$c^L(lm, lm)$		
$\| \phi_{n,l,m} \|^2$	$L=0$	2	4
$\| s \|^2$	1	0	0
$\| p_{\pm 1} \|^2$	1	−1/5	0
$\| p_0 \|^2$	1	+2/5	0
$\Sigma \| p_i \|^2$	3	0	0

[22] A. L. Companion and F. O. Ellison, J. Chem. Phys. 28, 1 (1958).

TABLE III. The terms $r^L \rho_{L,0}(r)$ in the angular expansion of the charge density [Eq. (25)].[a]

			$L=0$[b]		$L=2$
Configuration and state		$\| M_L \|$	$\| R_s \|^2$	$\| R_p \|^2$	$\| R_p \|^2$
s	^2S	0	1		
s^2	^1S	0	2		
p	^2P	1		1	−1/5
		0		1	+2/5
p^2	^3P	1		2	1/5
		0		2	−2/5
	^1D	2		2	−2/5
		1		2	+1/5
		0		2	+2/5
	^1S	0		2	
sp	$^{1,3}P$	1	1	1	−1/5
		0	1	1	+2/5
p^3	^4D	2		3	
		1		3	
		0		3	
	^2P	1		3	
		0		3	
	^4S	0		3	
sp^2	$^{2,4}P$	1	1	2	1/5
		0	1	2	−2/5
	^2D	2	1	2	−2/5
		1	1	2	+1/5
		0	1	2	+2/5
	^2S	0	1	2	
p^4	^3P	1		4	−1/5
		0		4	+2/5
	^1D	2		4	+2/5
		1		4	−1/5
		0		4	−2/5
	^1S	0		4	
sp^3	$^{3,5}S$	0	1	3	
	$^{1,3}D$	2	1	3	
		1	1	3	
		0	1	3	
	$^{1,3}P$	1	1	3	
		0	1	3	
p^5	^2P	1		5	1/5
		0		5	−1/5
sp^4	$^{2,4}P$	1	1	4	−1/5
		0	1	4	+2/5
	^2D	2	1	4	+2/5
		1	1	4	−1/5
		0	1	4	−2/5
	^2S	0	1	4	
p^6	^1S	0		6	
sp^5	$^{1,3}P$	1	1	5	1/5
		0	1	5	−2/5

[a] Here only the spherically symmetric ($L=0$) term $\rho_{0,0}(r)$ and the term with $L=2$ $r^2\rho_{2,0}(r)$ occur. Example: for sp^2 ^2D, $M_L=\pm 2$ we have $\rho_{0,0}(r)=R_p^2+2R_p^2$ and $r^2\rho_{2,0}(r)=-2/5R_p^2$.

[b] Since $c^0(lm, lm)=1$ for all lm, it follows from Eq. (31) and (29a) that $\rho_{0,0}(r)=\Sigma_{n,l}N_{nl}\cdot R_{nl}^2$.

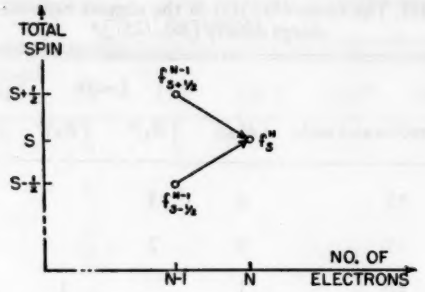

FIG. 1.

where the quantities

$$c^L(lm, lm)$$
$$=[2/(2L+1)]^{\frac{1}{2}}\int(\Pi_l^{|m|}(\cos\theta))^2\Pi_L^0(\cos\theta)d(\cos\theta)$$

are the Condon-Shortley coefficients.[23] Table II gives those which are necessary for this calculation. With the help of Tables I and II and Eq. (31), Table III can be constructed which gives the actual decomposition of the states considered here into terms of different angular momentum L. It should be noted that only terms with $M=0$ appear. This is in agreement with the general formula (25), since the charge densities considered here are the $\gamma_{\nu'S'M_{S'}L'M_{L'},\nu'S'M_{S'}L'M_{L'}}$ of Eq. (25). They turn out to be independent of $M_{S'}=M_{S''}$, which also follows quite generally from this equation. Finally, inspection of Table III shows that the L values which occur are in agreement with Eq. (23′). This limitation on the values of L which was derived in Sec. IV from general considerations, follows here from the special properties of the Condon-Shortley coefficients c^L.

APPENDIX

Any N-electron wave function with definite quantum numbers S, M of total spin and its component in a fixed direction can be expressed in the form[24]

$$\Phi_{S,M}^{(m)}=(f_S^N)^{-\frac{1}{2}}\sum_{k=1}^{f_S^N}\Psi_{S,k}^{(m)}(\mathbf{r}_1, \mathbf{r}_2, \cdots \mathbf{r}_N)\cdot\Theta_{S,M;k}^N(s_1, s_2, \cdots s_N). \quad (A1)$$

The spin functions $\Theta_{S,M,k}^N$ for fixed S and M form a basis for the irreducible representation $\mathfrak{D}_S^N$ of the permutation group of dimension

$$f_S^N=\binom{N}{N/2+S}-\binom{N}{N/2+S+1}.$$

[23] E. U. Condon and G. H. Shortley, *The Theory of Atomic Spectra* (Cambridge 1951), p. 178.
[24] M. Kotani, A. Amemiya, E. Ishiguro, and T. Kimura, *Table of Molecular Integrals* (Tokyo, 1955), Part I.

The space functions $\psi_{S,k}^{(m)}$ for fixed S and m form a basis for the dual representation† $\mathfrak{D}_S^N$. The N-electron spin functions are built up from those for $N-1$ electrons according to the branching rule (see Fig. 1)

$$\Theta_{S,M;k}^N=-[(S-M+1)/(2S+2)]^{\frac{1}{2}}\Theta_{S+\frac{1}{2},M-\frac{1}{2};k}^{N-1}\cdot\alpha(N)$$
$$+[(S+M+1)/(2S+2)]^{\frac{1}{2}}\Theta_{S+\frac{1}{2},M+\frac{1}{2};k}^{N-1}\cdot\beta(N)$$
$$(k=1, 2\cdots f_{S+\frac{1}{2}}^{N-1})$$
$$\Theta_{S,M;k}^N=[(S+M)/2S]^{\frac{1}{2}}\Theta_{S-\frac{1}{2},M-\frac{1}{2};k}^{N-1}\cdot\alpha(N)$$
$$+[(S-M)/2S]^{\frac{1}{2}}\Theta_{S-\frac{1}{2},M+\frac{1}{2};k}^{N-1}\cdot\beta(N).$$
$$(k=f_{S+\frac{1}{2}}^{N-1}+h,$$
$$h=1, 2\cdots f_{S-\frac{1}{2}}^{N-1}) \quad (A2)$$

These spin functions are orthonormal:

$$\int\Theta_{S,M;k}^N\Theta_{S',M',k'}^N(ds)^N=\delta_{S,S'}\delta_{M,M'}\delta_{k,k'}. \quad (A3)$$

Making use of the decomposition (A1) the first order density matrix (2) can now be expressed as

$$\gamma(\mathbf{x}'\mid\mathbf{x})=(N/f_S^N)\sum_{k,k'}\int\Psi_{S,k}^{(m)*}(\mathbf{r}_1\cdots\mathbf{r}_{N-1}, \mathbf{r}')$$
$$\times\Psi_{S,k'}^{(m)}(\mathbf{r}_1\cdots\mathbf{r}_{N-1}, \mathbf{r})(d\mathbf{r})^{N-1}\cdot J_{kk'} \quad (A4)$$

where

$$J_{k,k'}=\int\Theta_{S,M;k}^N(S_1\cdots S_{N-1}S')\Theta_{S,M;k'}^N$$
$$\times(s_1\cdots s_{N-1}s)(ds)^{N-1}. \quad (A5)$$

Substituting (A2) into the spin integral (A5) one has the following possibilities (see Fig. 1):

(a) k and k' both from $S+\frac{1}{2}$: here

$$J_{k,k'}=$$
$$\frac{S-M+1}{2(S+1)}\int\Theta_{S+\frac{1}{2},M-\frac{1}{2};k}^{N-1}\Theta_{S+\frac{1}{2},M-\frac{1}{2};k'}^{N-1}(ds)^{N-1}\cdot\alpha(s')\alpha(s)$$
$$+\frac{S+M+1}{2(S+1)}\int\Theta_{S+\frac{1}{2};M+\frac{1}{2};k}^{N-1}\Theta_{S+\frac{1}{2},M+\frac{1}{2};k'}^{N-1}(ds)^{N-1}\cdot\beta(s')\beta(s)$$
$$-\left(\frac{(S-M+1)(S+M+1)}{(2S+2)^2}\right)^2\times$$
$$\left\{\int\Theta_{S+\frac{1}{2},M-\frac{1}{2};k}^{N-1}\Theta_{S+\frac{1}{2},M+\frac{1}{2};k'}^{N-1}(ds)^{N-1}\cdot\alpha(s')\beta(s)\right.$$
$$\left.+\text{similarly with } k\leftrightarrow k'\cdot\beta(s')\alpha(s)\right\}.$$

From (A3) the first two integrals are equal to $\delta_{k,k'}$ and the last two are zero (the functions have different M's), therefore

$$J_{k,k'}=\delta_{k,k'}(2S+2)^{-1}\{(S-M+1)\cdot\alpha(s')\alpha(s)+(S+M+1)\cdot\beta(s')\beta(s)\}.$$

(b) k and k' both from $S-\frac{1}{2}$: In the same way as (a) we get

$$J_{k,k'}=\delta_{k,k'}(2S)^{-1}\{(S+M)\cdot\alpha(s')\alpha(s)+(S-M)\cdot\beta(s')\beta(s)\}.$$

(c) k from $S+\frac{1}{2}$, k' from $S-\frac{1}{2}$: from (A3) it follows that $J_{k,k'}$ is zero (the functions have different S's).

(d) k from $S-\frac{1}{2}$, k' from $S+\frac{1}{2}$: same as (c).

Collecting these results, (A4) gives the desired formula

$$\gamma(\mathbf{x}'\mid\mathbf{x})=\gamma_+(\mathbf{r}'\mid\mathbf{r})\cdot\alpha(s')\alpha(s)+\gamma_-(\mathbf{r}'\mid\mathbf{r})\cdot\beta(s')\beta(s) \quad (A6)$$

where the partial density matrices γ_+ and γ_- are given by

$$\gamma_\pm(\mathbf{r}'\mid\mathbf{r})=(1/f_S{}^N)\Big\{[(S\mp M+1)/(2S+2)]\cdot\sum_{k=1}^{f_{S+\frac{1}{2}}{}^{N-1}}N\int\Psi_{S,k}{}^{(m)*}(\mathbf{r}_1\cdots\mathbf{r}_{N-1},\mathbf{r}')\times\Psi_{S,k}{}^{(m)}(\mathbf{r}_1\cdots\mathbf{r}_{N-1},\mathbf{r})(d\mathbf{r})^{N-1}+[(S\pm M)/2S]\sum_{k>f_{S+\frac{1}{2}}{}^{N-1}}^{f_S{}^N}N\int\Psi_{S,k}{}^{(m)*}(\mathbf{r}_1\cdots\mathbf{r}_{N-1},\mathbf{r}')\times\Psi_{S,k}{}^{(m)}(\mathbf{r}_1\cdots\mathbf{r}_{N-1},\mathbf{r})(d\mathbf{r})^{N-1}\Big\}. \quad (A7)$$

From Eq. (A7) it follows that

$$\gamma_+(\mathbf{r}'\mid\mathbf{r})+\gamma_-(\mathbf{r}'\mid\mathbf{r})=(N/f_S{}^N)\sum_{k=1}^{f_S{}^N}\int\Psi_{S,k}{}^{(m)*}(\mathbf{r}_1\cdots\mathbf{r}_{N-1},\mathbf{r}')\times\Psi_{S,k}{}^{(m)}(\mathbf{r}_1\cdots\mathbf{r}_{N-1},\mathbf{r})(d\mathbf{r})^{N-1}.$$

But this is equal to $\gamma(\mathbf{r}'\mid\mathbf{r})$ of (3) with the Φ of (A1). Therefore

$$\gamma_+(\mathbf{r}'\mid\mathbf{r})+\gamma_-(\mathbf{r}'\mid\mathbf{r})=\gamma(\mathbf{r}'\mid\mathbf{r}). \quad (A8)$$

Equation (A7) shows how the partial density matrices γ_+ and γ_- of (A6) depend on the space functions $\Psi_{S,k}{}^{(m)}$ of the decomposition (A1).

Now it is possible to define the diagonal elements of these quantities directly in terms of the total wave function Φ, namely, as expectation values of the operators

$$\sum_{i=1}^{N}\delta(\mathbf{r}_i-\mathbf{r})(\tfrac{1}{2}\pm S_{zi}).$$

Using again the decomposition (A1) we find

$$\langle\Phi\mid\sum_{i=1}^{N}\delta(\mathbf{r}_i-\mathbf{r})(\tfrac{1}{2}\pm S_{zi})\mid\Phi\rangle=(N/f_S{}^N)\sum_{k,k'}^{N}\int\Psi_{S,k}{}^{(m)*}(\mathbf{r}_1\cdots\mathbf{r}_{N-1},\mathbf{r})\times\Psi_{S,k'}{}^{(m)}(\mathbf{r}_1\cdots\mathbf{r}_{N-1},\mathbf{r})(d\mathbf{r})^{N-1}\cdot I_{k,k'}{}^{\pm} \quad (A9)$$

where

$$I_{k,k'}{}^{\pm}=\int\Theta_{S,M;k}{}^{N}(\tfrac{1}{2}\pm S_{zN})\Theta_{S,M;k'}{}^{N}(ds)^N. \quad (A10)$$

The calculation of $I_{k,k'}{}^{\pm}$ proceeds in the same way as for the corresponding integrals (A5). Use of (A2) and the additional rules

$$(\tfrac{1}{2}+S_z)\alpha=\alpha,\qquad(\tfrac{1}{2}+S_z)\beta=0,\qquad(\tfrac{1}{2}-S_z)\alpha=0,\qquad(\tfrac{1}{2}-S_z)\beta=\beta \quad (A11)$$

gives for

(a) k and k' both from $S+\frac{1}{2}$:

$$(\tfrac{1}{2}+S_{zN})\Theta_{S,M;k'}{}^{N}=-[(S-M+1)/(2S+2)]^{\frac{1}{2}}\cdot\Theta_{S+\frac{1}{2},M-\frac{1}{2};k'}{}^{N-1}\cdot\alpha(N)$$

$$(\tfrac{1}{2}-S_{zN})\Theta_{S,M;k'}{}^{N}=+[(S+M+1)/(2S+2)]^{\frac{1}{2}}\cdot\Theta_{S+\frac{1}{2},M+\frac{1}{2};k'}{}^{N-1}\cdot\beta(N)$$

$$I_{k,k'}{}^{+}=+[(S-M+1)/(2S+2)]\cdot\int\Theta_{S+\frac{1}{2},M-\frac{1}{2};k}{}^{N-1}\Theta_{S+\frac{1}{2},M-\frac{1}{2};k'}{}^{N-1}(ds)^{N-1}\cdot\int\alpha^2(N)ds_N=[(S-M+1)/(2S+2)]\cdot\delta_{k,k'} \quad (A12)$$

and in the same way

$$I_{k,k'}{}^{-}=[(S+M+1)/(2S+2)]\cdot\delta_{k,k'}.$$

(d) k from $S-\frac{1}{2}$, k' from $S+\frac{1}{2}$: (A2) and (A12) give

$$I_{k,k'}{}^{+}=-\left(\frac{(S-M+1)(S+M)}{2S(2S+2)}\right)^{\frac{1}{2}}\cdot\int\Theta_{S-\frac{1}{2},M-\frac{1}{2};k}{}^{N-1}\Theta_{S+\frac{1}{2},M-\frac{1}{2};k'}{}^{N-1}(ds)^{N-1}\cdot\int\alpha^2(N)ds_N.$$

The first integral is zero according to (A3) (different S's). The same results for $I_{k,k'}{}^{-}$, therefore $I_{k,k'}{}^{\pm}=0$.

(b) k and k' both from $S-\frac{1}{2}$:

$$(\tfrac{1}{2}+S_{zN})\Theta_{S,M;k'}{}^{N}=+[(S+M)/2S]^{\frac{1}{2}}\cdot\Theta_{S-\frac{1}{2},M-\frac{1}{2};k'}{}^{N-1}\cdot\alpha(N)$$

$$(\tfrac{1}{2}-S_{zN})\Theta_{S,M;k'}{}^{N}=+[(S-M)/2S]^{\frac{1}{2}}\cdot\Theta_{S-\frac{1}{2},M+\frac{1}{2};k'}{}^{N-1}\cdot\beta(N)$$

$$I_{k,k'}{}^{\pm}=[(S\pm M)/2S]\delta_{k,k'} \tag{A13}$$

(c) k from $S+\frac{1}{2}$, k' from $S-\frac{1}{2}$: $I_{k,k'}{}^{\pm}=0$, same as (d).

Summarizing, one gets

$$\langle\Phi\mid\sum_{i=1}^{N}\delta(\mathbf{r}_i-\mathbf{r})(\tfrac{1}{2}\pm S_{zi})\mid\Phi\rangle=(N/f_S{}^{N})\Big\{[(S\mp M+1)/(2S+2)]\sum_{k=1}^{f_{S+\frac{1}{2}}{}^{N-1}}\int\mid\Psi_{S,k}{}^{(m)}(\mathbf{r}_1\cdots\mathbf{r}_{N-1}\mathbf{r})\mid^2(d\mathbf{r})^{N-1}$$

$$+[(S\pm M)/2S]\sum_{k>f_{S+\frac{1}{2}}{}^{N-1}}^{f_S{}^{N}}\int\mid\Psi_{S,k}{}^{(m)}(\mathbf{r}_1\cdots\mathbf{r}_{N-1}\mathbf{r})\mid^2(d\mathbf{r})^{N-1}\Big\}. \tag{A14}$$

Comparison with (A7) shows that

$$\gamma_{\pm}(\mathbf{r}\mid\mathbf{r})\equiv\gamma_{\pm}(\mathbf{r})=\langle\Phi\mid\sum_{i=1}^{N}\delta(\mathbf{r}_i-\mathbf{r})(\tfrac{1}{2}\pm S_{zi})\mid\Phi\rangle. \tag{A12}$$

This is the desired formula defining the partial charge densities $\gamma_{+}(r)$ and $\gamma_{-}(\mathbf{r})$ in terms of the total wave function Φ. Equation (A12) can be generalized for the nondiagonal elements where

$$\gamma_{\pm}(\mathbf{r}'\mid\mathbf{r})=N\int\Phi^{*}(\mathbf{r}'s,\,\mathbf{x}_2\cdots\mathbf{x}_N)\times(\tfrac{1}{2}\pm S_{z1})\Phi(\mathbf{r}s,\,\mathbf{x}_2\cdots\mathbf{x}_N)(d\mathbf{x})^{N-1}ds \tag{A13}$$

as can be shown by a derivation similar to the one leading to Eq. (A12).

Crystal Field Splitting of Energy Levels of Thulium Ethylsulfate*

JOHN B. GRUBER AND JOHN G. CONWAY

Lawrence Radiation Laboratory, University of California, Berkeley, California

(Received October 2, 1959)

The operator-equivalent method was employed to calculate the theoretical splitting of electronic energy levels $^3P_2$, $^1D_2$, $^3F_2$, $^3F_3$, $^3F_4$, $^1G_4$, and $^3H_6$ in $Tm(C_2H_5SO_4)_3 \cdot 9H_2O$. Intermediate field corrections were made to α, β, and γ. A first-order perturbation treatment on Tm^{3+} ($4f^{12}$) in C_{3h} symmetry, using crystal-field parameters $A_2^0\langle r^2\rangle = 13$ cm^{-1}, $A_4^0\langle r^4\rangle = -80$ cm^{-1}, $A_6^0\langle r^6\rangle = -32$ cm^{-1}, and $A_6^6\langle r^6\rangle = 300$ cm^{-1}, predicts the position of the crystal quantum states in reasonable agreement with experiment.

INTRODUCTION

In a $Tm(C_2H_5SO_4)_3 \cdot 9H_2O$ single crystal, where the Tm^{3+} configuration is $4f^{12}$, the perturbing influence of the water and ethylsulfate groups on the energy-level system of the free ion can be calculated by expanding the crystal-field electric potential in a series of spherical harmonics. A first-order perturbation treatment is possible since the crystal field splitting of the various electronic levels is of the order of 100 cm^{-1}, whereas the spin orbit splitting between adjacent levels is generally greater than 1000 cm^{-1}. The work of Ketelaar has shown that the point symmetry at the metal-ion site in rare earth ethylsulfates is predominantly C_{3h}.[1] Johnsen[2] and the present authors[3] have found C_{3h} point symmetry to be consistent with the interpretation of the $Tm(C_2H_5SO_4)_3 \cdot 9H_2O$ absorption spectra. However, a few transitions were observed that are forbidden in C_{3h} symmetry but are allowed in C_{3v} symmetry. The theoretical splitting of $^3H_6$, $^3F_4$, $^3F_3$, $^3F_2$, $^1G_4$, $^1D_2$, and $^3P_2$ levels presented here is based on the experimental work of these investigators.

CALCULATION OF INTERMEDIATE-FIELD OPERATOR EQUIVALENTS

The potential energy of a $4f$ electron in the electrostatic field of the lattice is taken to be

$$A_2^0(3z^2-r^2)+A_4^0(35z^4-30z^2r^2+3r^4)$$
$$+A_6^0(231z^6-315z^4r^2+105z^2r^4-5r^6)$$
$$+A_6^6(x^6-15x^4y^2+15x^2y^4-y^6).$$

The contribution to the free-Tm^{3+} Hamiltonian consists of two expressions of this form, corresponding to the two $4f$ electron "holes." The quantities A_n^m are characteristic of the lattice and appear with the corresponding quantities $\langle r^n\rangle$, the mean value of r^n for a single $4f$ electron.

As Stevens has shown,[4] within a given manifold of J the matrix elements of the potential form V_n^m associated with the parameter A_n^m are related to the matrix elements of certain angular-momentum operators through a factor $\theta_n\langle r^n\rangle$. Here θ_n is the so-called "operator-equivalent" factor, usually written as α, β, and γ for $n=2$, 4, and 6. This theory has been generalized by Elliott *et al.* for all rare earth ions.[5] Judd has given the equations for evaluating the pure L-S operator equivalent for $Pr^{3+}(4f^2)$.[6] He has tabulated these values for $^3H_4$, $^1G_4$, $^3F_4$, $^3F_3$, $^1D_2$, $^3P_2$, and $^3P_1$ in the same paper with the crystal-field-splitting results for Pr^{3+} in $LaCl_3$. For $Tm^{3+}(4f^{12})$, the L-S α, β, and γ may be calculated from the Pr^{3+} set of equations. The only difference will be a change in sign. However, L-S coupling breaks down in Tm^{3+}, and it is necessary to consider intermediate coupling effects on the L-S operator equivalents.

In an earlier paper[3] the electronic energy levels for Tm^{3+} in the intermediate field were obtained from a plot of E/F_2 vs χ, where $\chi=\zeta/F_2$, ζ is the spin orbit parameter used by Spedding,[7] and F_2 is a Slater integral. The best fit of theory to experiment was obtained at $\chi=3$. The eigenvectors at $\chi=3$ for $^3H_4$, $^3F_4$, $^1G_4$, and $^3F_2$, $^3P_2$, $^1D_2$, used in calculating α, β, and γ in the intermediate field were obtained from an IBM-650 program. The eigenvectors for $^3H_6$ and $^1I_6$ were calculated by hand using Spedding's equations. Table I includes values of operator equivalents for $Tm(C_2H_5SO_4)_3 \cdot 9H_2O$ with intermediate-field corrections in brackets.

Suppose we wish to calculate α, β, and γ for $^1G_4$ in an intermediate field at $\chi=3$. In a $4f^{12}$ configuration there are three $J=4$ levels. We write

$$|\,^1G_4'\rangle = 0.6119\,|\,^3H_4\rangle + 0.7260\,|\,^1G_4\rangle - 0.3137\,|\,^3F_4\rangle, \quad (1)$$

where 0.6119, 0.7260, and -0.3137 are the corre-

* This work was performed under the auspices of the U. S. Atomic Energy Commission.

[1] J. A. A. Ketelaar, Physica (Haag) **4**, 619 (1937).

[2] U. Johnsen, Z. Physik **152**, 454 (1958).

[3] J. B. Gruber and J. G. Conway, UCRL-8839 (August, 1959); J. Chem. Phys. **32**, 1178 (1960).

[4] K. W. H. Stevens, Proc. Phys. Soc. (London) **A65**, 209 (1952).

[5] R. J. Elliott, B. R. Judd, and W. A. Runciman, Proc. Roy. Soc. (London) **A240**, 509 (1957).

[6] B. R. Judd, Proc. Roy. Soc. (London) **A241**, 414 (1957).

[7] F. H. Spedding, Phys. Rev. **58**, 255 (1940).

TABLE I. Operator equivalents in the intermediate field, Tm^{3+} $(4f^{12})$.

Level	$\langle J \Vert \alpha \Vert J \rangle$		$\langle J \Vert \beta \Vert J \rangle$		$\langle J \Vert \gamma \Vert J \rangle$	
$^3P_1$	(1/5)	[1.000]	0		0	
$^3P_2$	(−1/15)	[1.095]	(−4/7·27)	[0.629][a]	0	
$^1D_2$	(−22/15·21)	[0.678]	(−4/7·27)	[−0.105]	0	
$^3F_2$	(−8/21·15)	[1.636]	(2/7·81)	[−1.859]	0	
$^3F_3$	(−1/90)	[1.000]	(1/45·99)	[1.000]	(1/39·99)	[1.000]
$^3F_4$	(−1/126)	[−1.357]	(1/45·77)	[1.527]	(−1/13·63·99)	[5.945]
$^1G_4$	(2/11·35)	[1.799]	(46/11·45·77)	[0.866]	(4/13·33·77)	[0.537]
$^1I_6$	(2/99)	[0.995]	(−4/11·15·99)	[0.984]	(2/13·33·21·99)	[0.967]
$^3H_6$	(1/99)	[1.010]	(8/3·11·1485)	[0.976]	(−5/13·33·2079)	[0.986]

[a] The pure L-S operator equivalent, β, is zero for $^3P_2$, since the corresponding Racah coefficient is zero. However, if we allow for intermediate coupling effects, the entry becomes (−4/7·27) [0.629].

sponding eigenvectors, and $|\,^1G_4'\rangle$ corresponds to the intermediate field $^1G_4$. Now we have

$$\langle {}^1G_4' \Vert \overset{\alpha}{\underset{\gamma}{\beta}} \Vert {}^1G_4' \rangle = (0.6119)^2 \langle {}^3H_4 \Vert \overset{\alpha}{\underset{\gamma}{\beta}} \Vert {}^3H_4 \rangle + (0.7260)^2 \langle {}^1G_4 \Vert \overset{\alpha}{\underset{\gamma}{\beta}} \Vert {}^1G_4 \rangle + (0.3137)^2 \langle {}^3F_4 \Vert \overset{\alpha}{\underset{\gamma}{\beta}} \Vert {}^3F_4 \rangle - 2(0.3137)(0.6119) \langle {}^3H_4 \Vert \overset{\alpha}{\underset{\gamma}{\beta}} \Vert {}^3F_4 \rangle. \quad (2)$$

There will be no cross terms involving $^1G_4$ with $^3F_4$ and $^3H_4$, since matrix elements between different spin states are zero. Each of the pure L-S operator equivalents in Eq. (2) can be evaluated from the equations given by Judd.[6] It is possible to factor out $^1G_4$, L-S α, β, and γ expressions from the right-hand side of Eq. (2), which leaves a sum of numbers that denotes the importance of intermediate-field corrections to the L-S operator-equivalent values. In this way, $^3F_4$, $^3F_2$, $^3P_2$, $^1D_2$, and $^3H_6$ operator equivalents were calculated. The $^3P_1$, $^3F_3$, and $^3H_5$ operator equivalents are not affected by spin-orbit interaction.

SELECTION OF PARAMETERS

Having found α, β, and γ for a particular level, we can now express the crystal splitting in terms of parameters $A_n^m \langle r^n \rangle$. These parameters were defined earlier. The values that these parameters can assume must be consistent with the point symmetry at the rare earth ion in the lattice.

In addition to containing some physical significance as a scale factor for the crystalline electric potential, A_n^m is also the repository for errors due to neglect of configuration interaction and interactions between crystal quantum states of one J level with those of a nearby J level. Since configuration interaction has greater effect on J levels in the ultraviolet than in the infrared, the $A_n^m \langle r^n \rangle$ parameters can not be expected to be really constant in going from $^3H_6$ to $^3P_2$, some 38 000 cm^{-1} away. Likewise, somewhat different parameter values are needed if a simultaneous perturbation treatment is carried out on the $^3F_2$, $^3F_3$, and $^3F_4$ levels and if a general second-order perturbation treatment is carried out.

If we neglect the effects mentioned in the preceding paragraph, the structure of $^3P_1$ (split into 2 sublevels $\mu=0, \pm1$) gives at once a preliminary value for $A_2^0\langle r^2 \rangle$. Unfortunately, our photographic plates unambiguously confirmed only the position of the $\mu=\pm1$ sublevel in $^3P_1$. Another line appearing in both σ and π polarization with a line width of some 10 cm^{-1} may have been 2 lines close together. More careful polarization experiments, in which the σ and π spectra are taken as a function of the rotation of the crystal, are necessary to confirm the actual energy value of the splitting. Parameters $A_6^6\langle r^6 \rangle$ and $A_6^0\langle r^6 \rangle$ were chosen so as to give the proper splitting of the $\mu=3$ and $\mu=\pm2$ sublevels in $^3F_4$, $^1G_4$, and $^3H_6$. Parameter $A_4^0\langle r^4 \rangle$ was chosen so as to give reasonable splitting of the $^3P_2$, $^3F_2$, and $^3H_6$ levels. The best over-all fit for this first-order perturbation treatment was obtained by using $A_2^0\langle r^2 \rangle = 13$ cm^{-1}, $A_4^0\langle r^4 \rangle = -80$ cm^{-1}, $A_6^0\langle r^6 \rangle = -32$ cm^{-1}, and $A_6^6\langle r^6 \rangle = 300$ cm^{-1}.

FITTING TO EXPERIMENTAL DATA

A. The $^3H_6$ Level

The theoretical predictions for $\mu=0, \pm1, 3$ are in good agreement with those crystal quantum states reported by experiment (see Fig. 1). The prediction of additional states between ±1 and 3 has led us to restudy our plates. Our reported analysis included only

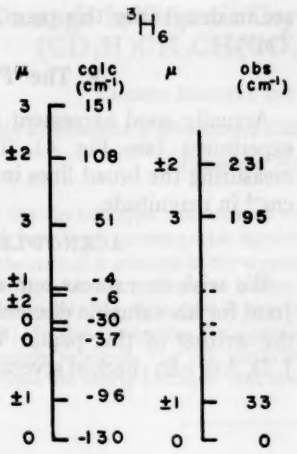

FIG. 1. The $^3H_6$ level. The dotted lines represent possible crystal quantum states not yet confirmed by experiment. The theoretical splitting of a particular J level is given on the left; the observed energy-level scheme on the right. Here μ is the crystal quantum number.

those intense lines in which polarization was complete.[3] As many as 3 or 4 weak lines appear between those due to transitions from the ±1 and 3, but these are not well polarized. These lines may be due to sublevels $\mu=0'$, $\pm1'$, and $\pm2'$ in $^3H_6$ as the theory predicts or satellite levels, but our experiments cannot really confirm this. Forbidden transitions observed in $^3P_2$, $^1D_2$, and $^1G_4$ may also confirm these predicted states in the $^3H_6$ level.

B. The $^3F_4$ Level

The splittings of the $\mu=\pm2$ and 3 are in reasonable agreement with experiment (see Fig. 2). However, the presence of the $^3F_3$ some 200 cm^{-1} away will cause certain states to be depressed more than others. This may explain the relative position of the theoretical value of $\mu=\pm1$.

C. The $^3F_3$ and $^3F_2$ Levels

Since $^3F_3$ and $^3F_2$ (see Figs. 3 and 4) are separated by 400 cm^{-1}, a simultaneous perturbation treatment is

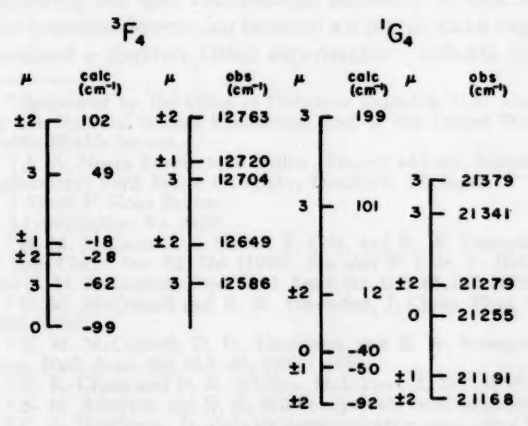

FIG. 2. The $^3F_4$ and $^1G_4$ levels.

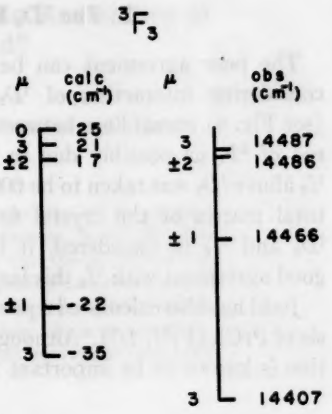

FIG. 3. The $^3F_3$ level.

necessary in order to get better fit. Such a treatment may reverse the positions $\mu=\pm1$, $\mu=\pm2$ in $^3F_2$, now given as a result of first-order methods. As yet, $\mu=0$ has not been reported for either of these levels.

D. The $^1G_4$ Level

The splitting between the lower $\mu=3$ and $\mu=\pm1$, between $\mu=\pm2$ and $\mu=\pm1$, and between $\mu=\pm1$ and lower $\mu=\pm2$ fits that found by experiment (see Fig. 2). The experimental positions of both $\mu=3$ sublevels are reasonably well established. The theoretical value of upper $\mu=3$ cannot be brought into better agreement by this present treatment. A slightly different set of parameters, $A_2{}^0\langle r^2\rangle=13$ cm^{-1}, $A_4{}^0\langle r^4\rangle=-80$ cm^{-1}, $A_6{}^0\langle r^6\rangle=-20$ cm^{-1}, and $A_6{}^6\langle r^6\rangle=200$ cm^{-1} gives the following somewhat better agreement: $\mu\pm2=-79$ cm^{-1}, $\mu\pm1=-50$ cm^{-1}, $\mu\pm2'=23$ cm^{-1}, $\mu3=101$ cm^{-1}, $\mu3'=166$ cm^{-1}.

That a slightly different set of parameters fits theory better to data may be due to increased importance of configuration interaction on excited levels. However, the internal inconsistency within the $^1G_4$ may be due to interactions between crystal quantum states of $^1G_4$ with those in $^3F_2$, $^3F_3$, and $^1D_2$.

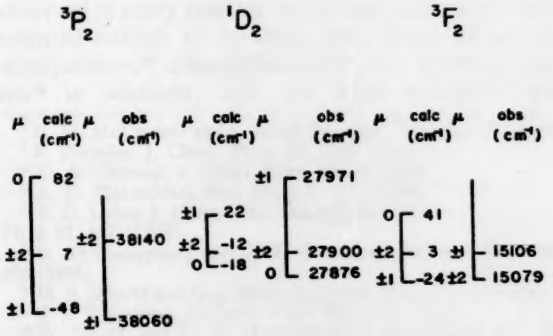

FIG. 4. The $^3F_2$, $^1D_2$, and $^3P_2$ levels.

E. The $^1D_2$ Level

The poor agreement can be partially remedied by considering interaction of $^1D_2$ with $^1I_6$. Our plates (see Fig. 4) reveal lines between $^3P_1$ and $^3P_0$ and to the red of $^3P_0$ as possibly due to the $^1I_6$. The energy of $^1I_6$ above $^1D_2$ was taken to be 6000 cm^{-1}. Even when the total matrix of the crystal field interaction between $^1D_2$ and $^1I_6$ is considered, it is impossible to obtain good agreement with $^1I_6$ this far removed from $^1D_2$.

Judd has also calculated a poor fit for $^1D_2$ in the analysis of $PrCl_3$ (Pr^{3+}, $4f^2$).[6] Although configuration interaction is known to be important for $^1D_2$, it is difficult to see in detail why this poor agreement occurs again in Tm^{3+}.

F. The $^3P_2$ Level

Actually good agreement exists between theory and experiment (see Fig. 4). The experimental error in measuring the broad lines in the ultraviolet is some 13 cm^{-1} in magnitude.

ACKNOWLEDGMENT

We wish to express our appreciation to Dr. B. R. Judd for his valuable discussion and suggestions during the writing of this paper. We also extend thanks to J. D. Axe who checked several of the calculations.

Radiation Damage in Organic Crystals. II. Electron Spin Resonance of $(CO_2H)CH_2\dot{C}H(CO_2H)$ in β-Succinic Acid*

CHONON HELLER† AND HARDEN M. MCCONNELL‡

Gates and Crellin Laboratories of Chemistry,§ California Institute of Technology, Pasadena 4, California

(Received November 23, 1959)

An analysis of the electron spin resonance of x-irradiated single crystals of β-succinic acid shows that: (a) the principal long-lived paramagnetic species produced by the radiation damage is $(CO_2H)CH_2\dot{C}H(CO_2H)$; (b) the radical is oriented in the crystal lattice in nearly the same way that the parent succinic acid molecule is oriented in the undamaged lattice; (c) the strongly anisotropic hyperfine interaction due to the σ proton is very nearly the same as that previously found for the σ proton in the malonic acid radical, $(CO_2H)\dot{C}H(CO_2H)$. In these molecules the σ proton is directly bonded to the carbon atom on which the odd electron is largely localized. The two methylene protons in the radical are not equivalent, and their hyperfine interactions are nearly isotropic, and in the range 80–100 Mc.

INTRODUCTION

IN previous work[1] electron spin resonance has been used to show that it is possible to prepare radicals with the formula $\dot{C}H(CO_2H)_2$ by 50-kv x irradiation of crystals of malonic acid. This radical has a fixed orientation in the crystal lattice and is stable at room temperature. The conclusions that were reached[1] on the orientation and electronic structure of this radical have been further substantiated by (a) the observation of C^{13} hyperfine splittings in the electron resonance of this radical,[2] and (b) the observed absorption of radio-frequency energy of the expected frequency and linear polarization by $\dot{C}H(CO_2H)_2$ in single crystals of x-ray damaged malonic acid in zero applied magnetic field.[3] This work[1–3] determines the parameters of the spin Hamiltonian that describes the hyperfine interaction between a *single* π electron and a σ proton. A "σ proton" is one that is directly bonded to an unsaturated carbon atom so that the σ proton lies in the nodal plane of the π-electron spin distribution. Ghosh and Whiffen,[4] and Atherton and Whiffen[5] have carried out studies of the paramagnetic resonance of γ-irradiated glycine and glycolic acid and have reached similar conclusions regarding the spin Hamiltonian necessary to describe the hyperfine interaction between a σ proton and a single localized π electron. Other experiments[6,7] indicate that these same parameters may be used for describing σ-proton hyperfine interaction with π-electron distributions centered on several carbon atoms in an aromatic or olefinic radical. Since (σ proton)-(π electron) hyperfine interactions appear to be rather well understood, both experimentally[1–7] and theoretically,[8] the present work was undertaken for the purpose of studying (π electron)-(π proton) hyperfine interactions. A "π proton" is one that is attached to an aliphatic carbon atom and lies above or below the plane of the π-electron spin distribution. As will be clear later, a detailed knowledge of the (σ proton)-(π electron) hyperfine interaction plays an essential role in the problem of distinguishing between (σ proton)-(π electron) and (π proton)-(π electron) hyperfine splittings in the observed spectra of $(CO_2H)_2\dot{C}HCH_2(CO_2H)$.

Isotropic (π proton)-(π electron) hyperfine interactions were first studied theoretically by Bersohn,[9] who applied molecular orbital theory to methyl proton splittings in semiquinones.

Chesnut[10] has used molecular orbital theory for π-proton hyperfine splittings in aliphatic radicals. Valence bond theoretical calculations of isotropic (π proton)-(π electron) hyperfine interactions in a number of molecules have been made by McLachlan,[11] and Lykos.[12] Hyperfine splittings due to π protons have now been observed in many radicals in solutions, and in randomly oriented radicals in the solid state. Examples are the semiquinones,[13] dimesitylmethyl,[14] and Wursters blue ion[15] in solutions, and the ethyl radical[16,17] and

* Sponsored by the Office of Ordnance Research, U.S. Army, by the National Science Foundation, and by the United States Public Health Service.

† A. A. Noyes Postdoctoral Fellow. Present address: Scientific Laboratory, Ford Motor Company, Dearborn, Michigan.

‡ Alfred P. Sloan Fellow.

§ Contribution No. 2529.

[1] H. M. McConnell, C. Heller, T. Cole, and R. W. Fessenden, J. Am. Chem. Soc. **82**, 766 (1960). See also T. Cole, C. Heller, and H. M. McConnell, Proc. Natl. Acad. Sci. U.S. **45**, 525 (1959).

[2] H. M. McConnell and R. W. Fessenden, J. Chem. Phys. **31**, 1688 (1959).

[3] H. M. McConnell, D. D. Thompson, and R. W. Fessenden, Proc. Natl. Acad. Sci. U.S. **45**, 1600 (1959).

[4] D. K. Ghosh and D. H. Whiffen, Mol. Phys. **2**, 285 (1959).

[5] N. M. Atherton and D. H. Whiffen (private communication).

[6] C. A. Hutchison, Jr. (private communication concerning the anisotropic proton hyperfine structure that is seen in the paramagnetic resonance of the triplet state of naphthalene).

[7] M. Hanna and H. M. McConnell (to be published).

[8] H. M. McConnell and J. Strathdee, Mol. Phys. **2**, 129 (1959).

[9] R. Bersohn, J. Chem. Phys. **24**, 1066 (1956).

[10] D. B. Chesnut, J. Chem. Phys. **29**, 43 (1958).

[11] A. D. McLachlan, Mol. Phys. **1**, 233 (1958).

[12] P. G. Lykos J. Chem. Phys. **32**, 625 (1960). Phys. **31**, 447 (1960).

[13] B. Venkataraman and G. K. Fraenkel, J. Chem. Phys. **23**, 588 (1955).

[14] H. S. Jarnett and G. J. Sloan, J. Chem. Phys. **22**, 1783 (1954).

[15] S. I. Weissman, J. Chem. Phys. **22**, 1135 (1954).

[16] W. Gordy and C. G. McCormick, J. Am. Chem. Soc. **78**, 3244 (1956).

[17] B. Smaller and M. S. Matheson, J. Chem. Phys. **28**, 1169 (1958).

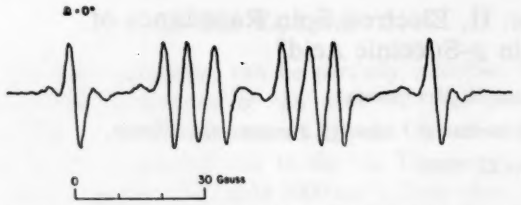

FIG. 1. Paramagnetic resonance of x-irradiated single crystal of β-succinic acid. Applied field is perpendicular to crystal b axis, and parallel to a.

$(CH_3)_2COH$[18] in polycrystalline solids or glasses. The present work differs from all previous work in that it provides an experimental determination of the anisotropy of π-proton hyperfine interactions for a molecular system where there can be no free rotation of the π protons.

EXPERIMENTAL

The crystal structure of β-succinic acid, the modification that is stable at room temperature, has been investigated by a number of workers.[19,20] The unit cell is monoclinic, $a=5.126$, $b=8.880$, $c=7.619$ A, and $\beta=133.6°$. The space group is $P\,2_1/a(C_{2h}^5)$. There are two molecules per unit cell. The asymmetric unit is half a molecule; the two halves of each molecule are related by a center of symmetry. The four carbon atoms are in a plane which we denote by **P**. The two molecules in the unit cell are transformed into one another by a twofold rotation about the b axis. The b axis passes through the center of symmetry of one molecule. The two carboxyl groups make an angle of about 11° with **P**. The molecules form chains parallel to the c axis, and the c axis lies in **P**.

Single crystals were grown by the slow evaporation of ethyl acetate solutions. The crystals were several millimeters in size and had well-developed faces [(001), (010), (110)] which were identified with an optical goniometer. The crystals were placed 5 cm from the tungsten target of an x-ray tube operating at 50 kv (30 ma) and were irradiated for 55 min. Spin resonance spectra were observed at room temperature using a conventional spectrometer with a microwave frequency of 9500 Mc and a field modulation of 100 kc. Succinic acid showed the same resonance spectrum immediately after irradiation as after prolonged aging at room temperature, or annealing for several days at 100°C. This is in contrast to the previous results obtained with malonic acid.[1]

The spin resonance spectra that are observed at most crystal orientations are complex and contain a number of unresolved lines. This result is related to the fact that in the undamaged lattice there are two molecules per unit cell, and at most crystal orientations these molecules—and the corresponding radicals produced by the x-ray damage—are not equivalent with respect to their interaction with the applied field. However, if the radicals produced by the radiation damage are related to one another by the space group symmetry operations of the undamaged crystal structure, then particularly simple spectra are expected when the applied field $\mathbf{H}_0$ is perpendicular to the b axis, since for this orientation the two radicals "per unit cell" should give the same spectrum. This was found to be the case. These "perperdicular" ($\mathbf{H}_0 \perp b$) spectra consisted of eight strong signals which for certain orientations coalesced into six. Two representative spectra are shown in Figs. 1 and 2, for $\Omega=0°$ and $\Omega=100°$. Here Ω refers to the angle between the applied field and the a axis of the unit cell, when the applied field is perpendicular to b. The two radicals per unit cell are also equivalent when the applied field is parallel to b, and a simple eight line spectrum was also obtained for this "parallel" ($\mathbf{H}_0 \parallel b$) orientation. In Figs. 1 and 2 there are weak satellite lines separated from the strong line by ca. 14 Mc. These weak lines were always 8–10 times less intense than the strong lines, and arise from a flip of the proton spin, which requires about 14 Mc, the proton resonance frequency in a field of 3300 gauss.[1,21]

ANALYSIS OF THE SPECTRA

The two basic assertions that we make in the following interpretation of the observed spectra are:

(A) The radicals giving the spectra have the formula

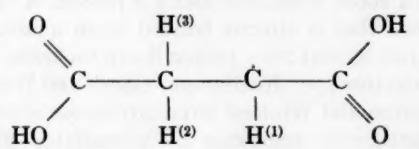

(I)

where the protons are numbered 1, 2, 3.

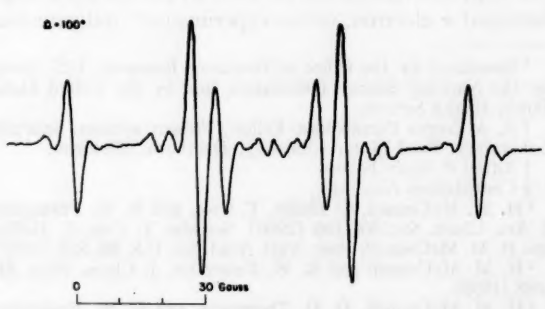

FIG. 2. Paramagnetic resonance of x-irradiated single crystal of β-succinic acid. Applied field is perpendicular to crystal b axis, and makes an angle of 100° with the a axis.

[18] J. F. Gibson, D. J. E. Ingram, M. C. R. Symons, and M. G. Townsend, Trans. Faraday Soc. **53**, 914 (1957).

[19] H. J. Verweel and C. H. MacGillary, Z. Krist. **102**, 60 (1939).

[20] J. D. Morrison and J. M. Robertson, J. Chem. Soc. **1949**, 980; J. S. Broadley, D. W. J. Cruickshank, J. D. Morrison, J. M. Robertson, and H. M. M. Shearer, Proc. Roy. Soc. (London) **A251**, 441 (1949).

[21] G. T. Trammell, H. Zeldes, and R. Livingston, Phys. Rev. **110**, 630 (1958).

(B) The radicals are related to one another by the point and space group symmetry operations of the undamaged crystal. According to assertion (B), any two radicals M_1 and M_2 are related to one another by (a) a center of inversion, or (b) a twofold rotation about the b axis, or, (c) a combination of (a) and (b). In the "parallel" ($\mathbf{H}_0 \| b$) and "perpendicular" orientations ($\mathbf{H}_0 \perp b$) each of the four different radical orientations are equivalent. Thus, for the parallel and perpendicular orientations we expect proton hyperfine structure due to only three protons, say $H^{(1)}$, $H^{(2)}$, and $H^{(3)}$ in (I). [One does not expect acid proton hyperfine structure from (I)[1,3-5]]. In general, a single proton gives rise to a hyperfine structure of four lines, the intensities of the outer two being the same, and the intensities of the inner two being the same.[1] For three protons the hyperfine structure pattern consists of $4\times4\times4=64$ lines, so that even for the perpendicular and parallel orientations a total of sixty-four hyperfine structure components are possible. One is lead, however, to the observed six and eight strong resonance signals in Figs. 1 and 2 by the following arguments. On the basis of purely theoretical considerations (see Discussion) the methylene π-proton hyperfine interactions should be nearly isotropic. Each of these protons [(2) and (3) in (I)] then contributes only a doublet structure to the hyperfine pattern. The second pair of signals from each proton quartet has negligible intensity for a nearly isotropic hyperfine interaction.[1] Now, consider the hyperfine structure arising from the σ proton. If we assume that this proton is very similar in its strongly anisotropic hyperfine interaction to the σ proton in malonic acid,[1] then at 3300 gauss this proton will give a hyperfine quartet of two strong and two quite weak hyperfine lines at most crystal orientations.[1] It is to be emphasized that the apparent simplicity of this hyperfine structure is a subtle accident. For example at 10 000 gauss the malonic acid radical σ proton can give a hyperfine quartet with all signals of equal intensity.[1] The observed spectra of eight lines are then accounted for in terms of a doublet from each of the three nonequivalent protons in the parallel and perpendicular orientations. Six-line hyperfine spectra occur when the splittings by two protons are the same.

Let the hyperfine splittings by the three protons be u, v, and w. The observed spectra can be interpreted in terms of u, v, and w, and the results are given in Table I for the parallel orientation, and for various perpendicular orientations. Note that $\Omega=0°$ for $\mathbf{H}_0 \| a$, and $\Omega=133.6°$ for $\mathbf{H}_0 \| c$. In the range $\Omega=90-160°$ six-line spectra are observed, that is, $v=w$. Now the question arises, which splitting u, v, w arises from which proton $H^{(1)}$, $H^{(2)}$, $H^{(3)}$? One possibility is immediately suggested by the symmetry of the problem. When $\mathbf{H}_0 \| c(\Omega=133.3°)$ all the methylene protons of the undamaged molecule are probably equivalent. Splittings (v and w) become equal in this range of crystal orientations (cf. Table I). Thus, it is tempting to suggest that

TABLE I. Experimental hyperfine splittings in x-irradiated succinic acid.

Angle Ω	No. of strong lines	Observed splittings u ±2 Mc	v ±2 Mc	w ±2 Mc	Calculated σ−CH proton splitting ±2 Mc
0	8	96.1	78.1	62.6	67.9
10	8	96.5	97.7	58.3	63.6
20	8	96.2	80.9	54.7	60.1
30	8	96.2	82	53.2	58.6
40	8	96.6	82.7	54.1	59
50	8	96.5	83.1	57.3	61.5
60	8	97.6	84.2	63.3	65.6
70	8	97.8	83.5	68.9	70.4
80	8	98.6	83.5	75.3	75.2
90	6	98.8	81.3	81.3	79.6
100	6	99.0	83	83	83.1
110	6	98.4	83	83	85.4
120	6	98.8	83.6	83.6	86.3
130	6	99.3	83.2	83.2	86
133.6	6	98.7	82	82	85.8
140	6	97.7	80.1	80.1	84.2
160	6	98.2	76.2	76.2	77.4
170	8	96.1	78.3	68.3	72.8
$\mathbf{H}_0 \| b$	8	107	83.8	50.7	48.3

the π protons of the radical [$H^{(2)}$ and $H^{(3)}$] give rise to splittings v and w. However, this leaves the third splitting, u, large (96 Mc) and very nearly isotropic. This is not what is expected on the basis of electronic structure theory,[8] and the known anisotropy of the σ-proton hyperfine splitting in the malonic acid radical.[1] We have therefore calculated the expected hyperfine splittings due to a malonic acid σ proton under the assumption that in the succinic acid radical the σ-proton C—H bond bisects the H—C—H angle of the undamaged succinic acid methylene group. The calculated splittings are given in the last column in Table I. It is seen that there is very good agreement between these calculated splittings and the observed splittings w. *The agreement is particularly striking for the parallel orientation.* It therefore appears safe to conclude that the splitting w arises from the σ proton [$H^{(1)}$ in (I)], and that the assumed direction of the σ-proton CH bond is correct. And this close agreement further suggests that there is no major reorientation of the carbon skeleton when the radical is formed from the parent molecule. However, the foregoing assignment of the splitting w to the σ proton forces us to the conclusion that the two methylene π protons $H^{(2)}$ and $H^{(3)}$ in the radical do not have the same orientation and elements of symmetry as they did in the undamaged parent molecule. In fact, the near isotropy of the couplings, and the fact that the apparent anisotropy of u and v is small compared to the difference between u and v, strongly suggests that these protons are chemically distinct; i.e., that the local electronic structure is different at the two protons. This nonequivalence of the methylene π protons could be achieved by a twist of the methylene H—C—H group so that the H—C—H angle is no longer bisected by the

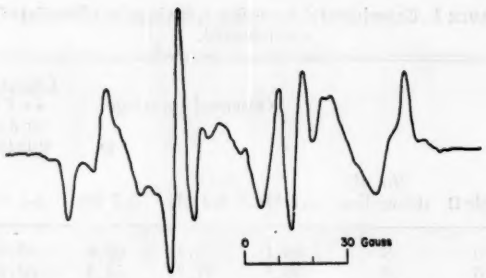

FIG. 3. Paramagnetic resonance of a polycrystalline sample of x-irradiated succinic acid.

molecular plane **P**. However, if this nonequivalence of the π protons is achieved by a twist of the H—C—H group, we must ask: Does the H—C—H group twist "up" or "down" relative to the molecular plane **P**? Since the molecular symmetry plane **P** is not a symmetry plane of the crystal lattice, it is possible that the H—C—H always twists in one direction. Call this alternative (i). With alternative (i) we may say that the simplicity of the observed spectra in the parallel and perpendicular orientations, and the complexity of the observed spectra in other orientations, may be taken as strong evidence for the validity of assertion (B).

However, let alternative (ii) correspond to the situation in which the H—C—H group twists "up" or "down," say, for simplicity, with equal probability. Here assertion (B) would remain valid as far as the point group operations of the crystal were concerned, but all radicals would not be related to one another by the space group symmetry operations of the undamaged lattice. Unfortunately the π-proton hyperfine splittings are so nearly isotropic that we cannot distinguish between alternatives (i) and (ii). If these splittings were more anisotropic there could be additional splittings in the parallel and perpendicular orientations with alternative (ii).

DISCUSSION

In previous work[22] it has been shown that the hyperfine splitting due to a σ proton, a_N, is directly proportional to the π-electron spin density ρ_N on the adjacent carbon atom. These quantities are related through the equation

$$a_N = Q\rho_N \qquad (1)$$

where Q has the semiempirical value of -22.5 gauss. A quite general theoretical derivation of (1) has recently been obtained by McLachlan, Dearman, and Lefebvre.[23] On the basis of this and other theoretical work[11] there is good reason to believe that the isotropic hyperfine interaction b_N due to a π proton is directly proportional to the spin density on the neighboring unsaturated carbon atom

$$b_N = R(\theta)\rho_N. \qquad (2)$$

In (2) it has been explicitly indicated that the constant of proportionality depends on the angle θ of rotation of the alkyl group attached to the unsaturated carbon atom. The angle θ is defined so that $\theta=0$ corresponds to the "eclipsed" orientation of the π-proton C—H bond relative to the π-orbital symmetry axis, and when $\theta=\frac{1}{2}\pi$ this proton lies in the nodal plane of the π-electron spin distribution. Thus, when $\theta=\frac{1}{2}\pi$ the alkyl group proton is a σ proton. Up to the present relatively little quantitative experimental information has been available on the constant of proportionality R. Thus, proton hyperfine splittings due to methyl-substituted aromatic radicals in solutions could give $\langle R\rangle$ if the neighboring π-electron spin densities were known accurately. Here $\langle R\rangle$ represent the average of $R(\theta)$ over "free" rotations of the methyl group. Unfortunately radicals in liquids that are suitable for this determination of $\langle R\rangle$ have not yet been studied.

Hyperfine splittings due to π protons have certainly been observed in the spin resonance of a number of irradiated materials in glassy or polycrystalline materials at low temperatures.[16–18] Unfortunately, the interpretation of such spectra is extremely difficult when σ protons contribute to the hyperfine interactions, since the σ-proton hyperfine interaction is so anisotropic. Also g-factor anisotropy contributes to the difficulty of interpreting these spectra. To exemplify this point we give in Fig. 3 the spin resonance of a polycrystalline sample of x-irradiated β-succinic acid. Since π-proton hyperfine interactions are nearly isotropic (see the following), we may however obtain some information on $\langle R\rangle$ from irradiated polycrystalline materials if they contain no σ protons with significant hyperfine interaction. This is the case for the radical $(CH_3)_2\dot{C}OH$ which shows seven well-resolved hyperfine lines even in a glass at low temperature.[18] Here the observed splittings are 56 Mc and this is probably the best value of $\langle R\rangle$ presently available.

The angular dependence of $R(\theta)$ can be approximated satisfactorily by the equation,

$$R(\theta) = A + B\cos^2\theta. \qquad (3)$$

Theoretical calculations of methyl proton hyperfine interactions[11,12] indicate that when $\theta=\frac{1}{2}\pi$, $R\simeq 0$. Thus, $A=0$ in (3). The foregoing experimental value of $\langle R\rangle$ determines B:

$$\langle R(\theta)\rangle = \tfrac{1}{2}B = 56 \text{ Mc}; \qquad B = 112 \text{ Mc}.$$

For the π protons in the succinic acid radical, we would then expect an isotropic splitting of the order of (112) $(\cos^2 30°) = 84$ Mc if the two protons were oriented in

[22] H. M. McConnell and D. B. Chesnut, J. Chem. Phys. **28**, 107 (1958).
[23] A. D. McLachlan, H. Dearman, and R. Lefebvre (to be published).

exactly the same way that they (probably) are in the undamaged succinic acid molecule. It is clear that a moderate twist of one, or both, of the π-proton CH bonds could account for the observed u and v splittings given in Table I.

Let us now consider the anisotropy that is expected theoretically for π-proton hyperfine interactions. The distribution of spin in the succinic can be represented by a normalized spin density distribution function[24] $\rho(\mathbf{r})$ and this distribution function can be expanded in terms of atomic orbitals centered on the carbon and hydrogen nuclei of the radical:

$$\rho(\mathbf{r}) = \Sigma_{\lambda\mu}\rho_{\lambda\mu}\phi_\mu{}^*\phi_\lambda. \quad (4)$$

The numbers $\rho_{\lambda\mu}$ are the elements of the atomic orbital spin density matrix.[24] The only orbitals we need consider in (4) are $2s$ and $2p$ atomic orbitals centered on carbon, and $1s$ atomic orbitals centered on hydrogen. Irrespective of whether one used valence bond theory[10-12] or molecular orbital theory[9] to calculate the elements $\rho_{\lambda\mu}$, the calculations all give $\rho_{\pi\pi}\sim 1$ where ϕ_π is the p atomic orbital centered on the unsaturated atom that holds "the" odd electron, and all other $\rho_{\lambda\lambda}$ (or $\rho_{\lambda\mu}$) are of the order of magnitude of 0.1—0.01, or less. In particular, the diagonal matrix elelments ρ_{ii} for the spin density centered on the σ and π protons are of the order of 0.05. Under these circumstances one can use previously calculated dipolar interaction integrals[8] to show that all terms in (4)—except terms involving the orbital ϕ_π—make a negligible contribution to the hyperfine interaction. The pure π-electron dipolar hyperfine interaction, arising from $\rho_{\pi\pi}\phi_\pi{}^*\phi_\pi$ in (4), contributes of only $\sim$4 Mc to the π-proton hyperfine interaction. It can be seen that the variation in the splittings u and v are of this order of magnitude. No attempt will be made here to interpret this small anisotropy of the π-electron hyperfine interaction evident in Table I in view of the uncertainty in the orientation of the methylene group in the radical. It may, however, be possible to give an analysis of this type for a similar radical produced in the x-irradiation of adipic acid.[25] This analysis would permit the determination of the sign of the π-proton isotropic hyperfine interaction, which has been predicted to be positive.[11]

Note added in proof. Similar results on γ-irradiated succinic acid have recently been obtained by D. Pooley and D. H. Whiffen (private communication).

ACKNOWLEDGMENT

We are greatly indebted to Dr. Richard Fessenden for helpful discussions and for much assistance with the spin resonance instrumentation.

[24] H. M. McConnell, J. Chem. Phys. 28, 1188 (1958).

[25] H. H. Dearman and H. M. McConnell (unpublished).

Sputtering of Silver by Light Ions with Energies from 2 to 12 kev

FINN GRØNLUND AND WALTER J. MOORE

Chemical Laboratory, Indiana University, Bloomington, Indiana

(Received December 29, 1959)

Electromagnetically analyzed ionic beams from a radio-frequency source were used to study the sputtering yield S (atoms per ion) for light ions normally incident on silver targets at energies from 2 to 12 kev. The yields displayed broad maxima with energy in the range studied. At 5 kev the following values of S were found: H^+, 0.035; D^+, 0.090; H_2^+, 0.077; D_2^+, 0.21; H_3^+, 0.11; D_3^+, 0.33; He^+, 0.48; N^+, 4.0; O^+, 4.4; Ne^+, 5.5. The angular distribution of sputtered silver followed a cosine dependence about the normal to the target surface even when the beam hit the target at oblique incidence.

BETWEEN the high-energy (mev) range of nuclear reactions and the low-energy (ev) range of chemical reactions, lies a region of energy in which the modes of interaction between particles are as yet relatively unexplored. One suitable approach to the interesting physicochemical processes in this region is the study of the sputtering of solids by ionic beams with energies from 100 ev to 100 kev, and the interpretation of the results in terms of solid-state collision theories.

With the development of isotope separators capable of delivering to a target an intense beam of electromagnetically analyzed positive ions, it has become possible to investigate sputtering with a close control of the chemical identities of the interactants. A small isotope separator might yield ion currents of several milliamperes, and a large machine of the Calutron type, currents up to a few tenths of an ampere. Interesting results have already been published by Kistemaker[1] and his co-workers using the Amsterdam isotope separator, and studies have been made by Yonts with the Oak Ridge Calutron.[2] In our laboratory, we utilized[3] a smaller apparatus, especially designed for the study of lighter ions, which yields current densities of about 100 μa cm^{-2}. Results previously reported gave the yields for the ions H^+, H_2^+, and D^+ at energies around 10 kev. To measure sputtering with these light ions, it is essential to use an analyzed ion beam, since heavy ions such as H_3O^+ occur in the unanalyzed output of the source.[4]

In the present paper, we give results for the hydrogen ions, H^+, H_2^+, H_3^+, D^+, D_2^+, and D_3^+, normally incident on silver targets over the range of energies from 2 to 12 kev. Results are also reported for the ions He^+, N^+, O^+, and Ne^+. We describe in this paper a new system for obtaining data on the angular dependence of the ejection of sputtered material.

Sputtering by the ions N^+ and O^+ plays an important part in computations of the energy losses of meteorites.[5] Sputtering by deuterium ions has become of special interest in the problems involved in materials research for the fusion reaction.[6]

EXPERIMENTAL METHODS

The system previously employed[3] has been considerably modified and improved, and its essential features are shown in Fig. 1.

An important change has been the substitution of an einzel lens for the two-element electrostatic lens previously employed to focus the ionic beam. With the new lens, the apparatus can provide a focused beam at energies from 2 to 12 kev. Except for problems of insulation, there should be no difficulty in extending this range to considerably higher energies. Below 2 kv, however, the output of the rf source drops rapidly. In principle it might be possible to extract the ions at high voltages and to decelerate them before they hit the target, but the spreading of the beam due to space charge would complicate such a procedure, and the experimental details have not yet been worked out. In any case, the energy spread of the ions, about 100 ev, would set a lower limit of about 500 ev to the production of essentially monoenergetic beams from this type of source.[7]

With the present system, ion currents at the target of up to 100 μa were obtained, compared to the 30 μa previously used. The usual current densities in the bombarded region were about 100 μa cm^{-2}. The use of a recorder to monitor the beam current considerably increased the accuracy of the determination of the sputtering yield.

The target system was also modified. The new target block was constructed entirely of copper and the target heater was placed outside the vacuum system in a quartz tube that penetrated the block. The collectors could be cooled as before with liquid nitrogen. However, special experiments showed that cooling the collectors had no effect on the measured sputtering yield, and heating the targets to 200° also was without effect.

[1] P. K. Rol, J. M. Fluit, and J. Kistemaker, *Proceedings of Symposium on Isotope Separation, Amsterdam, 1957* (North-Holland Publishing Company, Amsterdam, 1958), p. 657.
[2] O. C. Yonts, C. E. Normand, and D. E. Harrison, J. Appl. Phys., **31**, 447 (1960).
[3] C. D. O'Briain, A. Lindner, and W. J. Moore, J. Chem. Phys. **29**, 3 (1958).
[4] F. Grønlund and W. J. Moore, J. Chem. Phys. **31**, 1132 (1959).
[5] R. M. L. Baker, J. Appl. Phys. **30**, 550 (1959).
[6] J. L. Craston, R. Hancox, A. E. Robson, S. Kaufman, H. T. Miles, A. A. Ware, and J. A. Wesson, Proc. Second Conf. Peaceful Uses Atomic Energy (Geneva, 1958), Paper 15/P/34 (U.K.).
[7] G. Forst, Z. angew. Phys. **10**, 546 (1958).

We still use radioactive targets electroplated on platinum supports. The target was mounted in a Faraday cage, so that the sputtering yields are automatically corrected for emission of secondary electrons. Correction also was made for the loss of sputtered material through the orifice of the cage.

The vacuum system used a mercury diffusion pump with a liquid nitrogen trap. The backing pump was separated from the diffusion pump through a dry-ice trap. The system was constructed of brass with hard-soldered joints. The seals were made with Teflon O rings throughout. The system could be baked out at about 100° and the ultimate vacuum obtainable with the source turned off was below 10^{-7} mm.

With this improved vacuum system, and with the somewhat higher current densities employed, we believe that the possibility of contamination of the targets has been considerably reduced. There was no correlation of the sputtering yields with the ultimate vacuum in the system over a range from 10^{-7} to 2×10^{-6} mm. A special set of runs was made with the ions H_2^+ at current densities from 30 to 220 μa cm^{-2}. There was no significant variation in the sputtering yield with current density. These results provide internal evidence that contamination of the targets by condensation of impurities from the ambient gas was not lowering the observed yields.

As a further test of the possibility of contamination, electron diffraction examinations were made of electropolished aluminum targets bombarded with He^+ or H^+. The original electropolished specimens showed no electron diffraction diagram due to aluminum, but only a diffuse halo due to the thin film of oxide left on the the surface by the polishing procedure. After two hours bombardment, the diffraction pattern of aluminum was clearly revealed. Thus not only did the bombardment remove the thin oxide layer in this case, but also it evidently introduced no other contamination detectable by means of electron diffraction. The apparent passivity conferred upon the aluminum by the bombardment procedure will form the subject of a subsequent research.

In addition to the experiments with hydrogen ions, observations were made with the ions He^+, N^+, O^+, and Ne^+. The rf source proved to be suitable for the production of sufficiently intense beams (5 to 20 μa cm^{-2}) of all these ions. The source was fed with highly purified gases, obtained in Pyrex bulbs from the Air Reduction Company, and admitted through Bayard-Alpert valves. The mass spectrometric analyses in mole percent of the reagent gases, as reported by the supplier, were as follows: neon: He 0.01, N_2 0.002, $CO_2<0.0001$, hydrocarbons<0.003; oxygen: H_2 0.006, N_2 or CO 0.40, $CO_2<0.006$; nitrogen: $H_2<0.005$, O_2 0.0005, hydrocarbons, CO, and $CO_2<0.0002$, $H_2O<0.0005$. When operating on nitrogen and oxygen, about 10 to 20% of the output of the source was in the form of the atomic ions, N^+ or O^+, the remainder being molecular ions. With helium, there was some evidence for the ion He_2^+ at a level less than 2% of the He^+.

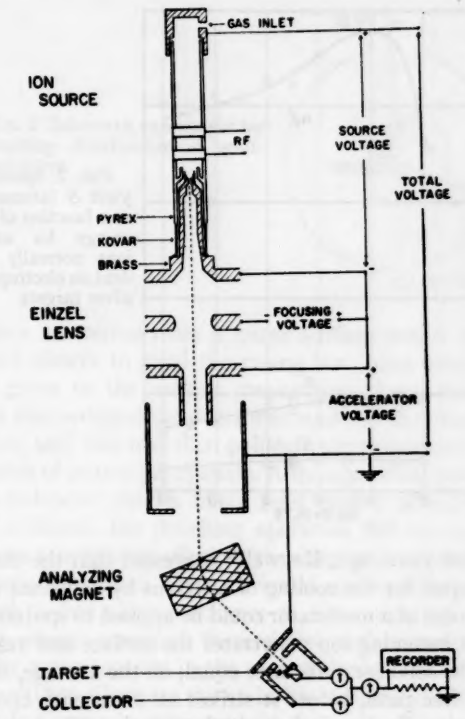

FIG. 1. Apparatus for measurement of sputtering by analyzed ionic beams.

RESULTS

Until quite recently, it was widely accepted that sputtering was due to the formation at the points of ionic impact of localized hot spots from which ordinary evaporation of target atoms occurred. This mechanism was given a fairly quantitative treatment by Townes.[8] According to his equation, the sputtering yield S (atoms of target sputtered per incident ion) should depend on the energy of the ion, but not on the ratio of its mass to that of the target atom. There is now abundant evidence that such simple energy transfer does not suffice to explain sputtering. Besides a definite dependence on the mass ratio, there are the observations that S depends on the angle of ionic incidence. Thus the current theories of sputtering are what might be called *momentum-transfer* or *collision theories*. Apparently Lamar and Compton[9] were the first to suggest that momentum transfer to a surface atom might occur when an ion penetrated the surface, was reflected from a lower layer, and recoiled to strike the surface atom in the outward direction. This model is close to that used in current theories of sputtering, except that most of the recoil particles are now believed to be displaced target atoms.

[8] C. H. Townes, Phys. Rev. **65**, 319 (1944).
[9] E. S. Lamar and K. T. Compton, Science **80**, 541 (1934).

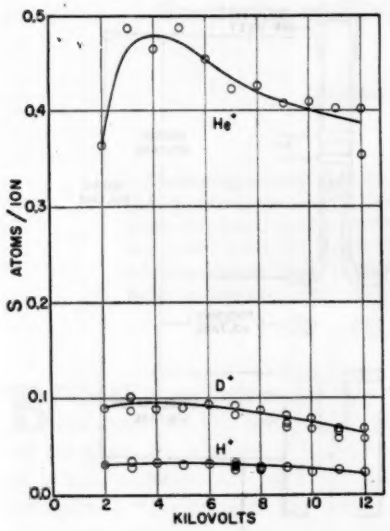

FIG. 2. Sputtering yield S (atoms/ion) as a function of ionic energy for atomic ions normally incident on electroplated silver targets.

A few years ago, Keywell[10] suggested that the theory developed for the cooling of neutrons by collisions with the atoms of a moderator could be applied to sputtering. A fast incoming ion penetrates the surface and travels into the solid for a distance equal, on the average, to its mean free path, before it strikes an atom with enough energy to displace it from its lattice site. The primary displaced atom is not itself sputtered but in its turn collides with neighboring atoms and produces secondary displacements. This branching chain of collisions continues until the displaced atoms have cooled to such an extent that they can no longer cause further displacements. In the meantime, the incoming ion has traveled a further distance into the solid and initiated one or more new primary displacements. The subsequent migrations of the displaced atoms are similar to a diffusion process, or a random walk of mobile atoms. Some of these mobile atoms reach the layer next to the surface, and if they still possess sufficient energy, may collide with surface atoms and drive them from the target.

According to this model, one expects that the sputtering yield S will rise quite rapidly from a certain threshold value as the energy is increased. The initial rise is steep because of the rapid increase in the probability of collisions sufficiently energetic to cause atomic displacements, but this probability levels off at higher energies to an approximately logarithmic dependence on E. However, with increasing energy, the mean free path of the ion in the solid also increases; in other words, the cross section for the collisional interaction decreases with energy. As a result of these two opposite effects of increasing energy, the yield vs energy curve will display a maximum. The maximum may be expected to be quite broad, since the cross section over a considerable region is not very sensitive to the increasing energy; it becomes more so only as the collisions result in a deeper penetration of the electrons shielding the atomic nuclei.

[10] F. Keywell, Phys. Rev. **97**, 1611 (1955).

Figure 2 shows the curves for sputtering yield vs energy for bombardments at normal incidence on silver by the atomic ions H^+, D^+, and He^+. With these light ions, the energy maximum occurs in the range studied, somewhere around 5 kev.

In Fig. 3 results are given for the impacts of the hydrogen molecular ions, H_2^+, H_3^+, D_2^+, and D_3^+, all normally incident on silver. To a first approximation the sputtering yield from any one of these molecular ions is equal to that calculated from its component atomic particles with the assumption that the energy is equally divided. For example, the sputtering by D_3^+ at 9 kev is approximately the same as that from 3 D^+ ions each at 3 kev. This result allows us to make a reasonable estimate of the sputtering by D^+ ions and H^+ ions at energies below the lower limit of 2 kev used in these experiments. For example, we can calculate the sputtering by D^+ ions at 1000 ev to be approximately one-third that observed for D_3^+ ions at 3000 v. Nevertheless, there is a consistent deviation from this sum rule. The values calculated from the sum of the atomic ions always lie somewhat too low at the lower end of our energy scale, and considerably too high at the upper end of our scale, being in exact equivalence only at about 6 kev. It might be suggested that at the lower energies the molecular ions sometimes produce surface sputtering before they have dissociated, and thus provide a greater momentum transfer than would be estimated from the sum of the atoms they contain. Another effect in the same direction would be a consequence of the angular dispersion of the atomic particles on dissociation of the molecular ion at the surface. If the dissociated atoms enter the solid at glancing angles, their distance of penetration will be less and consequently the sputtering yield somewhat higher than for the same atoms entering normally. At present, however, we have no explanation to offer as to why such effects evidently disappear at higher energies and the resultant yield from the molecular ions actually falls below that estimated from the constituent atoms.

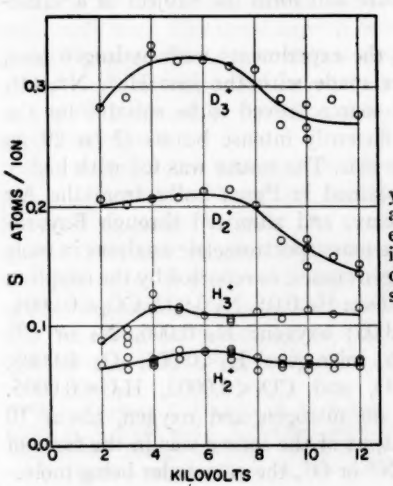

FIG. 3. Sputtering yield S (atoms/ion) as a function of ionic energy for molecular ions normally incident on electroplated silver targets.

Figure 4 shows the yield as a function of the mass of the ion for a series of atomic ions, all normally incident at 5 kev on silver targets. One factor governing the mass dependence is the increased probability of energy transfer to the heavy silver atoms as the mass of the bombarding ion increases. From the laws of the conservation of momentum and of energy applied to an elastic collision between an ion of mass m_1 and a target atom of mass m_2, the maximum energy that can be transferred at impact is found to be $E_m = 4Em_1m_2/(m_1+m_2)^2$. The second important factor is the increase in the collision cross section with increasing nuclear charge of the incoming ion. Thus the cross section varies approximately as the nuclear charge cubed, in the unscreened region, and hence the depth of penetration varies inversely with Z_1^3. The combination of these two factors explains semiquantitatively the dependence of sputtering yield on the mass and nuclear charge of the incoming ion.

ANGULAR DISTRIBUTION

The question of the angular distribution of the sputtered atoms has been investigated with an improved technique. In the previous measurements in our laboratory, the angular distribution of sputtered material was studied after bombardment of silver targets by normally incident ions. This choice of incident angle is the least favorable for distinguishing possible departures from the cosine law, which governs uniform emission from a surface. Therefore, in the present studies, the distribution of sputtered material was measured after ionic bombardment at glancing angles. A special target holder was devised, in which the angle of incidence of the ionic beam could be accurately adjusted and measured. The sputtered material was collected on a copper strip circularly disposed around the target, so that the position of the deposit on the strip corresponded to the angle of sputtering. After the run an autoradiograph was made of the collector strip on ordinary x-ray film, and after development this was scanned by means of a microphotometer. The schematic arrangement of the experiments is shown in Fig. 5.

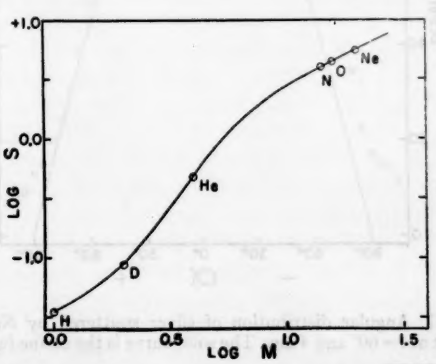

FIG. 4. Sputtering yield S as a function of mass of ion for ions normally incident on electroplated silver targets at 5-kev energy.

FIG. 5. Schematic experiment for measuring distribution of sputtered silver.

Since scattering from a rough surface would be expected always to yield the cosine law, some attention was given to the surface preparation. A particularly thick electrodeposit of silver was made on the platinum holder, and this was then polished electrolytically in a solution of potassium cyanide. Although visual observation indicated that a fairly good degree of polishing was achieved, the polishing operation did not appear to have a significant effect on the angular distribution of sputtered material. Thus we would not have been surprised to find exact obedience to the cosine law in all cases, simply owing to the residual surface roughness.

The typical results in the case of the ion D^+ incident at $\theta = 60°$ on silver are shown in Fig. 6. One notices that there is a general agreement with the cosine distribution, except for a considerable amount of additional sputtering in the forward direction, that is, along the direction parallel to that of specular reflection of the incoming beam. Having confirmed this result with D^+, we next tried the same experiment with the ion Ne^+, anticipating that there would be a much more marked momentum-transfer effect in this case, owing both to the lesser penetration of the Ne^+ ion and to its more effective momentum-transfer factor. The results with Ne^+ are shown in Fig. 7, and appear to follow almost perfectly the cosine distribution about the normal to the surface.

No theory at present exists to predict the angular distribution of sputtered material, but we may expect two factors to be especially important, the roughness of the surface, and the randomization of the atomic displacements as a result of the internal collisions which finally lead to sputtering. The effect of focusing along close-packed lines in solid-state collisions[11] would be averaged out in these microcrystalline targets. It is unlikely that any clear-cut demonstration of persistence of momentum in sputtering can be obtained from the angular distribution until experiments are done on single crystals with surfaces that are more nearly smooth on an atomic scale.

It may be recalled that about 10% of the H^+ or D^+ ions normally incident on silver at 9250 v were reflected from the surface after a 180° collision.[3] If some of these reflected ions were to knock off a silver atom the atoms so removed might account for the enhanced sputtering in the forward direction which is observed in Fig. 6.

[11] R. H. Silsbee, J. Appl. Phys. **28**, 1246 (1957).

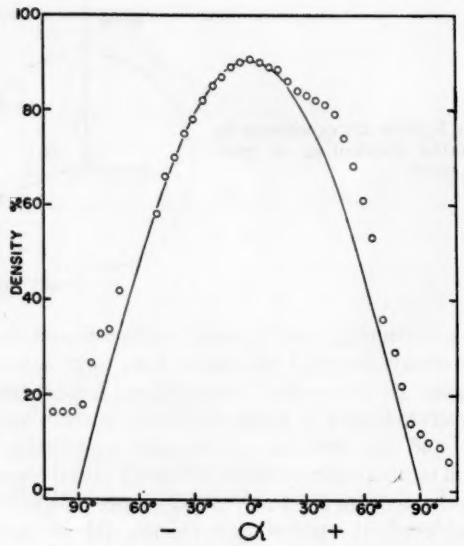

FIG. 6. Angular distribution of silver sputtered by D^+ ions incident at $\theta = 60°$ and 9 kev. The solid curve is the cosine function.

DISCUSSION

A number of advances have been made in the theoretical treatment of the sputtering process during the past several years. In connection with the problem of angular dependence just discussed, the theory of Henschke[12] may be of interest. According to his model, the sputtering occurs entirely as a result of collisions between the impinging ions and the surface atoms of the target. This theory is therefore especially applicable to sputtering near the threshold energy, and it apparently should give a sputtering yield which is markedly dependent on the roughness of the surface

A very general mathematical description of the sputtering process was provided in the theory of Harrison,[13] which, however, is difficult to apply to actual cases because of the number of adjustable parameters that it contains. An analytical theory for sputtering at rather high energies (>20 kev) was given by Goldman and Simon.[14] This was based on Rutherford collisions in the primary displacements of target atoms by incident ions; the subsequent secondary collisions were treated as hard-sphere interactions. It was further assumed that all the displaced atoms originated in a small layer beneath the surface, and adjustment was made for the actual volume distribution of displaced atoms by introducting a correction factor into the mean free path. A Monte Carlo calculation was done[15] with an IBM high-speed calculator to determine the sputtering yield based on the same model as that in the theory of Harrison. At energies of about 200 kev these two calculations agreed quite well, but at 30 kev the Goldman and Simon approximation gave a sputtering yield about twice that of the Monte Carlo calculation. Available experimental data indicate that the analytic approximation is more nearly correct in this instance.

A much simplified mean free path theory has been given by R. S. Pease.[16] He has estimated the range of validity of the various collision models, hard sphere, screened coulombic, and coulombic. For comparison with our present results, it is best to use a screened coulombic interaction for the ions H^+, D^+, and He^+, and a hard-sphere interaction for the heavier ions. In all cases, the collision cross section was assumed to be constant throughout the surface layer. Pease obtained for the sputtering yield the following equation:

$$S = (\bar{E}/4E_d)\{1+[\ln(\bar{E}/E_s)/\ln 2]^{\frac{1}{2}}\}\sigma_p n^{\frac{1}{3}}.$$

This equation contains no adjustable parameters. $\bar{E}$ is the average energy transferred from ion to target atom in collision. E_d is the energy required to displace an atom from its lattice site. This energy can be obtained from studies of radiation damage; for silver, it is about 21 ev. This value may seem surprisingly high, but it has been explained by saying that in the absence of lattice defects an atom displaced from a normal site must surmount a considerable barrier of activation energy before it comes to rest in a relatively stable interstitial site. E_s is the energy necessary to remove an atom from the surface, about 3 ev for silver. The displacement cross section in collisions is σ_p and n is the number of atoms per unit volume.

If we compare the calculated and observed sputtering

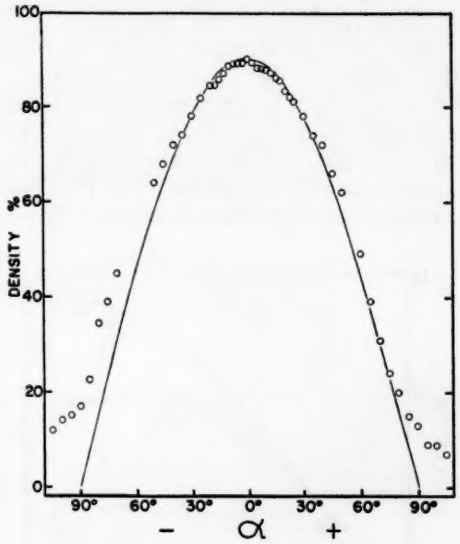

FIG. 7. Angular distribution of silver sputtered by Ne^+ ions incident at $\theta = 60°$ and 4 kev. The solid curve is the cosine function.

[12] E. B. Henschke, Phys. Rev. **156**, 737 (1957).
[13] D. E. Harrison, Phys. Rev. **105**, 1202 (1957); **102**, 1473 (1956).
[14] D. T. Goldman and A. Simon, Phys. Rev. **111**, 383, (1958).
[15] D. T. Goldman, D. E. Harrison, and R. Coveyou, Oak Ridge National Laboratory, Report ORNL-2729 (July 29, 1959).
[16] R. S. Pease, Nuovo Cimento (to be published); Repts. Progr. Phys. **18**, 1 (1955).

yields, using the equation of Pease, for 5-kev ions at normal incidence on silver, we obtain the following results: H^+, S(observed)=0.035, S(calculated)=0.025; D^+, S(obs)=0.090, S(calc)=0.050; He^+, S(obs)=0.48, S(calc)=0.24; N^+, S(obs)=4.00, S(calc)=2.40. The calculated values are consistently about one-half the observed values. The general parallelism between the predictions of Pease and the experimental results seems to indicate that the picture provided by the collision theory is essentially correct. It should therefore be possible to use precise sputtering data to obtain a deeper insight into collisional interactions in solids.

It does not appear to be profitable at the present to seek further refinements in the theoretical calculations for this energy range until the question of the effect of surface asperities on the sputtering rate and the contribution from inelastic collisions can be decided. It would appear that a particularly sensitive test of the theoretical models will be their ability to predict the variation of sputtering yield with incident angle. We have not yet obtained data on this subject, but some preliminary observations by Kistemaker for N^+ ions on copper indicate that the angular dependence will be considerable.

ACKNOWLEDGMENTS

This work was carried out with the support of the National Science Foundation and the U.S. Atomic Energy Commission. William Caldwell was responsible for the construction of specialized instruments and equipment. We wish to thank the Indiana University Electronics Department (George Siddons, Director) for advice and assistance. We are grateful to Dr. Pease for permission to use his theoretical results in advance of publication, and to P. Haymann for the electron diffraction examinations of the bombarded targets.

Kinetics of Unimolecular Decomposition of Excited Alkylamine Ions*

WILLIAM A. CHUPKA AND JOSEPH BERKOWITZ

Argonne National Laboratory, Lemont, Illinois

(Received November 4, 1959)

The unimolecular reaction $RCH_2NH_2^+ \rightarrow R + CH_2NH_2^+$ has been studied for the *n*-alkylamines from ethyl- to *n*-heptylamine inclusive by a mass spectrometric technique. The intensity of the metastable ion produced in the above reaction was measured and used to determine the variation of the specific rate constant with the internal energy of the molecular ion. The results are compared with those predicted by various theories. The agreement of the data with the theories of Kassel and of Rosenstock is bad for the smallest molecules but improves with increasing number of oscillators in the molecule. Earlier evidence for intramolecular vibrational relaxation in the parent molecular ions is discussed in relation to the assumptions of Slater's theory. A simplified application of Slater's theory seems unable to explain all the data.

INTRODUCTION

THE kinetic behavior of a polyatomic molecule which has been given more than enough energy to cause dissociation is of interest to many fields of chemistry. Recently, Wahrhaftig, Eyring, and their associates[1,2] have developed a statistical theory to explain the mass spectra of polyatomic molecules in terms of competing and successive reactions of excited molecular ions. Friedman *et al.*[3] and King and Long[4] have indicated the inadequacy of at least a simplified application of the theory to the calculation of mass spectra of certain molecules. Chupka[5] has shown that many of the assumptions and consequences of the theory may be checked more directly by experiment. Such experiments indicate that the vitally important assumption of energy randomization is valid in some cases but not in others and that even when energy randomization seems to occur, the rate constants calculated by the method of Rosenstock *et al.*[2] are badly in error. The purpose of this experiment was to investigate the dependence on internal energy of the rate constant for dissociation as the number of oscillators in the molecule is varied and to compare the results with theory.

The molecules chosen for this study were the *n*-alkylamines from ethyl- to *n*-heptylamine inclusive. This series of compounds was chosen because the process of dissociation of the parent ion occurring at the lowest energy is free of competing reactions and other complications and because a relatively large amount of information concerning the initial excitation is available.

The photoionization of ethyl- and *n*-propylamine was studied by Hurzeler *et al.*[6] and that of *n*-propylamine by Chupka.[5] The data obtained are shown in Fig. 1. The significance of the first derivative of the ionization efficiency curve is discussed by Hurzeler *et al.* and by Chupka. The ordinate of the derivative curve is proportional to the number of parent ions formed with total energy equal to the value E given by the abscissa. The internal energy of the molecule is given by $E-\mathrm{IP}$ where IP is the ionization potential of the molecule.

The data of Fig. 1 were interpreted by Chupka in the following manner. The sum of parent and fragment derivative curves in the region shown represents the band evelope of the transition to the ground electronic state of the alkylamine ion. This ground electronic state is formed by removal of a nonbonding electron from the nitrogen atom. This results in such a change in bond angles that, by the Frank-Condon principle, most of the vibrational energy represented by the width of the band envelope appears in strong bending vibrations of the two hydrogen atoms attached to the nitrogen atom. When the internal energy reaches a certain value, the following reaction occurs:

$$R-CH_2NH_2^+ \rightarrow R + CH_2NH_2^+.$$

However, this reaction is not instantaneous but rather a unimolecular reaction whose rate constant is an increasing function of the excess internal energy above that just necessary to permit the reaction to occur. When the rate constant is in the range 10^5–10^6 sec^{-1}, "metastable" ions are observed with an intensity which is proportional to the increment of internal energy required to change the rate constant from 10^5 to 10^6 sec^{-1}. The thermal internal energy of the original alkylamine molecule also contributes effectively to the total internal energy of the molecular ion.

Several theories[2,7,8] propose that the specific rate constant k_E for unimolecular decomposition is given

* Work performed under the auspices of the U. S. Atomic Energy Commission.

[1] Wallenstein, Wahrhaftig, Rosenstock, and Eyring, "Chemical reactions in the gas phase connected with ionization," in *Symposium on Radiobiology* (John Wiley & Sons, Inc., New York, 1952).

[2] Rosenstock, Wallenstein, Wahrhaftig, and Eyring, Proc. Natl. Acad. Sci. U. S. **38**, 667 (1952).

[3] L. Friedman, F. A. Long, and M. Wolfsberg, J. Chem. Phys. **27**, 613 (1957); **30**, 1605 (1959).

[4] A. B. King and F. A. Long, J. Chem. Phys. **29**, 374 (1958).

[5] W. A. Chupka, J. Chem. Phys. **30**, 191 (1959).

[6] H. Hurzeler, M. G. Inghram, and J. D. Morrison, J. Chem. Phys. **28**, 76 (1958).

[7] L. S. Kassel, *Kinetics of Homogeneous Gas Reactions* (Chemical Catalog Company, New York, 1932).

[8] N. B. Slater, Proc. Roy. Soc. (London) **A194**, 112 (1948); Trans. Roy. Soc. (London) **A246**, 57 (1953).

by the expression

$$k_E = \nu[(E-\epsilon/E]^{n-1},$$

where E is the total energy less zero-point energy of the molecular ion, ϵ the minimum energy required for the decomposition, and the other symbols have somewhat different significance in the various theories. Rosenstock *et al.* calculate ν, the frequency factor, to be of the order of $10^{14}-10^{15}$ sec^{-1} while Slater's model gives a value of about 3.5×10^{13} sec^{-1} for the simple bond dissociation process studied here. In Kassel's theory ν is an ill-defined quantity which is determined empirically to be in the range 10^{12}–10^{14} sec^{-1}. Rosenstock and Kassel both consider n to be the number of oscillators in the molecule, while Slater considers n to be the number of oscillators which are effective in the dissociation process.

Chupka showed that, if ν was taken to be of the order of 10^{14}, the value of n in Eq. (1) must be about one-fifth the theoretical number of oscillators in order to account for the experimental intensity of the metastable ion from propylamine as shown in Fig. 1.

An obvious direct method of measuring the variation of the rate constant with internal energy would consist of measuring the amount by which ionization efficiency curves shift along the energy axis as the residence time of the ions in the ionization chamber is varied. However, this residence time can be varied easily only by about one order of magnitude and the resulting shift in energy is usually so small that it can be measured with sufficient accuracy only by photoionization techniques. Since a photoionization apparatus was not available, these studies employed electron impact and the more indirect method of using the metastable ion intensity as a measure of the variation of rate constant with internal energy. For exact comparison with theory, what is needed is the area under the normalized derivative curve for the metastable ion.[5] (The *second* derivative must be used in the case of electron impact.) Because of the usual large energy spread of our electron beam and the difficulty of getting accurate second derivatives of the ionization efficiency curves, such a normalized derivative curve was not obtained in this experiment. Rather, it is assumed that the sum of the derivative curves for parent and fragment ions has nearly the same shape (although shifted slightly in energy) for all the *n*-alkalyamines and further that the relative areas under the parent and fragment derivative curves are nearly the same for all cases. As can be seen from Fig. 1, this is the case for ethyl and *n*-propylamine and can also be expected to hold with fair accuracy for other *n*-alkalyamines, since the removal of such a localized electron on the nitrogen atom will be little affected by lengthening the hydrocarbon chain. As long as these assumptions hold, the intensity of the parent ion may be used as a normalizing factor, corrected by comparison of the electron impact data with the photoionization data on *n*-propylamine. This may be done since the ratio of intensities of metastable and parent ions formed by 75-v electrons will be very nearly equal to the ratio of the definite double integrals of the respective derivative curves between the limits of 0 and 75 v. Since these derivative curves have nonzero value for only a short interval at very nearly the same voltage, which is much lower than 75 v, the ratio of the definite double integrals will be very nearly equal to the ratio of the areas under the respective derivative curves. This conclusion is not affected by the fact that the variation of the electron-impact ionization cross section with energy departs from linearity below 75 v, since this departure will be virtually identical for both the parent and metastable ions which result merely from different vibrational levels of the same electronic state. Some error could result if parent ions were formed in excited states above the energy range shown in Fig. 1 and did not dissociate in the ion source because of the inefficiency of radiationless transitions. This possibility is investigated in this experiment. Thus, the normalizing factor used in the foregoing procedure is really the area under the derivative curve for the parent ions rather than the ordinate of the total ion derivative curve in the region of metastable ion formation. However, to the degree that the foregoing assumptions regarding the constancy of the shapes of the derivative curves hold, these two quantities differ by a constant factor, which may be determined by comparison with the photoionization data on *n*-propylamine.

Alternatively one might assume that the cross section for formation of the ground state of the parent ion was

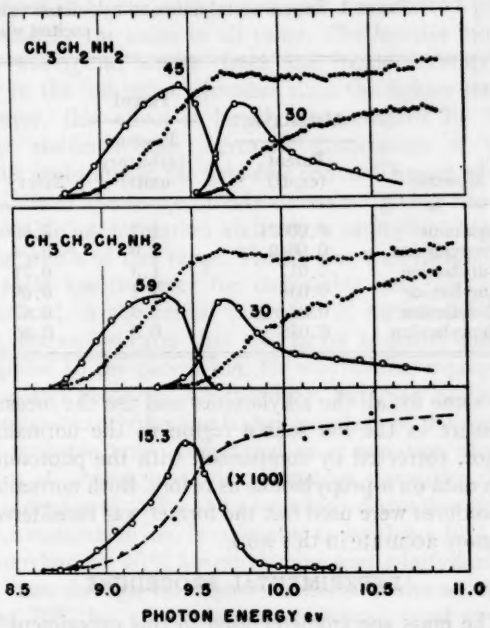

FIG. 1. Photoionization efficiency curves (closed circles) and their first derivatives (open circles and solid lines) for parent and fragment ions of ethylamine ($CH_3CH_2NH_2$) and *n*-propylamine ($CH_3CH_2CH_2NH_2$) and for the metastable ion of *n*-propylamine.

TABLE I. Experimental data and calculated values of the effective number of oscillators for the dissociation of excited *n*-alkylamine molecular ions.

Molecule	Metastable / Parent (exptl)	Parent / Pressure (arbitrary units)	Σ_0(ev)	Theoretical number of oscillators ($3N-6$)	Metastable / Parent (calculated using $n=3N-6$)	Effective number of oscillators	Effective n / Theoretical n
Ethylamine	0.00024	1.2	0.80	24	0.037	4	0.17
n-Propylamine	0.0049	1.0	0.74	33	0.049	7	0.21
n-Butylamine	0.017	1.3	0.71	42	0.060	15	0.36
n-Amylamine	0.038	1.2	0.69	51	0.072	28	0.55
n-Hexylamine	0.034	1.0	0.67	60	0.082	27	0.45
n-Heptylamine	0.038	0.8	0.66	69	0.095	29	0.42

the same for all the alkylamines and use the measured pressure in the ion source region as the normalizing factor, corrected by comparison with the photoionization data on *n*-propylamine as before. Both normalizing procedures were used but the former was considered to be more accurate in this work.

EXPERIMENTAL PROCEDURE

The mass spectrometer used in this experiment is a single-focusing, 60° instrument with a 12-in. radius of curvature. The source and analyzer regions are pumped separately, so that the pressures may differ by as much as a factor of thirty. The detector system consists of an electron multiplier immediately after the final defining slit and a fine wire grid of known transmission just before this slit. Another adjustable slit, which can be opened as much as 4 in. wide, is located immediately before the wire grid.

Some preliminary studies of the shapes of metastable peaks were carried out with the ion beam focused on the final defining slit immediately before the electron multiplier. This focusing arrangement, which is the normal one for this mass spectrometer, permits the use of high resolution while adequate sensitivity is provided by the electron multiplier. However, the relative intensities reported here were all measured with the mass spectrometer adjusted so that the ions were focused at the slit just before the wire grid. Measuring these ion intensities by use of the grid collector obviated any correction for variation in the sensitivity of the electron multiplier. In all cases, metastable ion intensities were measured with the slit before the wire grid opened wide enough to collect at least 95% of the metastable ions. It was possible to do this and still resolve the metastable peaks from other mass peaks since the broadest metastable peaks occurred at apparent masses below mass twelve, where the spectrum is almost devoid of peaks.

The preliminary study of the shapes of metastable peaks frequently indicated that some other diffuse peak of lower intensity overlapped the peak of interest. This was particularly important in the case of *n*-amylamine. In this case, with 75-v electrons, the interfering diffuse peak was roughly one-third as intense as the metastable peak of interest and only a few tenths of a mass unit away. When the electron bombardment voltage was lowered to within a few volts of the appearance potential of the metastable ion, the interfering peak disappeared, and the metastable peak was left with its characteristic nearly symmetrical shape. The intensities of metastable ions were corrected for such extraneous contributions, the correction amounting to less than 10% in most cases.

The measurements of the intensities of parent and metastable ions were made with 75-v electrons and such voltages in the ion source that the parent ions spent roughly 3–5 μsec in the ion source region before entering the field-free region of the analyzer tube, where they spent about 5–8 μsec, depending on the mass of the ion. During the measurements, the pressure of the sample gas in the ion source region was maintained at about 10^{-6} mm as indicated by an ionization gauge calibrated for air. Thus, the actual pressure was probably several times this value. The pressure in the analyzer section was always well below 10^{-7} mm, as indicated by an ionization gauge. These measurements were then repeated with the pressure in the analyzer tube at least doubled. The fact that the ratio of parent to metastable ion intensity remained the same, within experimental error, indicated that collision-induced dissociation made a negligible contribution to the intensity of metastable ions.

RESULTS AND DISCUSSION

The measured ratios of metastable and parent ions are shown in the second column of Table I. In the third column are listed the measured ratios of the parent ion intensities to the pressure in the ionization region of the mass spectrometer. The pressure read from the ionization gauge was corrected for the differing total ionization cross sections by assuming that each CH_2, CH_3, or NH_2 group in the molecule had equal ionization cross sections which were additive.[9] The values in this column have been normalized to unity for *n*-propylamine. Thus the departure from unity for other molecules is a measure of the difference between the two

[9] J. W. Otvos and D. P. Stevenson, J. Am. Chem. Soc. **78**, 546 (1956).

methods of normalizing the metastable ion intensity as mentioned earlier. The pressure normalization is not used since it was felt to be less reliable than that employing the parent ion intensity. In any case, the difference between the two methods is too small to affect the general conclusions reached from the data.

The fourth column lists the values of ϵ for the dissociation being studied. The values for ethylamine and *n*-propylamine are determined from the photoionization data in the manner described previously.[5] The others are estimated from the values for ethylamine and *n*-propylamine and cannot be in error enough to affect significantly the calculations in which they are used, since the dissociation is so similar in all cases.

In the sixth column of Table I are given theoretical values of the ratio of metastable to parent ion intensities calculated in the following manner. Equation (1) is assumed to hold, ν is given the value 10^{14} sec^{-1}, and ϵ is taken from column four of the table. The value of ΔE, the energy increment necessary to change the rate constant from 10^5 to 10^6 sec^{-1}, is then calculated for *n*-propylamine, for the value $n=7$, which was found to give the correct dependence in earlier work.[5] Then ΔE was set equal to a constant times the observed ratio of metastable to parent ion intensities for *n*-propylamine and the constant was evaluated. The calculated ratios given in column six were then obtained by multiplying this constant by the values of ΔE obtained for each alkylamine on the assumption that $n=3N-6$. The calculations were repeated for smaller values of n until agreement with the observed values of column two was obtained. The values of n which gave this agreement are listed in column seven and may be termed the effective number of oscillators. Column eight then gives the ratios of effective to theoretical values of n.

The major errors involved in these measurements are now considered. The assumptions regarding constancy of the relative areas under parent and fragment derivative curves holds well for ethyl- and *n*-propylamine, as seen from Fig. 1. For the higher members of the series, two effects are expected. The energy difference $(E-\epsilon)$ which determines the position at which the parent derivative curve drops and the fragment derivative curve rises will increase with the number of oscillators. However, this increase will be compensated by an increase of similar magnitude in the original thermal energy of the molecule as seen from Table II of reference 5. The assumption that the undissociated parent ions observed were formed in the ground electronic state was checked experimentally by taking ionization efficiency curves for the parent ions. Though detection of a second break in such a curve is quite difficult, there appeared to be some evidence for one. However, this higher energy process was less intense than that involving the formation of the ground state and furthermore seemed to be of roughly similar intensity in all cases. Since the normalization constant was determined by reference to *n*-propylamine, no error would be encountered if higher energy processes contributed proportionately the same in all cases. The heavier molecules will spend longer times and hence decompose more in the ionization chamber than the lighter ones. However, this effect is largely compensated by the longer residence and increased dissociation of the heavier molecules in the field-free region. The net effect is a shift of the range of rate constants giving rise to metastable ion formation and only a negligible change in the width of this range. Finally the transmission of the mass spectrometer for metastable ions must be considered. A theoretical analysis[10] of metastable ion peak shapes indicates that this factor is nearly unity, compared to the parent ion, for ethylamine, *n*-propylamine and probably *n*-butylamine, but may begin to drop significantly for the higher members of the series. The probable error, considered as a deviation of the values of column two from quantities proportional to the correct area under the normalized derivative curve of the metastable ion, is estimated to be about 30% for *n*-propylamine, 40% for ethylamine and *n*-butylamine, and rises through the higher members of the series to about 70% for *n*-heptylamine. However, most of the error should be systematic and should vary monotonically through the series of compounds. Thus the general trends shown by the data should be little affected.

The general trend of the values of the effective number of oscillators is such that the disagreement with the theoretical number diminishes as the number of oscillators in the molecule increases. For the three highest members of the series the effective number of oscillators is approximately one-half the theoretical number. The slight decrease from one-half in going from *n*-amylamine to *n*-heptylamine is quite likely due to the error caused by decreasing transmission of their respective metastable ions. This correction cannot be made very quantitatively at present. Hence it is not certain from these data whether the ratio of the effective to the theoretical number of oscillators levels off at a value of about one-half or continues to approach unity.

There is obviously a certain degree of arbitrariness in the choice of the value of ν, the frequency factor. However, in order to make a significant increase in the calculated effective number of oscillators, the value for ν would have to be made much larger. There is no justification in any of the statistical theories for much larger values of ν than the one chosen, except by recourse to the effects of nonrandomization of energy or, in Slater's theory, formation of the excited molecular ion with a particularly favorable set of amplitudes and phases of the normal vibrational modes. If the value of ν were made smaller, the calculated effective number of oscillators would become still smaller and thus deviate more from the theoretical number.

[10] W. A. Chupka (to be published).

Perhaps the most striking results listed in Table I are the low values of the effective number of oscillators for *n*-propylamine (obtained previously[5]) and ethylamine. In the case of the latter, it can easily be shown that the actual number of oscillators participating in some way in the dissociation process is larger than four (the effective number). This follows from the fact that all or nearly all the original thermal energy of the molecule is available for the dissociation as shown previously (see Fig. 12 of reference 5). If dissociation is to occur, at least one of the participating vibrational modes must involve stretching of the bond to be broken. Also several normal modes which involve bending of the hydrogen atoms of the NH_2 group are excited in the ionization act. More than one such mode must be excited since the bending motion of these hydrogen atoms is not by itself a normal mode and must be a combination of several normal modes of appropriate phases and amplitudes. Even the two stretching modes and the two torsional modes of lowest frequency (an unlikely combination) account for little more than half the thermal energy of the molecule. Thus the low number of oscillators very probably has no direct physical significance in the theories of Kassel and of Rosenstock *et al.*, but must rather be attributed to inadequacies of the approximations used by these workers in obtaining Eq. (1).

In the present case, perhaps one of the more drastic approximations made by Rosenstock *et al.* is their use of integrations over state density functions rather than summations over discrete quantum states. It is probably significant that the calculations of Marcus,[11] in which he used summations for the higher vibrational frequencies and integrals for the lower frequencies, give a much larger value for the rate constant of the reaction $C_3H_8^* \rightarrow C_2H_5 + CH_3$ than would be obtained by the use of Eq. (1). Thus, for $\nu = 10^{14}$, n must be given a value of about 10 (about one-third the theoretical number) in order for the value of the rate constant from Eq. (1) to agree with that calculated by Marcus. It would be of great interest, though very tedious, to apply to the reactions studied here a calculation such as done by Marcus, but with no semiclassical approximations.

Before attempting to compare Slater's theory with the present data, it is necessary to discuss one of the essential differences between it and the theories of Kassel and of Rosenstock *et al.* One of the basic assumptions of the latter theories is that complete intramolecular vibrational relaxation occurs while Slater assumes it to be completely absent. The theories of Slater, Kassel, and Rosenstock *et al.* all give expressions of the form of Eq. (1) for the specific rate constant k_E of an assembly of molecules, each containing total internal energy E. According to Kassel and Rosenstock, all molecules of the assembly have equal *a priori* probabilities of discussion given by k_E. However, according to Slater, each molecule in the assembly has a different, exact lifetime which is completely determined by its vibrational configuration immediately after the last collision, and k_E represents a particular kind of average of these lifetimes. If the assembly of molecules were suddenly isolated from all collisions, according to Kassel and Rosenstock *et al.* they would decompose exponentially while according to Slater they would decompose in a more complicated manner and in fact many would never decompose at all. This is a direct consequence of the different assumptions regarding intramolecular vibrational relaxation.

Earlier work (see Fig. 12 and accompanying discussion in reference 5) indicates strongly that vibrational energy put into specific modes of the molecular ion in the ionization process is indistinguishable in effect from the original random thermal energy of the molecule, and that, within experimental error, all the thermal energy is effective in producing dissociation. Expecially significant is the fact that most of this thermal energy is contained in modes such as torsions and bendings of the carbon-nitrogen skeleton, which would not be most effective, according to Slater, in the process of dissociation. Thus the evidence points strongly to a large degree of intramolecular vibrational relaxation in less than about 10^{-6} sec for at least ethyl- and *n*-propylamine ions with total vibrational energies of about 0.8 ev. Since Slater's assumption of no vibrational relaxation apparently does not hold in this case, the original formulation of the theory cannot be applied.

Two extreme cases are possible in this instance. The rate-controlling process may be either (1) the flow of energy into the effective vibrational modes or (2) the dissociation of a molecular ion containing sufficient energy in the effective vibrational modes. In case (1) the appropriate model is then similar to that of Kassel with one important difference, namely that the criterion of reaction is not the presence of sufficient energy in only *one* vibrational mode but rather in the *several* effective modes in such amounts as to satisfy Slater's condition of reactivity [see Eq. (25) of reference 8(a)]. This change in Kassel's model would result in a larger specific rate constant for a given internal energy and thus is in such a direction as to lower the value of the exponent in Eq. (1) in qualitative agreement with experiment. A more detailed analysis of this case will not be attempted here.

In case (2) vibrational relaxation is complete in a time which is very short compared to dissociation. Hence, such relaxation rather than collision can be considered to be the mechanism for maintaining a vibrational energy distribution and Slater's theory then becomes formally identical with Kassel's and k_E (but not some of the other symbols) of Eq. (1) then has the same meaning as in the theories of Kassel and of Rosenstock *et al.* Slater's theory has the advantage that the

[11] R. A. Marcus, J. Chem. Phys. **20**, 355 (1952).

value of ν is particularly easy to calculate for the simple dissociation studied here. According to Slater, "where dissociation is due to the breaking of an isolated bond between two atoms, ν is equal to the vibration frequency of an imaginary diatomic molecule consisting of these two atoms connected by the same bond force as in the polyatomic molecule." For the carbon-carbon bond rupture considered here, ν is easily calculated to be 3.5×10^{13} sec^{-1}. Use of this value of ν rather than 10^{14} in the calculation of the effective number of oscillators from the experimental data results in very slightly smaller values than those given in Table I. According to Slater's theory, n is the number of normal modes effectively contributing to the coordinate whose stretching leads to dissociation. Thus n is expected to be equal to or less than the total number of normal modes, in agreement with experiment. However the determination of the number of modes which are effective, in Slater's sense, is no simple matter. Slater's theory is properly applicable only to molecules of which the vibrational structure is completely known, and this is not the case with the molecular ions studied here. While on cursory examination there appears to be no simple class or classes of vibrations, such as stretching vibrations or skeletal vibrations, which would explain the experimental number of oscillators, it cannot be said with certainty that Slater's theory, as applied in the foregoing, is inadequate.

In the only careful application of the theory to date, Slater[12] found that, in the isomerization of cyclopropane, all but one of the distinct modes were effective. However, the critical coordinate in this case was a nonbonded CH distance. In the same paper, Slater determined that if the primary process occurred by excessive stretching of a C—C bond, the number of effective oscillators would be three. The latter process is related to the primary process investigated here, and the number of effective oscillators might be expected to be of roughly the same magnitude for ethylamine, and to increase somewhat for the larger molecules. A generous estimate would probably be given by the number of skeletal vibrations (i.e., normal modes of a hypothetical nonlinear molecule made up of the carbon and nitrogen atoms of the actual molecule). Only a fraction of these modes would be very effective but this might be compensated for by some other modes of the actual molecule which might be effective. The number of skeletal modes is $3N-6$ where N is the number of skeletal atoms. Thus, a simple application of Slater's theory might explain the results for ethylamine and propylamine. However, for the larger molecules the effective numbers of oscillators found experimentally are much too large to be explained by Slater's theory in terms of a simple stretching of a C—C bond as the reaction coordinate. The results for the larger molecules are in accord with some results of conventional investigations of quasi-unimolecular reactions[13–16] which indicate that the number of effective oscillators is in the range of one-half to one times the total number of normal modes (less degeneracies). The values of n determined from conventional data are very sensitive to the accuracy of the data and to the method of calculation used. Thus, Rabinowitch and Michel[13] and Powell,[14] using the same experimental data, calculate values of n which differ by a factor of two for the cases of cyclobutane and trioxymethylene. The latter results are further subject to errors arising from certain of Slater's approximations which become worse with higher values of n. Rabinowitch and Michel conclude that the large experimental values of n indicate a more complex reaction coordinate than generally assumed. Such a complex reaction coordinate for a C—C bond scission might involve motions of all atoms attached to the two carbon atoms being split apart. This would result from the fact that in the resulting fragments each of these two carbon atoms would be coplanar, or very nearly so, with the atoms directly attached to it. The reaction coordinate might then consist of stretching of the C—C bond together with movement of the attached atoms to coplanar positions. The process of bond dissociation in the alkylamine ions may be complicated further by the fact that the resulting charged fragment is isoelectronic with ethylene and very probably has the analogous double-bonded structure $H_2C=NH_2^+$ in which all atoms are coplanar. If this double bond is formed as the C—C bond is broken, various motions of the NH_2 group and a shortening of the C—N bond may also be included in the reaction coordinate. Perhaps the most disturbing result of attempting to explain the data in terms of Slater's theory is that the large range of experimental values of n would seem to indicate that the form of the reaction coordinate varies greatly for similar reactions within a homologous series. A careful analysis of vibrational structure and more accurate photoionization studies should be made before such a conclusion could be drawn reliably. If true, such behavior would be difficult to explain.

The hypothesis that the critical coordinate is complex in the sense described above can be supported by the following considerations. The energy of reaction for the dissociation process studied here may be calculated roughly as the difference in energy of one C=C double bond and two C—C single bonds. The approximation is justified since the nitrogen atom with one nonbonding electron removed is isoelectronic with a carbon atom and thus the $CH_2NH_2^+$ fragment is isoelectronic with ethylene. The values of bond energy given by Pitzer[17] yield $\Delta E=2\times80-145=15$ kcal or 0.65 ev which is

[12] N. B. Slater, Proc. Roy. Soc. (London) **A218**, 224 (1953).

[13] B. S. Rabinovitch and K. W. Michel, J. Am. Chem. Soc. **81**, 5065 (1959).

[14] R. E. Powell, J. Chem. Phys. **30**, 724 (1959).

[15] E. Thiele and D. J. Wilson, Can. J. Chem. **37**, 1035 (1959).

[16] E. K. Gill and K. J. Laidler, Proc. Roy. Soc. (London) **A250**, 121 (1959).

[17] K. S. Pitzer, J. Am. Chem. Soc. **70**, 2140 (1948).

in good agreement with the experimental activation energies for ethyl and *n*-propylamine given in Table I. If tetrahedral bond angles were maintained on the average in the dissociation, the activation energy would be expected to be higher by about $2\times0.5=1.0$ ev. This value is obtained by comparison with the data on the positive ions of ammonia and the alkylamines which are isoelectronic with methyl and substituted methyl radicals. These data[5] indicate that the difference in energy between planar and pyramidal configurations is about 0.6 ev. Since the tetrahedral angle (109.3°) is slightly smaller than the angle in NH_3(106.8°), a better estimate for the energy difference is 0.5 ev. While the $CH_2NH_2^+$ ion probably cannot be considered a substituted methyl radical, the difference in energy between the planar and tetrahedral positions of the hydrogen atoms attached to the carbon atom must also be very nearly the same as for RNH_2^+ and NH_3^+. This conclusion follows from the fact that the analogous hydrogen bending frequencies (and thus force constants) for ethylene (Herzberg's[18] $\nu_7=950$ cm^{-1}) and and for NH_3^+ ($\sim$1000 cm^{-1})[5] are very nearly the same. While the foregoing estimates, particularly of ΔE, are not very precise, they are probably accurate enough to provide support for the proposed complex reaction coordinate.

The same argument can be made to support a similar complex reaction coordinate for the general case of C—C or C—X bond scission, where X is a monovalent atom such as H or Cl. Although the data are often unreliable, it is generally accepted that the activation energy for such bond scission is very nearly equal to the bond energy. If the tetrahedral configuration about each carbon atom were preserved in the dissociation, the activation energy would be greater than the bond energy by about 1.0 ev for C—C bond scission and 0.5 ev for C—X bond scission. The proposed complex reaction coordinate would greatly increase the number of effective oscillators and might easily account for the large values obtained experimentally.[13–19]

Since Slater's assumption of the absence of intramolecular vibrational relaxation apparently does not hold under our conditions and with the molecular ions studied here, it is of interest to compare these conditions with those encountered in the more conventional studies of unimolecular decompositions. We conclude here that intramolecular vibrational relaxation is essentially complete in about 10^{-6} sec. The time between collisions will be of this magnitude at a pressure of about 10^{-4} atm for the gases considered here. Since it is by no means certain that every collision results in the transfer of vibrational energy, we may conclude that with the systems studied here intramolecular relaxation would be competitive with collisional relaxation at some pressures above about 10^{-4} atm and would predominate at lower pressures. Since studies[13] of quasi-unimolecular decomposition have been carried out at pressures as low as 10^{-5} atm, we may reasonably expect that there will be at least some cases in which Slater's assumption will be invalid at experimentally accessible pressures. Slater[8] has dicussed this possibility.

The evidence for intramolecular vibrational relaxation cited before applied only to ethyl- and *n*-propylamine molecular ions. The photoionization data on *n*-propanol[5,6] exhibit apparently thermal tails, very similar to those observed for the two alkylamines, at the thresholds of the differential ionization efficiency curves for the fragments, a fact which indicates a large degree of relaxation. Since the fragmentation process of highest energy probably occurred in a time several orders of magnitude less than 10^{-6} sec, appreciable relaxation in such short times is suggested. It may be noted further that the above evidence for vibrational relaxation in less than 10^{-6} sec applies to molecules containing about 0.8 ev of vibrational energy. The activation energies of quasi-unimolecular reactions of molecules of similar complexity which have been studied by conventional techniques are about three times larger than this amount. In these cases the activated molecules have much more closely spaced vibrational levels and the vibrations, being more highly excited, are more anharmonic and thus more strongly coupled. Vibrational relaxation is then expected to be much more efficient (except possibly where restricted by symmetry) than for the alkylamines. These considerations suggest that Slater's assumption may often be invalid over the entire pressure range of conventional experiments.

Relaxation times are expected to vary from molecule to molecule and, in fact, a spectrum of relaxation times would be expected for a complex molecule. More detailed phonionization studies may make it possible to determine for a large number of molecular ions whether relaxation occurs in times as short as 10^{-10} sec. Since there seems to be no reason why such relaxation phenomena should be fundamentally different for molecular ions and neutral molecules, such studies should provide further evidence regarding the validity (or lack thereof) of Slater's assumption.

The mass spectrometric technique, particularly using photoionization, promises to be a powerful new tool for the study of unimolecular decomposition of isolated systems. It has a great advantage in that at the low pressures usually employed there is practically an infinite number of such decompositions amenable to such study while the number of clean unimolecular reactions occurring under more standard conditions is very small. It is capable of yielding information on such details as intramolecular relaxation times. From the study of metastable ion intensities (or, more directly, normalized differential ionization efficiency curves as a

[18] G. Herzberg, *Infrared and Raman Spectra* (D. Van Nostrand Company, Inc., Princeton, New Jersey, 1945).

[19] B. S. Rabinovitch, E. W. Schlag, and K. B. Wiberg, J. Chem. Phys. **28**, 504 (1959).

function of residence time in the ionization chamber), it is possible to determine the variation of the rate constant with internal energy of the molecule. While the systems studied are, of necessity, molecular ions rather than the neutral molecules of interest to most chemical kineticists, the same theory should apply to both. A slight qualification might be added to the latter statement. Because one of the separating fragments is electrically charged in the case of decomposition of a molecular ion, there will be an induced dipole (and sometimes a permanent one also) so the potential energy as a function of the distance of separation will contain an ion-dipole term which is absent in the case of the neutral molecule.This term leads to a slower asymptotic approach of the potential to the dissociation limit and hence to an adverse effect on the applicability of a theory, such as Slater's, that employs the harmonic oscillator approximation up to the point of dissociation. We shall not attempt to determine the seriousness of this factor at present. Another complicating factor which must be considered in many cases is the efficiency of radiationless electronic transitions. Frequently the excitation necessary to produce the desired dissociation appears initially as electronic energy in the ionization process. The rate constant for dissociation will depend greatly on whether dissociation occurs directly from the excited state or whether the system first goes to lower states by radiationless transitions, since both E and ϵ will be quite different in these cases. A further complication is introduced if the system makes radiative transitions with half-lives shorter than 10^{-5} sec. Fortunately, the dissociations of *n*-alkylamines investigated in this experiment have no such complications caused by excited electronic states.

Potential Energy Constants, Rotational Distortion Constants, and Thermodynamic Properties of $H_2C=C=O$ and $D_2C=C=O$

S. SUNDARAM AND FORREST F. CLEVELAND

Spectroscopy Laboratory, Department of Physics, Illinois Institute of Technology, Chicago 16, Illinois*

(Received August 18, 1959)

As a check on the assignments of the fundamentals of ketene ($H_2C=C=O$), a normal coordinate analysis has been carried out and the constants for the general quadratic potential energy function for this molecule have been obtained. Using these constants, the fundamental vibrational wave numbers for the deuteroketene have been calculated, and compared with the observed bands reported for this molecule. The moments of inertia tensor derivatives for the general X_2YXW molecule have been obtained. The rotational distortion constants for $H_2C=C=O$ and $D_2C=C=O$ have been determined. The molar thermodynamic properties—heat content, free energy, entropy, and heat capacity—have been calculated for both molecules for various temperatures from 100° to 1000°K at atmospheric pressure for the rigid-rotor, harmonic-oscillator approximation.

INTRODUCTION

THE Raman spectrum of ketene ($H_2C=C=O$) in the liquid state has been observed by Kopper,[1] and the infrared spectrum of the vapor has been obtained under low resolution by Gershinowitz and Wilson.[2] Halverson and Williams,[3] and Harp and Rasmussen,[4] have studied the infrared spectrum of the vapor under high resolution. Drayton and Thompson[5] have reported the infrared spectrum above 1000 c/cm (cycles/cm), and Bak and Anderson[6] also have investigated the infrared spectrum in the 500–1200 c/cm region. Recently, analysis of the infrared spectrum of ketene and deuteroketene has been made by Arendale and Fletcher.[7]

It may be seen that while there is a general agreement as to the assignments of the fundamentals in the region 1100–3500 c/cm, there is considerable difficulty and therefore differences in the interpretations of the spectrum and the assignments by the various authors, particularly in the region of 500–1100 c/cm. The normal coordinate analyses have been done by Halverson and Williams,[3] and by Arendale and Fletcher.[7] However, in order to provide a check on the assignments of the fundamentals and to obtain better values for the potential energy constants, using also the improved microwave data[8,9] for the molecular parameters, it was felt that a revision of the normal coordinate treatment was necessary. This is therefore one of the aims of the present investigation.

NORMAL COORDINATE TREATMENT

There are 10 internal coordinates which would account for the in-plane and out-of-plane motions of the atoms of the ketene molecule. The orthonormal set of symmetry coordinates used in this investigation is that given by Arendale and Fletcher.[7] The symmetry coordinate used by Halverson and Williams[3] for the symmetrical H—C—H bending mode is not orthogonal to the redundant coordinate,

$$S_0=(\Delta\alpha+\Delta\beta_1+\Delta\beta_2)/3^{\frac{1}{2}}\equiv 0,$$

since α is not independent of β. Using the theory given by Gold *et al.*[10] for the molecules with redundant coordinates, analytical expressions relating the valence force constants **f** to the symmetry force constants **F** have been derived. The elements of the kinetic energy matrices **G** were obtained by the method of the s_{kt} vectors as described by Meister and Cleveland,[11] Ferigle and Meister,[12] and by Wilson *et al.*[13]

In the determination of the potential energy constants, a suitable choice of the matrix elements, corresponding to the bond stretchings, was made after a number of trials. The other elements were then adjusted to give satisfactory agreement between the calculated and observed wave numbers. From these symmetry force constants, the valence force constants have been calculated by using the analytical expressions mentioned earlier.

The quadratic potential energy constants obtained in this investigation are given in Table I. The descriptive

* Publication No. 132.

[1] H. Kopper, Z. physik. Chem. **B34**, 396 (1936).

[2] H. Gershinowitz and E. B. Wilson, Jr., J. Chem. Phys. **5**, 500 (1937).

[3] F. Halverson and V. Z. Williams, J. Chem. Phys. **15**, 552 (1947).

[4] W. R. Harp, Jr., and R. S. Rasmussen, J. Chem. Phys. **15**, 778 (1947).

[5] L. G. Drayton and H. W. Thompson, J. Chem. Soc. **1948**, 1416.

[6] B. Bak and F. A. Anderson, J. Chem. Phys. **22**, 1050 (1954).

[7] W. F. Arendale and W. H. Fletcher, J. Chem. Phys. **26**, 793 (1957).

[8] H. R. Johnson and M. W. P. Strandberg, J. Chem. Phys. **20**, 687 (1952).

[9] B. Bak, E. S. Knudsen, E. Madsen, and J. Rastrup-Anderson, Phys. Rev. **79**, 190 (1950).

[10] R. Gold, J. M. Dowling, and A. G. Meister, J. Mol. Spectroscopy **2**, 9 (1958).

[11] A. G. Meister and F. F. Cleveland, Am. J. Phys. **14**, 13 (1946).

[12] S. M. Ferigle and A. G. Meister, J. Chem. Phys. **19**, 982 (1951).

[13] E. B. Wilson, Jr., J. C. Decius, and P. C. Cross, *Molecular Vibrations* (McGraw-Hill Book Company, Inc., New York, 1955), pp. 58–59.

TABLE I. Potential energy constants for ketene ($H_2C{=}C{=}O$).[a]

Bond stretching and bond-bond interaction constants (md/A)		Bond-angle interaction constants (md/rad)		Angle bending and angle-angle interaction constants (md A/rad²)	
f_o	14.8500	f_o^{hh}	0.0008	f_{hh}	0.2317
f_c	10.0500	f_o^{ch}	−0.0004	f_{ch}	0.2329
f_h	5.2850	f_c^{hh}	0.0024	f_{co}	0.8776
f_o^c	1.3306	f_c^{ch}	−0.0012	f_χ	0.2200
f_o^h	0.0035	f_h^{hh}	0.0866	f_{hh}^{ch}	−0.1158
f_c^h	0.0707	f_h^{ch}	0.0067	f_{ch}^{ch}	−0.1171
f_h^h	0.0400	$f_h^{ch'}$	−0.0933	f_{ch}^{co}	0.0354
		f_h^{co}	0.0707	f_{co}^{χ}	0.2226
		$f_h^{\prime co}$	−0.0707		

[a] All other constants are zero; χ is the angle made by the CH_2 plane with the equilibrium plane of the molecule.

notation used here is the same as that given by Davis *et al.*[14] It may be seen that the C=O stretching constant is 14.85 md/A, which is almost as large as for CO_2. This is to be expected as the C=O distance of 1.16A is considerably shorter than the normal C=O distance. The C=C stretching constant is 10.05 md/A which is also reasonable. The constant for the out-of-plane motion of the CH_2 group is 0.2200 md A/rad² which is very close to the value of 0.23077 md A/rad² for ethylene obtained by Dowling.[15]

Comparing some of the constants obtained in this investigation with those given by Arendale and Fletcher,[7] particularly the stretching constants, one notices the value of 19.5 md/A for the C=O stretching constant given by them seems very large, especially since they have used a larger C=O distance than in the present study. They have obtained a low value of 7.6 md/A for the C=C stretching constant which may perhaps be due to their having assumed a larger C=C distance of 1.35 A. For the out-of-plane motion of the CH_2 group, the value of 0.071 md/A is very low compared to the present value. These differences and others are also due to the differences in the assignments of the fundamentals of ketene.

TABLE II. Calculated and observed wave numbers (in c/cm) for ketene ($H_2C{=}C{=}O$).

Species	Designation	Calc	Obs
a_1	σ_1	2126	2150
	σ_2	1113	1120
	σ_3	3056	3060
	σ_4	1418	1391
b_1	σ_5	3148	3162
	σ_6	950	942
	σ_7	543	545
b_2	σ_8	588	588
	σ_9	916	916

[14] A. Davis, F. F. Cleveland, and A. G. Meister, J. Chem. Phys. **20**, 454 (1952).
[15] J. M. Dowling, J. Chem. Phys. **25**, 284 (1956).

TABLE III. Calculated and observed wave numbers (in c/cm) for deuteroketene ($D_2C{=}C{=}O$).

Species	Designation	Calc	Obs[a]
a_1	σ_1	2079	2117
	σ_2	844	862
	σ_3	2253	2268
	σ_4	1323	(1293)[b]
b_1	σ_5	2349	2375
	σ_6	847	(815)[b]
	σ_7	451	450
b_2	σ_8	585	...
	σ_9	709	712

[a] Reference 7.
[b] The numbers in parentheses are those reported for HDC=C=O (reference 7) but which might well be those of deuteroketene.

Table II lists the wave numbers calculated for the fundamental vibrations of ketene compared with those proposed by Bak and Anderson[6] from the observed bands. It may be seen that the agreement is very satisfactory.

Using the same potential energy constants, the fundamental vibrational wave numbers for deuteroketene have been calculated. These are given in Table III. The bands assigned by Arendale and Fletcher[7] as fundamentals are also included for comparison. There is very good agreement for most of the bands reported by them. The bands at 1229 and 798 c/cm, described by them as fundamentals of $D_2C{=}C{=}O$, might be due to absorption by $HDC{=}C{=}O$, which according to them was inevitable in their sample. Also, some of the bands assigned by them for $HDC{=}C{=}O$ may belong to the $D_2C{=}C{=}O$ molecule. These differences might perhaps be unambiguously settled if further work is done on $D_2C{=}C{=}O$, particularly in the low-frequency region. Also, there still remain some uncertainties in the perpendicular fundamentals of $D_2C{=}C{=}O$ as stated by Arendale and Fletcher.[7]

The very close agreement between the calculated and observed wave numbers together with the very reasonable values of the force constants indicate that the potential energy constants reported here form decidedly an improved set.

TABLE IV. Rotational distortion constants for ketene and deuteroketene in Mc.[a]

Constants	$H_2C{=}C{=}O$	$D_2C{=}C{=}O$
D_J	0.0032	0.0027
D_{JK}	0.2920	0.2015
D_K	21.7848	5.3117
R_5	−0.0882	0.0608
R_6	-2.2080×10^{-6}	-9.7400×10^{-6}
δ_J	0.0002	0.0002

[a] This number of significant figures is not necessary except to have internal consistency in calculations.

TABLE V. Heat content, free energy, entropy, and heat capacity for $H_2C{=}C{=}O$ for the ideal gaseous state at 1 atm pressure.[a]

T(°K)	$(H°-E_0°)/T$	$-(F°-E_0°)/T$	$S°$	$C_p°$
100	7.96	39.06	47.02	8.02
200	8.27	44.64	52.91	9.38
273.16	8.77	47.29	56.06	10.92
298.16	8.97	48.06	57.03	11.46
300	8.99	48.12	57.11	11.49
400	9.87	50.82	60.69	13.46
500	10.76	53.12	63.88	15.09
600	11.59	55.16	66.75	16.43
700	12.37	57.00	69.37	17.55
800	13.08	58.70	71.78	18.51
900	13.73	60.28	74.01	19.34
1000	14.32	61.76	76.08	20.05

[a] The values are in cal deg^{-1} mole^{-1}.

ROTATIONAL DISTORTION CONSTANTS

Having obtained a valid set of potential energy constants, one may proceed to calculate the rotational distortion constants for these asymmetric rotor molecules by use of the first-order perturbation theory given by Kivelson and Wilson.[16] In the case of these molecules of the type X_2YZW, one needs to determine all the moment of inertia tensor derivatives of the form $[J_{\alpha\beta}{}^i]_0$, where α and β may be x, y, or z, based on a center-of-mass principal-axes system. These derivatives with respect to the internal coordinates, and therefore with respect to the symmetry coordinates, were obtained in the present study, assuming arbitrary displacements of the atoms of the molecule. There are 6 distortion constants in the energy expression for the asymmetric rotors. These have been calculated for ketene and deuteroketene, and are listed in Table IV. Although D_J and D_{JK} are of the same order of magnitude as those given by Johnson and Strandberg,[8] no rigorous comparison is possible, since their investigation has been handicapped by the lack of definite assignments for the fundamentals of ketene. The values of D_J and δ_J reported here compare extremely well with the values obtained by Sheridan.[17]

[16] D. Kivelson and E. B. Wilson, Jr., J. Chem. Phys. **20**, 1575 (1952); **21**, 1229 (1953).

[17] J. Sheridan (private communication, July 30, 1959).

TABLE VI. Heat content, free energy, entropy, and heat capacity for $D_2C{=}C{=}O$ for the ideal gaseous state at 1 atm pressure.[a,b]

T(°K)	$(H°-E_0°)/T$	$-(F°-E_0°)/T$	$S°$	$C_p°$
100	7.97	40.15	48.12	8.12
200	8.45	45.79	54.24	10.04
273.16	9.13	48.52	56.65	11.90
298.16	9.39	49.33	58.72	12.50
300	9.41	49.39	58.80	12.54
400	10.46	52.24	62.70	14.59
500	11.46	54.68	66.14	16.24
600	12.37	56.85	69.22	17.61
700	13.20	58.82	72.02	18.77
800	13.96	60.64	74.60	19.75
900	14.65	62.32	76.97	20.57
1000	15.28	63.90	79.18	21.26

[a] The values are in cal deg^{-1} mole^{-1}.

[b] Calculated wave numbers reported in Table IV, reliable to about 2%, were used to obtain the results in this table.

THERMODYNAMIC PROPERTIES

Though Drayton and Thompson[5] have calculated the thermodynamic properties of ketene, it seems desirable to do such a calculation in the present investigation with the revised values of the fundamental vibrational wave numbers and the new molecular structural parameters. Bak and Anderson[6] have calculated only the free energy for ketene for some temperatures. In the present study, the heat content, free energy, entropy, and heat capacity have been calculated for ketene and deuteroketene for temperatures from 100° to 1000°K. These are listed in Tables V and VI, respectively, for the two molecules. For ketene, the observed wave numbers of Table II have been used and for deuteroketene, the calculated wave numbers of Table III have been used.

ACKNOWLEDGMENTS

This work was aided by a grant from the National Science Foundation and the authors are thankful for this assistance. Thanks are due also to Dr. M. G. Krishna Pillai for pointing out a missing factor in the calculations of the rotational distortion constants in time to permit appropriate corrections in the proof.

Enrichment of Nitrogen-15 by Chemical Exchange of NO with Liquid N_2O_3*

E. U. Monse,† W. Spindel,† Lois Nash Kauder,† and T. I. Taylor

Chemistry Department, Columbia University, New York

(Received December 31, 1959)

The characteristics of the two-phase exchange system: $N_2{}^{14}O_3(liq)+N^{15}O(gas)\rightleftarrows N^{14}N^{15}O_3(liq)+N^{14}O(gas)$ have been studied in laboratory exchange columns to evaluate its usefulness for concentrating nitrogen-15. The effective single stage separation factor α has been determined both by direct equilibration of liquid and gas phases, and by measuring the over-all separation in an exchange column as a function of the rate of product withdrawal. The factor α varies from 1.035 ± 0.005 at $-14°C$ to 1.016 ± 0.004 at $+14°C$. The system is complicated by the presence of additional oxides of nitrogen in both phases, and it is not yet possible to evaluate the contributions of each of the individual molecular species to the effective separation factor. The over-all separations achieved at total reflux in a 40-stage bubble plate column corresponded to a maximum plate efficiency of $\backsim 60\%$ at an interstage flow of $\backsim 50$ mM N/min cm². Similarly, the separations obtained in a 95-cm column packed with stainless steel wire helices corresponded to stage heights of 1.1 and 1.2 cm for interstage flows of 23 and 31 mM N/min cm², respectively. A comparison of the present system with the nitric acid-nitric oxide exchange system indicates that approximately equal volumes of column would be required for the same isotope separation task in spite of a considerably lower α for the N_2O_3 system. This is due to the higher rate of exchange as evidenced by lower stage height. The favorable stage height for this process makes it possible to prepare highly concentrated nitrogen-15 in shorter columns than those used for the nitric acid exchange.

INTRODUCTION

UREY and Greiff[1] first suggested the possibility of concentrating nitrogen-15 by exchange of NO and NO_2. That the exchange is rapid was demonstrated by Leifer.[2] The gas phase reaction was used for concentrating nitrogen-15 by chemical exchange in thermal diffusion columns.[3,4] At lower temperatures, a two-phase exchange system results, which may be represented as

$$N_2{}^{14}O_3(liq)+N^{15}O(gas)\rightleftarrows N^{14}N^{15}O_3(liq)+N^{14}O(gas). \quad (1)$$

Preliminary results on the use of this exchange reaction have been reported previously.[5] This paper reports the results of an investigation of the characteristics of this exchange system and a study of those factors that are important in evaluating its use in concentrating nitrogen-15.

EXPERIMENTAL METHOD

Many of the characteristics of an isotope exchange system are conveniently studied in an exchange column by determining the behavior of the system as the operating conditions are varied. The experimental system used for most of the experiments is illustrated schematically in Fig. 1. It is essentially similar to the apparatus used for studying the exchange of N^{15} between NO and HNO_3,[5–9] except for several modifications required because of the low boiling point of the compounds. Since two different exchange columns were used detailed characteristics are not indicated in Fig. 1. One column was a bubble plate type containing 40 actual plates 1.6 cm in diam, spaced 2 cm apart. The other column was of the packed type, 95 cm long by 2.5 cm i.d., filled with Helipak No. 3013 stainless steel helices (Podbielniak, Inc., Chicago, Illinois).

In operation, liquid N_2O_4 in a tank (Allied Chemical Corporation, Hopewell, Virginia, technical grade) is vaporized and fed to the system as gaseous NO_2 through a rotameter type flow meter *F*. At the top of the exchange column, the NO_2 is liquified in a cooled Friedrichs condenser. The liquid then passes through a short (20-cm) column *S* packed with stainless steel helices, where it reacts with an ascending stream of NO to form an equilibrium amount of N_2O_3. From the equilibrating section, the liquid N_2O_3—N_2O_4 mixture flows into a rotatable graduated cylinder *CY* which is used to measure the liquid flow rate; and from there, it flows to the top of the exchange column, *E*. The liquid draining from the column enters the product refluxer *P* through a cooled U tube. In the product refluxer (80 cm long and 5 cm i.d., packed with glass helices), the liquid is warmed to vaporize and dissociate it into NO and NO_2. The NO gas ascends and passes into the exchange column, while the NO_2 reacts with the water in a descending stream of dilute sulfuric acid, and with an ascending stream of SO_2 to form NO according to the following equations:

$$3NO_2+H_2O\rightleftarrows 2HNO_3+NO$$

$$2HNO_3+3SO_2+2H_2O\rightleftarrows 3H_2SO_4+2NO. \quad (2)$$

* Supported in part by a grant from the U. S. Atomic Energy Commission.

† Present address: Rutgers, The State University, Newark, New Jersey.

[1] H. C. Urey and L. J. Greiff J. Am. Chem. Soc. **5**, 321 (1935).

[2] E. Leifer, J. Chem. Phys. **8**, 301 (1940).

[3] T I. Taylor and W. Spindel, J. Chem. Phys. **16**, 635 (1948).

[4] W. Spindel and T. I. Taylor, J. Chem. Phys. **23**, 1318 (1955).

[5] W. Spindel and T. I. Taylor, J. Chem. Phys. **23**, 981 (1955).

[6] W. Spindel and T. I. Taylor, J. Chem. Phys. **24**, 626 (1956).

[7] W. Spindel and T. I. Taylor, Trans. New York Acad. Sci. **19**, 3 (1956).

[8] T. I. Taylor and W. Spindel, *Proceedings International Symposium on Isotope Separation* (North-Holland Publishing Company, Amsterdam, 1958), p. 158.

[9] C. N. Kauder, T. I. Taylor, and W. Spindel, J. Chem. Phys. **31**, 232 (1959).

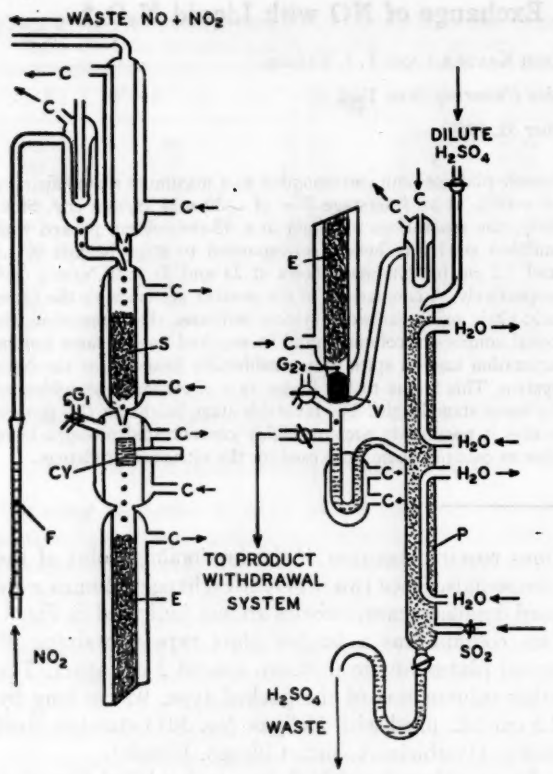

FIG. 1. System for the exchange between N_2O_3 and NO. C=coolant; CV=calibrated cylinder; E=exchange column; F=flowmeter; G_1, G_2=gas sample take-off; P=product refluxer; S=packed section; V=check valve, which was opened by rotating a rod through a ground joint.

Dilute sulfuric acid was used instead of water because the increased acidity speeds up the reflux reaction, as evidenced by a sharper and darker reaction zone.

The system is provided with stopcocks (G_1 and G_2, Fig. 1) to permit sampling of the gas phase at either end of the column for isotopic or chemical analysis. An opening at the bottom of the column permits the withdrawal of enriched product material at a measured rate (see also Fig. 3). The main exchange column, as well as the small packed column and the condensers, are jacketed and maintained at low temperature by circulating a refrigerated coolant. A waste refluxer identical with the unit used to absorb waste nitrogen oxides in the NO—HNO_3 system[5–8] was operated for the present system, but is not shown in Fig. 1. The waste gas from the top of the column is passed through a cooled condenser which removes excess NO_2 and returns it to the column before the gas passes into the waste refluxer.

CHEMICAL COMPOSITION AND MOLAR FLOWS

The system has been described in Eq. (1) as involving the exchange between liquid N_2O_3 and gaseous NO. However, at atmospheric pressure and at operating temperatures from $-13°$ to $+14°$C, a number of other chemical components are formed in appreciable quantities. The liquid contains N_2O_4, N_2O_3, and NO; the gas phase contains N_2O_4, N_2O_3, NO_2, and NO. Figure 2 shows the amounts of the principal components in the two phases (calculated from vapor pressure data of Purcell and Cheesman[10]) as a function of temperature at atmospheric pressure. The abscissa indicates the mole fraction of total nitrogen in the +4 oxidation state, the remainder being the mole fraction of nitrogen in the +2 state. The +4 nitrogen is NO_2, N_2O_4 plus half the number of moles of N_2O_3; the +2 nitrogen is NO plus half the number of moles of N_2O_3.

In order to maintain the liquid interstage flow constant along the length of the column, and to keep the chemical composition of the two phases constant, it is necessary to equilibrate liquid N_2O_4 with NO at the operating temperature before introducing the liquid into the exchange column. It is also important that the gas phase entering the column from the product refluxer contain about the equilibrium amounts in the corresponding oxidation states as shown in Fig. 2. The equilibrium gas phase composition is maintained by suitably adjusting the flow of cooling water and of dilute sulfuric acid into the product refluxer. Cooling the gas leaving the product refluxer to the column temperature condenses excess NO_2 and N_2O_4, and helps to maintain the equilibrium composition. The relative amounts of NO and $NO_2+N_2O_4$ in the gas phase were determined with a Cary spectrophotometer by comparison with standards containing known amounts of the two components.

The liquid interstage flow L (in mM N/min) was obtained in three different ways by direct and indirect determinations:

1. The flow, λ (in ml/min), of the liquid was directly measured by noting the time required to fill the small

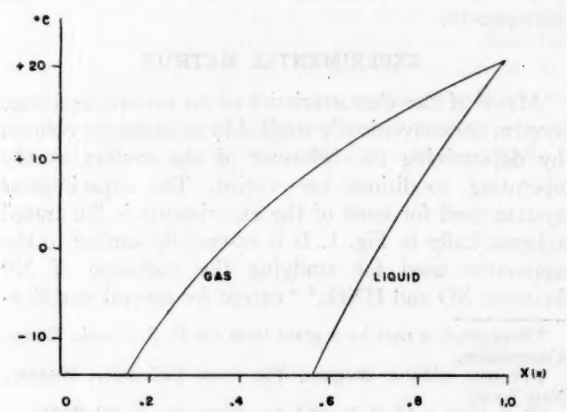

FIG. 2. System NO—$NO_2(N_2O_4)$ at 1 atm pressure. X, x=mole fraction of N in the +4 oxidation state in liquid and gas phase, respectively. The remaining nitrogen, $1-X$ and $1-x$, is the mole fraction of N in the +2 oxidation state in liquid and gas phase, respectively.

[10] R. H. Purcell and G. H. Cheesman, J. Chem. Soc. **1932**, 826.

TABLE I. Comparison of the measurements of the interstage flow L at −9°C.

λ ml/min	L_f mM N/min	$\Delta L_{SO_4^{2-}}$ mM SO_4^{2-}/min	(1) L from λ	(2) L from L_f	(3) L from $\Delta L_{SO_4^{2-}}$	L Av
			mM N/min			
2.36	48	37	87	90	91	90
3.10	60	47	115	112	116	114
3.35	60	51	124	115	125	119

cylinder (3.3±0.1 ml) at the top of the column (CY, Fig. 1). The interstage flow L was then calculated from λ by the relationship

$$L=1000\lambda d/[G_2+X(G_1-G_2)], \qquad (3)$$

where X is the mole fraction of N in the +4 state in the liquid (the remainder $1-X$ being the mole fraction of N in the +2 state), d is the density of the liquid (g/ml), G_1 is the gram-molecular weight of NO_2, and G_2 is the gram-molecular weight of NO.

2. The interstage flow L can also be determined from the N_2O_4 feed flow L_f and the chemical composition of the two phases. The flow L_f was measured with a flow meter (Fig. 1), which was calibrated by determining the weight loss from a vessel of N_2O_4 over a fixed time interval. The interstage flow, feed flow, and chemical compositions are related at total reflux by the equation

$$L=L_f[(1-x)/(X-x)], \qquad (4)$$

where x and X are the mole fractions of N in the +4 state in the gas and liquid phases, respectively. The remaining nitrogen in the two phases, $(1-x)$ or $(1-X)$, is the mole fraction of N in the +2 state.

Equation (4) follows from a consideration of material balance. At steady state and total reflux, the number of moles of $NO_2(N_2O_4)$ reduced to NO, at the bottom of the column per unit time is $(X-x)L$. This is equal to the number of moles of NO leaving the system per unit time, namely, $L_f(1-x)$.

It may be noted that if the column were operated at a considerably lower temperature, the liquid phase would consist essentially of $N_2O_3(X=0.5)$ and the gas phase would be essentially NO ($x=0$). The interstage flow L under these conditions would obviously be twice the feed flow L_f of N_2O_4.

3. Finally, the interstage flow can be determined at total reflux from the number of moles of H_2SO_4 formed in the product refluxer per unit time, during the reduction of NO_2 to NO with SO_2. From the over-all stoichiometry of reactions (2), it may be noted that one mole of H_2SO_4 is produced for each mole of NO_2 reduced to NO.

From the previous consideration of material balance, it follows that

$$L=\Delta L_{SO_4^{2-}}/X-x, \qquad (5)$$

where $\Delta L_{SO_4^{2-}}$ is the number of moles of H_2SO_4 formed in the refluxer per unit time. $\Delta L_{SO_4^{2-}}$ was determined by measuring the molarity and flow rate of the sulfuric acid entering and leaving the product refluxer. The concentration of the waste sulfuric acid was corrected for dissolved SO_2 by titrating with a standard iodine solution.

Intercomparison of the flow rates as measured by the three methods outlined permits an estimate of the constancy of the interstage flow along the column, since method 3 measures the interstage flow at the bottom of the column, while methods 1 and 2 yield values for the flow at the upper end. Several interstage flow measurements are shown in Table I. It may be noted that the values obtained by the three different methods agree within ±4%.

The isotopic analyses were carried out in a single collector Nier-type mass spectrometer.[11] Gas samples were withdrawn at the top and at the bottom of the column (G_1 and G_2 in Fig. 1), and reduced to elemental nitrogen for analysis in the mass spectrometer. Reduction was accomplished by passing the samples through a fused silica tube filled with a mixture of copper and copper oxide at about 750°C. Some of the samples were reduced by an electric arc (7500-v neon sign transformer) in a small discharge tube.[12] The residual nitrogen oxides were frozen out in a trap cooled with liquid nitrogen before introducing the sample into the mass spectrometer. Reduction of gas samples in an electrical discharge tube provided a rapid and convenient means for handling routine samples, since the sampling, reduction, and isotopic analysis were carried out in the same tube without any additional transfer of gas.

EFFECTIVE SINGLE STAGE FACTOR α

The effective single stage factor α was determined both by single stage equilibrations of gas and liquid

[11] A. O. C. Nier, Rev. Sci. Instr. **11**, 212 (1940).
[12] T. I. Taylor (to be published).

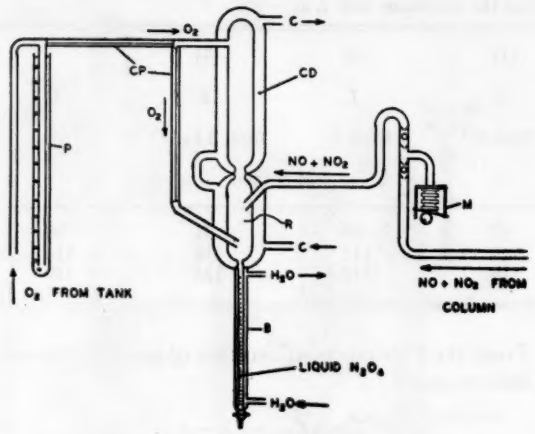

FIG. 3. System for measuring the product rate. B=jacketed burette; C=coolant; CP=capillaries; CD=condenser; M=metering pump; P=pressure regulator; R=reaction vessel.

phase, and by measuring the over-all separation as a function of the product withdrawal rate.

The single stage equilibrations were carried out in a 150-cc reaction vessel, which was jacketed to allow precise temperature control by circulating a refrigerated coolant. Measured volumes of NO were transferred from a gas burette into the vessel at the equilibrium temperature (either $-14°$ or $+10°$C), containing about 0.04 moles of N_2O_4 which was continuously stirred. The absorption of NO was continued until a vapor pressure of 1 atm was reached. The liquid was stirred for at least 24 hr before gaseous and liquid samples were taken for analysis. The NO used in these experiments was prepared by reaction of nitric acid with mercury in the presence of a large excess of sulfuric acid.[13] The NO_2 was obtained by reacting equimolar amounts of this NO with oxygen, freezing with liquid nitrogen, and evacuating to remove the excess oxygen. The effective single stage factor α, defined as the ratio of the concentrations of N^{15} and N^{14} in the liquid, divided by the ratio of N^{15} and N^{14} in the gas phase, was determined by directly measuring the isotopic composition in both phases or by analyzing the gas phase alone, before and after equilibration.[9] The separation factor α is related to the isotopic compositions in the gas before and after equilibrium by the relation:

$$\alpha = a + (m/M)(a-1) \tag{6}$$

where a is the quotient of N^{15}/N^{14} ratios in the gas phase before and after equilibration, m is the number of moles of nitrogen in the gas phase, and M is the number of moles of nitrogen in the liquid. This equation applies when both phases originally have the same isotopic composition.

[13] Friedel, Sharkey, Shultz, and Humbert, Anal. Chem. **25**, 1314 (1953).

The method of determining α from the over-all separation in a column at different product withdrawal rates has been employed by a number of authors.[9,14–16] The theory of isotope separation[17] relates the number n of theoretical plates in a column to the product flow P (in mM N/min), the interstage flow L, the single stage factor α, and the mole fractions, N_0 and N_p, of N^{15} at the feed and product ends of a column by the following equation:

$$n = \frac{1-P/L}{(\alpha-1)+P/L} \times \ln \frac{1}{(N_0/N_P)-[P/L(\alpha-1)](1-N_0/N_P)}. \tag{7}$$

Equation (7) is an approximation of a more general equation, and is valid for $\alpha-1$, N_P and $N_0 \ll 1$.

From Eq. (7) the following relation can be derived:

$$(1/S_0)^{(1+\theta)/(1-p)} = [(1-S_p)/S_p]\theta + (1/S_p), \tag{8}$$

where $S_0=\alpha^n$=over-all separation at total reflux$\cong (N_P/N_0)_{p=0}$, S_p=over-all separation during production $\cong (N_P/N_0)_{p>0}$, $p=P/L$, $\theta=[P/L(\alpha-1)]=p/(\alpha-1)$. The variables S_0, S_p, and p in Eq. (8) are experimentally determined, while θ (and consequently α) can be evaluated graphically by plotting the functions

$$F(\theta) = (1/S_0)^{(1+\theta)/(1-p)}$$

and

$$g(\theta) = [(1-S_p)/S_p]\theta + (1/S_p) \tag{9}$$

for various assumed values of θ and determining the point of intersection of the two curves.

Since it is difficult to keep the interstage flow constant over extended periods of time, it is necessary to measure $S_p=(N_P/N_0)_{p>0}$ for several different product rates p, and determine an average value of α from the intersection of several curves.

In practice, for each flow rate, the column was operated until a steady state separation S_p was obtained at a fixed product rate, then product withdrawal was stopped and operation was continued until a steady state separation S_0 at total reflux was reached.

Enriched product may be withdrawn at measured rates either as liquid or gas. In the present experiments, gas was withdrawn because this appeared to be more convenient. The gas withdrawn consisted of a mixture

[14] Thode, Smith, and Walkling, Can. J. Research **22B**, 127 (1944).

[15] Dostrovsky, Gillis, Llewellyn, and Vromen, J. Chem. Soc. **1952**, 3517.

[16] Begun, Palko, and Brown, J. Phys. Chem. **60**, 48 (1956).

[17] K. Cohen, J. Chem. Phys. **8**, 588 (1940); *The Theory of Isotope Separation* (McGraw-Hill Book Company, Inc., New York, 1951).

of NO, NO_2, N_2O_3, and N_2O_4, and it was necessary to convert this mixture into a well-defined compound, such as N_2O_4, in order to measure the product flow in mM N/min. Figure 3 shows the apparatus used for withdrawing constant quantities of product gases, converting these completely to N_2O_4 and measuring the equivalent amount of N_2O_4 withdrawn (i.e., mM N/unit time). Enriched gas was pumped from the bottom of the column by a microbellows metering pump *M* into a vessel *R* where it reacted with oxygen to form N_2O_4 (and NO_2). Oxygen was admitted to the reaction vessel at constant pressure as required for reaction with NO, and entered from two directions to provide satisfactory mixing. Capillary tubes in the lines prevented back diffusion of N_2O_4 and NO_2 into the oxygen supply. The reaction vessel was kept at a temperature of about −5°C because the rate of the NO-O_2 reaction increases at lower temperatures. The liquid N_2O_4 produced was collected in the jacketed burette shown, and the quantity collected was measured volumetrically. The flow of liquid N_2O_4 was fairly constant, fluctuations being less than ±3%.

TABLE II. Single stage factor α measured by single stage equilibrations.

Temp °C	X[a]	α
−15	0.55	1.034
−14.5	0.55	1.044
−13.5	0.57	1.032
−14.5	0.56	1.028
−14.0	0.55	1.036
−7.0	0.65	1.021
−7.5	0.59	1.029
+8.8	0.82	1.009
+8.8	0.80	1.015

[a] See Fig. 2. X is the mole fraction of nitrogen in the +4 oxidation state in the liquid, the remaining nitrogen $(1-X)$ being the mole fraction of nitrogen in the +2 oxidation state.

RESULTS

The single state separation factor α obtained by two independent methods at various temperatures, and the over-all separation achieved in two different types of laboratory exchange columns at various temperatures and flow rates are summarized in Tables II–VI.

Table II shows the separation factor α obtained by single stage equilibrations. The precision of the separation factor obtained by this method is limited by the mass spectrometric error in measuring isotopic ratios. The magnitude of this error in the present instrument is indicated by the scatter of the measured α at a given temperature, ±0.003–0.005. The mole fractions X in the table were determined from the moles of $NO_2+N_2O_4$ (+4N) and NO (+2N) introduced into the equilibration flask. It may be noted that the measured compositions agree quite well with the values reported by Purcell and Cheesman,[10] as shown in Fig. 2.

TABLE III. Single stage factor α from product withdrawal experiments.

Temp °C	Interstage flow L mM N/min	Product flow P mM N/min	Product rate p (P/L)	Over-all separation S_p	Over-all separation S_0	α
−8.5	90	2.87	0.0319	1.53	1.78	1.030
−8.5	114	2.12	0.0186	1.75	2.01	1.031
−9	119	6.40	0.0539	1.44	1.85	1.031
+14	83	4.70	0.0566	1.19	1.28	1.016
+13.5	72	7.64	0.1062	1.14	1.38	1.016

In Table III, the data from several product withdrawal experiments are listed. The last column shows the single stage factor α as determined from the over-all separation S_0, at zero withdrawal, and the separation S_p, at a given product rate p. All these product withdrawal experiments were carried out using the bubble plate exchange column. The experimental error in α is mainly determined by the fluctuations of the over-all separation at steady state, which was about ±2%. This results in an error of about ±0.005 in α.

The average values of the effective single stage factor α, as determined by both methods, are summarized in Table IV. These values are in fairly good agreement with each other. Their dependence on composition and temperature will be discussed later.

Tables V and VI show the over-all separation S_0, at total reflux in the bubble plate and packed columns at various temperatures and interstage flow rates, and also indicate several column parameters derived from the overall separation. In the experiments with the bubble plate column, a steady state separation was reached within 8–12 hr. The equilibrium time for the packed column, which contained many more separating stages, was between 100 and 150 hr. Figure 4 shows the approach to equilibrium in one of the experiments done with the packed column. The solid curve represents the theoretical time dependence of the over-all separation

TABLE IV. Average effective single stage factor α between about −14° and +14° C.

Temp °C	Composition X[a]	Composition x[a]	Single stage factor α	Method
−14±1	0.57	0.15	1.035±0.005	Single stage equilibration
−9±1	0.61	0.20	1.031±0.005	Product withdrawal experiment
−7±1	0.64	0.24	1.025±0.004	Single stage equilibration
+9±1	0.83	0.68	1.012±0.003	Single stage equilibration
+14±1	0.91	0.74	1.016±0.004	Product withdrawal experiment

[a] X, x mole fraction of nitrogen in the +4 oxidation state in liquid and gas, the remaining nitrogen, $1-X$ or $1-x$, being the mole fraction of nitrogen in the +2 state in liquid and gas, respectively.

TABLE V. Over-all separation S_0 at total reflux in bubble plate column.[a]

Temp °C	Interstage flow L mM N/min	Over-all separation S_0	Plate efficiency %
−13.0	107	1.78	42
−8.5	90	1.78	47
−8.5	114	2.01	57
−9.0	119	1.85	50
−2.0	108	2.10	60[b]
−2.0	158	1.81	47[b]
−2.0	205	1.70	42[b]
+14.0	83	1.28	39
+13.5	72	1.38	50

[a] Number of actual plates, 40; i.d., 1.6 cm.
[b] Minimum values assuming $\alpha=1.031$, since α for this temperature was not determined.

calculated from the following parameters: the over-all separation S_0 at steady state; the single stage factor α; the interstage flow L; and the holdup of enriched material in the column and in the product refluxer.[17] The slow approach to steady state separation is largely caused by the holdup in the product refluxer, which was about 20% of the holdup in the column.

DISCUSSION

Effective Single Stage Factor α

In a system such as the present one, where several exchangeable species are present in the exchanging phases, all of the chemical species in the liquid and gas phases contribute, each according to its quantity and individual molecular structure, to the total exchange, and the effective single stage separation factor α is a weighted average of all the equilibrium constants for exchange.

In the N_2O_3–NO system, there are four different molecular species (N_2O_3, N_2O_4, NO, and NO_2) in the gas phase, and three (N_2O_3, N_2O_4, and NO) in the liquid, allowing for twelve possible independent exchange reactions. For further consideration, we shall neglect the structural difference of one and the same molecule in the liquid and gas phase. This restricts the number of independent exchange reactions to three, for example:

$$N_2{}^{14}O_3+N^{15}O \rightleftarrows N^{14}N^{15}O_3+N^{14}O, \qquad K_{13}, \qquad (10)$$

$$N_2{}^{14}O_4+N^{15}O \rightleftarrows N^{14}N^{15}O_4+N^{14}O, \qquad K_{23}, \qquad (11)$$

$$N^{14}O_2+N^{15}O \rightleftarrows N^{15}O_2+N^{14}O, \qquad K_{43}. \qquad (12)$$

With the further assumption that the concentration of N^{15} is always small compared to the concentration of N^{14}, the effective single stage factor α may be expressed in terms of the individual equilibrium constants in the form

$$\alpha=\frac{M_1K_{13}+M_2K_{23}+M_3}{m_1K_{13}+m_2K_{23}+m_3+m_4K_{43}}. \qquad (13)$$

Here M_i and m_i are the mole fractions of total nitrogen in the species i in the liquid and gas phase, respectively; the subscript 1 refers to N_2O_3, 2 to N_2O_4, 3 to NO, and 4 to NO_2. K_{13}, K_{23}, and K_{43} are the individual equilibrium constants of the exchange reactions (10), (11), and (12), respectively.

Kirshenbaum and co-workers[18] have used a similar mathematical treatment to evaluate individual exchange constants from the effective separation factor in the $NH_4^+-NH_3$ system, but since α has been determined for the present system at only one composition of liquid and gas for each temperature (Table IV), it is not possible to evaluate the three unknown individual equilibrium constants, K_{13}, K_{23}, and K_{43} directly from Eq. (13). Only in those cases where the concentrations of one compound in the liquid and another compound in the gas are much larger than the concentrations of the remaining components, can the equilibrium constant for exchange between those highly concentrated compounds be estimated from the experimental value of α.

Table VII shows the chemical composition of the gas and liquid at 1 atm pressure for three experimental temperatures, as calculated from data on the dissociation of N_2O_3[19] and N_2O_4[20] in the gas phase, together with vapor pressure data of Purcell and Cheesman[10] (see Fig. 2). The composition of the liquid phase is shown in the table consisting either of N_2O_3 and N_2O_4 only ($M_3=0$), or consisting of N_2O_4 and NO only (primed letters M_2', M_3', where $M_1'=0$). The true composition of the liquid will probably be somewhere

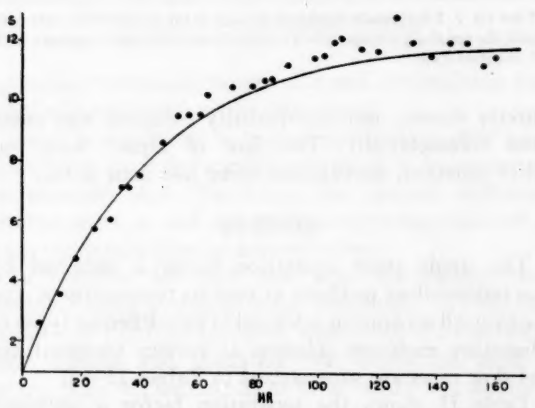

FIG. 4. Typical approach to equilibrium in packed column (see Table VI). ⊙ = experimental point. The solid curve is a theoretical curve calculated from the single stage factor α; the steady state separation S_0; the flow rate L; the holdups H in column and H' in product refluxer; $\alpha=1.031$; $S_0=12.0$; $L=150$ mM of N/min; $H=2.20$ moles of N; $H'=0.41$ moles of N.

[18] Kirshenbaum, Smith, Crowell, Graff, and McKee, J. Chem. Phys. **15**, 440 (1947).
[19] E. Abel and J. Proisl, Z. Elektrochem. **35**, 712 (1929).
[20] M. Bodenstein, Z. physik. Chem. **100**, 75 (1922).

TABLE VI. Over-all separation S_0 at total reflux in packed column at −9°C.[a]

Feed L_f	Flow rate Interstage L	Liquid rate		HETP	Holdup	Average process time per stage
mM N/min		ml/cm² min	Over-all separation	cm	mM/cm	min
60	112	0.62	13.5	1.13	18.6	0.19
80	150	0.83	12.0	1.19	23.1	0.18

[a] 95 cm long by 2.5 cm i.d. (4.9 cm² area) packed with stainless steel helices, Helipak No. 3013, Podbielniak, Inc., Chicago, Illinois.

TABLE VII. Individual equilibrium constants for exchange.

	Gas phase				Liquid phase $N_2O_3+N_2O_4$		Liquid phase N_2O_4+NO		Equilibrium constants K_{13} (max)	K_{23}' (min)	K_{23}
Temp °C	m_1	m_2	m_3	m_4	M_1	M_2	M_2'	M_3'	($M_3=0$)	($M_1'=0$)	calc[a]
−14	0.082	0.100	0.804	0.014	0.870	0.130	0.565	0.435	1.044±0.006	1.072±0.011	1.084
−9	0.104	0.130	0.745	0.021	0.780	0.220	0.610	0.390	1.044±0.008	1.065±0.010	1.082
+14	0.078	0.594	0.222	0.106	0.180	0.820	0.910	0.090	...	1.051±0.016	1.072

[a] From spectroscopic data.

between these two extremes.[21] At −14° and −9°C, the NO in the gas phase (m_3) and the N_2O_3 in the liquid (M_1) (if the liquid is treated as an N_2O_3-N_2O_4 mixture) predominates over other components in the two phases. In this case, the equilibrium constant K_{13} for the exchange between N_2O_3 and NO can be estimated from the experimental data using Eq. (13). This result is shown in the column labeled K_{13} (max) in Table VII. K_{13} is a maximum value because the minimum value of K_{23}, namely, $K_{23}=1.00$, was inserted into Eq. (13). For simplicity, a value of $K_{43}=1.00$ was used here. The value of K_{43} does not influence the result, since NO_2 in the gas phase (m_4) is only about 2% of the total nitrogen at these temperatures. Similarly, K_{23}' (min), as shown in Table VII was calculated (using $K_{13}=1=K_{43}$), whereby the liquid is treated as an N_2O_4-NO mixture.

The magnitudes of K_{23}' are in reasonable agreement with values of K_{23} shown in the last column of Table VII, as calculated from spectroscopic data for N_2O_4.[22]

A similar calculation of K_{13} is not now possible, since the necessary spectroscopic data for the N_2O_3 molecule are still incomplete.[23] The estimated values of K_{13} and K_{23}' may not be compared with each other, since they are based on two different hypothetical compositions of the liquid.

Apart from a better understanding of the liquid composition, further investigations are necessary to evaluate exactly the individual equilibrium constants K_{13} and K_{23} (and K_{43}). This could be done by measuring the effective single stage factor α at a constant temperature, but different compositions, the change in composition being accomplished by varying total pressure of the system.

Rate of Exchange

The results of the experiments with the bubble plate column listed in Table V show a high column efficiency, approaching a value of 60% at −2°C. This magnitude of efficiency is about that usually obtained by distillation of organic compounds in the same type of column. Thus, the high separation efficiency indicates that the rate of phase transfer for the N_2O_3-NO or N_2O_4-NO exchange is probably very high. The same behavior is even more evident in the results obtained with the packed column (Table VI), where over-all separations of 12–13.5 and stage heights of about 1.2 cm were realized at interstage flows of 112–150 mM N/min. Similar experiments with the HNO_3-NO system using 10 M acid in the same column gave a maximum separation of about 7, and a stage height of 2.7–2.8 cm at a lower flow rate of 80 mM N/min. The lower stage height and therefore higher reaction rate of the N_2O_3-NO system may be due to the higher molar density of nitrogen in the liquid N_2O_3-N_2O_4 mixture.

From the theory of isotope separation,[17] one would expect the efficiency to vary inversely with L, the liquid interstage flow. This, however, corresponds to a greater decrease in over-all separation with increasing flow rate than was observed experimentally. In some cases, (Table V), the over-all separation even increased with increasing flow rate. The experimental results may be due to the fact that maximal wetting of

[21] For numerous references see Gmelin, *Handbuch der Anorganishe Chemie* (Verlag Chemie, G.m.b.H., Berlin, 1936), 8th ed., p. 737.

[22] We are indebted to Dr. I. C. Hisatsune of Kansas State College, Manhattan, Kansas, for furnishing us his unpublished set of fundamental vibration frequencies for the N_2O_4 molecule. Details of the calculations of the equilibrium constants are to be published separately.

[23] L. d'Or and P. Tarte, Bull. soc. roy. sci. Liège **22**, 276 (1953).

TABLE VIII. Comparative data on several processes for producing 1 g per day of 99 atom % nitrogen-15; over-all separation, $S=27$ 100.

Process	HNO_3-NO exchange	N_2O_3-NO exchange	NO distillation	NH_4^+-NH_3 exchange
1. Feed material	10*M* HNO_3	Liquid N_2O_4	Liquid NO	60% NH_4NO_3
2. Product reflux material	SO_2	SO_2	Heat energy	NaOH
3. Operating temperature (°C)	25	−9	−161	25
4. Operating pressure (atm)	1	1	0.3	0.24
5. Single stage factor α	1.055	1.031	1.0315	1.023
6. Minimum number of stages n_{min}	191	334	329	449
7. Minimum interstage flow, L_{min} (mM N/min)	228	405	399	546
8. L_{min}/P	4900	8800	8600	12,000
9. Minimum feed flow, L_f (mM N/min)	215	206	399	546
10. Minimum flow of product reflux material	265 mM SO_2/min	166 mM SO_2/min	1.314 kcal/min	546 mM OH^-/min

the plates or packing was not achieved at the lower flow rates.

Comparison of Processes for Concentrating Nitrogen-15

Chemical exchange of N^{15} between NO and HNO_3 has proven to be a particularly efficient and economical process for concentrating nitrogen isotopes because of the favorable single stage factor α, the inexpensive chemicals used for reflux at both ends of the system, and the production of a useful by-product, sulfuric acid, in the product reflux reaction. Since the present N_2O_3-NO exchange process is chemically similar, and utilizes the same product reflux reaction, it seems of interest to compare these two systems. Further, Clusius and Schleich[24] have recently described a very promising new process for separating nitrogen isotopes by the distillation of nitric oxide, and it appears worthwhile to compare the characteristics of this process with the exchange processes.

In Tables VIII and IX, significant comparative data on the several isotope separation processes are summarized. For completeness, available data on the NH_4^+-NH_3 exchange system, developed by Urey and co-workers[25] and extensively used during the past twenty years by others[26–29] for the separation of nitrogen isotopes, have been included in this table. As a basis for comparison, the operating requirements for a plant to produce 1 g per day of 99 atom % N^{15} were calculated for each of the processes. For simplicity, a square cascade, consisting of a single exchange column packed with stainless steel wire helices (Helipak) was assumed. The entire column functions as a rectifier, with no stripping section provided.

The feed materials required and the product reflux reagents for each process are indicated in the row 1 of Table VIII. For the distillation process, heat, which must be supplied to the boiler, is required in the place of a reflux reagent. The minimum number of stages n_{min} and the minimum interstage flows L_{min} were calculated from the experimental single stage factor α for the required product flow P, of 1 g per day of 99 atom % N^{15}, using the following equations:

$$n_{min}=\ln S_0/(\alpha-1), \tag{14}$$

$$L_{min}=\left[\frac{N_P[(\alpha-1)(1-N_0)+1]-N_0}{(\alpha-1)N_0(1-N_0)}\right]P. \tag{15}$$

Here, $S_0=N_P(1-N_0)/(1-N_P)N_0$, where N_P is the mole fraction of N^{15} in the product, i.e., 0.99, and N_0 is the mole fraction in the feed material, 0.00365. Any actual system designed to produce N^{15} at the required rate and product concentration would, of course, need to contain a larger number of stages than n_{min}, and would require an interstage flow greater than L_{min}, but the relative magnitudes of these parameters for the several processes would remain unchanged.

Although Eqs. (14) and (15) indicate that n_{min} and interstage flow L_{min} are directly proportional to $1/(\alpha-1)$, the minimum feed flow L_f and the minimum amount of reflux reagent required are dependent in some cases upon other factors as well. For example, in the N_2O_3-NO system, as indicated in Eq. (4), the feed flow of N_2O_4 in mM N per unit time is considerably less than the interstage flow, and depends on the relative amounts of +4 and +2 nitrogen in the two phases. Similarly, the required molar flow of SO_2 is less

[24] K. Clusius and K. Schleich, Helv. Chim. Acta **42**, 232 (1959). published separately.
[25] Urey, Huffman, Thode, and Fox, J. Chem. Phys. **5**, 856 (1937); H. G. Thode and H. C. Urey, *ibid.* **7**, 34 (1939).
[26] D. W. Stewart, Nucleonics **1**, No. 2, 25 (1947).
[27] E. W. Becker and H. Baumgartel, Z. Naturforch. **1**, 514 (1946).
[28] Sugimoto, Nakane, and Watanabe, Bull. Chem. Soc. Japan **24**, 153 (1951).
[29] Panchenkov, Semiokhin, Reuzaera, Molchanov, and Kalashnikova, Zhur. fiz. khim. **31**, 1352 (1957).

TABLE IX. Further comparison of the exchange systems and nitric oxide distillation for concentrating nitrogen-15.

Process	NO-HNO_3			NO-N_2O_3		NO distillation	
1. Interstage flow per unit area (mM N/cm² min)	17	32	53	23	31	1.89	6.25
2. Liquid flow (ml/cm² min)	1.6	3.0	5.0	0.62	0.83	0.045	0.15
3. HETP (cm)	2.8	4.0	5.8	1.13	1.19	0.49	0.78
4. Minimum length of column (cm)	535	764	1110	378	398	161	256
5. Minimum area of column (cm²)	13	7.1	4.3	18	13	211	64
6. Minimum volume of column (cm³)	7200	5400	4800	6700	5200	34 000	16 000
7. Holdup per stage (mM N)	17	...	...	21	28	...	...
8. Average process time per stage h (min)	0.20	...	...	0.19	0.18	...	...
9. Relative equil. time[a] $t=h/(\alpha-1)^2$ (min)	66	...	...	198	187	...	...

[a] The actual equilibrium time is equal to t times a constant which depends only upon the feed and product concentrations.

than the interstage flow as indicated by Eq. (5), Fig. 2, and Table I. In the HNO_3-NO system, the feed flow of HNO_3 is slightly smaller than the interstage flow because the liquid flowing in the exchange column is saturated with dissolved nitrogen oxides.[9] The number of moles of SO_2 per unit time required for reflux is determined by the feed flow of HNO_3 and the relative amounts of NO_2 and NO in the equilibrium gas phase. Thus, it may be noted that although the separation factor is considerably smaller for the N_2O_3 system than for the HNO_3 system, only 63% as much SO_2 is required for reflux.

For the nitric oxide distillation system, where no reflux chemicals are used, the minimum number of calories for the required boil-up rate are indicated in row 10 of Table VIII. London[30] has shown that power consumption for distillation processes can be kept very small by vapor recompression. This technique could considerably reduce the power required for the nitric oxide reflux. The NH_4^+-NH_3 system, which has the smallest separation factor, requires the largest number of stages, and the highest material flow rates.

The size of a column or cascade, i.e., its length area, and volume, needed to accomplish a given task of isotope separation, is determined by the stage heights observed at particular interstage flows per unit area, as well as by the α for the process. As indicated before, the magnitude of α establishes only the number of stages and the interstage flow for a given production rate. In Table IX, the experimental values for the height equivalent to a theoretical plate (HETP) at various flows per unit area are listed for the HNO_3, N_2O_3, and NO distillation systems. All of these HETP values have been measured in similar columns packed with stainless steel wire helices. Unfortunately, data on stage heights for the NH_4^+ system using this type of packing are not available to us, and so this system has been omitted from the comparison in Table IX. As indicated earlier, because of the higher rate of exchange, the stage height, for the N_2O_3 system, at a comparable flow rate, is considerably smaller than in the HNO_3 system. For NO distillation, the HETP is less than that observed in the N_2O_3 system, but the NO flow per unit area, as calculated from the applied power for reflux[31] is considerably smaller. At comparable flow rates of about 30 mM N/min cm², the HETP for the N_2O_3 system is only 1/3 of the value for the HNO_3 system.

In calculating the minimum cascade size (length and cross-sectional area of column) to produce 1 g/day of 99% nitrogen-15, we have used experimental values of HETP and flow per unit area. It may be noted that for each process the length of column required increases as the flow per unit area (and hence the HETP) is increased, but the volume of the column needed is smallest at the highest flow rate listed. It is difficult to compare the processes directly as to sizes of columns required, since the variations of HETP with flow per unit area is known only for a relatively narrow range for each process. Further, the flow rate observed for the NO distillation process is lower than that measured for the other two systems. At a flow rate of about 30 mM N/min cm², where comparable data exist for HNO_3 and N_2O_3, it may be noted that although the N_2O_3 system requires about twice as large a cross-sectional area as the HNO_3 system, the required column length is only about half as great. The actual minimum square cascade volume is slightly smaller for the N_2O_3 process, 5200 cm³, as opposed to 5400 cm³ for HNO_3. Although the minimum cascade volume for NO distillation (Table IX, line 6) is much larger than for the exchange processes, it should be emphasized that these values were calculated from data at lower flow rates. It may be expected that the volume will approach that for the exchange systems at higher flows per unit area.

The equilibrium time for a cascade can be estimated from the average process time per stage by the relation-

[30] H. London in reference 8, p. 319.

[31] K. Clusius and M. Vecchi, Helv. Chim. Acta (to be published).

ship $t=K\cdot h/(\alpha-1)^2$, where the constant K depends only on mole fractions of the product and feed materials,[17] and h, the process time, is the ratio of holdup (moles/stage) to interstage flow (moles/unit time). The relative equilibrium times, $h/(\alpha-1)^2$, for the HNO_3 and N_2O_3 processes are shown in row 9 of Table IX. The N_2O_3 process takes about 3 times longer to reach steady state. Actual equilibrium times are not shown for these cascades, because naturally, a much faster approach to equilibrium would be achieved in a tapered cascade.[17] As stated earlier, the square cascade was used as a basis of comparison, only because of its simplicity. The relative magnitudes of the parameters for the various processes would not change in other types of cascades.

The N_2O_3-NO process has some advantages as compared to the HNO_3 process in spite of an appreciably smaller α. About equal column volumes are required for the two processes, but a shorter column can be used with N_2O_3. About equal quantities of feed material are required for the two processes, but a smaller amount of SO_2 is needed for reflux in the N_2O_3 system. The longer time required to attain steady state and the power costs for refrigerating the liquid N_2O_3 column to a temperature of 0°C or lower are disadvantageous as compared to the HNO_3 system. Any conclusions regarding the NO distillation process for concentrating nitrogen-15 must await further data on the efficiency of this process at higher flow rates and pressures. Certainly, the possibility of simultaneously concentrating oxygen and nitrogen isotopes by NO distillation is a very attractive one. It is possible also to use the waste stream of NO from the NO-HNO_3, or the NO-N_2O_3 process to concentrate oxygen-18 by a chemical exchange process.[32]

Since the HETP for N_2O_3 exchange is so favorable, a relatively short, tapered cascade for producing 99% N^{15} appears feasible. Two packed columns, each about 250 cm long, operating at interstage flows between 20 and 30 mM/min cm^2 should provide the required number of stages.

ACKNOWLEDGMENTS

The authors gratefully acknowledge the assistance of Heiko H. Ohlenbusch and Burhan Hakioglu with the operation of the columns and the help of Vincent G. Saltamach with the mass spectrometric analyses. The exchange columns and reflux systems were constructed by Karl Schumann.

[32] T. I. Taylor and J. C. Clarke, J. Chem. Phys. **31**, 277 (1959).

Letters to the Editor

THE Letters to the Editor section is subdivided into three parts entitled Communications, Comments and Errata, and Notes. These three sections are all subject to the same limitations on length. The textual material of each Letter is limited to a number of words equal to 950 minus the following: (a) 200 words for each average-sized figure; (b) 50 words for each displayed equation; (c) 7 words for each line of table including headings and horizontal rulings. No proof will be sent to the authors of "Communications" and "Comments and Errata." Proof will be sent to the authors of "Notes." The publication charge for Letters is $30 per page, with a minimum of $30 per Letter. If honored, the Institution will be entitled to 100 reprints without covers. See issues of May–September, 1957, for descriptions of categories.

Communications

Tracer Experiments on the Reaction of UH_3 with Aqueous Acid

UMESH AGARWALA, J. B. HUNT, AND H. TAUBE

George Herbert Jones Laboratory, University of Chicago
Chicago, Illinois

(Received March 11, 1960)

SALTLIKE hydrides such as NaH react in H_2O so that in each molecule of hydrogen which forms, one atom is derived from the hydride and one from the solvent. The equation for the reaction in the tracer experiment which provides the basis for this conclusion may be represented as

$$CH+DA=HD+C^+ +A^-.$$

It seemed of interest to learn whether a similar mechanism operates when a metallike hydride such as UH_3 reacts in an acid solution. Interest in these experiments derives also from the consideration that the results obtained from them may be relevant to the mechanism of oxidation in water of certain metals which appear to involve hydride formation in the course of the reaction.[1,2]

The reaction of UH_3 in solutions of ordinary acidity is quite slow. One of our experiments was done using very concentrated DCl in D_2O, ca 16M. When this solution is added to UH_3, there is an initial violent reaction, in the course of which much gas is formed, and a red solution is produced. This phase is followed by a much slower reaction, resulting in the formation of more gas and the transformation of the red solution, which presumably contains U^{+++}, to green-olive, a color characteristic of U^{4+}. The gas formed in the initial phase of the reaction (this comprised ca 80% of the total) was collected separately from that formed later, and both samples were analyzed for the relative amounts of H_2, HD, and D_2. These were found to be 0.11:1:0.20 and 0.26:1:0.44 for the two fractions, respectively. Substantially all of the hydrogen in the UH_3 appears in the gas, and it appears largely as HD. The increase in the relative amount of D_2 in the second sample compared to the first can be attributed to the reaction

$$U^{3+}+H^+=U^{4+}+\tfrac{1}{2}H_2$$

which takes place largely in the second stage.

When the acidity of the reaction medium is lowered only slightly, the course of the reaction is dramatically altered. With the DCl concentration at 11M, at no stage is the reaction violent, and a slow evolution of gas continues over a period of weeks. The reaction leaves as products U^{4+} in solution, and a residue of material which has been reported by others who have studied the dissolution of UH_3 in acid to have a composition approximating U_3O_4.[3] In our experiment, gas was collected after 5 days, then after 3 more days, and finally after 13 more, at the end of which time gas evolution had practically ceased. The bulk of the gas (ca 90%) is contained in the first two samples. For the first sample the relative abundances of H_2:HD:D_2 were found to be 9.6:1:9.0, and for the second, the relative abundance of HD was increased perhaps 5%. For the third sample, the relative abundances of H_2:HD:D_2 were observed as 3.6:1:2.6.

The striking result is that at low acid, very little mixing of the isotopes occurs, and again, the delivery of the hydrogen from the solid to the gas phase is substantially complete. We attribute the course of the reaction at low acid to the formation and maintenance of an oxide film, which prevents direct attack of D^+ on UH_3. Marker experiments[4] on the oxidation of U by O_2 have shown that in this system, film growth takes place at the metal-oxide rather than at the oxide-gas interface. If in our system also O^{--} rather than the metal cation is the diffusing species, we must consider as the complementary processes D^+ moving in the same direction or electrons moving in the opposite direction. It seems quite reasonable that the electron mobility in the (black) oxide formed will be greater than that of D^+. Thus, D^+ is discharged as D_2 at the oxide-water interface, and, as uranium cations are transferred from the metal to the oxide phase, H_2 is formed. We infer that in the more acidic solutions, at least during the major part of the reaction, the oxide film does not develop, and D^+ attacks the metal hydride directly. Consistent with this view is the fact that in the more acidic solution, a much smaller fraction of the uranium is left as the inert oxide.

It is surprising that even for a metallike hydride, the reaction with acid takes place with so little exchange of hydride-hydrogen with solvent. Thus, when the oxide

film is prevented from developing, attack of D^+ must be specifically at sites on the surface occupied by hydrogen. There is no evidence from these experiments for the formation of a film of atomic hydrogen, which would of necessity lead to much mixing of the forms of hydrogen, even if not to exchange with solvent.

The water used in these experiments contained at least 99.5% D_2O. DCl was prepared by the reaction of D_2O with PCl_3. The sample of UH_3 was prepared by H. Flotow and supplied through courtesy of B. Abraham of the Argonne National Laboratory. We are happy to acknowledge their cooperation, the cooperation of Dr. H. S. Anker in making available to us the use of the mass spectrometer, and the assistance of the Office of Naval Research in providing financial support for this investigation.

[1] J. Draley and W. E. Ruther, J. Electrochem. Soc. **104**, 329 (1957).
[2] H. W. Salzberg, J. Electrochem. Soc. **100**, 146 (1953).
[3] R. C. Young, J. Inorg. & Nuclear Chem. **7**, 418 (1958).
[4] J. G. Schnizlein, J. D. Woods, J. D. Bingle, and R. C. Vogel, experiments done at Argonne National Laboratory, to be published in J. Electrochem. Soc.

A New Phototropic Substance and Its ESR

TARŌ HAYASHI AND KŌKO MAEDA
Ochanoizu University, Ootsuka, Bunkyo-ku, Tokyo
AND
SHŌJI SHIDA AND KAZUO NAKADA
Tokyo Institute of Technology, Ookayama, Meguro-ku, Tokyo

(Received March 7, 1960)

ALTHOUGH a considerable number of organic substances which exhibit phototropy in solid and in solution are known, the mechanisms of only a few have been clarified. Especially in phototropic solids, the reversible changes of colors of which is usually assumed to be due to the formation of free radicals or triplet states, the paramagnetism characteristic of these states has been demonstrated only for tetrachloro-α-ketonaphthalene by susceptibility measurement.[1] Gutowsky *et al.*[2] investigated several phototropic solids by the ESR method, but failed to detect any absorption except for a sidonone derivative; and even for this compound it is doubtful whether the absorption detected is really due to the phototropic species itself. Recently Hayashi and Maeda[3] found, in the course of investigation of chemiluminescence appearing in oxidation of lophine (2, 4, 5-triphenylimidazole) with potassium ferricyanide, a new phototropic substance [mp 198–201°C, a light lemon-yellow prism (recrystallized from ethanol)], which is considered to be the oxidation product of lophine. The molecular weight is determined to be ca 300 by the cryoscopic method and does not change under the irradiation of ultraviolet light. This compound is soluble in ordinary organic solvents, giving colorless or pale yellow solutions. The ultraviolet absorption spectrum in ethanol has a λ_{max} at 265 mμ. The empirical formula of this compound is $C_{21}H_{15}N_2$ (found: C 85.20, H 5.50, N 9.41. $C_{21}H_{15}N_2$ requires C 85.38, H 5.11, N 9.49), but the chemical structure has not yet been established.

This substance shows a marked phototropy; on irradiation with sunlight or a quartz mercury lamp, both in air and *in vacuo* at room temperature, the color changes rapidly into reddish purple. On irradiation, the absorption spectrum of benzene solution, for example, gives rise to two new absorption bands of λ_{max} at 350 and 550 mμ, while the ultraviolet absorption mentioned above weakens. On shutting off the light the color fades to recover the original one in about one day in the case of solids, and fades rapidly in benzene or dioxane solutions even at room temperature. This reversible phenomenon can be observed repeatedly, especially in nitrogen atmosphere or *in vacuo*.

ESR absorption was measured on the first derivative curve recorded by an instrument of Japan Electron Optics Laboratory of the JEP-1 type (9420 Mc) and detected for solutions as well as for the solid state, irrespectively in air or *in vacuo*, its intensity being far stronger in solution than in solid. The pattern has a single peak with no structure with the width of 7.5 gauss and a *g* factor of 2.003 close to that of DPPH. The spin concentration observed for the benzene solution (0.1%) was about 10^{18} spin/cc immediately after irradiation by direct sunrays.

In addition to phototropy this compound also shows thermochromism at temperatures higher than room temperature. After taking this into account the rate of phototropic decay reaction in solution is expressed by the first-order kinetics, the half-life period being a few minutes at room temperature (25°C), as measured by visible absorption spectrophotometry and ESR experiments. Measurements of the rate of decay in benzene solution at several temperatures between 15° and 60°C gives 14 kcal/mole as the activation energy of the reaction. The ΔH of the reaction is determined to be −5 kcal/mole from thermochromic coloration and ESR absorption of benzene solutions in equilibrium state at each temperature.

This seems to be the first case of a phototropic compound for which ESR has been detected in solution and/or in crystalline state. Thanks are due to Dr. S. Sato and Dr. H. Yamazaki for their spectrophotometric measurements.

[1] F. Dörr and F. Engelmann, Naturwissenschaften **39**, 397 (1952).
[2] H. S. Gutowsky, R. L. Rutlage, and I. M. Hunsberger, J. Chem. Phys. **29**, 1183 (1958).
[3] The preparation of the new phototropic substance from lophine will be shortly published in Bull. Chem. Soc. Japan.

Comments and Errata

On the Structure of Trimethylamine-Trimethylboron

S. GELLER

Bell Telephone Laboratories, Inc., Murray Hill, New Jersey

(Received December 1, 1959)

RECENTLY, Lide *et al.*[1] reported on the microwave absorption in $(H_3C)_3N$–$B(CH_3)_3$, the trimethylamine-trimethylboron addition complex. They found a value of $B_0=1573.7\pm3$ Mc from which the moment of inertia, $I_B=321.2\pm0.6$ amu A^2 is obtained. Lide *et al.* assume certain distances and angles in this molecule and then conclude that B—N distance lies between 1.70 and 1.95 A.

To date, seven accurately determined molecular structures have been reported (Table I) in which boron is bonded to four atoms at least one of which is nitrogen. The limits of B—N distance in these compounds are 1.53−1.635 A. The longest of these distances occurs in $H_3CC{\equiv}N{-}BF_3$ which is virtually completely dissociated in the vapor state at 50°C.[2] An electron diffraction investigation of $(H_3C)_3N{-}BH_3$ by Bauer[3] led to a B—N distance of 1.62 ± 0.15 A in this molecule. The $(CH_3)_3N{-}BH_3$ crystal,[4] however, is isostructural with $(H_3C)_3N{-}BF_3$[5] and it is very probable that the B—N distances in the two compounds are very similar[4] (Table I); that is, the value obtained for the B—N distance in $(H_3C)_3N{-}BH_3$ is very likely correct to within much narrower limits than those imposed on it by the electron diffraction analysis. In ammonia-borane, a distance of 1.6 A for B—N has been found to be consistent with the powder diffraction data.[6]

TABLE I. B-N distances in accurately determined crystal structures.

Molecule	B—N distance	Reference
$H_3N{-}BF_3$	1.60 A	a, b
$H_3CH_2N{-}BF_3$	1.57	c, b
$(H_3C)_3N{-}BF_3$	1.585	d, b
$H_3CC{\equiv}N{-}BF_3$	1.635	e, b
$C_5H_5N{-}BF_3$	1.53	f
$[(NH_3)_2BH_2]Cl$	1.57, 1.60	g
$H_3NB_3H_7$	1.581	h

[a] Hoard, Geller, and Cashin, Acta Cryst. **4**, 396 (1951).
[b] See reference 10.
[c] S. Geller and J. L. Hoard, Acta Cryst. **3**, 121 (1950).
[d] See reference 5.
[e] Hoard, Owen, Buzzell, and Salmon, Acta Cryst. **3**, 130 (1950).
[f] Z. V. Zvonkova, Kristallografiia **1**, 73 (1956).
[g] C. E. Nordman and C. R. Peters, J. Am. Chem. Soc. **81**, 3551 (1959).
[h] C. E. Nordman and C. Reimann, J. Am. Chem. Soc. **81**, 3538 (1959).

In a recent note[7] by the present author, it has been pointed out that the B—N distance 1.57 A in the cubic form of boron nitride[8] may be considered as the ideal tetrahedral single B—N bond length. It was also indicated in that note that the energy of this bond, approximately 35 kcal/mole, is less than half that of a tetrahedral covalent C—C bond. Further, a rough estimate of the energy required to lengthen a B—N bond by 0.01 A is about 4 kcal/mole.[7]

At this point the evidence is rather overwhelmingly in favor of the conclusion that it is extremely unlikely that the B—N bond in $(H_3C)_3N{-}B(CH_3)_3$ is as long as 1.70 A which is only the lower limit of the "best estimate for r_{NB}" given by Lide *et al.* In fact it is very probable that the B—N bond distance in this compound is very close to 1.60 A.

In their assumptions regarding the geometry of the adducts, Lide *et al.* have taken the B—C distance in the compound to be 1.56 A, the same as that in the free $(CH_3)_3B$ molecule.[9] However, they have also assumed tetrahedral C—B—C angles in the adduct. The two assumptions are incompatible; there is little doubt that there is a significant lengthening of the B—C bond as it changes from sp^2 type to essentially sp^3 type.

As to the trimethylamine part of the molecule, large changes in bond length are not expected. However large charges in angle and small changes in distance do occur as indicated by the structure of $(CH_3)_3N{-}BF_3$.[5,10]

It is recognized that changes in angle do not ordinarily involve much energy (i.e., per degree). The C—N—C angle reported[11] for trimethylamine is 108°40′±1°; in $(H_3C)_3N{-}BF_3$, this angle is 114°. However, in $(H_3C)_3N{-}B(CH_3)_3$ the mutual repulsion of the neighboring hydrogens of the adducts, as described by

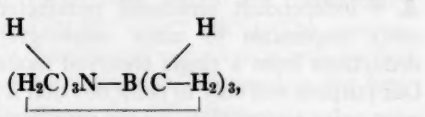

would result in smaller C—N—C angles than in the BF_3 compound.

In view of the foregoing analysis, it is reasonable to estimate a maximum of 1.62 A for the B—N bond distance in $(H_3C)_3N{-}B(CH_3)_3$. In the BF_3 compounds in which the F—B—F angle is approximately tetrahedral the B—F distance is lengthened 0.09 A[10] over its value in BF_3 itself. Therefore, it seems reasonable to assume a B—C distance of 1.65 A in $(H_3C)_3N{-}B(CH_3)_3$. Also a lengthening of the C—N distance to 1.50 A as in $(H_3C)_3N{-}BF_3$[5,10] is a valid assumption. We may further assume, as did Lide *et al.*, C—H distances of 1.09 A and H—C—H angles of 108.5° in all of the methyl groups. With these assumptions we may try to estimate the C—N—C and C—B—C angles: When both of these angles are equal to 107° the calculated value of I_B is 312 amu A^2; when, $\angle$C—N—C=107° and $\angle$C—B—C=106°, $I_B=315$ amu A^2;

when both angles are equal to 106°, $I_B = 317$ amu A². Thus we may estimate that when these angles are simultaneously between 105 and 106°, a calculated value equal to that observed for I_B will be obtained.

Therefore, contrary to the conclusion reached by Lide *et al.*, the microwave absorption in $(H_3C)_3N{-}B(CH_3)_3$ does not show an inconsistency with the well-established pattern for such compounds.

[1] D. R. Lide, Jr., R. W. Taft, Jr., and P. Love, J. Chem. Phys. **31**, 561 (1959).
[2] A. W. Laubengayer and D. S. Sears, J. Am. Chem. Soc. **67**, 164 (1945).
[3] S. H. Bauer, J. Am. Chem. Soc. **59**, 1804 (1937).
[4] S. Geller, E. W. Hughes, and J. L. Hoard, Acta Cryst. **4**, 380 (1951).
[5] S. Geller and J. L. Hoard, Acta Cryst. **4**, 399 (1951).
[6] E. L. Lippert and W. N. Lipscomb, J. Am. Chem. Soc. **78**, 503 (1956); E. W. Hughes, *ibid.* **78**, 502 (1956).
[7] S. Geller, J. Phys. Chem. Solids **10**, 340 (1959).
[8] R. A. Wentorf, Jr., J. Chem. Phys. **26**, 956 (1957).
[9] H. A. Levy and L. O. Brockway, J. Am. Chem. Soc. **59**, 2085 (1937).
[10] Hoard, Geller, and Owen, Acta Cryst. **4**, 405 (1951).
[11] D. R. Lide, Jr., and D. E. Mann, J. Chem. Phys. **28**, 572 (1958). See also L. O. Brockway and H. O. Jenkins, J. Am. Chem. Soc. **58**, 2036 (1936).

Reply to "On the Structure of Trimethylamine-Trimethylboron"

DAVID R. LIDE, JR.*

William Ramsay and Ralph Forster Laboratories, University College, London W.C.1

(Received February 1, 1960)

In a molecule such as $(CH_3)_3N{:}B(CH_3)_3$, with at least 9 independent structural parameters, it is obviously impossible to make meaningful quantitative deductions from a single observed moment of inertia. Our purpose was only to point out that if one makes the most naive assumptions for the remaining distances and angles, the N—B distance turns out to be appreciably longer than similar distances observed in crystalline addition compounds. Specifically, we stated that the N—B distance becomes 1.80±0.15 A if the CNC and CBC angles are both assumed to be 109.5±4°; therefore, one possible structure involves an N—B distance of 1.65 A and ∠CBC = ∠CNC = 105.5°. This statement is clearly consistent with Geller's calculation that the observed moment of inertia may be satisfied by an N—B distance of 1.62 A, with the CNC and CBC angles between 105 and 106°. (As Geller points out, the B—C distance is likely to be longer than in free $B(CH_3)_3$; however, this has a very minor effect on the calculation, and one can certainly draw no conclusions whatsoever concerning the B—C and N—C distances from the present data.)

There is complete agreement, then, that one must accept either a long N—B bond or unusually small CBC and CNC angles. There is no further experimental information *on this compound* to suggest which abnormality is to be preferred, and any choice at this stage must be based on inferential evidence. It still appears to the present author that the small angles would be at least as surprising as a long N—B bond. In all known compounds in which two or more CH_3 groups are attached to a second-period element the CXC angle is equal to or greater than tetrahedral (with the possible exception of $(CH_3)_3N$, where ∠CNC = 108.7±1°). Furthermore, in the most directly comparable molecule for which a structure is available, crystalline $(CH_3)_3N{:}BF_3$, the CNC angle is 114°. It would be indeed surprising if the replacement of F atoms by CH_3 groups were to cause a decrease of 9° in angles at the other end of the molecule. The arguments based on mutual repulsion between CH_3 groups are not very convincing. Reasoning of this type would predict, for example, ∠CNC in $(CH_3)_3N$ to be larger than ∠CNH in CH_3NH_2, and the CCC angle in isobutane to be greater than that in propane, while the reverse is found in both cases.

This is all in the realm of speculation, and the answer can come only from further experiments, which we hope will be forthcoming. However, it should be remembered that all previous structure determinations on B—N addition compounds, with the exception of the early electron diffraction study of $(CH_3)_3N{:}BH_3$ (and here, in spite of Geller's arguments, we prefer to retain the original investigator's estimate of his experimental uncertainty), were carried out on the solid phase. Where a bond as weak as the B—N bond is involved, it is conceivable that measurable differences exist between the structure in the crystalline and vapor phases.

* National Science Foundation Senior Postdoctoral Fellow, 1959–1960. Permanent address: National Bureau of Standards, Washington 25, D.C.

Notes

Organic Semiconductors. I. Some Characteristics of the *p*-Phenylenediamine-Chloranil Complex

MORTIMER M. LABES, ROBERT SEHR, AND MONISHA BOSE

The Franklin Institute, Laboratories for Research and Development, Philadelphia 3, Pennsylvania

(Received December 30, 1959)

RELATIVELY high conductivities have been reported for organic molecular complexes in several cases: complexes between polycyclic aromatic hydrocarbons and halogens,[1,2] tetrahalogen-*p*-benzoquinones and dimethylaniline,[3] *p*-phenylenediamine-chloranil,[4]

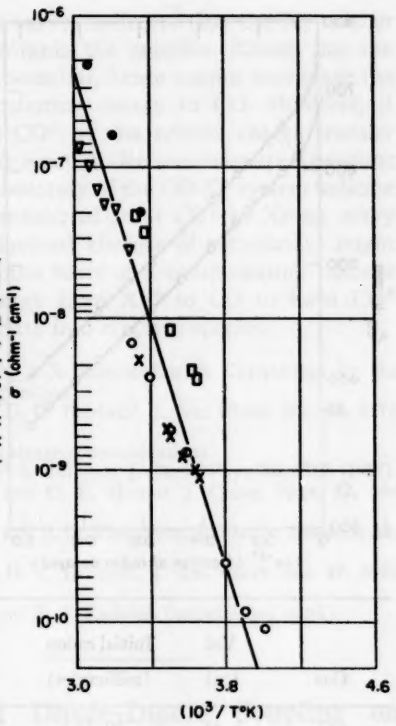

FIG. 1. Log electrical conductivity as a function of temperature between −23° and +57°C. Filled circles: rectangular sample 1; squares: rectangular sample 2; crosses: sample 3; triangles: sample 4; open circles: sample 5.

and aromatic hydrocarbons with halogens or alkali metals.[5-7]

There are only two references to our knowledge concerning measurement of Seebeck coefficients on organic materials, excluding carbons and pyrolized polymers on which more extensive work has been done.[8] Fielding and Gutman[9] report a value of 5×10^{-5} v deg^{-1} for metal-free phthalocyanine. Nelson[10] cites the work of Schroeder[11] on the Seebeck coefficient of crystal violet, giving a value of -3×10^{-4} v deg^{-1}.

We have studied the electronic properties of a wide variety of molecular complexes in the solid state, measuring the electrical conductivities and Seebeck coefficients as functions of temperature.[12] The present communication deals only with the *p*-phenylenediamine-chloranil complex which has been examined in part by Bijl *et al.*[4] We find a Seebeck coefficient which is the highest thus far reported for organic materials.

Microcrystalline samples of complex were pressed at 2900 atm; further increase of pressure gives only a slight increase in electrical conductivity. The measurements were made on samples of two different shapes. Rectangular samples had the dimensions $2\times0.5\times0.2$ cm; either two or four platinum electrodes were embedded during pressing, allowing the electrical conductivity to be measured by both a two- and four-probe method. The contact resistance of the current electrodes was thus found to be neglible. Round samples had the dimensions, 1.3 cm diam$\times$0.3 cm, with embedded perforated copper foil electrodes. Samples were mounted in evacuable glass holders with provision for heating one end of the sample. A Keithley Model 610 electrometer was used, and all the apparatus was contained in a steel Faraday cage which provided capacitative and inductive shielding.

The complex was prepared by mixing 1:1 molar ratios of the two components separately dissolved in hot benzene; however multicomplexing can and does occur. The microcrystalline complex which separates could not be recrystallized from the common solvents. Microanalyses do not agree with any simple stoichiometric ratio of amine-quinone, but an attempt is made in Table I to indicate the approximate ratio. Schlenk's analytical data[13] on the same complex are included in Table I; he performed only nitrogen analysis on this complex. No analytical data are reported by Bijl *et al.*[4]

Figure 1 gives the measured electrical conductivity as a function of temperature involving two separate preparations of complex on both round and rectangular samples. The average activation energy [from $\sigma=\sigma_0\exp(-E/kT)$] determined from these data is 0.57 ev. which does not agree with that reported by Bijl *et al.*[4] However, their conductivity values are considerably higher than ours (2×10^{-6} ohm^{-1} cm^{-1}). The nonstoichiometry of this complex and variations in composition from preparation to preparation discussed in the foregoing may easily explain this difference.

The Seebeck coefficient was measured on one round and one rectangular sample. Thirty-two readings were taken in the temperature range +49° to −36°C. The cold end was always positive indicating hole conduction. Deviations from a straight temperature independent line lie within the experimental scatter. The mean value is 1.1×10^{-3} v deg$^{-1}\pm20\%$.

TABLE I. Microanalytical data on *p*-phenylenediamine-chloranil complex.

Sample	Calc for ratio amine:quinone	%C calc	%C found	%H calc	%H found	%N calc	%N found
1, 2[a]	3:2	44.1	44.2	2.9	3.1	10.3	7.8, 7.9
3–5[b]	5:3	45.1	45.4	3.1	3.3	10.9	9.5
Schlenk[c]	1:1	40.7	...	2.3	...	7.9	7.9

[a] Rectangular samples.
[b] Round samples.
[c] Footnote 13.

We also measured the thermal conductivity on two round samples by the Joffe method.[14] It was found to be 2.0×10^{-3} w cm^{-1} deg^{-1} with an accuracy of about 15%. With these values, a figure of merit of $Z=S^2\sigma/\kappa\approx10^{-11}$ is calculated. It should be noted, however, that this poor value is solely caused by the low conductivity σ while S and κ are better than inorganic thermoelectric materials.

The technical assistance of P. J. Hackett and Mrs. F. R. Taylor is gratefully acknowledged.

[1] H. Akamatu, H. Inokuchi, and Y. Matsunaga, Bull. Chem. Soc. Japan **29**, 213 (1956).
[2] H. Akamatu, Y. Matsunaga, and H. Kuroda, Bull. Chem. Soc. Japan **30**, 618 (1957).
[3] D. D. Eley and H. Inokuchi, *Proceedings of the Third Conference on Carbon* (Pergamon Press, New York, 1959), p. 91.
[4] D. Bijl, H. Kainer, and A. C. Rose-Innes, J. Chem. Phys. **30**, 756 (1959).
[5] J. P. V. Gracey and A. R. Ubbelohde, J. Chem. Soc. **1955**, 4089.
[6] W. A. Holmes-Walker and A. R. Ubbelohde, J. Chem. Soc. **1954**, 720.
[7] F. R. M. McDonnell, R. C. Pink, and A. R. Ubbelohde, J. Chem. Soc. **1951**, 191.
[8] See, for example, E. E. Loebner, Phys. Rev. **102**, 46 (1956); and F. H. Winslow, W. O. Baker, and W. A. Yager, J. Am. Chem. Soc. **77**, 4751 (1955).
[9] P. E. Fielding and F. Gutman, J. Chem. Phys. **26**, 411 (1957).
[10] R. C. Nelson, J. Chem. Phys. **22**, 890 (1954).
[11] C. Schroeder, M.S. thesis, Ohio State University, 1952 (unpublished).
[12] We will report in the near future studies of these properties on several molecular complexes, as well as details of electrical apparatus, sample holder designs, and the problems involved in measurements on organic materials in general.
[13] W. Schlenk, Ann. **368**, 281 (1909).
[14] A. F. Joffe, Can. J. Phys. **34**, 1342 (1956).

Alpha Radiolysis of CO with and without Xe

P. S. Rudolph and S. C. Lind

Oak Ridge National Laboratory, Oak Ridge, Tennessee*

(Received January 14, 1960)

THE influence of chemically inert gases on the alpha radiolysis of gases has been extensively studied by Lind and Bardwell.[1] They found that the inert gases accelerated the rate of reaction and explained this effect as due to charge transfer. However, they observed two cases of acceleration where the inert gas had a lower ionization potential than the reactant gas (viz., HCN and C_2N_2 with Xe). This latter effect may be explained on the basis that Xe^+ forms an active addition complex with the reactant molecule.[2] The first reported retardation of a radiolytic gaseous reaction by a foreign gas was the retardation of the polymerization of C_2H_2 by C_6H_6.[3] The retardant in this case had the lower ionization potential and retardation was explained on the basis of charge transfer from $C_2H_2^+$ to C_6H_6. This charge transfer reaction was subsequently confirmed by studies in the alpha mass spectrometer.[4] Schaeffer and Thompson[5] observed the retardation of the H_2-D_2 exchange by the rare gases. They postulated ion-molecule reactions between H_2^+ (chain initiator), H_3^+ (chain carrier) and a rare gas atom, to form a rare gas-hydride ion, which retard the reaction. To our knowledge no case has been reported wherein the chemically inert additive had no effect on the rate of reaction. Such a case is reported herein.

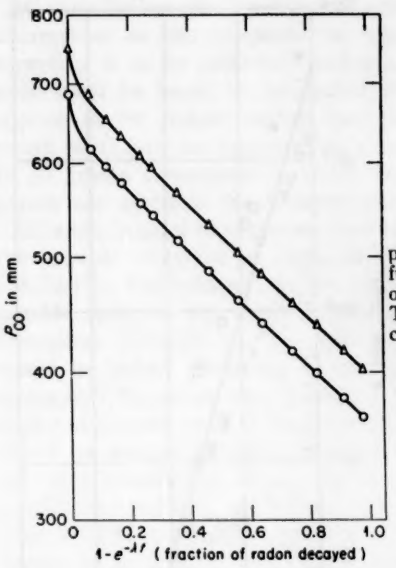

FIG. 1. Log of CO pressure at 25° as a function of fraction of radon decayed. Triangles: CO; circles CO+Xe.

Gas	Vol (cc)	Initial radon (millicuries)	Initial pressure CO	Initial pressure Xe
CO	8.43	79.32	747.9	0
CO+Xe	8.35	79.68	685.0	54.2

Since Xe has a lower ionization potential than CO (12.13 ev and 14.01 ev, respectively), it was deemed possible that Xe would retard the radiolytic condensation of CO. Hence, we studied the effect of Xe on the alpha induced radiolysis of CO. To simplify the comparison of the rates of reaction of CO with and without Xe, the mixture and the pure gas were studied concurrently in two small spheres of approximately equal volumes with about the same initial charges of radon (see Fig. 1).

During the course of the reactions, the total pressures were read at increasing time inervals. From the total pressures, the pressures of CO and CO_2 were calculated on the basis of the equation, $3CO \rightsquigarrow CO_2+\text{solids}$.[6] When about half of the radon was decayed, cryogenic separations of the gases were made *in situ* using liquid oxygen. These measured pressures agreed with the calculated pressures to within 1.5%.

In Fig. 1, the pressure of CO (calculated) is plotted against the fraction of the radon decayed. The paral-

lelism of the two curves indicates that the Xe neither accelerates nor retards the reaction. Xenon has the lower ionization potential, hence cannot accelerate the reaction by transferring charge to CO. However, it could deactivate CO^+ by the reverse charge transfer thus retarding the reaction. Recent mass-spectrometric studies[7] in this laboratory of the CO-Xe system indicate that charge is transferred from CO^+ to Xe on every collision. The observed absence of retardation might be explained on the basis of a compensating transfer of excitation energy from Xe* to CO to form CO* which can dissociate into reactive species.

* Operated for the U.S. Atomic Energy Commission by the Union Carbide Corporation.

[1] S. C. Lind and D. C. Bardwell, J. Am. Chem. Soc. **48**, 1575 (1926).
[2] Henry Eyring (private communication).
[3] S. C. Lind and P. S. Rudolph, J. Chem. Phys. **26**, 1768 (1957).
[4] P. S. Rudolph and C. E. Melton, J. Chem. Phys. **32**, 586 (1960).
[5] O. A. Schaeffer and S. O. Thompson, Radiation Research **10**, 671 (1959).
[6] S. C. Lind and D. C. Bardwell, J. Am. Chem. Soc. **47**, 2675 (1925).
[7] C. E. Melton and P. S. Rudolph (unpublished work).

Influence of Dipole-Dipole Coupling on Specific Heat of a Paramagnetic Salt

R. I. JOSEPH AND J. H. VAN VLECK
Harvard University, Cambridge, Massachusetts

(Received January 27, 1960)

IN the evaluation of the zero field partition function and from it the specific heat as a series in powers of T^{-1}, Van Vleck[1] has omitted certain contributions to the cofficient of T^{-4}. The method of Rushbrooke and Wood[2] is used here to revaluate this coefficient. We only treat the case of a simple cubic lattice.

Consider a Hamiltonian of the form

$$H=P-\alpha Q, \tag{1}$$

where

$$P=\sum_{j>i} w_{ij}, \qquad Q=\sum_i J_{zi}, \qquad \alpha=g\beta H_0$$

$$w_{ij}=g^2\beta^2 r_{ij}^{-3}[(1+v_{ij})\mathbf{J}_i\cdot\mathbf{J}_j-3r_{ij}^{-2}(\mathbf{J}_i\cdot\mathbf{r}_{ij})(\mathbf{J}_j\cdot\mathbf{r}_{ij})]. \tag{2}$$

It then follows that for a simple cubic lattice in zero field

$$C_v/Nk=[C/(kT)^2]\{1+\sum_{n=1}^{\infty}[C_n/(kT)^n]\}, \tag{3}$$

where

$$C_n=(-)^n\Gamma_N\langle P^{n+2}\rangle/n!C,$$
$$C=(2.8+v^2)g^4\beta^4J^2(J+1)^2r^{-6}. \tag{4}$$

$\Gamma_N\langle A\rangle$ means that part of $\langle A\rangle$ proportional to N, $\langle A\rangle=(2J+1)^{-N}\,\mathrm{Tr}\,A$ and v is the value of v_{ij} connecting adjacent atoms. Exchange is neglected except between nearest neighbors.

From Van Vleck[1] we obtain $\langle P\rangle$, $\langle P^2\rangle$, and $\langle P^3\rangle$ corresponding to his Eqs. (15), (17), and (27), respectively. Five kinds of terms contribute to $\langle P^4\rangle$:

(a) w_{ij}^4, (b) $w_{ij}^2w_{jk}^2$,

(c) $w_{ij}^2w_{kl}^2$, (d) $w_{ij}^2w_{jk}w_{ki}$,

(e) $w_{ij}w_{jk}w_{kl}w_{li}$.

Equations (29), (32), and (28) of Van Vleck[1] correspond to (a), (b), and (c), respectively. A rough allowance of the interaction between nonneighbors can be made by multiplying the dipole-dipole parts (i.e., parts independent of v) of (b) and (c) by $(1.4)^2$. The contributions to $\langle P^4\rangle$ from (d) and (e) have been calculated and are

$$(\mathrm{d})=(64/15)Ng^8\beta^8r^{-12}J^3(J+1)^3(1+v_4), \qquad v_4=-(v/8)(v-7)$$

$$(\mathrm{e})=(244/25)Ng^8\beta^8r^{-12}J^4(J+1)^4(1+v_5), \qquad v_5=(v/183)(50v^3+16v+354). \tag{5}$$

The coefficient of T^{-4} in C_v is then determined. Our results may be compared with the results of Rushbrooke and Wood[2] for pure exchange coupling by considering $\lim_{\beta\to 0}g^2\beta^2r^{-3}v=-2J$. The two are found to agree exactly.

If we set $v=0$ and assume J is large, we then find for the specific heat

$$C_v=Nk[2.8(\tau\tfrac{1}{2}T)^2-3.7(\tau/T)^3+0.9(\tau/T)^4+\cdots], \tag{6}$$

where τ is a characteristic temperature defined by

$$\tau=g^2\beta^2NJ(J+1)/k. \tag{7}$$

Equation (6) corresponds to (35) of Van Vleck[1] but with the coefficient of $(\tau/T)^4$ 0.9 instead of -4.0. Equation (6) is valid only for a simple cubic lattice but may be adapted to face-centered and body-centered cubic lattices by replacing the coefficient of T^{-2} by 2.4 and of T^{-3} by 3.4 and 3.5, respectively. If the temperature is high enough to give good convergence of (6) we may use the coefficient of T^{-4} for a simple cubic lattice without too much error. For temperatures on the order of τ (6) cannot be used since higher order terms come into play.

We now compare the results with experiment. We specialize to the case of a face-centered lattice for which $J=S=\frac{1}{2}$. Then the specific heat is

$$C_v=R[2.4(\tau/T)^2-4.4(\tau/T)^3-5.8(\tau/T)^4+\cdots], \tag{8}$$

which corresponds to (13) of Hebb and Purcell[3] but with the coefficient of $(\tau/T)^4-5.8$ instead of -13.5. This means that the plot of C_v vs T of Hebb and Purcell[3] (their Fig. 3) is of the same shape but shifted upward slightly. Thus their conclusion that better agreement

between theory and experiment is achieved if only the first term of (8) is used is still valid.

One of us (JHVV) wishes to thank Professor Opechowski for originally pointing out this error to him.

[1] J. H. Van Vleck, J. Chem. Phys. **5**, 322 (1937).
[2] G. S. Rushbrooke and P. J. Wood, Mol. Phys. **1**, 257 (1958).
[3] M. H. Hebb and E. M. Purcell, J. Chem. Phys. **5**, 338 (1937).

Difference of Upper and Lower State Rotational Constants of Symmetrical-Top Molecules from Infrared Intensity Measurement

TSUNEO YOSHINO

Tokyo Institute of Technology, Ohokayama, Meguro, Tokyo, Japan

(Received December 14, 1959)

THE difference of the rotational constants of the upper and lower levels of a vibrational transition α can be a kind of fingerprint for the assignment of the band, because α is related to the normal coordinate of the vibration,[1] and the α's of a fundamental band and its harmonics are in a ratio of integral numbers. α is generally very small and has not been measured in infrared spectroscopy except for very light molecules and some linear molecules. By the following method, however, relative values of α are obtainable from the infrared intensity measurement for a large number of fairly heavy symmetrical-top molecules. Here and hereafter α means $B'-B''$ or $A'-B'-A''+B''$, where A'' and B'' are the lower state rotational constants with axes parallel and perpendicular to the top axis, respectively, and A' and B' the upper state rotational constants.

An absorption band of a symmetrical-top molecule can be divided into groups of lines, in each of which line separations are linear functions of one of the α's of the band. The absorption of an infrared beam by a single line k in the jth group of the ith band is expressed by Eq. (1) when overlaps with other lines are in the linear absorption range,

$$A_{ijk}=\int_{-\infty}^{+\infty}[1-\exp(-\kappa_{ijk}u_{ij})]d\nu=(\gamma_{ijk}/2)$$

$$\times\int_{-\infty}^{+\infty}[1-\exp\{-f_{ijk}(x_{ijk})u_{ij}S_{ijk}/\gamma_{ijk}a_{ijk}\}]dx_{ijk}, \quad (1)$$

where κ_{ijk} is the absorption coefficient, u_{ij} the reduced path length, ν the frequency, γ_{ijk} the line width, S_{ijk} the line intensity, $S_{ijk}/\gamma_{ijk}a_{ijk}$ the peak height, $x_{ijk}=2(\nu-\nu_{ijk})/\gamma_{ijk}$, ν_{ijk} the frequency at the line center, and $f_{ijk}(x_{ijk})$ the function of x_{ijk} determining the line shape as Lorentzian or Gaussian. The absorption of an infrared beam by lines of the jth group A_{ij} is equal to or smaller than $\sum_k A_{ijk}$, depending on whether the overlaps of the lines are in the linear absorption range.

If the ratios $S_{i'jk}/S_{ijk}$ and $\gamma_{i'jk}/\gamma_{ijk}$ between the corresponding kth lines in the jth groups of the i'th and the ith bands are expressed by b_j and y_j, respectively, which are independent of k, and if $f_{i'jk}(x_{i'jk})$ and $f_{ijk}(x_{ijk})$ are the same between these corresponding lines, Eq. (2) is satisfied, as can be seen from Eq. (1), when $y_j=\alpha_{i'j}/\alpha_{ij}$ and $u_{i'j}/u_{ij}=y_j/b_j$,

$$A_{i'j}/A_{ij}=\sum_k A_{i'jk}/\sum_k A_{ijk}=\alpha_{i'j}/\alpha_{ij} \quad (2)$$

where α_{ij} is one of the α's determining the line separation in the jth group of the ith band. When $A_{i'j}/A_{ij}$ is measured for varying $\gamma_{i'jk}$ or γ_{ijk} under the condition of $u_{i'j}/u_{ij}=y_j/b_j$ and plotted against y_j, the intersection of the obtained curve with the straight line for $A_{i'j}/A_{ij}=y_j$ gives the value of $\alpha_{i'j}/\alpha_{ij}$ provided b_j and y_j are known. The angle β between the straight line and the tangent of the curve at $y_j=\alpha_{i'j}/\alpha_{ij}$ has a value between zero and $\tan^{-1}(A_{i'j}\alpha_{ij}/A_{ij}\alpha_{i'j})$ depending on the values of u_{ij} and γ_{ijk}. Better accuracy of $\alpha_{i'j}/\alpha_{ij}$ is obtainable for larger β, so far as the absorption by the jth group does not overlap with those of other groups in both the ith and i'th bands.

The line width γ_{ijk} can be most easily changed for a Lorentzian shape due to molecular collision by changing the gas pressure. Especially when the ratio of the partial pressures of all the component gases is unchanged the measurement of $A_{i'j}/A_{ij}$ is facilitated by the automatic satisfaction of the condition $u_{i'j}/u_{ij}=y_j/b_j$ for varying y_j without changing the optical path length. From the requirement of invariant $f_{ijk}(x_{ijk})$ in going from γ_{ijk} to $\gamma_{i'jk}$, both γ_{ijk} and $\gamma_{i'jk}$ must be several ten times larger than the Doppler broadening, which is around 10^{-3} cm^{-1} at room temperature. The collision width for a gas with total pressure of several tens of mm Hg generally has a sufficient magnitude.

The present method is most easily applicable to a group of lines for which absorption measurement can be made almost separately from other groups of lines, as for the Q branch of a linear or a spherical-top molecule. But in the Q, P, or R branch of a parallel band or the Q branch of a perpendicular band of a symmetrical top molecule, several groups of lines may appear in the interval of a measuring spectral slit width. However, for line groups in ith and i'th bands satisfying the conditions that $a_{i'j}/\alpha_{ij}$ and b_j are independent of j and overlaps between the groups are in the linear absorption range, we have a relation similar to Eq. (2), in which $A_{i'j}$, A_{ij}, $\sum_k A_{i'jk}$ and $\sum_k A_{ijk}$ in Eq. (2) are replaced by $\sum_j A_{i'j}$, $\sum_j A_{ij}$, $\sum_i\sum_k A_{i'jk}$, and $\sum_i\sum_k A_{ijk}$, respectively. The latter condition gives the upper limits to the line width and the number of lines with appreciable intensities in each of the groups. The latter limitation can be roughly estimated from relative intensities of lines[2] in the group. The

effect of the overlapping of line groups on the observed value of $\alpha_{i'j}/\alpha_{ij}$ is revealed as the dependency of $\alpha_{i'j}/\alpha_{ij}$ on frequencies.

The value of $S_{i'ji}/S_{ijk}$ is not exactly independent of k and j when the bands compared belong to molecules with different values of rotational constants, which appear in the Bolzmann factors in the intensity expressions of lines.[2] There are many cases, however, where the Bolzmann factor remains almost constant for the change of rotational constants. In these cases $\alpha_{i'j}/\alpha_{ij}$ is obtainable from the measurement of $A_{i'j}/A_{ij}$ or $\sum_i A_{i'j}/\sum_i A_{ij}$ between the ith and i'th bands belonging to molecules with different values for the rotational constants.

[1] H. H. Nielsen, Phys. Rev. **60**, 794 (1941); Revs. Modern Phys. **23**, 90 (1951).
[2] G. Herzberg, *Infrared and Raman Spectra* (D. Van Nostrand Company, Inc., New York, 1950), p. 421.

Substitutional Incorporation of Divalent Iron in Yttrium Iron Garnet

R. A. LEFEVER AND A. B. CHASE
Hughes Research Laboratories, Culver City, California

(Received February 3, 1960)

A RECENT theoretical paper on ferrimagnetic resonance in rare earth iron garnets[1] and low temperature line width measurements on high purity yttrium iron garnet (YIG)[2] have emphasized the fact that incorporation of certain rare earth ions as impurities in the YIG structure leads to an increase in resonance line widths. Certain transition metal ions, including divalent iron, may also contribute to line widths exhibited by ferrimagnetic materials.[1,3] The suggestion has been made that divalent iron may be incorporated in YIG samples as a result of silicon contamination in materials normally employed for synthesis.[4] The ability of silicon to provide a mechanism for incorporation of divalent iron in the YIG structure is illustrated by the following observations.

In an absorption spectroscopic study of the silicate ion in the garnet structure, the concentration of silicon substitutionally incorporated in YIG samples was found to be approximately proportional to silicon concentrations in the melts from which the crystals were grown.[4] On the other hand, silicon concentrations in yttrium gallium garnet (YGaG) crystals were much lower than anticipated on the basis of experience with YIG and silicon contents of the materials employed for synthesis. The addition of silicon (as SiO_2) to YGaG melts did not result in an increase in substitutionally incorporated silicon unless calcium oxide was also added, indicating that silicon incorporation was limited by the availability of suitable charge-compensating ions. The mechanism involved is probably the substitution of a pair of trivalent cations by a divalent calcium ion and a tetravalent silicon ion, thereby maintaining the garnet cation-to-anion ratio of 2/3. The substitution of one divalent ion and one tetravalent ion for two of the trivalent ions in a garnet has been demonstrated in several reports in the literature.[5]

In order to determine whether divalent iron was responsible for the ability of YIG samples to incorporate higher concentrations of silicon, crystals were grown under an atmosphere of oxygen rather than air (previously employed). When an oxygen atmosphere was employed, YIG crystals grown from reagent grade materials contained less silicon than normally encountered and the color of 25-μ sections (by white light) was altered from reddish orange to yellow. The change in color was most pronounced in crystals occurring near the melt surfaces.

In a paper on the optical and magnetic properties of ferrimagnetic garnets, the color of a 25-μ thick piece of YIG was reported to be reddish orange by transmitted light, and a 125-μ piece a very deep red.[6] We have obtained essentially the same results with thin sections of YIG crystals grown from melts containing reagent grade PbO and Fe_2O_3. However, 25-μ sections of YIG crystals grown from spectroscopically pure PbO and Fe_2O_3 and triple-purification (Lindsay Grade 3A) Y_2O_3 are yellow by transmitted white light, with no indication of a reddish trend with increasing thickness (to 70 μ). The addition of as little as 0.005 wt % SiO_2 to the high purity melts introduced a distinct reddish tinge to the color of YIG sections. As the silicon concentrations in the melts were increased, the thin-section color became increasingly red. At silicon concentrations approximating those encountered (approx 0.05 wt %) in melts prepared from reagent grade materials, the color of 25-μ sections was identical with that observed in equivalent sections of YIG crystals grown from reagent grade materials. The yellow sections are more transparent than reddish orange sections of equivalent thickness. In view of the high purity of the melts employed for synthesis and the fact that silicate frequencies fall outside of the visible spectrum, the reddish orange color and decreased transparency are attributed to the incorporation of divalent iron in the structure through a mechanism involving silicon.

The color of YIG thin sections was also altered from reddish orange to yellow by the addition of calcium oxide (50 mole % of the PbO replaced by CaO) to melts prepared from reagent grade materials. The effect is interpreted as resulting from a reduction in divalent iron in the structure due to greater availability of divalent calcium during growth.

A recent report by Dillon[7] and work in these laboratories indicate that the addition of small concentrations of silicon to melts prepared from materials of exceptionally high purity produces a low temperature peak in ferrimagnetic line widths exhibited by YIG crystals.

The effect is most likely the result of divalent iron in the structure, present as a result of cooperative incorporation with silicon.

[1] P. G. de Gennes, C. Kittel, and A. M. Portis, Phys. Rev. **116**, 323 (1959).
[2] J. F. Dillon, Jr., and J. W. Nielsen, Phys. Rev. Letters **3**, 30 (1959); E. G. Spencer, R. C. LeCraw, and A. M. Clogston, *ibid.* **3**, 32 (1959).
[3] R. L. White, Phys. Rev. Letters **2**, 465 (1959).
[4] K. A. Wickersheim, R. A. Lefever, and B. M. Hanking, J. Chem. Phys. **32**, 271 (1960).
[5] See for example, H. S. Yoder, Jr., and M. L. Keith, Am. Min. **36**, 519 (1951); S. Geller and C. E. Miller, *ibid.* **44**, 1115 (1959); R. M. Bozorth and S. Geller, J. Phys. Chem. Solids **11**, 263 (1959).
[6] J. F. Dillon, Jr., J. Appl. Phys. **29**, 1286 (1958).
[7] J. F. Dillon, Jr., presented at the Detroit Magnetics Conference, November, 1959, J. Appl. Phys. Supplement **32**, 43S (1960).

Chemisorption of CO on Ni Using a Radioactive Tracer*

A. D. Crowell
Department of Physics, University of Vermont, Burlington, Vermont

(Received January 25, 1960)

In previous studies of radioactively tagged gases adsorbed on small metal surfaces, either the metal specimen was removed from the adsorption chamber and placed before a counter[1] or the adsorption chamber contained an internal counter[2] which was designed to operate at low pressures.[3] This note reports some preliminary studies using a new technique in which a metal specimen with an area of about one square centimeter was exposed to a gas tagged with C^{14} and then moved by magnetic controls in front of a mica window which was thin enough to pass a measurable amount of the β radiation but thick enough to withstand atmospheric pressure. A commercial GM counter was located on the other side of this window as shown in Fig. 1. This method has the advantage over the technique of Crowell and Farnsworth[1] of not breaking the vacuum and exposing the surface to contamination between measurements and the advantage over the technique of Dillon and Farnsworth[2] of using a commercial counter. It has the disadvantage of a low counting efficiency.

A mica window 4 mg/cm^2 thick was sealed to the all-glass adsorption chamber by the method of Wu *et al.*[4] The counting efficiency was determined by depositing carefully measured amounts of a calibrated $Na_2C^{14}O_3$ solution obtained from Tracerlab, Inc., on a nickel surface and was found to be $1.25\pm0.01\%$.

In order to determine the feasibility of the method, a preliminary investigation of the adsorption of CO on a polycrystalline nickel disk 1.1 cm in diam was made.

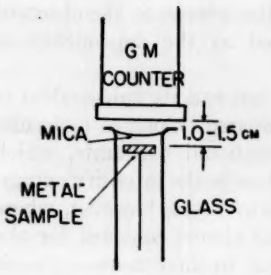

Fig. 1. Diagram of relative positions of metal sample, mica window, and GM counter during counting. During outgassing, adsorption, and background determinations, sample is lowered magnetically by about 8 cm.

The specimen was etched in dilute aqua regia, rinsed many times in distilled water and placed in the adsorption chamber which was evacuated through an all-metal valve (Granville Phillips Type C) and a dry ice trap by an oil diffusion pump (CVC GF-25) to a pressure of about 5×10^{-9} mm Hg. After the specimen was outgassed by induction heating at a dull orange heat for several hours and allowed to cool for 20 to 30 min, CO (obtained from New England Nuclear Corporation with a specific activity of 2.00 mC/mm) was admitted at room temperature through a dry ice trap and a second all-metal valve to pressures in the 10^{-2} to 10^{-1} mm Hg range. After exposures of 5 to 30 min, the CO was withdrawn and the specimen was raised to the position shown in Fig. 1. Counting rates were then taken for 5 to 30 min periods in between which the specimen was lowered for the determination of background. The mica window acquired a small irreversible contamination which was included in the background count.

The results of these studies showed that the gas adsorbed on small surfaces can be quantitatively studied by the method described. In the case of CO adsorbed on the nickel surface, total adsorption varied in several trials from 2 to 3×10^{14} adsorbed molecules per square centimeter of geometric area. The CO was observed to desorb at a rate proportional to the amount still adsorbed with a half-life of about 165 min in all cases.

Since the total number of nickel surface atoms was probably of the order of 10^{16} only a small fraction of the potential adsorption sites were occupied. This result is consistent with the earlier studies[1,2] and is probably due to surface contamination, only a small part of which was removed by the outgassing procedure.

While little can be said of the character of the nickel surface, it is of some interest to estimate the activation energy of desorption at room temperature as an example of the type of information which can be obtained by this method. Assuming the adsorption to be unactivated,[5] this energy is also the heat of adsorption. Using the Polanyi-Wigner equation as given by Garner[5,6] and assuming a normal vibration frequency of admolecules on the surface of 10^{13} sec^{-1}, one finds an activation energy of about 25 000 cal/mole, which is somewhat less than the 35 000 cal/mole reported by

Beeck[7] for calorimetric studies of the adsorption of CO on evaporated nickel films.

* Supported by the National Science Foundation.

[1] A. D. Crowell and H. E. Farnsworth, J. Chem. Phys. **19**, 1206 (1951).
[2] J. A. Dillon, Jr., and H. E. Farnsworth, J. Chem. Phys. **22**, 1601 (1954).
[3] J. A. Dillon and H. E. Farnsworth, Rev. Sci. Instr. **25**, 96 (1954).
[4] Wu, Meaker, and Glassford, Rev. Sci. Instr. **18**, 693 (1947).
[5] B. M. W. Trapnell, *Chemisorption* (Academic Press, Inc., New York, 1955).
[6] W. E. Garner, J. Chem. Soc. **1947**, 1239.
[7] O. Beeck, Advances in Catalysis **2**, 151 (1950).

Microwave Spectra and Structure of H_3SiCN and D_3SiCN*

NORBERT MULLER AND RONALD C. BRACKEN

Department of Chemistry, Purdue University, Lafayette, Indiana

(Received January 5, 1960)

FOR a number of compounds of the types X—CN and X—C≡CH it has been observed[1] that the X—C bond length, r(X—C), is quite appreciably less than the corresponding length in X—CH_3. This difference is about 0.04 A for the H—C bond, 0.08 A for C—C bonds, and about 0.15 A when X is Cl, Br, or I. Several explanations have been proposed to account for these differences, including the change in the covalent radius of carbon with changing hybridization, hyperconjugation, and, for the cyanogen halides, resonance contributions of the type

$$\overset{+}{\text{Cl}}\text{=C=N}^-.$$

In the hope of contributing to the understanding of this phenomenon we have examined the microwave spectra of H_3SiCN and D_3SiCN and derived a value for r_0(Si-C) which may be compared with the value[2] of 1.8668 A in H_3SiCH_3.

The compounds were prepared by the reaction[3] of H_3SiI or D_3SiI with AgCN and purified by bulb-to-bulb distillation until the infrared spectra showed only small traces of the strong bands of the major impurities, $(H_3Si)_2O$ and HCN. Since H_3SiCN decomposed fairly rapidly in the waveguide, we observed the microwave spectra with the guide cooled with dry ice, using a spectrometer with 100 kc Stark modulation.[4] For each isotopic species we measured the $J=1\rightarrow2$ and $J=2\rightarrow3$ transitions and derived B_0 values of 4972.7±0.5 Mc for H_3SiCN and 4535.0±0.5 Mc for D_3SiCN. The transitions were broadened by the nuclear quadrupole fine structure, which we were not able to resolve.

Recently, Dr. J. Sheridan[5] has communicated to us microwave data on normal H_3SiCN and the species containing Si^{29} and Si^{30} which indicate that the Si nucleus must lie 1.103 A from the center of gravity of the Si^{28}-containing species. To use our data with this additional condition to derive a structure, it is still necessary to assume a value for one structural parameter[6] and to postulate some relation between the geometries of the normal and the deuterated silyl groups. We chose, first, to assume r_0(C—N) = 1.58 A, since this parameter lies within a few thousandths of an angstrom of this value for all other X—CN compounds investigated.[1] This assumption is supported by the fact that the C—N stretching band[7] of D_3SiCN is at 2212 cm^{-1}, as compared with 2249 cm^{-1} for acetonitrile[8] and 2201 cm^{-1} for cyanogen chloride.[9] We further assumed[10] that r_0(Si—H) = r_0(Si—D) + 0.010 A and ∠H—Si—H = ∠D—Si—D. The Si—H parameters are very sensitive to a change in the latter assumption, but neither assumption strongly influences the value of r_0(Si—C). The structure obtained is

$$r_0(\text{Si—H}) = 1.49 \pm 0.05 \text{ A}$$
$$\angle \text{C—Si—H} = 107.5° \pm 2°$$
$$r_0(\text{Si—C}) = 1.847 \pm 0.005 \text{ A}.$$

Very similar values were proposed independently by Sheridan and Turner.[5]

It is rather surprising that r_0(Si—C) is only 0.02 A less in H_3SiCN than in H_3SiCH_3. Both values are considerably smaller than the sum of the Pauling covalent radii,[11] 1.94 A. It might be inferred that both Si—C bonds acquire nearly the same amount of double bond character through resonance. In the methyl compound this would imply a significant contribution by hyperconjugative structures such as I in which the 3*d* orbitals of Si participate in the bonding. Because of the much lower electron releasing tendency of −CN as compared to —CH_3 it would be expected that the analogous forms II for the cyanide would contribute little, perhaps less than the alternative hyperconjugative structures, III:

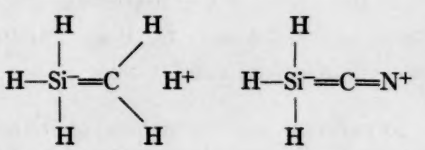

I II

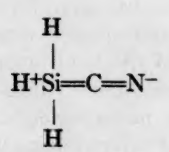

III.

We cannot at present decide between this interpretation and the possibility that the Si—C bond in methyl

silane is made with a carbon orbital of unusually high s character and is therefore shortened nearly as much as the bond in the cyanide. A study of the C^{13}—H coupling in the proton magnetic resonance spectrum of H_3SiCH_3 would be desirable, since such data may be used[12] to estimate the state of hybridization of the carbon atom.

We wish to thank Mr. William E. Baitinger for help with the preparation of H_3SiCN. One of us (RCB) thanks the Purdue Research Foundation for financial support during a part of this work.

* Supported by the U.S. Atomic Energy Commission under contract with the Purdue Research Foundation.

[1] For relevant data see W. Gordy, W. V. Smith, and R. F. Trambarulo, *Microwave Spectroscopy* (John Wiley & Sons, Inc., New York, 1953), p. 371.

[2] R. W. Kilb and L. Pierce, J. Chem. Phys. **27**, 108 (1957).

[3] A. G. MacDiarmid, J. Inorg. & Nuclear Chem. **2**, 88 (1956). See, however, references 5 and 7 which show that the normal cyanide is indeed obtained and not the isocyanide.

[4] We are indebted to Professor Walter Edgell for the use of this instrument.

[5] J. Sheridan and A. G. Turner, Proc. Chem. Soc. **1960**, 21.

[6] In collaboration with Professor R. L. Livingston and Dr. C. N. R. Rao, one of us (RCB) is attempting to obtain the necessary value using the electron diffraction technique.

[7] H. R. Linton and E. R. Nixon, Spectrochim. Acta **10**, 299 (1958).

[8] G. Herzberg, *Infrared and Raman Spectra* (D. Van Nostrand Company, Inc., Princeton, New Jersey, 1945), p. 333.

[9] W. West and M. Farnsworth, J. Chem. Phys. **1**, 402 (1933).

[10] This assumption of course does not imply that the true, equilibrium Si—H distance differs significantly from the Si—D distance, but applies only to the "effective" parameters derived from the I° values. See C. C. Costain, J. Chem. Phys. **29**, 864 (1958).

[11] L. Pauling, *The Nature of the Chemical Bond* (Cornell University Press, Ithaca, New York, 1945), p. 164.

[12] N. Muller and D. E. Pritchard, J. Chem. Phys. **31**, 1471 (1959).

Appearance Potential Study of Tetrafluorohydrazine*

E. Dan Loughran and Charles Mader

Los Alamos Scientific Laboratory, Los Alamos, New Mexico

(Received January 11, 1960)

THE preparation and properties of tetrafluorohydrazine (N_2F_4) have been reported by Colburn and Kennedy.[1] A recent study of the microwave spectrum of the compound has given further information as to the structure of tetrafluorohydrazine.[2] We wish to report an estimate of the bond dissociation energy of the N—N bond in tetrafluorohydrazine as derived from appearance potential measurements.

A sample of tetrafluorohydrazine was obtained from Rohm and Haas Company, Redstone Arsenal Research Division, Huntsville, Alabama. The purity was quoted at 95+% and was found to be 97% by mass spectral analysis. The major impurities of air and nitrous oxide were removed by standard low temperature distillation techniques, increasing the purity to 99%.

Table I. Mass spectrum of tetrafluorohydrazine.

Species	Relative abundance (70 v)	AP (v)
NF_2^+	57.6	11.8±0.2
NF^+	100.0	15.0±0.2
N_2^+	0.2	
F^+	6.6	
NF^{++}	0.3	
N^+	11.4	

The mass spectrum of tetrafluorohydrazine and the observed appearance potentials are presented in Table I. The data were obtained using a Consolidated Electrodynamics Corporation Model 21-103C mass spectrometer modified for appearance potential and excess kinetic energy studies.[3] The appearance potentials were determined by the method of initial breaks. Excess kinetic energies were measured by using the metastable ion suppressor as a retarding potential device. Both procedures have been described previously.[3] Krypton and argon were added as calibration standards for the appearance potential and excess kinetic energy measurements, respectively.

Since the fragmentation process producing NF_2^+ is probably complex, several mechanisms resulting in its formation may be postulated. However, reasonable arguments can be made for the preference of a single possibility, which is presented in Table II. A value for the bond dissociation energy, $D(F_2N\text{-}NF_2)$, may be calculated using the observed appearance potential (AP) for NF_2^+ if one knows the ionization potential (IP) of NF_2 and the bond dissociation energy, D(FN-F). From our measured value of 14.6 v for the AP-(NF_2^+) from NF_3, and Reese and Dibeler's estimate of 3.2 v for $D(F_2N—F)$,[4] a value of 11.4 v for the $IP(NF_2)$ was estimated. The value for D(FN—F) was taken to

Table II. Fragmentation mechanisms postulated.

m/e 52 $\qquad AP(NF_2^+) = 11.8 \pm 0.2$

$$e + N_2F_4 \rightarrow NF_2^+ + NF + F^- + e$$

$$D(F_2N-NF_2) = AP(NF_2^+) - IP(NF_2) - D(FN-F) + EA(F)^a$$
$$= 11.8 \quad -11.4 \quad -2.7 \quad +3.6$$
$$= 1.3 \pm 0.3 \text{ v (30 kcal)}$$
$$\text{or} = 1.7 \text{ using 11.0 for } IP(NF_2)^b$$

m/e 33 $\qquad AP(NF^+) = 15.0 \pm 0.2$

$$e + N_2F_4 \rightarrow NF^+ + NF + F^- + F + e$$

$$D(F_2N-NF_2) = AP(NF^+) - IP(NF) - 2D(FN-F) + EA(F)^a$$
$$= 15.0 \quad -12.0 \quad -5.4 \quad +3.6$$
$$= 1.2 \pm 0.3 \text{ v (28 kcal)}$$

[a] Excess kinetic measurements indicated that both NF_2^+ and NF^+ are formed with less than 0.2 v excess kinetic energy.

[b] Footnote 4.

be 2.7 v.[4] The proposed mechanism appears to be supported by the shape of the ionization efficiency curve, which exhibits a rather long tail in the appearance potential region. This would suggest, in the absence of excess kinetic energy of the ion, that the NF_2^+ fragment is being formed by a multiple fragmentation process.[5]

Table II also contains the most probable fragmentation mechanism for the formation of the NF^+ species. It can be seen that the mechanism is comparable to that written for the formation of NF_2^+ and gives a value for $D(F_2N—NF_2)$ in good agreement with the number calculated from the $AP(NF_2^+)$. The value for $IP(NF)$ was taken to be 12.0 v[4] and for $EA(F)$ 3.6 v.[4]

From this study and the known physical properties of the compound, it has been concluded that the bond dissociation energy of the $F_2N—NF_2$ bond in tetrafluorohydrazine undergoing electron bombardment is 1.3 ± 0.3 ev.

* Work performed under the auspices of the U.S. Atomic Energy Commission.

[1] C. B. Colburn and A. Kennedy, J. Am. Chem. Soc. **80**, 5004 (1958).
[2] D. R. Lide, Jr., and D. E. Mann, J. Chem. Phys. **31**, 1129 (1959).
[3] R. J. Kandel, J. Chem. Phys. **22**, 1496 (1954).
[4] R. M. Reese and V. H. Dibeler, J. Chem. Phys. **24**, 1175 (1956).
[5] F. H. Field and J. L. Franklin, *Electron Impact Phenomena* (Academic Press, Inc., New York, 1957), p. 12.

Spin Distribution in Naphthalene Negative Ion*

T. R. Tuttle, Jr.

Department of Chemistry and Chemical Engineering, Stanford University, Stanford, California

(Received December 18, 1959)

THE ESR absorption spectrum of naphthalene negative ion with 53 atom percent C^{13} in one β position has been observed in dilute 1,2-dimethoxyethane solution at room temperature. This spectrum is well represented by a superposition on the spectrum of ordinary naphthalene negative ion of a spectrum in which each line has been doubled with a splitting of 1.2 gauss. One may relate this β C^{13} splitting and the previously determined α C^{13} splitting[1] with unpaired π-electron densities through an empirical equation suggested by the application of simple valence bond[2] or molecular orbital theory[3] to a C—C fragment. This relationship may be written as follows:

$$S_n=3k_1\rho_n+k_2\sum_i\rho_i,$$

where S_n is the hyperfine splitting from a C^{13} at position n, ρ_n is the unpaired π-electron density at this position, ρ_i's are π densities on adjacent carbon atoms or more generally the corresponding diagonal elements of the spin density matrix.[4] This is an approximate expression which neglects contributions from unpaired π density on noncontiguous atoms and from terms corresponding to off-diagonal elements of the spin density matrix. The data for C^{13} splittings in naphthalene negative ion combined with values of ρ_α and ρ_β calculated from proton hyperfine splittings[5,2] yield $k_1=13.5$ gauss, $k_2=-5.9$ gauss. These constants are in agreement with C^{13} splittings[6] and π spin densities[7,8] in triphenylmethyl-C^{13} and methyl[9]-C^{13}. In the case of triphenylmethyl-C^{13} the best agreement is obtained if the three rings are considered coplanar.[8]

I wish to acknowledge encouragement and inspiration given me by Professor S. I. Wiessman.

* This research was supported in part by the U. S. Air Force under contract monitored by the Air Force Office of Scientific Research of the Air Research and Development Command.

[1] T. R. Tuttle, Jr., and S. I. Weissman, J. Chem. Phys. **25**, 189–190 (1956).
[2] H. M. McConnell, J. Chem. Phys. **24**, 764 (1956).
[3] S. I. Weissman, J. Chem. Phys. **25**, 890–891 (1956).
[4] H. M. McConnell, J. Chem. Phys. **28**, 1188 (1958).
[5] T. R. Tuttle, Jr., R. L. Ward, and S. I. Weissman, J. Chem. Phys. **25**, 189 (1956).
[6] S. I. Weissman and J. C. Sowden, J. Am. Chem. Soc. **75**, 503 (1953).
[7] P. Brovetto and S. Ferroni, Nuovo Cimento **5**, 142–153 (1957).
[8] F. C. Adam and S. I. Weissman, J. Am. Chem. Soc. **80**, 2059 (1958).
[9] T. Cole, H. O. Pritchard, N. R. Davidson, and H. M. McConnell, Mol. Phys. **1**, 406 (1958).

Some Observations on Atomic Exchange in NO*

W. Spindel and Marvin J. Stern

Department of Chemistry, Rutgers, The State University, Newark 2, New Jersey

(Received September 8, 1959)

CLUSIUS and Schleich[1] have recently found that the vapor pressure ratios of isotopic nitric oxides, $N^{14}O^{16}/N^{15}O^{16}$ and $N^{14}O^{16}/N^{14}O^{18}$, are three to five times greater than the corresponding ratios for other diatomic molecules of comparable molecular weight and boiling point. They have used the strikingly high single-stage separation factor to enrich nitrogen-15 by distillation of nitric oxide, and have pointed out the attractive possibility of using this process to simultaneously concentrate the heavy isotopes of nitrogen and oxygen.[2] In order to obtain highly concentrated nitrogen-15 or oxygen-18 by distillaton of a mixture of $N^{14}O^{16}$, $N^{15}O^{16}$, and $N^{14}O^{18}$, it is necessary to establish the equilibrium: $N^{15}O^{16}+N^{14}O^{18}\rightleftharpoons N^{14}O^{16}+N^{15}O^{18}$. In view of this it seemed of interest to measure the rate of exchange between isotopically labeled nitric oxide molecules.

TABLE I. Comparison of observed spectra[a] and predicted compositions of isotopic nitric oxides.

		(1)		(2)		(3)		
		Nitric oxide enriched in O^{18} and O^{17} (9.13% O^{18}, 0.332% O^{17})		Nitric oxide enriched in N^{15} (99.4% N^{15})		Mixture of equal amounts of (1) and (2)		
m/e	Contributing molecular species	calc	obs	calc	obs	calc for 0% equil	calc for 100% equil	obs
30	$N^{14}O^{16}$	90.1	89.4	0.61	0.52	45.4	47.7	47.9
31	$N^{15}O^{16}$, $N^{14}O^{17}$	0.66	0.68	99.2	98.9	49.9	47.6	46.7
32	$N^{14}O^{18}$, $N^{15}O^{17}$	9.09	9.84	0.04	0.40	4.57	2.43	2.98
33	$N^{15}O^{18}$	0.03	0.03	0.20	0.21	0.12	2.33	2.41

[a] The observed spectra have been corrected for the presence of secondary species, N_2, O_2, and CO, which are produced by reactions of NO in the mass spectrometer source, and normalized to make the sum of peaks 30–33 equal to 100.

Leifer[3] showed that exchange between NO and NO_2 takes place rapidly in the gas phase at or below room temperature, and so the primary interest in the present study was to explore the rate of equilibration in nitric oxide samples purified to minimize the concentration of higher oxides, and to determine whether exchange in such samples could proceed through the formation of a dimer intermediate, $(NO)_2$, of a square structure,[4] as well as by the known higher oxide mechanism.

Nitrogen-15 labeled nitric oxide was prepared by reducing potassium nitrate containing 99 atom % N^{15} with mercury in an excess of sulfuric acid. Oxygen-18 labeled gas was prepared by equilibrating normal nitric oxide overnight with a large excess of acidified water containing about 10 atom % O^{18}. N_2O_4 and N_2O_3 were removed from the samples by freezing the gas with liquid nitrogen and quickly replacing the nitrogen with dry ice to preferentially vaporize the NO. The frozen oxides were separated from the bulk of the gas, allowed to warm to room temperature, and then pumped off. This purification process was repeated several times.

Exchange was observed by mixing equal volumes of the two labeled nitric oxides in the sample inlet system of a Consolidated-Nier mass spectrometer and measuring the intensity of the $m/e=33$ peak due to $N^{15}O^{18+}$. This instrument utilizes a capillary leak into the ion source, and the inlet gas pressure required for sufficient ion beam intensity is about 1–4 cm Hg. Samples were mixed at a total pressure of ~2 cm Hg. Complete exchange occurred under these conditions in less than the time required for measurement, i.e., about 15–30 sec. Spectra of the isotopic nitric oxide samples and the mixed sample are shown in Table I, together with the mole percents of the various NO species calculated from the isotopic abundances in the samples. For the sample of mixed nitric oxide the spectrum is compared to that calculated for zero and complete exchange. The $m/e=33$ peak expected for zero exchange is simply the average of this peak in the two enriched samples; for complete exchange the 33 peak corresponds to random distribution of N and O atoms among the various species. It may be noted that for the samples used, the 33 peak expected for complete exchange is about twenty times larger than for zero exchange, and the observed peak agrees closely with that calculated for complete equilibration.

These experiments indicated that equilibration of nitric oxide species should occur continuously in a distillation column without any added catalyst, but the rapidity of the exchange did not permit any conclusions as to mechanism. To decrease the rate of exchange and explore the mechanism, samples were mixed and exchange was observed at much lower pressures of ~60–100 μ Hg. This was done in the inlet system of a mass spectrometer equipped with a pinhole leak. Samples were introduced into a small metering volume (~11 cm^3) at pressures of 1–3 cm Hg and allowed to mix in an evacuated 3.5-liter vessel which connected to the ion source via the pinhole. At these low pressures the exchange rate was about 100–1000 times slower than at 2 cm Hg; the $N^{15}O^{18+}$ peak only increased a total of about 3% in 10 min after mixing. The "catalytic" effect of oxygen on the exchange by a mechanism such as: $O_2+NO\rightarrow NO_2$, $N^{15}O_2+N^{14}O\rightleftharpoons N^{14}O_2+N^{15}O$, etc., was observed by adding ~20 μ of O_2 to the vessel which contained ~60 μ of nitric oxide. The exchange rate increased considerably; a fourfold increase in the $N^{15}O^{18}$ peak was observed in the first 5 min after the oxygen was added.

The possibility that the exchange could also proceed through a dimer intermediate, of structure

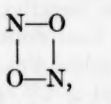

in the solid state[4] was explored in another low pressure experiment. Two samples, each at a partial pressure of ~90 μ Hg were mixed; about 30% of the mixture was frozen into a side tube with liquid nitrogen, kept solid for several minutes, and allowed to revaporize directly back into the low pressure reservoir. No increase in the 33 peak was observed after this freezing and vaporization process, indicating that the dimer formed in solid nitric oxide does not have a square structure containing

N—O bridges, but is probably of a bent chain structure,

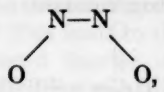

such as that proposed by several authors from spectroscopic data.[5]

The exchange rate increased after cooling, perhaps due to the increased reaction rate of nitric oxide with traces of oxygen at low temperature. Further studies of the kinetics of the exchange at low pressures are planned.

We are indebted to Professor T. I. Taylor of Columbia University for use of his mass spectrometer in the low pressure studies, and to Paul Tag for assistance with mass spectrometric analyses.

* This work was supported in part by a grant from the U.S. Atomic Energy Commission.

[1] K. Clusius and K. Schleich, Helv. Chim. Acta **41**, 1342 (1958).
[2] K. Clusius and K. Schleich, Helv. Chim. Acta **42**, 232 (1959).
[3] E. Leifer, J. Chem. Phys. **8**, 301 (1940).
[4] Dulmage, Meyers, and Lipscomb, J. Chem. Phys. **19**, 1432 (1951); Acta Cryst. **6**, 760 (1953).
[5] Smith, Keller, and Johnston, J. Chem. Phys. **19**, 189 (1951); L. D'Or and P. Tarte, Bull. Soc. Roy. Sci. Liège, 6–7, 276 (1953); W. G. Fateley, H. A. Bent, and B. Crawford, Jr., J. Chem. Phys. **31**, 204 (1959).

Study of Infrared Reflection Spectrum of Liquid C_6H_6

DAVID A. DOWS AND J. L. HOLLENBERG

Department of Chemistry, University of Southern California, Los Angeles 7, California

(Received January 11, 1960)

RECENT measurements of absolute intensities of infrared absorption bands in condensed phases are of considerable potential value in the study of intermolecular interactions. Examples of recent work of this type are studies on benzene by Hisatsune and Jayadevappa,[1] and Swenson and Person[2] and on the ammonium ion in various environments.[3] It is well known that strong light absorption is accompanied by a region of anomalous dispersion and a reflection band. It seems desirable that absolute intensity measurements be corrected for any appreciable reflection effect, but it is not clear just how intense a transition must be to necessitate an important correction.

We have measured the reflection spectrum of liquid benzene (at 20°C) behind a potassium bromide plate, the angle of incidence being 11° (close enough to normal incidence to allow neglect of any correction). The light beam traversed the KBr plate and was partially reflected at the KBr-air and the KBr-benzene interfaces, and the unreflected portion was absorbed in the benzene or removed from the optical path by the "light-trap" design of the cell.

The reflection between 650 and 4000 cm^{-1} consisted of a general background due primarily to the KBr-air surface, with only one detectable band, at 675 ± 1 cm^{-1}. This band was quite symmetrical, with a peak reflectance of 0.14 ± 0.01 (the background was about 0.03) and a width at 0.085 reflectance of 14 cm^{-1}. The frequency and width correspond closely to the observations by Hisatsune and Jayadevappa[1] on the absorption band.

In the study of absolute absorption intensities[4] it is the quantity $A=\int\alpha d\nu$ which is required. With the assumption of Beer's law connecting α, the absorption coefficient, with the concentration n, the path length l, and the ratio of incident to transmitted light intensity, A is obtained as the limit at low absorption of a quantity B, given by

$$B=(1/nl)\int\ln(T_0/T)d\nu. \qquad (1)$$

Actually, if a reflectivity R exists at both surfaces of the sample, the relation between fraction transmission and absorption coefficient is (instead of Beer's law)

$$I/I_0=(1-R)^2\exp(-\alpha nl). \qquad (2)$$

Thus A (in the limit) is given by

$$A=B+(2/nl)\int\ln(1-R)d\nu. \qquad (3)$$

It would appear from this formula (3) that a correction to integrated band areas could easily be made, by integrating the term $(1-R)$. This integration was carried out for the 675 cm^{-1} benzene band, giving $\int\ln(1-R)d\nu=-2.8\pm.1$ cm^{-1}. In integrating, the general background reflection was taken to be zero, and integration was performed over the frequency range 655–705 cm^{-1}, where R was above the background. This corresponds to adjustment of the wings of an absorption band to the 100% line. The correction would be about 11–28% of Hisatsune and Jayadevappa's observed B values.

There exists a complication, however, which makes the correction as derived in the preceding of questionable validity. This is the interference phenomenon in liquid (or solid) phases in which the thickness is smaller than the wavelength of light. The benzene film thicknesses ranged from 0.6 to 6.9$_3$ μ. As pointed out previously this interference, in very thin layers, may cancel the reflection. This cancellation can occur, however, only if the reflectivity and percent absorption are not too high. The calculation of an accurate reflection correction to thin film absorption intensities, based on bulk reflectivity as measured in this work, is thus a considerably more complicated problem.

In conclusion, from this brief study of benzene, it seems that only the very intense bands (the 671 cm^{-1}

band is by far the most intense in the benzene spectrum) produce measurable reflection. These bands can reflect enough light[5] to make consideration of a reflection correction necessary, though treatment of the interference phenomena found in thin films will be a necessary complication.

It might be pointed out that measurements of the reflection spectra of liquids may themselves be used to determine absolute intensities. The relations are analogous to those discussed by Haas and Hornig[6] for solids, and are closely connected to the dispersion method recently used on benzene by Schatz.[7] A study is now underway, in cooperation with Professor Schatz, of the reflection spectra of several liquids, the calculation of their reflection from dispersion data, and the measurement of absolute intensities by reflection studies. Preliminary results on benzene are encouraging, and the work will be forthcoming.

We wish to thank Professor Hisatsune, Professor Hornig, and Professor Person for making available their results before publication. The Office of Ordnance Research has assisted in the support of this work.

[1] I. C. Hisatsune and E. S. Jayadevappa, J. Chem. Phys. **30**, 848 (1959).
[2] C. S. Swenson, thesis, State University of Iowa, 1959; C. S. Swenson and W. B. Person J. Chem. Phys. (to be published).
[3] C. C. Ferriso and D. F. Hornig (private communication).
[4] E. B. Wilson and A. J. Wells, J. Chem. Phys. **14**, 578 (1946).
[5] Reflection measurements on some other organic substances are reported by Cameo-Bosco [Compt. rend. **248**, 1642 (1959)], who uses a method similar to our own.
[6] C. Haas and D. F. Hornig, J. Chem. Phys. **26**, 707 (1957).
[7] P. N. Schatz, Ohio State Symposium on Molecular Structure and Spectroscopy, 1959, paper M-4.

Group Electronegativities from Bond Lengths

HENRY A. BENT

School of Chemistry, Institute of Technology, University of Minnesota, Minneapolis, Minnesota

(Received January 27, 1960)

IT has been pointed out by Mulliken[1] and Walsh[2] that the more *s* character in a carbon valency, the more electronegative is the carbon atom in that valency. Strong confirmation of the importance of atom hybridization on electronegativity has been given recently by Petro,[3] who calculates from dipole moment and infrared dispersion data the following carbon-carbon moments: $(sp^3)^+-(sp^2)^-=0.68$ debye, $(sp^2)^+-(sp)^-=1.15$ debyes, $(sp^3)^+-(sp)^-=1.48$ debyes (he finds, also, that chlorine constitutes the positive end of the C—Cl bond moment in HC≡CCl); and by Taft,[4] who lists the following inductive constants:

$$H_3C-=-0.100,\quad CH_3\overset{O}{\overset{\|}{C}}-=+0.60,\quad NC-=+1.300(Cl-=+1.10).$$

It is apparent, too, that atom hybridization also affects not only bond angles, as is well known, but bond lengths as well. Data concerning this point has been summarized recently by Brown.[5] Typically, the length (in A) of the carbon-carbon single bond for the two carbon atoms in the hybrid states sp^3-sp^3, sp^3-sp^2, sp^3-sp, sp^2-sp^2, sp^2-sp, sp-sp, decreases as follows: 1.54, 1.50, 1.46, 1.47 (?), 1.42. 1.38; i.e., by about 0.04 A each time a carbon atom changes its hybridization from sp^3 to sp^2 or from sp^2 to sp.

Since a change in hybridization ratio affects both the electronegativity of an atomic orbital and its effective radius, it should be possible to predict trends in bond lengths from inductive constants, or conversely, to infer from measured bond lengths trends in group electronegativities. For example, as the electronegativity of A in the system A—X—B increases, or as X changes from sp^3- to sp^2- or sp-type hybridization, the *s* character in the orbital toward B increases. This tends to make the X—B bond shorter. However, counteracting this foreshortening of the X—B bond is an inductively induced rehybridization of B; for as the *s* character in the X-to-B orbital increases, X becomes effectively more electronegative with respect to B, making it advantageous for B to remove some of its *s* character from the B-to-X orbital. This tends to increase the length of the X—B bond. To preserve the full effect of the change in hybridization of X on the length of the X—B bond, B should be a group that uses most of its *s* character elsewhere than in its bond to X. Such an atom is fluorine with three lone pairs.

The data listed in Table I illustrate the composite effect of inductive influences and nominal changes in states of hybridization of carbon on the C—F bond length. If a foreshortening of the C—F bond is taken to imply an increase in *s* content of the carbon-to-fluorine orbital, and an increase in *s* content is taken to mean an increase in electronegativity, the order from top to bottom is the order of increasing group electronegativity. By and large, this order agrees well with chemical intuition and Taft's inductive constants. Additional electronegativity sequences that can be inferred from sequences b-d-i and g-h are $-F>-H>-CH_3$ and $=CF_2>=CH_2$.

In a quantitative sense, one may ask whether it is reasonable, even as a first approximation, to attribute these changes in bond lengths entirely to changes in the hybridization ratio of the carbon orbital of the C—F bond. Although the state of hybridization of carbon in these compounds is not known with great

accuracy, it is known that the HCH angle in the methyl halides tends to be several degrees greater than the tetrahedral value.[6] This leads to the estimate that the carbon orbital toward fluorine in CH_3—F contains 15–20% *s* character.[7] The relatively large uncertainty in this figure arises from the uncertainty in the position of the hydrogen atoms, owing to their smallness of mass, or scattering power, and the sharp dependence of pyramidal hybridization ratios on the interbond angle between equivalent groups when there are three such groups attached to the central atom. In F_2CO, the carbon orbital toward fluorine may be estimated to contain 27–29% *s* character. Thus the change in *s* content from compound (a) to (i) is perhaps 7–14%, the corresponding change in bond length being 0.09 A. This may be compared with the numbers cited earlier for carbon-carbon bonds. It was seen that the $C(sp^3)$-$C(sp)$ bond is typically 0.08 A or so shorter than the $C(sp^2)$-$C(sp^3)$ bond, which corresponds to a nominal change in *s* content of 25%. The actual change in *s* content is probably much less than this figure, first, because the carbon orbitals of the C—C bond such as ethane are slightly richer in *s* character than the notation sp^3 indicates, and second and more importantly, because the lone σ orbital projecting from a triple bond is undoubtably significantly poorer in *s* character than the notation *sp* indicates. How much poorer is, of course, a moot question. If one adopts, as we have here, the $\sigma-\pi$ description of multiple bonds and assumes that a triple bond preempts *s* character per π bond as efficiently as does a double bond, and while this is unlikely, it does afford some kind of a first approximation, the lone "*sp*" orbital might contain as little as 35–40% *s* character. While exceedingly rough, these estimates do give for the carbon-carbon case a change in hybridization ratio and concomitant change in bond length that is comparable to that found for the carbon-fluorine bond. This makes it seem not unreasonable to suppose that perhaps the same effects are operative in the two cases.

TABLE I. Nine fluorine-containing compounds in order of decreasing C—F bond length.

Molecule	C—F distance	Reference
a. H_3C—F	1.391 A	a
b. $CH_3\overset{O}{\overset{\|}{C}}$—F	1.37	b
c. FH_2C—F	1.358	c
d. $HC(=O)$—F	1.351	d
e. F_2HC—F	1.332	e
f. F_3C—F	1.323	a
g. $FC(=CH_2)$—F	1.321	f
h. $FC(=CF_2)$—F	1.313	f
i. $FC(=O)$—F	1.32	g

[a] L. O. Brockway, Acta Cryst. **7**, 682 (1954).
[b] P. W. Allen and L. E. Sutton, Trans. Faraday Soc. **47**, 236 (1951).
[c] D. R. Lide, Jr., J. Am. Chem. Soc. **74**, 3548 (1952); R. L. Livingston and D. H. Lyon, J. Chem. Phys. **24**, 1283 (1956).
[d] M. E. Jones, K. Hedberg, and V. Schomaker, J. Am. Chem. Soc. **77**, 5278 (1955).
[e] S. N. Ghosh, R. Trambarulo, and W. Gordy, J. Chem. Phys. **20**, 605 (1952).
[f] I. L. Karle and J. Karle, J. Chem. Phys. **18**, 963 (1950).
[g] T. T. Broun and R. L. Livingston, J. Am. Chem. Soc. **74**, 6084 (1952).

[1] R. S. Mulliken, J. Phys. Chem. **41**, 318 (1937).
[2] A. D. Walsh, Trans. Faraday Soc. **43**, 60 (1947).
[3] A. J. Petro, J. Am. Chem. Soc. **80**, 4230 (1958).
[4] R. W. Taft, Jr., in *Steric Effects in Organic Chemistry*, edited by M. S. Newman (John Wiley & Sons, Inc., New York, 1956), Chap. 13.
[5] M. G. Brown, Trans. Faraday Soc. **55**, 694 (1959); also, see C. C. Costain and B. P. Stoicheff, J. Chem. Phys. **30**, 777 (1959).
[6] S. L. Miller, L. C. Aamodt, G. Dousmanis, and C. H. Townes, J. Chem. Phys. **20**, 1112 (1952).
[7] C. A. Coulson in *Victor Henri Commemoratif Volume* (Maison Desoer, Liège, 1947–1948), p. 15.

Spectral and Reactivity Differences of Transition Metal Ions in H_2O and D_2O*

JACOB BIGELEISEN
Chemistry Department, Brookhaven National Laboratory, Upton, New York

(Received December 28, 1959)

HALPERN and Harkness[1] have recently reported shifts in the absorption maxima in the solution spectra of transition metal ions between H_2O and D_2O as solvents. They point out that the shifts are limited to those ions where the water enters the first coordination sphere of the cation. The shift between H_2O and D_2O as solvent is ascribed to the difference in ligand field splitting of the 3*d* electrons by virtue of the difference in dipole moments of H_2O and D_2O. In any complete theory such an effect would have to be considered. It is the purpose of this note to point out several additional effects which contribute to the spectral shifts and to the difference in chemical properties, both rate and equilibrium processes, of transition metal ions in H_2O and D_2O solvents.

If we consider the solvation of any solute in H_2O and D_2O, we recognize that D_2O will be a poorer solvent due to the greater strength of the hydrogen bonds in D_2O. Anions, which are capable of forming hydrogen bonds with the solvent, are more strongly solvated in D_2O than H_2O as compared with neutral solutes. This

hydrogen bonding of the water by anions will serve to decrease the stability of complexes between anions and cations in D_2O compared with H_2O. Additional contributions to the difference in solvent properties of H_2O and D_2O arise when a cation solute forms an inner sphere hydration complex. This interaction, which we will discuss in somewhat greater detail, will lead to a decreased stability of cations in D_2O compared with H_2O and will enhance complex formation in the former solvent as compared with H_2O. It will also lead to a spectral shift.

We restrict our attention to the first coordination sphere of the transition metal ions, where the formulas will be assumed to be $M(H_2O)_6^{Z+}$ and $M(D_2O)_6^{Z+}$ at equilibrium in H_2O and D_2O, respectively. (It is not clear whether the measurements of Halpern and Harkness correspond to $Cr(H_2O)_6^{3+}$ or $Cr(D_2O)_6^{3+}$ in D_2O.) A number of inner sphere complexes and solvates are sufficiently inert to exchange with the solvent that definite formulae of this type can be written.[2] If the lifetime of such a complex is long compared to 10^{-13} sec, there is associated with each cation a zero point energy. To the extent that the normal modes of the water molecules are not appreciably perturbed in forming the inner sphere complex, there are three internal vibrations per water molecule. Thirty-three vibrational modes arise from the translational and librational modes of six water molecules. The zero point energies of complexes $M(H_2O)_6^{3+}$ and $M(D_2O)_6^{3+}$ will differ by some 7500 cm^{-1}. The characteristic large breadth of the absorption bands of the hydrated transition metal ions, even in crystals at low temperatures, is indicative of coupling between the electronic motion and the ligands. The coupling and bonding of the ligands will be different in the various electronic states arising from the splitting of the *d* shell by the ligand field. A 1–4% change in the zero point energy will lead to a shift in the 0–0 transition sufficient to explain the spectral shifts observed by Halpern and Harkness. Additional shifts will result from changes in the vibrational quantum numbers accompanying the electronic transition. Small second order effects are to be expected when the solvent is in the outer coordination sphere, as in $Cr(C_2O_4)_3^{3-}$ and MnO_4^-.

The stretching vibrational frequencies associated with the individual water molecules of the inner sphere complex will be lower than that in the bulk liquid as a result of the electrostatic interaction of the cation with the water dipoles. A calculation of this effect by Sartori *et al.*[3] for a cation of charge 3+ hydrated by one water molecule leads to a decrease of about 400 cm^{-1} for each of the two stretching frequencies in the H_2O molecule. Within the approximations of this calculation, the zero point energy difference associated with the internal vibrations between H_2O and D_2O is reduced by about 120 cm^{-1} between a water molecule in the solvent and in the first coordination sphere. On formation of a complex between a cation and an anion, a water molecule from the first coordination sphere is presumably replaced by an anion. This makes the complex more stable in D_2O by 340 cal mol^{-1} from the change in the internal stretching vibrations. There will also be a contribution, presumably smaller, from the other vibrations. In any case, this is an appreciable fraction of the observed enchanced stability of $FeCl^{2+}$ in the two solvents.[4] The introduction of the negative charge of the anion into the first coordination sphere will asymmetrically screen the charge of the cation and reduce the interaction between the cation and the dipoles on the five other water molecules in the first coordination sphere. This will further increase the stability of complexes in D_2O compared to H_2O. A combination of some of these effects will also be involved in electron transfer reactions and could explain the reduced reaction rates observed[4–7] in D_2O compared with H_2O in the absence of a proton or hydrogen atom transfer mechanism.

A number of the points discussed here have been sharpened through helpful discussions with Dr. R. W. Dodson and Dr. N. Sutin.

* Research performed under the auspices of the U.S. Atomic Energy Commission.

[1] J. Halpern and A. C. Harkness, J. Chem. Phys. **31**, 1147 (1959).
[2] H. Taube, *Advances in Inorganic and Radiochemistry*, edited by H. J. Emeleus and A. G. Sharpe (Academic Press, Inc., New York, 1959), Vol. 1, pp. 1–50.
[3] G. Sartori, C. Furlani, and A. Damiani, J. Inorg. & Nuclear Chem. **8**, 119 1958).
[4] N. Sutin and R. W. Dodson, Paper 53, Division of Inorganic Chemistry, 136th meeting American Chemical Society, September, 1959.
[5] J. Hudis and R. W. Dodson, J. Am. Chem. Soc. **78**, 911 (1956).
[6] A. Zwickel and H. Taube, J. Am. Chem. Soc. **81**, 1288 (1959).
[7] A. Zwickel and H. Taube, Paper 54, Division of Inorganic Chemistry, 136th meeting American Chemical Society, September, 1959.

Proton Hyperfine Spectra of Diphenyl Picryl Hydrazyl*

YASUO DEGUCHI†

Department of Chemistry, Washington University, St. Louis, Missouri

(Received January 25, 1960)

MANY authors[1–5] have investigated the electron spin resonance spectra of diphenyl picryl hydrazyl (DPPH) either in the crystalline state or liquid solution. In diluted benzene solution of DPPH, five lines have been observed. This structure has been interpreted by Hutchison *et al.*[2] as arising from an equal coupling of the unpaired electron to the nuclei of the two central nitrogen atoms of DPPH. However, no hyperfine

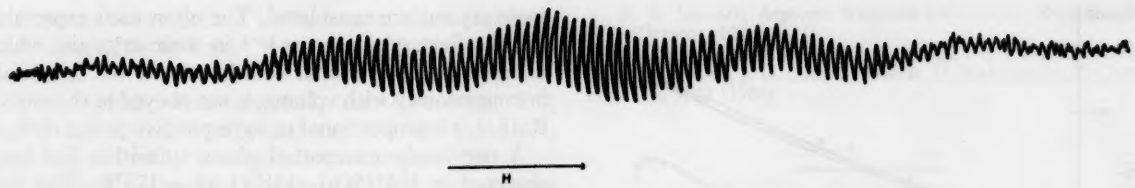

FIG. 1. Electron spin resonance spectrum of DPPH in tetrahydrofuran.

components arising from an interaction with the edge protons adjacent to the ring carbon atoms have been reported in DPPH solution.

It has been suggested[6] that the unpaired electron is localized on the center two nitrogens of DPPH. On the other hand, Beljers *et al.*[7] have detected an Overhauser effect for these protons, showing that there must be some small coupling to the unpaired electron.

If we dissolve DPPH in unpurified solvents which are commercially available, such as diethyl ether, 1,2-dimethoxyethane, tetrahydrofuran, cyclohexane, or carbon disulfide, we can only resolve hyperfine spectra due to nitrogen nuclear moment and none from the protons. But when we use the solvents which have been prepared by the same process as that of Lewis *et al.*[8], i.e., dried, degassed, and distilled in a vacuum line, we can observe well-resolved proton hyperfine lines. The broadening in the unpurified solvents is probably due to dissolved oxygen.

We prepared the liquid solution of DPPH using the aforementioned solvents in vacuum and observed the electron spin resonance spectra.

Figure 1 shows the resonance spectrum of DPPH in tetrahydrofuran in which the concentration of DPPH is less than 10^{-3} mole/liter. We can see proton hyperfine lines throughout the spectrum. The lines at the low-field side of the spectrum are sharper than those at the high-field side. This may be because of the anisotropic effect of the DPPH molecule.[9,10] We have obtained this spectrum for all solvents mentioned earlier. Further observation is now going on.

The author is much indebted to Professor S. I. Weissman for his helpful discussion and encouragement of the present work. He also wishes to express his heartful thanks to Professor J. Townsend for offering the opportunity to use the EPR apparatus which he constructed and supplying DPPH for the present work.

* This work was supported by the U.S. Air Force through the AIR Force Office of Scientific Research of the Air Research and Development Command under contract. Reproduction in whole or in part is permitted for any purpose of the U.S. Government.

† On leave from Kyoto University, Kyoto, Japan, Fulbright Scholar, 1958–1959.

[1] A. N. Holden, C. Kittel, F. R. Merritt, and W. A. Yager, Phys. Rev. **77**, 147 (1950).
[2] C. A. Hutchison, R. C. Pastor, and A. G. Kowalsky, J. Chem. Phys. **20**, 534 (1952).
[3] V. N. Cohen, C. Kikuchi, and J. Turkevich, Phys. Rev. **85**, 379 (1952).
[4] C. Kikuchi and V. N. Cohen, Phys. Rev. **93**, 394 (1954).
[5] G. E. Pake, S. I. Weissman, and J. Townsend, Discussions Faraday Soc. **19**, 147 (1955).
[6] D. J. E. Ingram, *Free Radicals* (Academic Press, Inc., New York, 1958), p. 142.
[7] H. G. Beljers, Van der Kint, and J. S. Van Wieringen, Phys. Rev. **95**, 1683 (1954).
[8] G. N. Lewis, D. Lipkin, and T. Magel, J. Am. Chem. Soc. **66**, 1579 (1944).
[9] H. M. McConnell, J. Chem. Phys. **25**, 709 (1956).
[10] D. Kivelson (to be published).

Nuclear Quadrupole Coupling in the Alums

GERALD BURNS

International Business Machines Research Laboratory, Poughkeepsie, New York

(Received December 30, 1959)

A NUMBER of alums have been shown to be ferroelectric by Pepinsky and co-workers.[1] The nuclear quadrupole coupling constant, eQq/h, for Al^{27} has been measured in several alums as part of a general program of studying nuclear quadrupole interactions in ferroelectrics. It is hoped that this will complement the large amount of work that has been done on the electron resonance in the alums[2] and the recent study of the pressure dependence of the paramagnetic resonance of Cr^{3+} in $NH_4Al(SO_4)_2 \cdot 12H_2O$ that has been done by Walsh.[3]

The temperature dependence of the Al^{27} eQq/h for four cubic α alums[4] is reported. The crystals were grown by slow evaporation from a water solution at room temperature.[5] They were mounted so that they could be rotated about a (100) direction which in turn was perpendicular to the magnetic field. In all cases the splittings were found to be proportional to $\sin 2\theta$ where θ is the angle between a (100) direction and H_0. Thus, the field gradient tensor is axially symmetric with the principal axis along a (111) direction. This is what one would have expected from the electron resonance results and is also in agreement with the results of Segleken and Torrey[6] who have measured eQq/h of Al in NH_4 and K alums at room temperature.

The results of the measurements are shown in Fig. 1. As can be seen from the diagram, in all cases eQq/h increases with increasing temperature. This is unusual

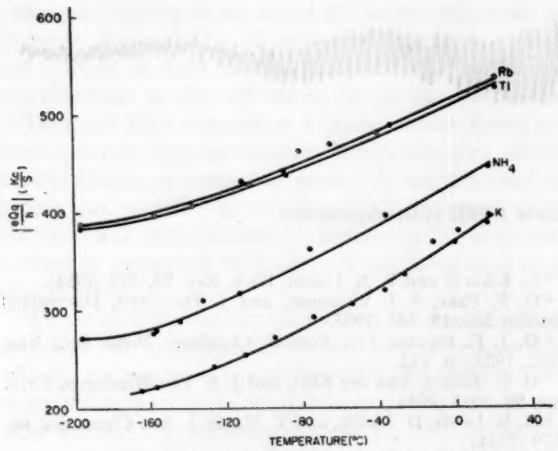

FIG. 1. The quadrupole coupling constant, eQq/h, for Al^{27} vs temperature in M Al $(SO_4)_2 \cdot 12H_2O$ for several M's. The circled points are for M=Rb.

and has only been observed in several other cases.[7-9] The room temperature values for NH_4 and K alums are in good agreement with the previous measurements.[6]

Assuming that the quadrupole interaction, $\nu = eQq/h$, depends only on the lattice frequencies, the volume and the temperature, then, for an isotropic crystal where the lattice frequencies depend only on the volume it can be shown[10,8]:

$$(1/\nu)(\partial\nu/\partial T)_P = -(\beta/\chi)(1/\nu)(\partial\nu/\partial P)_T + (1/\nu)(\partial\nu/\partial T)_V. \quad (1)$$

The volume coefficient of thermal expansion β has been measured by Klug and Alexander[11] and the bulk compressibility χ by Bridgman[12] for several alums. Values typical of all the alums are 3×10^{-5} deg^{-1} and 6.3×10^{-6} kg^{-1} cm^2 for β and χ, respectively. From Fig. 1 $(1/\nu)(\partial\nu/\partial T)_P = +2.3\times10^{-3}$ deg^{-1} at room temperature is a typical value for all four alums.

The first term on the right of Eq. (1) can be estimated by noting that the largest reported value of $(1/\nu)(\partial\nu/\partial P)_T$ is 7.7×10^{-6} kg^{-1} cm^2 for Na in $NaClO_3$[10] and that other values lie between this value and one that is an order of magnitude smaller,[8,10,13-15] Assuming this largest value is of the order of magnitude to be expected for the alums, one arrives at a value for $(\beta/\chi)(1/\nu)(\partial\nu/\partial P)_T$ which is two orders of magnitude smaller than the observed value of $(1/\nu)(\partial\nu/\partial T)_P = +2.3\times10^{-3}$ deg^{-1}. Thus, it appears probable that $(1/\nu)(\partial\nu/\partial T)_V \approx 1/\nu(\partial\nu/\partial T)_P = +2.3\times10^{-3}$ deg^{-1} at room temperature. Walsh[3] finds similar behavior for the zero field splitting δ by directly measuring $(\partial\delta/\partial P)_T$, i.e., $(1/\delta)(\partial\delta/\partial T)_P \approx (1/\delta)(\partial\delta/\partial T)_V = +5.6\times10^{-3}$ deg^{-1} at room temperature.

Theoretical[16] calculations on the basis of molecular torsional vibrations yield negative values for $(1/\nu)(\partial\nu/\partial T)_V$. It is not clear what one would predict when the many low-frequency lattice vibrations[17] in this ionic crystal are considered. The often used expression for the field gradient $q \propto V^{-1}$ in ionic crystals, which assumes all the internal coordinates of the ions scale homogeneously with volume, is not obeyed in the alums. Rather, q is proportional to some positive power of V.

A previously unreported phase transition has been observed in $KAl(SO_4)_2 \cdot 12H_2O$ at -175°C. The low temperature behavior of this and several other alums that have phase transitions is being studied. The electron resonance of Cr^{3+} doped alums is also being studied.

[1] R. Pepinsky, F. Jona, and G. Shirane, Phys. Rev. **102**, 1181 (1956); and R. Pepinsky (private communication).
[2] See K. D. Bowers and J. Owen, Repts. Progr. in Phys. **18**, 305 (1955).
[3] W. M. Walsh, Phys. Rev. **114**, 1485 (1959). I wish to thank Dr. Walsh for communicating his results prior to publication.
[4] H. Lipson and C. A. Beevers, Proc. Roy. Soc. (London) **148**, 664 (1935). H. Lipson, Proc. Roy. Soc. (London) **151**, 347 (1935).
[5] I am indebted to Dr. T. Dunne and M. L. Wang for growing the crystals and to J. E. Scardefield for cutting them.
[6] W. G. Segleken and H. C. Torrey, Phys. Rev. **98**, 1537 (1955). See also M. H. Cohen and F. Reif, *Solid State Physics* (Academic Press, Inc., New York, 1956), Vol. 5.
[7] R. P. Hamlen and W. S. Koski, J. Chem. Phys. **25**, 360 (1956); S. Ogawa, J. Phys. Soc. Japan **12**, 618 (1958).
[8] R. G. Barns and R. D. Engardt, J. Chem. Phys. **29**, 248 (1958).
[9] G. Burns, Bull. Am. Phys. Soc. Ser. II, **3**, 371 (1958). A full account of the results on GASH and its isomorphic compounds including electron resonance is in preparation.
[10] H. S. Gutowsky and G. A. Williams, Phys. Rev. **105**, 464 (1957).
[11] H. P. Klug and L. Alexander, J. Am. Chem. Soc. **64**, 1819 (1942).
[12] P. W. Bridgman, Proc. Am. Acad. Arts Sci. **64**, 51 (1929).
[13] T. Kushida, G. B. Benedek, and N. Bloembergen, Phys. Rev. **104**, 1364 (1956).
[14] D. Dautreppe and B. Dreyfus, Compt. rend. **241**, 795 (1955).
[15] D. Dautreppe and B. Dreyfus, Compt. rend. **242**, 766 (1956).
[16] H. Bayer, Z. Physik **130**, 227 (1951).
[17] V. M. Padmanabhan, Proc. Indian Acad. Sci. **34A**, 396 (1951).

Luminescence Spectrum of $PmCl_3$*

JOHN G. CONWAY AND JOHN B. GRUBER

Lawrence Radiation Laboratory, University of California, Berkeley, California

(Received January 29, 1960)

MANY rare earth compounds are known to fluoresce. However, promethium, element 61, has not been extensively studied, in fact, only the solution and emission spectra have been observed.[1-5] The difficulties stem from the fact that promethium is intensely radioactive and is not available from natural sources. Promethium is available in large quantities as a fission product of uranium. The isotope of promethium that is available in quantities is Pm^{147} which has a 2.6-year half-life and a 0.22-Mev β^- ray. The decay product is stable Sm^{147}. Carlson and Dieke have noted that most

rare earths fluoresce in a $LaCl_3$ matrix.[6] It is therefore very reasonable to expect that promethium would also fluoresce.

Two crystals were prepared, one containing 1 g $LaCl_3$ and 20 mg $PmCl_3$ and the second, 1 g $LaCl_3$ and 2 mg of $PmCl_3$. The crystals were prepared following the method outlined by Gruen *et al.*[7] The promethium was purified by ion-exchange techniques before incorporation into the crystal.

These crystals exhibited several interesting features. (a) The crystals are self-luminescent. In this case the luminescence is activated by the energy given to the crystal by the radioactive decay. (b) As the crystal cools to room temperature, it gradually blackens. This darkening saturates in about ½ to 1 hr, depending on the concentration of promethium. The crystal is almost opaque at saturation time. The darkening may be bleached with heat or light. We believe the darkening is due to the trapping of free electrons into crystal defects (color centers). The source of the electrons is the soft β^-'s emitted by the decaying Pm^{147}. The β^-'s are degraded in the crystal and finally captured in the defects. (c) The crystal fluoresces. In the 2% crystal, the multiplet at 8300 A is intensified by irradiation with ultraviolet light. This multiplet is more than 10 times as intense under ultraviolet irradiation as in self-luminescence. This of course depends on the intensity of the incident ultraviolet radiation. The visible spectrum is not noticably enhanced by ultraviolet irradiation. In the 0.2% crystal, all lines were intensified by ultraviolet irradiation.

Spectra were taken on a Hilger $f/4$ spectrograph with quartz optics. Under this low dispersion, 34 lines could be seen on the photographic plate. Most of the lines were in seven groupings. The groupings of the promethium luminescence lines were at 4610, 4980, 5410, 5900, 6600, 7420, and 8300 A. Spectra of $SmCl_3$ in $LaCl_3$ were also taken to determine the extent to which this element had grown into the promethium crystal. The strong fluorescent lines of samarium, which appear in a region free of promethium lines, were not detected, and it is concluded that all the luminescence is due to promethium.

The luminescence is due to transitions from excited levels to the ground-state multiplet which according to Hund's rules is a ^5I having J values of 4, 5, 6, 7, and 8, with $J=4$ the lowest. The variation of intensity of the 8300-A multiplet should be an aid in analyzing this spectrum. The fluorescence and absorption spectrum are being investigated with higher-resolution instruments and at low temperatures.

* This work was done under the auspices of the U.S. Atomic Energy Commission.

[1] C. Feldman, J. Am. Chem. Soc. **71**, 3841 (1949).
[2] D. Timma, J. Opt. Soc. Am. **39**, 898 (1949).
[3] G. W. Parker and P. M. Lantz, J. Am. Chem. Soc. **72**, 2834 (1950).
[4] W. F. Meggers, B. F. Scribner, and W. R. Bozman, J. Research Natl. Bur. Standards **46**, 85 (1951).
D. S. Stewart, Argonne National Laboratory Report ANL 4812 (October, 1956).
[6] E. Carlson and G. H. Dieke, J. Chem. Phys. **29**, 229 (1958).
[7] D. M. Gruen, J. G. Conway, and R. D. McLaughlin, J. Chem. Phys. **25**, 1102 (1956).

Photooxidation of Biacetyl

GERALD B. PORTER

Department of Chemistry, University of British Columbia, Vancouver, Canada

(Received December 28, 1959)

THE photochemistry and luminescence of biacetyl have been interpreted in terms of excited singlet and triplet electronic states.[1-3] The only piece of information still missing concerns the relative importance of internal conversion (intramolecular degradation) of these two states. Unambiguous evidence can only come from a comparison of natural and experimental lifetimes. The photooxidation studies reported here provide evidence that internal conversion of the singlet state is negligible.

Quenching of phosphorescence but not of fluorescence by oxygen shows that oxygen interacts only with the triplet state under normal experimental conditions. The photooxidation has been studied at a wavelength, 4358 A, at which there is no photodissociation into radicals in the absence of oxygen. As in an earlier study of this system at shorter wavelength, quantum yields of products showed considerable irreproducibility.[4] The major product was carbon dioxide and there was a correspondingly large consumption of oxygen (see Table I). Carbon monoxide and methanol quantum yields were about one-fourth of the carbon dioxide quantum yield. Formaldehyde, acetone, acetaldehyde, and some high molecular weight substances were minor products, but were not analyzed quantitatively.

Since there is no evidence for a chain reaction in this system at 30°C,[4] the relatively high quantum yields of products indicate triplet molecules are formed with almost unit efficiency. In this case, the measured lifetime, 1.80×10^{-3} sec,[5] and the quantum efficiency, 0.145,[6] for phosphorescence can be combined to give 1.2×10^{-2} sec for the natural lifetime of the triplet state.

TABLE I. Quantum yields in biacetyl photooxidation ($t=30$°C, biacetyl=30 mm, $\lambda=4358$ A).

P_{O_2}(mm)	$-\Phi_{O_2}$	Φ_{CO_2}	Φ_{CO}	Φ_{CH_3OH}
0.10	1.2	0.95	0.17	...
0.23	2.3	1.49	0.34	...
0.20	1.9	1.28	0.33	...
1.27	2.1	...	0.15	0.13

Further, since the natural lifetime of the singlet state is 8.5×10^{-6} sec,[7] estimated from the integrated absorption coefficient, and the fluorescence yield is 2.5×10^{-3} the rate constant for intersystem crossing (singlet to triplet) is ca 4×10^{7} sec.$^{-1}$

This research was supported in part by a grant from The Petroleum Research Fund administered by the American Chemical Society. Grateful acknowledgment is hereby made to the donors of said fund. The research was also sponsored in part by the National Research Council of Canada.

[1] See W. A. Noyes, Jr., G. B. Porter, and J. E. Jolley, Chem. Revs. **56,** 49 (1956), for earlier references.
[2] H. Okabe and W. A. Noyes, Jr., J. Am. Chem. Soc. **79,** 801 (1957).
[3] J. Heicklen, J. Am. Chem. Soc. **81,** 3863 (1959).
[4] R. P. Taylor and F. E. Blacet, Ind. Eng. Chem. **48,** 1505 (1956).
[5] W. E. Kaskan and A. B. F. Duncan, J. Chem. Phys. **18,** 427 (1950).
[6] G. M. Almy and P. R. Gillette, J. Chem. Phys. **11,** 188 (1943).
[7] G. M. Almy and S. Anderson, J. Chem. Phys. **8,** 805 (1940).

Microwave Spectrum of *trans*-Crotononitrile

VICTOR W. LAURIE*
National Bureau of Standards, Washington 25, D. C.

(Received January 25, 1960)

As part of a program of study of molecules with hindered internal rotation the microwave spectrum of crotononitrile, *trans*-$H_3CCH{=}CHCN$, has been investigated in the region from 13–36 kMc.

The spectrograph was a conventional apparatus employing 80 kc Stark modulation and has been described elsewhere.[1]

The spectrum is characteristic of a near-prolate symmetric rotor and contains groups of broad overlapping absorption lines spaced at intervals of ~4500 Mc. These correspond to parallel transitions grouped about $(b+c)(J+1)$ where $J\rightarrow J+1$. Most of the lines are essentially K degenerate and exhibit very rapid first order Stark effects. A number of lines have been measured and assigned to the ground vibrational state on the basis of a slightly asymmetric rigid rotor with a small centrifugal distortion correction. The identified lines and their measured frequencies are given in Table I together with frequencies calculated from the rotational constants of Table II. The fit is within the estimated experimental uncertainty of $\leq$0.15 Mc. The spectrum also contains a number of bands attributable to excited vibrational states, but no detailed analysis of these has been carried out. Because of the smaller component of dipole moment, perpendicular transitions are considerably reduced in intensity and none have been identified.

TABLE I. Identified transitions of crotononitrile.

$J\rightarrow J+1$	K	obs (Mc)	calc[a]
	0	13475.89	13475.91
	1	13324.45	13323.97
2→3	1	13629.06	13629.46
	2	13477.2[b]	13477.08
	2		13477.97
	0	17966.75	17966.83
	1	17765.04	17765.00
	1	18172.15	18172.33
3→4	2		17969.23
	2	17970.0[b]	17970.34
	3		17971.48
	0	22456.90	22456.85
	1	22205.78	22205.79
	1	22714.99	22714.94
4→5	2	[c]	22461.21
	2	[c]	22465.56
	3	22463.68	22463.07
	4		22463.69
	0	26945.74	26945.74
	1	26646.22	26646.26
	1	27257.39	27257.24
	2	26953.3[c]	26952.97
	2	26961.1[c]	26960.57
	3	26956.48	26955.89
5→6	4		26956.50
	5	26957.60	26957.48
	0	35919.24	35919.24
	1	35526.03	35526.07
	1	36340.65	36340.61
	2	35936.2[c]	35935.64
	2	25954.3[c]	35953.89
7→8	3	35942.6[c]	35941.91
	4		35942.24
	5	35943.5[c]	35943.59
	6	35945.6[c]	35945.57
	7	35948.4[c]	35948.04

[a] No allowance has been made for possible hyperfine or internal rotation effects on the position of the peak intensities.
[b] Broad unresolved clump undoubtedly containing hyperfine and internal rotation splittings.
[c] Measurement interfered with by Stark components of nearby lines.

None of the lines studied showed fine structure arising from the quadrupole moment of the N^{14} nucleus or splitting from the internal rotation of the methyl group although all of the lines were rather broad. It is probable, however, that the $K=2$ lines would exhibit such splittings if they could be clearly resolved from the other K components. Of the cleanly resolved transitions the most sensitive to internal rotation effects are

TABLE II. Rotational constants[a] and moments of inertia[b] for ground vibrational state of crotomonitrile.

a	$38._2\times10^3$	I_a	1.3_2
b	2297.05	I_b	220.078
c	2195.22	I_c	230.287
D_J	$0.3_4\times10^{-3}$	D_{JK}	-12.6×10^{-3}

[a] In Mc.
[b] In amu A^2 with a conversion factor of 5.05531×10^5 Mc amu A^2 used.

those where $J=2\rightarrow3$, $K=1$. If a minimum possible resolution of 0.5 Mc is assumed, failure to observe any splitting implies a lower limit for the internal barrier of 2.1 kcal/mole. This may be compared with values of 1.98, 2.20, 2.21, and 2.44 kcal/mole found in propene,[2] *trans*-fluoropropene,[3] isobutene,[4] and 2-fluoropropene,[5] respectively.

The present data are insufficient for a complete structural determination, but it might be pointed out that the observed moments of inertia are consistent with r_{CC} $(CH_3)=1.49$ A, $r_{C=C}=1.34$ A, and other parameters assumed to be the same as in propene[2] or vinyl cyanide.[6]

* National Research Council—National Bureau of Standards Research Associate, 1957–1959.

[1] D. R. Lide, Jr., D. E. Mann, and R. M. Fristrom, J. Chem. Phys. **26**, 734 (1957).
[2] D. R. Lide, Jr., and D. E. Mann, J. Chem. Phys. **27**, 868 (1957).
[3] S. Siegel, J. Chem. Phys. **27**, 989 (1957).
[4] V. W. Laurie, Symposium on Molecular Structure and Spectroscopy, Columbus, Ohio, June, 1959.
[5] L. Pierce and J. M. O'Reilly, J. Mol. Spectroscopy **3**, 536 (1959).
[6] C. C. Costain and B. P. Stoicheff, J. Chem. Phys. **30**, 777 (1959).

On the Correlation Correction to the Fermi-Thomas-Dirac Equation*

HERBERT PAYNE

Physics Department, University of Detroit, Detroit, Michigan

(Received January 11, 1960)

IN the statistical model of the atom the energy components of the system—the kinetic, exchange, potential, and correlation energies—may be expressed as[1]

$$E_k=\kappa_k\int\rho^{5/3}dv,$$

$$E_a=-\kappa_a\int\rho^{4/3}dv,$$

$$E_p=-\int\rho(V_k+\tfrac{1}{2}V_e)dv,$$

and

$$E_w=-\int\rho g(\rho^{\frac{1}{2}})dv,$$

where $\rho(r)$ represents the electronic density at distance r from the nucleus. Atomic units will be used throughout.

Gombas[2] has proposed that inasmuch as the correlation effect assumes importance near $r=r_0$, the atomic radius, g be approximated by

$$g^*=g(\rho_0^{\frac{1}{2}})+\lambda_0(\rho^{\frac{1}{2}}-\rho_0^{\frac{1}{2}}), \qquad (1)$$

where $\rho_0=\rho(r_0)$ and $\lambda_0=|\,dg/d\rho^{\frac{1}{2}}|_{\rho=\rho_0}$. With the substitution of $\kappa_a'=\kappa_a+\lambda_0$ for κ_a the form of the Fermi-Thomas-Dirac equation, as well as of the boundary conditions given by Jensen, is preserved. This enables one to use existing tables[3] of solutions to the Fermi-Thomas-Dirac equation. Some of the r_0 values reported by Gombas, who used the Wigner relation for g, are given in Table I.

TABLE I. Atomic radii in a.u.

Atom	r_0 from FTD equation	r_0 from FTD equation with correlation correction from: Gombas	Eqs. (1) and (2)	Eqs. (3) and (2)
Ar	4.2818	4.05	3.950	4.102
Kr	4.5275	4.16	4.189	4.360
Xe	4.6577	4.33	4.315	4.497

Tomishima[4] has derived $g(\rho_0^{\frac{1}{2}})$ and λ_0 from the relation

$$g=0.0645+0.01565\ln\rho^{\frac{1}{2}}+(0.00016/\rho^{\frac{1}{2}}), \qquad (2)$$

obtained from Pines' expression[5] for the correlation energy per electron in an electron gas of density ρ. Application of the variational principle upon which the Fermi-Thomas-Dirac equation and Jensen's boundary conditions rest gives $\rho_0^{\frac{1}{2}}=0.146$ and $\lambda_0=0.0999$.

In extending expression (1) to

$$g^*=g(\rho_0^{\frac{1}{2}})+\lambda_0(\rho^{\frac{1}{2}}-\rho_0^{\frac{1}{2}})+\mu_0(\rho^{\frac{1}{2}}-\rho_0^{\frac{1}{2}})^2, \qquad (3)$$

where $\mu_0=\frac{1}{2}\,|\,d^2g/d\rho^{\frac{1}{2}\,2}|_{\rho=\rho_0}$, one may still make use of Thomas' tables by employing $Z'=Z(\kappa_a/\kappa_a')^{\frac{1}{2}}$, $N'=N(\kappa_a/\kappa_a')^{\frac{1}{2}}$, and $r_0'=r_0(\kappa_a'/\kappa_a)^{\frac{1}{2}}(\kappa_k/\kappa_k')$, where $\kappa_k'=\kappa_k-\mu_0$ and $\kappa_a'=\kappa_a+\lambda_0-2\rho_0^{\frac{1}{2}}\mu_0$, in place of Z, N, and r_0. From Eq. (2) one finds $\mu_0=-0.317$.

Since formula (1) overcorrects for correlations for $r<r_0$ while formula (3) undercorrects—even leading to a reversal of sign at higher densities—their use should provide limiting values for an atomic property determined from the statistical model with correlations. Between these values should lie that obtained after the more accurate treatment of correlations proposed by Lewis.[6]

In Table I are listed the values of r_0 determined for three atoms from Thomas' tables without the correlation correction and with the correlation correction provided by fomulas (1) and (3) with the foregoing values of $\rho_0^{\frac{1}{2}}$, λ_0, and μ_0.

For positive ions it turns out that the value of r_0

as calculated with the use of Eq. (3) exceeds the value from the uncorrected Fermi-Thomas-Dirac equation. This seems to invalidate for these cases the simplified relations (1) and (3).

* Supported by the Physics Branch of the Office of Naval Research.

[1] P. Gombas, *Die Statistische Theorie des Atoms und ihre Anwendungen* (Springer-Verlag, Vienna, 1949).
[2] P. Gombas, Z. Physik **121**, 523 (1943).
[3] L. H. Thomas, J. Chem. Phys. **22**, 1758 (1954).
[4] Y. Tomishima, Progr. Theoret. Phys. (Kyoto) **22**, 1 (1959).
[5] D. Pines, *Solid State Physics*, edited by F. Seitz and D. Turnbull (Academic Press, Inc., New York, 1955), Vol. 1, p. 397.
[6] H. W. Lewis, Phys. Rev. **111**, 1554 (1958).

Structure and Magnetic Properties of $LiCuCl_3 \cdot 2H_2O$

P. H. Vossos, L. D. Jennings, and R. E. Rundle

Institute for Atomic Research and Department of Chemistry, Iowa State University of Science and Technology, Ames, Iowa*

(Received June 17, 1959)

PRELIMINARY x-ray and magnetic studies of $LiCuCl_3 \cdot 2H_2O$ have produced results of unusual interest, and possibly of significance to the understanding of magnetic interactions in crystals.

The red-brown, monoclinic crystals have lattice constants $a=6.078$, $b=11.145$, $c=9.145$A, $\beta=108°50'$.

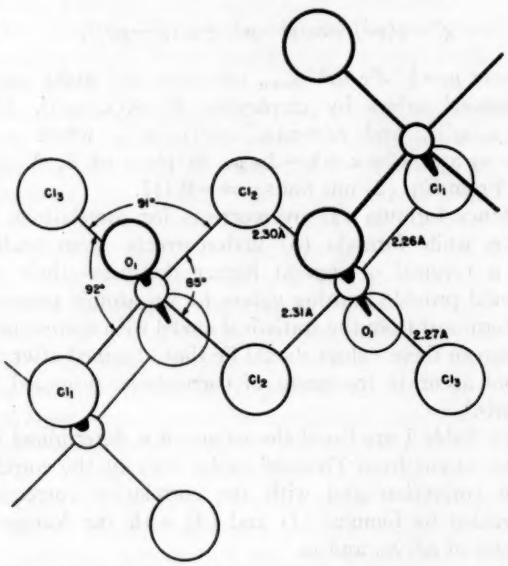

FIG. 1. The structure of $LiCuCl_3 \cdot 2H_2O$.

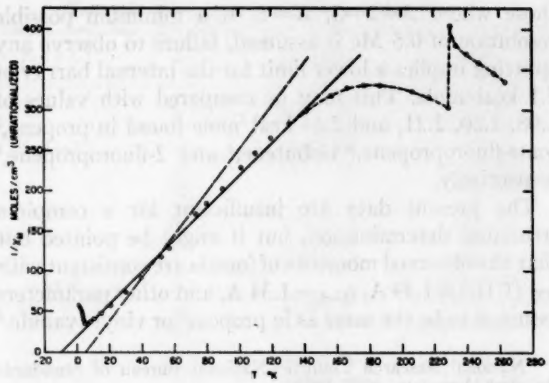

FIG. 2. The reciprocal molar susceptibility of $LiCuCl_3 \cdot 2H_2O$ vs temperature. The solid line shows the slope to be expected if the two Cu ions in a dimer form a triplet. The straight dashed line shows the slope expected for independent ions, $g=2$. Circles represent experimental determination.

Systematic absences establish the space group as $P2_1/c$; the density, 2.36 g/cc, requires that $z=4$.

Positional parameters, omitting hydrogen and lithium, have been refined by minimizing the function

$$R_3=\sum w(\,|F_0|-|F_c|\,)^2/\sum wF_0^2,$$

using 2076 reflections recorded with a Weissenberg camera and Mo radiation;

$$R_1=\sum(\,|F_0|-|F_c|\,)/\sum|F_0|$$

is 0.128.

Prominent in the structure, Fig. 1, are planar $Cu_2Cl_6^{--}$ ions with symmetrical Cu—Cl—Cu bridges; the ions are weakly linked by longer Cu···Cl bonds to form chains. The copper acetate hydrate dimers appear to contain direct Cu—Cu bonds, and the ground state is a singlet about 300 cm^{-1} below the triplet state.[1,2] The $Cu_2Cl_6^{--}$ ion is structurally different, and there are reasons to expect a ground state triplet.[3]

The triplet state is supported by the paramagnetism of $LiCuCl_3 \cdot 2H_2O$ to 5.9°K where it becomes magnetically ordered (Fig. 2). A ground state singlet for the dimer should produce diamagnetism at low temperature, as in copper acetate. The unlikely possibility of independent magnetic electrons in the dimer would lead to the dashed curve of Fig. 2 if $g=2$.[4] The experimental slope of $1/\chi_m$ vs T, is closer to that expected for the triplet state (solid curve).

The initial susceptibility of this salt is not reversible at temperatures above 220°K; the points shown connected with a short dashed line in Fig. 2 are typical ones obtained on heating. (The crystal structure is unchanged in this region.)

This work suggests that anhydrous $CuCl_2$,[5] and other similarly bridged structures (infinite planar chains, symmetrically bridged) should contain ferromagnetically aligned chains. (The antiferromagnetism

of $CuCl_2$ [6] must, then, come from interactions between chains.) It has also been suggested that for certain antiferromagnetic iron group halides with layered structures the nearest neighbor interactions (within layers) are ferromagnetic[7]; since these are symmetrically bridged structures the causes are presumably related.[3]

Ferromagnetic alignment in symmetrical, strongly bridged halides is to be distinguished from alignment in asymmetric, weakly bridged halides, e.g., $CuCl_2 \cdot 2H_2O$,[8] where the nearest neighbor interaction is antiferromagnetic.[9] Such weaker bridges are found between dimers in $LiCuCl_3 \cdot 2H_2O$, (Fig. 1) so that in the dimer chains an alignment $\alpha\alpha\beta\beta\alpha\alpha\cdots$ is to be expected.

Further studies on $LiCuCl_3 \cdot 2H_2O$ are to be made by neutron diffraction and an NMR method recently suggested.[10]

* Contribution No. 770. Work was performed in the Ames Laboratory of the U.S. Atomic Energy Commission. Taken in part from the MS thesis of Peter H. Vossos, Iowa State College, 1958.

[1] B. Bleaney and K. D. Bowers, Proc. Roy. Soc. (London) **A214**, 451 (1952).

[2] J. N. van Niekerk and F. R. L. Schrening, Acta Cryst. **6**, 227 (1953).

[3] R. E. Rundle (to be published).

[4] In a preliminary study of ESR, Dr. Michael Baker at the Clarendon Laboratory, Oxford, has found that extreme values of g are 2.13 and 2.10 in the ac place, 2.23 and 2.06 in the ab plane.

[5] A. F. Wells, J. Chem. Soc. (L) **1947**, 1670.

[6] W. J. deHaas and C. J. Gorter, Comm. Phys. Lab. Leiden No. 215a (1931); C. Starr, F. Bitter, and A. R. Kaufmann, Phys. Rev. **58**, 977 (1940).

[7] L. Landau, Physik Z. Sowjet union **4**, 675 (1933). Neutron diffraction has recently confirmed this supposition [M. K. Wilkinson, J. W. Cable, E. O. Wollan, and W. C. Koehler, Phys. Rev. **113**, 497 (1959)].

[8] D. Harker, Z. Krist **93**, 136 (1938).

[9] N. J. Poulis and G. E. G. Hardeman, Physica **18**, 201 (1952).

[10] R. E. Rundle, J. Am. Chem. Soc. **79**, 3372 (1957).

Energy Levels of a Slightly Asymmetric Top

JAMES A. NORRIS* AND VICTOR W. LAURIE†

Department of Chemistry, University of California, Berkeley 4, California

(Received December 28, 1959)

THE energy levels for the rigid asymmetric rotor can be written in the form[1]

$$W=\tfrac{1}{2}(B+C)J(J+1)+[A-\tfrac{1}{2}(B+C)]w. \quad (1)$$

Whenever the asymmetry is small[2] w may be expanded as a series

$$w=K^2+c_1b_p+c_2b_p^2+c_3b_p^3+\cdots \quad (2)$$

where $b_p=(C-B)/(2A-B-C)$, and c_n is a function of the energy level under consideration. Schwendeman[3] has tabulated the coefficients through c_5 for values of J through 40. For high values of the quantum number K convergence is very good and the expansion is a good approximation even in the case of fairly large asymmetry. The levels $J_{0,J}$ and $J_{2,J-2}$ are strongly perturbed by asymmetry, however, and require the inclusion of higher order terms for rather small values of the asymmetry parameter. Since these levels occur frequently in microwave spectra, it has been found convenient to tabulate c_6 for $J=5$ through 40. These coefficients are given in Table I under the headings of $K=0$ and $K=2$. Coefficients in a given row are to be multiplied by the power of 10 given in the last column. Values of c_6 for other levels are much smaller and often can be neglected even when c_6 makes an important contribution to the $J_{0,J}$ and $J_{2,J-2}$ levels.

TABLE I. Sixth order coefficients in expansion of energy levels of asymmetric rotor.

J	$K=0$	$K=2$	$\times 10^n$
5	−0.1344803	0.1300071	06
6	−0.1028274	0.1011189	07
7	−0.5840270	0.5787353	07
8	−0.2658561	0.2644570	08
9	−0.1019890	0.1016629	09
10	−0.3414187	0.3407349	09
11	−0.1022772	0.1021466	10
12	−0.2793704	0.2791417	10
13	−0.7058849	0.7055186	10
14	−0.1668500	0.1667970	11
15	−0.3722673	0.3722007	11
16	−0.7897306	0.7896660	11
17	−0.1602487	0.1602467	12
18	−0.3125801	0.3125918	12
19	−0.5885659	0.5886097	12
20	−0.1073588	0.1073697	13
21	−0.1902868	0.1903100	13
22	−0.3285847	0.3286297	13
23	−0.5540425	0.5541247	13
24	−0.9140310	0.9141745	13
25	−0.1477957	0.1478199	14
26	−0.2345949	0.2346344	14
27	−0.3660402	0.3661032	14
28	−0.5621158	0.5622142	14
29	−0.8505262	0.8506767	14
30	−0.1269242	0.1269469	15
31	−0.1869754	0.1870090	15
32	−0.2721194	0.2721685	15
33	−0.3915519	0.3916226	15
34	−0.5573979	0.5574987	15
35	−0.7855141	0.7856562	15
36	−0.1096477	0.1096675	16
37	−0.1516791	0.1517065	16
38	−0.2080367	0.2080743	16
39	−0.2830300	0.2830810	16
40	−0.3821023	0.3821710	16

* National Science Foundation Predoctoral Fellow 1959–1960.
† National Science Foundation Postdoctoral Fellow 1959–1960.

[1] For example, see C. H. Townes and A. L. Schawlow, *Microwave Spectroscopy* (McGraw-Hill Book Company, Inc., New York, 1955), p. 83.

[2] The discussion is appropriate to a near prolate rotor, but similar considerations hold for the near oblate case. See reference 1 for more detail and further references.

[3] R. H. Schwendeman, J. Chem. Phys. **27**, 986 (1957).

C^{13} Hyperfine Splitting in Benzonitrile Negative Ion*

RAYMOND L. WARD

University of California, Ernest O. Lawrence Radiation Laboratory, Livermore, California

(Received January 29, 1960)

BENZONITRILE negative ion has been prepared with potassium in 1,2-dimethoxyethane at temperatures below −50°C. The hyperfine structure of this negative ion was observed at temperatures below −50°C in a conventional spectrometer using 250 kcs field modulation.

The hyperfine pattern in Fig. 1(A) consists of 10 resolvable lines extending over 20 gauss measured from the centers of extreme lines. A detailed analysis of the spectrum has not been made at this time, but information about the C^{13} splitting in the nitrile group has been obtained.

Benzonitrile, containing 64 atom % C^{13} in the nitrile group, has been synthesized and the negative ion prepared. The resulting spectrum in Fig. 1(B) is therefore a superposition of the isotopically substituted species and the unsubstituted species. This spectrum extends over 26.4 gauss. Since C^{13} has spin $\frac{1}{2}$, its hyperfine splitting doubles all lines. The C^{13} splitting is 6.4 gauss.

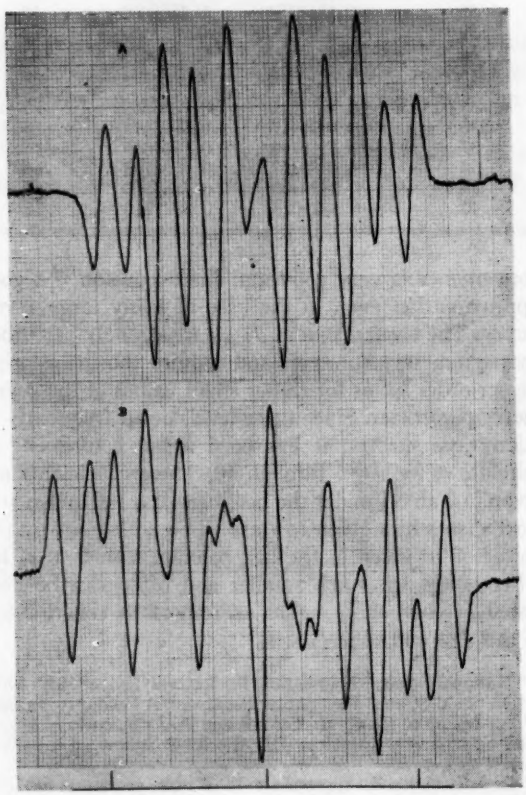

FIG. 1. The derivative of the absorption for the electron spin resonance spectrum of benzonitrile negative ion (A) and 64% C^{13}- and 36% C^{12}-benzonitrile negative mixture (B) prepared with K and 1,2-dimethoxyethane at −50°C.

he spin density at the C^{13} nucleus is therefore 0.051 compared to the hydrogen atom in its $1S$ state. A carbon spin density of 4.25[1] has been estimated for a configuration $2s(2p)^3$.

I wish to thank Dr. R. E. Anderson for his assistance with the 250 kc field modulation system.

* This work was performed under the auspices of the U.S. Atomic Energy Commission.

[1] This is the value for a $2S$ function with $z=3.25$.

Microwave Spectrum of O^{18} Formic Acid and Structure of Formic Acid*

GEORGE HSING KWEI†

Mallinckrodt Chemical Laboratory, Harvard University, Cambridge, Massachusetts

AND

R. F. CURL, JR.‡

Department of Chemistry, The Rice Institute, Houston, Texas

(Received January 18, 1960)

THE microwave spectra of $HCO^{18}OH$ and $HCOO^{18}H$ have been assigned and the rotational constants have been combined with data of Lerner *et al.*[1] to determine the structure of formic acid. Several structural studies have been made, but there are large discrepancies in the results[1,2] (Table I). Although the C^{13} and the deuterated species were studied in the previous microwave work of Lerner *et al.*, their structural calculations were necessarily subject to the serious limitation that most of the errors must be absorbed in the oxygen coordinates.

The two O^{18} species were prepared by hydrolyzing trimethyl orthoformate with 65% H_2O^{18}. The methyl formate produced was hydrolyzed with equivalent amounts of sodium methoxide and 65% H_2O^{18}. The resulting sodium formate was dried and dissolved in an excess of dichloracetic acid. The O^{18} formic acid was pumped off and vacuum distilled. Since some water is always present, a mixture of both isotopic species is obtained by any method.

A conventional Stark effect microwave spectrometer[3] with a modulation frequency of 100 kc was used in this work. The frequencies of measured rotational transitions and the rotational constants of the two isotopic species are listed in Table II. The calculated transition frequencies were obtained from the observed rotational constants. The rotational constants B and C were fitted to the 0_{00}–1_{01} and 1_{10}–2_{11} transitions. Since we did not measure any b-type transitions, the rotational constants A were calculated from the B and C and from the iner-

TABLE I. Structure of formic acid.

	Schomaker and O'Gorman	Karle and Karle	Lerner *et al.*	This work
r_{C-H}(A)	1.09[a]	1.09[a]	1.085±0.02	1.097±0.005
$r_{C=O}$(A)	1.213±0.026	1.23±0.01	1.245±0.002	1.202±0.010
r_{C-O}(A)	1.368±0.034	1.36±0.01	1.312±0.002	1.343±0.010
r_{O-H}(A)	0.97[a]	0.97±0.05	0.95±0.02	0.972±0.005
∠OCO	123.5±3°	122.4°±1°	124° 18′±10′	124° 53′±1°
∠HC=O	...	...	...	124° 8′±2°
∠COH	...	105°[a]	107° 48′±1°	106° 19′±1°
r_{O-O}(A)	2.275±0.025	2.27±0.005	2.261±0.004	2.257±0.005

[a] Assumed.

tial defect given by Trambarulo *et al.*[4] for normal formic acid. The discrepancies between calculated and observed transition frequencies for the higher J lines are attributed to the centrifugal distortion and are of the magnitude expected in a light molecule.

When isotopic substitutions have been made on all atoms, Costain[5] has shown that the best method of obtaining the structure is by Kraitchman's method,[6] which gives the coordinates of each atom with respect to the principal axes of the normal species in terms of the differences between the moments of inertia of the isotopic and normal species. However, when an atom is near a principal axis, zero point vibrational effects become significant and it is no longer possible to obtain an accurate determination of the coordinate. In this case, it is necessary to use some additional conditions on the coordinates. Unfortunately, in formic acid both oxygen atoms are near the a axis while the carbon hydrogen and the carbon atom are near the b axis. The a coordinates of both oxygen atoms and of the hydroxyl hydrogen atom and the b coordinates of both hydrogen atoms and the carbon atom were obtained by Kraitchman's method. The a coordinate of the carbon hydrogen atom was calculated using a method for doubly substituted isotopes described by Pierce and Krisher.[7,8] The three remaining coordinates were then obtained by conditions on the center of mass and the condition that the sum of the products of inertia vanish in the principal axis system. Table I gives the structure of formic acid obtained in this manner and a comparison with the structures obtained by several other investigators.[9]

Because the moments of inertia of the two O^{18} species are so similar further discussion is necessary to show how the moments of inertia were identified with the chemical positions of the oxygen atoms. In the species I with rotational constant $A_I=76.5\times10^3$ Mc, the substituted oxygen atom I is definitely further from the a axis than is the substituted oxygen atom II with $A_{II}=77.2\times10^3$ Mc. In order for the product of inertia to be near zero, it is necessary that atom I be in the first quadrant by itself and that atom II be in the fourth quadrant with the hydroxyl hydrogen.

In a light molecule with so many atoms near principal axes, it is difficult to obtain the accuracy that is generally achieved in microwave structural determinations because of the relatively large zero point vibrational

TABLE II. Rotational constants and frequencies of rotational transitions (Mc).

	$HCO^{18}OH$		$HCOO^{18}H$	
	obs	calc	obs	calc
Rotational constants				
A	76521±100[a]		77206±100[a]	
B	11396.91±0.3		11383.58±0.3	
C	9904.76±0.3		9906.06±0.3	
Transition frequencies[b]				
0_{00}—1_{01}	21301.67	21301.67[c]	21289.64	21289.64[c]
1_{10}—2_{11}	44095.5	44095.46[c]	44056.8	44056.83[c]
4_{13}—4_{14}	14919.20	14919.54	14773.56	14773.72
5_{14}—5_{15}	22372.49	22374.42	22154.85	22155.93
6_{15}—6_{16}	31309.00	31311.70	31003.73	31006.42

[a] A was not directly obtained from transition frequencies (see text).
[b] All frequencies in the 14–32 kMc range are accurate to 0.1 Mc. All frequencies in the 40 kMc range are accurate to 0.2 Mc.
[c] These transitions were used to calculate the rotational constants.

effects. Our results are in fair agreement with those obtained by electron diffraction; the O—O bond distance provides the most reliable comparison between the two methods and agrees within the experimental errors.

This work was suggested by Professor E. B. Wilson, Jr., and the major portion of it was done in his laboratory.

* The research reported here was made possible by support extended to Harvard University by the Office of Naval Research and by a grant to the Rice Institute from the Research Corporation.

† Present address: Department of Chemistry, University of California, Berkeley 4, California.

‡ At Harvard University, 1957–1958.

[1] R. G. Lerner, B. P. Dailey, and J. P. Friend, J. Chem. Phys. **26**, 680 (1957).

[2] D. P. Stevenson and J. A. Ibers, Ann. Rev. Phys. Chem. **9**, 359 (1958).

[3] K. B. McAfee, Jr., R. H. Hughes, and E. B. Wilson, Jr., Rev. Sci. Instr. **20**, 821 (1949).

[4] R. Trambarulo, A. Clark, and C. Hearns, J. Chem. Phys. **28**, 736 (1958).

[5] C. C. Costain, J. Chem. Phys. **29**, 864 (1958).

[6] J. Kraitchman, Am. J. Phys. **21**, 17 (1953).

[7] L. Pierce, J. Mol. Spectroscopy **3**, 575 (1959).

[8] L. Pierce and L. C. Krisher (to be published).

[9] V. Schomaker and J. M. O'Gorman, J. Am. Chem. Soc. **69**, 2638 (1947); I. L. Karle and J. Karle, J. Chem. Phys. **22**, 43 (1954). Both of these studies were by electron diffraction.

Photochemical Evidence for Triplet State Quenching by Paramagnetic Species

WILLIAM M. MOORE, GEORGE S. HAMMOND, AND ROBERT P. FOSS

Gates and Crellin Laboratories of Chemistry, California Institute of Technology, Pasadena, California

(Received November 25, 1959)

WE have observed that inclusion of small amounts of paramagnetic solutes reduces quantum yields in photoreduction reactions of benzophenone. An adequate chemical mechanism for these reactions involves production of free radicals by hydrogen transfer from the reductant to an excited state of the ketone. Various reaction products are formed by radical coupling and disproportionation reactions.

$$(C_6H_5)_2C{=}O^* + RH \xrightarrow{k_r} (C_6H_5)_2\dot{C}OH + R\cdot$$

$$\rightarrow \text{coupling and disproportionation.}$$

Under ordinary circumstances, deactivation is a first-order process which varies little in rate in different solvents (benzene, toluene, acetonitrile, *tert*-butyl alcohol).

$$(C_6H_5)_2C{=}O^* \xrightarrow{k_d} (C_6H_5)_2C{=}O + \text{thermal energy.}$$

In the presence of paramagnetic compounds, specific, bimolecular quenching steps are added.

$$(C_6H_5)_2C{=}O^* + Q \xrightarrow{k_Q} (C_6H_5)_2CO.$$

We recently have reported[1] a study of the reaction of benzophonene with benzhydrol ($RH = (C_6H_5)_2CHOH$) in which it was found that the reduction reaction persists even when the hydrogen donor is present in low concentration. Quantitative consideration of the data indicated that the chemically active state must be a long-lived triplet. The conclusion is consistent with the fact that irradiation of benzophenone at 77° K results in phosphorescence with high quantum yield.[2]

Most of our observations of quenching effects have been made with paramagnetic metal chelate compounds in which the ligand is the dipivaloylmethide ion

$$[(CH_3)_3CCO\bar{C}HCOC(CH_3)_3].$$

Quantum yields for reduction of benzophenone by toluene or cumene $C_6H_5CH(CH_3)_2$ are reduced in the presence of trace amounts ($10^{-4}M$) of chelates of iron(III), samarium, and erbium. The corresponding aluminum chelate has no measurable effect. Oxygen effects on reduction by toluene and cumene cannot be studied because oxygen is very rapidly removed from the system by chemical reactions. However, oxygen effects on the reaction with benzhydrol are observed even after massive amounts of photoreaction have been carried out. This is consistent with the report by Bäckstrom[3] that photooxidation of benzhydrol is a very slow, nonchain reaction. In our experiments the number of excited ketone molecules deactivated exceeds the number of quencher molecules present by as much as one hundred-fold.

Figure 1 shows plots of $1/\Phi$ against $1/[\text{benzhydrol}]$ for degassed benzene solutions, for solutions containing dissolved air under one atmosphere pressure, and for solutions containing 10^{-4} ferric dipivaloylmethide. From the slopes of the lines one can evaluate $k_Q[Q]/k_r$ for the two quenchers. If the oxygen concentration remains near that of the saturated solution ($10^{-3}M$), the results indicate that $k_{Q(O_2)} = 3.6\ k_{Q(\text{Fe chelate})}$. The fact that the efficiencies of the two quenchers are similar implies that both quenching processes may be diffusion controlled. Bäckstrom and Sandros[4] reported a value of 5×10^9 liter mole^{-1} sec^{-1} for the quenching of biacetyl phosphorescence by oxygen and Livingston and Tanner[5] reported a rate of 2×10^9 liter mole^{-1} sec^{-1} for oxygen quenching of anthracene triplet. Both values are about those expected for diffusion-controlled reactions.

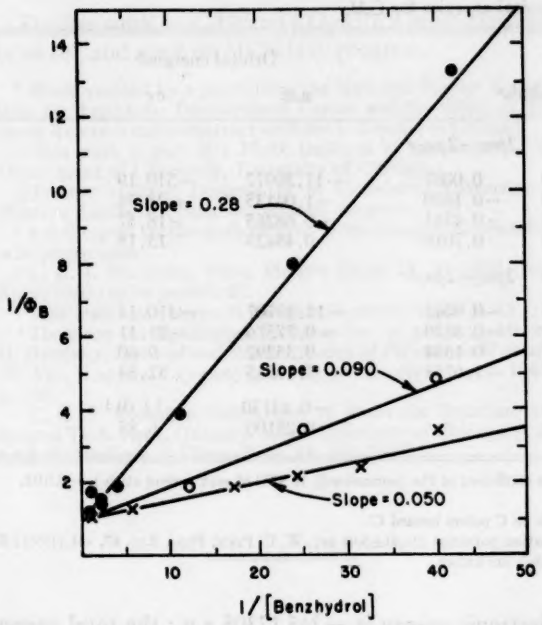

FIG. 1. Photoreduction of $0.1M_4$ benzophenone by benzhydrol in benzene solution. Crosses: no additive; open circles: $10^{-4}M$ Fe(DPM)$_3$; filled circles: oxygen ($\sim 10^{-3}M$).

Although one could not be sure that quenching did not involve chemical reaction in the earlier experiments, we can be reasonably certain that in the benzophenone-benzhydrol system quenching is a physical process and is at least close to diffusion controlled in the systems studied.

Ample precedent exists for the chemical effects observed. The most direct analogy is found in the work of Porter and Wright[6] who observed directly the quenching of anthracene triplets, produced by flash photolysis, by oxygen, nitric oxide, and paramagnetic metal ions. It is interesting to note that in their work the efficiency of oxygen quenching exceeded that of metal ions by a substantial margin. Phosphorescence quenching has been mentioned and singlet-triplet absorption bands have been observed in the presence of paramagnetic solutes.[7,8] *Cis-trans* isomerization of olefins is catalyzed by nitric oxide[9,10] in a process which is believed to involve a triplet transition state. McConnell[11] has suggested a reasonable mechanism to account for the catalytic effect and there seems to be no reason to doubt that a similar mechanism applies to triplet deactivation by triplets (such as O_2) or by paramagnetic substances having higher degeneracy (such as iron chelates).

Because of their lower chemical reactivity metal chelates are much more attractive than oxygen for the study of quenching phenomena. Such compounds should be generally useful for the investigation of the mechanisms of photochemical processes and for the estimation of lifetimes of triplet states.

[1] G. S. Hammond and W. M. Moore, J. Am. Chem. Soc. (to be published).
[2] E. H. Gilmore, G. E. Gibson, and D. S. McClure, J. Chem. Phys. **20**, 829 (1952); **23**, 399 (1955).
[3] H. L. J. Bäckstrom, *The Svedberg Memorial Volume* (Alnaquist and Wiksells Boktryckeri, Uppsala, Sweden, 1944).
[4] H. J. L. Bäckstrom and K. Sandros, J. Chem. Phys. **23**, 2197 (1950).
[5] R. Livingston and D. W. Tanner, Trans. Faraday Soc. **54**, 765 (1958).
[6] G. Porter and M. R. Wright, J. Chim. Phis. **55**, 705 (1958).
[7] D. F. Evans, J. Chem. Soc. **1958**, 1351.
[8] J. N. Chauduri and S. Basu, Trans. Faraday Soc. **54**, 1605 (1958).
[9] J. L. Magee, W. Shand, and H. Eyring, J. Am. Chem. Soc. **63**, 677 (1941).
[10] B. S. Rabinovitch and F. S. Lowry, J. Chem. Phys. **23**, 2439 (1955).
[11] H. M. McConnell, *ibid.* **20**, 1043 (1952); **23**, 2440 (1955).

LCAO-MO-SCF Ground State Calculations on C_2H_2 and CO_2*†

A. D. McLEAN‡

Laboratory of Molecular Structure and Spectra, University of Chicago, Chicago 37, Illinois

(Received December 14, 1959)

THIS communication reports the first work on linear polyatomic molecules carried out in LCAO-MO-SCF approximation using a recently completed program for a Univac Scientific 1103 A digital computer. The program was written by the author (integrals[1]), Mr. A. Weiss (control program) and Mr. M. Yoshimine (Roothaan open and closed shell SCF procedures[2]), and operates completely automatically with a minimum of input data (basis functions, internuclear distances, electronic configuration, symmetry, and nuclear charges). Restrictions are that the basis functions be Slater type orbitals (STO's) whose principal quantum number is $\leqslant 8$ and that there are $< \approx 16$. The number of nuclei in the molecule must be $\leqslant 4$. All integrals are computed accurate to at least five decimal places; the total energy and orbital energies[3] are believed accurate to at least four decimal places. Coefficients in the molecular orbitals are accurate to four decimal places.

The C_2H_2 calculation was done for the ground state configuration $1\sigma_g^2 1\sigma_u^2 2\sigma_g^2 2\sigma_u^2 3\sigma_g^2 1\pi_u^4$ with $R_{CH}=2.002$ a.u. (1.0595 A), $R_{CC}=2.281$ a.u. (1.207 A).[4] The MO's were constructed from $1s(\zeta=1.00)$ STO's on each H, and $1s(\zeta=5.6726)$, $2s(\zeta=1.6082, 2p\sigma, 2p\pi$ $(\zeta=1.56805)$ STO's on each C. The carbon ζ's are "best atom" values.[5] Table I lists the molecular orbitals and orbital

TABLE I. LCAO–MO's and orbital energies for C_2H_2.

MO's	Coefficients of symmetry orbitals[a]				Orbital energies[b] a.u.	ev
	$1s_H+1s_{H'}$	$1s_C+1s_{C'}$	$2s_C+2s_{C'}$	$2p\sigma_C-2p\sigma_{C'}$[c]		
$1\sigma_g$	0.0033	−0.7045	−0.0100	0.0007	−11.39977	−310.19
$2\sigma_g$	−0.1033	0.1722	−0.4670	−0.1850	−1.04135	−28.34
$3\sigma_g$	0.3109	−0.0009	0.0965	−0.4761	−0.68265	−18.57
$4\sigma_g$	1.0594	0.0647	−0.8256	0.7016	0.48423	13.18
	$1s_H-1s_{H'}$	$1s_C-1s_{C'}$	$2s_C-2s_{C'}$	$2p\sigma_C+2p\sigma_{C'}$		
$1\sigma_u$	0.0031	−0.7049	−0.0193	−0.0042	−11.39707	−310.11
$2\sigma_u$	0.2957	−0.1118	0.3237	−0.3139	−0.77576	−21.11
$3\sigma_u$	0.9259	0.1360	−1.1807	0.1334	0.35292	9.60
$4\sigma_u$	−0.5989	0.0595	−1.3291	−1.6753	1.19545	32.53
$1\pi_u$		$0.6071(2p\pi_C+2p\pi_{C'})$			−0.44130	−12.01[d]
$1\pi_g$		$0.8814(2p\pi_C-2p\pi_{C'})$			0.25100	6.83

[a] For example, the entry −0.7045 under $1s_C+1s_{C'}$ for the MO $1\sigma_g$ means that the coefficient of the (normalized) 1s STO of *each* carbon atom is −0.7045.
[b] 1 a.u.=27.210 ev.
[c] All z axes are taken in the same direction along the internuclear axis. The z axis on C points toward C'.
[d] The computed $1\pi_u$ $\epsilon(-12.01$ ev) agrees well with the observed minimum ionization potential (11.41±0.01 ev). W. C. Price, Phys. Rev. **47**, 444 (1935); K. Watanabe, J. Chem. Phys. **26**, 542 (1957). No higher experimental ionization potentials are known.

energies obtained. The total electronic energy is −101.28327 a.u.; the total energy −76.54383 a.u. Approximately two hours of computer time was used.

The CO_2 calculation was done for the ground state configuration $1\sigma_u^2 1\sigma_g^2 2\sigma_g^2 3\sigma_g^2 2\sigma_u^2 4\sigma_g^2 1\pi_u^4 3\sigma_u^2 1\pi_g^4$ with $R_{CO}=2.1944$ a.u. (1.1613 A).[4] The basis functions were 1s ($\zeta=7.658$), 2s ($\zeta=2.2461$), and $2p\sigma$, $2p\pi$ ($\zeta=2.22625$) STO's on each O, 1s ($\zeta=5.6726$), 2s ($\zeta=1.6082$), $2p\sigma$, $2p\pi$ ($\zeta=1.56805$) on the C. The total electronic energy is −245.17305 a.u.; the total energy −186.84275 a.u. Computer time used was approximately three hours. Table II lists the molecular orbitals and orbital energies and compares the ϵ's with those computed by Mulligan[6] in a calculation differing from the present one mainly by approximating certain integrals and neglecting inner-outer shell mixing, and with the reliable (±0.01 ev) experimental ionization potentials.

TABLE II.[a] LCAO–MO's and orbital energies for CO_2.

MO's	Coefficients of symmetry orbitals					Orbital energies a.u.	ev	Mulligan[b]	Exptl. Ion Pot'ls
	$1s_O+1s_{O'}$	$2s_O+2s_{O'}$	$2p\sigma_O-2p\sigma_{O'}$	$1s_C$	$2s_C$				
$1\sigma_g$	0.7049	0.0106	0.0031	0.0002	0.0067	−20.72473	−563.92	−560	524[c]
$2\sigma_g$	0.0003	0.0025	−0.0002	−0.9969	−0.0146	−11.60351	−315.73	−314	284[c]
$3\sigma_g$	−0.1408	0.5144	0.1603	−0.1497	0.3265	−1.51199	−41.14	−44.9	
$4\sigma_g$	−0.1028	0.5390	−0.4156	0.1411	−0.5448	−0.72513	−19.73	−19.1	19.38[d]
$5\sigma_g$	−0.0739	0.5719	0.6974	0.1470	−1.3571	0.44149	12.01	16.8	
	$1s_O-1s_{O'}$	$2s_O-2s_{O'}$	$2p\sigma_O+2p\sigma_{O'}$		$2p\sigma_C$				
$1\sigma_u$	0.7048	0.0131	0.0044		0.0093	−20.72500	−563.93	−560	524[c]
$2\sigma_u$	0.1531	−0.5241	−0.1298		0.3156	−1.44104	−39.21	−42.4	
$3\sigma_u$	0.0766	−0.4753	0.5099		−0.4435	−0.62949	−17.13	−17.9	18.07[d,e]
$4\sigma_u$	0.0925	−1.0097	−0.7802		−1.7889	1.25843	34.24	18.5	
$1\pi_u$	$0.4504(2p\pi_O+2p\pi_{O'})+0.5729\ 2p\pi_C$					−0.68654	−18.68	−18.8	17.36[e]
$2\pi_u$	$0.6066(2p\pi_O+2p\pi_{O'})-0.9059\ 2p\pi_C$					0.26233	7.14	9.3	
$1\pi_g$	$0.7094(2p\pi_O-2p\pi_{O'})$					−0.44033	−11.98	−11.5	13.79[d]

[a] See footnotes a–c, Table I.
[b] Reference 6.
[c] J. Thibaud, Compt. rend. **186**, 308 (1928); *K*-shell x-ray absorption limits.
[d] Price and Simpson; Henning; Tanaka *et al.* (see Y. Tanaka, A. S. Jursa, and F. J. Le Blanc, J. Chem. Phys. **28**, 350 (1958) and forthcoming paper), from Rydberg series spectra of CO_2. $4\sigma_g$ from Tanake *et al.* only.
[e] From emission spectra of CO_2^+ combined with $1\pi_g$ potential of 13.79 ev; see S. Mrozowski; Revs. Modern Phys. **14**, 216 (1942); Phys. Rev. **60**, 730 (1941); **62**, 270 (1942); **72**, 682, 691 (1947); cf. R. S. Mulliken, Revs. Modern Phys. **14**, 204 (1942), and Can. J. Chem. **36**, 10 (1958).

Further work on C_2H_2 and CO_2 with a more extensive basis set, and work on HCN is in progress.

* Work assisted by a grant from the National Science Foundation, by Wright Air Development Center and the Office of Ordnance Research under contract with the University of Chicago.

† This work is part of a Ph.D. thesis to be submitted to the Department of Chemistry, University of Chicago.

‡ Present address: Department of Chemistry, University of Western Australia, Nedlands, Western Australia.

[1] A full report on the analysis used in the integral computation is in preparation.

[2] C. C. J. Roothaan, Revs. Modern Phys. **23**, 69 (1951); also April, 1960 (to be published).

[3] This statement refers to energies in atomic units (a.u.).

[4] These are the equilibrium distances for the ground state; see G. Herzberg, *Infrared and Raman Spectra of Polyatomic Molecules* (D. Van Nostrand Company, Inc., Princeton, New Jersey, 1945), p. 398.

[5] C. C. J. Roothaan, Laboratory of Molecular Structure and Spectra Tech. Rept. (January, 1955), University of Chicago, p. 24.

[6] J. F. Mulligan, J. Chem. Phys. **19**, 347 (1951).

K-Type Doubling in Phosphine*

J. M. Hoffman, H. H. Nielsen, and K. Narahari Rao

Department of Physics and Astronomy, The Ohio State University, Columbus 10, Ohio

(Received December 15, 1959)

In the perpendicular band, ν_4, of phosphine, we have observed for the first time a doubling of the ${}^RR(J, 3)$ lines. This doubling is indicated as a broadening of the ${}^RR(7, 3)$ line, but is clearly resolved in the ${}^RR(8, 3)$, ${}^RR(9, 3)$, and ${}^RR(10, 3)$ lines (Fig. 1). The effect resembles that observed in the microwave spectra of NH_3 and explained by Nielsen and Dennison[1] as due to the splitting of the rotational levels in the ground state where $K=3q(q=1, 2, 3, \cdots)$. This splitting is approximately 10^{-3} cm^{-1} in NH_3 and is even smaller in PH_3. The doubling we observe in PH_3 is of the order of 0.1 cm^{-1} and must therefore primarily be due to a splitting of the level $K=\pm 4$, $l=\pm 1$ in the excited state ν_4.

A term of second order importance in the Hamiltonian for a molecule like PH_3 which will cause this splitting in the excited state, but not in the ground state, has been discussed by Nielsen[2] and referred to as a second order rotational resonance. In the notation of Amat *et al.*[3] this term has the form

$$H_2' = \cdots + \sum_{\alpha\beta} \sum_{ab, a\leq b} ({}^{\alpha\beta}{}_{(2)}Y^{ab} p_a p_b + {}^{\alpha\beta}{}_{(2)}Y_{ab} q_a q_b) P_\alpha P_\beta. \quad (1)$$

The matrix elements, which contribute to the energy in the second order only when resonance between the ν_2 and ν_4 levels exists, are:

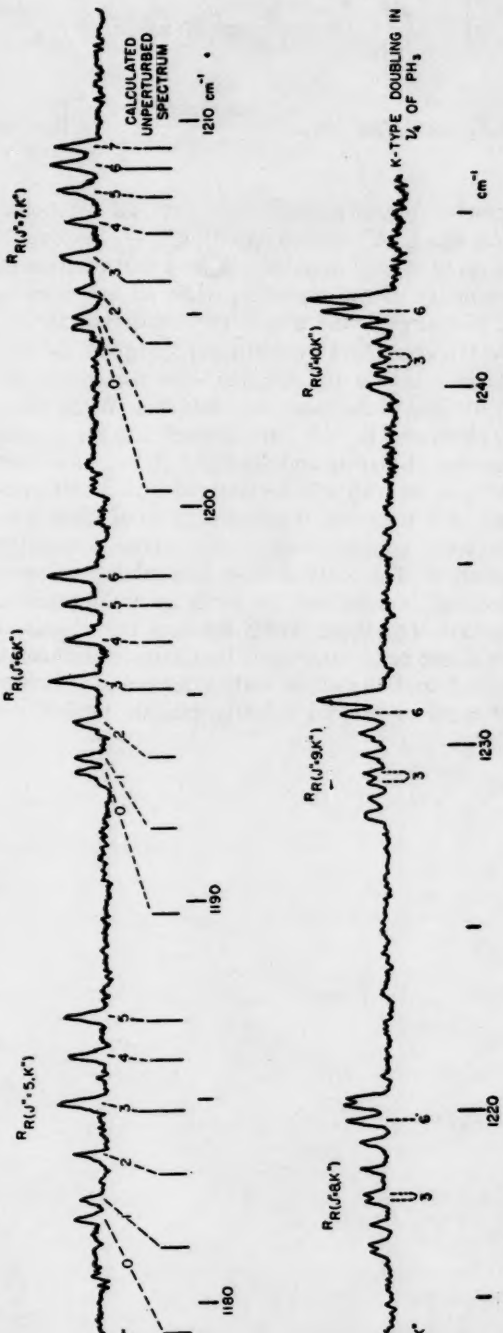

FIG. 1. The ν_4 perpendicular band of PH_3 from $J''=5$ to $J''=10$. The lower spectrum shows K-type doubling of ${}^RR(J, 3)$ lines. Separations of the doublets are 0.16_6, 0.26_7, and 0.33_9 cm^{-1}, respectively, for $J''=8$, 9, and 10. The unperturbed spectrum is calculated on the assumption of no Coriolis resonance between ν_2 and ν_4 vibrations.

$$(v_2-1,\ v_4,\ l_4,\ K \mid H'_2/hc \mid v_2,\ v_4-1,\ l_4\mp 1,\ K\pm 2)$$

$$=(v_2,\ v_4-1,\ l_4\mp 1,\ K\pm 2 \mid H'_2/hc \mid v_2-1,\ v_4,\ l_4,\ K)$$

$$=\left[\mp\frac{B_e^2}{2(\omega_2\omega_4)^{\frac{1}{2}}}\left\{\frac{3}{2}\frac{a_2^{(xx)}a_{41}^{(xx)}}{I_x}+2\zeta_{2,32}^{(x)}\zeta_{41,32}^{(x)}\frac{(\omega_2^2\omega_4^2-\omega_3^4)}{(\omega_2^2-\omega_3^2)(\omega_4^2-\omega_3^2)}\right\}\right.$$

$$\left.\mp B_e^2(\omega_2\omega_4)^{\frac{1}{2}}\zeta_{2,32}^{(x)}\zeta_{41,32}^{(x)}\frac{(\omega_4^2+\omega_2^2-2\omega_3^2)}{(\omega_2^2-\omega_3^2)(\omega_4^2-\omega_3^2)}\right]\{v_2(v_4\pm l_4)\}^{\frac{1}{2}}[(J\mp K)(J\mp K-1)(J\pm K+1)(J\pm K+2)]^{\frac{1}{2}}. \quad (2)$$

Symmetry considerations show that all rotational levels for which $|K'-l|=3q$ $(q=0, 1, 2, \cdots)$ belong to species A_1 or A_2 and may be split by a perturbation of the symmetry of the molecule, while all other levels belong to species E and remain twofold degenerate.

Only the case $J=4$ in the upper state will be discussed since this is the simplest case for which the ${}^RR(J, 3)$ lines could show this doubling. When these matrix elements [Eq. (2)] are inserted into the secular determinant of Garing and Nielsen,[4] it becomes more complicated but can still be factored into 3 subdeterminants of 9 rows and 9 columns. Two of these subdeterminants contain only levels whose symmetry species are E. The roots of these two subdeterminants are identical showing that the levels remain degenerate as required. The third, which contains only levels of species A, can be factored again into 2 subdeterminants, one with 5 and the other with 4 rows and columns. The 9 roots of these 2 subdeterminants predict the following results:

the splitting of the $K=\pm 1$, $l=\pm 1$ levels ("giant" l-type doubling),
the splitting of the $K=\pm 2$, $l=\mp 1$ levels,
the splitting of the $K=\pm 4$, $l=\pm 1$ levels,
and some of the perturbed levels in ν_2.

* One of us (HHN) acknowledges the support of the National Science Foundation. Thanks are also due the Office of Ordnance, U. S. Army, and the Cambridge Air Force Research Center for their partial support through contracts with The Ohio State University Research Foundation.

[1] H. H. Nielsen and D. M. Dennison, Phys. Rev. 72, 1101 (1947).
[2] H. H. Nielsen, Revs. Modern Phys. 23, 90 (1951); H. H. Nielsen, *Handbuch der Physik* (Springer-Verlag, Berlin, 1959), Bd. XXXVII/1, p. 304.
[3] G. Amat, M. Goldsmith, and H. H. Nielsen, J. Chem. Phys. 27, 838 (1957).
[4] J. S. Garing and H. H. Nielsen, Proc. Natl. Acad. Sci. U.S. 44, 467 (1958); J. S. Garing, H. H. Nielsen, and K. Narahari Rao, J. Mol. Spectroscopy 3, 496 (1959).